Tangled Circuits

Characterizing Errors in Experimental Superconducting Quantum Processors

by

Gabriel Orr Samach

B.A., Williams College (2015)
S.M., Massachusetts Institute of Technology (2021)

Submitted to the Department of Electrical Engineering and Computer Science
in partial fulfillment of the requirements for the degree of

Doctor of Philosophy

at the

MASSACHUSETTS INSTITUTE OF TECHNOLOGY

February 2023

Author .....
Department of Electrical Engineering and Computer Science
November 9, 2022

Certified by .....
William D. Oliver
Professor of Electrical Engineering and Computer Science
Thesis Supervisor

Accepted by .....
Leslie A. Kolodziejski
Professor of Electrical Engineering and Computer Science
Chair, Department Committee on Graduate Students

Tangled Circuits

Characterizing Errors in Experimental Superconducting Quantum Processors

by

Gabriel Orr Samach

Submitted to the Department of Electrical Engineering and Computer Science
on November 9, 2022, in partial fulfillment of the
requirements for the degree of
Doctor of Philosophy

Abstract

As progress is made towards the first generation of error-corrected quantum computers based on physical quantum bits (qubits), researchers require robust techniques for designing, operating, and characterizing coupled multi-qubit systems in the laboratory, and for understanding the errors which arise in such systems. This doctoral thesis is structured around three interconnected bodies of technical work which span the field of superconducting quantum information science. In Part II, we consider the design, simulation, and measurement of high coherence quantum bits mediated by tunable coupler elements, a fundamental building block of extensible quantum processors based on superconducting Josephson circuits. In Part III, we consider the calibration of high fidelity single- and two-qubit gate operations, and we show how these operations were harnessed to perform a demonstration of Density Matrix Exponentiation, a deep Trotter-like quantum algorithm. In Part IV, we consider an array of techniques for the characterization, verification, and validation of quantum computing hardware, and we put forth a novel quantum characterization technique for reconstructing the dynamic loss channels of multi-qubit systems, known as Lindblad tomography. Framing the dissertation on each end, Parts I and V offer a complementary account of quantum computing grounded in feminist science and technology studies, situating quantum computing as a historical, social, and material-semiotic enterprise, complicating the narrative of progress which animates our work in the laboratory.

Thesis Supervisor: William D. Oliver
Title: Professor of Electrical Engineering and Computer Science

This doctoral thesis has been examined by a Committee of the Department of Electrical Engineering and Computer Science as follows:

Professor William D. Oliver .....
Thesis Supervisor
Henry Ellis Warren Professor of EECS, MIT

Dr. Robin Blume-Kohout .....
Member, Thesis Committee
Principal Member of Technical Staff, Sandia National Labs

Professor Stefan Helmreich .....
Member, Thesis Committee
Elting E. Morison Professor of Anthropology, MIT

Dr. Andrew J. Kerman .....
Member, Thesis Committee
Senior Staff, MIT Lincoln Laboratory

Professor Kevin O'Brien .....
Member, Thesis Committee
Emanuel E. Landsman Assistant Professor of EECS, MIT

The text you are holding, physically or digitally, is a work in progress and in process. As a consequence, the reader may find—in the course of this volume of errors—errors of different sorts.

If you would like to discuss this work or read an updated version of this text, please get in touch.

gabriel.samach@mit.edu

However long you spend here, thank you for your time.

This document was typeset on:

November 9, 2022

Acknowledgments

There is one name on the title page of this thesis, but that name does not belong to the sole author of this work. Here, I would like to gratefully acknowledge all of the mentors, colleagues, friends, family members, and guides who—together, in community and collaboration—gave this thesis form and meaning. This is the true author list of this work.

First, thank you to the members of my thesis committee, all of whom contributed to this work long before a single word of it was written. Foremost, to Will Oliver, for your mentorship, support, and friendship throughout this journey. We're in this for the long haul. To Jamie Kerman, for being the first scientist to truly trust me as a peer, an honor I'm still trying to live up to. None of this would exist if our paths hadn't crossed in Thompson Physics Lab back in late October 2014. To Stefan Helmreich, for your incredible generosity, encouragement, and conversation in the moments when the path ahead seemed least clear. I would not be the scholar I am today without you. To Robin Blume-Kohout, for your valuable feedback and discussion during the final stages of the Lindblad tomography work; for your generous and extensive bibliography of quantum characterization literature; and for your warm welcome to the QCVV community. I have learned so much from our conversations together, and I look forward to continuing those conversations for years to come. To Kevin O'Brien, for your profound support and friendship during my transition back to graduate school. As I look ahead to life beyond graduate school, the training, mentorship, and care you demonstrate to the members of your group inspire me enormously.

Next, thank you to all of my colleagues in the Engineering Quantum Systems (EQuS) group at MIT, past and present, for supporting me from my earliest days as an interloper in the group back in 2015 all the way through grad school: Aziza

For a complementary narrative account of the people, places, and events which shaped this text, see Section 1.5 of this thesis.

Almanakly, Junyoung An, Lamia Ateshian, Will Banner, Franck Belemkoabga, Charlotte Boettcher, Jochen Braumueller, Dan Campbell, Shoumik Chowdhury, Agustin Di Paolo, Leon Ding, Andy Ding, Alex Greene, Jeff Grover, Aranya Goswami, Simon Gustavsson, Patrick Harrington, Max Hays, Shantanu Jha, Archana Kamal, Harry Kang, Bharath Kannan, Amir Karamlou, Morten Kjaergaard, Junghyun Kim, Philip Krantz, Dani Rodan Legrain, Ben Lienhard, Rebecca Li, Chris McNally, Tim Menke, Miguel Moreira, Sarah Muschinske, Will Oliver, Terry Orlando, David Pahl, Lukas Pahl, Elaine Pham, Mirabella Pulido, Jack Qiu, Ilan Rosen, David Rower, Youngkyu Sung, Miuko Tanaka, Francisca Vasconcelos, Antti Pekka Vepsalainen, Joel Wang, Chihiro Watanabe, Roni Winik, Megan Yamoah, Fei Yan, Beatriz Yankelevich, Daniela Zaidenberg, Sameia Zaman.

Among my colleagues in EQuS, I would like to offer special thanks to the following individuals, without whom the work in this volume literally would not have been possible. To Morten Kjaergaard: for the late nights in lab, crumpled on the floor cackling over gate fidelities; for the NA brews and Saturday morning climbing outings with Maria and Baby A; for the hardcore album recommendations, concert nights in Allston, and trips to Buk Kyung II; for encouraging me to stick with this journey, to keep chopping the wood, to keep carrying the water. When I joined EQuS, I was told I could work with whoever I wanted; I've never regretted my choice for a second. To Alex Greene, the best experimentalist I know. Thank you so much for all of your support, care, and patience showing me the ropes early in grad school and throughout our time working together. To Chris McNally, for reminding me to practice what I preach, and for showing me that, at their best, all our experiments are art projects. To Elaine Pham, for your deep patience and infectious enthusiasm during my first attempts at mentorship. You helped me see a different side of my work, at a moment when I most needed a change of perspective. To Chihiro Watanabe and Mirabella Pulido, for all of your work in the group office. EQuS would not exist without the two of you. To Jeff Grover, for your incredible friendship throughout our long and mutually winding paths through campus and Lincoln, and for your immense support during the writing of this thesis. We both know that MIT is a much kinder, gentler,

and more thoughtful place with you in it. To Simon Gustavsson and Terry Orlando, for your warm welcomes to campus back in 2015, and for both of your support and guidance throughout my time in grad school. And finally, a special thanks to all of the graduate students who have joined EQuS in the years since I started in the group, especially during the COVID-19 pandemic. The care that you all show for one another and for your work inspires me totally. You are building something incredible together, and I am not talking about a quantum computer. I will always have your backs.

I owe a deep gratitude to my colleagues in the Quantum Information and Integrated Nanosystems group at MIT Lincoln Laboratory, many of whom supported and mentored me during my earliest days as a researcher: Sam Alterman, Kate Azar, Peter Baldo, James Basham, Vlad Bolkhovsky, Jeff Birenbaum, Colin Bruzewicz, Greg Calusine, John Chiaverini, John Cummings, Rabi Das, Steve Disseler, Eric Dauler, Alexandra Day, Bryce Fisher, George Fitch, Evan Golden, Mark Gouker, Tom Hazard, Cyrus Hirjibehedin, Gerry Holland, David Hover, Bethany Niedzielski Huffman, Erin Jones-Ravgiala, Paul Juodawlkis, Jamie Kerman, Dave Kharas, David Kim, Jeff Knecht, Arthur Kurlej, Justin Mallek, Lee Mailhiot, Alex Melville, Jovi Miloshi, Peter Murphy, Dan Oates, Kevin Obenland, Mike O'Keeffe, Will Oliver, Mallika Randeria, Danna Rosenberg, Jeremy Sage, Barbara Santorella, Andrew Savage, Meghan Schuldt, Mollie Schwartz, Adam Sears, Kyle Serniak, Arjan Sevi, Rick Slattery, Katrina Sliwa, Sergey Tolpygo, Shireen Warnock, Steve Weber, Terry Weir, Wayne Woods, Jonilyn Yoder, Donna-Ruth Yost.

Among my colleagues at Lincoln Lab, I owe a special gratitude to the following individuals for their support at different points in my career. First, to the generation of researchers who supported me in the period between 2015 and 2018, before my transition to graduate school. To Steve Weber, for taking me under your wing early in this journey and showing me the ropes in the laboratory. To Greg Calusine, David Hover, David Kim, Danna Rosenberg, Mollie Schwartz, and Jonilyn Yoder, for your friendship and camaraderie throughout this journey. I became an experimentalist because I wanted to work with all of you, and I am so glad I did. To the generation of

researchers who joined Lincoln during my time in graduate school: Kate Azar, Bryce Fisher, Tom Hazard, Mallika Randeria, Kyle Serniak, Katrina Sliwa. Among these colleagues, I owe a deep and particular gratitude to Kyle Serniak, for your friendship and encouragement during my time in grad school, particularly during the transition period back to Lincoln in the final year. Together, you all make me so excited for the next chapter of this journey.

Thank you to all of my mentors and professors during my time as an undergraduate at Williams College. Among my many mentors during this period, I owe a deep and lasting gratitude to my thesis advisor, Bill Wootters. You were the first person to show me that quantum mechanics was beautiful, and I have been chasing that feeling ever since. I don't always find it in my work, but over the years I keep finding that same feeling in the strangest and most wonderful places. I would not be here with you. To Chris Bolton, for teaching me that everything is a text, that everything can be read. To all of my college professors, on both sides of Route 2: Christopher Bolton, Julie Cassiday, Margeaux Cowden, Bill Darrow, Charlie Doret, Eugene Johnson, Kevin Jones, Mike Lewis, Ward Lopes, Tiku Majumder, Anjuli Raza-Kolb, Mike Seifert, David Tucker-Smith, Janneke van de Stadt, William Wootters, Li Yu.

To all of my friends for their support and care throughout this journey. To Teddy Amdur and Cole Meisenhelder, for convincing me to give physics another shot all the way back in 2012, and for carrying me through the next three years of problem sets. You taught me that physics is something that you do with people. I've never forgotten that, and I'm still here. To all of my friends in the Williams physics department for their support and for the wild research summers we shared on campus back in 2013 and 2014: Ilya Amburg, Weng-Him Cheung, Julia Cline, Dan Evangelakos, Sarah Fleming, Chip Herman, Isaac Hoenig, Kitty Kistler, Max LaBerge, Kamuela Lau, Brandon Ling, Bijan Mazaheri, Cesar Melendez, Sarah Peters, Corey Smith, Kirk Swanson, Scott Wieman. To my college friends beyond physics, for bringing balance to my life in so many ways, especially in the years after graduation: Jeremy Boissevain, Liz Dietz, Adrienne Favis, Kate Flanagan, Jack Hoover, Wei Li, David Yan. To all of the friends and comrades who joined this journey during grad school,

for your encouragement, feedback, and conversation on so many things over the years: Maria Genckel, Lindsay Johnson, Will Julian, Julia Menzel, Taylor Southworth, Mike Sugarman, Nina Wexelblatt. Our dinner parties, climbing sessions, and evenings at Rebel Rebel sustained me in so many ways.

A thesis is, first and foremost, a written document, and I owe a deep gratitude to so many writers for their impact and influence during the development of this document. First, to Marvin Lin and the entire crew at Tiny Mix Tapes, for all of your support and encouragement in the publication of my first written work all the way back in 2013. To the writers whose work has impacted my own throughout this journey, past and present: Hanif Abdurraqib, Camae Ayewa, James Baldwin, Karen Barad, Ruha Benjamin, Andrea Long Chu, Samuel Delaney, Ruth Wilson Gilmore, Stefano Harney, Cheryl Harris, Shigesato Itoi, Ilya Kaminsky, Thebe Neruda Kgositsile, Ursula K. Le Guin, Emma McKay, Herman Melville, Fred Moten, Rasheedah Phillips, Chanda Prescod-Weinstein, Anthony Veasna So, Ocean Vuong.

To the gardeners, pollinators, vegetables and wildflowers of Sacramento Street Community Garden, where much of this thesis was written and dreamed. To Inky, Bozeman, and all the neighborhood outdoor cats whose companionship enriched the meditative walks between writing sessions. To the workers at Cambridge Public Works, for their maintenance of the roads, bike lanes, public parks, and countless other infrastructures which made this work possible. To all of the workers and organizers in the MIT Graduate Student Union, for keeping it rolling.

Through it all, thank you to my family. To my sisters, Maya and Ariel Samach, for being my role models when we were growing up. When I tell friends and coworkers about the two of you, they sometimes comment on how we chose such different paths. I think the three of us know that, actually, we're on the same path. We always will be. I've learned more from the two of you over these past three decades than anyone, and this thesis proves that. To my parents, Beth and Raffie Samach, for reminding me to always be myself and to never forget where I came from. Those two lessons have kept me grounded through all stages of this journey. I would not be here without your love and support in so many different ways.

And finally, to my best friend, to my collaborator in all things, to my careful editor, and to my partner, in the truest sense of the word. To Sarah McClain Fleming. None of this would have been possible without you. Looking back through this thesis, I see you everywhere.

The first epigraph on page 19 has been excerpted from the conclusion of "Information, Physics, Quantum: The Search for Links" by John Archibald Wheeler [468]; the second, an exchange between the blinded Earl of Gloucester and the mad King Lear during their final reunion on the heath, is taken from Act IV Scene 5 of Shakespeare's *The Tragedy of King Lear* (the folio text) [416].

Land Acknowledgment

In March 2020, my employer—the Massachusetts Institute of Technology—issued the following land acknowledgment, drafted by members of MIT's Indigenous community, including students, staff, visiting scholars, and alumni, as well as officials from local tribal organizations and staff from the ICEO and the Office of Intercultural Engagement:

> MIT acknowledges Indigenous Peoples as the traditional stewards of the land, and the enduring relationship that exists between them and their traditional territories. The land on which we sit is the traditional unceded territory of the Wampanoag Nation. We acknowledge the painful history of genocide and forced occupation of their territory, and we honor and respect the many diverse indigenous people connected to this land on which we gather from time immemorial.

During the writing of this thesis, MIT announced that it was initiating a formal process to develop a new statement based on feedback the Institute had received since this original statement was released, including disagreements among Native American tribes regarding historical land claims in Cambridge and surrounding areas. At the time of writing, this revised statement is still forthcoming.

Funding Acknowledgment

The author acknowledges financial support from the Lincoln Scholars Program fellowship at MIT Lincoln Laboratory for the duration of their graduate studies at MIT.

Portions of the research presented in Parts II, III, and IV of this thesis were funded in part by the U.S. Army Research Office Grant W911NF-18-1-0411 and the Assistant Secretary of Defense for Research & Engineering under Air Force Contract No. FA8721-05-C-0002.

Opinions, interpretations, conclusions, and recommendations expressed in this thesis are those of the author and are not necessarily endorsed by the United States Government.

A single question animates this report: Can we ever expect to understand existence? Clues we have, and work to do, to make headway on that issue. Surely someday, we can believe, we will grasp the central idea of it all as so simple, so beautiful, so compelling that we will say to each other, "Oh, how could it have been otherwise! How could we have been blind so long!"

—John Archibald Wheeler

LEAR *Read.*

GLOUCESTER *What—with the case of eyes?*

LEAR *O ho, are you there with me? No eyes in your head, nor no money in your purse? Your eyes are in a heavy case, your purse in a light; yet you see how this world goes.*

GLOUCESTER *I see it feelingly.*

LEAR *What, art mad? A man may see how this world goes with no eyes; look with thine ears.*

Tangled Circuits

Contents

List of Figures

List of Publications

[481] Fei Yan, Simon Gustavsson, Archana Kamal, Jeffrey Birenbaum, Adam P Sears, David Hover, Ted J. Gudmundsen, Danna Rosenberg, Gabriel Samach, S. Weber, Jonilyn L. Yoder, Terry P. Orlando, John Clarke, Andrew J. Kerman, and William D. Oliver. "The flux qubit revisited to enhance coherence and reproducibility". In: *Nature Communications* 7.1 (2016), p. 12964. DOI: 10.1038/ncomms12964. URL: https://doi.org/10.1038/ncomms12964

[174] Simon Gustavsson, Fei Yan, Gianluigi Catelani, Jonas Bylander, Archana Kamal, Jeffrey Birenbaum, David Hover, Danna Rosenberg, Gabriel Samach, Adam P. Sears, Steven J. Weber, Jonilyn L. Yoder, John Clarke, Andrew J. Kerman, Fumiki Yoshihara, Yasunobu Nakamura, Terry P. Orlando, and William D. Oliver. "Suppressing relaxation in superconducting qubits by quasiparticle pumping". In: *Science* 354.6319 (2016), pp. 1573–1577. DOI: 10.1126/science.aah5844. eprint: https://www.science.org/doi/pdf/10.1126/science.aah5844. URL: https://www.science.org/doi/abs/10.1126/science.aah5844

[463] Steven J. Weber, Gabriel O. Samach, David Hover, Simon Gustavsson, David K. Kim, Alexander Melville, Danna Rosenberg, Adam P. Sears, Fei Yan, Jonilyn L. Yoder, William D. Oliver, and Andrew J. Kerman. "Coherent Coupled Qubits for Quantum Annealing". In: *Phys. Rev. Applied* 8 (1 July 2017), p. 014004. DOI: 10.1103/PhysRevApplied.8.014004. URL: https://link.aps.org/doi/10.1103/PhysRevApplied.8.014004

[390] D. Rosenberg, D. Kim, R. Das, D. Yost, S. Gustavsson, D. Hover, P. Krantz, A. Melville, L. Racz, G. O. Samach, S. J. Weber, F. Yan, J. L. Yoder, A. J. Kerman, and W. D. Oliver. "3D integrated superconducting qubits". In: *npj Quantum Information* 3.1 (2017), p. 42. DOI: 10.1038/s41534-017-0044-0. URL: https://doi.org/10.1038/s41534-017-0044-0

[460] Joel I-Jan Wang, Daniel Rodan-Legrain, Landry Bretheau, Daniel L. Campbell, Bharath Kannan, David Kim, Morten Kjaergaard, Philip Krantz, Gabriel O. Samach, Fei Yan, Jonilyn L. Yoder, Kenji Watanabe, Takashi Taniguchi, Terry P. Orlando, Simon Gustavsson, Pablo Jarillo-Herrero, and William D. Oliver. "Coherent control of a hybrid superconducting circuit made with graphene-based van der Waals heterostructures". In: *Nature Nanotechnology* 14.2 (2019), pp. 120–125. DOI: 10.1038/s41565-018-0329-2. URL: https://doi.org/10.1038/s41565-018-0329-2

[428] Youngkyu Sung, Leon Ding, Jochen Braumüller, Antti Vepsäläinen, Bharath Kannan, Morten Kjaergaard, Ami Greene, Gabriel O. Samach, Chris McNally, David Kim, Alexander Melville, Bethany M. Niedzielski, Mollie E. Schwartz, Jonilyn L. Yoder, Terry P. Orlando, Simon Gustavsson, and William D. Oliver. "Realization of High-Fidelity CZ and ZZ-Free iSWAP Gates with a Tunable Coupler". In: *Phys. Rev. X* 11 (2 June 2021), p. 021058. DOI: 10.1103/PhysRevX.11.021058. URL: https://link.aps.org/doi/10.1103/PhysRevX.11.021058

[168] A. Greene, M. Kjaergaard, M. E. Schwartz, G. O. Samach, A. Bengtsson, M. O'Keeffe, D. K. Kim, M. Marvian, A. Melville, B. M. Niedzielski, A. Vepsalainen, R. Winik, J. Yoder, D. Rosenberg, S. Lloyd, T. P. Orlando, I. Marvian, S. Gustavsson, and W. D. Oliver. *Error mitigation via stabilizer measurement emulation.* 2021. DOI: 10.48550/ARXIV.2102.05767. URL: https://arxiv.org/abs/2102.05767

[246] M. Kjaergaard, M. E. Schwartz, A. Greene, G. O. Samach, A. Bengtsson, M. O'Keeffe, C. M. McNally, J. Braumüller, D. K. Kim, P. Krantz, M. Marvian, A. Melville, B. M. Niedzielski, Y. Sung, R. Winik, J. Yoder, D. Rosenberg, K. Obenland, S. Lloyd, T. P. Orlando, I. Marvian, S. Gustavsson, and W. D. Oliver. "Demonstration of Density Matrix Exponentiation Using a Superconducting Quantum Processor". In: *Phys. Rev. X* 12 (1 Jan. 2022), p. 011005. DOI: 10.1103/PhysRevX.12.011005. URL: https://link.aps.org/doi/10.1103/PhysRevX.12.011005

[399] Gabriel O. Samach, Ami Greene, Johannes Borregaard, Matthias Christandl, Joseph Barreto, David K. Kim, Christopher M. McNally, Alexander Melville, Bethany M. Niedzielski, Youngkyu Sung, Danna Rosenberg, Mollie E. Schwartz, Jonilyn L. Yoder, Terry P. Orlando, Joel I-Jan Wang, Simon Gustavsson, Morten Kjaergaard, and William D. Oliver. *Lindblad Tomography of a Superconducting Quantum Processor*. 2021. DOI: 10.48550/ARXIV.2105.02338. URL: https://arxiv.org/abs/2105.02338

Part I

Quantum Circuits

Chapter 1

Searching for Links

1.1 Physics of Information

In the spring of 1989, a group of forty scientists convened at St. John's College in Santa Fe, a pueblo-clad liberal arts college nestled in the high desert valley between the Sangre de Cristo and Jemez mountains.[1] Gathering under the auspices of the Sante Fe Institute—a small independent research center founded five years prior by theoretical physicists from nearby Los Alamos—the scientists in attendance had been enticed to Santa Fe by a short "manifesto" issued by the Polish-American physicist Wojciech Zurek. The document, which Zurek titled "Complexity, Entropy, and the Physics of Information—A Manifesto," opens on a supernatural note: "The specter of information is haunting the sciences.[2]

> Thermodynamics, much of the foundation of statistical mechanics, the quantum theory of measurement, the physics of computation, and many of the issues of the theory of dynamical systems, molecular biology, genetics, and computer science share information as a common theme. [491]

Taking information as the core analytic, Zurek challenged like-minded scientists to

[1] For an anthropological analysis of Santa Fe architecture, geography, and the research interests of the Santa Fe Institute, see Ref. [197].

[2] The opening to Zurek's distinctly twentieth-century manifesto is, of course, a playful and oblique reference to the spectral first line of the nineteenth century's most famous manifesto [297].

consider the deep connections which might be found between physics and computer science, between the entropy of thermodynamics and the entropy of information theory [417]. What links might be unearthed between these seemingly separate disciplines, and what profound secrets of the universe might they guide the intrepid scientist to?

These questions, heady and abstract as they were, attracted eager participants. Charles Bennett, a founding figure in the theory of quantum teleportation and cryptography [49, 50], presented a paper weighing candidates for a formal measure of complexity [48]. Benjamin Schumacher, who later coined the term *qubit* [410], considered the mathematical connection between information and energy by way of Holevo's theorem for the entropy of a quantum system [204, 409]. Murray Gell-Mann, winner of the 1969 Nobel Prize in Physics for his contributions to the theory of elementary particles, coauthored a piece with James Hartle offering insights on quantum mechanics gleaned from quantum cosmology [157]. William Wootters, coauthor with Zurek of the no-cloning theorem [472], offered a meditation on the relationship between the linearity of quantum theory and the resources required to reconstruct a quantum state [475].

When the proceedings of the 1989 meeting on Complexity, Entropy, and the Physics of Information were published in print the following year—collected as volume eight of the Santa Fe Institute's iconic terracotta red series on the science of complexity—Zurek chose to open the collection with a contributed essay by his postdoctoral advisor, the physicist John Archibald Wheeler. Widely considered one of the great American physicists of the twentieth century for his early contributions to quantum theory and general relativity,[3] by the 1980s Wheeler had largely shifted his passion towards an emerging field of research captivating many of his students: quantum information. In this endeavor, the elder Wheeler proved even more radical than his pupils.

[3]More popularly, Wheeler is perhaps best known for coining the term "black hole" and for his leading role in the US effort to design the hydrogen bomb. For a contemporary critique of the term "black hole," see the recent work of cosmologist Chanda Prescod-Weinstein [358]; for a reflection on the legacy of US nuclear colonialism in the aftermath of the hydrogen bomb, see the work of particle physicist Karen Barad [31].

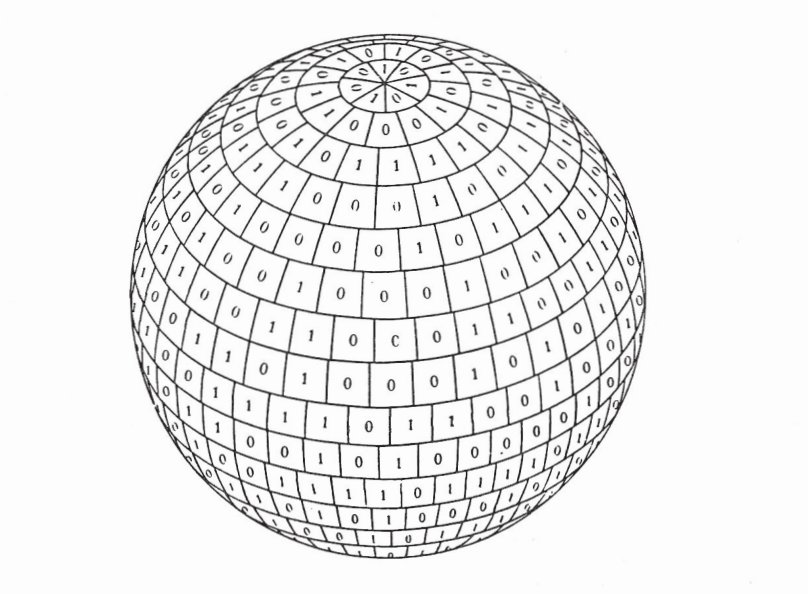

Figure 1-1: Figure from John Wheeler's "Information, Physics, Quantum: The Search for Links," depicting the event horizon of a black hole digitized as a surface of binary measurement outcomes for each Planck area. "Symbol, also, in a broader sense," Wheeler notes in the figure caption, "of the theme that *every* physical entity, every it, derives from bits." [468]

In his essay for the Santa Fe collection, "Information, Physics, Quantum: The Search for Links," Wheeler offered an expansive and provocative theory for the connection between physics and information science. By the late 1980s a few scientists, including Wheeler's former graduate student Richard Feynman, had begun to see the potential of new computing devices based on the principles of physics, an insight which would radically alter the classical theory of computation [141]. Wheeler, however, saw the inverse. Perhaps, he argued, it was physics itself which would be forever changed from its encounter with computer science. Following quantum mechanics to its logical conclusion, Wheeler argued that the fundamental substratum of the universe was composed not of particles and fields, as classical physics would suggest, but of information: binary quantum measurements yielding zeroes and ones. "The yes or no that is recorded," Wheeler writes, "constitutes an unsplittable bit of information"—a bit which, as his pupils Wootters and Zurek demonstrated years prior, cannot be divided into multiple copies [472]. Partitioning the universe up into irreducible pieces and performing a measurement on each (Fig. 1-1), wouldn't we find

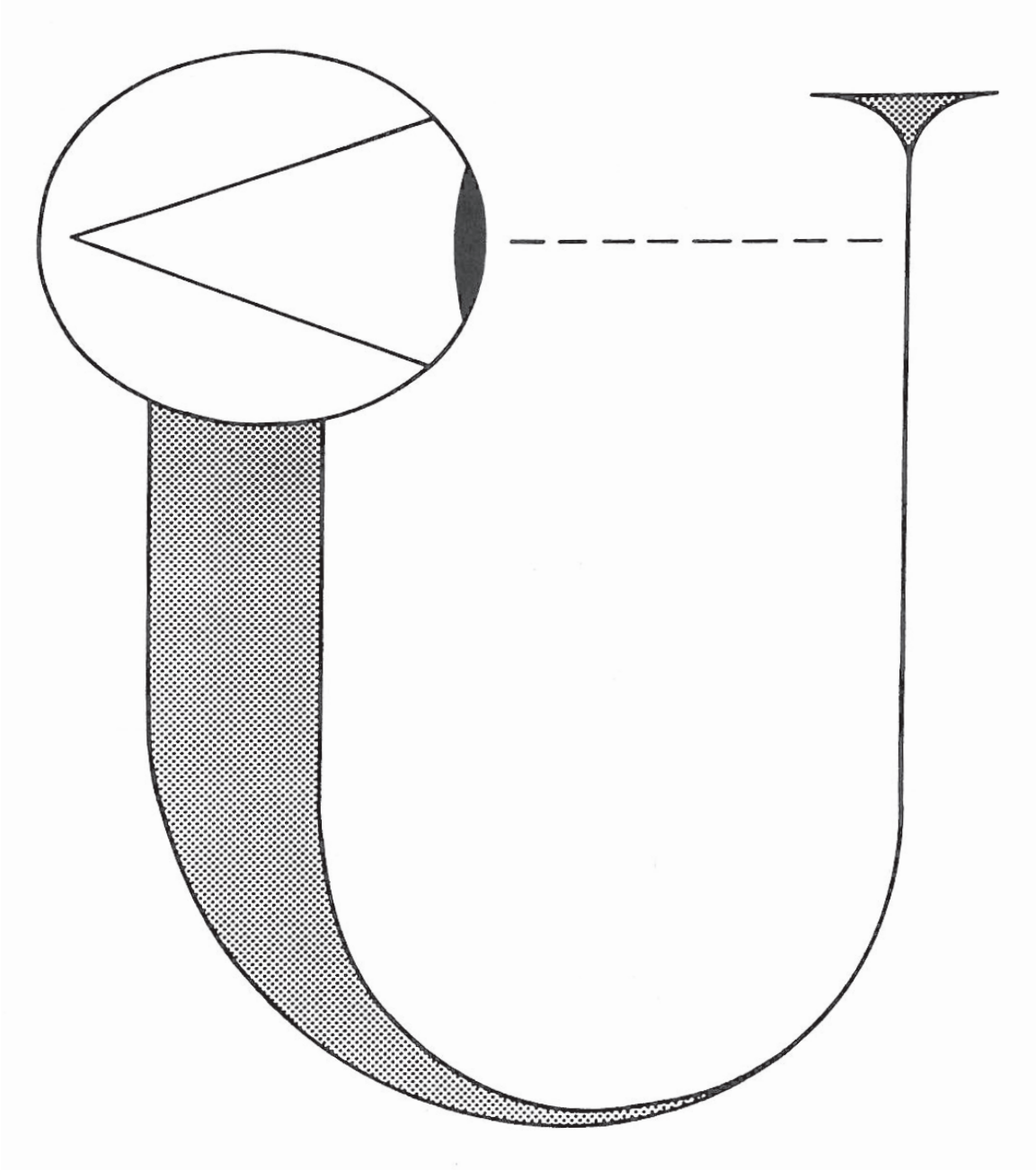

Figure 1-2: Frontispiece to *Complexity, Entropy, and the Physics of Information*, depicting the universe bending back upon itself in self-observation [468]. Illustration originally published by John Wheeler in Ref. [467], where it is captioned "The universe viewed as a self-excited circuit. Starting small (thin U at upper right), it grows (loop of U) and in time gives rise (upper left) to observer-participancy—which in turn imparts 'tangible reality' (cf. the delayed-choice experiment [...]) to even the earliest days of the universe."

that all phenomena are—at their most foundational level—digital? Wheeler gave his theory a lyrical name, *it from bit*:

> Otherwise put, every *it*—every particle, every field of force, even the space-time continuum itself—derives its function, its meaning, its very existence entirely [...] from the apparatus-elicited answers to yes-or-no questions, binary choices, *bits*.
>
> It from bit symbolizes the idea that every item of the physical world has at bottom—at a very deep bottom, in most instances—an immaterial source and explanation; that which we call reality arises in the last analysis from the posing of yes-or-no questions and the registering of equipment-evoked responses; in short, that all things are information-theoretic in origin and this is a *participatory universe*. [468]

For Feynman, as for most scientists today, quantum information was an application of quantum mechanics. For Wheeler, it was its foundation.

Unique among the papers in the volume, Wheeler's is accompanied by a cryptic frontispiece. Opposite the opening to his essay, a full page is devoted to an abstract hieroglyph of a serpent-like creature, its body expanding and tapering out from a thin line on one end to a single bulbous eyeball on the other (Fig. 1-2). Like the ouroboros of a medieval alchemical text, the figure bends back upon itself, forming not a continuous O but a great U. Contorted in alphabetic significance, the Universe-creature looks back on its own tail, a thin dashed line connecting it back to its origin, looping back through space and time to where it began. The gaze completes the circuit.

Bending backwards thirty years later, the collection of papers in the Santa Fe Institute volume will appear utterly alien to most scientists in the accelerating field of quantum computing. While many of the authors in the collection will be immediately recognizable for their contributions to the theory of quantum computing—such as Tommaso Toffoli [434], for whom the three-qubit CCNOT or *Toffoli gate* is named [435]—Zurek and his colleagues appear largely uninterested in the industrial implications or commercial utility of their research. Gathered in the New Mexico

desert in 1989, the scientists in attendance embraced the notion that they were part of something deeply unorthodox, perhaps even subversive. Well outside the disciplinary borders of traditional physics, further still beyond the boundaries of computer science or engineering, the Santa Fe cohort saw quantum information foremost as a branch of quantum foundations, a window into the fundamental mathematical and existential structure of the universe. For them, the relationship between physics and information was one of true natural philosophy, answering every practical question with a deeper spiritual one. "What kind of computer," Feynman famously asked eight years earlier, "are we going to use to simulate physics?" [141] *"How come existence?"* his mentor blithely retorts. *"How come the quantum?"* [468]

Such existential questions typically have no place in a quantum computing thesis, and yet they too are part of our history, part of our past. And the past is not yet done with us. So, like the cryptic serpent staring back at its own tail, I turn towards Santa Fe. I turn towards Santa Fe at the outset of this thesis because I am trying to make sense of the present, and this means I must contend with what came before me. I am searching, like Wheeler, for links, and links there are plenty. Indeed, as I write this thesis, Wheeler's questions weigh heavily on me—though likely not in the sense he originally meant them. If the question of *existence* for Wheeler and the Santa Fe cohort was one of cosmological and theological proportion—a question whose answer would unlock the deepest secrets of the universe, explain what it all means and why—I am far more interested in a different sort of existence, one humbler in scale, though calibrated to the times we are living and working in. *How come the quantum computer?* I ask. *How come its existence, now?*

Put another way, how do we make sense of this machine we are trying to build? How do we understand the physics which animates it, the engineering which gives it shape, the institutions which house it, the social life it has lived, and the people who have poured so much labor, so much money, so much time into its creation? So much time, at a time when time itself seems to be running out. For so many, has long since run out, has been cut short. Some of these questions are scientific, and this thesis is a ledger of my attempts to answer at least a few of them in kind. Others are not;

this thesis is an account of my attempts to answer some of those as well.

These questions, I have learned time and time again, are utterly tangled with each other. I will not attempt to slice the Gordian knot binding them. Instead, this thesis is a document of my attempts to follow, feelingly, the contours of their tangle—winding through circuit diagrams, cryostats, Python simulations, microwave attenuators, peer review, PowerPoint, the Oval Office. What follows is a partial trace of the tangled circuitry at the heart of quantum computing.

1.2 Tangled Circuits

In 2022, as the field of quantum computing enters its fifth decade, the opening salvo of Zurek's manifesto rings truer than ever before. The sciences are indeed haunted. For many younger scientists such as myself, it is difficult to imagine a time before this haunting, before the specter of information possessed the sciences so completely. In the decades since the Santa Fe meeting, computers have become integral to the daily lives and activities of most industrialized humans in ways that Zurek and Wheeler could not have imagined. If information for the Santa Fe scientists was still an object of inquiry that could be held at a distance and examined, today it is the opaque lens through which we experience so much of the world, woven into the fabric of our reality no less profoundly than the electric or magnetic fields of classical physics. The extent to which the computing revolution of the last half-century has impacted the methods and aspirations of our research cannot be understated.

Following in the footsteps of the classical computing revolution of the late twentieth century, in the past decade alone, efforts to design and engineer real quantum processors based on physical quantum bits have accelerated like never before. Indeed, after decades gestating as a largely theoretical, mathematical, and philosophical curiosity, high coherence and high fidelity quantum processors based on a range of hardware modalities—such as trapped ions, neutral atoms, and nitrogen-vacency centers in diamond—are gradually becoming technical reality. Among these modalities, quantum processors based on superconducting Josephson circuits have proven

particularly compelling, and progress towards the first generation of fault-tolerant, error-corrected quantum processors based on these artificial atoms is well underway. This thesis is a partial account of that journey.

And yet, while the past ten years have been ones of enormous scientific and engineering progress, the modern quantum engineer finds themselves in something of a liminal space. Operating between the dual poles of science and engineering, of quantum theory and computer science, of physics and information, the quantum computer scientist is both chimera and polyglot: a disciplinary and intellectual shapeshifter of sorts, versed in a dozen languages and tasked with winding them together in a single sentence. We are not the first to find ourselves here. Though the questions animating our work may differ, like the scientists in Santa Fe, we too are interested in tying things together, in dancing at the borders between more established disciplines, asking profound questions at the interface between multiple levels of abstraction.

These interfaces are absolutely physical, and they have profound and material consequences for the task of building a quantum computer. In the research reported in this thesis, I am largely interested in the interface between two distinct levels of abstraction which coincidentally—indeed, zeugmatically [41, 195]—share a common name. The first is the logical circuit of a quantum algorithm. This circuit is a mathematical object, describing the set of operations performed on a collection of qubits to implement some interesting computational task:

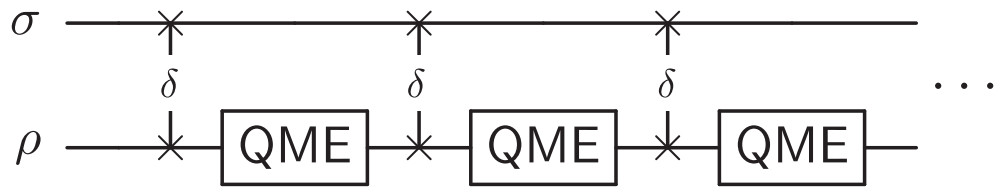

The second is the electrical circuit of the superconducting quantum processor which attempts to perform this computation. This circuit is a physical object, precision fabricated in a cleanroom and painstakingly calibrated in the laboratory using a dilution refrigerator and racks of microwave electronics:

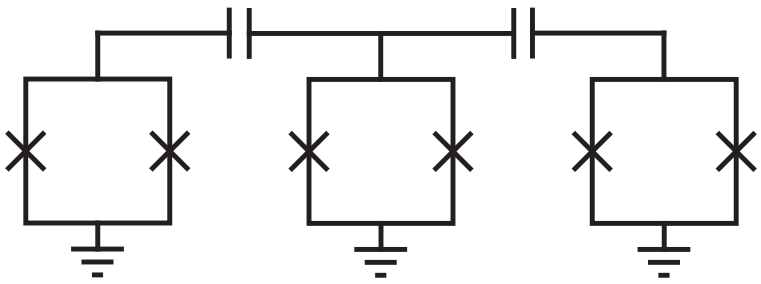

The logical circuit in the first diagram above corresponds to a hardware-efficient formulation of the Density Matrix Exponentiation algorithm using two qubits; the electrical circuit in the second, to three capacitively-coupled flux-tunable transmon qubits fabricated on a silicon wafer. While these two circuits, no less hieroglyphic than Wheeler's serpent, share many of the same schematic elements—lines, boxes, crosses—their interpretation could not be more different: the SWAP operation between two qubits in a logical circuit has no inherent relationship to a series pair of Josephson junctions in an electrical circuit, though they are both signified using the exact same symbol (two $\times$'s joined with a line). And yet, as we will see in Part III of this thesis, the logical circuit and the electrical circuit above can, in principle, be made to map perfectly onto each other, giving the mathematical abstraction of the former flesh in the latter. In practice, they do not. When these two circuits fail to align, errors arise in the computation. These errors can be difficult to characterize and mitigate—in many cases, as we'll see in Parts III and IV, deceptively so—but they must be contended with. These errors are the main characters of this story.

However, before I turn to these errors at the interface of logical circuit and superconducting circuit, there are a few other interfaces which must be addressed to set the stage for the work which follows. These interfaces are variously historical, social, linguistic, philosophical, and they too define the material conditions of our research. It is to these interfaces that I turn for the remainder of this introduction.

1.3 Quantum Computing, Historically

When quantum engineers and computer scientists are called upon to tell the history of our discipline, tradition compels us to recite the same general tale:

In 1982, the American physicist Richard Phillips Feynman delivered a keynote address at the first conference on Physics and Computation, hosted at MIT's Endicott House. In the address, titled "Simulating Physics with Computers," Feynman considered the difficulty of simulating quantum mechanical processes on computers. The problem, as quantum physicists had long known and as I will demonstrate formally in Part II of this thesis, was that the state space of a quantum system scales exponentially with the number of subsystems it is composed of. As such, in order to simulate the dynamics of two systems interacting with one another, one required computational resources equal not to the sum of the resources required to simulate each system in isolation, but to their *product*. This fundamental exponential scaling of quantum mechanics effectively thwarted any attempt to simulate all but the smallest quantum systems in their full quantum mechanical complexity; for larger systems, such as the atomic and molecular reactions of even the most elementary chemistry problem, scientists were forced to resort to clever semi-classical approximations, effectively cutting down the dimensionality of the problem at the cost of complete numerical and analytic accuracy.

To bypass this fundamental simulation penalty imposed by quantum mechanics, Feynman imagined a computer built according to a new rule. "The rule of simulation that I would like to have," Feynman mused,

> is that the number of computer elements required to simulate a large physical system is only to be proportional to the space-time volume of the physical system. I don't want to have an explosion. That is, if you say I want to explain this much physics, I can do it exactly and I need a certain-sized computer. If doubling the volume of space and time means I'll need an exponentially larger computer, I consider that against the rules (I make up the rules, I'm allowed to do that). [141]

That is, if one wanted to double the size of the quantum system they were simu-

Physics of Computation Conference Endicott House MIT May 6-8, 1981

1 Freeman Dyson
2 Gregory Chaitin
3 James Crutchfield
4 Norman Packard
5 Panos Ligomenides
6 Jerome Rothstein
7 Carl Hewitt
8 Norman Hardy
9 Edward Fredkin
10 Tom Toffoli
11 Rolf Landauer
12 John Wheeler
13 Frederick Kantor
14 David Leinweber
15 Konrad Zuse
16 Bernard Zeigler
17 Carl Adam Petri
18 Anatol Holt
19 Roland Vollmar
20 Hans Bremerman
21 Donald Greenspan
22 Markus Buettiker
23 Otto Floberth
24 Robert Lewis
25 Robert Suaya
26 Stan Kugell
27 Bill Gosper
28 Lutz Priese
39 Madhu Gupta
30 Paul Benioff
31 Hans Moravec
32 Ian Richards
33 Marian Pour-El
34 Danny Hillis
35 Arthur Burks
36 John Cocke
37 George Michaels
38 Richard Feynman
39 Laurie Lingham
40 Thiagarajan
41 ?
42 Gerard Vichniac
43 Leonid Levin
44 Lev Levitin
45 Peter Gacs
46 Dan Greenberger

Figure 1-3: Group photograph of the participants at the first Physics of Computation Conference, hosted at MIT's Endicott House in May 1981 [432]. Among those in attendance were Richard Feynman (number 38, standing in the back right) and his graduate advisor John Wheeler (number 12, seated in the front center).

lating, Feynman demanded a computer at most twice as large to complete the task. Feynman's made-up rule, impetuous though it was, had clear basis in reality. After all, when two molecules are placed together in a chemical reaction, one might say that all the molecules are doing is simulating themselves in interaction, a process they innately accomplish with no need for an external buffer to store the exponential details of their tryst. Put another way, quantum mechanical systems clearly simulated quantum mechanics just fine. No, the problem of simulation lay in *translation*, in the mapping between the physics of quantum systems and the binary bits of our definitively "classical" computers. In one of his characteristic and irreverent rhetorical flourishes, Feynman concluded his talk by summarizing this point in a single dramatic proclamation: that "nature isn't classical, dammit, and if you want to make a simulation of nature, you'd better make it quantum mechanical, and by golly it's a

wonderful problem, because it doesn't look so easy."

Indeed, the problem was not, in fact, so easy. And yet, in the forty years since the MIT conference, substantial progress has been made towards the design and engineering of exactly the sort of devices Feynman was imagining. These machines, which we today call *quantum simulators*, encode difficult quantum mechanical problems onto devices composed of programmable and well controlled quantum systems, systems which are then manipulated into mimicking the desired process and outputting a particular quantity of interest [158]. Among the myriad applications which have been explored theoretically and experimentally in the past decades, great strides have been made towards simulation of the Hubbard model of condensed matter physics [86, 117, 169, 219], properties of spin models and spin glasses [77, 156, 191, 222, 241, 265, 426], and chemical reaction rates and molecular energies [26, 127, 268, 276], to name only a few.

While the idea of quantum simulation offered a promising path towards solving a large and imminently useful range of classically-intractable problems, Feynman's vision fell well short of what we would call a "computer," let alone a *universal computer*: a device which, as the pioneering computer scientist Alan Turing showed in 1936, was capable of performing any computational task [445]. Throughout the 1980s, the promise of quantum computation was, in some sense, pleasantly tautological: quantum systems representing other quantum systems for solving hard quantum mechanical problems. Indeed, for over a decade it was entirely unclear whether or not a programmable quantum system would be able to perform any task other than pure simulation, let alone hard *classical* problems.

This changed in 1994. In November of that year, a young mathematician from Bell Laboratories named Peter Shor presented a paper at the Annual Symposium on Foundations of Computer Science [419]. In his paper, Shor proposed an algorithm for performing prime factorization—a problem so notoriously hard that it has become the backbone of many modern cryptographic protocols [316]—in an amount of time which scaled polynomially with the size of the number to be factored, an exponential improvement over any known prior algorithm for accomplishing the task. The trick,

Shor discovered, was to perform the algorithm on a very different sort of computer: a computer so unusual, in fact, that it did not exist yet. For his algorithm, Shor required a quantum computer.

Shor's discovery, that a computer composed of coherent quantum bits could outperform a classical computer in performing certain classical tasks, set in motion three decades of experimental progress towards the creation of such a device. During this time, quantum computers began their transition from small-scale science experiments—systems of 5–10 physical qubits capable of performing trivial computations, such as factoring the number 15 into 5×3 [448]—to industrial-scale, precision-engineered devices. While these systems—composed, at present, of 50–100 qubits—remain too small and error-prone to run Shor's algorithms on a classically-intractable factorization problem, the vast Hilbert space occupied by even these modestly-sized quantum processors already exceeds the number of classical bits in all but the largest supercomputers. Harnessing this fact, attempts to demonstrate improved performance on certain, contrived problems—a feat known variously as *quantum advantage* or *quantum supremacy* [22, 469]—are currently underway.[4]

Although the progress towards experimental universal quantum computers has proceeded slowly, at least in terms of the number of quantum bits in the processor, a comparison can be made to the slow but steady progress made during the early days of classical computing. While the building block of the modern classical computer, the transistor, was first invented in 1947, it wasn't until 1971 that the first commercial microprocessor based on the transistor became available. This first device, the 4-bit Intel 4004, consisted of 2300 transistors; by 1993, the first Intel Pentium processor contained over 3 million transistors. This exponential increase in the size of commercial classical processors over time, a phenomenon commonly known as Moore's law, continues to the present day, and some quantum computing evangelists argue that a similar law will govern the increase in quantum processors in the coming decades.

At the same time that quantum computers have increased in size, enormous work

[4]For a deeper consideration of these experiments and the language games at play in claims of quantum supremacy, see Part V of this thesis.

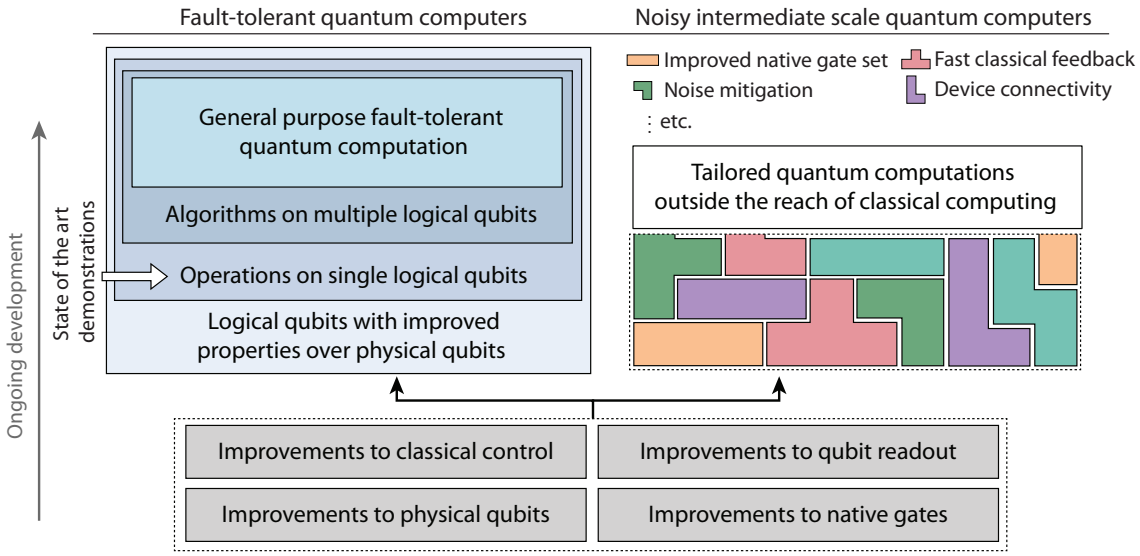

Figure 1-4: The garden of forking paths: left, the path towards fault-tolerant quantum error-corrected quantum computers; right, the path towards noisy intermediate scale quantum (NISQ) computing. While fault-tolerant quantum computers offer the promise of performing arbitrarily long programs to arbitrary precision using logical (i.e. encoded and error-corrected) qubits, NISQ computers [365] attempt to perform highly optimized quantum algorithms and quantum simulations which take into account the details and imperfections of the processor, avoiding the need for error correction. Image taken from Ref. [248], designed in collaboration with the author.

has gone into improving the coherence and operation of physical qubits, as well as towards the creation of error-corrected and fault-tolerant *logical qubits*, resilient to the intrinsic errors of their constituent components [10, 14, 217]. Here, the path forward has partly bifurcated. While many scientists and research institutions remain committed to the slow path towards fault-tolerant quantum computing—a path where successful error correction is *required* in order to demonstrate useful quantum applications—others have begun to branch out and explore the capabilities of the current generation of noisy intermediate-scale quantum ('NISQ' [365]) devices in the absence of error correction. Along this latter path, research has tended towards the study of highly optimized quantum algorithms and quantum simulations which take into account the details and imperfections of the processor, avoiding the need for error correction. However, while the NISQ path towards useful applications is conceivably shorter than the one for fault-tolerance, these NISQ applications forfeit many of the

theoretical guarantees of quantum speedup which hold for fault-tolerant computation (as in Shor's algorithm), and to date it remains an open question whether or not such devices can demonstrate a computational enhancement over classical processors.

1.4 Quantum Computing, Historically (Remix)

The conventional history of quantum computing sketched above is true. It is also, like all histories, the result of deliberate and methodical curation. It is a tool for making sense of our past and speculating about our future. Arranging the events of the last half century in a line from Feynman at one end to industrial quantum computing on the other, one is given the impression of continuous and unmitigated scientific progress. For many scientists, this narrative is optimistic and comforting. Indeed, while the dream of a universal fault tolerant quantum computer remains unfulfilled at present, one need only connect the dots of this history to conclude that someday, with enough time, such a machine will surely exist.

Could we tell the history of quantum computing differently? Like archaeologists huddled over the scattered bones of some prehistoric leviathan, could we arrange the facts of our discipline in a different sequence to tell a different story, create a different beast? I believe we can, and we must. Placing the conventional history of quantum computing within the broader historical and political context of the past century, we might find that the history of our young field is not linear at all, but cyclical. In this section, I will trace out two complete turns of this cycle over four distinct movements in the journey from quantum mechanics to quantum computing, movements which I believe shed considerable light on the current conditions of our research and offer, dimly, a vision of our field's future. In this task, I am indebted to the work of the MIT physicist and historian David Kaiser, whose essential history of early quantum information provides the first three of these movements [231]. The fourth movement, which was inaugurated the same year Kaiser published his text and thus falls outside the scope of his analysis, is my own.

Figure 1-5: Niels Bohr (left) and Albert Einstein (right) in conversation, Leiden 1930. Throughout the prewar period, the architects of quantum theory frequently crossed paths to discuss and debate the philosophical interpretation of their new theory. Photograph taken by the physicist Paul Ehrenfest in his home. Image adapted from Ref. [229].

1.4.1 Quantum Theory and Philosophy in Weimar Europe

The first era of this history begins with the birth of quantum theory in the first quarter of the twentieth century, a movement which reached its apex in the period of the German Weimar Republic, between the two World Wars. This is the period of Niels Bohr, Werner Heisenberg, and Erwin Schrödinger (to name only a few actors), and it centers primarily in the physics capitals of Northern Europe: Göttingen, Munich, Copenhagen, Cambridge.

During this period, the principle architects of quantum mechanics understood their project as, first and foremost, a new way of *thinking*. Something was clearly wrong with the classical Newtonian picture of nature, and physics required a dramatic change of perspective. For these scientists, quantum theory belonged as much to the

domain of philosophy as to that of physics. To make sense of their theory, they drew liberally from texts as varied as Immanuel Kant's *Critique of Pure Reason*, ancient Hindu scripture, and the analytical psychology of Carl Jung, arguing vigorously with each other over how to correctly ground their work in the larger landscape of ideas. Indeed, even quantum theory's greatest detractors, such as Albert Einstein, agreed that the deficiency of quantum theory lay not in any lack of mathematical consistency or agreement to experiment, but in its failure to stand up to rigorous philosophical tests. The history of early quantum theory is peppered with deep and blistering arguments over the puzzles and paradoxes of the new theory, and many of its architects would go on to write long and searching volumes on the philosophical interpretation of their work [61–64, 408].

The influence of history and philosophy on early quantum theory wasn't merely cosmetic. Just as Bohr and Schrödinger were looking to the past to validate and ground their theories, their work was responding to the historical and political demands of their present. Indeed, as the historian of physics Paul Forman famously showed in his landmark 1971 essay "Weimar culture, causality, and quantum theory," quantum mechanics came of age in an extraordinarily hostile—and, relevant for many of the scientists involved, increasingly anti-Semitic—intellectual environment [147]. In this context, many of the core tenets of quantum theory can be seen as strategic maneuvers to ensure greater cultural acceptance and survival. In particular, Forman notes that the quantum mechanical refutation of classical causality (long seen as one of the theory's strangest twists) was, in fact, predated by a wider intellectual revolt in Germany against rationalism and causal-realism—two philosophies which, many intellectuals of the time believed, contributed to the crisis of German national identity which led to the nation's defeat in the first World War. Forman's argument, that quantum theory emerged at the fertile intersection of science, history, and a particular set of cultural values, would become foundational to the late twentieth-century discipline of Science, Technology, and Society studies (STS).

1.4.2 Quantum Mechanics in the Corridors of Power

The second era of quantum mechanics arrived with the rise fascism in Europe and the ensuing outbreak of World War II. During this period, the geopolitical epicenter of quantum research shifted rapidly from the medieval colleges of Northern Europe to the government laboratories and research institutes of the United States. This is the period where quantum theory first became 'useful.' It is the period of Los Alamos and the Manhattan Project, of the Trinity nuclear test in August 1945, and of the American atomic bombings of Japanese civilian populations in Hiroshima and Nagasaki the following month. It is the period, also, of the MIT Radiation Laboratory (the "Rad Lab"), the invention of radar and microwave technologies, and the birth of a new persona who would consummate the wartime alliance between physics and industry for the remainder of the century: the electrical engineer.[5]

Following the war, the industrial apparatuses of US wartime physics research would find a new home in the military-industrial complex of the Cold War against the Soviet Union, a period which saw the vast expansion of federally-funded research and development centers (FFRDCs) under the auspices of the US Departments of Energy (such as Sandia and Lawrence Livermore National Laboratories) and Defense (such as the Rad Lab's successor, MIT Lincoln Laboratory). For the United States, these centers, largely tasked with developing the guidance systems for the American nuclear arsenal and maintaining the nation's vast stockpiles, were not simply sites of scientific inquiry, but of vital national security interests. To staff these laboratories and ensure a ready standing army of scientists in the event that the Cold War turned hot, the United States needed more physicists. A lot more physicists.

World War II and the Cold War had a profound influence on how a generation of physicists came to understand their profession and its role in the new world order. "Before the war," Kaiser writes,

[5]This work, though ostensibly classical in nature, nonetheless had an enormous and indelible impact on the trajectory of quantum mechanics research in the mid-twentieth century, particularly in the development of quantum electrodynamics (QED). For a history and analysis of the MIT Rad Lab, see Ref [151].

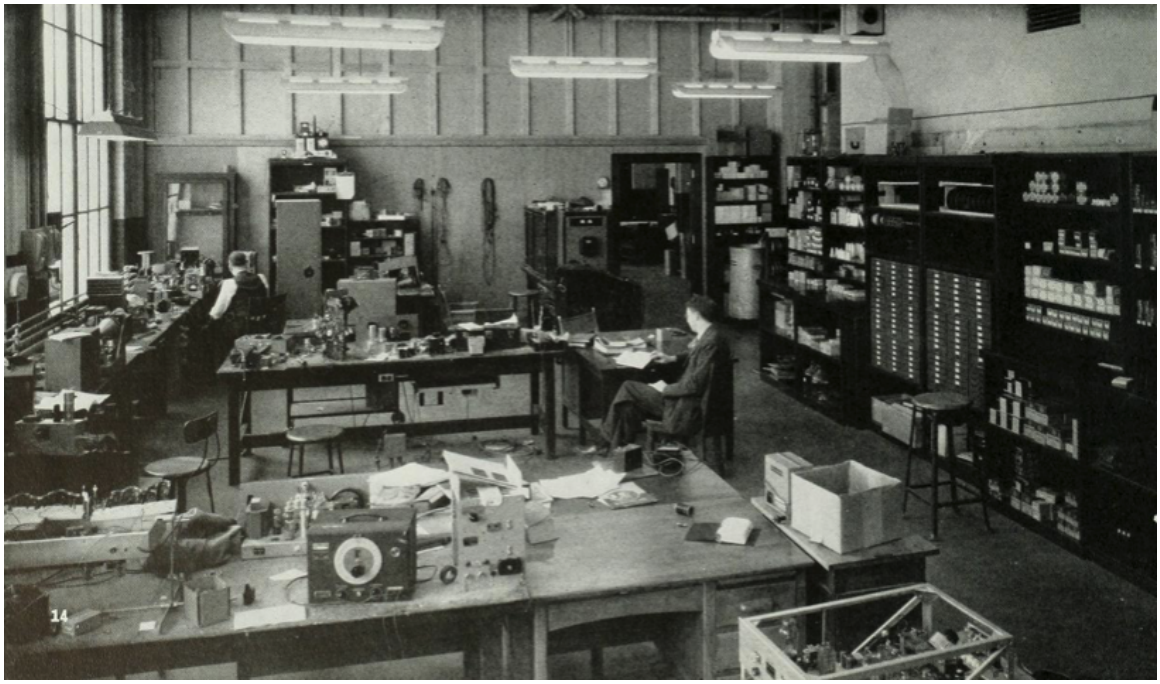

Figure 1-6: The Modulator Laboratory at the MIT Radiation Laboratory, Cambridge 1941. During the early 1940's, the 'Rad Lab' became a model for industrial-scale physics research in service of the war effort. Image taken from Ref. [145].

> Einstein, Bohr, Heisenberg, and Schrödinger had held one model in mind for the aspiring physicist. A physicist should aim, above all, to be a Kulturträger—a bearer of culture—as comfortable reciting passages of Goethe's *Faust* from memory or admiring a Mozart sonata as jousting over the strange world of the quantum. The physicists who came of age during and after World War II crafted a rather different identity for themselves. Watching their mentors stride through the corridors of power, advising generals, lecturing politicians, and consulting for major industries, few sought to mimic the otherworldly, detached demeanor of the prewar days. Philosophical engagement with quantum theory, which had once seemed inseparable from working on quantum theory itself, rapidly fell out of fashion. Those few physicists who continued to wrestle with the seemingly outlandish features of quantum mechanics found their activity shoved ever more sharply to the margins. [231]

This shift was reflected in the pedagogy of the postwar period. In the United States throughout the 1920s and 30s, general exams for PhD candidacy routinely required students to compose essays on the implications of wave-particle duality and interpretations of the double-slit experiment. After the war, with the number of PhD candidates skyrocketing by an order of magnitude in response to new government

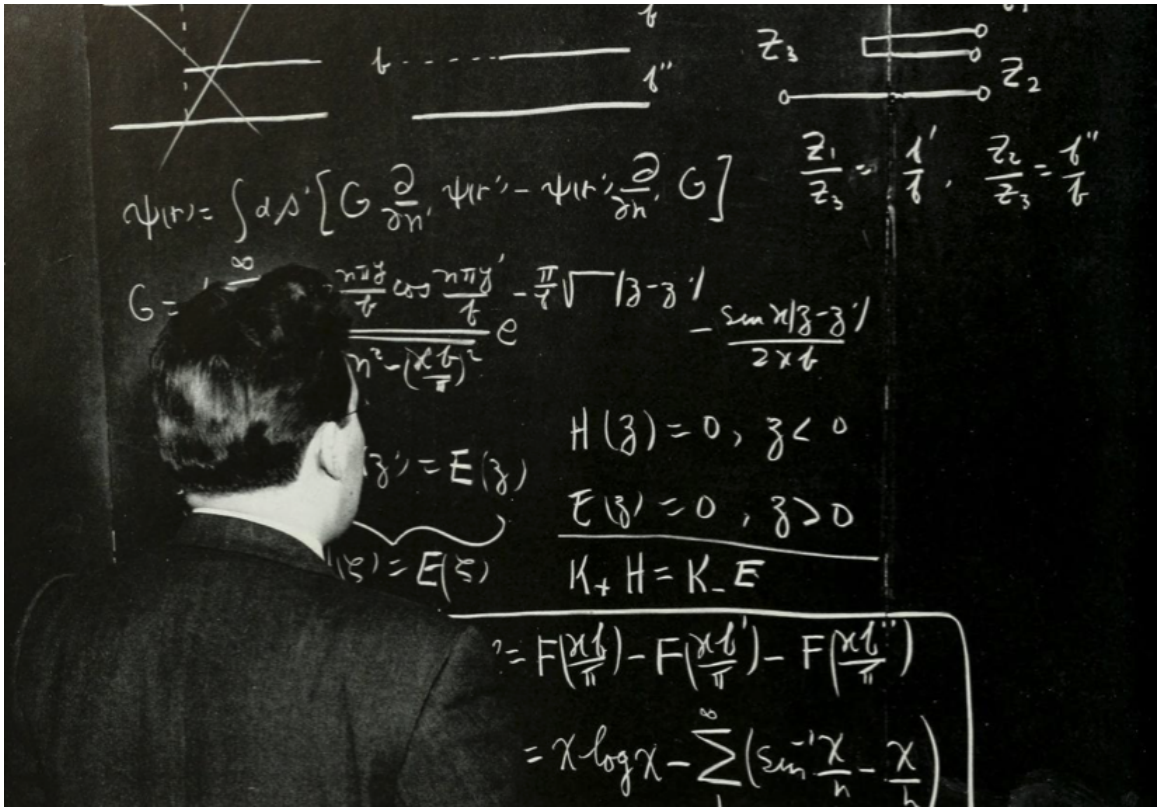

Figure 1-7: Julian Schwinger, calculating the quantum mechanical description of the electromagnetic field in a transmission line at the MIT Radiation Lab, circa 1941. Schwinger would later go on to win the 1965 Nobel Prize in Physics for his contributions to quantum electrodynamics, an award he shared with Shin'ichirō Tomonaga and Richard Feynman. Image taken from Ref. [145], adapted from Ref. [151].

fellowships and instructors struggling to manage the newly built stadium-style lecture halls, physics curricula quickly dispensed with the philosophical musings in favor of a stricter and more quantitative curriculum aggressively focused on results and applications.

This philosophy—for of course, the impulse to repudiate philosophy is, too, part of a larger worldview, part of a philosophy—was exemplified in a new rallying cry, widely attributed to the postwar physicist *par excellence*, Richard Feynman: "Shut up and calculate!"

1.4.3 Quantum Counterculture and Revival

The broad strokes of the two preceding periods will be familiar to most quantum information scientists, and it is tempting to draw a straight line between these two movements, connecting them in a continuous chain of progress which persists to the present day. Here, however, Kaiser stages a crucial historical intervention.

While undeniable traces of the wartime research period persist to the present day, its reign was not eternal. The third period of quantum mechanics, to which Kaiser directs the bulk of his analysis [231], begins with the crash in physics funding during the early 1970s. After three decades of continual growth, with the Cold War slowly thawing and government sponsors reevaluating their allocation of dwindling resources, the bottom suddenly fell out for the physics economy. Within a decade, the number of physicists enrolled in the United States plummeted by fully one half, a plunge exacerbated by the military revoking draft deferments for undergraduates (in 1967) and graduate students (in 1969) during the height of the Vietnam War. While all academic disciplines felt the shock of this sudden sea change, none were hit as hard as physics, a field which had become uniquely dependent on the deep pockets of the Department of Defense. Throughout the 1960s, the American Institute of Physics—the umbrella organization which houses the American Physical Society—recorded more open employment opportunities than applicants. By 1971, the organization reported 53 available jobs for 1053 applicants.

And yet, the ruins of the postwar physics economy proved—not unlike the literal ruins of the German Empire during the Weimar period—to be fertile ground for a new generation of physics research. Underemployed and newly unmoored from the professional demands of their floundering discipline, a motley crew of young physics PhDs began informally convening in a seminar room housed in the Theoretical Physics Division of Lawrence Berkeley National Laboratory. The "Fundamental Fysics Group," as the cohort called themselves, became standard bearers for a new generation of physicists eager to push the boundaries of 'acceptable' physics, countering the austere pragmatism of their postwar mentors with a return to the wild speculation and

Figure 1-8: Members of the Fundamental Fysics Group, 1975. (Standing, left to right) Jack Sarfatti, Saul-Paul Sirag, Nick Herbert; (kneeling, right) Fred Alan Wolf. Image adapted from Ref. [232].

heady questions of their prewar elders. These questions—fueled in equal parts by rigorous formal inquiry, New Age spirituality, appropriated Buddhist iconography, and a liberal dose of psychedelics—laid the foundation for a new way of imagining the relationship between physics and the world.

While many of the group's efforts would be derided by following generations—such as their fusion of quantum mechanics and pseudo-Buddhist pop mysticism in books such as *The Tao of Physics* and *The Dancing Wu Li Masters* [88, 490], or their attempts to connect quantum theory with ESP and telepathy—others proved extremely prescient. In particular, it was the members of the Fundamental Fysics Group who first rediscovered the long obscure work of the Irish physicist John Stewart Bell and

his forgotten 1964 paper "On the Einstein Podolsky Rosen paradox" [42], a work they latched onto with extraordinary zeal. Originally published in the short-lived trilingual journal *Physics Physique Физика*, Bell's paper elegantly refuted Einstein's famous argument that the nonlocality of quantum mechanics—the notion that two systems could become 'entangled' with one another, such that measurement of one would instantaneously affect the state of the other, even after separation across vast distances—was evidence of its incompleteness, necessitating the introduction of 'hidden variables' which would restore locality and fix the theory. Bell's theorem revealed the error in Einstein's logic.Entanglement, he showed, wasn't the weak link of quantum theory; it was what made quantum mechanics possible.

Up until 1964, the EPR paradox was widely regarded as little more than a philosophical artifact of the prewar period. Bell not only resolved this paradox: he showed that its resolution had physical consequences. It could be measured. Seeing the implications of Bell's theorem, members of the Fundamental Fysics Group quickly began cooking up proposals for superluminal communication devices—communication which utilized entanglement between polarized photons to send messages across vast distances faster than the speed of light. In 1982, the proposal for one of these devices—Nick Herbert's scheme for the "First Laser-Amplified Superluminal Hookup," or "FLASH" [200]—found its way onto the desk of John Wheeler, a longtime recipient of the Fysics Group's fan letters and preprints, and into the hands of two of his students at the University of Texas, William Wootters and Wojciech Zurek [230]. Working through Herbert's manuscript, Wootters and Zurek hit upon the flaw in the FLASH proposal, a flaw which escaped the paper's referees. In order for superluminal communication to work, one would need a way to amplify a photon with unknown polarization into many copies. This sort of amplification, Wootters and Zurek showed, fundamentally violated the linearity of quantum mechanics [472]. Quantum information was fundamentally different from classical information. While the "no-cloning theorem"—as Wheeler christened his students' theory—shattered the possibility of superluminal communication, it soon set in motion a new area of inquiry inspired by the impossibility of copying quantum data: quantum cryptography.

Figure 1-9: Wheeler and his students, 1981. (Left to right) William Wootters, Kip Thorne, John Wheeler, Wojciech Zurek, and William Unruh. Photograph taken at the NATO Advanced Study Institute conference on Quantum Optics and Experimental General Relativity in Bad Windsheim, West Germany. [473]

By the time that Zurek convened the Santa Fe conference on the physics of information in 1989 [491], the strange seeds planted by the Fundamental Fysics Group had blossomed into a full-fledged quantum revival. If the Cold War had defined strict boundaries within which quantum theory might be useful, by the end of the century it appeared that these borders were rapidly disintegrating. It was clear that the story of quantum mechanics was not yet finished, that there was still much work to be done if physicists wanted to get to the bottom of it all, if they wanted to understand existence itself. This endeavor, like those of the eras before it, was very much of its time. Looking back on the work of the Fundamental Fysics Group, it is impossible to ignore the group's particular politics, teetering uneasily between political activism and psychedelic escapism, haunted in equal parts by an orientalist obsession with 'Eastern mysticism' and an acquiescence to the patronage of the CIA and the Pentagon.

As for the cohort at the Santa Fe conference, though none of the participants were directly associated with the Fysics Group—Wheeler, for his part, tried to shield his students as much as possible from direct contact with the group [230]—these early investigations into quantum information share a certain faith in the transcendent, a conviction that the secrets of the universe were theirs to unlock and harness. These early quantum information theorists were not alone in this conviction, and one can see a distinct resonance between Wheeler's 'it from bit' theory and another contemporaneous area of research circulating around the Santa Fe Institute at the same time: the field of Artificial Life [196, 262]. Indeed, both fields share a common commitment to computation as a unifying principle of the cosmos, and both attempted to ground the secrets of the universe in the digital, reducing all of creation to a massive computer, waiting to be programmed. This hubris too is part of our inheritance as quantum engineers.

1.4.4 "The Era of Quantum Supremacy"

History, Hegel tells us, has a way of repeating itself: arriving first as tragedy, then as farce [295]. If the countercultural revival of the late century recalled—in playful pantomime—the solemn philosophizing of Bohr and Einstein, today we find that the pendulum has once again swung. Here, we must tread cautiously. While it is foolish to attempt a history of the present—to tell a story we are deep in the middle of, the conclusion yet unwritten—we can nonetheless trace a number of themes which animate quantum research in the present day, themes not altogether dissimilar from those which animated the wartime scientists of the mid-century.

I call this fourth movement in the history of quantum mechanics "the era of quantum supremacy," a phrase which I taken in full from physicist John Preskill's 2011 keynote address at the Solvay Conference on Physics [364]. In this phrase—a phrase which, significantly, marked the first appearance of the term *quantum supremacy* in the English language—Preskill presciently acknowledged that quantum mechanics was once again at a turning point, at the cusp of a new era which would radically depart from the one which preceded it.

Figure 1-10: Promotional photograph of Google's newly built Quantum AI research campus in Santa Barbara, California [447].

Here, however, I have chosen to alter the phrase's meaning. In his original remarks, Preskill was referring to the anticipated period of scientific history when quantum computers—devices which harness quantum mechanics to perform programmed computational tasks—would enable computations far surpassing the capabilities of classical computers. This era, by Preskill's definition, has not yet arrived. And yet, I believe that this phrase provides as succinct a summary as any of the period in which it appeared and of the period in which we currently find ourselves.

Quantum supremacy, as I argue at length in Part V of this thesis, is not simply a quantifiable technical milestone: it is an overarching narrative and *myth*, in the poststructuralist sense [37], which has guided quantum mechanics research throughout the early decades of the twenty-first century. As such, the 'era of quantum supremacy' in which we currently find ourselves is not, *pace* Preskill, the era of demonstrable quantum advantage—though it may prove to be that too—but rather *the era governed by the aspiration of supremacy and advantage*.

This definition will make many scientists uneasy, but the broad strokes are relatively uncontroversial. As quantum mechanics has entered the twenty-first century, a renewed emphasis has been placed on harnessing quantum theory towards 'useful' ends—towards designing coherent physical systems which are faster, more powerful, and more secure than those which came before. Among the success stories of this era, we would include the successful deployment of quantum encryption between Vienna and Beijing in September 2017,[6] the generation of large and controllable entangled states consisting of tens of qubits, and the first claimed demonstration of quantum supremacy by Google Quantum AI in 2019 [22].

For many scientists, these accomplishments stand as inarguable proof that the arc of scientific history bends towards progress. And yet, as we have seen in the preceding movements sketched above, the meaning of *progress* is not time invariant. Indeed, the aspiration of quantum computational advantage is a new invention, one which diverges profoundly from the aspirations of the Fysics Group and Sante Fe cohort, as well as their prewar antecedents. Instead, the dream of quantum supremacy brings quantum mechanics back into resonance with the pragmatic aims of the wartime period, where philosophy is once again subordinated to results, to quantitative metrics, to progress.

The aspiration of quantum supremacy is not some ethereal thing hanging dimly in thin air, a figment of the imagination; it is a guiding principle which concretely shapes where research happens, which research is deemed acceptable, and what sort of pedagogy must be practiced to discipline a new generation of scientists accordingly. What do the corridors of power look like in this era? Just as the medieval academies of Northern Europe gave way to the government laboratories of the United States, the geographic center of quantum research has once again shifted profoundly, from the psychedelic ashrams and privately endowed research centers of the late century to the corporate laboratories of tech giants such as Google, IBM, Microsoft, Amazon, Alibaba, as well as a teeming network of fledgling tech startups, each vying for their

[6]Notably, Kaiser's history opens with an account of this experiment's 2004 predecessor, in which quantum key distribution enabled a secure bank transfer between the mayor of Vienna and the national bank. While Kaiser portrays this experiment as the culmination of the counterculture period, with the benefit of hindsight, I argue that it instead suggests the waning of that era and the emergence of a new one.

Figure 1-11: Promotional image posted on the LinkedIn account of Atlantic Quantum, a Cambridge, Massachusetts, quantum hardware startup [125].

shot an IPO or a lucrative acquisition. Today, the quantum isn't simply an object of intellectual curiosity, a key which might unlock the deepest secrets of creation. It's a buzzword on a corporate press release. It's a keyword, a hashtag.

To carry out this work and bear the torch of progress, the current era once again demands more scientists and engineers. Just as the aspirations of the wartime period were made flesh in the figure of the electrical engineer—a figure who mobilized physics in the name of national security and strategic dominance—the era of quantum supremacy demands new offspring in its image. This is the era of the *quantum engineer*, of a new breed of scientists tasked with bending quantum mechanics towards productive and industrious ends. Such scientists do not emerge out of thin air: they are molded, inspired, disciplined. They are taught, but by who? Whereas the Cold War period saw an enormous expansion of the United States university system,

today we find that much of the pedagogical infrastructure for training new quantum engineers is housed, not in the academy, but in the online PR and outreach apparatuses of for-profit corporations—corporations which, incidentally, have deep financial interests in the success of quantum computing. Indeed, while the academy has been slow to adapt to the new pedagogical demands of quantum engineering—uncertain, for example, whether to offer such courses in the Physics or the Electrical Engineering departments, hesitant to adapt the traditional syllabus of an introductory quantum mechanics or microwave engineering course to cover such topics—companies such as IBM and Google, have been quick to promulgate their own textbooks and educational resources. These texts, such as IBM's Qiskit Textbook [7] or Google's Cirq tutorials and education workshops [130], draw liberally from a variety of conventional academic disciplines, teaching students just enough quantum mechanics as necessary to start operating quantum processors and playing with real devices hosted on the cloud. These educational resources are strategic and, like the textbooks of the wartime period, are intended to guide students towards a particular set of useful skills. Here, however, the tactics differ. Where the students of the 1950s and '60s were instructed to shut up and calculate, to bend their minds rigidly towards useful ends, students today are encouraged to play with quantum mechanics, to be creative. Creative, at least, within certain limits. Today, creativity is valuable; which is to say, it has a price tag. This sentiment, like Feynman's apocryphal invective to calculate, is embodied in a new mantra of progress: *"We are only one creative algorithm away from valuable near-term applications."* [22]

This era of quantum research has not developed in a vacuum, and here again history threatens to repeat itself. Just as the rise of fascism in Europe cut short the era of the quantum Kulturträger, ushering in the age of the Bomb and the physicist-soldier, the era of quantum supremacy has emerged simultaneously with a new era of geopolitical upheaval. Notably, many of these movements of upheaval have also taken shape in language of advantage and supremacy. In particular, the last decade has been marked by an enormous resurgence in movements of ethnic nationalism worldwide—in Western and Central Europe, with the rise of the far-right National

Rally and AfD parties in France and Germany; in Russia, with Vladamir Putin's invasion of Ukraine in the name of militant cultural unity; in India, with the Hindu nationalist movement of Narendra Modi; in China, with the consolidation of power under Xi Jinping and the genocide of Uygher communities in Xinjiang province; and in the United States, with the election of Donald Trump and the return of an overt politics of white supremacy. In the latter two cases, these governments have proven to be to most reliable sponsors of quantum computing research. The consequences of this entanglement warrant further study.

1.5 Situating the Text

When I was a kid, I told my dad that I didn't want to be Jewish anymore. I dreaded the Shabbat and Rosh Hashanah services at our suburban New York synagogue; I didn't like evening Hebrew school, or the rich straight kids who bullied me during Torah class, or the lavish Bat Mitzvahs a few of their parents forced them to invite me to; and I was starting to realize that I probably didn't believe in the Old Testament god that these things were supposed to represent. They didn't seem to believe in me. So I had done the research, and I had decided that I would try to be something else, something other than Jewish.

My dad was not impressed. He told me that I could call myself whatever I wanted, but either way, he was going to hold me to the Nuremberg Laws. And according to those laws—laws passed in Nazi Germany in 1935 which codified the racial criteria of German personhood, effectively revoking the citizenship of every German with a Jewish grandparent and laying the legal foundation for the project of mass extermination which would begin six years later—I was Jewish. So I could call myself whatever I wanted. I didn't have to go to services anymore, didn't have to believe in a higher power. But if I were in Europe in 1941, I would be in the camps, same as him. And if history repeated itself, as it had threatened to time and again during his life, we might both still find ourselves there. So we had to stick together, and we had to make sure that never happened again. That was what it meant to be Jewish. That was

what it meant to be a custodian of history—to be responsible to a past you didn't choose, but would not be possible without. A past that is never past at all.

The kid in the story above has no place in a physics thesis—no place, except the author page. After that, the author of a physics text must become a ghost. But equations do not derive themselves. Before there is a proof, there is a hand, poised at a blackboard or draped prone over a keyboard. Experiments do not simply happen of their own accord. Before there is a spectroscopy peak heralding a great result, there are bodies: bodies in a cleanroom to fabricate the device; bodies on ladders around a dilution refrigerator to open the vacuum cans and wire up the device; bodies hunched over a computer in the laboratory watching data come in, sometimes late into the night. These bodies, physics tells us, occupy space and time. And yet, reading through an account of a physics result—either in a published research paper or in a thesis such as this one—the body of the scientist is forced to retreat, fatally, behind the arras of the text.

This narrative convention is consistent, of course, with the way most physicists are taught to understand their relationship to the systems they study. Scientific objectivity, we are told, demands that we always hold the subject of our work at arm's length, removing ourselves from the story such that the data—and, by extension, Nature—speaks for itself. The modern scientific impulse towards detached objectivity, historically and socially contingent as it is [32, 111, 184, 201, 271, 405, 418, 438], has its utility. It also necessitates a sort of narrative sleight of hand, disappearing the author totally and creating what the great historian Donna Haraway once famously called the scientist's "conquering gaze from nowhere." [184]

I have never been to nowhere. Nor has the kid in the story above, the kid whose whose hands are now my hands, hunched over this keyboard, typing these words. And so, we cannot in good conscience claim to have done any of this work there. We refuse our disappearance.

It could be otherwise. In many social science disciplines, such as anthropology and STS, it is considered good practice to begin a text with a brief and self-contained autobiographical sketch describing the author's relationship to the work which fol-

lows [194]. This self-description provides the reader with context for the research, context for why a particular set of questions were asked and why particular conclusions are drawn from their answers. It grounds the text in a body, in a place, and in a time. It *situates* the text, to borrow again from Haraway [184], and it sketches the boundaries of the partial perspective from which it emerged. The work in this thesis happened somewhere. It happened, in every instance, with people. Many of these people are listed as coauthors on the associated publications; many are not, though their contributions were no less essential. In what follows, I will attempt to offer a thorough account of my situation—of my relationship to quantum computing over the past decade, and of the people, places, and events through which that relationship took shape.

When physicists tell their stories, most begin with love: love of the science, love of Nature and its mysteries, love tested, love affirmed, love lost, sometime irrevocably. Mine does not begin with love, though it may still end with it. My first exposure to physics came in high school. I didn't know much about love back then, but I did know about competition—like many unhappy teenagers, I readily exchanged the former for the latter and convinced myself I had gotten a pretty good deal. And so, when I was given the choice between taking biology, chemistry, or physics late in high school, I chose the 'hard' science—hard both in terms of rumored difficulty and in terms of some imagined intellectual purity in comparison to the 'soft' sciences. Looking back, I do not remember how I became naturalized to this notion—how it became obvious or sensible to me that physics was an exceptional pursuit—but I internalized it deeply. Physics made me feel exceptional, even as my test scores suggested otherwise.

Like most things in high school, however, I compartmentalized physics, and it ended at the bell. Physics was a part of my life, but it was not my life. Outside of school, I was an actor in a Shakespeare company, made long pilgrimages to the local library to rip stacks of CDs onto my iPod, binged on video games and anime. As far as physics was concerned, my primary extracurricular activity consisted of long

and precocious debates about time travel with my friend Zach. In retrospect, those rambling afternoons at the local Starbucks were my first intimation that physics was something you did with people, something that emerged in conversation, grasping at ideas you don't yet have the language for. That physics, perhaps, had something to do with love.

I started college in fall 2011 and again enrolled in physics, because it was a thing I had done in high school and figured I could probably do again. My physics grades that first semester were even worse than they were in high school, and I quickly realized that my old strategy of memorizing equations before an exam wasn't going to work anymore. So I decided to quit physics and try something else. It was around this time that I first encountered comparative literature, a discipline which fluidly brought together my interests outside of the sciences, in language, storytelling, art history, aesthetics, philosophy. Comparative literature, in turn, introduced me to critical theory and the study of narrative structure—structures which extended their reach well beyond the page, shaping our creation of meaning in every facet of our life. I owe a deep thanks to my mentors along this path: Christopher Bolton, Margeaux Cowden, Anjuli Raza-Kolb, Janneke van de Stadt, Julie Cassiday, Bill Darrow, Li Yu, Eugene Johnson, Mike Lewis. Through them, I learned that everything was a text, that everything could be read, and that good reading was always a practice of care.

In those early days, my studies in comparative literature were inseparable from my evolving interest in music. My friend Stan Monfront encouraged me to join the college radio station my first semester of college, and I began hosting a weekly—and, with each passing semester, increasingly byzantine—music program on WCFM; here, Isabel Vazquez, Andrew Langston, Will Hayes, Wade Phenicie, and Norman Walczak were invaluable co-conspirators. Following my interests in literary criticism and experimental music, I secured a writing gig as a music critic at Tiny Mix Tapes, an online music site which had shaped my listening since high school; I owe a deep gratitude to my editor, Marvin Lin, for taking a chance on me and for his encouragement throughout my time at the site.

My path back to physics was accidental and fortuitous. In 2012, during a delirious

late-summer week on campus before the start of my second year, I became entangled with a group of people who would become my lifelong friends: Teddy Amdur, Cole Meisenhelder, Liz Dietz, David Yan, Jeremy Boissevain, Adrienne Favis, Jack Hoover. Cole and Teddy were planning to become physics majors, and they suggested that I take electromagnetism with them that semester. For the first time, I had friends to work on problem sets with; for the first time, I saw other people struggling with physics the way I thought I alone had struggled. By the end of the semester, I had committed to a double major in comparative literature and physics: the first, for love of the material; the second, for love of the people.

Physics and comparative literature offered two very different windows into what it meant to do research. In general, we tend to think of the humanities as deeply social disciples—invested, as they are, in the study of people, their beliefs, their interactions—while the sciences are regarded as fundamentally anti-social. In practice, I found the opposite was true. When it was time to write an essay for a literature class, I holed up in the library or in my room, alone with my computer. I savored the pride that came with finishing an ambitious essay and receiving praise from a professor I admired, but it was a solitary pride—perhaps even an anxious, paranoid pride. I knew it could be taken away as easily as it was given. My successes and failures in the humanities were two sides of a coin, deeply individuated, intensely private.

In stark contrast, my accomplishments in physics always felt far more modest, but they were shared richly and widely. Weekly physics problem sets were always completed in a group, and our work was permeated everywhere by play. Throughout college, this usually took the form of weekly ten-hour marathon sessions the night before the due date, usually from 5pm to 3am the following morning. Huddled in the physics common room or in the basement of the math building, the music was always loud and the tangents innumerable. Working through the derivation of a single formula, conversation would invariably turn to politics, art criticism, petty gossip, grave conspiracy. Midnight snack runs were ritual and required. Coffee cups overflowed and accumulated next to calculators and textbooks. By the time we handed it into our professor the following morning, the official document of equations

and (variously) completed problems always felt like an incidental and perfunctory product of the night before.

This was, I realize now, one of my earliest experiences of that wild unruly thing which we might call *study* [185]. Yes, there was 'work' happening somewhere in the midst of it all, but the line between labor and play was never fixed, with each contributing obliquely and abstractly to a collective practice of worldbuilding, of figuring our situation out. I am deeply grateful to my physics professors for encouraging us to create this space: Kevin Jones, Ward Lopes, Mike Seifert, David Tucker-Smith, Charlie Doret, William Wootters, Tiku Majumder.

During the summers after my sophomore and junior years of college, I worked on campus as a research assistant in the physics department: the first summer, in theoretical particle physics under the mentorship of David Tucker-Smith; the second, in theoretical quantum foundations with William Wootters. These were my first encounters with physics research outside the classroom, and they exposed me to yet another model for what it meant to be a scientist. Words cannot begin to describe those two iridescent summers in the Berkshires, and they would not have been possible without the riotous crew of physics comrades who made them possible: Julia Cline, Corey Smith, Max LaBerge, Kitty Kistler, Sarah Peters, Kirk Swanson, Dan Evangelakos, Brandon Ling, Chip Herman, Kamuela Lau, Cesar Melendez, Ilya Amburg, Weng-Him Cheung, Bijan Mazaheri, Scott Wieman, Isaac Hoenig, Sarah Fleming, Teddy Amdur, Cole Meisenhelder.

And yet, even as I continued to apply for summer RAs and committed to writing a senior research thesis, I had no plans to continue physics after graduation. As far as I understood it, physics after college meant graduate school, and grad school was for the brilliant students. As much as I enjoyed the problem set camaraderie and the sprawling research summers, I knew I was not one of those students. And so, as my classmates began prepping for the GRE and pulling together their applications, I looked on from the outside, trying to figure out my path forward. With little other guidance from the bewildered counselors at my college career office, I began applying to jobs in management consulting.

The fact of this thesis already spoils the twist of the story, and I owe its existence to two interventions which occurred in the fall of 2014 during my final year of college. The first was the mentorship of my undergraduate thesis advisor, Bill Wootters. At the time, I was convinced that my work in comparative literature made me a worse scientist, that it distracted me from committing fully to the life of a physicist. Bill embraced my interests outside physics and encouraged me to incorporate them into my work—when I shared with him my discovery of Karen Barad's *Meeting the Universe Halfway*, he excitedly offered for me to switch thesis topics and write about the philosophy of quantum mechanics. I demurred, but the sincerity and the spirit of his offer left a lasting impression on me. At a moment when I failed to see myself as a scientist, Bill taught me that there were many ways to be a scientist. It was up to me to define which sort I wanted to be, on my own terms.

The second intervention came in the form of a surprise colloquium talk. In late October 2014, Jamie Kerman visited my college campus on behalf of MIT Lincoln Laboratory. Lincoln Lab had recently secured a major research program to develop a high-coherence quantum annealer using superconducting circuits, and Jamie was returning to his alma mater to recruit undergraduates for the project. Before the talk, my life after college felt like an ultimatum: either continue physics in grad school, or leave research to join the workforce. All at once, a third path seemed to open up before me, a path which allowed me to continue doing research outside of academia, testing the waters before committing to grad school later down the line. In conversation after the colloquium, Jamie described the program he was hiring for as the Manhattan Project of quantum computing. I asked him where I could sign up.

On July 13, 2015, I began work as an Assistant Staff scientist in the Quantum Information and Integrated Nanonsystems group at MIT Lincoln Laboratory. For the next three years, I worked as a researcher on QEO (short for 'Quantum Enhanced Optimization'), a government research program sponsored by IARPA to investigate the viability of quantum annealing systems beyond the capabilities of the D-Wave system. During this time, I gradually transitioned from a role on Lincoln Lab's small theory team to a more interdisciplinary position, spanning both the theory

and experimental teams. Early on, I had begun to notice that the theorists and the experimentalists in the group spoke very different technical dialects—as a literature student at heart, I stepped in as a translator of sorts. With the measurement team, I worked to articulate their technical capabilities and limitations to the theorists; with the theory team, I digested volumes of derivations into actionable results for the experimentalists to test. I am profoundly grateful to Jamie Kerman for his mentorship during this period and for his incredible trust and faith in me during those early years.

Like all work of translation, the role I carved out at Lincoln was deeply creative. It also demanded fluency in both sides of the conversation, and I soon found myself thrust, for the first time, into the laboratory as an experimentalist. While my undergraduate thesis work had given me a firm foundation in quantum information theory, little could prepare me for my new role designing and measuring novel superconducting qubits. Fortunately, I found myself surrounded by eager mentors, and I owe deep thanks to Steve Weber, Danna Rosenberg, Greg Calusine, Mollie Schwartz, David Kim, Jonilyn Yoder, Kevin Obenland, Mike O'Keeffe, Jovi Miloshi, Adam Sears, Eric Dauler, and David Hover for their generosity, support, and friendship during these early years. During this period, Will Oliver's role and influence cannot be understated. As the leader of the measurement team at Lincoln at the time, Will actively encouraged my transition into the laboratory, offering me a level of trust and responsibility which far exceeded my extremely limited experience. I tried my best to rise to the challenge. Will and Jamie saw that I knew how to tell a story, and I soon found myself presenting research at conferences and program reviews on behalf of the entire team.

Life outside the laboratory, however, was starting to look different. In January 2016, in the middle of a particularly difficult first winter in Cambridge, I came out to my family and a few of my closest friends. This revelation, years in the making, somehow managed to explain everything and nothing about my life up to that point. All these years later, it is still difficult to find the right words to articulate this, and I have long since given up trying to. Folks who have gone through this process will know what I mean. But I can say this: for the first time in my life, many of the

closely guarded compartments I had divided my life into began to dissolve. Working through the messy tangle between them, I began to make some sense of it all, and I started to feel at peace with what I saw in the mirror. At work, however, I struggled to negotiate the boundary between my new personal and professional lives, and I once again defaulted to compartmentalizing. Even now, this part of the story will likely come as a surprise to many of my oldest coworkers. So be it.

I was twenty-three in 2016—old enough, in retrospect, to start seeing myself as more than just myself, as a body adrift in history, a living artifact—and it is around this point that biographical time and historical time began to intertwine for me. I was twenty-three and newly employed when, browsing the shelves of Lincoln's subterranean library one day, I first came across Zurek's *Complexity, Entropy, and the Physics of Information*; reading through that volume, I began to situate some of the lessons Bill Wootters had instilled in me years earlier, and I began to understand myself as part of a tangled quantum lineage, one which placed me well outside the mainstream of the field as I was coming to understand it. I was twenty-three and newly queer when, alone in an unfamiliar city I had just begun to call home, I first heard the news of the massacre at Pulse, saw the pageantry of couples lined up at the blood banks to donate to the survivors, realized my own blood was newly worthless. I was twenty-three when Donald Trump was elected president and my dad's childhood warnings came flooding back like air raid sirens. I started dreaming of the camps, of leaving my luggage on station platforms, looking back at the bags as they fade into the distance, realizing I am never getting off the train. I still have those dreams. During this period, my college friends Liz Dietz and Kate Flanagan generously opened up their home in Newburgh as a weekend refuge, and I cannot thank them enough for their support, care, and hospitality during this period.

As the world around me began contorting into monstrous new shapes, quantum computing thrived like never before. And so, I contorted. I thrived. It was during this period that I first became enmeshed in the Engineering Quantum Systems (EQuS) group at MIT campus. The group, led by Will Oliver and Terry Orlando, operated under a "One Team" model with the Quantum Information group up in Lexington, and

Will warmly encouraged me to see the group on campus as an extension of my home at Lincoln. When I first joined the team in 2015, EQuS consisted of only a handful of postdocs and research scientists; I am grateful to Terry Orlando, Simon Gustavsson, Jeff Grover, Archana Kamal, Fei Yan, Dan Campbell, and Phillip Krantz for their warm welcome to MIT during those early years. In 2016, the first generation of grad students arrived at EQuS: Alex Greene, Youngkyu Sung, and Bharath Kannan. It was late in 2016 that I first met Morten Kjaergaard, a postdoc newly arrived from the University of Copenhagen. Morten and I quickly bonded over our shared interest in hardcore music, and he and his wife Maria Genckel became close friends. Morten had ambitions of starting a quantum algorithms subteam on campus, and he graciously invited me to join brainstorming sessions on campus. Together with Alex Greene and Mollie Schwartz from Lincoln, these weekly journal clubs became the foundation of the nascent algorithm team in EQuS. Through those early meetings, I slowly began to wrap my head around a vision of graduate school. I started planning my return to academia.

In the fall of 2018, I transitioned to graduate school as a PhD candidate in Electrical Engineering and Computer Science at MIT. Will Oliver generously offered me a position in his group, and I began settling into my new role in EQuS. These first years were a period of enormous adjustment. On the technical side, I quickly realized that I had much to learn in the transition from quantum annealing to the gate model; I am enormously indebted to Alex Greene for showing me the ropes and for their patience and care throughout that journey, and I am grateful to the rest of the growing EQuS team for their support and friendship those first two years: Jochen Braumueller, Leon Ding, Simon Gustavsson, Bharath Kannan, Amir Karmalou, Rebecca Li, Chris McNally, Tim Menke, Mirabella Pulido, Jack Qiu, Youngkyu Sung, Fran Vasconcelos, Antti Vepsalainen, Joel Wang, Roni Winik, and Megan Yamoah. On the academic side, I sharply felt the toll of three years away from exams and my undergrad problem set support network; I am grateful to all my professors during this period, particularly to Kevin O'Brien for his enormous support and understanding during one especially difficult semester.

The autumn of 2018 brought another change to my life, one which influenced the trajectory of this work in innumerable, immeasurable ways. In November of that year, I once again crossed path with Sarah Fleming, an old friend who I first met during summer physics research in college years earlier. After college, Sarah had switched career paths to become a hospital chaplain, and she had recently moved to Cambridge to attend graduate school at Harvard Divinity School. In the years since our chance encounter in 2018, our friendship matured into a partnership, and we began to build a life together. Sarah's service to her patients—often during their final moments of hospice or in the neonatal ICU—inspires me every day, and her work has served as a constant reminder to put my own in perspective. Through Sarah, years of cultivated cynicism began to thaw, and I gradually began to think of my own work as a practice of care. In time, I started to wonder—eyes wide open, with all the naivete and wisdom of love—if my work was actually making the world a better place.

During my early years of graduate school as a member of the EQuS algorithm team, our efforts all aligned towards a first demonstration of Density Matrix Exponentiation (DME), an algorithm we had arrived at during lively conversations with the theorists Iman and Milad Marvian, as well as their postdoctural advisor Seth Lloyd. The amount of technical and theoretical infrastructure we developed during this period was extraordinary, and I learned an enormous amount from all of my colleagues during this period: Morten Kjaergaard, Alex Greene, Mollie Schwartz, Chris McNally, Andreas Bengtsson, Mike O'Keeffe, Kevin Obenland. It was during this period that Morten first introduced me to Matthias Christandl, a theorist on sabbatical at MIT from the University of Copenhagen, and his postdoc Johannes Borregaard; Johannes, Matthias, and I would continue to collaborate for the remainder of my graduate studies—culminating, after a number of twists and turns, in our joint development of Lindblad tomography—and I am immensely thankful for their incredible contributions to this journey.

In late 2019, two events occurred which profoundly changed my relationship to the field of quantum computing. In July 2019, during the final stages of the DME experiment, the financier and socialite Jefferey Epstein was arrested on federal charges

for the sex trafficking of minors in New York and Florida. Epstein died in prison a month later. Over the coming months, the extent of Epstein's crimes and his entanglements with the scientific community quickly came to light, and it was revealed that Epstein had made significant financial contributions to prominent researchers at Harvard and at MIT. Following this news, my colleagues in EQuS and I first became aware of Epstein's name in the acknowledgment section of the original DME theory paper. It is difficult to articulate the depth of my anger and frustration following this revelation, or my dissatisfaction with the profound indifference expressed by the quantum computing community during this period.

The shock waves cast by this first event were quickly quelled by the arrival of the second. In October 2019, the team at Google Quantum AI published the first claimed demonstration of quantum supremacy using a superconducting quantum processors. At the time, this result was widely heralded as the crowning achievement of my field to date, and it was greeted with excitement and euphoria by many of my colleagues. It was, many of us believed at the time, the beginning of a new era. In the fanfare around the result, a few colleagues began passing me online discussions and articles they had come across over the years regarding the term 'quantum supremacy' and its possible association with white supremacy: Karoline Wiesner's 2017 arXiv article on "the careless use of language in quantum computing" [469], the ensuing debate it provoked on SciRate among many senior members of the quantum information community [105], Scott Aaronson's popular blog posts on the subject [3]. As a student of language, I took a keen interest in these texts. These two words were doing something powerful, though I struggled at the time to fully articulate exactly what I thought they were doing. I tucked these words away, like a splinter in the back of my brain, and I tried to focus on my research.

A few months later, in March 2020, COVID-19 hit North America. This was the start of the folding years. All at once, time began to bend back and forth upon itself, collapsing 2020 and 2021 and 2022 onto each other, looping and distorting memory. During this period, Cambridge became a ghost town—undergraduates were abruptly ejected from campus and sent home, graduate dorms were placed on lockdown and

surveilled, wealthy townies invested in real estate and fled to their new *pieds-à-tierre* in Maine and Vermont. As the world around my apartment rapidly came undone, life in Cambridge took on a new rhythm: paranoid, twice-monthly trips to the grocery store for lentils and cans of non-perishables; anxious excursions though the empty streets of our Potemkin city, masked up with no one else in sight; group meeting and research updates over Zoom, colleagues and labmates now permanently flattened into small boxes in a grid of faces; eyestrain; migraines.

This thesis is inseparable from the COVID-19 pandemic, and those years cast a shadow over every chapter of this document, those in Part IV especially. The Lindblad tomography project took shape during a period of mass quarantine, and that work would not exist without the support, patience, and care of all my coauthors on that work. In particular, I am incredibly thankful to Morten Kjaergaard, Johannes Borregaard, and Matthias Christandl for generously offering so much of their time and attention during our virtual transatlantic collaboration (particularly the late-night Zoom calls between Copenhagen, Delft, and Cambridge), and to Alex Greene and Youngkyu Sung for maintaining our dilution fridge at MIT campus while I collected data remotely from my apartment during the height of lockdown in July 2020. Our work together kept me afloat through many difficult weeks and months.

Physics research happened during COVID, but it was not my primary motivator during that period. Looking back, the period of the pandemic was an enormously clarifying time for me. It was an opportunity to recalibrate, and to focus on what was really meaningful and important in my life. The company of my friends and my family—too often taken for granted in the busy years after college, now mediated by a computer monitor or an empty six feet of social distance—became infinitely precious again. Words cannot express my gratitude to Teddy Amdur for our weekly morning walks around Radcliffe campus, and to David Yan, Wei Li, and Cole Meisenhelder for our gaming nights playing Final Fantasy XIV over Discord. I started seriously listening to music again: the work of Matana Roberts, Elysia Crampton, aya, DJ Rashad, Moor Mother, billy woods, E L U C I D, keiyaA, MIKE, Graham Lambkin, Jim O'Rourke, Claire Rousay, Geneviève Castrée, Phil Elverum, Klein, and SOPHIE held

me down throughout it all.[7] I reconnected with the online community of writers I had worked with at Tiny Mix Tapes so many years earlier; after half a decade writing little more than research manuscripts and PowerPoint presentations, I started to think seriously about writing longform criticism again. I started an online study circle with friends from college, and I began reading theory again—Fred Moten and Stefano Harney's *The Undercommons* had a particularly powerful impact on me [185], and their work helped crystallize my thoughts on the labor economy of academic research. I began mentoring an undergraduate researcher in EQuS over Zoom—through teaching, I caught a glimpse of something I thought I had lost back in the Berkshires, and I started to think seriously about the transformative power of pedagogy. I started taking long afternoon walks with my partner Sarah, wading through public parks overrun with weeds and wildflowers. I started biking.

In the background of these tremendous joys, however, the COVID years were a sustained and unrelenting nightmare. While I stayed home and tried to focus on research, my partner Sarah became a frontline worker at Brigham and Women's Hospital, and she witnessed the surges firsthand—the ventilator shortages, the transfer of cancer patients to nearby Dana Farber to free up beds, cots lining the hallway to accommodate the sick. At the time of writing, 1.04 million people have died of COVID-19 in the United States since January 2020; worldwide, the number is reported at 6.48 million, though that figure is almost certainly an underestimate. And the COVID years are not over. The death toll continues to rise.

It must also be remembered that, during this period of mass death, the novel coronavirus was not the only actor. In February 2020, Ahmaud Arbery was pursued and murdered by three white men while jogging in Glynn County, Georgia. The following month, Breonna Taylor was murdered in her apartment by officers of the Louisville Metro Police Department. I was 27 in 2020. Ahmaud Arbery was 25; Breonna Taylor, 26. In May, George Perry Floyd Jr. died beneath the knee of a Minneapolis police officer in broad daylight; his murder set off the largest mass movement for racial jus-

[7]For a partial discography of the works which supported and shaped me during the COVID years, see Refs. [27, 28, 97, 98, 123, 124, 180, 235, 249, 260, 261, 305, 306, 315, 338–340, 381–384, 391, 392, 422, 423, 431].

tice in US history. Unfortunately, like so many things during the COVID years, the events of that summer have faded for many into collective amnesia. Faded, forgotten, but not fixed.

In May 2022, Ruth Whitfield, Pearl Young, Katherine Massey, Heyward Patterson, Celestine Chaney, Geraldine Talley, Aaron Salter Jr., Andre Mackniel, Margus Morrison, and Roberta Drury were killed by a white gunman in a mass shooting at a Buffalo supermarket. I was writing a chapter of this thesis when the news broke. This thesis has taken shape against a backdrop of festering white supremacy—that too is part of its situation. In the period since I started graduate school in September 2018, 96 Black Americans have been murdered at the hands of law enforcement or civilian hate crimes.[8] Like the death toll of COVID, this number is almost certainly underreported and continues to rise, even in the parts of this country where we tell ourselves that both crises are long past. When I mention this fact to my colleagues in quantum computing, most express concern, though almost all attempt to convince me that this has nothing to do with me or with our research. I'm sure that many of them actually believe this.

The fact remains, however, that half of my family is from the South. My mother was born in Marietta, Georgia—the same town where Leo Frank, a Jewish pencil factory superintendent, was lynched in 1915. The former governor of Georgia and two Marietta mayors were among the lynch mob, flanked by sheriffs. I was raised with this story, and it served as another cautionary tale of what might happen to me and to my body if I find myself at the wrong place at the wrong time. But history is not that simple. My mother's parents were not Jewish, and the Orr family goes way back in Cobb County. My ancestors fought for the Confederacy. They owned slaves. To the best of my knowledge, my middle name does not appear among the records of the mob that lynched Leo Frank. But my ancestors were part of that history. That history made them possible, and they in turn made it possible. And they made me possible. I do not know the names of the people my ancestors enslaved, but they did

[8]For a living record of the Black lives taken in the United States by law enforcement and civilian hate crimes, see the work of the #SayTheirNames project [1].

have names. I am responsible to them, and I am responsible to that history. That history is my history. It is American history. I must reckon with the consequences of that. We all do.

As for the connection between quantum computing and white supremacy—the splinter I had pushed to the back of my brain began to throb. Here too there was something to reckon with, but my thoughts remained tangled. I needed comrades, so I went looking for help. Fortunately, the graduate program in EECS at MIT has a minor requirement, and students are required to take two courses in a single discipline outside of their research area as a 'broadening experience.' By the end of 2020, it had become clear to me that many of the most pressing questions facing quantum computing could not be answered within physics, electrical engineering, or computer science. So, inspired by the graduate work of my dear friend Liz Dietz, I proposed a minor in Science, Technology, and Society (STS) studies. In the spring of 2021, I enrolled in the first of my minor courses, a graduate seminar on Social Theory and Analysis. I am grateful to the students I shared that experience with: Bridget Burns, Kelcey Gibbons, Tomas Guarna, Enjoli Hall, James Heard, Will Julian, Rustam Khan, Elitza Koeva, Zachary La Rock, Antonio Pacheco, Mike Sugarman, Salina Suri, JS Tan, and Hina Walajahi. If it weren't for all of their work, conversation, debate, and feedback throughout that difficult and formative semester, this thesis would not be what it is today.

It was during through that spring semester seminar that I first met Stefan Helmreich. I am profoundly grateful to Stefan for his incredible support and feedback during those first forays back into writing, and for passing along my early essays to his colleagues—including, to my great surprise and excitement, Karen Barad, who generously provided detailed comments on a rough piece exploring crowd theory through the poetics of entanglement and coherence. That following fall, Stefan graciously agreed to advise an independent study exploring the social-scientific entanglements of quantum computing in closer detail. Our semester together quickly turned into a crash course in the philosophy, history, sociology, and anthropology of science. Bit by bit, I began to find new language. By the end of the semester, I had produced

an extended manuscript on the material-semiotics of quantum supremacy; that piece, the culmination of half a decade of subconscious data taking during my time as a quantum engineer, is included unabridged in Part V of this thesis, where it serves as the conclusion of this document. I am grateful to Julia Menzel and Cristopher Moore for their feedback on early drafts of that essay, and I thank all the colleagues I passed drafts to throughout the development process of that work.

During the years of remote work under COVID, I lost contact with many of my friends and colleagues in EQuS and at Lincoln. In late 2021, as the pandemic thawed and I slowly returned to in-person work on campus and at Lincoln, I quickly realized how much the world had changed and how much I had changed with it. All at once, I found myself surrounded by friends old and new—I resolved not to take these communities for granted again, and I resolved to help make them better than I had left them. At MIT campus, I was thrilled to see my old friend and colleague Jeff Grover return to EQuS as a research scientist, and I suddenly found myself the 'old grad student' amidst a new generation of students who had joined the group during the lockdown—the generosity and care these younger students show for each other and for their work inspires me totally: Aziza Almanakly, Junyoung An, Lamia Ateshian, Will Banner, Shoumik Chowdhury, Andy Ding, Shantanu Jha, Sarah Muschinske, David Rower, Sameia Zaman. Outside of MIT, I was thrilled to start up new conversation and collaboration with Robin Blume-Kohout and Kevin Young at the Quantum Performance Lab at Sandia, and I am grateful to them and to their team for their support and invaluable conversation during my entry into the QCVV community. And back at Lincoln, I began to settle in among a new generation of friends and comrades: Kyle Serniak, Kate Azar, Tom Hazard, Bryce Fischer, Katrina Sliwa, Mallika Randeria. I am thankful to them for their support and patience during my impending transition back to Lincoln after grad school. We have our work cut out for us.

This self-description brings us, at last, to the present. This document arrives at

the end of one story arc in my life, the beginning of another, and somewhere in the middle of countless others. There are loose ends which must be attended to. In February 2022, Russia invaded the sovereign nation of Ukraine, bringing the horrors of industrial warfare back to the European continent and the Western imagination. At the time of writing, the struggle for Ukrainian independence persists—the civilian death toll and the ledger of atrocities continue to rise. In June, the United States Supreme Court overturned the landmark 1973 decision of *Roe v. Wade*, stripping access to safe and legal abortions for pregnant people in much of the United States. This decision—along with renewed efforts in many states to criminalize gender-affirming treatment for transgender youths—poses a devastating threat to the bodily autonomy of countless Americans, particularly low-income communities and communities of color. And in the background of it all, the climate crisis rages on across the globe, simultaneously ushering in unprecedented droughts in the American West and calamitous flooding in Pakistan. In Massachusetts where I am writing this, each summer feels hotter than the last; each winter, colder; each spring and fall, shorter.

These loose threads are tangled with each other, and they are harbingers of the world that is to come. They are foreshadows of the world which will likely shape the duration of my adult life. But they also suggest the terms of our struggle. None of these crises are new, nor are their solutions. In the face of resurgent white supremacy, the struggle for racial justice and abolition continues worldwide. In the face of rising income inequality and labor exploitation, workers are organizing and fighting to take back the means of their production. The academy is not a bystander in these struggles. In April 2022, MIT graduate students overwhelmingly voted in favor of unionization—only the latest of many universities in the United States to do the same—demanding a say in the conditions of our intellectual labor and demanding protections for the most vulnerable members of our community. I am grateful to all of the students and workers who worked to make this possible.

And finally, in the midst of everything, the story of quantum computing is not yet written. With each passing year, the hype continues to grow, the funding continues to pour, and the whispers of an impending quantum winter grow louder. Time moves

quickly these days, and this thesis already feels dated. I cannot predict the world into which the text will arrive. Perhaps readers decades from now will look back on this work as the start of something extraordinary, something bigger than my colleagues and I could ever dream. But then again, maybe they will hold this document as an artifact of a dead field, an account of the delirious rise before an unceremonious fall. I do not know. So, sitting in the present, I ask the reader: was quantum computing really the future, or was it a refracted mirage of our past, history bent back upon itself in a great tangled circuit? And if it was indeed the future, what sort of future did it become a part of? Did the quantum computer become an instrument of power, or a tool of liberation? As researchers in quantum computing, we cannot wait passively for these answers. We have a say in them. We must have a say in them.

This story does not end with love, because this story does not end. Rather, it arrives at love, arrives at community, arrives at both having never left either. This thesis is a work of science, but it is also a work of criticism. This will be jarring to some readers, and to them I say this: at its best, criticism is a sort of poetry, which is to say that it is an act of love. I wrote this thesis as an act of love—I hope that much is clear in the reading of it. I wrote it as a living monument to the people, the places, and the communities which have shaped me throughout this journey. I am responsible to these communities. I simply ask that they continue to hold me responsible. I promise to do the same.

1.6 Circuit Diagram

A text is a sort of algorithm. A reader arrives at the page in some initial state and, through some series of operations, twists, and turns, emerges on the other side in an altered state. It is fitting that this particular document—concerned as it is with the nature of quantum algorithms and circuits—is itself a sort of logical circuit, with each chapter contributing a rotation in the algorithmic sequence of the text. Like all algorithms, the reader's final state will depend in part on their initial, and younger quantum computing students will likely get something different from the text than

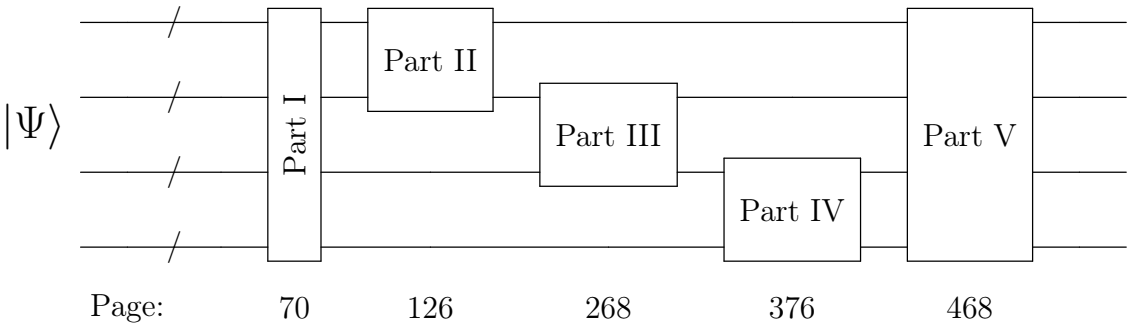

Figure 1-12: The outline of this thesis, abstractly rendered as the circuit diagram of a quantum algorithm. Each part of the text is represented as a gate operation, and the collective action of these operations executes the function of the text.

seasoned researchers. However, I venture that no one will encounter this thesis in an eigenstate of the text and pass through it without perturbation, least of all its author. Language is strange that way.

The technical work reported in this thesis is divided into three main parts: Quantum Bits in Part II, Quantum Algorithms in Part III, and Quantum Characterization in Part IV. We can think of these three coarse blocks as the logical operations of this thesis-algorithm, and they are in turn composed of many smaller physical operations—chapters, sections, and subsections, in the language of the text. The arrangement of the chapters within each part follows a deliberate rhythm: the opening chapter of each part presents an introduction to the mathematical and technical formalisms which structure the work, and each proceeding chapter builds in complexity until a novel result is presented at the conclusion. The part then concludes, the topic changes, and the pattern repeats. These three parts are bookended by Part I and Part V, which serve as introduction and conclusion respectively.

The content of this thesis proceeds as follows:

Part I: Quantum Circuits

Part I—and this, its lone chapter—provides the 'state preparation' portion of the algorithm. Like the initial preparatory gates of a quantum algorithm, we can think of this chapter in two equivalent ways. From one vantage, this introduction prepares

the state of the reader for a particular encounter with the remainder of the text, initializing them in geographic space and historical time. From another perspective, however, this introduction may be seen to rotate everything which follows it, warping the remainder of the text relative to the reader.[9] Take your pick.

Part II: Quantum Bits

Following this introduction, our technical discussion of quantum computing begins in earnest in Part II, where we consider the fundamental building block of a quantum computer: the qubit. In Chapter 2, we begin this part with a review of the fundamental mathematical machinery of quantum bits, unitary rotations, coherent superposition, and entanglement. This chapter is based in large part on a series of lectures I prepared to train undergraduate researchers in the Engineering Quantum Systems group at MIT—lectures which were significantly informed by my early experiences as an undergraduate researcher under the mentorship of William Wootters.

Chapter 3 begins the transition from pure theory to engineering reality. In this chapter, I focus on how to realize the mathematical abstraction of a quantum bit in a piece of physical hardware: a superconducting Josephson circuit. An introduction is made to the formalism of circuit quantization, and we consider a couple examples in the zoology of artificial atoms, species which arise from the different arrangements of electrical circuit elements at our disposal. Portions of this chapters are based on notes I developed under the mentorship of Jamie Kerman, during my early experiences simulating novel flux qubits as a research scientist at Lincoln Lab.

Part II concludes with Chapter 4, where we extend the discussion of superconducting qubits from the previous chapter to multi-qubit systems composed of coupled circuits. In particular, we discuss the design considerations of engineering coupled superconducting circuits with high coherence, delicately balancing a qubit's coupling

[9] That is, given the state of the reader $|\Psi\rangle$ and the text-operators U_{intro} and U_{thesis}, we can absorb the action of the introduction into either the state or the other operator

$$U_{\text{thesis}}\, U_{\text{intro}}\, |\Psi\rangle = U_{\text{thesis}}\, |\widetilde{\Psi}\rangle = \widetilde{U}_{\text{thesis}}\, |\Psi\rangle$$

where $|\widetilde{\Psi}\rangle$ and $\widetilde{U}_{\text{thesis}}$ are the introduction-modified reader-state and thesis-operator respectively.

to its neighbor with its coupling to the noise environment around it. This chapter is based in large part on the work reported in Ref. [463], and I am deeply thankful to all of my coauthors for their contributions to this work, with particular acknowledgment to Steven Weber, David Hover, William Oliver, and Jamie Kerman.

Part III: Quantum Algorithms

Building upon the foundation of single- and coupled-qubit systems laid in Part II, Chapter 5 transitions to a discussion of quantum algorithms composed of discrete gate operations. This chapter reviews the requirements for a universal quantum gate set, and it considers an example algorithm as a case study: the SWAP test. The discussion of universal gate sets in this chapter is heavily inspired by conversations with Morten Kjaergaard early in my graduate studies, and the discussion of the SWAP test is based on discussions with Matthias Christandl and Johannes Borregaard during their time at MIT in 2019.

Chapter 6 picks up the discussion of gate operations and brings it into the laboratory. In this chapter, we discuss the device theory behind the implementation of single- and two-qubit gates using tunable transmon qubit, and we walk through an example calibration of high-fidelity single-qubit gates in the lab. This chapter is based in large part on the gate calibration techniques my colleagues and I employed during the Density Matrix Exponentiation [247] and Lindblad tomography [399] experiments reported in Chapters 7 and 10, and I gratefully acknowledge my colleagues Alex Greene and Morten Kjaergaard for their contributions to the calibration protocol reported in this chapter.

In Chapter 7, we wrap up our discussion of quantum algorithms by presenting the first demonstration of the Density Matrix Exponentiation algorithm on a superconducting quantum processor. This algorithm leads us to a deeper consideration of the relationship between data and instructions in quantum algorithms, and it explores the tradeoffs we must face when performing quantum algorithms on noisy physical hardware. This chapter is based in large part on the work reported in Ref. [247], and I gratefully acknowledge all of my coauthors for their contributions to that work, with

particular acknowledgment to Morten Kjaergaard, Mollie Schwartz, Alex Greene, Christopher McNally, Mike O'Keeffe, Kevin Obenland, Milad Marvian, Iman Marvian, and William Oliver.

Part IV: Quantum Characterization

Part IV will initially seem like a backstep. Having focused on applications and algorithms in Part III, we then turn our attention back to constituent building blocks of a quantum computer and ask: how do we understand these components better? Phrased another way, how do we make intelligent statements about a quantum system when its Hilbert space exceeds the limits of classical description? How do we figure out what our quantum computer is doing? How do we say anything about the states it prepares or the processes it executes? How do we determine whether our processor did any of these things well? In Chapter 8, we consider seven broad categories of questions we might ask about a quantum processor, questions which each define a different technique in the field of Quantum Characterization, Verification, and Validation (QCVV).

In Chapter 9, we focus in on one particular category of QCVV techniques: the characterization of quantum processes. In this chapter, we introduce a number of mathematical formalisms for representing general quantum processes—such as the Kraus and χ-matrix representations—and we consider the relationship between these discrete black boxes and the continuous dynamics of open quantum systems evolving under the Lindblad master equation. This discussion inevitably brings us to the subject of Markovianity and to its foil: non-Markovian errors.

Part IV concludes with Chapter 10, where we consider a novel technique for tomographically reconstructing the time dynamics of a physical quantum system, which we call Lindblad tomography (LT). Performing LT on a physical quantum device, we show how our technique reconstructs the most likely set of Hamiltonian and Lindblad operators governing the particular evolution of a physical multi-qubit system, and we consider how this reconstruction is affected by the presence of non-Markovian errors arising from always-on electrical coupling between qubits. This chapter is based in

large part on original work reported in Ref. [399], and I gratefully acknowledge all of my coauthors for their contributions to this work, with particular acknowledgment to Johannes Borregaard, Morten Kjaergaard, Alex Greene, Matthias Christandl, Joseph Barreto, and William Oliver.

Part V: Quantum Supremacy

Together, Parts II, III, and IV form a useful algorithm, and the reader will hopefully arrive at the end of them with a deeper understanding of what it takes to design, engineer, and characterize a superconducting quantum processor. Equations have been derived, data has been presented, progress has been made. Part V complicates this progress. The work in this part will not help anyone build a quantum computer—on the contrary, some will walk away from this part of the story wondering if we should build quantum computers at all. Like the final inversion gate at the end of a randomized benchmarking sequence, the work presented in Part V bends the thesis back upon itself, unwinding whatever progress we believe we have made up to that point. It completes the loop—or, rather, it reveals the loop we have been circling all along.

This inversion gate takes the form of an extended essay in Chapter 12, which I include in full as the conclusion of this thesis. This conclusion eschews the optimistic outlook of a traditional physics text, offering instead a sustained meditation on the current state of quantum computing as a human enterprise, and on the role of language in the sciences more broadly. This chapter is based in large part on work I developed under the mentorship of the anthropologist Stefan Helmreich during my final years of graduate school, and it centers around the term 'quantum supremacy'—where it came from, what scientists believe it means, what it does. Taking these two words as a starting point, I draw on a century of language studies to deconstruct the tangled myth of supremacy which sits at the heart of contemporary quantum computing, a myth which fatally short-circuits our work to projects of racial, national, and intellectual supremacy.

If the conclusion of this thesis succeeds—if the inversion is total, if the circuit

completes—where does this leave us? Now we are starting to ask the right questions. This thesis ends with only a shadow of an answer, but I will say this: as in a quantum circuit, total inversion requires both a perfect circuit and a perfect inversion gate, a unitary operator matched to its absolute adjoint. This thesis offers neither. Then, perhaps the accumulated errors of this tangled document will serve to splinter the circuit, crack the artifice just enough to imagine something different beyond it, leave us somewhere other than where we began. And then we can begin again.

Part II

Quantum Bits

Chapter 2

Qubits, Rotations, Entanglements

In this chapter, I provide a thorough introduction to the mathematical formalism of quantum bits. Starting from the definition of the two orthogonal states $|0\rangle$ and $|1\rangle$, requiring only that they evolve according to the Schrödinger equation with a hermitian Hamiltonian $\hat{H}$, we derive the Bloch sphere representation of a general qubit state. In the process, we encounter the first hallmark of quantum mechanics, coherent superposition. Going from a single qubit to a pair of qubits evolving under a general two-qubit Hamiltonian, we quickly encounter its second hallmark: entanglement.

2.1 Waves of Probability

Classical physics is the study of bodies in motion: atoms, electrons, bowling balls, artillery shells, planets, stars. Plotting their trajectories across space and time, we find that these bodies are compelled by the same fundamental set of forces, regardless of their size. This observation, commonly attributed to the seventeenth-century English mathematician and natural philosopher Isaac Newton, had enormous consequences—physical, political, philosophical, and theological [418]. With a small set of fundamental equations, this new science of the natural world successfully predicted the motion of both an apple falling from a tree and the orbit of Venus across the heavens, uniting the cosmos under common laws. It was not until the nineteenth century that

practitioners of this science were given a name: 'physicist,' a term first coined in English in 1836 by the theologian and 'scientist'[1] William Whewell [363]. And so it happened that, a century after his death, Isaac Newton posthumously became the first physicist.

Encountering quantum theory by way of classical mechanics or electromagnetism, most students quickly find themselves on unfamiliar terrain. Gone are the free-body diagrams, forces, trajectories through space and time. The primary object of quantum mechanics is not a body, nor is it motion—at least in the senses that we commonly associate either of those words. Quantum mechanics is, first and foremost, a science of *wavefunctions*. Unlike a billiard ball or an electron in the classical description of the world, a wavefunction is not an 'object'—which is to say, it is not a thing which exists at some discrete coordinate in both space and time. Rather, a wavefunction is a thing which captures the *probability* of measuring a given property of a system, like position or momentum. For some systems, these probabilities are localized such that we can say, with certainty, that the system is located *here* and it is not located *there*. For other systems, these probabilities are distributed across space more evenly: in such cases, quantum mechanics will tell us that there is some probability of measuring the system *here*, but there is also some nonzero probability of measuring it *there*.

In either of these two cases, the distribution of probabilities can be mathematically described as a wave. Like waves on an ocean surface, some are sharp and pointy (the position is narrowly localized, as in the former case) while others are spread in rolling peaks and troughs across great distances (the position is delocalized, as in the latter case). In this sense, we can think of a quantum mechanical wavefunction as a *wave of probability*, mapping out the likelihood of measuring a particular property at a particular coordinate. Like all waves, wavefunctions can interact and superpose on top of each other, creating intricate interference patterns. These patterns, abstract as they are, have enormous predictive power for characterizing phenomena across all scales of matter. Indeed, it is this process of interaction and interference which gives

[1]Incidentally, the invention of the English term 'scientist' is also credited to Whewell in the nineteenth century, as is the term 'linguistics.'

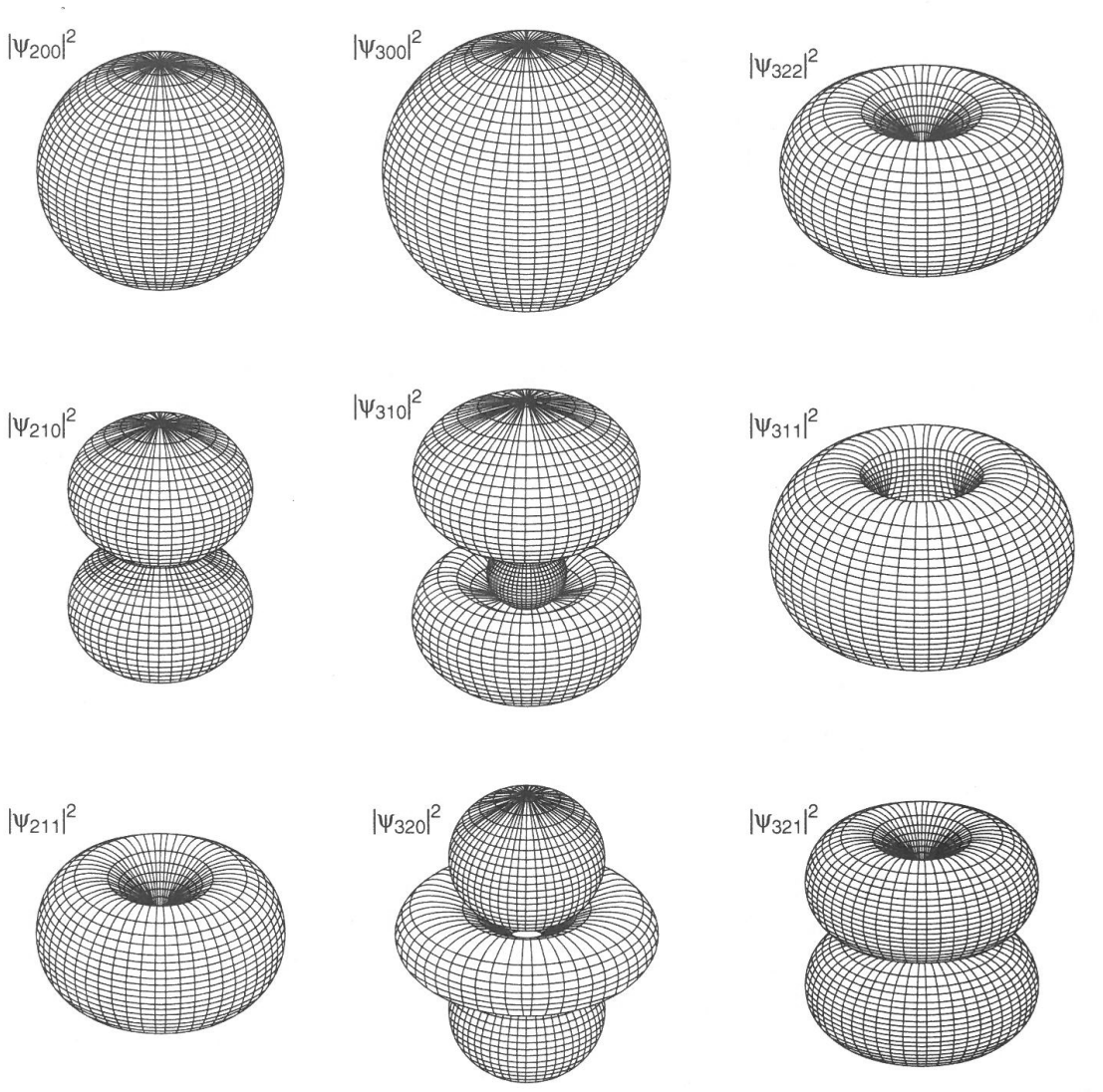

Figure 2-1: The first several electronic wavefunctions of the hydrogen atom ψ_{nlm} from Eq. (2.1), plotted as surfaces of constant probability $|\psi|^2$ around the nucleus at $r = 0$. Image reproduced from Ref. [72], as it appears in Ref. [170].

rise to the bodies of classical mechanics in the first place.

The first successes of quantum theory in the early twentieth-century came in the domain of atomic theory. Here, the tools of Schrödinger, Bohr, and Heisenberg provided powerful and detailed quantitative descriptions of the orbitals of electrons around the nucleus of an atom. In doing so, however, quantum theory demanded that physicists abandon the picture of an atom as a tiny solar system—electrons circling the nucleus like planets around a star. Instead of imagining the electrons as spheres

in motion, like the bodies of classical mechanics, quantum theory ascribed to each atom distributed clouds of probability in which one *might* find an electron. Indeed, when most students first learn quantum theory, one of their first tasks is to retrace this atomic lineage, rederiving the electronic wavefunctions of the hydrogen atom

$$\psi_{nlm}(r,\theta,\phi) = \sqrt{\left(\frac{2}{na}\right)^3 \frac{(n-l-1)!}{2n\left[(n+l)!\right]^3}} e^{-r/na} \left(\frac{2r}{na}\right)^l \left[L_{n-l-1}^{2l+1}(2r/na)\right] Y_l^m(\theta,\phi) \quad (2.1)$$

where $a = 5.29177 \times 10^{-11}$m is the Bohr radius, $L_{q-p}^{p}(r)$ are the associated Laguerre polynomials which define the radial structure of the wavefunctions, and $Y_l^m(\theta,\phi)$ are the spherical harmonics which define their polar and azimuthal structure.[2] In Fig. 2-1, we can see the structure of a few of these wavefunctions, centered around the nucleus of the atom.

While the interpretation of these wavefunctions is abstract, the results they yield are anything but. Taking the expectation value of these electronic wavefunctions with a quantum operator, one can calculate properties such as the energy of a particular electronic transition, properties which quantum theory predicts with unprecedented accuracy. Indeed, though the hydrogen atom remains the only atom on the periodic table whose wavefunctions can be solved analytically, the development of perturbative methods throughout the twentieth century has allowed physicists to obtain accurate numerical results for a large range of atomic, molecular, and condensed matter systems, such as binding energies of quantum chemistry or the electronic band structures of semiconducting solids.

In this chapter, however, we are interested in a different handling of quantum wavefunctions, one which eschews the literalness of atoms and electrons in favor of a more abstract, though mathematically simpler treatment of quantum states. Here, we are interested in the simplest possible quantum system—much simpler, in fact, than the hydrogen atom itself. This system, which we will call a quantum bit or *qubit*, has only two possible wavefunctions, which we will label $|0\rangle$ and $|1\rangle$ in analogy to

[2]For definitions and helpful tables of the associated Laguerre polynomials and spherical harmonics, see an introductory quantum mechanics textbook such as Ref. [170, 179].

the binary bits of classical computer science. These wavefunctions, while intimately related to those of atomic and condensed matter systems—as we will quickly see in the following chapter when we try to build a quantum bit in the laboratory—are largely mathematical abstractions, and thy have their own internal rhyme and logic. Studying the dynamics of these simple two-level systems, we quickly come face to face with the strangeness and beauty of quantum theory at its most fundamental level. Having established this mathematical foundation, the remainder of this thesis will be spent attempting to reconcile this ideal with the reality of physical quantum processors built out of imperfect bits.

2.2 Its and Bits

For the purpose of this thesis, I will be primarily concerned with only two principle wavefunctions. These wavefunctions, curiously, have no immediate physical interpretation. They are simply wavefunctions, no more, no less. In fact, all we can say about these two wavefunctions is that they are as dissimilar from each other as possible, in the following sense: if I ask a particular question, one wavefunction corresponds to answering *YES* with 100% probability, and the other corresponds to answering *NO* with 100% probability. Now, for the moment, it doesn't matter which question these wavefunctions are answering, just that they provide opposite answers.

Let's call these two wavefunctions $|1\rangle$ and $|0\rangle$ respectively. Here, we will use the labels 1 and 0 to denote the binary answer the wavefunction predicts, 1 for *YES* and 0 for *NO*. As for the peculiar bracket around the labels—a notation commonly attributed to the nineteenth-century English physicist Paul Dirac—these are simply mathematical shorthand for *'the wavefunction which, when queried, will always answer _____,'* or interchangeably *'the ____-state.'* As stated above, the only thing which we can say with absolute certainty is that these two states have no overlap with one another—they are orthogonal and have an inner product of zero

$$\langle 1|0\rangle \equiv \int_V \psi_1^* \psi_0 \, dv \equiv 0 \tag{2.2}$$

where the integral is taken over all space.

Note that we have not specified any functional form for the wavefunctions ψ_0 and ψ_1. This is crucial: in general, it is the orthogonality condition in Eq. (2.2) which defines these two states, not the specific details of their wavefunctions. The significance of this statement will become immediately clear in the following chapters when we try to map these states onto physical systems in the laboratory. For now, it simply means we can clean up our notation a bit. Since these wavefunctions do not depend on any spatial coordinate (or any other parameter for that matter), it is convenient to dispense with the ψ's altogether and define these states as simple two-dimensional vectors, as such

$$|0\rangle \equiv \begin{bmatrix} 1 \\ 0 \end{bmatrix} \tag{2.3}$$

$$|1\rangle \equiv \begin{bmatrix} 0 \\ 1 \end{bmatrix} \tag{2.4}$$

Writing the states in this form, we can confirm that the orthogonality condition in Eq. (2.2) is indeed enforced

$$\langle 1|0\rangle = \begin{bmatrix} 0 & 1 \end{bmatrix} \begin{bmatrix} 1 \\ 0 \end{bmatrix} = 0 \tag{2.5}$$

where $\langle\psi|$ is defined as the conjugate transpose of $|\psi\rangle$.

In quantum information and computer science, we call systems which possess the wavefunctions $|0\rangle$ and $|1\rangle$ quantum bits or *qubits*—a term first coined in 1995 by the American theoretical physicists Benjamin Schumacher and William Wootters [410]. Like the binary 0's and 1's of classical information, a quantum bit is an irreducible piece of quantum information out of which all other systems can be constructed, though the significance of that statement won't be apparent until much later in this chapter. For now, it suffices to think of the two states as a simple pair of wavefunctions which always contradict each other. As we'll see, the power and beauty of quantum bits—and, indeed, quantum mechanics itself—emerges quickly from a very small set

of principles.

Having defined these two unremarkable quantum states, the question naturally arises: *ok, so what do they do?* How do they change? How do they move? Like all wavefunctions, these states evolve in time according to the Schrödinger equation, which we can write in time-independent form as

$$\frac{d}{dt}|\psi\rangle = -\frac{i}{\hbar}\hat{H}|\psi\rangle \tag{2.6}$$

where $|\psi\rangle$ is shorthand for a general quantum mechanical wavefunction, $i \equiv \sqrt{-1}$ is the imaginary unit,[3] $\hbar = 1.055 \times 10^{-34}\text{J} \cdot \text{s}$ is the reduced Planck constant, and $\hat{H}$ is the Hamiltonian of the system. Solving this first-order differential equation, we arrive at solutions of the form

$$|\psi(t)\rangle = e^{-\frac{i}{\hbar}\hat{H}t}|\psi(t=0)\rangle \tag{2.7}$$

where $|\psi(t=0)\rangle$ is the state of the system at some initial time $t = 0$ and $|\psi(t)\rangle$ is the wavefunction at some later time t.

Looking at the differential equation in Eq. (2.6) and its solution in Eq. (2.7), it is immediately clear that the time dynamics of the wavefunction $|\psi\rangle$ are entirely determined by the Hamiltonian operator $\hat{H}$. From dimensional analysis, we see that the Hamiltonian has units of energy: indeed, in classical mechanics the Hamiltonian is defined as the sum of a system's kinetic energy T and potential energy U

$$H = T + U \tag{2.8}$$

So too in continuous-variable quantum mechanics, except that the Hamiltonian, kinetic, and potential energies are now promoted to quantum operators

$$\hat{H} = \hat{T} + \hat{U} \tag{2.9}$$

[3]For a deeper consideration of the role of the imaginary unit in the Schrödinger equation and the implications of a real-amplitude theory of quantum mechanics *without* the imaginary unit, see Ref. [13, 397, 427].

In both the classical and quantum mechanical cases, the Hamiltonian captures the balance of energies at play in the system, and this balance defines the conditions of the system's evolution for all times, past, present, and future.

We will return to Eq. (2.9) in the following chapter, but for now it isn't immediately clear what this equation has to do with our states $|0\rangle$ and $|1\rangle$. After all, these states don't have any sense of position, let alone kinetics. For now, it suffices to treat the Hamiltonian as a simple mathematical abstraction and look at what it can do to our two states.

Since we've written our states $|0\rangle$ and $|1\rangle$ as simple 2×1 vectors, we can write our Hamiltonian $\hat{H}$ as a 2×2 matrix, demanding only that the matrix is hermitian

$$\hat{H} = \hat{H}^\dagger = \hbar\omega \begin{bmatrix} a+b & c-id \\ c+id & a-b \end{bmatrix} \tag{2.10}$$

where a, b, c, d are real numbers, the prefactor $\hbar\omega$ has units of energy, and $\hat{H}^\dagger$ is the conjugate transpose of the matrix $\hat{H}$. Since $\hat{H}$ is hermitian, we can decompose the matrix into a linear combination of four basic matrices

$$\hat{H} = E_I\hat{I} + E_X\hat{X} + E_Y\hat{Y} + E_Z\hat{Z} \tag{2.11}$$

where $\hat{I}$ is the 2×2 identity matrix

$$\hat{I} = \begin{bmatrix} 1 & 0 \\ 0 & 1 \end{bmatrix} \tag{2.12}$$

$\hat{X}, \hat{Y}, \hat{Z}$ are the three Pauli matrices

$$\hat{X} = \begin{bmatrix} 0 & 1 \\ 1 & 0 \end{bmatrix} \tag{2.13}$$

$$\hat{Y} = \begin{bmatrix} 0 & -i \\ i & 0 \end{bmatrix} \tag{2.14}$$

$$\hat{Z} = \begin{bmatrix} 1 & 0 \\ 0 & -1 \end{bmatrix} \tag{2.15}$$

and the coefficients E_k are the energies associated with each term.

Returning to the solution to the Schrödinger equation in Eq. (2.7), we can define a new operator which is equal to the exponentiation of the Hamiltonian evaluated at a particular time t

$$\hat{U}(\hat{H}, t) = \exp\left(-\frac{i}{\hbar}\hat{H}t\right) \tag{2.16}$$

Rewriting the solution to the Schrödinger equation in terms of $\hat{U}$

$$|\psi(t)\rangle = \hat{U}(\hat{H}, t)\,|\psi(t=0)\rangle \tag{2.17}$$

we can see that the evolution of the state $|\psi\rangle$ is completely determined by the action of the operator $\hat{U}$ on the initial wavefunction $|\psi(t=0)\rangle$, where $\hat{U}$ is a 2×2 matrix which is unitary

$$\hat{U}^\dagger\hat{U} = \hat{U}\hat{U}^\dagger = \hat{I} \tag{2.18}$$

To see that $\hat{U}$ must be unitary, recall that we required that the Hamiltonian is a hermitian 2×2 matrix such that $\hat{H} = \hat{H}^\dagger$. As such, taking the conjugate transpose of Eq. (2.16) amounts to simply flipping the sign in front of the imaginary unit

$$\hat{U}^\dagger(\hat{H}, t) = \exp\left(+\frac{i}{\hbar}\hat{H}^\dagger t\right) \tag{2.19}$$

$$= \exp\left(+\frac{i}{\hbar}\hat{H}t\right) \tag{2.20}$$

Taking the product of $\hat{U}$ and $\hat{U}^\dagger$, the complex exponentials will cancel out to the identity, in agreement with the unitarity condition

$$\hat{U}(\hat{H}, t)\hat{U}^\dagger(\hat{H}, t) = e^{-\frac{i}{\hbar}\hat{H}t}e^{+\frac{i}{\hbar}\hat{H}t} \tag{2.21}$$

$$= \hat{I} \tag{2.22}$$

Note that the unitarity condition has a nice physical interpretation. Looking at Eq. (2.20) and shuffling around the signs, we can see that this is equivalent to

Eq. (2.16), except with a minus sign in front of the time t

$$\hat{U}^\dagger(\hat{H},t) = \exp\left(+\frac{i}{\hbar}\hat{H}t\right) \tag{2.23}$$

$$= \exp\left(-\frac{i}{\hbar}\hat{H}(-t)\right) \tag{2.24}$$

$$= \hat{U}(\hat{H},-t) \tag{2.25}$$

If $\hat{U}(\hat{H},t)$ is an operator which evolves the state forward in time by some duration t, $\hat{U}(\hat{H},-t)$ is that same operator evolving the state *backwards* in time by a duration t. Evolving the state forward in time and then back in time by that same amount, we expect the state to return to its initial state

$$|\psi\rangle = \hat{U}^\dagger(\hat{H},t)\hat{U}(\hat{H},t)\,|\psi(t=0)\rangle \tag{2.26}$$

$$= \hat{U}(\hat{H},-t)\left(\hat{U}(\hat{H},t)\,|\psi(t=0)\rangle\right) \tag{2.27}$$

$$= \hat{U}(\hat{H},-t)\,|\psi(t=t)\rangle \tag{2.28}$$

$$= |\psi(t=0)\rangle \tag{2.29}$$

which is equivalent to simply enforcing the unitarity condition on the first line and cancelling the two operators out.

To see how our states $|0\rangle$ and $|1\rangle$ evolve under the influence of a general Hamiltonian, let's take the decomposition in Eq. (2.11) and find the corresponding unitary operator for each of the four terms. Starting with the case where $\hat{H} = E_I\hat{I}$

$$\hat{U}_I = \exp\left(-\frac{i}{\hbar}\hat{H}t\right) \tag{2.30}$$

$$= \exp\left(-\frac{i}{\hbar}E_I\hat{I}t\right) \tag{2.31}$$

$$= \exp\left(-i\omega_I\hat{I}t\right) \tag{2.32}$$

where $\omega_I = E_I/\hbar$ is the angular frequency corresponding to the energy E_I. To resolve

the matrix exponential on the RHS, we can take a Taylor expansion of the exponent

$$\hat{U}_I = \exp\left(-i\omega_I \hat{I} t\right) \tag{2.33}$$

$$= \sum_{k=0}^{\infty} \frac{\left(-i\omega_I \hat{I} t\right)^k}{k!} \tag{2.34}$$

$$= \sum_{k=0}^{\infty} \frac{\hat{I}^k \left(-i\omega_I t\right)^k}{k!} \tag{2.35}$$

Since $\hat{I}$ is the identity matrix and $\hat{I}^k = \hat{I}$ for all k, we can factor a single $\hat{I}$ out of all terms in the sum

$$\hat{U}_I = \hat{I} \sum_{k=0}^{\infty} \frac{\left(-i\omega_I t\right)^k}{k!} \tag{2.36}$$

Now that we've pulled the matrix $\hat{I}$ out of the sum, we can collapse the sum back into an exponent of scalars and arrive at our unitary matrix

$$\hat{U}_I = \hat{I} e^{-i\omega_I t} \tag{2.37}$$

$$= \begin{bmatrix} e^{-i\omega_I t} & 0 \\ 0 & e^{-i\omega_I t} \end{bmatrix} \tag{2.38}$$

Applying this unitary operator to our two states $|0\rangle$ and $|1\rangle$, we find that the operator simply applies a phase in front of the state

$$\hat{U}_I |0\rangle = \begin{bmatrix} e^{-i\omega_I t} & 0 \\ 0 & e^{-i\omega_i t} \end{bmatrix} \begin{bmatrix} 1 \\ 0 \end{bmatrix} \tag{2.39}$$

$$= \begin{bmatrix} e^{-i\omega_I t} \\ 0 \end{bmatrix} \tag{2.40}$$

$$= e^{-i\omega_i t} |0\rangle \tag{2.41}$$

$$\hat{U}_I |1\rangle = \begin{bmatrix} e^{-i\omega_I t} & 0 \\ 0 & e^{-i\omega_I t} \end{bmatrix} \begin{bmatrix} 0 \\ 1 \end{bmatrix} \tag{2.42}$$

$$= \begin{bmatrix} 0 \\ e^{-i\omega_I t} \end{bmatrix} \tag{2.43}$$

$$= e^{-i\omega_I t} |1\rangle \tag{2.44}$$

This result is unsurprising, since $|0\rangle$ and $|1\rangle$ are both eigenvectors of the matrix $\hat{I}$. Indeed, all vectors are trivial eigenstates of the identity matrix, so this result will hold for any general vector

$$|\psi\rangle = \begin{bmatrix} a \\ b \end{bmatrix} \tag{2.45}$$

$$\hat{U}_I |\psi\rangle = e^{-i\omega_I t} |\psi\rangle \tag{2.46}$$

Ok, what did this Hamiltonian do to our states? While it would appear that the Hamiltonian $\hat{H} = E_I \hat{I}$ did *something* to the states $|0\rangle$ and $|1\rangle$, the global phase $\exp(-i\omega_I t)$ is not physical. In quantum mechanics, physical observables—position, momentum, energy, for example—are calculated by taking the expectation value of the operator corresponding to the observable. For a general wavefunction $|\psi\rangle$, the expectation value of a general observable $\hat{O}$ is a scalar

$$\langle \hat{O} \rangle \equiv \langle \psi | \hat{O} |\psi\rangle \tag{2.47}$$

Comparing this to the expectation value calculated given the evolved state $\hat{U}_I |\psi\rangle$, we find that the global phases will always factor out of the expectation value and cancel out

$$\langle \hat{O} \rangle_I = \left(\langle \psi | e^{+i\omega_I t} \right) \hat{O} \left(e^{-i\omega_I t} |\psi\rangle \right) \tag{2.48}$$

$$= e^{+i\omega_I t} e^{-i\omega_I t} \langle \psi | \hat{O} |\psi\rangle \tag{2.49}$$

$$= \langle \hat{O} \rangle \tag{2.50}$$

In other words, while the Hamiltonian $\hat{H} = E_I \hat{I}$ modifies the wavefunction, the global phase it applies will never affect the result of a measurement performed on that wavefunction.

Something much more interesting happens when we consider the other three terms of the Hamiltonian decomposition in Eq. (2.11). To see this, let's start by finding the unitary operator corresponding to a Hamiltonian $\hat{H} = E_X \hat{X}$. As we'll quickly see, the three Pauli matrices share a common set of useful properties, so this derivation will suffice for all three cases. Starting again from the definition of the unitary operator in Eq. (2.16), we can once again expand the exponent as a Taylor series

$$\hat{U}_X = \exp\left(-\frac{i}{\hbar}\hat{H}t\right) \tag{2.51}$$

$$= \exp\left(-i\omega_X \hat{X}t\right) \tag{2.52}$$

$$= \sum_{k=0}^{\infty} \frac{\left(-i\omega_X \hat{X}t\right)^k}{k!} \tag{2.53}$$

At this point, we cannot trivially pull $\hat{X}^k$ out of the sum, as we did with the identity. However, we can play a similar trick if we first break the infinite sum into two parts, one for all even values of k is and one for all the odd

$$\hat{U}_X = \sum_{k=0,2,4,\ldots}^{\infty} \frac{\left(-i\omega_X \hat{X}t\right)^k}{k!} + \sum_{k=1,3,5,\ldots}^{\infty} \frac{\left(-i\omega_X \hat{X}t\right)^k}{k!} \tag{2.54}$$

Here, we can exploit an important property of the Pauli matrices: in all three cases, the matrices square to the identity $\hat{X}^2 = \hat{Y}^2 = \hat{Z}^2 = \hat{I}$. Seeing this, we can now factor out all the Pauli matrices in the even and odd sums as

$$\hat{U}_X = \hat{I} \sum_{k=0,2,4,\ldots}^{\infty} \frac{(-i\omega_X t)^k}{k!} + \hat{X} \sum_{k=1,3,5,\ldots}^{\infty} \frac{(-i\omega_X t)^k}{k!} \tag{2.55}$$

where the two infinite sums are simply the Taylor expansions of cosine and sine

respectively

$$\hat{U}_X = \hat{I}\cos(\omega_X t) - i\hat{X}\sin(\omega_X t) \tag{2.56}$$

Since this derivation depended only on the property that $\hat{X}^2 = \hat{Y}^2 = \hat{Z}^2 = \hat{I}$, the same result immediately follows for Hamiltonians proportional to each of the other two Pauli matrices

$$\hat{U}_Y = \hat{I}\cos(\omega_Y t) - i\hat{Y}\sin(\omega_Y t) \tag{2.57}$$

$$\hat{U}_Z = \hat{I}\cos(\omega_Z t) - i\hat{Z}\sin(\omega_Z t) \tag{2.58}$$

Substituting in the full matrices from Eq. (2.12)–(2.15) and multiplying out the terms in the three equations above, we can now explicitly write out the unitary matrices corresponding to each of these three Hamiltonians

$$\hat{U}_X(\omega, t) = \begin{bmatrix} \cos(\omega t) & -i\sin(\omega t) \\ -i\sin(\omega t) & \cos(\omega t) \end{bmatrix} \tag{2.59}$$

$$\hat{U}_Y(\omega, t) = \begin{bmatrix} \cos(\omega t) & -\sin(\omega t) \\ \sin(\omega t) & \cos(\omega t) \end{bmatrix} \tag{2.60}$$

$$\hat{U}_Z(\omega, t) = \begin{bmatrix} e^{-i\omega t} & 0 \\ 0 & e^{i\omega t} \end{bmatrix} \tag{2.61}$$

These operators depend only on the product ωt, which has units of radians, so let's replace this product with an angle $\omega t = \theta/2$

$$\hat{U}_X(\theta) = \begin{bmatrix} \cos(\theta/2) & -i\sin(\theta/2) \\ -i\sin(\theta/2) & \cos(\theta/2) \end{bmatrix} \tag{2.62}$$

$$\hat{U}_Y(\theta) = \begin{bmatrix} \cos(\theta/2) & -\sin(\theta/2) \\ \sin(\theta/2) & \cos(\theta/2) \end{bmatrix} \tag{2.63}$$

$$\hat{U}_Z(\theta) = \begin{bmatrix} e^{-i\theta/2} & 0 \\ 0 & e^{i\theta/2} \end{bmatrix} \tag{2.64}$$

The operators $\hat{U}_X, \hat{U}_Y, \hat{U}_Z$ are rotation matrices. Indeed, when we decomposed a

general Hamiltonian into the sum of Pauli matrices in Eq. (2.11), we were essentially defining a coordinate system within the space of possible two-dimensional hermitian operators. In group theory, this space is known as the two-dimensional special unitary group, SU(2). In this space, the three Pauli operators $\hat{X}, \hat{Y}, \hat{Z}$ function in perfect analogy to the unit vectors $\hat{x}, \hat{y}, \hat{z}$ in three-dimensional real space—also known as O(3), in group theoretic terms (Fig. 2-2a). Like the familiar unit vectors in O(3), the Pauli matrices are orthonormal such that

$$\sigma_i \cdot \sigma_j = \begin{cases} 1, & \text{for } i = j \\ 0, & \text{for } i \neq j \end{cases} \tag{2.65}$$

$$\sigma_i \times \sigma_j = \begin{cases} 0, & \text{for } i = j \\ \sigma_k, & \text{for cyclic permutation of } i, j, k \end{cases} \tag{2.66}$$

where $\vec{\sigma} \equiv (\hat{X}, \hat{Y}, \hat{Z})$ is the vector of Pauli matrices, and the dot and cross products are defined as the symmetric and anti-symmetric matrix products

$$\sigma_i \cdot \sigma_j \equiv \frac{1}{2}\left(\sigma_i\sigma_j + \sigma_j\sigma_i\right) \tag{2.67}$$

$$\sigma_i \times \sigma_j \equiv -\frac{i}{2}\left(\sigma_i\sigma_j - \sigma_j\sigma_i\right) \tag{2.68}$$

Indeed, there is a homomorphic relationship between the group of unitary two-dimensional operators SU(2) and the group of three-dimensional rotation matrices SO(3). As a result, we can robustly think of the unitary operators $\hat{U}$ as rotations in a three dimension space defined by the three Pauli matrices, where the operators $\hat{U}_X(\theta), \hat{U}_Y(\theta), \hat{U}_Z(\theta)$ are rotations around the axes defined by the Pauli matrices $\hat{X}, \hat{Y}, \hat{Z}$ respectively (Fig. 2-2b).

Let's play around with these rotations and see how they evolve our states $|0\rangle$ and $|1\rangle$ for particular products of time and frequency. Starting with the unitary $\hat{U}_X$, we

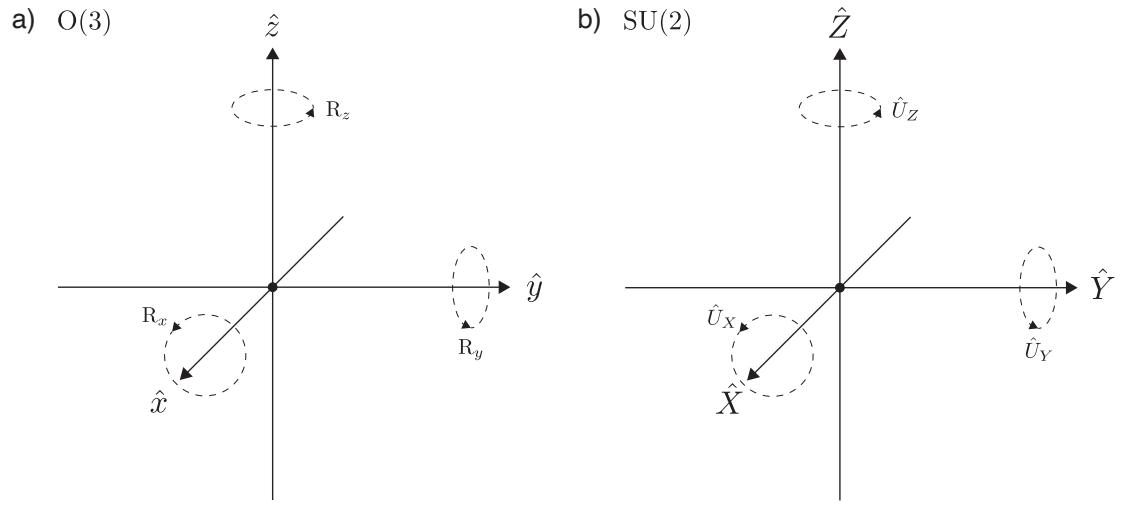

Figure 2-2: **(a)** Cartesian coordinate system in three-dimensional real space O(3). The space of possible vectors is defined by the orthogonal unit vectors $\hat{x}, \hat{y}, \hat{z}$, where $\mathrm{R}_x, \mathrm{R}_y, \mathrm{R}_z$ are rotation matrices around the three cardinal axes respectively. **(b)** The space of possible two-dimensional hermitian operators SU(2), homomorphically mapped onto O(3). In this mapping, the Pauli matrices $\hat{X}, \hat{Y}, \hat{Z}$ define the orthogonal axes of the space of matrices, and the unitary operators $\hat{U}_X, \hat{U}_Y, \hat{U}_Z$ generate rotations around these axes.

can first evaluate the matrix for the case where $\theta = \pi$

$$\hat{U}_X(\theta = \pi) = \begin{bmatrix} 0 & -i \\ -i & 0 \end{bmatrix} \tag{2.69}$$

$$= \begin{bmatrix} 0 & 1 \\ 1 & 0 \end{bmatrix} \tag{2.70}$$

where we have dropped the global phase of $-i$ in the second line for simplicity since, as we just showed, it has no affect on physical measurables. Applying this unitary to our two states $|0\rangle$ and $|1\rangle$

$$\hat{U}_X(\theta = \pi)\,|0\rangle = \begin{bmatrix} 0 & 1 \\ 1 & 0 \end{bmatrix} \begin{bmatrix} 1 \\ 0 \end{bmatrix} \tag{2.71}$$

$$= \begin{bmatrix} 0 \\ 1 \end{bmatrix} \tag{2.72}$$

$$= |1\rangle \tag{2.73}$$

$$\hat{U}_X(\theta = \pi)\,|1\rangle = \begin{bmatrix} 0 & 1 \\ 1 & 0 \end{bmatrix} \begin{bmatrix} 0 \\ 1 \end{bmatrix} \tag{2.74}$$

$$= \begin{bmatrix} 1 \\ 0 \end{bmatrix} \tag{2.75}$$

$$= |0\rangle \tag{2.76}$$

we find that our two states have flipped. If $|0\rangle$ was a wavefunction which always yielded the answer *NO* when measured, after evolving for some time according to the Hamiltonian $\hat{H} \propto \hat{X}$ we now find that is always answers *YES*.

Notice that, as long as we're rotating around the same axis, we can apply multiple unitary operators in a row to rotate our state by their combined angle[4]

$$\hat{U}_i(\theta_A + \theta_B) = \exp\left(-\frac{i}{2}(\theta_A + \theta_B)\hat{\sigma}_i\right) \tag{2.77}$$

$$= \exp\left(-\frac{i}{2}\theta_A\hat{\sigma}_i\right) + \exp\left(-\frac{i}{2}\theta_A\hat{\sigma}_i\right) \tag{2.78}$$

$$= \hat{U}_{\sigma_i}(\theta_A)\hat{U}_{\sigma_i}(\theta_B) \tag{2.79}$$

Applying the unitary $\hat{U}_X(\theta = \pi)$ to each state twice such that they are rotated by a combined angle $\theta = 2\pi$

$$\hat{U}_X(\theta = \pi)\hat{U}_X(\theta = \pi)\,|0\rangle = \begin{bmatrix} 0 & 1 \\ 1 & 0 \end{bmatrix} \begin{bmatrix} 0 & 1 \\ 1 & 0 \end{bmatrix} \begin{bmatrix} 1 \\ 0 \end{bmatrix} \tag{2.80}$$

$$= \begin{bmatrix} 0 & 1 \\ 1 & 0 \end{bmatrix} \begin{bmatrix} 0 \\ 1 \end{bmatrix} \tag{2.81}$$

$$= |0\rangle \tag{2.82}$$

[4]While this result appears to be a trivial application of the exponential of sums, note that this only holds if the matrices in the exponential are the same

$$e^{(a+b)\hat{A}} \equiv e^{a\hat{A}}e^{b\hat{A}}$$

As we'll see later, this does not hold in general when there is a sum of different matrices in the exponential, particularly non-commuting matrices.

$$\hat{U}_X(\theta=\pi)\hat{U}_X(\theta=\pi)\left|1\right\rangle = \begin{bmatrix}0 & 1\\ 1 & 0\end{bmatrix}\begin{bmatrix}0 & 1\\ 1 & 0\end{bmatrix}\begin{bmatrix}0\\ 1\end{bmatrix} \tag{2.83}$$

$$= \begin{bmatrix}0 & 1\\ 1 & 0\end{bmatrix}\begin{bmatrix}1\\ 0\end{bmatrix} \tag{2.84}$$

$$= \left|1\right\rangle \tag{2.85}$$

we find that the two states return to their initial states.

So far, none of these operations have done anything particularly quantum mechanical. Indeed, the unitary operator above is no different from a NOT operation in classical logic, inverting the state such that a 0 becomes a 1 and vice versa. But what happens if we interrupt our wavefunction during its journey from $\left|0\right\rangle$ to $\left|1\right\rangle$? For example, what if we only allow it to evolve for half the amount of time required to completely invert, such that $\theta = \pi/2$? Calculating the resulting unitary operator

$$\hat{U}_X(\theta=\pi/2) = \frac{1}{\sqrt{2}}\begin{bmatrix}1 & -i\\ -i & 1\end{bmatrix} \tag{2.86}$$

and applying it to each of our states

$$\hat{U}_X(\theta=\pi/2)\left|0\right\rangle = \frac{1}{\sqrt{2}}\begin{bmatrix}1 & -i\\ -i & 1\end{bmatrix}\begin{bmatrix}1\\ 0\end{bmatrix} \tag{2.87}$$

$$= \frac{1}{\sqrt{2}}\begin{bmatrix}1\\ -i\end{bmatrix} \tag{2.88}$$

$$= \frac{1}{\sqrt{2}}\left(\left|0\right\rangle - i\left|1\right\rangle\right) \tag{2.89}$$

$$\hat{U}_X(\theta=\pi/2)\left|1\right\rangle = \frac{1}{\sqrt{2}}\begin{bmatrix}1 & -i\\ -i & 1\end{bmatrix}\begin{bmatrix}0\\ 1\end{bmatrix} \tag{2.90}$$

$$= \frac{1}{\sqrt{2}}\begin{bmatrix}-i\\ 1\end{bmatrix} \tag{2.91}$$

$$= \frac{1}{\sqrt{2}}\left(\left|0\right\rangle + i\left|1\right\rangle\right) \tag{2.92}$$

Similarly, if we apply the unitary $\hat{U}_Y$ for an angle of $\theta = \pi/2$,

$$\hat{U}_Y(\theta = \pi/2) = \frac{1}{\sqrt{2}} \begin{bmatrix} 1 & -1 \\ 1 & 1 \end{bmatrix} \tag{2.93}$$

we find that $|0\rangle$ and $|1\rangle$ evolve into the states

$$\hat{U}_Y(\theta = \pi/2)\,|0\rangle = \frac{1}{\sqrt{2}} \begin{bmatrix} 1 & -1 \\ 1 & 1 \end{bmatrix} \begin{bmatrix} 1 \\ 0 \end{bmatrix} \tag{2.94}$$

$$= \frac{1}{\sqrt{2}} \begin{bmatrix} 1 \\ 1 \end{bmatrix} \tag{2.95}$$

$$= \frac{1}{\sqrt{2}} \left(|0\rangle + |1\rangle\right) \tag{2.96}$$

$$\hat{U}_Y(\theta = \pi/2)\,|1\rangle = \frac{1}{\sqrt{2}} \begin{bmatrix} 1 & -1 \\ 1 & 1 \end{bmatrix} \begin{bmatrix} 0 \\ 1 \end{bmatrix} \tag{2.97}$$

$$= \frac{1}{\sqrt{2}} \begin{bmatrix} 1 \\ -1 \end{bmatrix} \tag{2.98}$$

$$= \frac{1}{\sqrt{2}} \left(|0\rangle - |1\rangle\right) \tag{2.99}$$

As for the rotations around the Pauli-Z axis $\hat{U}_Z(\theta)$, we can see that these rotations simply apply a global phase to our two states, regardless of θ

$$\hat{U}_Z(\theta)\,|0\rangle = \begin{bmatrix} e^{-i\theta/2} & 0 \\ 0 & e^{i\theta/2} \end{bmatrix} \begin{bmatrix} 1 \\ 0 \end{bmatrix} \tag{2.100}$$

$$= \begin{bmatrix} e^{-i\theta/2} \\ 0 \end{bmatrix} \tag{2.101}$$

$$= |0\rangle \tag{2.102}$$

$$\hat{U}_Z(\theta)\,|1\rangle = \begin{bmatrix} e^{-i\theta/2} & 0 \\ 0 & e^{i\theta/2} \end{bmatrix} \begin{bmatrix} 0 \\ 1 \end{bmatrix} \tag{2.103}$$

$$= \begin{bmatrix} 0 \\ e^{i\theta/2} \end{bmatrix} \tag{2.104}$$

$$= |1\rangle \tag{2.105}$$

Together with the states $|0\rangle$ and $|1\rangle$, the four states in Eq. (2.89), (2.92), (2.96), and (2.99) are special, so we'll give them their own names, based on the coefficient in front of $|1\rangle$

$$|+\rangle \equiv \frac{1}{\sqrt{2}}\left(|0\rangle + |1\rangle\right) \tag{2.106}$$

$$|-\rangle \equiv \frac{1}{\sqrt{2}}\left(|0\rangle - |1\rangle\right) \tag{2.107}$$

$$|+i\rangle \equiv \frac{1}{\sqrt{2}}\left(|0\rangle + i\,|1\rangle\right) \tag{2.108}$$

$$|-i\rangle \equiv \frac{1}{\sqrt{2}}\left(|0\rangle - i\,|1\rangle\right) \tag{2.109}$$

The set of six states $\{|0\rangle, |1\rangle, |+\rangle, |-\rangle, |+i\rangle, |-i\rangle\}$ are the ± 1 eigenstates of the three Pauli matrices

Pauli matrix	Eigenvalue	Eigenstate
$\hat{X}$	+1	$\|+\rangle$
	-1	$\|-\rangle$
$\hat{Y}$	+1	$\|+i\rangle$
	-1	$\|-i\rangle$
$\hat{Z}$	+1	$\|0\rangle$
	-1	$\|1\rangle$

Since the eigenstates of a given Pauli matrix σ_i are stationary under application of the corresponding unitary operator $\hat{U}_i$ (up to a global phase), these six wavefunctions serve as cardinal states of the three-dimensional space defined by the Pauli matrices (Fig. 2-2b). Moreover, when these wavefunctions are rotated according to one of the other two Pauli matrices $\sigma_{j\neq i}$, they trace out the equator and meridians of a spherical shell in SU(2), known as the Bloch sphere (Fig. 2-3).

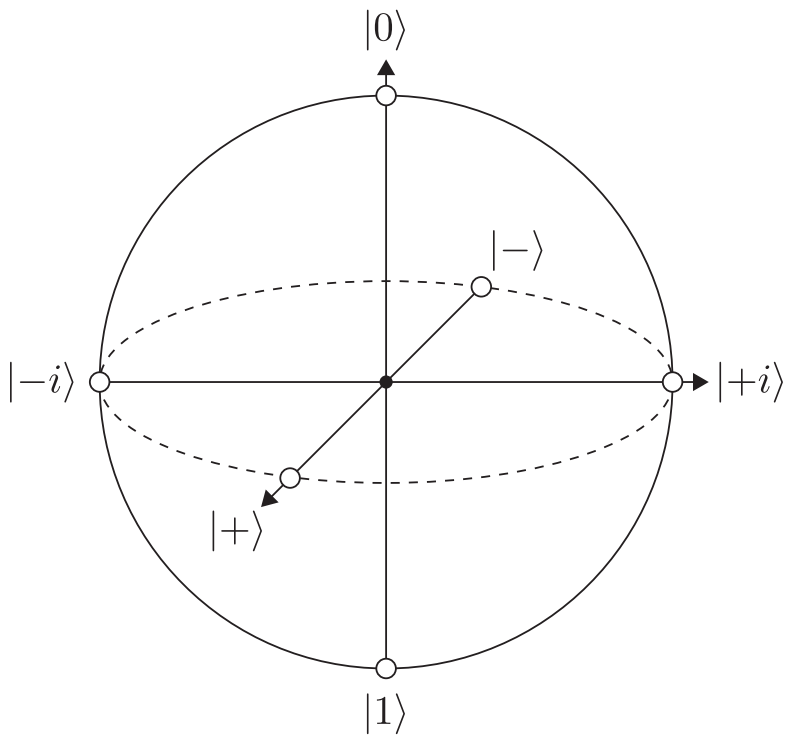

Figure 2-3: The Bloch sphere, inscribed atop the axes of the matrix space SU(2) in Fig. 2-2b. The spherical shell of constant radius represents the complete set of possible single-qubit pure states $|\psi\rangle$ under evolution of a general 2×2 Hamiltonian $\hat{H}$.

2.3 General Rotations

In the previous section, we showed how Hamiltonians proportional to each of the Pauli matrices generate rotations along the equator and medians of the Bloch sphere, transforming the states $|0\rangle$ and $|1\rangle$ into each of the six cardinal states $\{|0\rangle, |1\rangle, |+\rangle, |-\rangle, |+i\rangle, |-i\rangle\}$. In this section, we'll briefly derive the unitary operator corresponding to a general Hamiltonian of the form in Eq. (2.11), and we'll show that this produces the full set of states on the surface of the Bloch sphere.

Starting from the Pauli decomposition of the general 2×2 Hamiltonian in Eq. (2.11)

$$\hat{H} = E_I \hat{I} + E_X \hat{X} + E_Y \hat{Y} + E_Z \hat{Z} \tag{2.110}$$

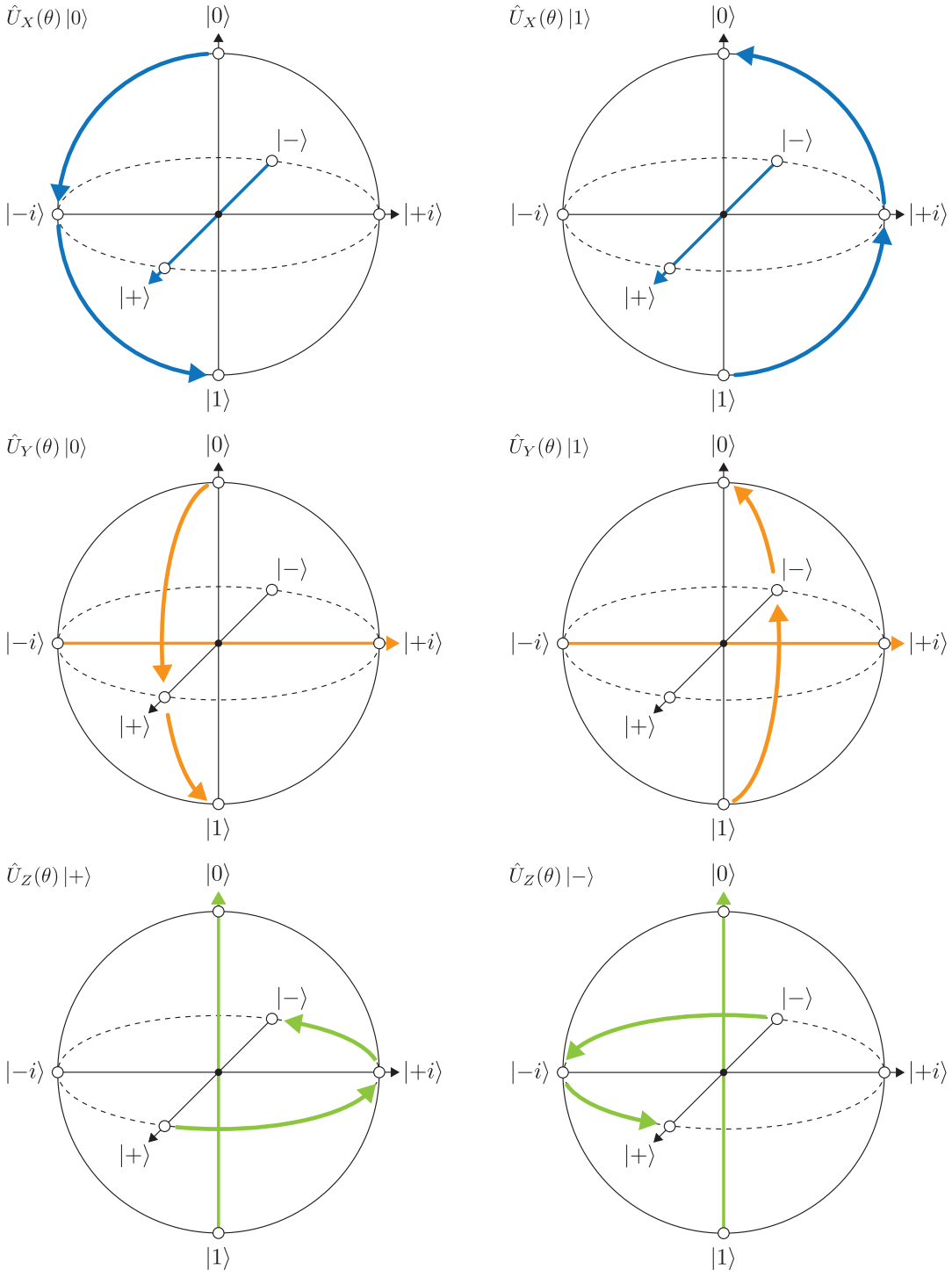

Figure 2-4: Examples of rotations generated by the unitary operators $\hat{U}_X$, $\hat{U}_Y$, and $\hat{U}_Z$ for a set of initial states. In each plot, two arcs of angle $\theta = \pi/2$ are drawn along the surface of the Bloch sphere—adding up to a combined rotation angle $\theta = \pi$—and the rotation axis is highlighted for emphasis.

we can exponentiate this Hamiltonian and write the completely general unitary

$$\hat{U}(\hat{H},t) = \exp\left(-\frac{i}{\hbar}\hat{H}t\right) \tag{2.111}$$

$$= \exp\left(-\frac{i}{\hbar}(E_I\hat{I} + E_X\hat{X} + E_Y\hat{Y} + E_Z\hat{Z})t\right) \tag{2.112}$$

Since the identity matrix $E_I\hat{I}$ commutes with the sum of Pauli matrices $E_X\hat{X}+E_Y\hat{Y}+E_Z\hat{Z}$, we can factor it out and rewrite the unitary as the product of two exponentials

$$\hat{U}(\hat{H},t) = \exp\left(-\frac{i}{\hbar}E_I\hat{I}\right)\exp\left(-\frac{i}{\hbar}(E_X\hat{X} + E_Y\hat{Y} + E_Z\hat{Z})t\right) \tag{2.113}$$

$$= \hat{U}_I(\theta)\exp\left(-\frac{i}{\hbar}(E_X\hat{X} + E_Y\hat{Y} + E_Z\hat{Z})t\right) \tag{2.114}$$

As we showed previously in our derivation of Eq. (2.46), the unitary $\hat{U}_I$ only applies a global phase, so we can drop this factor without loss of generality

$$\hat{U}(\hat{H},t) = \exp\left(-\frac{i}{\hbar}(E_X\hat{X} + E_Y\hat{Y} + E_Z\hat{Z})t\right) \tag{2.115}$$

Since the Pauli matrices form an orthonormal basis in SU(2), we can rewite the sum in the exponential above as a dot product

$$\hat{U}(\hat{H},t) = \exp\left(-\frac{i}{\hbar}E(\hat{n}\cdot\vec{\sigma})t\right) \tag{2.116}$$

$$= \exp\left(-i\omega(\hat{n}\cdot\vec{\sigma})t\right) \tag{2.117}$$

where the unit vector $\hat{n} = (n_X, n_Y, n_Z)$ captures the relative weighting of the three Pauli components in the Hamiltonian. Taking the general unitary operator in Eq. (2.117), we can exploit the fact that $(\hat{n}\cdot\vec{\sigma})^2 = \hat{I}$ and follow the exact same derivation from Eqs. (2.51)–(2.56). Doing this, we arrive at the general rotation matrix

$$\hat{U}_{\hat{n}} = \hat{I}\cos(\omega t) - i(\hat{n}\cdot\vec{\sigma})\sin(\omega t) \tag{2.118}$$

which we can write in terms of an angle θ around the axis $\hat{n}$ as

$$\hat{U}_{\hat{n}}(\theta) = \hat{I}\cos(\theta/2) - i(\hat{n}\cdot\vec{\sigma})\sin(\theta/2) \tag{2.119}$$

Let's apply this general rotation to the state $|0\rangle$ and see what it does. Writing the matrix in Eq. (2.119) and applying it to the vector $|0\rangle$

$$\hat{U}_{\hat{n}}(\theta)\,|0\rangle = \begin{bmatrix} \cos(\theta/2) - in_Z\sin(\theta/2) & (-n_Y - in_X)\sin(\theta/2) \\ (n_Y - in_X)\sin(\theta/2) & \cos(\theta/2) + in_Z\sin(\theta/2) \end{bmatrix} \begin{bmatrix} 1 \\ 0 \end{bmatrix} \tag{2.120}$$

$$= \begin{bmatrix} \cos(\theta/2) - in_Z\sin(\theta/2) \\ (n_Y - in_X)\sin(\theta/2) \end{bmatrix} \tag{2.121}$$

$$= a\begin{bmatrix} 1 \\ 0 \end{bmatrix} + b\begin{bmatrix} 0 \\ 1 \end{bmatrix} \tag{2.122}$$

$$= a\,|0\rangle + b\,|1\rangle \tag{2.123}$$

where a and b are complex numbers which depend on the axis $\hat{n}$ and angle θ of rotation

$$a = \cos(\theta/2) - in_Z\sin(\theta/2) \tag{2.124}$$

$$b = (n_Y - in_X)\sin(\theta/2) \tag{2.125}$$

Notice that, since $\hat{n}$ is a unit vector $n_X^2 + n_Y^2 + n_Z^2 = 1$, the complex coefficients a and b are constrained such that

$$|a|^2 + |b|^2 = |\cos(\theta/2) - in_Z\sin(\theta/2)|^2 + |(n_Y - in_X)\sin(\theta/2)|^2 \tag{2.126}$$

$$= \cos^2(\theta/2) + n_Z^2\sin^2(\theta/2) + +n_Y^2\sin^2(\theta/2) + +n_X^2\sin^2(\theta/2) \tag{2.127}$$

$$= \cos^2(\theta/2) + (n_X^2 + n_Y^2 + n_Z^2)\sin^2(\theta/2) \tag{2.128}$$

$$= \cos^2(\theta/2) + \sin^2(\theta/2) \tag{2.129}$$

$$= 1 \tag{2.130}$$

for all values of θ, n_X, n_Y, n_Z.

Recall that the unitary $\hat{U}_{\hat{n}}(\theta)$ represents the complete set of possible evolutions

given the general 2×2 Hamiltonian in Eq. (2.11). Thus, we have just arrived at the complete set of quantum mechanical states $|\psi\rangle$ which are possible given evolution of the states $|0\rangle$ and $|1\rangle$ under the Schrödinger equation

$$|\psi\rangle = a\,|0\rangle + b\,|1\rangle \tag{2.131}$$

where

$$|a|^2 + |b|^2 = 1 \tag{2.132}$$

These vectors live on the surface of the Bloch sphere in Fig. 2-3 and form a Hilbert space of possible quantum states. Thus, when we ask how a quantum bit moves in time, we can imagine our qubit tracing out elaborate trajectories across the surface of this sphere, its path through state space determined by the Hamiltonian governing its evolution.

2.4 Coherent Superposition

Before we proceed, it is worth sitting with the consequences of what we have just done. Starting from the Schrödinger equation in Eq. (2.6) and the requirement that $\hat{H}$ is hermitian, our states $|0\rangle$ and $|1\rangle$ have evolved into new states of the general form

$$|\psi\rangle = a\,|0\rangle + b\,|1\rangle \tag{2.133}$$

When we defined the states $|0\rangle$ and $|1\rangle$, recall that we required only that they were orthogonal to one another—that is, that they were are dissimilar from each other as possible. How do we interpret this new state $|\psi\rangle$, which appears to contain both itself and its opposite?

To answer this question we need to return to a point that we brushed under the rug at the beginning of the section: when the wavefunctions $|1\rangle$ and $|0\rangle$ were answering *YES* and *NO* with absolute conviction, *what question were they responding to?* Playing with this riddle for a minute, it's easy to see that there is only one question

which would generically—albeit tautologically—produce these responses: *"will you answer YES?"* Formally, we can write this question as a quantum operator

$$\hat{M}_1 = \begin{bmatrix} 0 & 0 \\ 0 & 1 \end{bmatrix} \tag{2.134}$$

where the probability p of a given wavefunction $|\psi\rangle$ answering this question in the affirmative is

$$p_1 \equiv \langle\psi| M_1 |\psi\rangle \tag{2.135}$$

Plugging in our states $|0\rangle$ and $|1\rangle$

$$\begin{aligned} p_1(|0\rangle) &= \langle 0| \hat{M}_1 |0\rangle && (2.136)\\ &= \begin{bmatrix} 1 & 0 \end{bmatrix} \begin{bmatrix} 0 & 0 \\ 0 & 1 \end{bmatrix} \begin{bmatrix} 1 \\ 0 \end{bmatrix} && (2.137)\\ &= 0 && (2.138) \end{aligned}$$

$$\begin{aligned} p_1(|1\rangle) &= \langle 1| \hat{M}_1 |1\rangle && (2.139)\\ &= \begin{bmatrix} 0 & 1 \end{bmatrix} \begin{bmatrix} 0 & 0 \\ 0 & 1 \end{bmatrix} \begin{bmatrix} 0 \\ 1 \end{bmatrix} && (2.140)\\ &= 1 && (2.141) \end{aligned}$$

we get exactly the answers which we used to label these two states in the first place. Indeed, $|0\rangle$ and $|1\rangle$ are the eigenstates of the operator $\hat{M}_1$, with eigenvalues 0 and 1 respectively. In this sense, it is the operator $\hat{M}_1$ which defines the 0 and 1 of our quantum bit—it is the 'question' which defines the 'answer' 0 or 1.

If the operator $\hat{M}_1$ corresponds to the question *"will you answer YES?"*, it is easy to see that there exists another operator $\hat{M}_0$ which corresponds to the question *"will*

you answer NO?"

$$\hat{M}_0 = \begin{bmatrix} 1 & 0 \\ 0 & 0 \end{bmatrix} \tag{2.142}$$

where the probability p of a given wavefunction $|\psi\rangle$ answering this question in the affirmative is

$$p_0 \equiv \langle\psi| M_0 |\psi\rangle \tag{2.143}$$

Plugging in our states $|0\rangle$ and $|1\rangle$, we find that the probabilities flip, as we would expect: $|0\rangle$ answers *NO* 100% of the time, $|1\rangle$ answers *NO* 0% of the time

$$p_0(|0\rangle) = \langle 0| \hat{M}_0 |0\rangle \tag{2.144}$$

$$= \begin{bmatrix} 1 & 0 \end{bmatrix} \begin{bmatrix} 1 & 0 \\ 0 & 0 \end{bmatrix} \begin{bmatrix} 1 \\ 0 \end{bmatrix} \tag{2.145}$$

$$= 1 \tag{2.146}$$

$$p_0(|1\rangle) = \langle 1| \hat{M}_0 |1\rangle \tag{2.147}$$

$$= \begin{bmatrix} 0 & 1 \end{bmatrix} \begin{bmatrix} 1 & 0 \\ 0 & 0 \end{bmatrix} \begin{bmatrix} 0 \\ 1 \end{bmatrix} \tag{2.148}$$

$$= 0 \tag{2.149}$$

Indeed, we can see that the labels we assigned to our two states were entirely contingent on the question we chose to ask—we could just as well have defined our states $|0\rangle$ and $|1\rangle$ in terms of the question posed by $\hat{M}_0$ instead of $\hat{M}_1$, which would simply amount to swapping which label we used for which state. Physically, this would amount to performing a simple basis transformation which rotates the Bloch sphere such that the poles swap, though all of the physics of the system would remain completely unchanged.

What happens when we ask these questions of a general wavefunction $|\psi\rangle$? Plugging in the general wavefunction $|\psi\rangle$ from Eq. (2.131), we can calculate the probabil-

ities p_0 and p_1

$$p_0(|\psi\rangle) = \langle\psi|\,\hat{M}_0\,|\psi\rangle \tag{2.150}$$
$$= (\langle 0|\,a^* + \langle 1|\,b^*)\,\hat{M}_0\,(a\,|0\rangle + b\,|1\rangle) \tag{2.151}$$
$$= \begin{bmatrix} a^* & b^* \end{bmatrix} \begin{bmatrix} 1 & 0 \\ 0 & 0 \end{bmatrix} \begin{bmatrix} a \\ b \end{bmatrix} \tag{2.152}$$
$$= |a|^2 \tag{2.153}$$

$$p_1(|\psi\rangle) = \langle\psi|\,\hat{M}_0\,|\psi\rangle \tag{2.154}$$
$$= (\langle 0|\,a^* + \langle 1|\,b^*)\,\hat{M}_0\,(a\,|0\rangle + b\,|1\rangle) \tag{2.155}$$
$$= \begin{bmatrix} a^* & b^* \end{bmatrix} \begin{bmatrix} 0 & 0 \\ 0 & 1 \end{bmatrix} \begin{bmatrix} a \\ b \end{bmatrix} \tag{2.156}$$
$$= |b|^2 \tag{2.157}$$

Here, we see that the state $|\psi\rangle$ does not answer *YES* or *NO* unequivocally: with probability $p_0 = |a|^2$, the state will yield the answer *NO*; with probability $p_1 = |b|^2$, *YES*. Since this is a binary response, these two probabilities should sum to 100%. Indeed, this is exactly the normalization condition we just proved in Eq. (2.132)! Geometrically, we can see that these probabilities correspond to taking state $|\psi\rangle$—visualized as a point on the surface of the Bloch sphere—and projecting it onto the $\hat{Z}$-axis: the closer to the $|0\rangle$ or $|1\rangle$ pole, the higher the probability of getting the corresponding outcome.

Which brings us back to the question we started this section with: how do we interpret this strange state $|\psi\rangle$ in the first place? Naïvely, we could say that $|\psi\rangle$ is simply a mathematical construct which captures a set of probabilities. In this interpretation, the wavefunction $|\psi\rangle$ isn't 'real,' but it has predictive power for estimating the answers to questions which are. For example, looking at the state $|+\rangle$, we see

that this state will answer *YES* and *NO* with 50% probability

$$p_0(|+\rangle) = \langle +| \hat{M}_0 |+\rangle \tag{2.158}$$

$$= \frac{1}{\sqrt{2}} (\langle 0| + \langle 1|) \begin{bmatrix} 1 & 0 \\ 0 & 0 \end{bmatrix} \frac{1}{\sqrt{2}} (|0\rangle + |1\rangle) \tag{2.159}$$

$$= 0.5 \tag{2.160}$$

$$p_1(|+\rangle) = \langle +| \hat{M}_1 |+\rangle \tag{2.161}$$

$$= \frac{1}{\sqrt{2}} (\langle 0| + \langle 1|) \begin{bmatrix} 0 & 0 \\ 0 & 1 \end{bmatrix} \frac{1}{\sqrt{2}} (|0\rangle + |1\rangle) \tag{2.162}$$

$$= 0.5 \tag{2.163}$$

In this sense, it's tempting to say that the state $|+\rangle$ is like the state of a coin flip before you look at the result. Before you look at which side the coin has landed on, all you can say is that there is a 50% chance of getting heads and a 50% chance of getting tails, just like there's a 50% chance of $|+\rangle$ yielding the answers 0 or 1. So can we just say that $|\psi\rangle$ is like the state of a biased coin flip, where the coefficients a and b capture the uneven probabilities of getting heads or tails?

And yet, $|+\rangle$ isn't the only state which predicts a 50/50 chance of *YES* or *NO*. Looking at the state $|-\rangle$, we find the exact same probabilities as we just found for $|+\rangle$

$$p_0(|-\rangle) = \langle -| \hat{M}_0 |-\rangle \tag{2.164}$$

$$= \frac{1}{\sqrt{2}} (\langle 0| - \langle 1|) \begin{bmatrix} 1 & 0 \\ 0 & 0 \end{bmatrix} \frac{1}{\sqrt{2}} (|0\rangle - |1\rangle) \tag{2.165}$$

$$= 0.5 \tag{2.166}$$

$$p_1(|-\rangle) = \langle -| \hat{M}_1 |-\rangle \tag{2.167}$$

$$= \frac{1}{\sqrt{2}} (\langle 0| - \langle 1|) \begin{bmatrix} 0 & 0 \\ 0 & 1 \end{bmatrix} \frac{1}{\sqrt{2}} (|0\rangle - |1\rangle) \tag{2.168}$$

$$= 0.5 \tag{2.169}$$

So too for the states $|+i\rangle$ and $|-i\rangle$. Indeed, since a and b are complex numbers and the probabilities only depend on the absolute value squared of the coefficients $|a|^2$ and $|b|^2$, we quickly see that there is a continuous degree of freedom in the phase between the two coefficients such that the probability of getting *YES* or *NO* is 50/50

$$\frac{a}{b} = e^{-i\phi} \tag{2.170}$$

Looking at the Bloch sphere in Fig. 2-3, it is easy to see that this condition corresponds to the infinite number of states on the equator of the sphere, equidistant from the poles $|0\rangle$ and $|1\rangle$.

If the wavefunction $|\psi\rangle$ only exists to keep track of probabilities, why is there this extraordinary redundancy in the number of states corresponding to an honest coin flip? Not only that, looking closer at the states on the equator of the Bloch sphere, we find pairs of states which clearly contradict each other. For example, though the states $|+\rangle$ and $|-\rangle$ yield the exact same probability of *YES* and *NO*, these two states are orthogonal

$$\langle +|-\rangle = \frac{1}{\sqrt{2}} \begin{bmatrix} 1 & 1 \end{bmatrix} \frac{1}{\sqrt{2}} \begin{bmatrix} 1 \\ -1 \end{bmatrix} \tag{2.171}$$

$$= 0 \tag{2.172}$$

The same is true of the states $|+i\rangle$ and $|-i\rangle$: $\langle +i| - i\rangle = 0$. This is deeply strange. Mathematically, the states $|+\rangle$ and $|-\rangle$ contradict each other as profoundly as $|0\rangle$ and $|1\rangle$ do. If this is true, surely there is something more going on than simple probabilities of binary responses. Surely these wavefunctions are 'real,' at least in the sense that they have some innate quality which is responsible for this absolute

disagreement between states yielding the same probabilities. It's as if these states both correspond to honest coin flips, but to such different types of flips that the two states have nothing in common with one another.

Here, the classical analogy of coin flips quickly starts to break down. *But wait!* Maybe the orthogonality of $|+\rangle$ and $|-\rangle$ is a simple mathematical artifact. After all, if we only ask these states questions of the form $\hat{M}_1$ or $\hat{M}_0$, surely there's no way to distinguish between these two states. This line of thinking has an easy rebuttal. As we just showed in the previous section, the states $|+\rangle$ and $|-\rangle$ may give the same probabilities of *YES* and *NO*, but they *evolve in opposite directions.* For example, consider the unitary operator which corresponds to rotation around the $\hat{Y}$ axis by an angle $\theta = \pi/2$

$$\hat{U}_Y(\theta = \pi/2) = \frac{1}{\sqrt{2}} \begin{bmatrix} 1 & -1 \\ 1 & 1 \end{bmatrix} \tag{2.173}$$

Applying this operator to the states $|+\rangle$ and $|-\rangle$, we find that they evolve into states which deterministically provide opposite answers to $\hat{M}_1$ and $\hat{M}_0$: namely our familiar states $|0\rangle$ and $|1\rangle$

$$\hat{U}_Y(\theta = \pi/2)\,|+\rangle = \frac{1}{\sqrt{2}} \begin{bmatrix} 1 & -1 \\ 1 & 1 \end{bmatrix} \frac{1}{\sqrt{2}} \begin{bmatrix} 1 \\ 1 \end{bmatrix} \tag{2.174}$$

$$= \frac{1}{2} \begin{bmatrix} 0 \\ 2 \end{bmatrix} \tag{2.175}$$

$$= |1\rangle \tag{2.176}$$

$$\hat{U}_Y(\theta = \pi/2)\,|-\rangle = \frac{1}{\sqrt{2}} \begin{bmatrix} 1 & -1 \\ 1 & 1 \end{bmatrix} \frac{1}{\sqrt{2}} \begin{bmatrix} 1 \\ -1 \end{bmatrix} \tag{2.177}$$

$$= \frac{1}{2} \begin{bmatrix} 2 \\ 0 \end{bmatrix} \tag{2.178}$$

$$= |0\rangle \tag{2.179}$$

Mathematically, this is not surprising—indeed, recalling our derivations leading up to Eqs. (2.96) and (2.99) from the previous section, this is exactly how we created the states $|+\rangle$ and $|-\rangle$ in the first place. Physically, this is utterly bizarre. It's as if, having flipped our coin, there was an operation we could perform which would yield heads or tails with absolute certainty.

In quantum mechanics, we call states of the form $|\psi\rangle = a\,|0\rangle + b\,|1\rangle$ *coherent superpositions*. As I've briefly sketched in this section, the properties of these states are deeply strange, and the philosophical implications of their existence are immense. Interpreting quantum theory through the lens of new materialism and queer theory, the physicist and philosopher Karen Barad famously noted that the difference between a classical coin flip and a quantum superposition is the difference between epistemological uncertainty and ontological indeterminacy [32]. It's not that we don't know whether the system is in either $|0\rangle$ or $|1\rangle$—that is, it's not an epistemological question of what we as observers know about the system, like a flipped coin that hasn't been checked yet—but rather that the system in fact occupies a state which is *both*—its reality defies the classical binary. If the states $|0\rangle$ and $|1\rangle$ are 'classical states'—in the sense that they correspond to classically binary properties—we have now shown how, from only a few core principles, quantum mechanics naturally gives rise to states which are decidedly 'nonclassical.' The creation, manipulation, and measurement of such states—and the consequences which arise in doing so—will occupy much of the remainder of this thesis.

2.5 Density Matrices

Throughout this chapter, we have described wavefunctions as state vectors of the form

$$|\psi\rangle = a\,|0\rangle + b\,|1\rangle \tag{2.180}$$

$$= \begin{bmatrix} a \\ b \end{bmatrix} \tag{2.181}$$

These vectors, we have shown, span the entire space of possible states which arise from evolving the qubit states $|0\rangle$ and $|1\rangle$ according to the Schrödinger equation with a hermitian 2×2 Hamiltonian. In the remainder of this thesis, it will be convenient to employ a complementary formalism for describing quantum states known as the *density matrix*.

For a general single-qubit state vector $|\psi\rangle = a\,|0\rangle + b\,|1\rangle$, the corresponding density matrix ρ is simply given by the outer product of the state vector with itself

$$\rho \equiv |\psi\rangle\langle\psi| \tag{2.182}$$

$$= \begin{bmatrix} a \\ b \end{bmatrix} \begin{bmatrix} a^* & b^* \end{bmatrix} \tag{2.183}$$

$$= \begin{bmatrix} |a|^2 & ab^* \\ a^*b & |b|^2 \end{bmatrix} \tag{2.184}$$

which has the nice property that the probabilities $p_0 = |a|^2$ and $p_1 = |b|^2$ are readily read off from the diagonal entries of the matrix. As such, we can see that the normalization condition from Eq. (2.132) places a constraint on the trace of the density matrix

$$\mathrm{Tr}[\rho] = 1 \tag{2.185}$$

Writing out the density matrices for the four cardinal states on the equator of the Bloch sphere

$$\rho_+ = \frac{1}{2} \begin{bmatrix} 1 & 1 \\ 1 & 1 \end{bmatrix} \tag{2.186}$$

$$\rho_- = \frac{1}{2} \begin{bmatrix} 1 & -1 \\ -1 & 1 \end{bmatrix} \tag{2.187}$$

$$\rho_{+i} = \frac{1}{2} \begin{bmatrix} 1 & -i \\ i & 1 \end{bmatrix} \tag{2.188}$$

$$\rho_{-i} = \frac{1}{2} \begin{bmatrix} 1 & i \\ -i & 1 \end{bmatrix} \tag{2.189}$$

we see that all these states have the same entries along the diagonal (i.e. they will

yield the same probabilities of measuring 0 or 1) but differ in the phases on the off-diagonal, the consequences of which we saw above in our discussion of the relationship between different superposition states. As for the qubit states $|0\rangle$ and $|1\rangle$

$$\rho_0 = \begin{bmatrix} 1 & 0 \\ 0 & 0 \end{bmatrix} \tag{2.190}$$

$$\rho_1 = \begin{bmatrix} 0 & 0 \\ 0 & 1 \end{bmatrix} \tag{2.191}$$

we see that these are exactly the same as the operators $\hat{M}_0$ and $\hat{M}_1$ we used to obtain the probabilities of measuring 0 and 1 above. This is not a coincidence. Notice the relationship between the state vector and density matrix in Eq. (2.182) implies that ρ must be hermitian. As a result, we can interpret the density matrix two different ways. First and foremost, we can interpret it as a quantum *state*—that is, as an account of the relative weighting of the basis states $|0\rangle$ and $|1\rangle$ and the phase between them. Second, we can interpret it as a quantum *operator*—it is the *projector* which captures the probability of collapsing another wavefunction onto the state corresponding to that density matrix.

In the density matrix formalism, we can write the time independent Schroödinger equation from Eq. (2.6) as

$$\frac{d}{dt}\rho = -\frac{i}{\hbar}\left[\hat{H}, \rho\right] \tag{2.192}$$

where $[A, B]$ is the commutator of the general square matrices A and B

$$[A, B] \equiv AB - BA \tag{2.193}$$

The density matrix form of the Schrödinger equation in Eq. (2.192) is commonly referred to as the von Neumann equation, and it has solutions of the form

$$\rho(t) = e^{-\frac{i}{\hbar}\hat{H}t}\rho(t=0)e^{\frac{i}{\hbar}\hat{H}t} \tag{2.194}$$

which is just the density matrix of $|\psi(t)\rangle$ from Eq. (2.7). Replacing the matrix

exponentials with the familiar unitary operators from Eq.(2.16), we find that the time evolved unitary $\rho(t)$ can be found by applying $\hat{U}$ and its complex conjugate $\hat{U}^\dagger$ to either side of the initial density matrix

$$\rho(t) = \hat{U}(\hat{H}, t)\rho(t = 0)\hat{U}^\dagger(\hat{H}, t) \tag{2.195}$$

Using the dynamic equations above, we can easily obtain all the results we calculated using state vectors in the previous section. However, as we'll see later in this chapter, the density matrix formalism is a more general way of expressing quantum states and can capture some important wavefunctions which the state vector representation cannot. For this reason, we will largely rely on density matrices going forward, using the equivalent state vectors when appropriate.

2.6 Dynamics of Multiple Qubits

So far, we have only considered the dynamics of a single quantum bit as it traces out a path across the surface of its Bloch sphere. How do we describe the dynamics of multiple qubits?

Let's consider two quantum mechanical systems A and B, where the wavefunction of each can be written as a quantum bit

$$|\psi\rangle_A = a_A |0\rangle + b_A |1\rangle \tag{2.196}$$

$$|\psi\rangle_B = a_B |0\rangle + b_B |1\rangle \tag{2.197}$$

We can write the combined wavefunction of these two systems $|\psi\rangle_A$ as the tensor product of the individual wavefunctions

$$|\psi\rangle_{AB} = |\psi\rangle_A \otimes |\psi\rangle_B \tag{2.198}$$

where the Kronecker product on the right hand side turns the two 2×1 vectors $|\psi\rangle_A$

and $|\psi\rangle_A$ into a single vector of dimension 4×1

$$|\psi\rangle_A \otimes |\psi\rangle_B = \begin{bmatrix} a_A \\ b_A \end{bmatrix} \otimes \begin{bmatrix} a_B \\ b_B \end{bmatrix} \tag{2.199}$$

$$= \begin{bmatrix} a_A \begin{bmatrix} a_B \\ b_B \end{bmatrix} \\ b_A \begin{bmatrix} a_B \\ b_B \end{bmatrix} \end{bmatrix} \tag{2.200}$$

$$= \begin{bmatrix} a_A a_B \\ a_A b_B \\ b_A a_B \\ b_A b_B \end{bmatrix} \tag{2.201}$$

From this definition, we can write down the state vectors for the four possible combinations of the states $|0\rangle$ and $|1\rangle$

$$|00\rangle_{AB} \equiv |0\rangle_A \otimes |0\rangle_B = \begin{bmatrix} 1 \\ 0 \\ 0 \\ 0 \end{bmatrix} \tag{2.202}$$

$$|10\rangle_{AB} \equiv |1\rangle_A \otimes |0\rangle_B = \begin{bmatrix} 0 \\ 0 \\ 1 \\ 0 \end{bmatrix} \tag{2.203}$$

$$|01\rangle_{AB} \equiv |0\rangle_A \otimes |1\rangle_B = \begin{bmatrix} 0 \\ 1 \\ 0 \\ 0 \end{bmatrix} \tag{2.204}$$

$$|11\rangle_{AB} \equiv |1\rangle_A \otimes |1\rangle_B = \begin{bmatrix} 0 \\ 0 \\ 0 \\ 1 \end{bmatrix} \tag{2.205}$$

Just as thee two states $|0\rangle$ and $|1\rangle$ formed an orthogonal basis for representing a general single-qubit state, we can see that these four states form an orthogonal basis

for representing a general two-qubit state

$$|\psi\rangle_{AB} = a\,|00\rangle + b\,|10\rangle + c\,|01\rangle + d\,|11\rangle \tag{2.206}$$

where the absolute value of the coefficients must sum to unity to preserve probability, as in the single-qubit case

$$|a|^2 + |b|^2 + |c|^2 + |d|^2 = 1 \tag{2.207}$$

Having written the wavefunction for a system of two qubits $|\psi\rangle_{AB}$, we can easily add a third qubit by taking the tensor product of the two-qubit wavefunction we just found with an additional single-qubit state

$$|\psi\rangle_{ABC} = |\psi\rangle_A \otimes |\psi\rangle_B \otimes |\psi\rangle_C \tag{2.208}$$

$$= |\psi\rangle_{AB} \otimes |\psi\rangle_C \tag{2.209}$$

$$= \begin{bmatrix} a_A a_B \\ a_A b_B \\ b_A a_B \\ b_A b_B \end{bmatrix} \otimes \begin{bmatrix} a_C \\ b_C \end{bmatrix} \tag{2.210}$$

$$= \begin{bmatrix} a_A a_B a_C \\ a_A a_B b_C \\ a_A b_B a_C \\ a_A b_B b_C \\ b_A a_B a_C \\ b_A a_B b_C \\ b_A b_B a_C \\ b_A b_B b_C \end{bmatrix} \tag{2.211}$$

which is now a linear combination of eight orthogonal basis states

$$|\psi\rangle_{ABC} = a\,|000\rangle + b\,|001\rangle + c\,|010\rangle + d\,|011\rangle + e\,|110\rangle + f\,|111\rangle \tag{2.212}$$

and so on and so forth for systems of four or more qubits.

What's significant here is that the number of basis states required to express

the wavefunction of an n-qubit state scales as 2^n. In one sense, this should not be surprising—after all, the number of possible outcomes of n coin flips also scales as 2^n. Indeed, like the outcomes of n coin flips, the exponential number of outcomes of measuring the states in Eq. (2.198) and (2.208) is somewhat misleading: the number of outcomes may scale as 2^n, but the probabilities of these outcomes are not independent. Looking at the wavefunctions, we can see that the number of independent parameters (i.e. the number of complex coefficients a_i and b_i) scales only as $2n$. That is, as long as we know the coefficients for each individual qubit in the ensemble, we can fully express the wavefunctions of these product states with resources that scale only linearly with the system size. However, as we're about to see, quantum mechanics quickly gives rise to states which are *not* product states. These states, unlike the classical example of multiple coin flips, cannot be expressed as the product of individual qubit states, and it is here that the exponential expanse of Hilbert space immediately unfolds before us.

How do these ensembles of qubits evolve in time? For simplicity, let's focus on states of only two qubits, since the results for two qubit can easily be extrapolated to systems of three or more qubits by taking tensor products of single- and two-qubit subsystems, as shown above. Given a general two-qubit wavefunction $|\psi\rangle_{AB}$, the evolution of this state is once again determined by the Schrödinger equation

$$\frac{d}{dt}|\psi\rangle = -\frac{i}{\hbar}\hat{H}|\psi\rangle \tag{2.213}$$

where the Hamiltonian $\hat{H}$ is now a 4×4 hermitian matrix. Just as we decomposed the general single-qubit Hamiltonian into a sum of Pauli matrices in Eq. (2.11), the general two-qubit Hamiltonian can be written as the sum of tensor products of Pauli matrices

$$\hat{H}_{AB} = \sum_{i,j=\{I,X,Y,Z\}} E_{ij}\sigma_i \otimes \sigma_j \tag{2.214}$$

We can pull out the terms proportional to the Identity matrix and break this sum

into a few more illustrative pieces

$$\hat{H}_{AB} = \sum_{i,j=\{I,X,Y,Z\}} E_{ij}\sigma_i \otimes \sigma_j \tag{2.215}$$

$$= \sum_{i=\{I,X,Y,Z\}} E_{iI}\sigma_i \otimes \hat{I} + \sum_{j=\{IX,Y,Z\}} E_{Ij}\hat{I} \otimes \sigma_i + \sum_{i,j=\{X,Y,Z\}} E_{ij}\sigma_i \otimes \sigma_j \tag{2.216}$$

Writing the two-qubit Hamiltonian in this form, notice that the first two terms are simply the general single-qubit Hamiltonians from Eq. (2.11) for each of the two qubits A and B, times the Identity for the other qubit. As a result, we can rewrite the Hamiltonian above as

$$\hat{H}_{AB} = \hat{H}_A \otimes \hat{I} + \hat{I} \otimes \hat{H}_B + \sum_{i,j=\{X,Y,Z\}} E_{ij}\sigma_i \otimes \sigma_j \tag{2.217}$$

$$= \hat{H}_{A\otimes B} + \hat{H}_{\text{int}} \tag{2.218}$$

where $\hat{H}_{A\otimes B}$ is the sum of the single-qubit Hamiltonians and $\hat{H}_{\text{int}}$ groups together the remaining products of Paulis

$$\hat{H}_{A\otimes B} \equiv \hat{H}_A \otimes \hat{I} + \hat{I} \otimes \hat{H}_B \tag{2.219}$$

$$\hat{H}_{\text{int}} \equiv \sum_{i,j=\{X,Y,Z\}} E_{ij}\sigma_i \otimes \sigma_j \tag{2.220}$$

Before we look at the terms in $\hat{H}_{\text{int}}$, let's set $\hat{H}_{\text{int}}$ to zero and consider what happens when our two qubits evolve according to a Hamiltonian of the form

$$\hat{H} = \hat{H}_{A\otimes B} \tag{2.221}$$

$$= \hat{H}_A \otimes \hat{I} + \hat{I} \otimes \hat{H}_B \tag{2.222}$$

Writing the unitary operator corresponding to this Hamiltonian, we can take advantage of the fact that $\hat{H}_A \otimes \hat{I}$ and $\hat{I} \otimes \hat{H}_B$ commute, allowing us to break apart the

exponential

$$\hat{U}(\hat{H}_{A\otimes B}, t) = \exp\left(-\frac{i}{\hbar}(\hat{H}_A \otimes \hat{I} + \hat{I} \otimes \hat{H}_B)t\right) \tag{2.223}$$

$$= \exp\left(-\frac{i}{\hbar}(\hat{H}_A \otimes \hat{I})t\right)\exp\left(-\frac{i}{\hbar}(\hat{I} \otimes \hat{H}_B)t\right) \tag{2.224}$$

$$= \hat{U}(\hat{H}_{A\otimes I}, t)\hat{U}(\hat{H}_{B\otimes I}, t) \tag{2.225}$$

Applying this unitary to the general two-qubit product state $|\psi\rangle_{AB} = |\psi\rangle_A \otimes |\psi\rangle_B$, we obtain the time-evolved state $|\psi(t)\rangle_{AB}$

$$|\psi(t)\rangle_{AB} = \hat{U}(\hat{H}_{A\otimes B}, t)\,|\psi\rangle_{AB} \tag{2.226}$$

$$= \hat{U}(\hat{H}_{A\otimes I}, t)\hat{U}(\hat{H}_{B\otimes I}, t)\,(|\psi\rangle_A \otimes |\psi\rangle_B) \tag{2.227}$$

$$= \hat{U}(\hat{H}_{A\otimes I}, t)\,(|\psi\rangle_A \otimes |\psi(t)\rangle_B) \tag{2.228}$$

$$= |\psi(t)\rangle_A \otimes |\psi(t)\rangle_B \tag{2.229}$$

which is just a product state of the time-evolved single-qubit states $|\psi(t)\rangle_A$ and $|\psi(t)\rangle_B$. Thus, for two-qubit Hamiltonians where $H_{\text{int}} = 0$, we see that the dynamics are separable and product states will always evolve into other product states determined by the single-qubit Hamiltonians $\hat{H}_A$ and $\hat{H}_B$.

What happens when $H_{\text{int}} \neq 0$? As a simple example, let's consider a two-qubit Hamiltonian where four of the coefficients E_{ij} in Eq. (2.214) are equal and all the rest are set to zero

$$E_{ij} = \begin{cases} E, & \text{for } i = j \\ 0, & \text{for } i \neq j \end{cases} \tag{2.230}$$

This will give us the corresponding two-qubit Hamiltonian

$$\hat{H}_{AB} = E(\hat{I} \otimes \hat{I} + \hat{X} \otimes \hat{X} + \hat{Y} \otimes \hat{Y} + \hat{Z} \otimes \hat{Z}) \tag{2.231}$$

which can be exponentiated into the unitary operator

$$\hat{U}(\hat{H}_{AB}, t) = \exp\left\{\left(-\frac{i}{\hbar}E(\hat{I}\otimes\hat{I} + \hat{X}\otimes\hat{X} + \hat{Y}\otimes\hat{Y} + \hat{Z}\otimes\hat{Z})t\right)\right\} \tag{2.232}$$

$$= \exp\left\{\left(-i\omega(\hat{I}\otimes\hat{I} + \hat{X}\otimes\hat{X} + \hat{Y}\otimes\hat{Y} + \hat{Z}\otimes\hat{Z})t\right)\right\} \tag{2.233}$$

where we can replace the product of frequency and time with an angle $\omega t \equiv \theta/2$, as we did in the single-qubit case

$$\hat{U}(\hat{H}_{AB}, \theta) = \exp\left\{\left(-i\frac{\theta}{2}(\hat{I}\otimes\hat{I} + \hat{X}\otimes\hat{X} + \hat{Y}\otimes\hat{Y} + \hat{Z}\otimes\hat{Z})\right)\right\} \tag{2.234}$$

Let's evaluate this unitary at a couple particular angles. First, consider the combination of frequency and time where $\theta = \pi/2$, factoring out and dropping global phases wherever possible

$$\hat{U}(\hat{H}_{AB}, \pi/2) = \begin{bmatrix} 1 & 0 & 0 & 0 \\ 0 & 0 & 1 & 0 \\ 0 & 1 & 0 & 0 \\ 0 & 0 & 0 & 1 \end{bmatrix} \tag{2.235}$$

To see what this operation does, we can apply this unitary to the four two-qubit basis states

$$\hat{U}(\hat{H}_{AB}, \pi/2)\left|00\right\rangle_{AB} = \begin{bmatrix} 1 & 0 & 0 & 0 \\ 0 & 0 & 1 & 0 \\ 0 & 1 & 0 & 0 \\ 0 & 0 & 0 & 1 \end{bmatrix}\begin{bmatrix} 1 \\ 0 \\ 0 \\ 0 \end{bmatrix} = \begin{bmatrix} 1 \\ 0 \\ 0 \\ 0 \end{bmatrix} = \left|00\right\rangle_{AB} \tag{2.236}$$

$$\hat{U}(\hat{H}_{AB}, \pi/2)\left|01\right\rangle_{AB} = \begin{bmatrix} 1 & 0 & 0 & 0 \\ 0 & 0 & 1 & 0 \\ 0 & 1 & 0 & 0 \\ 0 & 0 & 0 & 1 \end{bmatrix}\begin{bmatrix} 0 \\ 1 \\ 0 \\ 0 \end{bmatrix} = \begin{bmatrix} 0 \\ 0 \\ 1 \\ 0 \end{bmatrix} = \left|10\right\rangle_{AB} \tag{2.237}$$

$$\hat{U}(\hat{H}_{AB}, \pi/2)\left|10\right\rangle_{AB} = \begin{bmatrix} 1 & 0 & 0 & 0 \\ 0 & 0 & 1 & 0 \\ 0 & 1 & 0 & 0 \\ 0 & 0 & 0 & 1 \end{bmatrix}\begin{bmatrix} 0 \\ 0 \\ 1 \\ 0 \end{bmatrix} = \begin{bmatrix} 0 \\ 1 \\ 0 \\ 0 \end{bmatrix} = \left|01\right\rangle_{AB} \tag{2.238}$$

$$\hat{U}(\hat{H}_{AB}, \pi/2) \left|11\right\rangle_{AB} = \begin{bmatrix} 1 & 0 & 0 & 0 \\ 0 & 0 & 1 & 0 \\ 0 & 1 & 0 & 0 \\ 0 & 0 & 0 & 1 \end{bmatrix} \begin{bmatrix} 0 \\ 0 \\ 0 \\ 1 \end{bmatrix} = \begin{bmatrix} 0 \\ 0 \\ 0 \\ 1 \end{bmatrix} = \left|11\right\rangle_{AB} \tag{2.239}$$

Comparing the states on the left and right hand sides of the four equations above, we see that the unitary $\hat{U}(\hat{H}_{AB}, \pi/2)$ swaps the states of the two qubits. That is, if qubit A is in a general state $|\psi\rangle$ and B is in a different state $|\phi\rangle$

$$\left|\psi\phi\right\rangle_{AB} \equiv \left|\psi\right\rangle_{A} \otimes \left|\phi\right\rangle_{B} \tag{2.240}$$

this operation places A in $|\phi\rangle$ and B in $|\psi\rangle$

$$\hat{U}(\hat{H}_{AB}, \pi/2) \left|\psi\phi\right\rangle_{AB} = \left|\phi\psi\right\rangle_{AB} \tag{2.241}$$

Notice that, like the Hamiltonians where $\hat{H}_{\text{int}} = 0$ which we considered above, this operation turns product states into other product states. However, unlike the Hamiltonians where $\hat{H}_{\text{int}} = 0$, the state which each of the qubits evolves into clearly depends on the state of its partner. The qubits are now talking to each other.

Things get even more interesting if we interrupt these states during their evolution from one product state to another. Just as we showed how superposition states arise from interrupting the single-qubit states $|0\rangle$ and $|1\rangle$ midway through their evolution from one pole of the Bloch sphere to the other, let's look at what happens when we apply this same swapping operation for half the time, such that $\theta = \pi/4$

$$\hat{U}(\hat{H}_{AB}, \pi/4) = \begin{bmatrix} e^{-i\frac{\pi}{4}} & 0 & 0 & 0 \\ 0 & \frac{1}{\sqrt{2}} & -\frac{i}{\sqrt{2}} & 0 \\ 0 & -\frac{i}{\sqrt{2}} & \frac{1}{\sqrt{2}} & 0 \\ 0 & 0 & 0 & e^{-i\frac{\pi}{4}} \end{bmatrix} \tag{2.242}$$

Applying this operation to each of the four basis states

$$\hat{U}(\hat{H}_{AB}, \pi/4) \left|00\right\rangle_{AB} = \begin{bmatrix} e^{-i\frac{\pi}{4}} & 0 & 0 & 0 \\ 0 & \frac{1}{\sqrt{2}} & -\frac{i}{\sqrt{2}} & 0 \\ 0 & -\frac{i}{\sqrt{2}} & \frac{1}{\sqrt{2}} & 0 \\ 0 & 0 & 0 & e^{-i\frac{\pi}{4}} \end{bmatrix} \begin{bmatrix} 1 \\ 0 \\ 0 \\ 0 \end{bmatrix} = \begin{bmatrix} e^{-i\frac{\pi}{4}} \\ 0 \\ 0 \\ 0 \end{bmatrix} \tag{2.243}$$

$$= e^{-i\frac{\pi}{4}} \left|00\right\rangle_{AB} \tag{2.244}$$

$$\hat{U}(\hat{H}_{AB}, \pi/4) \left|01\right\rangle_{AB} = \begin{bmatrix} e^{-i\frac{\pi}{4}} & 0 & 0 & 0 \\ 0 & \frac{1}{\sqrt{2}} & -\frac{i}{\sqrt{2}} & 0 \\ 0 & -\frac{i}{\sqrt{2}} & \frac{1}{\sqrt{2}} & 0 \\ 0 & 0 & 0 & e^{-i\frac{\pi}{4}} \end{bmatrix} \begin{bmatrix} 0 \\ 1 \\ 0 \\ 0 \end{bmatrix} = \begin{bmatrix} 0 \\ \frac{1}{\sqrt{2}} \\ -\frac{i}{\sqrt{2}} \\ 0 \end{bmatrix} \tag{2.245}$$

$$= \frac{1}{\sqrt{2}}(\left|01\right\rangle_{AB} - i \left|10\right\rangle_{AB}) \tag{2.246}$$

$$\hat{U}(\hat{H}_{AB}, \pi/4) \left|10\right\rangle_{AB} = \begin{bmatrix} e^{-i\frac{\pi}{4}} & 0 & 0 & 0 \\ 0 & \frac{1}{\sqrt{2}} & -\frac{i}{\sqrt{2}} & 0 \\ 0 & -\frac{i}{\sqrt{2}} & \frac{1}{\sqrt{2}} & 0 \\ 0 & 0 & 0 & e^{-i\frac{\pi}{4}} \end{bmatrix} \begin{bmatrix} 0 \\ 0 \\ 1 \\ 0 \end{bmatrix} = \begin{bmatrix} 0 \\ -\frac{i}{\sqrt{2}} \\ \frac{1}{\sqrt{2}} \\ 0 \end{bmatrix} \tag{2.247}$$

$$= \frac{1}{\sqrt{2}}(\left|10\right\rangle_{AB} - i \left|01\right\rangle_{AB}) \tag{2.248}$$

$$\hat{U}(\hat{H}_{AB}, \pi/4) \left|11\right\rangle_{AB} = \begin{bmatrix} e^{-i\frac{\pi}{4}} & 0 & 0 & 0 \\ 0 & \frac{1}{\sqrt{2}} & -\frac{i}{\sqrt{2}} & 0 \\ 0 & -\frac{i}{\sqrt{2}} & \frac{1}{\sqrt{2}} & 0 \\ 0 & 0 & 0 & e^{-i\frac{\pi}{4}} \end{bmatrix} \begin{bmatrix} 0 \\ 0 \\ 0 \\ 1 \end{bmatrix} = \begin{bmatrix} 0 \\ 0 \\ 0 \\ 1 \end{bmatrix} \tag{2.249}$$

$$= e^{-i\frac{\pi}{4}} \left|11\right\rangle_{AB} \tag{2.250}$$

The states in Eq. (2.244) and (2.250) are unremarkable, just a phase applied to the initial state. The states in Eq. (2.246) and (2.248) are anything but. Looking at these two states, we see that the product states $|01\rangle$ and $|10\rangle$ have evolved into coherent positions of each other on their way to swapping places. Curiously, these states are no longer product states: try to write them as the tensor products of single-qubit

states as in Eq. (2.198), and you quickly run into a roadblock. You can't do it.

2.7 Entanglement

States like the ones in Eq. (2.246) and (2.248)—states which cannot be factored into product states of the form $|\psi\rangle \otimes |\psi\rangle$—are known as *entangled states*. If coherent superposition is the first hallmark of quantum theory, entanglement is the inseparable second. Like quantum superposition, entanglement gives rise to distinctively non-classical phenomenon.

As we showed in the previous section, a product state is separable, by definition. Consider a two-qubit state where each qubit is in an equal superposition of $|0\rangle$ and $|1\rangle$

$$|{+}{+}\rangle_{AB} = |+\rangle_A \otimes |+\rangle_B \tag{2.251}$$

$$= \frac{1}{\sqrt{2}}\left(|0\rangle_A + |1\rangle_A\right) \otimes \frac{1}{\sqrt{2}}\left(|0\rangle_B + |1\rangle_B\right) \tag{2.252}$$

$$= \frac{1}{2}\left(|00\rangle_{AB} + |01\rangle_{AB} + |10\rangle_{AB} + |11\rangle_{AB}\right) \tag{2.253}$$

Now, imagine we measure qubit A and get the answer *NO*. What can we say about the probability of qubit B answering one way or another? Mathematically, we can figure this out by applying the projector $\hat{M}_0$ to qubit A—since our measurement projected

it into the $|0\rangle$-state—and the identity $\hat{I}$ to qubit B—since we haven't touched it yet

$$(\hat{M}_0 \otimes \hat{I})\,|{+}{+}\rangle_{AB} = \left(\begin{bmatrix}1 & 0\\ 0 & 0\end{bmatrix} \otimes \begin{bmatrix}1 & 0\\ 0 & 1\end{bmatrix}\right) \begin{bmatrix}1/2\\ 1/2\\ 1/2\\ 1/2\end{bmatrix} \tag{2.254}$$

$$= \begin{bmatrix}1 & 0 & 0 & 0\\ 0 & 1 & 0 & 0\\ 0 & 0 & 0 & 0\\ 0 & 0 & 0 & 0\end{bmatrix} \begin{bmatrix}1/2\\ 1/2\\ 1/2\\ 1/2\end{bmatrix} \tag{2.255}$$

$$= \begin{bmatrix}1/2\\ 1/2\\ 0\\ 0\end{bmatrix} \tag{2.256}$$

$$= \frac{1}{2}(|00\rangle_{AB} + |01\rangle_{AB}) \tag{2.257}$$

This wavefunction is not normalized, since the projective measurement $\hat{M}_0$ is not a unitary operator, so we'll have to normalize it by hand such that the probabilities add up to unity again. Doing this, we see that we have arrived at the product state

$$(\hat{M}_0 \otimes \hat{I})\,|{+}{+}\rangle_{AB} = \frac{1}{\sqrt{2}}(|00\rangle_{AB} + |01\rangle_{AB}) \tag{2.258}$$

$$= |0\rangle_A \otimes \frac{1}{\sqrt{2}}(|0\rangle_B + |1\rangle_B) \tag{2.259}$$

$$= |0\rangle_A \otimes |{+}\rangle_B \tag{2.260}$$

That is, after projecting qubit A into the $|0\rangle$-state, qubit B remains in an equal superposition of $|0\rangle$ and $|1\rangle$, and there is still a 50/50 chance of measuring it in either state. In fact, this was clear from the expansion in Eq. (2.253). Looking at the four terms, we see there are two corresponding to qubit A being in the $|0\rangle$-state: $|00\rangle_{AB}$ and $|01\rangle_{AB}$. Since there is an equal probability of the combined two-qubit state being in either of these two states, we can see that there is a 50/50 chance of measuring qubit B in $|0\rangle$ (the combined system is projected into $|00\rangle_{AB}$ and B answers *NO*) or $|1\rangle$ (the combined system is projected into $|01\rangle_{AB}$and B answers *YES*). Indeed, we

find the exact same result if we imagine instead projecting qubit A into $|1\rangle$

$$(\hat{M}_1 \otimes \hat{I})\,|{+}{+}\rangle_{AB} = \frac{1}{\sqrt{2}}(|10\rangle_{AB} + |11\rangle_{AB}) \tag{2.261}$$

$$= |1\rangle_A \otimes \frac{1}{\sqrt{2}}(|0\rangle_B + |1\rangle_B) \tag{2.262}$$

$$= |1\rangle_A \otimes |+\rangle_B \tag{2.263}$$

Looking at these two cases, we can see that the state of qubit B is utterly unaffected by how we project qubit A. In both cases, B remains in exactly the same state it was in prior to measuring A.

In this sense, measuring the state $|{+}{+}\rangle_{AB}$ is like measuring the outcomes of two flipped coins. Look at the outcome of the first coin flip and, whatever side the coin landed on, the outcome of the second coin flip remains completely unknown. Indeed, as we discussed back when we derived the multi-qubit state vectors in Eq. (2.201) and (2.211), the probability of measuring a product state in any given basis state is determined entirely by the product of measuring each individual qubit in the corresponding state, just like the probability of finding n flipped coins in a particular state.

Something very different is going on with the entangled states in Eq. (2.246) and (2.248). To see this, let's take the state in Eq. (2.246) and imagine doing a projective measurement of qubit A. Taking the expectation value of the state with the two projectors M_0 and M_1, we see that there is a 50/50 chance of projecting qubit A into either the $|0\rangle$- or $|1\rangle$-state

$$\langle \hat{M}_0 \otimes \hat{I} \rangle = \frac{1}{\sqrt{2}}(\langle 01|_{AB} + i\,\langle 10|_{AB})(\hat{M}_0 \otimes \hat{I})\frac{1}{\sqrt{2}}(|01\rangle_{AB} - i\,|10\rangle_{AB}) \tag{2.264}$$

$$= 0.5 \tag{2.265}$$

$$\langle \hat{M}_1 \otimes \hat{I} \rangle = \frac{1}{\sqrt{2}}(\langle 01|_{AB} + i\,\langle 10|_{AB})(\hat{M}_1 \otimes \hat{I})\frac{1}{\sqrt{2}}(|01\rangle_{AB} - i\,|10\rangle_{AB}) \tag{2.266}$$

$$= 0.5 \tag{2.267}$$

Looking at these two possibilities, let's consider what happens in the case where we collapse qubit A into the $|0\rangle$-state

$$(\hat{M}_0 \otimes \hat{I})\frac{1}{\sqrt{2}}(|01\rangle_{AB} - i\,|10\rangle_{AB}) = \left(\begin{bmatrix}1 & 0\\ 0 & 0\end{bmatrix} \otimes \begin{bmatrix}1 & 0\\ 0 & 1\end{bmatrix}\right) \begin{bmatrix}0\\ \frac{1}{\sqrt{2}}\\ \frac{-i}{\sqrt{2}}\\ 0\end{bmatrix} \tag{2.268}$$

$$= \begin{bmatrix}1 & 0 & 0 & 0\\ 0 & 1 & 0 & 0\\ 0 & 0 & 0 & 0\\ 0 & 0 & 0 & 0\end{bmatrix} \begin{bmatrix}0\\ \frac{1}{\sqrt{2}}\\ \frac{-i}{\sqrt{2}}\\ 0\end{bmatrix} \tag{2.269}$$

$$= \begin{bmatrix}0\\ \frac{1}{\sqrt{2}}\\ 0\\ 0\end{bmatrix} \tag{2.270}$$

$$= \frac{1}{\sqrt{2}}\,|01\rangle_{AB} \tag{2.271}$$

This wavefunction is, again, not normalized, so we have to adjust the amplitudes by hand such that the probabilities add up to unity. But notice that the two qubits are no longer in a coherent superposition. Indeed, the two qubits are now in a single basis state

$$(\hat{M}_0 \otimes \hat{I})\frac{1}{\sqrt{2}}(|01\rangle_{AB} - i\,|10\rangle_{AB}) = |01\rangle_{AB} \tag{2.272}$$

$$= |0\rangle_A \otimes |1\rangle_B \tag{2.273}$$

What does this tell us? Having measured the state of qubit A and projected it into the $|0\rangle$-state, we see that there is a 100% chance of qubit B being in the $|1\rangle$-state. That is, having queried system A and received the answer *NO*, we can now say with certainty that system B will respond *YES* before we even ask the question. Indeed,

we find a similar result when we instead project qubit A into the $|1\rangle$-state

$$(\hat{M}_1 \otimes \hat{I})\frac{1}{\sqrt{2}}(|01\rangle_{AB} - i\,|10\rangle_{AB}) = \left(\begin{bmatrix} 0 & 0 \\ 0 & 1 \end{bmatrix} \otimes \begin{bmatrix} 1 & 0 \\ 0 & 1 \end{bmatrix}\right) \begin{bmatrix} 0 \\ \frac{1}{\sqrt{2}} \\ \frac{-i}{\sqrt{2}} \\ 0 \end{bmatrix} \tag{2.274}$$

$$= \begin{bmatrix} 0 & 0 & 0 & 0 \\ 0 & 0 & 0 & 0 \\ 0 & 0 & 1 & 0 \\ 0 & 0 & 0 & 1 \end{bmatrix} \begin{bmatrix} 0 \\ \frac{1}{\sqrt{2}} \\ \frac{-i}{\sqrt{2}} \\ 0 \end{bmatrix} \tag{2.275}$$

$$= \begin{bmatrix} 0 \\ 0 \\ \frac{-i}{\sqrt{2}} \\ 0 \end{bmatrix} \tag{2.276}$$

$$= \frac{-i}{\sqrt{2}}\,|10\rangle_{AB} \tag{2.277}$$

which, when properly renormalized, is simply

$$(\hat{M}_1 \otimes \hat{I})\frac{1}{\sqrt{2}}(|01\rangle_{AB} - i\,|10\rangle_{AB}) = |10\rangle_{AB} \tag{2.278}$$

$$= |1\rangle_A \otimes |0\rangle_B \tag{2.279}$$

Projecting qubit A into the $|1\rangle$-state, we now find that qubit B is unambiguously in the $|0\rangle$-state: we know that system B will answer *NO* without even asking the question.

Returning to the analogy of coin flips, how would we interpret what is going on here? Looking at the results above, it is as if we flipped two coins and, having determined the result of the first, we could say with absolute certainty the state of the second. The result is still random—repeating these coin flips, we would find that there is a 50/50 chance of finding the first coin in heads or tails—but the outcomes of the two coin flips are now absolutely correlated. How is this possible? It is as if, the moment we unclenched the fist holding the first flipped coin, it sent a message to the coin in our other hand, instructing it to give the opposite result.

This, on its own, is not impossible to understand classically: classical physics is built out of interactions between systems, gravitational and electromagnetic, which produce correlated outcomes. Move an electron, and a charged particle nearby will change its trajectory accordingly, due to the Coulomb interaction between the two particles. Perhaps, then, there is some force exchanged between the two qubits which induces the correlated outcomes as soon as we measure one. And yet, recall again that none of the states or operators above have any explicit spatial dependence. All we required was a Hamiltonian of the form in Eq. (2.231), applied for a sufficient time to generate a rotation $\theta = \pi/4$. The moment this is accomplished, we can turn off the interaction and separate the two qubits by an arbitrary distance, nanometers, kilometers, lightyears, whatever. After all, the operator $\hat{M} \otimes \hat{I}$ has no spatial dependence. Moreover, the operation is entirely local: we performed a measurement on one qubit at one point in space and time, and we did nothing to the other qubit, wherever it might be at the moment of measurement.

And yet, the moment the measurement is locally performed on one qubit, something *happened* to the other qubit, even if it was now on the other side of the universe. Here, we see that quantum mechanics has given rise to a phenomenon which is defiantly non-local, exerting an influence across spacetime which is faster than the speed of light, appearing to violate Einstein's theory of relativity. Indeed, for Einstein this represented a dire flaw of quantum theory. Surely, he and other skeptics reasoned, math of the form we have sketched above is an incomplete account of what is going on. Surely we must be hiding some 'hidden variables,' parameters which would capture the spatial and temporal dependence of the interaction between these two qubits at the moment of measurement, restoring locality. It was not until 1964 that the Irish physicist John Stewart Bell showed that such a hidden variable theory would result in demonstrably different measurement outcomes than a theory without hidden variables [42]. To date, all experimental tests of Bell's theorem have ruled against the presence of hidden variables [20, 25, 350, 393, 404, 465]. The nonlocality of quantum mechanics is, to the best of our understanding, fundamental to the theory.

In short, the presence of entanglement in quantum mechanics is not an anomaly

of the theory; it's the rule. As we've just showed, the emergence of entangled states is a direct consequence of the Pauli product terms in the multi-qubit Hamiltonian decomposition we started with in Eq. (2.214). Indeed, just as the equator of the Bloch sphere defines an infinite number of unique coherent superposition states for a single qubit, we can see that the states in Eq. (2.246) and (2.248) are only two of an infinite number of unique entangled states between two qubits. Here, it is helpful to define four special entangled states to orient ourselves

$$|\beta_{00}\rangle \equiv \frac{1}{\sqrt{2}}(|00\rangle + |11\rangle) \tag{2.280}$$

$$|\beta_{01}\rangle \equiv \frac{1}{\sqrt{2}}(|01\rangle + |10\rangle) \tag{2.281}$$

$$|\beta_{10}\rangle \equiv \frac{1}{\sqrt{2}}(|00\rangle - |11\rangle) \tag{2.282}$$

$$|\beta_{11}\rangle \equiv \frac{1}{\sqrt{2}}(|01\rangle - |10\rangle) \tag{2.283}$$

These four states are commonly referred to as the four *Bell states*—after J.S. Bell—or as the four *EPR pairs*—after the paradox of Einstein and coauthors which Bell resolved. Comparing these four states, we can see that they are all orthogonal to one another

$$\langle\beta_{ij}|\beta_{kl}\rangle = \begin{cases} 1, & \text{for } i = k, j = l \\ 0, & \text{else} \end{cases} \tag{2.284}$$

Thus, like the product states $\{|00\rangle, |01\rangle, |10\rangle, |00\rangle\}$ we used to construct our two-qubit states in Eq. (2.206), the four Bell states form a complete basis for expressing any general two-qubit state

$$|\psi\rangle_{AB} = \tilde{a}\,|\beta_{00}\rangle + \tilde{b}\,|\beta_{01}\rangle + \tilde{c}\,|\beta_{10}\rangle + \tilde{a}\,|\beta_{11}\rangle \tag{2.285}$$

In this sense, just as we are free to redefine our single-qubit Bloch sphere with the superposition states $|+\rangle$ and $|-\rangle$ at the poles—a basis in which case $|0\rangle$ and $|1\rangle$ would be interpreted as superpositions of superposition states—we are welcome to think of our product states as entanglements of entangled states. Mathematically, it is all a

matter of perspective.

2.8 Coherence

In the preceding section, we showed that the dynamics of quantum mechanics gives rise to entangled states, states which cannot be separated into a product of single-qubit states. What happens if we try to separate them? Mathematically, there is no great difficulty here. Just as we combined two single-qubit states $|\psi\rangle_A$ and $|\phi\rangle_B$ using the tensor product

$$|\psi\phi\rangle_{AB} \equiv |\psi\rangle_A \otimes |\phi\rangle_B \tag{2.286}$$

we can pull the two states apart again by taking the *partial trace* of the combined system. For reasons which will quickly become apparent, the partial trace must be performed on density matrices instead of state vectors, though we can convert to this representation easily enough using the tools from Section 2.5

$$\rho_\psi^A \equiv |\psi\rangle\langle\psi|_A \tag{2.287}$$

$$\rho_\phi^B \equiv |\phi\rangle\langle\phi|_B \tag{2.288}$$

$$\rho_{\psi\phi}^{AB} \equiv \rho_A \otimes \rho_B \tag{2.289}$$

where we will use the notation convention that superscripts label the associated qubits and the subscript denotes the corresponding pure state. Having converted our state vectors to density matrices, we define the partial trace Tr_x as the average over a full set of projective measurements of the subsystem x

$$\mathrm{Tr}_B\left[\rho^{AB}\right] := \sum_j (\hat{I}_A \otimes \langle j|_B)\rho^{AB}(\hat{I}_A \otimes |j\rangle_B) \tag{2.290}$$

$$\mathrm{Tr}_A\left[\rho^{AB}\right] := \sum_i (\langle i|_A \otimes \hat{I}_B)\rho^{AB}(|i\rangle_A \otimes \hat{I}_B) \tag{2.291}$$

where $\{|j\rangle\}, \{|i\rangle\}$ are orthonormal bases in the Hilbert space of subsystems B and A respectively. Notice that this is the same spirit as the exercise we performed in the

previous section with the operators $\hat{M}_0 \otimes \hat{I}$ and $\hat{M}_1 \otimes \hat{I}$, projecting on of the qubits into each possible basis and looking at the state of the other qubit.

Defining the partial trace above, the single-qubit density matrices ρ^A and ρ^B are given by the partial traces of their combined density matrix ρ^{AB} over the state of the other qubit

$$\mathrm{Tr}_B \left[\rho^{AB}\right] \equiv \rho^A \tag{2.292}$$

$$\mathrm{Tr}_A \left[\rho^{AB}\right] \equiv \rho^B \tag{2.293}$$

What happens when we take the partial trace of some of the two-qubit states we considered in the previous sections. For example, let's consider the product state of two superposition states

$$\rho^{AB}_{++} \equiv |{+}{+}\rangle\langle{+}{+}|_{AB} \tag{2.294}$$

$$= \frac{1}{4}\begin{bmatrix} 1 & 1 & 1 & 1 \\ 1 & 1 & 1 & 1 \\ 1 & 1 & 1 & 1 \\ 1 & 1 & 1 & 1 \end{bmatrix}_{AB} \tag{2.295}$$

Taking the partial trace over each of the qubits, using the orthonormal bases $\{|j\rangle\} =$

$\{|i\rangle\} = \{|0\rangle, |1\rangle\}$

$$\begin{aligned}
\mathrm{Tr}_B\left[\rho_{++}^{AB}\right] =& \sum_j (\hat{I}_A \otimes \langle j|_B)\rho_{++}^{AB}(\hat{I}_A \otimes |j\rangle_B) && (2.296)\\
=& (\hat{I}_A \otimes \langle 0|_B)\rho_{++}^{AB}(\hat{I}_A \otimes |0\rangle_B) \\
&+ (\hat{I}_A \otimes \langle 1|_B)\rho_{++}^{AB}(\hat{I}_A \otimes |1\rangle_B) && (2.297)\\
=& \left(\begin{bmatrix}1 & 0\\ 0 & 1\end{bmatrix}_A \otimes \begin{bmatrix}1 & 0\end{bmatrix}_B\right)\rho_{++}^{AB}\left(\begin{bmatrix}1 & 0\\ 0 & 1\end{bmatrix}_A \otimes \begin{bmatrix}1\\ 0\end{bmatrix}_B\right) \\
&+ \left(\begin{bmatrix}1 & 0\\ 0 & 1\end{bmatrix}_A \otimes \begin{bmatrix}0 & 1\end{bmatrix}_B\right)\rho_{++}^{AB}\left(\begin{bmatrix}1 & 0\\ 0 & 1\end{bmatrix}_A \otimes \begin{bmatrix}0\\ 1\end{bmatrix}_B\right) && (2.298)\\
=& \begin{bmatrix}1 & 0 & 0 & 0\\ 0 & 0 & 1 & 0\end{bmatrix}_{AB} \frac{1}{4}\begin{bmatrix}1 & 1 & 1 & 1\\ 1 & 1 & 1 & 1\\ 1 & 1 & 1 & 1\\ 1 & 1 & 1 & 1\end{bmatrix}_{AB} \begin{bmatrix}1 & 0\\ 0 & 0\\ 0 & 1\\ 0 & 0\end{bmatrix}_{AB} \\
&+ \begin{bmatrix}0 & 1 & 0 & 0\\ 0 & 0 & 0 & 1\end{bmatrix}_{AB} \frac{1}{4}\begin{bmatrix}1 & 1 & 1 & 1\\ 1 & 1 & 1 & 1\\ 1 & 1 & 1 & 1\\ 1 & 1 & 1 & 1\end{bmatrix}_{AB} \begin{bmatrix}0 & 0\\ 1 & 0\\ 0 & 0\\ 0 & 1\end{bmatrix}_{AB} && (2.299)\\
=& \frac{1}{4}\begin{bmatrix}1 & 1\\ 1 & 1\end{bmatrix}_A + \frac{1}{4}\begin{bmatrix}1 & 1\\ 1 & 1\end{bmatrix}_A && (2.300)\\
=& \frac{1}{2}\begin{bmatrix}1 & 1\\ 1 & 1\end{bmatrix}_A && (2.301)\\
=& |+\rangle\langle +|_A && (2.302)
\end{aligned}$$

and ditto for the trace over qubit A

$$\begin{aligned}
\mathrm{Tr}_A\left[\rho_{++}^{AB}\right] =& \sum_i (\langle i|_A \otimes \hat{I}_B)\rho_{++}^{AB}(|i\rangle_A \otimes \hat{I}_B) && (2.303)\\
=& (\langle 0|_A \otimes \hat{I}_B)\rho_{++}^{AB}(|0\rangle_A \otimes \hat{I}_B) \\
&+ (\langle 1|_A \otimes \hat{I}_B)\rho_{++}^{AB}(|1\rangle_A \otimes \hat{I}_B) && (2.304)\\
=& |+\rangle\langle +|_B && (2.305)
\end{aligned}$$

Running through the math above, we have confirmed that, yes, taking the partial

traces of the tensor product of two superposition states gives us a pair of superposition states—which is exactly what we demanded of the partial trace operation in the first place.

What happens when we take the partial trace of an entangled state? Consider, for example, one of the Bell states we defined in the previous section

$$|\beta_{00}\rangle_{AB} \equiv \frac{1}{\sqrt{2}}(|00\rangle_{AB} + |11\rangle_{AB}) \tag{2.306}$$

which we can write in density matrix form as

$$\rho_{\beta}^{AB} = |\beta_{00}\rangle\langle\beta_{00}|_{AB} \tag{2.307}$$

$$= \frac{1}{2}\begin{bmatrix} 1 & 0 & 0 & 1 \\ 0 & 0 & 0 & 0 \\ 0 & 0 & 0 & 0 \\ 1 & 0 & 0 & 1 \end{bmatrix}_{AB} \tag{2.308}$$

Taking the partial trace over qubit B, as above

$$\begin{aligned}
\mathrm{Tr}_B\left[\rho_\beta^{AB}\right] =& \sum_j (\hat{I}_A \otimes \langle j|_B)\rho_\beta^{AB}(\hat{I}_A \otimes |j\rangle_B) && (2.309)\\
=& (\hat{I}_A \otimes \langle 0|_B)\rho_\beta^{AB}(\hat{I}_A \otimes |0\rangle_B) \\
&+ (\hat{I}_A \otimes \langle 1|_B)\rho_\beta^{AB}(\hat{I}_A \otimes |1\rangle_B) && (2.310)\\
=& \left(\begin{bmatrix}1 & 0\\ 0 & 1\end{bmatrix}_A \otimes \begin{bmatrix}1 & 0\end{bmatrix}_B\right)\rho_\beta^{AB}\left(\begin{bmatrix}1 & 0\\ 0 & 1\end{bmatrix}_A \otimes \begin{bmatrix}1\\ 0\end{bmatrix}_B\right) \\
&+ \left(\begin{bmatrix}1 & 0\\ 0 & 1\end{bmatrix}_A \otimes \begin{bmatrix}0 & 1\end{bmatrix}_B\right)\rho_\beta^{AB}\left(\begin{bmatrix}1 & 0\\ 0 & 1\end{bmatrix}_A \otimes \begin{bmatrix}0\\ 1\end{bmatrix}_B\right) && (2.311)\\
=& \begin{bmatrix}1 & 0 & 0 & 0\\ 0 & 0 & 1 & 0\end{bmatrix}_{AB} \frac{1}{2}\begin{bmatrix}1 & 0 & 0 & 1\\ 0 & 0 & 0 & 0\\ 0 & 0 & 0 & 0\\ 1 & 0 & 0 & 1\end{bmatrix}_{AB} \begin{bmatrix}1 & 0\\ 0 & 0\\ 0 & 1\\ 0 & 0\end{bmatrix}_{AB} \\
&+ \begin{bmatrix}0 & 1 & 0 & 0\\ 0 & 0 & 0 & 1\end{bmatrix}_{AB} \frac{1}{2}\begin{bmatrix}1 & 0 & 0 & 1\\ 0 & 0 & 0 & 0\\ 0 & 0 & 0 & 0\\ 1 & 0 & 0 & 1\end{bmatrix}_{AB} \begin{bmatrix}0 & 0\\ 1 & 0\\ 0 & 0\\ 0 & 1\end{bmatrix}_{AB} && (2.312)\\
=& \frac{1}{2}\begin{bmatrix}1 & 0\\ 0 & 0\end{bmatrix}_A + \frac{1}{2}\begin{bmatrix}0 & 0\\ 0 & 1\end{bmatrix}_A && (2.313)\\
=& \frac{1}{2}\begin{bmatrix}1 & 0\\ 0 & 1\end{bmatrix}_A && (2.314)
\end{aligned}$$

and so too for the partial trace over qubit A

$$\begin{aligned}
\mathrm{Tr}_A\left[\rho_\beta^{AB}\right] =& \sum_i (\langle i|_A \otimes \hat{I}_B)\rho_\beta^{AB}(|i\rangle_A \otimes \hat{I}_B) && (2.315)\\
=& (\langle 0|_A \otimes \hat{I}_B)\rho_\beta^{AB}(|0\rangle_A \otimes \hat{I}_B) \\
&+ (\langle 1|_A \otimes \hat{I}_B)\rho_\beta^{AB}(|1\rangle_A \otimes \hat{I}_B) && (2.316)\\
=& \frac{1}{2}\begin{bmatrix}1 & 0\\ 0 & 1\end{bmatrix}_B && (2.317)
\end{aligned}$$

What is going on with these single-qubit states? Looking at the density matrices in Eq. (2.314) and (2.317), we find that these states are unlike any that we've en-

countered in this chapter so far. To see how these partially traced entangled states are different from, for example, the partial traces of the state $|{+}{+}\rangle_{AB}$, let's directly compare the density matrices in Eq. (2.301) and (2.314)

$$\mathrm{Tr}_B\left[\rho_{++}^{AB}\right] = \frac{1}{2}\begin{bmatrix}1 & 1\\ 1 & 1\end{bmatrix}_A \tag{2.318}$$

$$\mathrm{Tr}_B\left[\rho_{\beta}^{AB}\right] = \frac{1}{2}\begin{bmatrix}1 & 0\\ 0 & 1\end{bmatrix}_A \tag{2.319}$$

In one sense, these matrices are similar: looking at the matrix elements along the diagonal, we see that both these states give a 50/50 probability of measuring qubit A in either $|0\rangle$ or $|1\rangle$ ($p_0 = p_1 = 0.5$). And yet, if we try to separate each of these density matrices into the outer product of a state vector, we find that we succeed in the former case and fail in the latter

$$\mathrm{Tr}_B\left[\rho_{++}^{AB}\right] = \frac{1}{2}\begin{bmatrix}1 & 1\\ 1 & 1\end{bmatrix}_A \tag{2.320}$$

$$= |{+}\rangle\langle{+}|_A \tag{2.321}$$

$$\mathrm{Tr}_B\left[\rho_{\beta}^{AB}\right] = \frac{1}{2}\begin{bmatrix}1 & 0\\ 0 & 1\end{bmatrix}_A \tag{2.322}$$

$$= \frac{1}{2}(|0\rangle\langle 0|_A + |1\rangle\langle 1|_A) \tag{2.323}$$

That is, while the density matrix in Eq. (2.301) corresponds exactly to a state vector—in this case, $|{+}\rangle_A$—the density matrix in Eq. (2.314) does not: the best we can do is write it as sum of two other density matrices, each of which corresponds to a basis state vector. For shorthand, let's give this density matrix a question mark as a subscript, to denote our confusion at being unable to write it as a state vector

$$\rho_? \equiv \frac{1}{2}\begin{bmatrix}1 & 0\\ 0 & 1\end{bmatrix} \tag{2.324}$$

In Section 2.4, we discussed the difference between a coherent superposition state

and a classical coin flip. While both systems might give rise to the same probability distribution, we showed that superposition state has some internal sense of self which the coin flip does not: suspended in a superposition, we can deterministically rotate the state such that the wavefunction always collapses into $|1\rangle$ or $|0\rangle$, *YES* or *NO*, heads or tails. No such operation can be applied to our classically flipped coin—whatever we do to it prior to looking at the result, the outcome of measurement remains totally random.

In Eq. (2.318) and (2.319), we can see the mathematical difference between a superposition state and a coin flip. In the former case, we see that the density matrix has non-zero diagonals, corresponding to the $+1$ phase between the $|0\rangle$ and $|1\rangle$ in the superposition state

$$|+\rangle = \frac{1}{\sqrt{2}}(|0\rangle + |1\rangle) \tag{2.325}$$

$$\rho_+ = \frac{1}{2}\begin{bmatrix} 1 & 1 \\ 1 & 1 \end{bmatrix} \tag{2.326}$$

This $+1$ phase is what gives the state $|+\rangle$ its internal sense of self, its internal *coherence*. It knows what it is, and it knows what it is not: as we showed previously, the state $|+\rangle$ is orthogonal to the state $|-\rangle$, a coherent superposition which has the exact same probability of projection into either basis state but with a phase factor of -1 between the states

$$|-\rangle = \frac{1}{\sqrt{2}}(|0\rangle - |1\rangle) \tag{2.327}$$

$$\rho_- = \frac{1}{2}\begin{bmatrix} 1 & -1 \\ -1 & 1 \end{bmatrix} \tag{2.328}$$

which now corresponds to an opposite sign in the off-diagonals of the corresponding density matrix.

The state in (2.319) has no off-diagonal entries, which is to say it has no internal relationship between its constituent basis states—it has no internal sense of itself, no internal coherence. There is no state which is orthogonal to it, and there is no

rotation $\hat{U}$ which can alter it

$$\hat{U}\rho_?\hat{U}^\dagger = \hat{U}\ \frac{1}{2}\begin{bmatrix}1 & 0\\ 0 & 1\end{bmatrix}\ \hat{U}^\dagger \tag{2.329}$$

$$= \frac{1}{2}\ \hat{U}\hat{U}^\dagger \tag{2.330}$$

$$= \frac{1}{2}\begin{bmatrix}1 & 0\\ 0 & 1\end{bmatrix} \tag{2.331}$$

$$= \rho_? \tag{2.332}$$

In this sense, we can see that the state $\rho_?$ is a purely classical object: there is no single-qubit Hamiltonian which will cause it to evolve under the Schrödinger equation. Geometrically, we can represent this state as a point at the center of the Bloch sphere—rotate the sphere however you like, and the state remains fixed in position.

Here, we can see why the density matrix formalism is more general than the state vector representation: if the set of single-qubit state vectors gives us all the points on the surface of the sphere, the set of single-qubit density matrices gives us all the points in the volume of the sphere. This makes sense, since the density matrices are hermitian matrices and, as we discussed in Section 2.2, the Bloch sphere is just a representation of the matrix space SU(2), the space of possible hermitian matrices. Indeed, the spherical shell of the Bloch sphere in SU(2) captures a constraint of physical density matrices

$$\frac{1}{d} \leq \text{Tr}\left[\rho^2\right] \leq 1 \tag{2.333}$$

where d is the dimension of the Hilbert space of the Hilbert space of ρ ($d = 2^n$ for a system of n qubits) and the quantity $\text{Tr}\left[\rho^2\right]$ indicates how deep in the volume of the Bloch sphere the state is located

$$\text{Tr}\left[\rho^2\right] \begin{cases} = 1, \text{ surface of Bloch sphere (pure state)} \\ < 1, \text{ volume of Bloch sphere (mixed state)} \end{cases} \tag{2.334}$$

The quantity $\text{Tr}\left[\rho^2\right]$ is known as the Rényi entropy of order 2 or, more succinctly, the

purity of the state ρ. Calculating the purity of the states ρ_+ and $\rho_?$

$$\text{Tr}\left[\rho_+^2\right] = \text{Tr}\left[\frac{1}{2}\begin{bmatrix}1 & 1\\ 1 & 1\end{bmatrix}\frac{1}{2}\begin{bmatrix}1 & 1\\ 1 & 1\end{bmatrix}\right] \tag{2.335}$$

$$= \text{Tr}\left[\frac{1}{4}\begin{bmatrix}2 & 2\\ 2 & 2\end{bmatrix}\right] \tag{2.336}$$

$$= 1 \tag{2.337}$$

$$\text{Tr}\left[\rho_?^2\right] = \text{Tr}\left[\frac{1}{2}\begin{bmatrix}1 & 0\\ 0 & 1\end{bmatrix}\frac{1}{2}\begin{bmatrix}1 & 0\\ 0 & 1\end{bmatrix}\right] \tag{2.338}$$

$$= \text{Tr}\left[\frac{1}{4}\begin{bmatrix}1 & 0\\ 0 & 1\end{bmatrix}\right] \tag{2.339}$$

$$= 0.5 \tag{2.340}$$

we can see that the former is indeed a pure state (the upper bound of Eq. (2.333), purity = 1) while the latter is a maximally mixed state (the lower bound of Eq. (2.333), purity = 1/2, since $d = 2$ for a single-qubit).

As we showed at the beginning of this section, the maximally mixed state $\rho_?$ arises as a natural consequence of trying to separate the two-qubit entangled state $|\beta\rangle_{AB}$ into single-qubit states. This is critical. Indeed, it is easy to confirm from Eq. (2.306) that, prior to performing the partial trace separating qubits A and B, the two qubits jointly occupied a coherent superposition of $|00\rangle$ and $|11\rangle$. Calculating the purity of the corresponding two-qubit density matrix, we can confirm that their combined

state is pure

$$\mathrm{Tr}\left[(\rho_\beta^{AB})^2\right] = \mathrm{Tr}\left[\frac{1}{2}\begin{bmatrix}1&0&0&1\\0&0&0&0\\0&0&0&0\\1&0&0&1\end{bmatrix}\frac{1}{2}\begin{bmatrix}1&0&0&1\\0&0&0&0\\0&0&0&0\\1&0&0&1\end{bmatrix}\right] \tag{2.341}$$

$$= \mathrm{Tr}\left[\frac{1}{4}\begin{bmatrix}2&0&0&2\\0&0&0&0\\0&0&0&0\\2&0&0&2\end{bmatrix}\right] \tag{2.342}$$

$$= 1 \tag{2.343}$$

How do we interpret this? Together, qubits A and B are coherent, superposed, ontologically indeterminate. Separated, all the coherence shared between the two qubits has vanished, leaving each system empty, incoherent, epistemologically uncertain. They are mixed up, no different from a classical coin flips. This is, perhaps, the most interesting feature of quantum entanglement. Though we attribute the state $|\beta\rangle_{AB}$ to two distinct systems A and B, these labels are somewhat misleading. Yes, they may correspond to objects which appear distinct—for example, two superconducting circuits—but all the quantum information they contain is shared between them, with neither system owning a part to the exclusion of the other. The moment we individuate these systems, separating them into distinct actors and tracing out their partner, we irretrievably shatter this precious link, reducing each qubit to an inert, classical system.

We call the process by which a pure state becomes an incoherent mixture, moving from the surface of the Bloch sphere into its center, *decoherence*. We will return to this concept in many different contexts over the course of this thesis, but for now we can make a few general statements about this process. First, decoherence is intimately connected with entanglement. Like the two mixed states which arose when we separated the entangled Bell state above, qubits lose their coherence when they are ripped from their entanglements, either with other qubits or with systems elsewhere in their environment. Second, decoherence is not a unitary process. The

journey from the surface of the Bloch sphere to its center cannot be captured by the single-qubit Schrödinger equation with a 2×2 Hamiltonian, and it is thus not a reversible process (we cannot run the clock backwards by applying a single qubit operation $\hat{U}^\dagger$ which undoes the decoherence). Later in Part IV of this thesis, we will show that there are mathematical tools for robustly handling such processes, but for now notice that decoherence breaks the pristine mathematical picture of quantum bits we've developed in this chapter. Finally, decoherence is inevitable. The moment we attempt to build a quantum bit in the laboratory, decoherence processes will constantly attempt to tamper with our quantum state, degrading the coherence into a classical mixture. Indeed, much of the engineering work of building a quantum computer centers around mitigating the effects of decoherence, restoring as much as possible the coherent mathematical ideal we have developed in this chapter.

Chapter 3

Designing an Artificial Atom

In Chapter 2, we introduced the mathematical formalism of quantum bits evolving according to a general multi-qubit Hamiltonian. Starting from a minimal set of assumptions, we showed how such systems come to inhabit distinctly nonclassical states, such as coherent superpositions of orthogonal classical states and entanglements with other systems. In this chapter, we will explore one paradigm for realizing physical quantum bits in the laboratory using superconducting Josephson circuits. Starting from the quantum harmonic oscillator formed by a superconducting LC-circuit, we show that the introduction of a nonlinear element—the Josephson junction—results in an anharmonic oscillator whose lowest two levels can be treated as the $|0\rangle$- and $|1\rangle$-states of a qubit. This leads us quickly to the simplest possible superconducting qubit, know as the *transmon*, which will serve as the backbone for the experiments performed in Parts III and IV. Increasing the circuit complexity, we introduce a general formalism for writing the circuit Hamiltonian of a more complicated assemblage of electrical elements, known as circuit quantization. With the tools of circuit quantization in hand, we derive the Hamiltonian for another paradigm of superconducting qubit, known as the *flux qubit*. The chapter closes with results from the first measurement and simulation of a novel superconducting qubit design, known as the *capacitively-shunted* or *C-shunt* flux qubit.

3.1 Artificial Atoms

When we first introduced the notion of a quantum bit in Chapter 2, we started by noting that the wavefunctions $|0\rangle$ and $|1\rangle$ are, first and foremost, mathematical abstractions. Unlike the canonical orbitals of the hydrogen atom, these wavefunction, we argued, had no particular spatial structure or parameter dependence. All we asked was that the two states $|0\rangle$ and $|1\rangle$ obey an orthogonality condition

$$\langle 1|0\rangle = 0 \tag{3.1}$$

As long as this condition holds, we showed that these states form a complete basis in two-dimensional Hilbert space and can be combined to create superposition and entangled states of arbitrary dimension.

Now, just because the wavefunctions of our qubit don't *need* to have any special parameter dependence, this doesn't mean that they cannot or will not. As long as the orthogonality condition above holds, we are free to construct these wavefunctions however we'd like. Indeed, looking back at the orbitals of the hydrogen atom in Eq. (2.1), we see that all of these orbitals are orthogonal with respect to one another. In that sense, we could imagine choosing any two electron orbitals of the hydrogen atom—say, ψ_{100} and ψ_{200} for example—and declare that these two states together form one quantum bit. The task would then be to construct an experimental apparatus which captures hydrogen atoms and reliably manipulates them such that we can experimentally realize single- and multi-qubit Hamiltonians. While the atomic properties of hydrogen would make this an engineering nightmare, this exact same principle has been used to great effect in the construction of quantum processors using trapped ions and neutral atoms [129, 325]—systems where qubit states are mapped onto the wavefunctions of interacting atomic systems, such as the orbitals of a Ytterbium-171 ion or the Rydberg states of Rubium-87. While quantum processors based on atomic systems represent a compelling paradigm for realizing large systems of quantum bits—due in no small part to the fact that every Rubium atom will be

physically identical to every other Rubium atom in the universe—the homogenatity of atomic systems is also a design constraint: there are only as many varieties of atoms and ions in the universe as there are entries on the periodic table, so the set of possible wavefunctions on which one might map the states $|0\rangle$ and $|1\rangle$ is fundamentally limited by the laws of nature. With the menu thus set in stone, the best we can do is pick elements with the most favorable properties for a particular application and design their system accordingly.

And yet, over the past three decades there has been enormous progress in designing controllable quantum systems which are untethered from the design constraints of the periodic table. These systems, assembled freely from electrical components such as inductors and capacitors, can be thought of as 'artificial atoms' built out of an infinite permutation of protons, neutrons, and electrons. In this chapter, we explore the formalism for representing and engineering the Hamiltonian of such a system, and we explore two of the most common families of circuits employed for quantum computation: the transmon and the flux qubit.

3.2 Quantum Harmonic Oscillators

In Chapter 2, we treated the Hamiltonian operator $\hat{H}$ as a purely mathematical object. For a single qubit, we expressed the Hamiltonian as a general 2×2 hermitian matrix, and we showed that such an operator placed into the Schrödinger equation quickly gives rise to coherent superposition and entanglement, depending on the structure of the Hamiltonian matrix. Where does the Hamiltonian comes from, physically?

In classical physics, the Hamiltonian of a system is defined as the sum of the kinetic and potential energies as play inside the system

$$H = T + U \tag{3.2}$$

where T is the kinetic energy and U is potential energy. For a particle of mass m in motion, we can rewrite the kinetic energy in terms of the particle's velocity v or

momentum $p = mv$

$$H = \frac{1}{2}mv^2 + U \tag{3.3}$$

$$= \frac{p^2}{2m} + U \tag{3.4}$$

where the potential energy U depends on the particular set of forces acting on the particle which constrain its motion. In elementary classical mechanics, one of the first systems a student will study is the canonical mass on a spring, where the particle is bound to a spring which exerts an energy of the mass proportional to its displacement x from equilibrium

$$F(x) = -kx \tag{3.5}$$

where k is the spring constant which captures the elasticity of the particular coil the particle is bound to. Integrating this force over the displaced distance x, we find the potential energy stored in the spring scales with the displacement squared

$$U(x) = -\int_0^x F(x)\,dx \tag{3.6}$$

$$= \frac{1}{2}kx^2 \tag{3.7}$$

Substituting this potential energy expression into Eq. (3.4), we arrive at the Hamiltonian of the mass and spring system

$$H(p, x) = \frac{p^2}{2m} + \frac{1}{2}kx^2 \tag{3.8}$$

Having defined the Hamiltonian of this system, the classical equations of motion for the particle can be derived from Hamilton's equations

$$\frac{dx}{dt} = \frac{\partial}{\partial p}H(p, x) \tag{3.9}$$

$$\frac{dp}{dt} = -\frac{\partial}{\partial x}H(p, x) \tag{3.10}$$

where plugging into the first gives us back the definition of velocity

$$\frac{dx}{dt} = \frac{\partial}{\partial p} H(p,x) \tag{3.11}$$

$$= \frac{\partial}{\partial p}\left(\frac{p^2}{2m} + \frac{1}{2}kx^2\right) \tag{3.12}$$

$$= \frac{p}{m} \tag{3.13}$$

$$= v \tag{3.14}$$

and plugging into the second gives us Newton's second law

$$\frac{dp}{dt} = -\frac{\partial}{\partial x} H(p,x) \tag{3.15}$$

$$\frac{d}{dt}(mv) = -\frac{\partial}{\partial x}\left(\frac{p^2}{2m} + \frac{1}{2}kx^2\right) \tag{3.16}$$

$$m\frac{dv}{dt} = -kx \tag{3.17}$$

$$ma = F(x) \tag{3.18}$$

where $a = \dot{v} = \ddot{x}$ is the acceleration of the particle.

Hamiltonians of the form in Eq. (3.8) appear over and over in physics, and they are generally applicable to any system governed by a linear restoring force—such as a mass on a string or a pendulum in a gravitational field—or indeed any system in an arbitrary potential, displaced a small amount from a local minimum—around which the potential can be approximated, to first order, as a parabola. We call such systems *simple harmonic oscillators*, since their equations of motion have oscillatory solutions of the form

$$x(t) = A\cos(\omega t + \delta) \tag{3.19}$$

where A is the amplitude of oscillation, δ is a phase offset, and ω is the frequency of oscillation, which is related to the coefficients of the kinetic and potential terms of the Hamiltonian

$$\omega = \sqrt{\frac{k}{m}} \tag{3.20}$$

for the mass on a spring.

Transitioning from classical mechanics to quantum theory, one of the first elementary tasks is to derive the quantum mechanical equivalent of the classical harmonic oscillator, aptly called the *quantum harmonic oscillator*. Such a system has a Hamiltonian which is formally equivalent to the classical Hamiltonian of a mass on a spring, except the Hamiltonian, kinetic, and potential energies are now promoted to quantum mechanical operators

$$\hat{H} = \hat{T} + \hat{U} \tag{3.21}$$

which we can write in terms of the position and momentum operators $\hat{p}$ and $\hat{x}$ as

$$\hat{H} = \frac{\hat{p}^2}{2m} + \frac{1}{2}m\omega^2\hat{x}^2 \tag{3.22}$$

Having defined this Hamiltonian, we can plug it into the Schrödinger equation to find its energy eigenstates. Doing so, we arrive at wavefunctions of the form

$$\psi_n(x) = A_n(\hat{a}^\dagger)^n\psi_0(x) \tag{3.23}$$

where A_n is the normalization constant which preserves probability, $a^\dagger$ is the creation operator

$$\hat{a}^\dagger \equiv \frac{1}{\sqrt{2\hbar m\omega}}\left(-i\hat{p} + m\omega\hat{x}\right) \tag{3.24}$$

and ψ_0 is the ground state wavefunction of the oscillator

$$\psi_0(x) = \left(\frac{m\omega}{\pi\hbar}\right)^{1/4} e^{-\frac{m\omega}{2\hbar}x^2} \tag{3.25}$$

which is a Gaussian wavepacket centered around the equilibrium point $x = 0$. Taking the expectation value of the Hamiltonian for each of the wavefunctions ψ_n, we find a ladder of equally spaced energy levels, separated by an energy quanta proportional

to the fundamental frequency ω

$$E_n = \left(n + \frac{1}{2}\right)\hbar\omega \tag{3.26}$$

How might we realize a quantum harmonic oscillator, physically? In classical electromagnetism, it is shown that one can construct an electrical analog to the mechanical mass and spring system—one which realizes the same fundamental Hamiltonian as the simple harmonic oscillator, with a change of variables. This system, know as the LC-circuit, consists of a capacitor in parallel with an inductor, as shown in Fig. 3-1a. Each of these electrical elements stores a certain amount of energy: the energy stored in the capacitor is given by

$$E_C = \frac{1}{2}CV^2 \tag{3.27}$$

$$= \frac{1}{2C}q^2 \tag{3.28}$$

where C is the capacitance, V is the voltage across the capacitor, and q is the total stored; meanwhile, the inductor stores an amount of energy

$$E_L = \frac{1}{2}LI^2 \tag{3.29}$$

$$= \frac{1}{2L}\Phi^2 \tag{3.30}$$

where L is the inductance, I is the current passing through the inductor, and Φ is the magnetic flux across the inductor. Summing these two energies, we arrive at the classical Hamiltonian of the LC-circuit

$$H(q, \Phi) = \frac{1}{2C}q^2 + \frac{1}{2L}\Phi^2 \tag{3.31}$$

Comparing Eq. (3.31) with Eq. (3.8), we see that the capacitive and inductive energies mathematically mirror the kinetic and potential energies of the mass of a spring, with the momentum p and displacement x mapping onto the charge stored in the capacitor q and flux across the inductor Φ respectively. Since the differential

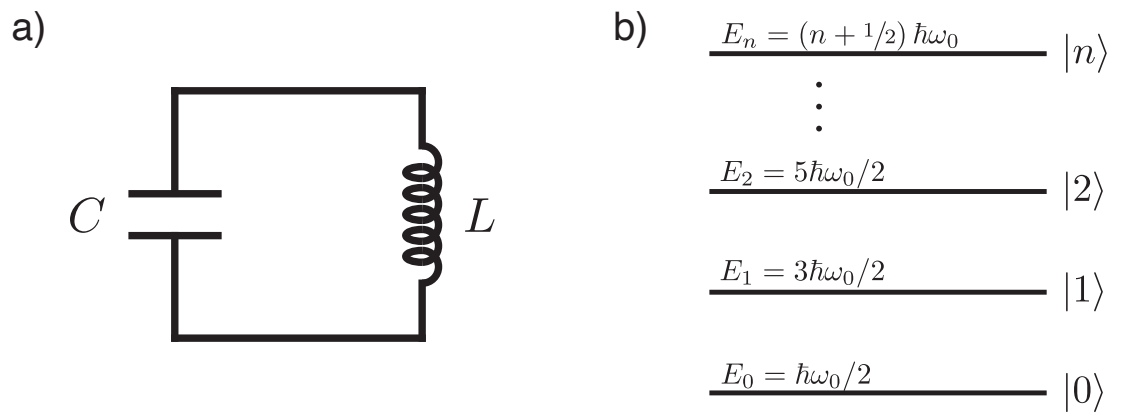

Figure 3-1: The LC Oscillator. **(a)** Electrical circuit diagram of the resonant circuit with a capacitor C in parallel with an inductor L. **(b)** The quantized energy levels of the corresponding quantum harmonic oscillator, where the levels are equally spaced by the fundamental frequency $\omega_0 = 1/\sqrt{LC}$, in accordance with Eq. (3.26).

equations for these two systems share a common form, we can easily show that the charge stored in the capacitor varies in time as an oscillating function of the same form as Eq (3.19)

$$q(t) = A\cos(\omega t + \delta) \tag{3.32}$$

where the fundamental frequency ω is now related to the capacitance and inductance as

$$\omega = \frac{1}{\sqrt{LC}} \tag{3.33}$$

Looking at the equation of motion for $q(t)$, we can see that electrical charge will oscillate back and forth around the circuit, alternating between filling up the capacitor at one point in time (maximizing the capacitive energy, like the mass achieving maximum kinetic energy as it passes through the equilibrium point of the spring), leaving the capacitor and flowing through the inductor (maximizing the inductive energy, like the mass achieving maximum potential energy as the extreme of the spring's displacement), and back and forth ad infinitum.

The classical equations above hold for LC-circuits at normal temperatures, but something interesting happens if we assemble the circuit out of a superconducting material and lower the temperature of the device below the critical temperature. Under

such a condition, the electrons in our LC-circuit will no longer act like tiny individual masses oscillating back and forth through the circuit. Instead, all of the electrons in the circuit will condense into a collective macroscopic wavefunction formed out of paired electrons (Cooper pairs with charge $2e$) known as the *fermionic condensate*, governed by the quantum mechanical Hamiltonian

$$\hat{H} = \frac{1}{2C}\hat{q}^2 + \frac{1}{2L}\hat{\Phi}^2 \tag{3.34}$$

This is a quantum harmonic oscillator, where the classical charge and flux have been promoted to their corresponding quantum operators $\hat{q}$ and $\hat{\Phi}$. Like the quantum harmonic oscillator describing a particle in a parabolic potential above, this system also has quantized energy levels

$$E_n = \left(n + \frac{1}{2}\right)\hbar\omega \tag{3.35}$$

where ω is now simply the resonant frequency of the LC-circuit from Eq. (3.33).

3.3 The Transmon

In the previous section, we showed how a superconducting resonant circuit composed of an inductor and capacitor creates a quantum harmonic oscillator with energy levels equally spaced by the fundamental frequency ω. Indeed, the wavefunctions associated with each of these levels, like the corresponding wavefunctions of the harmonic oscillator in Eq. (3.23), are mutually orthogonal

$$\langle\psi_n|\psi_m\rangle \equiv \int_V \psi_n^*\psi_m\, dv = \begin{cases} 1, \text{ for } n = m \\ 0, \text{ for } n \neq m \end{cases} \tag{3.36}$$

These wavefunctions, it would seem, are fair candidates for our qubit states $|0\rangle$ and $|1\rangle$. So, why not design a superconducting LC-circuit, pick any two energy eigenstates—say, the ones corresponding to $n = 0$ and $n = 1$, for example—and treat this subsys-

tem as a quantum bit?

Running with this idea, how would we generate rotations between these two states, like the ones we realized mathematically in Chapter 2? The most straightforward option is to perturb the system by applying a periodic drive at a frequency equal to the energy difference of the two qubit levels, a process known as *Rabi driving*. Here, the transition probability P of the fermionic condensate in the LC-circuit going from the $n = 0$ state to the $n = 1$ state and vice versa is

$$P_{0\leftrightarrow 1}(t) \cong \frac{|H_{01}|^2}{\hbar^2} \frac{\sin^2\left[(\omega_{01} - \omega_{\text{drive}})t\right]}{(\omega_{01} - \omega_{\text{drive}})^2} \tag{3.37}$$

where $\omega_{01} \equiv (E_1 - E_0)/\hbar$ is the frequency difference between the two states ψ_0 and ψ_1; ω_{drive} is the frequency of the external drive (say, the signal from a microwave generator); and H_{01} is the off-diagonal element of the Hamiltonian which couples the two states. This function reaches unity when the drive is resonant with the transition frequency $\omega_{\text{drive}} = \omega_{01}$ and the drive power is very strong $H_{01}/\hbar \gg (\omega_{01} - \omega_{\text{drive}})$, at which point the system will oscillate back and forth between total population of state ψ_0 and total population of ψ_1. This should sound familiar: in the Bloch sphere picture, the system is traversing a meridian of the sphere in time, coherently oscillating between the poles as if under the influence of the single-qubit Hamiltonian $\hat{H} = E_X\hat{X}$. Indeed, as we will see in Part III, this is exactly how we will realize a single-qubit rotation using a superconducting circuit.

While this idea is not too far from reality, there's one big problem. For a quantum harmonic oscillator such as an LC-circuit, the energy difference between adjacent eigenstates is equal, *by definition*. That is, the transition frequency ω_{01} is equal to the transition frequency ω_{12} between $n = 1$ and $n = 2$, which is equal to ω_{23}, and so on and so forth. As such, the moment we apply a drive at this frequency, we are as likely to drive the system from $n = 1$ down to $n = 0$ as we are to drive it up a level to $n = 2$ instead. Indeed, to moment we apply this drive, we will trigger transitions between all levels $n \leftrightarrow n + 1$, shuttling the system up and down the ladder of states

uncontrollably

$$P_{0\leftrightarrow 1}(t) = P_{1\leftrightarrow 2}(t) = P_{n\leftrightarrow n+1}(t) \tag{3.38}$$

In order to turn this system into a quantum bit—into a system with two well-controlled levels we can maneuver the system back and forth between—we need some way of individually addressing the $n = 0 \leftrightarrow n = 1$ transition, without accidentally triggering every other transition in the process. To achieve this, we need to disturb the harmonic structure of the energy levels and introduce some *anharmonicity* to the circuit. The greater the anharmonicity—that is, the greater the difference between ω_{01} and ω_{12}, for example—the further off-resonance the drive will be in relationship to the other transitions, and the lower the probability that we will unintentionally populate a state outside the qubit subspace.

Fortunately, superconductivity provides us with a circuit element which introduces exactly this sort of anharmonicity to our resonant circuit, known as the *Josephson junction*. To build a Josephson junction, one simply needs two pieces of superconducting metal separated by a thin insulating barrier—aluminum separated by a thin layer of aluminum oxide, for example. At room temperature, such an element would break the circuit: no charge can pass through the insulating barrier, so current cannot flow across it, like the two pads of a capacitor. However, at superconducting temperatures, the wavefunction of the superconducting condensate can tunnel through the thin barrier, creating a current through the junction which completes the circuit. The current through the junction I and the voltage across it V are given by the two Josephson relations

$$I = I_c \sin(\phi) \tag{3.39}$$

$$V = \frac{\Phi_0}{2\pi}\frac{d\phi}{dt} \tag{3.40}$$

where $\phi \equiv 2\pi\Phi/\Phi_0$ is the *gauge-invariant phase* across the junction, the critical current I_c is a parameter which depends on the size and material of junction, and the constant $\Phi_0 = h/(2e)$ is known as the *magnetic flux quantum*. Playing around with the two Josephson relations, we can ascribe an inductance to this element by

rewriting the relations in the form

$$\frac{dI}{d\phi} = I_c \cos(\phi) \tag{3.41}$$

$$\frac{d\phi}{dt} = \frac{2\pi}{\Phi_0} V \tag{3.42}$$

which we can combine to get the time derivative of the current

$$\frac{dI}{dt} = \frac{dI}{d\phi}\frac{d\phi}{dt} \tag{3.43}$$

$$= I_c \cos(\phi)\frac{2\pi}{\Phi_0} V \tag{3.44}$$

Rearranging this expression into the form of the current-voltage relationship for an inductor

$$V = L(\phi)\frac{dI}{dt} \tag{3.45}$$

we find that the kinetic inductance of the junction $L(\phi)$ is given by

$$L(\phi) = \frac{L_J}{\cos(\phi)} \tag{3.46}$$

where $L_J = \Phi_0/(2\pi I_c)$ is known as the *Josephson inductance* of a given junction with critical current I_c. From Eq. (3.46), we see that the Josephson junction can be thought of as a nonlinear inductor which depends on the phase across the junction ϕ, in contrast to the normal linear inductor with constant inductance L we used to construct the LC-circuit.

What happens when we replace the linear inductor in the LC-circuit with a Josephson junction? From the two Josephson relations, we can calculate the potential energy stored in this element by integrating the product of the current and voltage over time

$$E(t) = \int_{-\infty}^{t} I(t')V(t')\,dt' \tag{3.47}$$

Using the Josephson relationship from Eq. (3.40), we can perform a change of variables

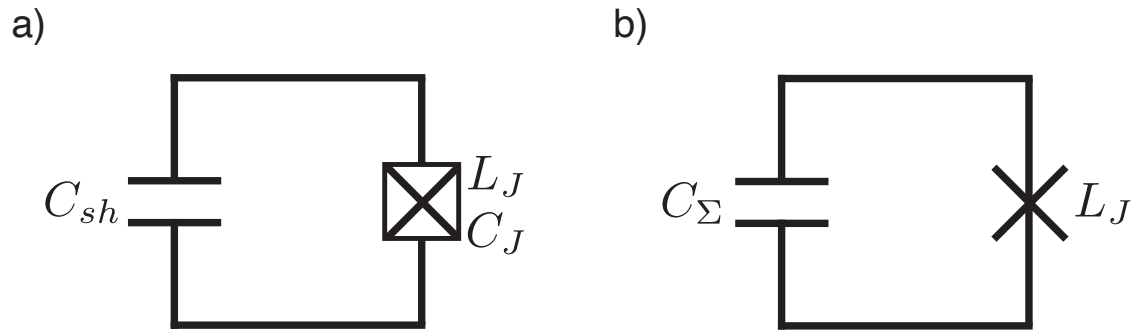

Figure 3-2: The Transmon Qubit. **(a)** Electrical circuit diagram of the transmon qubit, where the linear inductor of the LC-oscillator in Fig. 3-1a has been replaced with a Josephson junction with Josephson inductance L_J and intrinsic capacitance C_J. The combined Josephson inductance plus intrinsic capacitance is commonly denoted by a $\times$ enclosed in a square. **(b)** The exact same circuit as in (a), except now written with the intrinsic capacitance of the junction added to the capacitance of the shunt capacitor $C_\sigma = C_{sh} + C_J$. The Josephson junction without its intrinsic capacitance can be treated as a nonlinear inductor and is denoted by a $\times$ without a square.

from time to phase $V\,dt \to d\phi$

$$E(\phi) = \int_{-\infty}^{\phi} I(\phi') \left(\frac{\Phi_0}{2\pi}\, d\phi'\right) \tag{3.48}$$

$$= \frac{\Phi_0}{2\pi} \int_{-\infty}^{\phi} I_c \sin(\phi')\, d\phi' \tag{3.49}$$

$$= -E_J \cos(\phi) \tag{3.50}$$

where $E_J = \Phi_0 I_c/(2\pi)$ is known as the Josephson energy of a given junction.

To write the Hamiltonian for a Josephson junction in parallel with a capacitor, we can modify the LC Hamiltonian from Eq. (3.34) by replacing the inductive energy with the Josephson junction energy we found in Eq. (3.50), plus an additional capacitive energy due to the junction (since the Josephson junction also acts as a small parallel

plate capacitor)

$$\hat{H} = \frac{1}{2C_{sh}}\hat{q}^2 + \frac{1}{2C_J}\hat{q}^2 - E_J \cos\left(\hat{\phi}\right) \tag{3.51}$$

$$= \frac{1}{2C_\Sigma}\hat{q}^2 - E_J \cos\left(\hat{\phi}\right) \tag{3.52}$$

where C_{sh} and C_J are the capacitances of the shunt capacitor and Josephson junction respectively, and $C_\Sigma \equiv C_{sh} + C_J$ is their parallel sum. Finally, it is conventional to replace the charge operator $\hat{q}$ with a number operator $\hat{n}$, where $\hat{n}$ represents the number of Cooper pairs with charge $2e$ on the superconducting island

$$\hat{q} \equiv 2e\,\hat{n} \tag{3.53}$$

Making this substitution, we arrive at the Hamiltonian of the capacitor-junction circuit

$$\hat{H} = 4E_C\hat{n}^2 - E_J \cos\left(\hat{\phi}\right) \tag{3.54}$$

where $E_C = e^2/(2C_\Sigma)$ is the capacitive energy of the circuit.

The electrical circuit represented by the Hamiltonian in Eq. (3.54)—based on the simple LC-resonator, with a single Josephson junction in place of the linear inductor to provide the necessary anharmonicity—is the simplest possible realization of a qubit using superconducting circuits. Looking at this Hamiltonian, we can see that the dynamics of this circuit are entirely determined by the relative weighting of the two energies E_J/E_C, in much the same way that a heavy mass bound to a limp spring will differ from a light mass on a stiff spring. In the limit where the Josephson energy is much larger than the capacitive energy $E_J \gg E_C$, this circuit is commonly known as the *transmon qubit* [254]. This choice of parameters is strategic: the larger the weighting of one energy relative to the other, the more susceptible the circuit will be to noise in the corresponding circuit variable. That is, when $E_J \gg E_C$, the circuit will be more susceptible to magnetic flux noise in the environment, which shifts the phase $\hat{\phi}$ in time; when $E_C \gg E_J$, the circuit will be more susceptible to electric charge

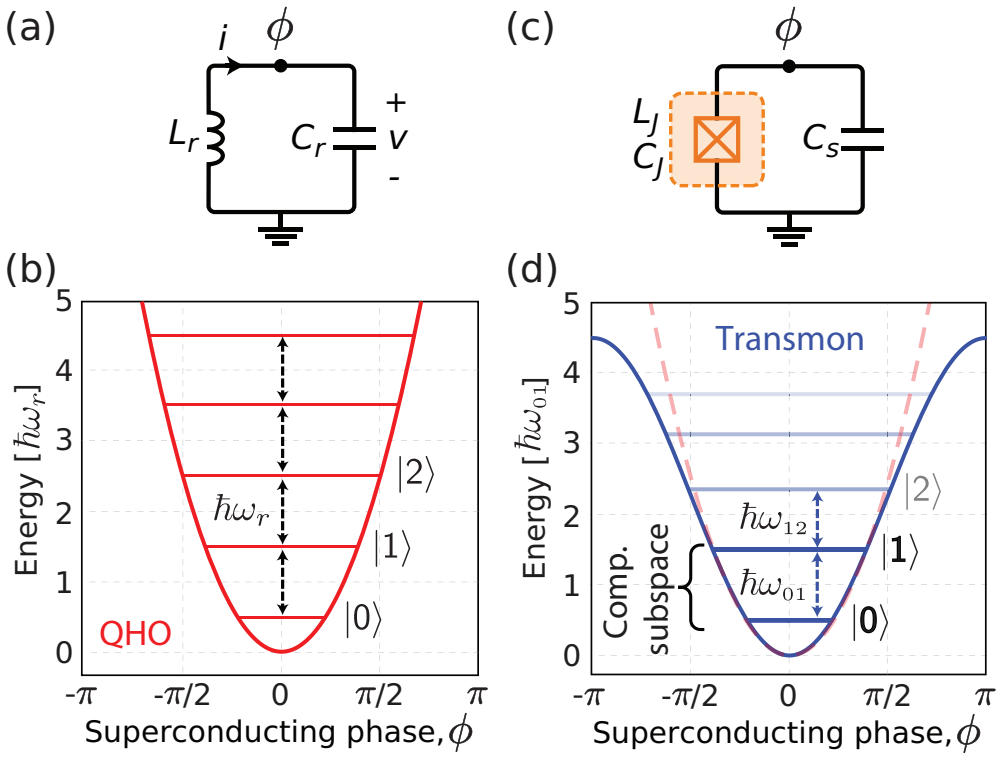

Figure 3-3: Quantum Harmonic and Anharmnonic Oscillators. **(a)** Electrical circuit diagram for a quantum harmonic oscillator (QHO) created using a simple LC-circuit with an inductor L in parallel with a capacitor C. **(b)** The parabolic energy potential of the LC-circuit, where the energy levels $|0\rangle, |1\rangle, |2\rangle$ are spaced evenly apart by the fundamental frequency $\hbar\omega_r$. **(c)** Circuit diagram of a single-junction transmon qubit, where the linear inductor in (a) has been replaced with a Josephson junction (inductance L_J, intrinsic capacitance C_J). **(d)** The cosinusoidal potential of the transmon qubit, where the energy levels of the circuit are spaced unevenly such that the lowest two energy states $|0\rangle$ and $|1\rangle$ can be uniquely addressed at their frequency difference ω_{01}. Together, the states $|0\rangle$ and $|1\rangle$ form the computational subspace of the quantum bit. Figure reproduced from Ref. [257].

noise in the environment, shifting the charge $\hat{q}$. Historically, charge noise has proven more difficult to mitigate than flux noise, hence the choice of $E_J \gg E_C$.

To access the transmon regime ($E_J/E_C \geq 50$), one technique is to increase the shunt capacitance C_{sh} in parallel to the Josephson junction, flattening the energy levels of the circuit with respect to charge and reducing the circuit's susecpibility to charge noise. In this limit, the anharmonicity of the qubit is simply given by the

charging energy of the capacitor

$$\omega_{12} - \omega_{01} = -E_C \tag{3.55}$$

and the qubit frequency can be found by diagonalizing the Hamiltonian in Eq. (3.54) and finding the difference in the eigenenergies of the lowest two states

$$\omega_{01} = (\sqrt{8E_J E_C} - E_C)/\hbar \tag{3.56}$$

Since E_C is small by design, we can see that the transmon is a weakly anharmonic circuit: for a typical device with a qubit frequency $\omega_{01} = 3$–6 GHz, the anharmociity $\omega_{01} - \omega_{12}$ is consequently on the order of 100–300 MHz [246].

We will return to the transmon qubit extensively in Part III, where it will serve as our hardware platform for performing multi-qubit algorithms using a universal gate set. For the remainder of this chapter, we will focus on a slightly more complex superconducting circuit known as the *flux qubit*, which will demand a more sophisticated handling of the circuit Hamiltonian than we were permitted to get away with for the transmon. This technique—known as *circuit quantization*—provides a powerful and flexible formalism for simulating general configurations of Josephson junctions, capacitors, and linear inductors, and it will lead us naturally to the consideration of multi-qubit circuits in the following chapter.

3.4 Circuit Quantization: The Flux Qubit

In this section, we will introduce the formalism of circuit quantization to derive the Hamiltonian of a more general superconducting qubit composed of an arbitrary arrangement of electrical elements. As an example, we will consider a circuit which contains multiple Josephson junctions in series, as well as shunt capacitors and—later in the section—linear inductors. This particular circuit, known as the flux qubit (Fig. 3-4), consists of three Josephson junctions in a loop, where two of the junctions A and B have Josephson energy E_J, and the third junction C has a smaller Josephson

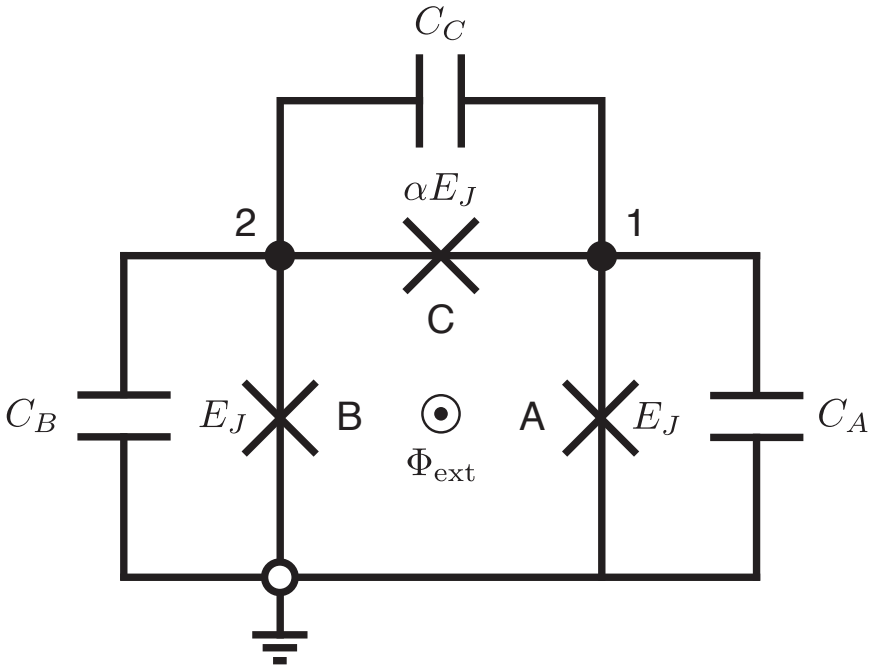

Figure 3-4: Electrical circuit diagram for a three-junction flux qubit, where two of the junctions (A and B) have Josephson energy E_J and the third junction (C) has Josephson energy αE_J ($\alpha < 1$, typically accomplished by making the overlap area of the junction a factor α smaller than the other two). The loop formed by the three series junctions is threaded by an external magnetic flux Φ_{ext}, and each junction is shunted by a capacitance C_n which includes the parallel combination of the intrinsic capacitance of the junction and any additional shunt capacitance. The two ungrounded circuit nodes (labeled 1 and 2) are the independent degrees of freedom of the circuit.

energy αE_J ($\alpha < 1$). This smaller junction will play a role similar to the single junction of the transmon in the previous section, while the two large junctions will serve as a shunt inductance across the smaller junction. As in the case of the transmon, each junction has a parallel capacitance C_n, which is the parallel combination of the intrinsic capacitance of the junction and an optional additional shunt capacitor.

We will first derive the Hamiltonian of this circuit for the simpler case of negligible linear inductance. From there, we will adjust add an additional degree of freedom to the circuit to account for the linear inductance of the loop.

3.4.1 Writing the Classical Hamiltonian

Before we treat the qubit quantum mechanically, let's consider the *classical* Hamiltonian of our qubit circuit. Having derived the classical Hamiltonian, the transition to the language of quantum mechanics—where the Hamiltonian is an operator on discrete energy states, rather than a continuous function of electrical variables—will emerge naturally.[1]

As we showed in Section 3.3, the Josephson potential energy U_J due to each junction in our circuit is given by

$$U_{Jn} = E_{Jn}\,(1 - \cos\phi_n) \tag{3.57}$$

where $E_{Jn} = \Phi_0 I_{cn}/(2\pi)$ is the Josephson energy of the nth junction with critical current I_{cn}, and ϕ_n is the gauge invariant phase across the superconducting junction. Summing over all three junctions, we get the total Josephson potential energy U of our circuit

$$\begin{aligned} U_J &= \sum_n E_{Jn}(1 - \cos\phi_n) && (3.58)\\ &= E_{JA}(1 - \cos\phi_A) + E_{JB}(1 - \cos\phi_B) + E_{Jc}(1 - \cos\phi_C) && (3.59)\\ &= E_J(2 + \alpha - \cos\phi_A - \cos\phi_B - \alpha\cos\phi_C) && (3.60) \end{aligned}$$

Now, let's define a set of circuit nodes between each of the electrical elements in our circuit. For the transmon, there were two nodes: the point between the junction and the capacitor on either side of the loop. One of these nodes is electrically grounded, so the circuit can be completely described by the electrical degree of freedom in the single ungrounded node (black dot labeled ϕ in Fig. 3-3c). For the flux qubit, the multiple junctions in series result in more circuit nodes: three in total (separating the three junctions and their parallel capacitances), two of which are ungrounded. Let's label these two nodes 1 and 2 (black dots in Fig. 3-4).

[1] The following derivation is loosely adapted from the original derivation of the persistent-current qubit in Ref. [345].

Having defined the nodes of the cicuit, we can make a change of variables. Rather than writing the Josephson potential in terms of the junction phases ϕ_A, ϕ_B, and ϕ_C (the so-called *branch variables* of our circuit), we can rewrite the potential in terms of the phase across the two circuit nodes ϕ_1 and ϕ_2 (the *node variables*). As we will see, these variables will effectively take into account the basic electrical constraints imposed by Kirchoff's laws and thus comprise the set of independent degrees of freedom in our circuit.

Unlike the branch variables, the definition of the node variables depends on how you describe the topology of the circuit, which is defined according to the following convention:[2]

1. Define the set of circuit nodes such that there is a node separating every circuit element.

2. From the set of circuit nodes, define a reference node at circuit ground.

3. Choose a set of circuit branches such that each node is connected to ground by a single chain of branches. Together, this set of branches defines the *spanning tree* of our circuit.

4. The remaining circuit paths which are not included in the spanning tree are defined as the *closure branches* of our circuit. These branches connect the spanning tree branches and complete the closed loops of the circuit.

For a given circuit, the exact choice of spanning tree and closure branches is not unique. This freedom in defining the spanning tree of the circuit is analogous to the freedom in choosing a particular gauge when defining the vector potential in electromagnetism.

Having defined the set of spanning tree branches T and the set of closure branches C, we can relate the phase across a given branch ϕ_b to the flux across its adjacent

[2]This method of defining the circuit topology is explained in detail in Ref. [119].

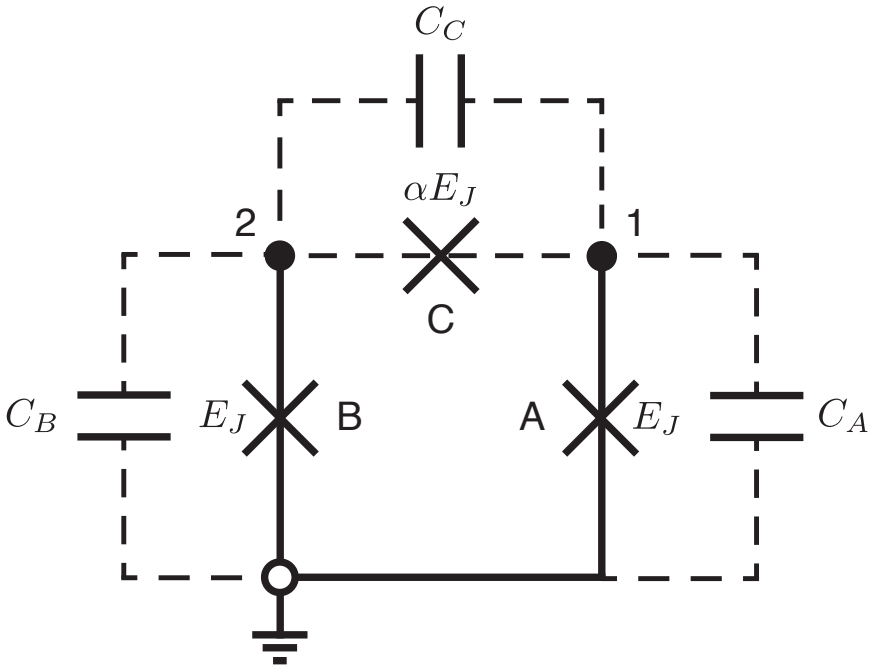

Figure 3-5: One choice of spanning tree for the circuit in Fig. 3-4. Here, solid lines denote spanning tree branches T, and dashed lines denote closure branches C. For this choice of spanning tree, the conversion between branch variables A, B, C and node variables $1, 2$ is given in Eq. (3.63)–(3.65).

nodes ϕ_n and $\phi_{n\prime}$

$$\phi_{b\in\mathsf{T}} = \phi_n - \phi_{n\prime} \tag{3.61}$$

$$\phi_{b\in\mathsf{C}} = \phi_n - \phi_{n\prime} + \frac{2\pi}{\Phi_0}\Phi_{l(b)} \tag{3.62}$$

where $\Phi_{l(b)}$ is the total external magnetic flux through loop l, the loop which branch b closes.

For the particular choice of spanning tree illustrated in Fig. 3-5, we would relate the flux across the three junctions in our qubit to the flux across the two nodes as

such:

$$\phi_A = \phi_1 \tag{3.63}$$

$$\phi_B = \phi_2 \tag{3.64}$$

$$\phi_C = \phi_1 - \phi_2 + \frac{2\pi}{\Phi_0}\Phi_{\text{ext}} \tag{3.65}$$

where Φ_{ext} is the magnetic flux bias applied through our qubit loop. Making this change of variables, we arrive at an expression for the Josephson potential energy in terms of the node fluxes

$$U_J = E_J\left(2 + \alpha - \cos\phi_1 - \cos\phi_2 - \alpha\cos\left(\phi_1 - \phi_2 + \frac{2\pi}{\Phi_0}\Phi_{\text{ext}}\right)\right) \tag{3.66}$$

Now that we have an expression for the Josephson potential energy of the qubit in terms of the node variables, let's consider the electrostatic energy T_C stored at each of the junctions

$$T_{Cn} = \frac{1}{2}C_n V_n^2 \tag{3.67}$$

where C_n is the total capacitance across the junction (a parallel sum of its intrinsic capacitance as well as its shunt capacitance) and V_n is the voltage across the junction. Summing over the capacitive energies of all three junctions, we get the total electrostatic energy stored in our qubit circuit

$$T_C = \frac{1}{2}\left(C_A V_A^2 + C_B V_B^2 + C_C V_C^2\right) \tag{3.68}$$

Now, just as with our expression for the Josephson potential energy, we want to make a change of variables and rewrite this expression in terms of the node variables of our circuit. Making this change of variable, we can write the voltage across each junction in terms of the voltages across the two nodes

$$T_C = \frac{1}{2}\left(C_A\left(V_1 - V_g\right)^2 + C_B\left(V_2 - V_g\right)^2 + C_C\left(V_1 - V_2\right)^2\right) \tag{3.69}$$

We are free to define the voltage at ground as zero ($V_g = 0$), so we can expand out this expression and drop the terms proportional to V_g

$$T_C = \frac{1}{2}\left(C_A V_1^2 + C_B V_2^2 + C_C\left(V_1^2 - 2\,V_1 V_2 + V_2^2\right)\right) \tag{3.70}$$

$$= \frac{1}{2}\left(\left(C_A + C_C\right)V_1^2 + \left(C_B + C_C\right)V_2^2 - 2\,C_C V_1 V_2\right) \tag{3.71}$$

Recall from Section 3.3 that the voltage across a Josephson junction is proportional to the time derivative of the phase across it

$$V_n = \frac{\Phi_0}{2\pi}\dot{\phi}_n \tag{3.72}$$

$$= \dot{\Phi}_n \tag{3.73}$$

We can thus rewrite the total electrostatic energy T_C stored in the qubit in terms of derivatives of the node *fluxes* $\dot{\Phi}_n$

$$T_C = \frac{1}{2}\left(\left(C_A + C_C\right)\dot{\Phi}_1^2 + \left(C_B + C_C\right)\dot{\Phi}_2^2 - 2\,C_C\dot{\Phi}_1\dot{\Phi}_2\right) \tag{3.74}$$

which we can express in a more compact matrix form as

$$T_C = \frac{1}{2}\,\vec{\dot{\Phi}}^{\,T}\cdot\mathbf{C}\cdot\vec{\dot{\Phi}} \tag{3.75}$$

where $\vec{\dot{\Phi}}$ is a column vector of our flux derivatives

$$\vec{\dot{\Phi}} = \begin{bmatrix}\dot{\Phi}_1\\ \dot{\Phi}_2\end{bmatrix} \tag{3.76}$$

and $\mathbf{C}$ is the capacitance matrix for our circuit[3]

$$\mathbf{C} = \begin{bmatrix} C_A + C_C & -C_C \\ -C_C & C_B + C_C \end{bmatrix} \tag{3.77}$$

Taking the electrostatic energy T_C as the qubit's kinetic energy T and the Josephson energy U_J as its potential energy U, we can write the Lagrangian of the circuit

$$\mathcal{L} = T(\dot{\vec{\Phi}}) - U(\vec{\Phi}) \tag{3.78}$$

where $U(\vec{\Phi})$ is the Josephson potential in Eq. (3.66) written in terms of the node fluxes $\Phi_n = \Phi_0\phi_n/(2\pi)$. Following Langrangian mechanics, the canonical momenta $P_i = \partial\mathcal{L}/\partial\dot{\Phi}_i$ are thus

$$\vec{P} = \mathbf{C} \cdot \dot{\vec{\Phi}} \tag{3.79}$$

$$= \mathbf{C} \cdot \vec{V} \tag{3.80}$$

$$= \vec{q} \tag{3.81}$$

which is the vector of total electric charge stored on the two circuit nodes q_1 and q_2.

Now that we have the Lagrangian of the circuit as well as the canonical momenta,

[3]In practice, we can bypass most of the steps in this derivation and go straight to the matrix expression in Eq. (3.75), provided we follow a couple simple rules in defining our capacitance matrix $\mathbf{C}$. For a completely general qubit with N circuit nodes, the N-dimensional capacitance matrix can be constructed as follows:

1. **The diagonal entry C_{nn} is the sum of the capacitances immediately adjacent to node n.** Since the nodes are independent degrees of freedom, only these capacitances immediately adjacent to a given node are actually affected by its voltage.

2. **The off-diagonal entry C_{nm} is the *negative* sum of the capacitances between node n and node m.** These off-diagonal entries give us the negative cross terms which arise when we take the square of the difference between adjacent node voltages.

3. **If nodes n and m are not adjacent—that is, there is at least one other node separating them—then $C_{nm} = 0$.**

we can now write the classical Hamiltonian:

$$H = \sum_i P_i \dot{\Phi}_i - \mathcal{L} \tag{3.82}$$

$$= \frac{1}{2}\, \dot{\vec{\Phi}}^{\,T} \cdot \mathbf{C} \cdot \dot{\vec{\Phi}} \; + U(\vec{\Phi}) \tag{3.83}$$

$$= \frac{1}{2}\, \vec{P}^{\,T} \cdot \mathbf{C}^{-1} \cdot \vec{P} \; + U(\vec{\Phi}) \tag{3.84}$$

$$= \frac{1}{2}\, \vec{q}^{\,T} \cdot \mathbf{C}^{-1} \cdot \vec{q} \; + U(\vec{\Phi}) \tag{3.85}$$

Working through the classical Langrangian mechanics, we have just shown that the classical node fluxes $\vec{\Phi}$ and node charges $\vec{q}$ are, respectively, the conjugate position and momentum variables of our circuit. That is, the Poisson bracket of the node flux and node charge at a given node n is unity

$$\{\Phi_n, q_n\} = 1 \tag{3.86}$$

3.4.2 Writing the Quantum Mechanical Hamiltonian

In order to consider our qubit circuit quantum mechanically, we need to translate our Hamiltonian from a classical function of conjugate variables $H(\vec{q}, \vec{\phi})$ to a quantum mechanical operator $\hat{H}$. To do this, we simply substitute our classically conjugate variables for their corresponding quantum mechanical operators

$$\Phi_n \rightarrow \hat{\Phi}_n \tag{3.87}$$

$$q_n \rightarrow \hat{q}_n \tag{3.88}$$

Since we just showed that the classical variables Φ and q are canonically conjugate variables, the corresponding quantum operators obey the position-momentum commutation relation

$$[\hat{\Phi}_n, \hat{q}_n] = i\hbar \tag{3.89}$$

The quantum mechanical Hamiltonian for our three-junction qubit circuit can thus be written be in terms of its node operators as

$$\begin{aligned}\hat{H} = &\frac{1}{2}\sum_{\substack{i=1,2\\j=1,2}}(\mathbf{C}^{-1})_{ij}\,\hat{q}_i\hat{q}_j \\ &+ E_J\left(2+\alpha-\cos\frac{2\pi}{\Phi_0}\hat{\Phi}_1-\cos\frac{2\pi}{\Phi_0}\hat{\Phi}_2-\alpha\cos\frac{2\pi}{\Phi_0}(\hat{\Phi}_1-\hat{\Phi}_2+\Phi_{\text{ext}})\right)\end{aligned} \tag{3.90}$$

We will now perform one last change of variables. Rather than express the Hamiltonian in terms of the node flux $\hat{\Phi}$ and charge $\hat{q}$, we can substitute these variables for their more evidently quantized counterparts

$$\hat{\Phi}_n \to \frac{\Phi_0}{2\pi}\,\hat{\phi}_n \tag{3.91}$$

$$\hat{q}_n \to 2e\,\hat{n}_n \tag{3.92}$$

where, once again, $\hat{\phi}$ is the gauge-invariant phase operator across a node and $\hat{n}$ is the number operator corresponding to the number of Cooper pairs (charge $2e$) on each node. These quantities are also conjugate variables, and the operators obey the commutation relationship

$$[\hat{\phi}_n, \hat{n}_n] = i \tag{3.93}$$

Making these substitutions, our Hamiltonian is now given by

$$\begin{aligned}\hat{H} = &\,2e^2\sum_{\substack{i=1,2\\j=1,2}}(\mathbf{C}^{-1})_{ij}\,\hat{n}_i\hat{n}_j \\ &+ E_J\left(2+\alpha-\cos\hat{\varphi}_1-\cos\hat{\varphi}_2-\alpha\cos\left(\hat{\varphi}_1-\hat{\varphi}_2+\frac{2\pi}{\Phi_0}\Phi_{\text{ext}}\right)\right)\end{aligned} \tag{3.94}$$

Now that we have a quantum mechanical expression for the Hamiltonian of our circuit in terms of conjugate node operators, we can find the energy levels on the circuit by numerically diagonalizing the Hamiltonian and recording its eigenvalues. Before we can explicitly write out our Hamiltonian matrix, we need to choose which basis we express our operators in. The two most obvious options are the flux basis

and the charge basis, which are equivalent to the position and momentum bases respectively.[4] While either basis will do the job, we will choose the charge basis for the remainder of this example.

Working in the charge basis, our basis states correspond to having an integer number of excess Cooper pairs at the node. By definition, the charge operator written in the charge basis is diagonal, and the number operator can thus be written as the diagonal matrix

$$\hat{n} = \begin{bmatrix} \ddots & & & & & & \\ & -2 & & & & & \\ & & -1 & & & & \\ & & & 0 & & & \\ & & & & 1 & & \\ & & & & & 2 & \\ & & & & & & \ddots \end{bmatrix} \tag{3.95}$$

In principle, this matrix has infinite dimension. However, since the energy required to put an additional Cooper pair on the island increases quadratically with n, the lowest energy eigenstates of the circuit (the ones we will use for our qubit states $|0\rangle$ and $|1\rangle$) will be most affected by small values of n. To make this computationally tractable, we will truncate our Hilbert space to allow for a finite number of states with a maximum of n_q Cooper pairs. Our charge operator for the nth node is now given by the finite matrix of dimension $2n_q + 1$

$$\hat{n}_n = \begin{bmatrix} -n_q & & & & \\ & -n_q+1 & & & \\ & & \ddots & & \\ & & & n_q - 1 & \\ & & & & n_q \end{bmatrix}_n \tag{3.96}$$

Now that we have a matrix form of the number operator at each node $\hat{n}_n$, we can

[4] Though, as we will see when we get to the case of non-negligible linear inductance, these are not the only options.

plug this matrix into out expression for the kinetic energy operator for our qubit

$$\hat{T} = 2e^2 \sum_{\substack{i=1,2 \\ j=1,2}} (\mathbf{C}^{-1})_{ij}\, \hat{n}_i \hat{n}_j \tag{3.97}$$

where the product $\hat{n}_i\hat{n}_j$ is a *tensor product* of the two matrices

$$\hat{n}_i\hat{n}_j \equiv \begin{bmatrix} -n_q & & & & \\ & -n_q+1 & & & \\ & & \ddots & & \\ & & & n_q-1 & \\ & & & & n_q \end{bmatrix}_i \otimes \begin{bmatrix} -n_q & & & & \\ & -n_q+1 & & & \\ & & \ddots & & \\ & & & n_q-1 & \\ & & & & n_q \end{bmatrix}_j \tag{3.98}$$

since each node is an independent degree of freedom and thus has its own Hilbert space.

Next, let's consider the potential energy operator

$$\hat{U} = E_J \left(2 + \alpha - \cos\hat{\phi}_1 - \cos\hat{\phi}_2 - \alpha\cos\left(\hat{\phi}_1 - \hat{\phi}_2 + \frac{2\pi}{\Phi_0}\Phi_{\text{ext}} \right) \right) \tag{3.99}$$

which we will now write in terms of complex exponentials

$$\begin{aligned} \hat{U} = {} & 2E_J + \alpha E_J \\ & - \frac{E_J}{2}\left(e^{-i\hat{\phi}_1} + e^{+i\hat{\phi}_1} \right) - \frac{E_J}{2}\left(e^{-i\hat{\phi}_2} + e^{+i\hat{\phi}_2} \right) \\ & - \frac{\alpha E_J}{2} e^{-i\frac{2\pi}{\Phi_0}\Phi_{\text{ext}}} \left(e^{-i\hat{\phi}_1} e^{+i\hat{\phi}_2} \right) - \frac{\alpha E_J}{2} e^{+i\frac{2\pi}{\Phi_0}\Phi_{\text{ext}}} \left(e^{+i\hat{\phi}_1} e^{-i\hat{\phi}_2} \right) \end{aligned} \tag{3.100}$$

Written explicitly in this form, we notice that the exponentials involving the node phase operators are in fact the charge displacement operators

$$\hat{D}^{\pm} = e^{\mp i\hat{\phi}} \tag{3.101}$$

and correspond to either adding or removing a single Cooper pair from the node.[5] In

[5] This is analogous to how, in position-momentum space, the momentum operator is the generator of spatial translations $\hat{D}(x) = \exp(-i\hat{p}_x/\hbar)$.

the charge basis, the charge displacement operators for the nth node are given by the off-diagonal matrices

$$\hat{D}_n^+ = \begin{bmatrix} \ddots & 1 & & & & & \\ & 0 & 1 & & & & \\ & & 0 & 1 & & & \\ & & & 0 & 1 & & \\ & & & & 0 & 1 & \\ & & & & & 0 & 1 \\ & & & & & & \ddots \end{bmatrix}_n \tag{3.102}$$

$$\hat{D}_n^- = \begin{bmatrix} \ddots & & & & & & \\ 1 & 0 & & & & & \\ & 1 & 0 & & & & \\ & & 1 & 0 & & & \\ & & & 1 & 0 & & \\ & & & & 1 & 0 & \\ & & & & & 1 & \ddots \end{bmatrix}_n \tag{3.103}$$

where, as with the charge operators, these infinite matrices can be truncated to finite dimension $2n_q + 1$.

Collecting these results and explicitly writing out the Hamiltonian in Eq. (3.94) as a $(2n_q + 1) \times (2n_q + 1)$ matrix, the energy spectrum of the circuit can be found by numerically solving for the eigenvalues of the matrix.

3.4.3 Dealing with Linear Inductance

In the circuit we have considered so far, all the inductance in the loop has come from the nonlinear Josephson junctions. In most circuits, this is a fair approximation. However, in circuits where the linear inductance of the loop is comparable to the Josephson inductance or smaller, the inductive energy term in the Hamiltonian will begin to dominate and must be accounted for. Schematically, we can model this by placing a lumped element inductor with inductance L in series with our three junctions, as illustrated in Fig. 3-6. Note that now that we've added a new circuit

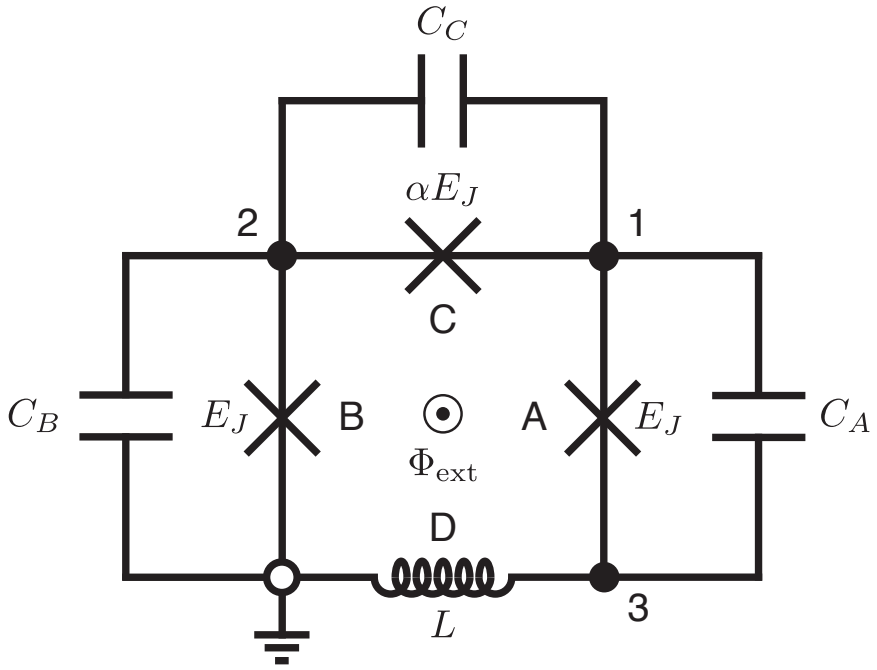

Figure 3-6: The qubit circuit from Fig. 3-4, now including a lumped-element inductor L which captures the combined linear inductance of the qubit loop. Adding this element requires the introduction of a third circuit node (labelled 3), which modifies the definition of the branch variables to those in Eqs. (3.105)–(3.108).

element, our circuit now has three ungrounded nodes rather than the two in the previous example.

To start, let's once again write down the total Josephson potential energy of our circuit

$$U_J = E_J \left(2 + \alpha - \cos\phi_A - \cos\phi_B - \cos\phi_C\right) \tag{3.104}$$

Translating from the branch phases ϕ_A, ϕ_B, ϕ_C, and ϕ_D to the node phases ϕ_1, ϕ_2,

and ϕ_3, we (arbitrarily) choose our spanning tree such that

$$\phi_A = \phi_1 - \phi_3 \tag{3.105}$$

$$\phi_B = \phi_2 \tag{3.106}$$

$$\phi_C = \phi_1 - \phi_2 + \frac{2\pi}{\Phi_0}\Phi_{\text{ext}} \tag{3.107}$$

$$\phi_D = \phi_3 \tag{3.108}$$

Making this change of variable, we can rewrite our expression for the total Josephson potential energy in terms of the three node variable

$$U_J = E_J \left(2 + \alpha - \cos(\phi_1 - \phi_3) - \cos\phi_2 - \cos\left(\phi_1 - \phi_2 + \frac{2\pi}{\Phi_0}\Phi_{\text{ext}}\right)\right) \tag{3.109}$$

Turning next to the electrostatic energy stored in the capacitive elements of our circuit, we can simply borrow the general expression we found in the previous example

$$T = \frac{1}{2}\,\vec{q}^{\,T} \cdot \mathbf{C}^{-1} \cdot \vec{q} \tag{3.110}$$

where, now that we have three nodes

$$\vec{q} = \begin{bmatrix} q_1 \\ q_2 \\ q_3 \end{bmatrix} \tag{3.111}$$

and the capacitive matrix $\mathbf{C}$ is now

$$\mathbf{C} = \begin{bmatrix} C_A + C_C & -C_C & -C_A \\ -C_C & C_B + C_C & 0 \\ -C_A & 0 & C_A \end{bmatrix} \tag{3.112}$$

Finally, now that we have introduced an inductance to our circuit, we must also consider the inductive energy it contributes to our circuit. The energy stored in the inductor is

$$U_{Ln} = \frac{1}{2} L_n I_n^2 \tag{3.113}$$

where I_n is the current flowing through the inductor, which can be related to the time derivative of the charge on the inductor's branch

$$I_n = \dot{q}_n \tag{3.114}$$

So, the energy U_L in our inductor can be written in terms of the time derivative of the charge on branch D

$$U_L = \frac{1}{2} L \dot{q}_D^2 \tag{3.115}$$

which can be rewritten in terms of the flux across the branch

$$U_L = \frac{1}{2L} \Phi_D^2 \tag{3.116}$$

which, for our particular choice of spanning tree, can be written in terms of the node flux

$$U_L = \frac{1}{2L} \Phi_3^2 \tag{3.117}$$

As we have already shown, the node fluxes Φ_n and node charges q_n are classically conjugate variables, and they can thus be substituted for their corresponding quantum mechanical operators $\hat{\Phi}_n$ and $\hat{q}_n$. Making this substitution, we get our quantum operators for the capacitive energy, the inductive energy, and the Josephson potential energy of our circuit

$$\hat{T}_C = \frac{1}{2} \sum_{\substack{i=1,2,3 \\ j=1,2,3}} (\mathbf{C}^{-1})_{ij} \, \hat{q}_i \hat{q}_j \tag{3.118}$$

$$\hat{U}_L = \frac{1}{2L} \hat{\Phi}_3^2 \tag{3.119}$$

$$\hat{U}_J = E_J \left(2 + \alpha - \cos \frac{2\pi}{\Phi_0} (\hat{\Phi}_1 - \hat{\Phi}_3) - \cos \frac{2\pi}{\Phi_0} \hat{\phi}_2 - \alpha \cos \frac{2\pi}{\Phi_0} \left(\hat{\Phi}_1 - \hat{\Phi}_2 + \Phi_{\text{ext}} \right) \right) \tag{3.120}$$

which combined give us the Hamiltonian of our circuit

$$\hat{H} = \hat{T} + \hat{U}_L + \hat{U}_J \tag{3.121}$$

Now that we have all the operators right in front of us, let's start writing them explicitly in matrix form. Once again, we'll replace the flux and charge variables at nodes 1 and 2 with the gauge-invariant phase and number operators

$$\hat{\Phi}_{1,2} \to \frac{\Phi_0}{2\pi}\,\hat{\phi}_{1,2} \tag{3.122}$$

$$\hat{q}_{1,2} \to 2e\,\hat{n}_{1,2} \tag{3.123}$$

from which we can get the relevant truncated matrices we found in Section 3.4.2

$$\hat{n}_{1,2} = \begin{bmatrix} -n_q & & & & \\ & -n_q+1 & & & \\ & & \ddots & & \\ & & & n_q-1 & \\ & & & & n_q \end{bmatrix}_{1,2} \tag{3.124}$$

$$e^{-i\hat{\phi}_{1,2}} = \hat{D}^{+}_{1,2} = \begin{bmatrix} 0 & 1 & & & \\ & 0 & 1 & & \\ & & \ddots & 1 & \\ & & & 0 & 1 \\ & & & & 0 \end{bmatrix}_{1,2} \tag{3.125}$$

$$e^{+i\hat{\phi}_{1,2}} = \hat{D}^{-}_{1,2} = \begin{bmatrix} 0 & & & & \\ 1 & 0 & & & \\ & 1 & \ddots & & \\ & & 1 & 0 & \\ & & & 1 & 0 \end{bmatrix}_{1,2} \tag{3.126}$$

What about node 3? Now that we've included the potential energy of our inductor,

our Hamiltonian now has a term which is parabolic in the flux across node 3:

$$\frac{1}{2L}\hat{\Phi}_3^2 \tag{3.127}$$

While we are free to write this term in the charge basis in much the same way we handled the Josephson junctions, the linear inductor lends itself naturally to a different choice of basis. Notice that node 3 essentially divides the circuit into two parts: on one side of ground, we have the linear inductance L; one the other, we have a collection of capacitive elements with combined series capacitance C_{Tot}

$$\frac{1}{C_{\text{Tot}}} = \frac{1}{C_A} + \frac{1}{C_B} + \frac{1}{C_C} \tag{3.128}$$

Indeed, when we invert the capacitance matrix in Eq. (3.112) to calculate the capacitive energy at each node

$$\mathbf{C}^{-1} = \begin{bmatrix} \frac{1}{C_B}+\frac{1}{C_C} & \frac{1}{C_B} & \frac{1}{C_B}+\frac{1}{C_C} \\ \frac{1}{C_B} & \frac{1}{C_B} & \frac{1}{C_B} \\ \frac{1}{C_B}+\frac{1}{C_C} & \frac{1}{C_B} & \frac{1}{C_A}+\frac{1}{C_B}+\frac{1}{C_C} \end{bmatrix} \tag{3.129}$$

we find that the matrix element corresponding to node 3 is simply the inverse of the total series capacitance in the circuit

$$\mathbf{C}_{33}^{-1} = \frac{1}{C_A} + \frac{1}{C_B} + \frac{1}{C_C} \tag{3.130}$$

$$= C_{\text{Tot}}^{-1} \tag{3.131}$$

We can thus think of our qubit as a simple LC-oscillator (Fig. 3-7), with node 3 as its single degree of freedom.

Following this train of thought, we can instead write the operators for node 3 in the *oscillator basis*, where we take as our basis states the quantized energy levels of the simple harmonic oscillator. Recalling the Hamiltonian for the quantum harmonic LC-oscillator in Section 3.2

$$\hat{H}_{\text{osc}} = \frac{\hat{q}^2}{2C} + \frac{\hat{\Phi}^2}{2L} \tag{3.132}$$

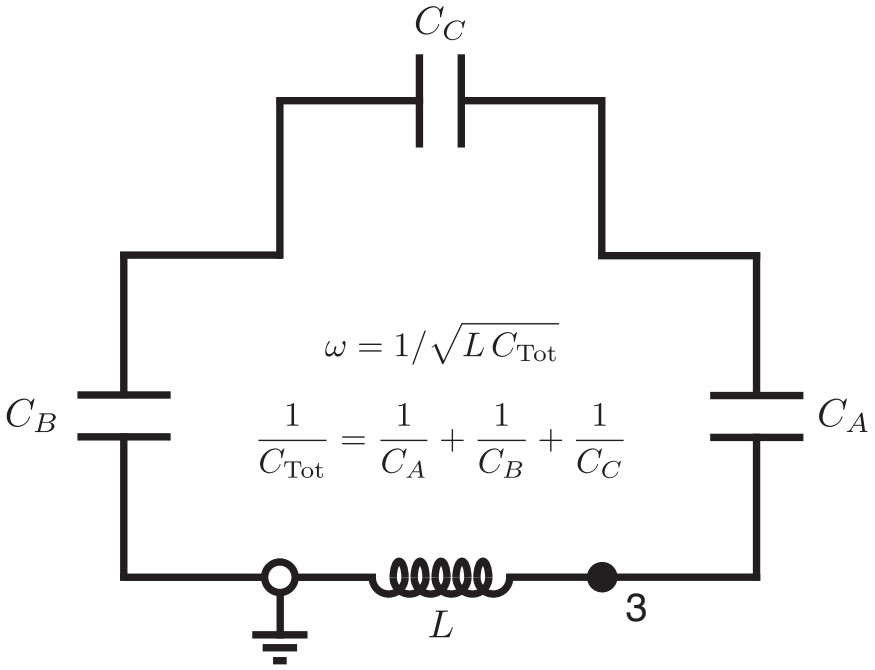

Figure 3-7: The qubit circuit from Fig. 3-6, where node 3 is now thought of as the single node of an LC circuit formed by the inductance L and the total series capacitance of the circuit C_{Tot} (fundamental frequency: $\omega = \sqrt{1/L\,C_{\text{Tot}}}$). The charge and flux operators at node 3 ($\hat{q}_3, \hat{\Phi}_3$) can thus be written in the oscillator basis as in Eq. (3.134) and (3.136).

we can thus rewrite the flux and charge operators in the oscillator basis as

$$\hat{\Phi} = \sqrt{\frac{\hbar\omega_0 L}{2}}(\hat{a}^\dagger + \hat{a}) \tag{3.133}$$

$$= \sqrt{\frac{\hbar Z_0}{2}}(\hat{a}^\dagger + \hat{a}) \tag{3.134}$$

$$\hat{q} = i\sqrt{\frac{\hbar\omega_0 C}{2}}(\hat{a}^\dagger - \hat{a}) \tag{3.135}$$

$$= i\sqrt{\frac{\hbar}{2Z_0}}(\hat{a}^\dagger - \hat{a}) \tag{3.136}$$

where $\hat{a}^\dagger$ and $\hat{a}$ are the creation and annihilation operators respectively, $Z_0 = \sqrt{L/C}$ is the characteristic impedance of the circuit, and $\omega_0 = 1/\sqrt{LC}$ is the characteristic frequency of the LC oscillator. Substituting these operators into the oscillator

Hamiltonian in Eq. (3.132), we get the familiar result

$$\hat{H}_{\text{osc}} = \hbar\omega_0 \left(\hat{a}^\dagger \hat{a} + \frac{1}{2}\right) = \hbar\omega_0 \left(\hat{N} + \frac{1}{2}\right) \tag{3.137}$$

where $\hat{N} \equiv \hat{a}^\dagger \hat{a}$ is the oscillator number operator

$$\hat{N} = \begin{bmatrix} 0 & & & \\ & 1 & & \\ & & 2 & \\ & & & \ddots \end{bmatrix} \tag{3.138}$$

With this in mind, we can easily write out the charge and flux operators for the third node in matrix form:

$$\hat{q}_3 = i\sqrt{\frac{\hbar}{2Z_0}}(\hat{a}_3^\dagger - \hat{a}_3) \tag{3.139}$$

$$= i\sqrt{\frac{\hbar}{2Z_0}} \begin{bmatrix} 0 & -\sqrt{1} & & & & \\ \sqrt{1} & 0 & -\sqrt{2} & & & \\ & \sqrt{2} & 0 & & & \\ & & & \ddots & & \\ & & & & 0 & -\sqrt{N-1} \\ & & & & \sqrt{N-1} & 0 \end{bmatrix} \tag{3.140}$$

$$\hat{\Phi}_3 = \sqrt{\frac{\hbar Z_0}{2}}(\hat{a}_3^\dagger + \hat{a}_3) \tag{3.141}$$

$$= \sqrt{\frac{\hbar Z_0}{2}} \begin{bmatrix} 0 & \sqrt{1} & & & & \\ \sqrt{1} & 0 & \sqrt{2} & & & \\ & \sqrt{2} & 0 & & & \\ & & & \ddots & & \\ & & & & 0 & \sqrt{N-1} \\ & & & & \sqrt{N-1} & 0 \end{bmatrix} \tag{3.142}$$

where the creation and annihilation operators have been truncated to allow for a maximum of N oscillator states.

The only matrices we still need to complete our Hamiltonian are the ones corresponding to the charge displacement operators $\hat{D}_3^{\pm} = \exp\left(\mp i 2\pi \hat{\Phi}_3/\Phi_0\right)$. Unfortu-

nately, writing the displacement operators in the oscillator basis is not as simple as it is in the charge basis. Instead, we can rely on the Taylor series definition of the exponential, expanding the operator out in powers of $\hat{\Phi}_3$

$$e^{\pm i\frac{2\pi}{\Phi_0}\hat{\Phi}_3} \equiv 1 + \left(\pm i\frac{2\pi}{\Phi_0}\hat{\Phi}_3\right) + \frac{1}{2!}\left(\pm i\frac{2\pi}{\Phi_0}\hat{\Phi}_3\right)^2 + \frac{1}{3!}\left(\pm i\frac{2\pi}{\Phi_0}\hat{\Phi}_3\right)^3 + \cdots \tag{3.143}$$

Alternatively, we can integrate the matrix elements of the displacement operator analytically, obviating the need for any series approximation.

Writing out the full Hamiltonian of our system

$$\hat{H} = \hat{T} + \hat{U}_L + \hat{U}_J \tag{3.144}$$

$$= \frac{1}{2}\sum_{\substack{i=1,2,3\\j=1,2,3}} (\mathbf{C}^{-1})_{ij}\,\hat{q}_i\hat{q}_j + \frac{1}{2L}\hat{\Phi}_3^2 + E_J\left(2 + \alpha - \cos\left(\hat{\phi}_1 - \frac{2\pi}{\Phi_0}\hat{\Phi}_3\right) - \cos\hat{\phi}_2 - \alpha\cos\left(\hat{\phi}_1 - \hat{\phi}_2 + \frac{2\pi}{\Phi_0}\Phi_{\text{ext}}\right)\right) \tag{3.145}$$

notice that we can now get rid of the parabolic potential energy term simply by replacing the capacitive and inductive energies at node 3 with the oscillator Hamiltonian

$$\hat{H}_{\text{osc}} = \frac{1}{2C}\hat{q}_3^2 + \frac{1}{2L}\hat{\Phi}_3^2 \tag{3.146}$$

$$= \hbar\omega_0\left(\hat{N}_3 + \frac{1}{2}\right) \tag{3.147}$$

Making this replacement and inserting all operators in their correct basis, we at last

get the Hamiltonian for our circuit

$$\hat{H} = \hat{T}' + \hat{H}_{\text{osc}} + \hat{U}_J \tag{3.148}$$

$$\begin{aligned} &= 2e^2 \sum_{\substack{i=1,2 \\ j=1,2}} (\mathbf{C}^{-1})_{ij}\, \hat{n}_i \hat{n}_j + e^2 \sum_{i=1,2} (\mathbf{C}^{-1})_{i3}\, \hat{n}_i \hat{q}_3 + e^2 \sum_{j=1,2} (\mathbf{C}^{-1})_{3j}\, \hat{q}_3 \hat{n}_j \\ &\quad + \hbar\omega_0 \left(\hat{N}_3 + \frac{1}{2} \right) \\ &\quad + E_J \left(2 + \alpha - \cos\left(\hat{\phi}_1 - \frac{2\pi}{\Phi_0} \hat{\Phi}_3 \right) - \cos\hat{\phi}_2 - \alpha \cos\left(\hat{\phi}_1 - \hat{\phi}_2 + \frac{2\pi}{\Phi_0} \Phi_{\text{ext}} \right) \right) \end{aligned} \tag{3.149}$$

This Hamiltonian is quite a bit more complicated than the one we found for the transmon qubit in Eq. (3.54). And yet, having picked a set of design values for the capacitances, inductances, and Josephson energies, we can simply plug these values into the equation above and diagonalize the resulting Hamiltonian matrix to find the energy levels of the resulting flux qubit. In the following section, we will do exactly this. Starting from measurements of a novel variation of the flux qubit (the capacitively-shunted or C-shunt flux qubit), we will optimize over the parameters in this Hamiltonian to find the most likely set of circuit parameters which the qubits are composed of.

3.5 The C-shunt Flux Qubit

In their simplest formulations, the transmon and the flux qubit are electrical duals of one another. As we showed in Section 3.3, the transmon can be thought of as a Josephson junction shunted by a capacitor (Fig. 3-8a). Indeed, when this circuit is operated outside the transmon limit ($E_J \gg E_C$), it is known simply as the *charge qubit*, since the basis states are well approximated as the charge states of the circuit [324].[6] Meanwhile, looking at the Hamiltonian we derived in Section 3.4, we can see that—in the limit where the shunt capacitors across each junction is simply

[6]This circuit was, in fact, the first realization of a coherent superconducting qubit and was originally know as a *Cooper-pair box* due to the paired electrons which tunnel on and off the superconducting island between the capacitor and junction [70, 273, 324].

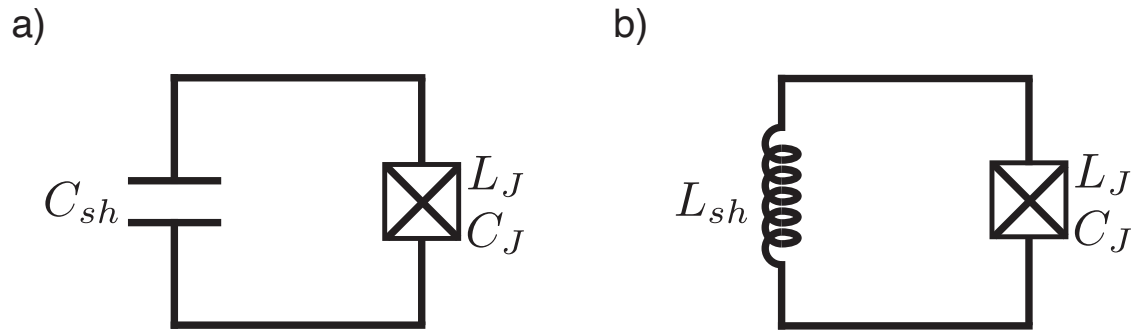

Figure 3-8: The Charge Qubit and the Flux Qubit. **(a)** Electrical circuit diagram of the general charge qubit, where the Josephson junction is shunted by a capacitor C_{sh}. In the limit where $E_J \gg E_C$ (large C_{sh}) this circuit is known as the transmon qubit. **(b)** Circuit diagram of the general flux qubit, where the Josephson junction is instead shunted by a linear inductor L_{sh}.

equal to the small intrinsic capacitor of the junction $C_\Sigma = C_J$—the flux qubit can be thought of as a Josephson junction shunted by the combined inductance of the large junctions and the linear inductor (Fig. 3-8b). In this circuit, the basis states of the circuit are well approximated as the flux states of the circuit, hence the name.

In this section, we will briefly introduce a novel superconducting circuit developed at MIT which combines aspects of both of these circuit paradigms: the capacitively-shunted flux qubit, or C-shunt flux qubit for short. In comparison to the first generation of flux qubits developed in the late 1990s [313, 345], the C-shunt flux qubits offered two key innovations which improved the resilience of the qubit to noise in the environment:

1. The critical currents of the Josephson junctions in the qubit loop are significantly reduced, both by decreasing the physical area of the junctions and by reducing the critical current density J_c of the superconductor-normal-superconductor (SNS) interface. This reduction in critical current reduces the sensitivity of the qubit energy levels to external flux bias, decreasing the susceptibility of the qubit to magnetic flux noise in the environment. This susceptibility to flux is given by the slope of the qubit's energy levels with respect to the external flux

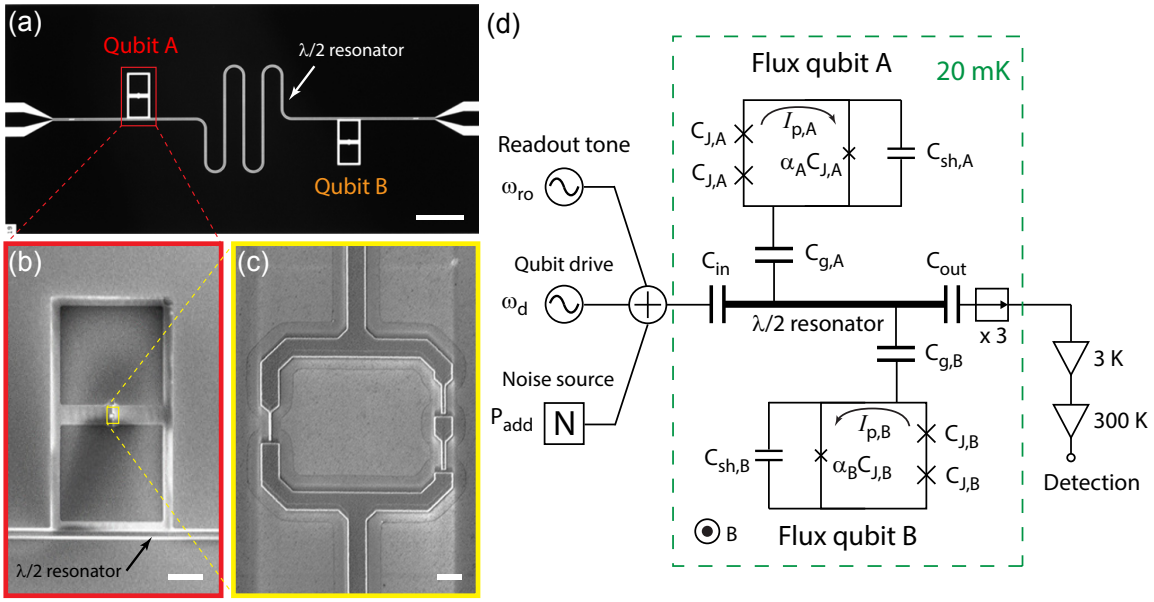

Figure 3-9: The C-shunt flux qubit, experimentally. **(a)** Optical micrograph of two capacitively-shunted flux qubits (labeled A and B) coupled to a common $\lambda/2$ coplanar waveguide for readout. The qubits and waveguide are fabricated out of superconducting aluminum (black) deposited on top of a sapphire substrate (white, where aluminum has been etched away). (Scale bar: 0.5mm.) **(b)** SEM image of qubit A. Together, the two 200×200 μm^2 square pads form a large parallel plate shunt capacitor across the Josephson junctions, the hallmark of the C-shunt flux qubit. (Scale bar: 50μm.) **(c)** Magnified SEM image of the qubit loop, with one small Josephson junction (left side of loop) in parallel with two larger junctions in series (right side). (Scale bar: 50μm.) **(d)** Equivalent electrical circuit diagram of the two qubits capacitively coupled to the $\lambda/2$ resonator, including signal generator for the qubit readout ω_{ro}, qubit drive ω_{d}, and external noise source for studying qubit coherence $\mathrm{P}_{\mathrm{add}}$. A global magnetic field B is applied perpendicular to the qubit chip, inducing an external flux Φ_b through each qubit loop. [481]

bias, a quantity known as the *persistent current* of the flux qubit I_p

$$I_p = \frac{dE}{d\Phi} \tag{3.150}$$

2. The effective capacitance of the small Josephson junction is dramatically increased by shunting the junction with a large capacitor ($C_{sh} \gg C_J$), in much the same way as the transmon qubit. Like the transmon, this shunt capacitor reduces the capacitive energy term in the qubit Hamiltonian, reducing the susceptibility of the qubit to electric charge noise. In addition, this large dramti-

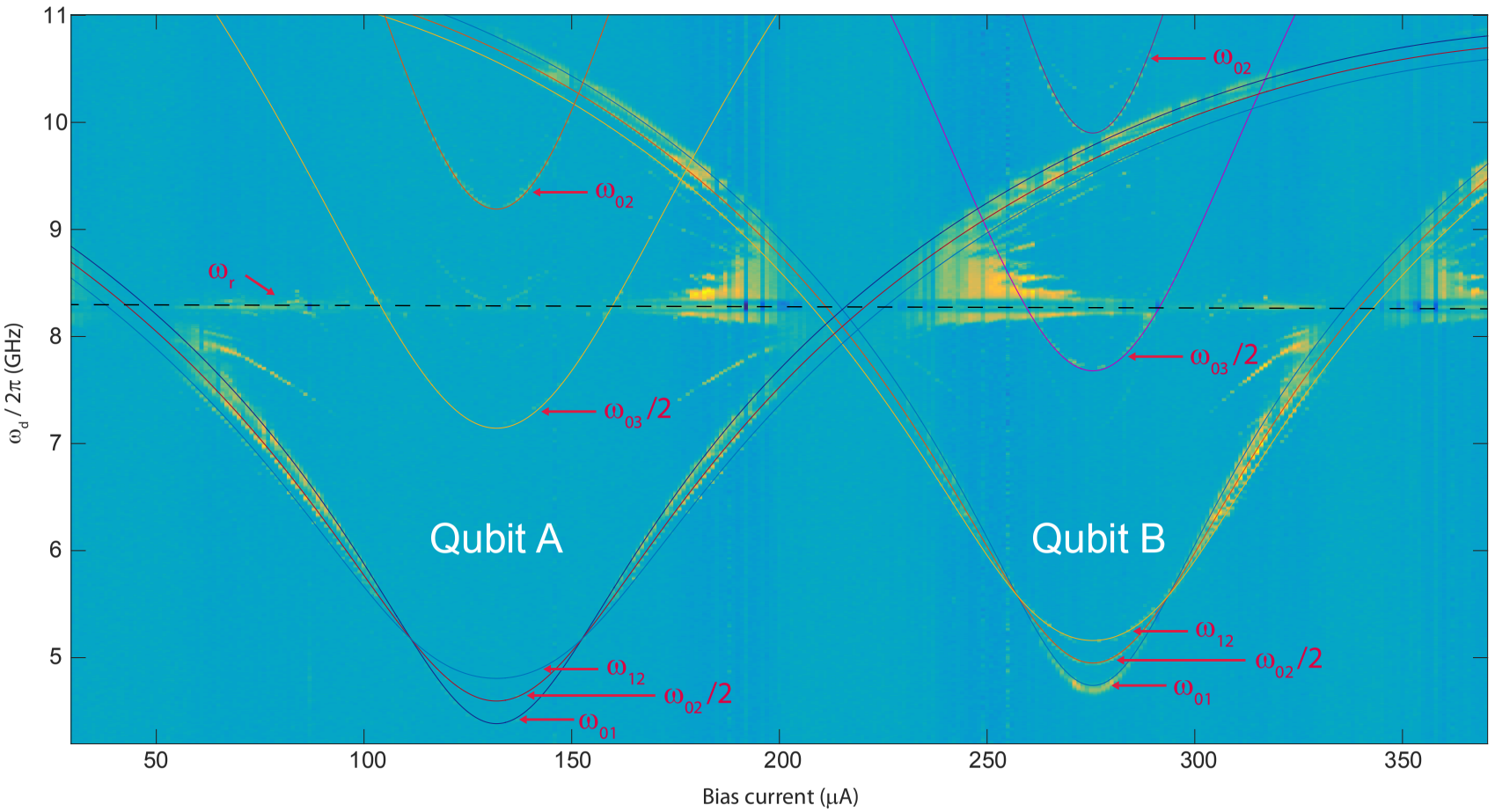

Figure 3-10: High-power spectroscopy of two C-shunt flux qubits A and B in Fig. 3-9, versus a magnetic flux bias Φ_b through the qubit loop of each. The energy levels are fitted to simulation (solid lines) by running a Nelder-Mead optimization of the quantized Hamiltonian over all design parameters of each qubit: the shunt capacitances, Josephson junction sizes, critical current density J_c, specific capacitance S_c, and linear inductance L. Running the optimizer, a set of parameters are found which fit numerous transitions of each qubit for a broad range of external flux bias Φ_{ext}. Figure courtesy of the author, as it appears in Ref. [481].

Parameter	Qubit A	Qubit B
Critical current density, J_c	$1.985\mu\text{A}/\mu\text{m}^2$	
Specific capacitance, S_c	$71.3\text{fF}/\mu\text{m}^2$	
Shunt capacitance, C_{sh}	49.712fF	
Loop inductance, L	24.964pH	
Area of small junction	$0.01876\mu\text{m}^2$	$0.02126\mu\text{m}^2$
Area of each large junction	$0.05542\mu\text{m}^2$	$0.06276\mu\text{m}^2$
Anharmonicity, $f_{12} - f_{01}$	423MHz	420MHz

Table 3.1: Table of device parameters for qubits A and B, extracted from fitting high power spectroscopy of both qubits (Fig. 3-10). Since both qubits were fabricated on the same wafer and designed to be geometrically identical except for the junction sizes, we simplified the optimization by contraining both qubits to have the same values of J_c, S_c, C_{sh}, and L. Running the optimization, we find a set of junction sizes for each qubit which successfully account for the difference in energy spectra between the two devices.

cally improves the reproducibility of the circuit. Since the intrinsic capacitance of the small Josephson junction is the only capacitance in the traditional flux qubit Hamiltonian (see C_J in Fig. 3-8b), small deviations in this value due to fabrication errors (for example, a deviation in the junction size by less than a nanometer) or stray capacitances will dramatically alter the energy spectrum of the resulting qubit. By shunting the junction with a large parallel capacitance, the role of the intrinsic junction capacitance is significantly depreciated, reducing the sensitivity of the circuit to systematic changes in this value.

In the previous sections, we saw how we can use circuit quantization to determine the energy spectrum of a superconducting qubit from a set of electrical parameters. Here, we can do the inverse. After fabricating and cooling the resulting circuit down to milliKelvin temperatures in a dilution refrigerator, we can measure the energy levels of the circuit in spectroscopy and use circuit quantization—coupled with a classical optimization algorithm such as Nelder-Mead [328]—to back out the most likely set of electrical parameters which gave rise to the observed spectrum.

To accomplish this, we performed high-power spectroscopy of both qubits as a function of drive frequency (Fig. 3-10, y-axis) and magnetic flux bias (x-axis), exciting

multiple single- and two-photon transitions between the $|0\rangle, |1\rangle, |2\rangle$, and $|3\rangle$-states of the qubits. Taking the set of transition frequencies observed in spectroscopy, we ran an optimizer over the full set of electrical parameters in the circuit, diagonalizing the Hamiltonian for each set of parameters and iterating until we converges on a spectrum which matches measurement. The results of the optimization are shown in Fig. 3-10, where the overlaid solid lines correspond to the simulated spectra which best fit the data (2D color map underneath, resonant features appearing in yellow). In Table 3.1, we record the set of electrical parameters extracted during the optimization.

Chapter 4

Coherent Coupled Qubits

In Chapter 3, we saw how to engineer a single quantum bit out of a superconducting Josephson circuit. Starting from an arrangement of capacitors, inductors, and Josephson junctions, we quantized the resulting circuit Hamiltonian and extracted the energy spectrum of the circuit. Harnessing the anharmonicity of these circuits, we were free to pick out a pair of energy levels—for example, the ground and first excited states—and call those wavefunctions the $|0\rangle$- and $|1\rangle$-states of our qubit. In this chapter, we will extend the discussion in the previous chapter from one qubit in isolation to two coupled qubits. In the process, we will show how to design and engineer multi-qubit Hamiltonians of the kind we saw in Section 2.6, consisting of products of Pauli operators.

Coupled qubits are the backbone of any quantum processor, and we will consider such circuits from multiple angles throughout the remainder of this thesis: in Part III, we will see how coupled transmon qubits can be harnessed to implement two-qubit entangling operations in quantum algorithms; in Part IV, we will study the errors which arise due to always-on coupling between qubits, particularly non-Markovian errors. However, as a first example, we will consider a different but related paradigm of

This chapter is based in large part on original work reported in Ref. [463], and I gratefully acknowledge all of my coauthors for their contributions to this work, with particular acknowledgment to Steven Weber, David Hover, William Oliver, and Jamie Kerman.

coupled qubits: C-shunt flux qubits galvanically coupled to an rf-SQUID for analogue quantum computation. This circuit, we will see, implements a ZZ-interaction between the two qubits whose strength and sign can be tuned *in situ* via an external flux through the coupler loop. In this way, the two qubits can be effectively mapped onto a pair of spins governed by the transverse Ising model, the elementary building block of a quantum annealer.

4.1 Quantum Annealing and the Ising Model

In Chapter 2, we showed how a system of interacting qubits will evolve under the influence of a multi-qubit Hamiltonian, becoming entangled with one another over time. In Part III, we will see how such Hamiltonians can be harnessed to perform discrete logic gates between qubits and concatenated to perform quantum algorithms. In this chapter, however, we will briefly consider the design considerations for an alternative paradigm of quantum computation known as *quantum annealing*. Unlike the gate-model quantum processors in Part III—where the algorithms are 'digital,' in the sense that the qubits are analogous to the bits of a classical computer and manipulated using discrete logic gates—quantum annealers are *analog* computing devices, in the sense that the computation of interest is encoded into the continuous time evolution of the system.

Consider a multi-qubit Hamiltonian of the form

$$\hat{H} = \sum_i \left(\epsilon_i \, \hat{Z}_i + \Delta_i \, \hat{X}_i \right) + \sum_{i,j} J_{ij} \, \hat{Z}_i \otimes \hat{Z}_j \tag{4.1}$$

where $\hat{Z}$ and $\hat{X}$ are the familiar Pauli operators, and the coefficients ϵ_i, Δ_i, and J_{ij} are energies which set the relative strength of the different terms in the Hamiltonian. Looking at the first sum in the Hamiltonian above, we see that each qubit i has a Hamiltonian with some weighting of single-qubit $\hat{Z}$ and $\hat{X}$ operators; looking at the second sum, we see that every pair of qubits i, j is coupled with a two-qubit interaction of the form $\hat{Z} \otimes \hat{Z}$. As we saw in Chapter 2, when all the interaction terms are set to

zero ($J_{ij} = 0$ for all pairs i, j), each qubit will traverse a path in its individual Bloch sphere, completely divorced from the evolution of every other qubit in the system. When the interaction are not set to zero, the qubits will begin to talk to each other and, in their conversation, become entangled.

What happens when we modify the coefficients in the Hamiltonian above as functions of time? As an example, let's regroup the terms in the Hamiltonian such that the terms proportional to $\hat{Z}$ and $\hat{Z} \otimes \hat{Z}$ change in time together according to some function $\Lambda(t)$, while the terms proportional to $\hat{X}$ change in time according to an independent function $\Gamma(t)$

$$\hat{H}(t) = \Lambda(t) \left(\sum_i \epsilon_i(t)\, \hat{Z}_i + \sum_{i,j} J_{ij}(t)\, \hat{Z}_i \otimes \hat{Z}_j \right) + \Gamma(t) \sum_i \Delta_i(t)\, \hat{X}_i \tag{4.2}$$

At $t = 0$, let $\Lambda(0) = 0$ and $\Gamma(0) = 1$ such that the Hamiltonian of the system only has single-qubit $\hat{X}$ terms

$$\hat{H}(t = 0) = \Delta \sum_i \hat{X}_i \tag{4.3}$$

where, for simplicity, we have set all the energies Δ_i equal to one another and pulled it out of the sum. Looking at this Hamiltonian, we can see that the lowest energy eigenstate of the system is trivial. As we showed in Chapter 2, the eigenstates of $\hat{X}$ are the superposition states $|+\rangle$ and $|-\rangle$, with eigenvalues $+1$ and -1 respectively. If Δ_i is positive, then the state $|-\rangle$ has the lower eigenvalue of the two and is thus the ground state of the Hamiltonian.

Since the qubits evolving under the Hamiltonian in Eq. (4.3) are totally uncoupled, the global ground state of the system of all N qubits is a product state of the single-qubit ground state

$$|\psi_0\rangle = |-\rangle^{\otimes N} \tag{4.4}$$

where the tensor product in the exponent is short-hand for the multi-qubit product state where all the qubits are in the same single-qubit state

$$|-\rangle^{\otimes N} \equiv |-\rangle_1 \otimes |-\rangle_2 \otimes \cdots \otimes |-\rangle_N \tag{4.5}$$

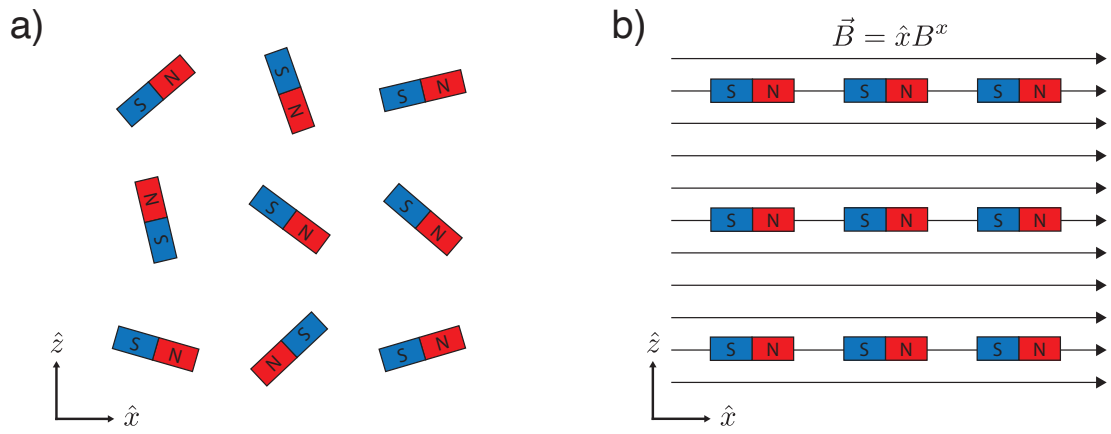

Figure 4-1: Spin systems, classically. **(a)** An array of classical bar magnets, arranged in the zx-plane. In the absence of an external magnetic field and interactions between the magnets, all orientations of the magnets are degenerate. **(b)** A uniform external magnetic field is applied in the $+\hat{x}$-direction, breaking the degeneracy. Once the field is applied, the lowest energy configuration of the system corresponds to all the magnets pointing in the $-\hat{x}$-direction. This classical picture is analogous to a multi-qubit system under the influence of the local Hamiltonians in Eq. (4.3), where the global ground state is the trivial product state in Eq. (4.5).

This global ground state has a nice physical interpretation from classical physics. Instead of thinking about qubits, imagine a large array of bar magnets as in Fig. 4-1. In this picture, the Hamiltonian in Eq. (4.3) is analogous to a uniform external magnetic field $\vec{B}$ applied to the array, pointing in the $+\hat{x}$-direction. Intuitively, we known what happens to the magnets under the influence of this external field: the moment the field turns on, all the bar magnets will align with the external magnetic field such that they each point in the $-\hat{x}$-direction, as in Fig. 4-1b. Once aligned, the magnets will have an energy Δ which is equal to the dot product of the magnetic field $\vec{B} = \hat{x}B^x$ and the dipole moment $\vec{\mu}$ of the magnet

$$\Delta = -\vec{B} \cdot \vec{\mu} \tag{4.6}$$

$$= -B^x \mu^x \tag{4.7}$$

Now, imagine that we slowly turn down the Δ coefficients in the Hamiltonian and turn up the ϵ and J coefficients such that, at the conclusion of the transition $t = T$,

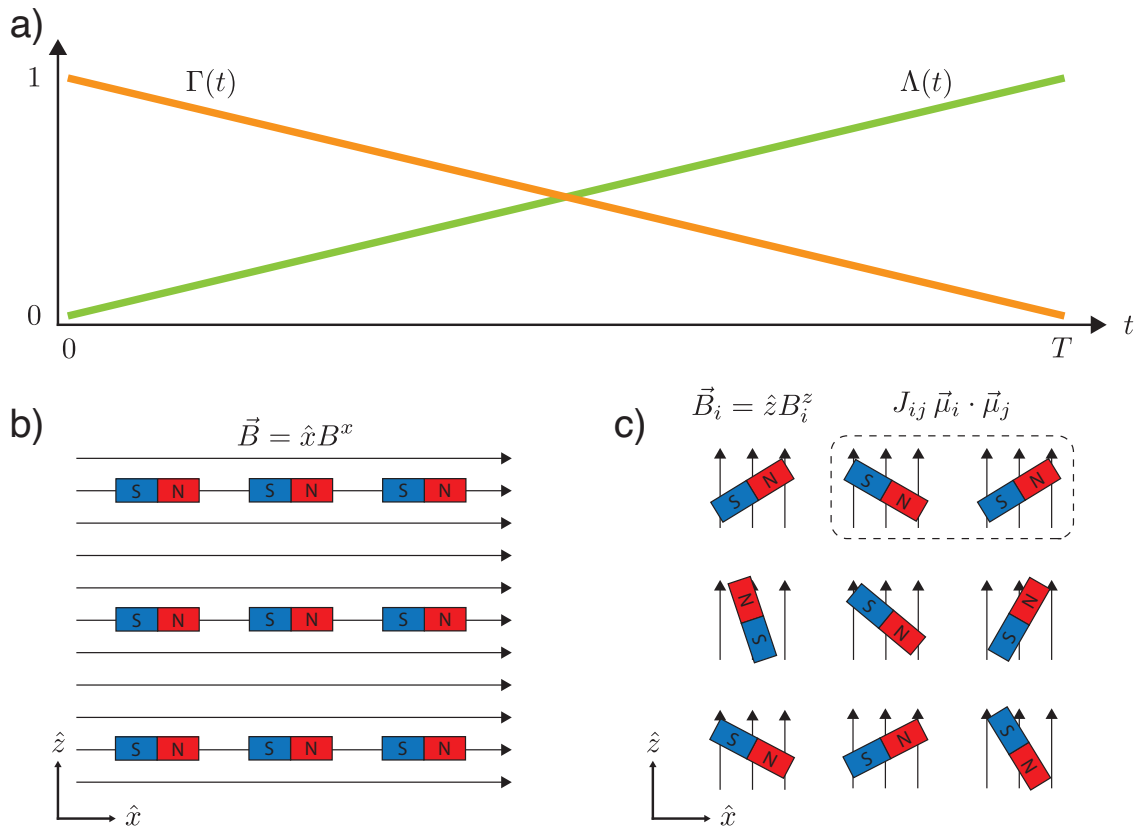

Figure 4-2: Quantum annealing, classically. **(a)** A simple quantum annealing schedule, where the coefficient $\Gamma(t)$ in Eq. (4.2) is linearly decreased and the coefficient $\Lambda(t)$ is increased. **(b)** Classical picture of the multi-qubit system at $t = 0$, where the qubits are governed by a uniform magnetic field and equilibriate to the trivial global ground state. **(c)** The system at $t = T$, where the uniform transverse field has been turned off and the Ising Hamiltonian in Eq. (4.8) has been turned on. At each site, a local magnetic field of variable strength is applied in the $\hat{z}$-direction, and interactions between pairs of sites are turned on. While the ground state of the general Ising Hamiltonian is extremely nontrivial, it can be obtained adiabatically by evolving the system from the initial trivial ground state in (b).

$\Lambda(T) = 1$ and $\Gamma(T) = 0$. The Hamiltonian will now have the form

$$\hat{H}(t = T) = \sum_i \epsilon_i \hat{Z}_i + \sum_{i,j} J_{ij}\, \hat{Z}_i \otimes \hat{Z}_j \tag{4.8}$$

In spin physics, this ubiquitous Hamiltonian is known as the Ising model. Classically, we can once again think of this Hamiltonian in terms of magnetic fields on an array of magnets, as in Fig. 4-2c. Here, the first sum corresponds to a set of local magnetic

fields on each of our bar magnets pointed in the $\hat{z}$-direction, where each magnet i has energy ϵ_i proportional to the strength of the local magnetic field $\vec{B}_i = \hat{z}B_i^z$

$$\epsilon_i = -\vec{B} \cdot \vec{\mu} \tag{4.9}$$

$$= -B_z \mu_z \tag{4.10}$$

As for the second sum in Eq. (4.8), these correspond to pairs of magnets experiencing the magnetic field generated by *each other*. Here, the energy of the interaction is proportional to the dot product of the two dipole moments

$$E_{\text{int}} = J_{ij}\, \vec{\mu}_i \cdot \vec{\mu}_j \tag{4.11}$$

In general, the strength of this interaction can be different for every pair of magnets in the array—for example, the magnets are varying distances away from each other and exert a different strength field on each of its neighbors.

Unlike the starting Hamiltonian in Eq. (4.3), the Hamiltonian in Eq. (4.8) does *not* have a trivial ground state: the moment the fields and interactions are suddenly turned on, there are a vast number of local minima which the system may find itself in, states which may have much larger energy than the global ground state. Indeed, for an array of magnets with completely general interaction strengths, solving for the global ground state in simulation is known to be an NP-complete problem [99, 215]. And yet, physics offers us an elegant way to solve this problem and find the ground state nonetheless. Imagine we tune our coefficients $\Lambda(t)$ and $\Gamma(t)$ very slowly in time. At $t = 0$, our system will be in the trivial ground state from Eq. (4.5), and we can verify this is the case by performing local measurements on each of the qubits. From here, we gradually turn down $\Gamma(t)$ and turn up $\Lambda(t)$ such that, at some later time $t = T$, our system is governed by the Ising Hamiltonian in Eq. (4.8). Now, if we tuned our coefficients slowly enough such that the system evolved *adiabatically*, the entire system will remain in the instantaneous ground state over the course of the entire evolution. Thus, the system at $t = T$ will be in the ground state of the Ising

Hamiltonian, solving the problem.

The protocol we just considered is known as *quantum annealing* [78, 137, 143, 227]: prepare a system in the ground state of a trivial Hamiltonian and gradually evolve the system into the ground state of a more complicated Hamiltonian. This final Hamiltonian may be interesting for physics reasons—for example, it corresponds to a complicated spin glass you wish to simulate the phase transitions of—but it could also be chosen such that it encodes a difficult classical problem. Indeed, in the limit that the evolution is purely adiabatic and the system remains in the ground state throughout the evolution, quantum annealing is equivalent to *adiabatic quantum computing* and is a form of universal quantum computation: for any arbitrary quantum algorithm, there exists a time-dependent Hamiltonian whose ground state encodes the algorithm's solution [11]. However, in practice, it is extremely difficult to ensure that the system remains in its ground state for the entirety of the evolution—as the size of the system grows, the gaps between energy eigenstates becoming exponentially small, increasing the likelihood of jumping out of the ground state as the Hamiltonian evolves—effectively thwarting the possibility of true adiabatic quantum computation.

Instead, modern quantum annealing systems are designed to solve hard optimization problems, where the final Hamiltonian encodes the cost function of the classical optimization—for example, the total distance traveled in a traveling salesman problem—is encoded into the final Hamiltonian. As such, even if the system fails to end up in the global ground state of the final Hamiltonian (corresponding to the most optimal solution of the problem), evolution to a higher excited state may still yield a solution which is more optimal than would be obtained using a classical optimizer. Unfortunately, unlike universal quantum computation, there is no formal proof of a quantum speedup using quantum annealing, and no experimental system to date has succeeded in demonstrating such a speedup [12, 65, 66, 116, 214, 234, 264, 292, 389].

4.2 Tunable ZZ-Coupling Between Coherent Flux Qubits

To date, it remains unclear why current-generation quantum annealers have not been able to demonstrate a quantum speedup. However, experience with existing quantum annealers—particularly the systems designed and engineered by D-Wave systems—suggests a number of potential avenues for improvement. The first generation of D-Wave annealers relied on niobium flux qubit with relatively short coherence times and pairwise couplings limited to a "Chimera" connectivity graph [79, 189]. These systems approximately realize the transverse Ising Hamiltonian in Eq. (4.1), where the eigenstates of the Pauli operator $\hat{Z}$ correspond to the persistent-current states of the individual flux qubits, which can be viewed as clockwise and counter-clockwise currents of magnitude I_{p} circulating around the qubit loop. The energies ϵ_i and Δ_i are then tuned *in situ* using local magnetic flux biases.

To implement the ZZ-interaction between the qubits, pairs of flux qubit are mutually coupled by way of an additional coupler circuit which mediates their interaction. These coupler elements [15, 16, 24, 75, 90, 188, 190, 228, 314, 334, 355, 356, 486] are themselves also flux qubits, though operated in a regime where they can be described as a simple flux-tunable effective inductance L_{eff}. Treating the coupler as such, the coupling energy between two qubits, each with persistent current I_{p} and mutual inductance M with the coupler, is given by

$$J = I_{\mathrm{p}}^2 M^2 / L_{\mathrm{eff}} \tag{4.12}$$

where M is the mutual inductance between each qubit and the coupler, and the quantity $1/L_{\mathrm{eff}}$ is known to as the *coupler susceptibility* [190].

As we can see in Eq. (4.12), the strength of the interaction between two flux qubits is largely determined by the magnitude of their persistent currents I_{p}: the larger the persistent current of each qubit, the stronger the coupling J. As it turns out, this is also the parameter which most directly affects the coherence of the flux

qubits. While qubits with large values of I_p strongly couple to one another, they also couple strongly to sources of magnetic flux noise in the environment, degrading their coherence. In this way, the persistent current I_p can be thought of as analogous to the magnetic dipole moment of a physical spin, setting the strength of interaction between pairs of spins and well as their sensitivity to fluctuations in the surrounding magnetic environment. For superconducting flux qubits, $1/f$ flux noise is the dominant noise source limiting the energy relaxation and the dephasing times, which roughly scale as $1/I_\mathrm{p}^2$ and $1/I_\mathrm{p}$ respectively [372, 480]. In the D-Wave system, the qubits are designed with large persistent currents $I_\mathrm{p} \sim 3$ μA [189] in order to achieve large coupling strength with modest values of coupler susceptibility and M, at the expense of dramatically reduced qubit coherence.

How might we design a system with strong coupling *and* long coherence? As we discussed in Section 3.5, the value of the persistent current can be significantly suppressed by capacitively shunting the qubit, leading to robust and long-lived devices with small persistent currents $I_\mathrm{p} \sim 50$ nA [480]. As we can see from Eq. (4.12), in order to realize strong coupling between qubits with small I_p, we must compensate by increasing either the mutual inductance M or the coupler susceptibility $1/L_\mathrm{eff}$. In exchange for a significant impovement in qubit coherence, this approach increases the qubit's sensitivity to flux noise in the coupler loop and requires more precise control over the coupler flux bias.

In the work which follows, we present the results of an experiment demonstrating tunable coupling between qubits with persistent currents reduced by nearly two orders of magnitude compared to existing quantum annealers. While coupled flux qubits with low persistent currents have been previously demonstrated [355], until the publication of this study, no work to date had investigated the implications that this design choice has on qubit coherence for quantum annealing. This work presented, for the first time, a systematic study of the coherence of coupled flux qubits in the context of quantum annealing. In particular, we investigate the effect of flux noise in the coupler loop on qubit coherence. Our results are in good agreement with simulations based on the full Hamiltonian of the coupled qubit system, as well

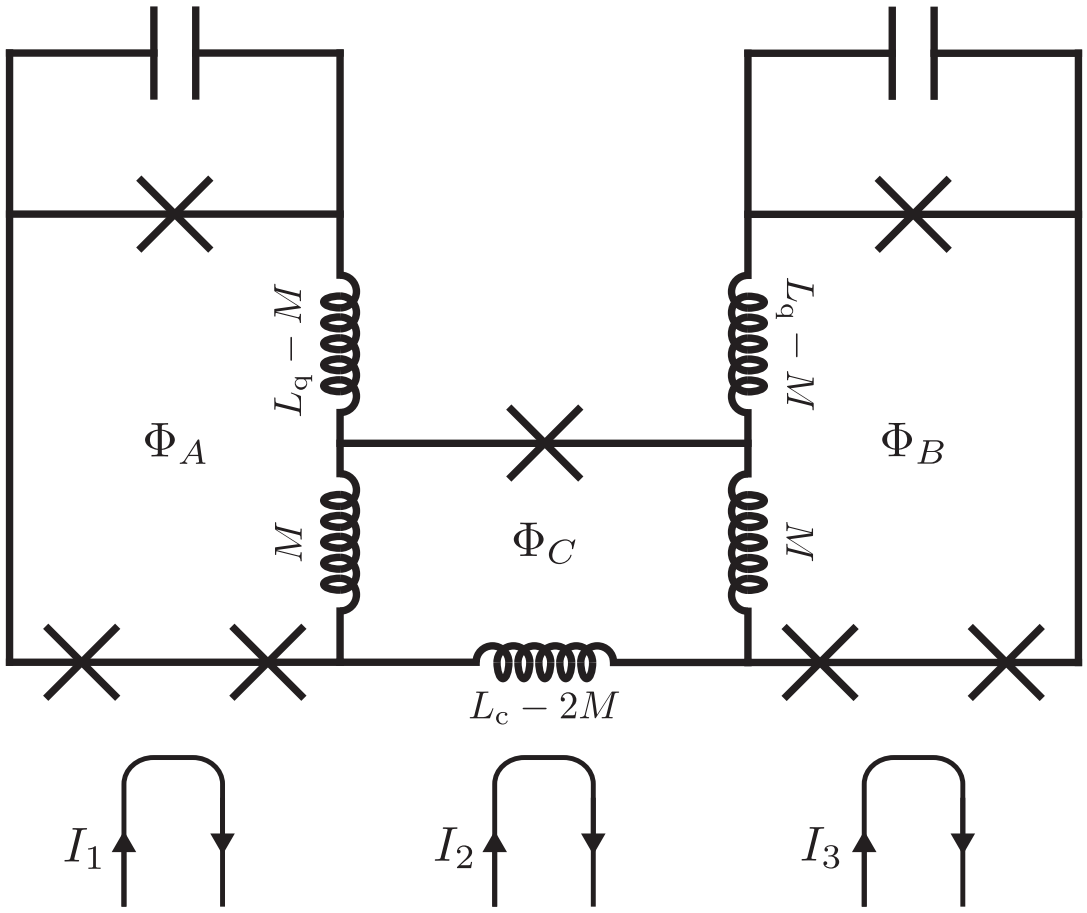

Figure 4-3: Schematic of ZZ-coupled C-shunt flux qubits. Qubit A (left loop) and Qubit B (right loop) are capacitively shunted three-junction flux qubits which are galvanically coupled to an rf-SQUID coupler C (center loop) which mediates their interaction. On-chip bias currents I_1, I_2, and I_3 induce the external fluxes Φ_A, Φ_C, and Φ_B through the qubit and coupler loops, tuning the individual qubit energies and the strength of their interaction. [463]

as a semi-classical model. This work serves as a proof-of-principle and provides a framework for evaluating coherence in future quantum annealing architectures.

4.2.1 Experimental Setup

In Fig. 4-3, we show a circuit diagram of the coupled qubit device used in this experiment. Here, two capacitively shunted three-junction flux qubits, Qubit A and Qubit B, are each galvanically coupled to an rf-SQUID coupler via a shared inductance of $M = 34$ pH, as shown in Fig. 4-4a–c. The parameters in the Ising Hamiltonian are

tuned via externally applied magnetic fluxes Φ_{A}, Φ_{B}, and Φ_{C} through the circuit loops. The qubits are measured using standard dispersive read out [55], with each qubit coupled to a separate readout resonator probed through a shared transmission line.

For this device, we designed the coupler to have a transition frequency $\omega_{\mathrm{C}}^{01}/2\pi \sim 20$ GHz between its ground- and first-excited state, which is significantly larger than the qubit transition frequencies at ~ 5 GHz. As a result, the coupled qubit system can be described by the approximate low-energy Hamiltonian [188]

$$H \approx H_{\mathrm{q}}^{(\mathrm{A})} + H_{\mathrm{q}}^{(\mathrm{B})} + H_{\mathrm{int}} \tag{4.13}$$

where

$$H_{\mathrm{q}}^{(i)} = \frac{\hbar}{2}\epsilon_i(\Phi_{\mathrm{A,B,C}})\hat{Z}^{(i)} + \frac{\hbar}{2}\Delta_i(\Phi_{\mathrm{A,B,C}})\hat{X}^{(i)} \tag{4.14}$$

$$H_{\mathrm{int}} = \hbar J(\Phi_{\mathrm{A,B,C}})\hat{Z}^{(\mathrm{A})}\hat{Z}^{(\mathrm{B})} \tag{4.15}$$

For the remainder of this chapter we will report the values of ϵ_i, Δ_i, and J in units of frequency rather than energy, hence the additional factors of $\hbar$ in the equations above. These effective parameters are determined by the circuit parameters of the individual qubits and coupler as well as by their couplings to each other, and can depend on all three flux biases. For each qubit, the degeneracy point is defined as the bias where $\epsilon_i = 0$.

In table 4.1, we record a list of sample parameters extracted from two different models of the coupled qubit system—a semi-classical model, where the individual qubits and coupler are treated quantum mechanically but their interactions are treated as a classical mutual inductance (see Section 4.3), and a quantum model of the full galvanically-coupled circuit shown in Fig. 4-9. Using the semi-classical model, we perform an optimization routine to determine the set of parameters which best fit the results in Fig. 4-5, 4-6, and 4-8. Note that the quantum model includes some effects—such as cross-capacitance between the qubits and coupler—which are

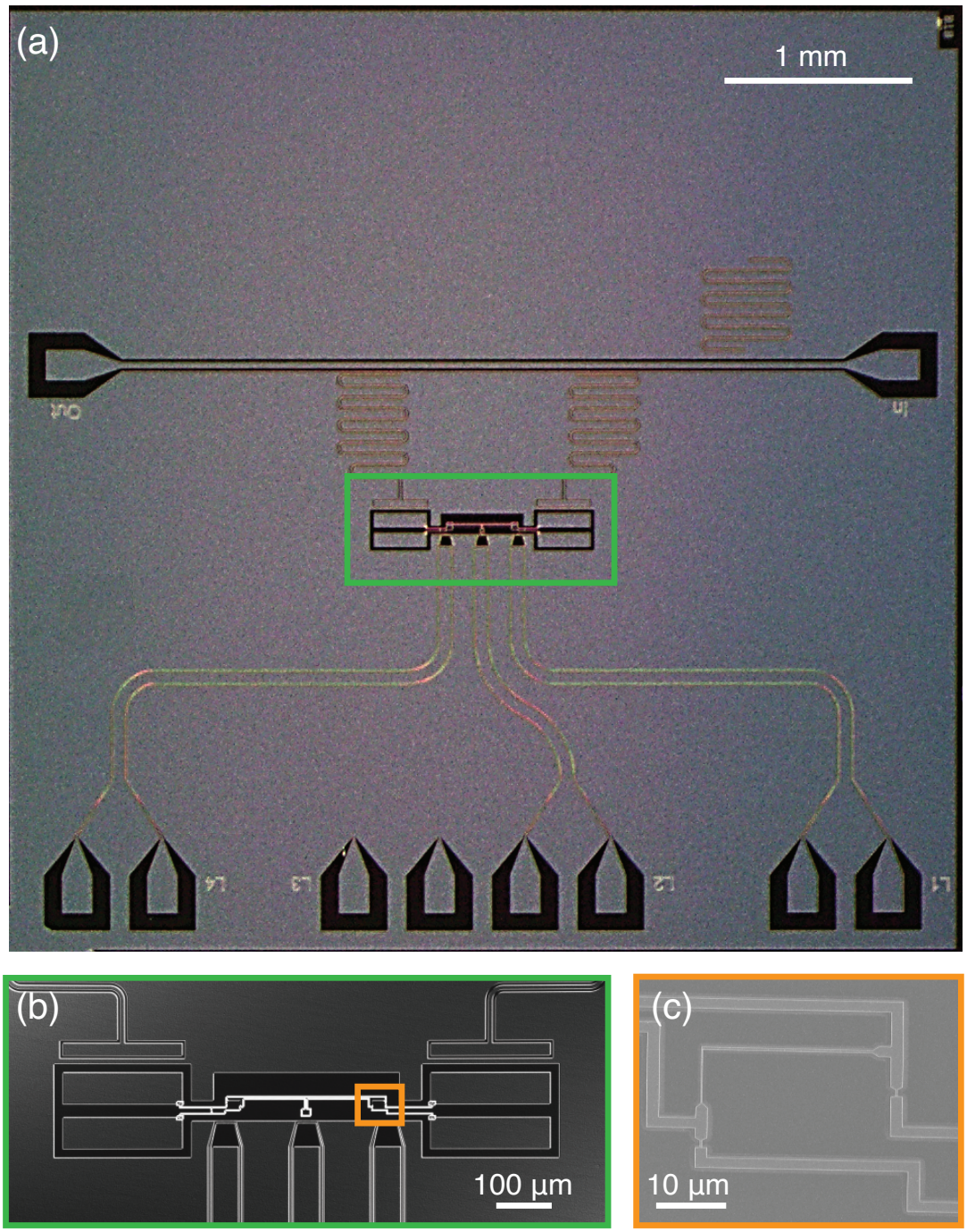

Figure 4-4: High-coherence flux qubits with tunable coupling. **(a)** Optical micrograph of the aluminum (light grey) device on a silicon (dark grey) substrate. **(b)** Optical image of the green highlighted region in (a), showing the qubits, coupler, and flux bias lines. **(c)** SEM image of the orange highlighted region in (b), showing the galvanic connection between Qubit B (lower-right) and the coupler (upper-left). [463]

	Parameter	Semi-classical model	Full galvanic circuit model
Common junction parameters	J_c (μA)	2.78	2.78
	S_c (fF/μm^2)	50	50
Qubit A	$I_0^{A,sm}$(nA)	78	78
	$I_0^{A,lg}$(nA)	206	206
	C_{sh}^A (fF)	53	53
	L_q^A (pH)	115	115
Qubit B	$I_0^{B,sm}$(nA)	78	78
	$I_0^{B,lg}$(nA)	209	209
	C_{sh}^B (fF)	53	53
	L_q^B (pH)	115	115
Coupler	M (pH)	39	43
	I_0^C(nA)	727	736
	L_C (pH)	467	542

Table 4.1: Table of parameters for the coupled flux qubit device in Fig. 4-4, extracted from simulation of both the semi-classical model of the circuit (see Section 4.3) and the full circuit Hamiltonian.

not included in the semi-classical model, and it was thus necessary to make small adjustments to the parameters extracted from the semi-classical model in order to achieve good agreement between the quantum model and the measured results.

The two qubits were each designed with shunt capacitance $C_{sh} = 50$ fF, loop inductance $L_q = 110$ pH, and $I_p = 45$ nA. All device components were patterned from a high-quality evaporated aluminum film on a high-resistivity silicon wafer, except for the superconducting loops and Josephson junctions, which were deposited using double-angle evaporation of aluminum [480]. In Fig. 4-5a,b, we show plots of qubit spectroscopy tracing the energy difference between the ground and first excited state for Qubits A and B as a function of the reduced flux $f_i \equiv \Phi_i/\Phi_0$ in the qubit loop, with the coupler biased at $f_C = 0$. At this coupler bias, $\Delta_A/2\pi = 5.042$ GHz and $\Delta_B/2\pi = 5.145$ GHz.

In Fig. 4-5c, we shows how the transition frequency of Qubit B depends on the coupler bias. This dependence is a consequence of the circulating current in the coupler loop $\langle I^C \rangle$, which induces an offset flux in the qubit loop through the shared inductance M, shifting the effective qubit bias (indicated by the yellow dashed line

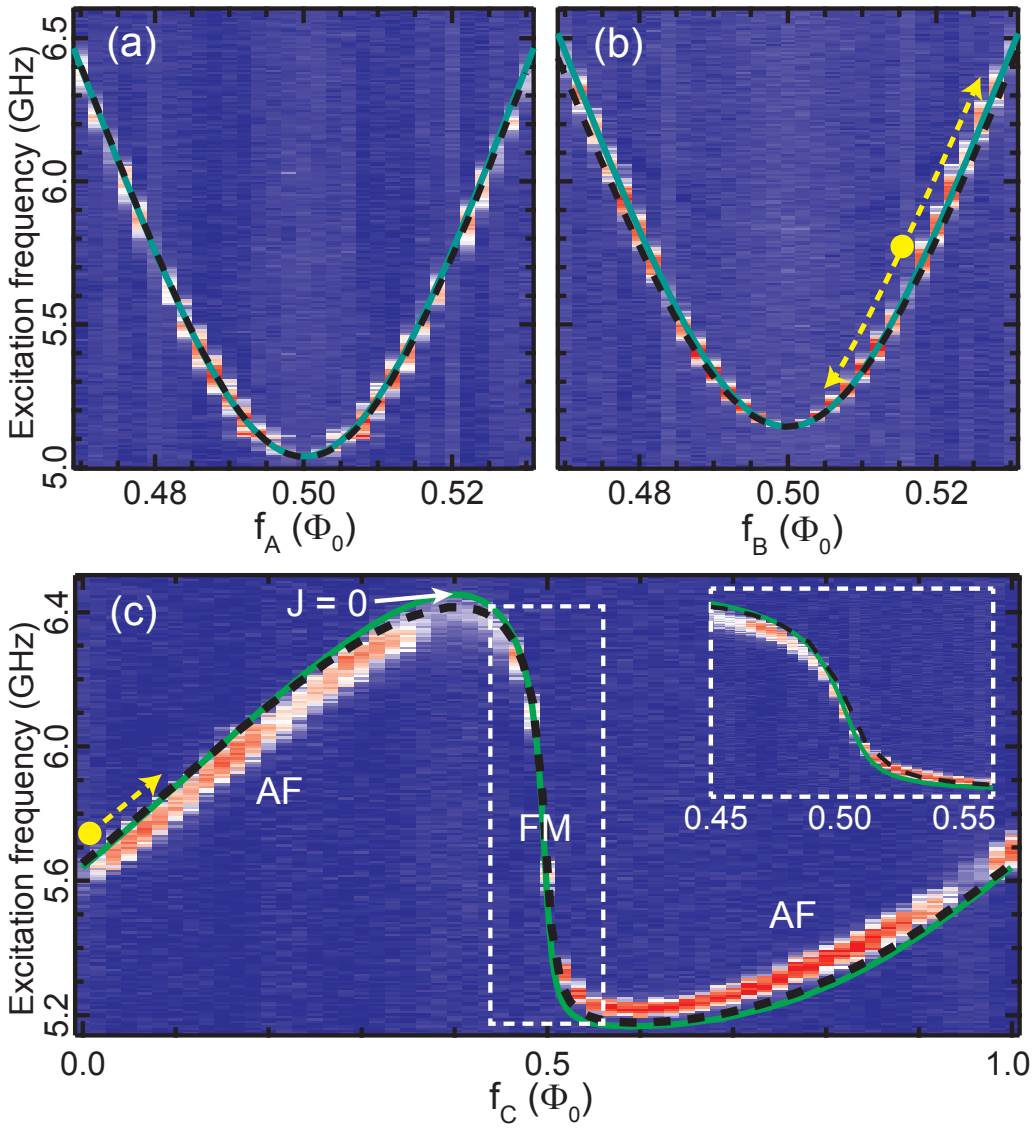

Figure 4-5: Spectroscopy of Qubits A and B. Overlaid curves match data to simulation results obtained from the semi-classical model (dashed black lines) and simulation of the full circuit Hamiltonian (solid green lines). **(a)** Spectroscopy of Qubit A as a function of the reduced flux through its qubit loop f_A, with $f_B = f_C = 0$. **(b)** Spectroscopy of Qubit B as a function of the reduced flux through its qubit loop f_B with $f_A = f_C = 0$. The yellow dot and dashed line represent the starting point and range of qubit frequencies in panel (c). **(c)** Spectroscopy of Qubit B as a function of the reduced flux through the coupler loop f_C, for $f_A = 0$ and $f_B = 0.516$. The regions of anti-ferromagnetic (AF), ferromagnetic (FM), and zero coupling are indicated. The inset shows detailed data for the FM region. [463]

in Figure 2b). Treating the interaction classically, the offset flux is given by

$$\delta f_{\mathrm{B}} = M\langle I^{\mathrm{C}}\rangle/\Phi_0 \tag{4.16}$$

Assuming that the coupler remains in its ground state, $\langle I^{\mathrm{C}} \rangle$ and L_{eff} are related to the first and second derivatives of the coupler ground state energy $E_0^{(\mathrm{C})}$ with respect to the flux through the coupler loop Φ_{C}

$$\langle I^{\mathrm{C}} \rangle \equiv \frac{\partial E_0^{(\mathrm{C})}}{\partial \Phi_{\mathrm{C}}} \tag{4.17}$$

$$\frac{1}{L_{\mathrm{eff}}} \equiv \frac{\partial \langle I^{\mathrm{C}} \rangle}{\partial \Phi_{\mathrm{C}}} = \frac{\partial^2 E_0^{(\mathrm{C})}}{\partial \Phi_{\mathrm{C}}^2} \tag{4.18}$$

Fitting our results to theory, we extract the rf-SQUID coupler loop inductance $L_{\mathrm{C}} = 470$ pH and junction critical current $I_{\mathrm{C}}^0 = 730$ nA.The circulating current $\langle I^{\mathrm{C}} \rangle$ and coupler susceptibility $1/L_{\mathrm{eff}}$ vary with applied flux f_C, ranging from -700 to 700 nA and $1/(1070$ pH) to $1/(-48$ pH) for these coupler parameters respectively. Looking at Eq. (4.18), notice that the slope of $\langle I^{\mathrm{C}} \rangle$ with respect to flux determines the sign of L_{eff} and, thus, the sign of the Ising interaction J. In this sense, Fig. 4-5c can be thought of as a map of the regions of anti-ferromagnetic ($J > 0$), ferromagnetic ($J < 0$), and zero coupling realized in this device.

4.2.2 Coupling Strength

In Fig. 4-6, we show two-qubit coupling between Qubits A and B, focusing primarily on the ferromagnetic coupling regime. Panels (a–f) show spectroscopy of both qubits as the transition frequency of Qubit A is tuned through resonance with that of Qubit B, which is held at a fixed bias. When the qubits are resonant their levels hybridize and split in frequency by $2|J|$, shown here for three coupler biases corresponding to different values of coupling strength J. Panel (g) shows the qubit frequencies for maximal coupling, as the reduced flux through Qubit A f_{A} is varied over a much larger range. At this coupler bias, we measure a maximal coupling strength of $|J|/2\pi = 94$ MHz. From this measurement and our experimental bound on the minimum coupling (see Fig. 4-7), we place a lower bound of 425 on the coupler on/off ratio. Finally, panel (h) shows the dependence of $|J|$ on the coupler bias, which agrees well with simulations of the full circuit Hamiltonian, as well as a semi-classical model (see

Section 4.3).

4.2.3 Qubit Coherence

Having demonstrated large qubit-qubit coupling, the question immediately arises: how does this coupling impact the coherence of the individual qubits? In Fig. 4-8, we report the properties of an individual qubit extracted for as range of coupler bias. Here, we present data for Qubit B, with f_{A} set to zero. Panels (a,b) display Δ_{B} versus f_{C}. For each value of f_{C}, we sweep f_{B} and perform qubit spectroscopy to find the minimum qubit frequency, $\omega_{\mathrm{B}}^{\mathrm{min}}(f_{\mathrm{C}}) \equiv \Delta_{\mathrm{B}}(f_{\mathrm{C}})$. The dependence of Δ_{B} on f_{C} can be understood semi-classically as loading of the qubit inductance by the effective inductance of the coupler,

$$L_{\mathrm{q}}^{\mathrm{loaded}} = L_{\mathrm{q}} - \frac{M^2}{L_{\mathrm{eff}}}, \tag{4.19}$$

as illustrated by the dashed lines in Figures 4-8a,b.

In Fig. 4-8c,d we show how the qubit energy relaxation time T_1 depends on f_{C}. For each coupler bias point, Qubit B is biased on degeneracy (at the point of minimum qubit frequency). Error bars correspond to the standard error for fitting the decay curve at each coupler bias point to an exponential function. In addition to any dependence on the coupler bias, T_1 also fluctuates on slow timescales [173, 480], and the grey band indicates the typical range of T_1 fluctuations when the coupler is biased away from degeneracy [463]. When the coupler is biased near degeneracy, we observe a reduction in T_1 substantially below the range of temporal fluctuations.

Finally, panels (e,f) show the dependence of the qubit dephasing times on f_{C}, for the same bias conditions as above. Here, we report the $1/e$ decay times T_2^{Ramsey} and T_2^{Echo} for Ramsey interferometry and spin echo experiments, respectively. When the coupler is biased away from degeneracy, T_2^{Ramsey} is essentially constant with respect to f_{C}, and the variation in T_2^{Echo} is roughly consistent with the range of values expected from the observed fluctuations in T_1.

Importantly, we observe a sharp reduction in the coherence times as the coupler

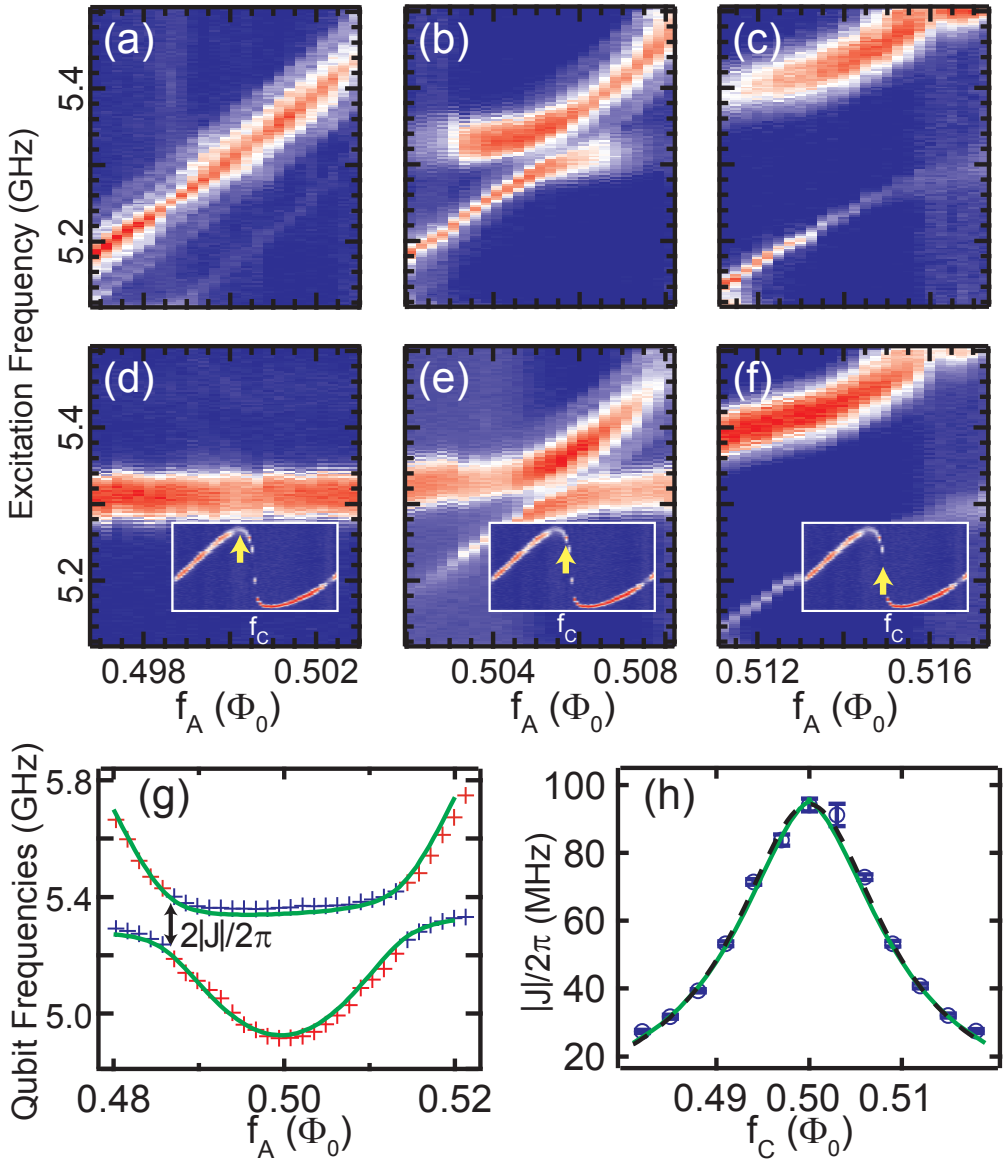

Figure 4-6: Measuring qubit-qubit coupling. **(a–f)** Spectroscopy of qubit level crossings for different coupling strength, where panels (a-c) and (d-f) show measurements using Resonator A and Resonator B, respectively. In each panel we scan f_A while holding f_B at a fixed bias point $\sim 10\mathrm{m}\Phi_0$ away from degeneracy. The left, middle, and right panels correspond to zero ($f_C = 0.402$), intermediate ($f_C = 0.48$), and maximum ($f_C = 0.5$) coupling, as indicated by the insets (see Fig. 4-5). **(g)** Avoided level crossings as Qubit A (red) is tuned across Qubit B (blue) with $f_C = 0.5$, compared to simulation of the energy levels of the full circuit Hamiltonian (solid green curve). **(h)** Coupling strength J vs coupler bias, compared to simulation using the semi-classical model (dashed black lines) and full circuit Hamiltonian (solid green lines). Error bars are derived from the error of fitting the qubit spectroscopy peaks to a double Gaussian function. [463]

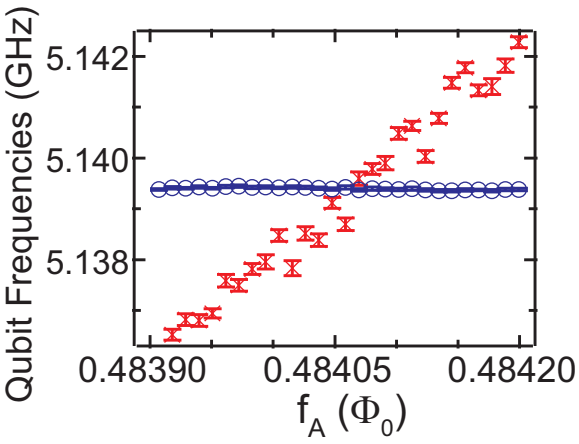

Figure 4-7: Bounding the minimum qubit-qubit coupling. Detailed data for the level crossing between Qubit A (red hourglasses) and Qubit B (blue circles) when the coupler nominally biased for zero coupling ($f_C = 0.5$). At this bias point, we observe no avoided crossing in spectroscopy, allowing us to bound any nonzero residual coupling to < 220 kHz, a limit determined by the resolution in f_A set by our bias current source. For each value of f_A, the frequency of Qubit A is determined by fitting the spectroscopy trace to a Gaussian function. Qubit B is biased on degeneracy, and its frequency is precisely determined through Ramsey spectroscopy.

bias approaches degeneracy, and a full recovery when the coupler is biased exactly on degeneracy. This effect can be understood as the result of the first-order sensitivity of Δ_B to the coupler bias, which is given by the slope of the data $\partial\Delta_B/\partial\Phi_C$ in panels (a,b). Fitting the measured dependence of Δ_B on f_C and assuming a $1/f^\alpha$ spectral density of fluctuations with $\alpha = 0.91$,[1] we see excellent agreement between our model and the coherence measurements for a flux noise amplitude of 15 $\mu\Phi_0/\sqrt{\text{Hz}}$, as indicated by the curves in Fig. 4-8f. Using the same amplitude and exponent, we calculate an upper limit on qubit T_1 due to flux noise in the coupler loop, as shown in Fig. 4-8c,d. In Section 4.4, we speculate on why the estimated flux noise amplitude is larger than previously reported values for flux qubits made with the same fabrication process [480] and the potential implications for future quantum annealing architectures designed to optimize for both coherence and coupling.

[1]In our previous work [480], we determined that $\alpha = 0.9$ for capacitively shunted flux qubits with 10×10 μm^2 loops produced using our fabrication process. Here, we have chosen to use $\alpha = 0.91$ in order achieve a good fit to our coherence data, as discussed in Section 4.4.

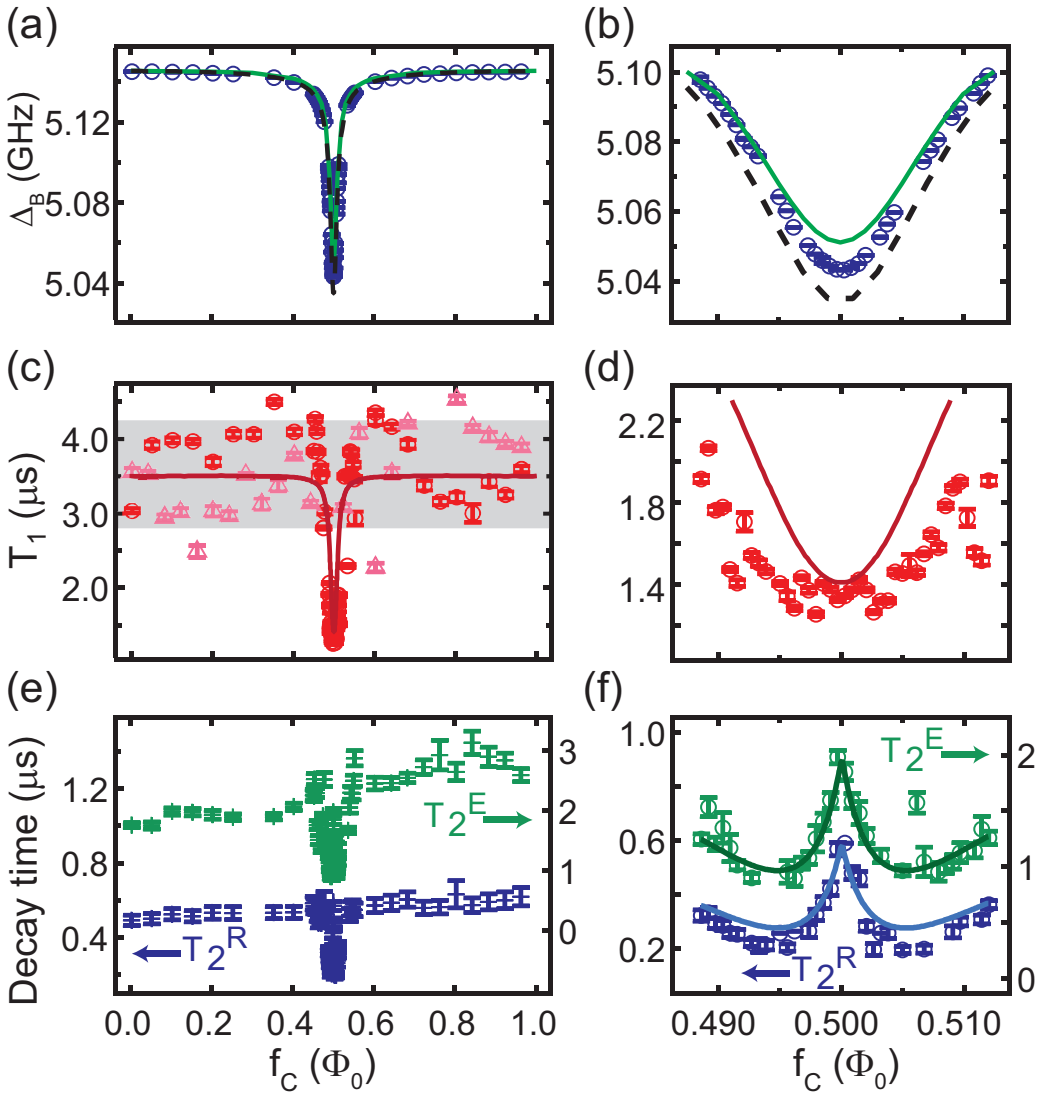

Figure 4-8: Properties of Qubit B ($f_A = 0$) vs coupler bias. Left column: full range of coupler biases. Right column: zoom in near coupler degeneracy $f_A = 0.5$. **(a,b)** Δ_B vs coupler bias. Dashed black traces: semi-classical model. Solid green traces: simulations of the full circuit Hamiltonian. **(c,d)** Qubit energy relaxation time T_1 vs coupler bias. The red circles and the magenta triangles correspond to measurements taken at different times. The grey band indicates the typical range of T1 variations when the coupler is biased away from degeneracy. The solid line represents an upper bound on qubit T_1 due to flux noise in the coupler loop with an exponent $\alpha = 0.91$ and an amplitude of $15\mu\Phi_0/\sqrt{\text{Hz}}$, combined in parallel with a coupler-independent relaxation time of $3.5\mu s$. **(e,f)** Ramsey (left axis) and echo (right axis) $1/e$ decay times (T_2) vs coupler bias. Solid lines show the expected dependence due to $1/f^\alpha$ flux noise in the coupler loop with the same amplitude and exponent as above. [463]

4.3 Semi-classical Model of Coupled Qubits

In Section 3.4, we showed how to simulate the energy spectrum of a superconducting qubit from the electrical elements and nodes of the circuit. For the coupled flux qubit device in the work above, this corresponds to simulating all nine nodes of the full galvanically-coupled circuit depicted in Fig. 4-9. In Fig. 4-5, 4-6, and 4-8, the results of this full quantum circuit simulation is shown as a green solid line, where we have hierarchically diagonalized the circuit Hamiltonian using the technique described in detail in Ref. [237].

In this section, we consider a simpler model of the coupled circuit which avoids the need to diagonalize the entire circuit. Instead, we will map this circuit onto a simpler and more computationally convenient semi-classical model, where the individual qubits and coupler are treated quantum mechanically, but their interactions are treated as a classical mutual inductance. Using this simplified model, we derive expressions for the coupling strength J, as well as the shifts in the qubit parameters Δ and ϵ due to interaction with the coupler.

4.3.1 Mutually-Inductive vs. Galvanic Coupling

To build up our model for the full coupled qubit system, let's first consider the simpler system depicted in Fig. 4-10. Here, two loops of inductance $L_{\mathrm{A,B}}$ threaded by magnetic flux $\Phi_{\mathrm{A,B}}$ are coupled through a mutual inductance M.

Defining the flux vector $\vec{\Phi}$, the mutual inductance matrix $\boldsymbol{M}$, and the self-inductance matrix $\boldsymbol{L}$ as

$$\vec{\Phi} \equiv \begin{bmatrix} \Phi_{\mathrm{A}} \\ \Phi_{\mathrm{B}} \end{bmatrix} \tag{4.20}$$

$$\boldsymbol{M} \equiv \begin{bmatrix} 0 & -M \\ -M & 0 \end{bmatrix} \tag{4.21}$$

$$\boldsymbol{L} \equiv \begin{bmatrix} L_{\mathrm{A}} & 0 \\ 0 & L_{\mathrm{B}} \end{bmatrix} \tag{4.22}$$

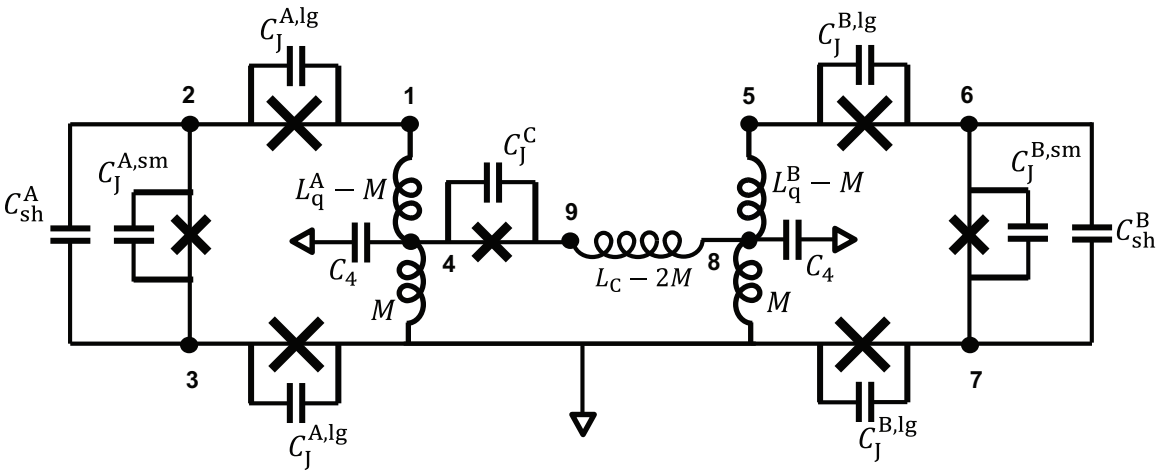

Figure 4-9: Schematic of the full galvanic circuit. The circuit nodes 1–9 are used to define the canonical flux and charge variables of the circuit, as discussed in Section 3.4. The green curves in Fig. 4-5, 4-6, and 4-8 are obtained by diagonalizing the entire nine node circuit. [463]

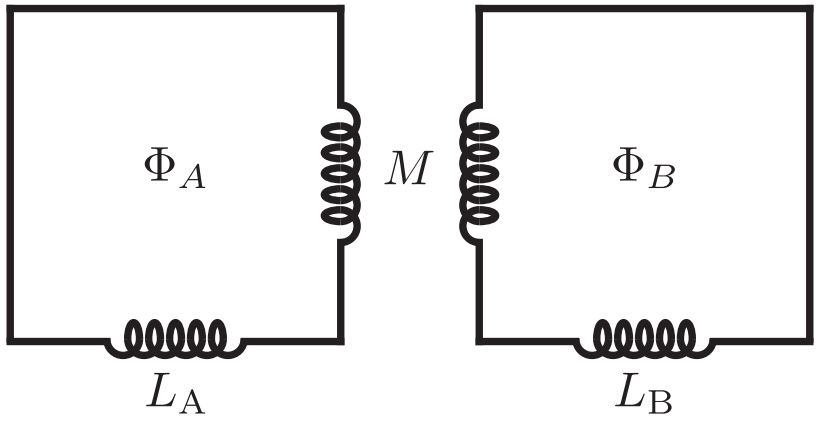

Figure 4-10: Circuit schematic for two loops of inductance $L_{A,B}$ coupled through a mutual inductance M.

the classical potential energy of the system is given by

$$U = \frac{1}{2}\vec{\Phi}^T \left(\boldsymbol{L}^{-1} + \boldsymbol{L}^{-1}\boldsymbol{M}\boldsymbol{L}^{-1}\right)\vec{\Phi} \tag{4.23}$$

$$= \frac{1}{2}\frac{\Phi_A^2}{L_A} + \frac{1}{2}\frac{\Phi_B^2}{L_B} + M\frac{\Phi_A}{L_A}\frac{\Phi_B}{L_B} \tag{4.24}$$

where the first two terms correspond to the energies of the individual loops, and the

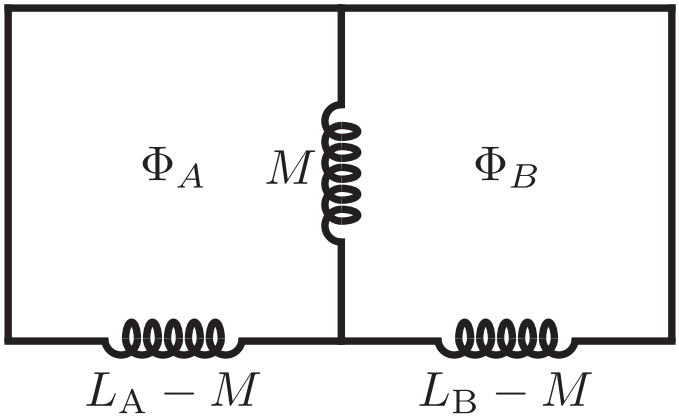

Figure 4-11: Circuit schematic for two loops which are galvanically coupled through a shared inductance M.

third term represents their interaction energy. The system can be re-expressed in terms of the classical circulating currents $I_{\mathrm{A,B}} = \Phi_{\mathrm{A,B}}/L_{\mathrm{A,B}}$, which yields

$$U = \frac{1}{2}L_\mathrm{A}I_\mathrm{A}^2 + \frac{1}{2}L_\mathrm{B}I_\mathrm{B}^2 + MI_\mathrm{A}I_\mathrm{B} \tag{4.25}$$

Next, we will compare this result for two mutually coupled loops to the case of two galvanically coupled loops, as depicted in Fig. 4-11. Here, the inductance matrix can be approximately defined as[2]

$$\boldsymbol{L} \equiv \begin{bmatrix} L_\mathrm{A} & -M \\ -M & L_\mathrm{B} \end{bmatrix} \tag{4.26}$$

and the potential energy is given by

$$U = \frac{1}{2}\vec{\Phi}^T\boldsymbol{L}^{-1}\vec{\Phi} \tag{4.27}$$

$$= \frac{1}{2}\frac{\Phi_\mathrm{A}^2}{L_\mathrm{A} - M^2/L_\mathrm{B}} + \frac{\Phi_\mathrm{B}^2}{L_\mathrm{B} - M^2/L_\mathrm{B}} + M\left(1 - \frac{M^2}{L_\mathrm{A}L_\mathrm{B}}\right)^{-1}\frac{\Phi_\mathrm{A}}{L_\mathrm{A}}\frac{\Phi_\mathrm{B}}{L_\mathrm{B}}. \tag{4.28}$$

[2]This 2x2 inductance matrix is appropriate in the limit of small island capacitance of the node connecting the three inductors. In this limit, independent phase fluctuations of this node can be neglected, and the circuit can be described by only two canonical phase variables with a 2x2 inductance matrix.

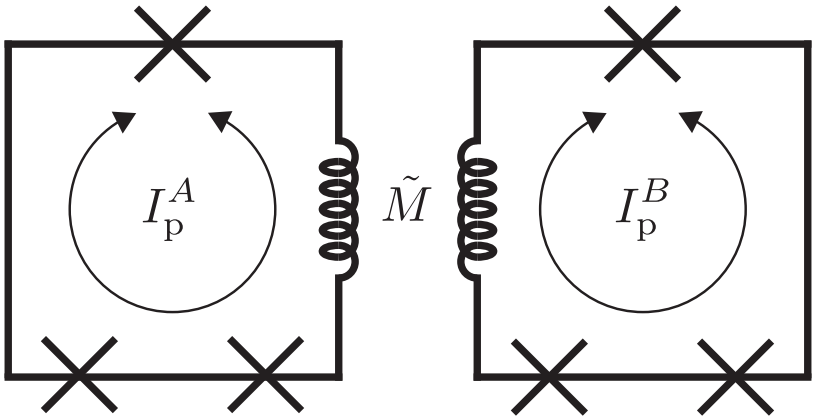

Figure 4-12: Circuit schematic for two flux qubits with persistent currents $I_{\mathrm{p}}^{\mathrm{A,B}}$ coupled through a mutual inductance $\tilde{M}$.

Note that this is equivalent to Eq. (4.24) after the following substitutions:

$$\tilde{L}_{\mathrm{A,B}} \equiv L_{\mathrm{A,B}} - \frac{M^2}{L_{\mathrm{B,A}}} \tag{4.29}$$

$$\tilde{M} \equiv M\left(1 - \frac{M^2}{L_{\mathrm{A}} L_{\mathrm{B}}}\right) \tag{4.30}$$

Thus, the galvanically-coupled circuits employed in this work can be approximately mapped onto simpler mutually-coupled circuits using the renormalized inductances $\tilde{L}$ and $\tilde{M}$.

4.3.2 Directly Coupled Qubits

Now, let's take the circuit above and replace each loop with a flux qubit (Fig. 4-12) described by the Hamiltonian $H_{\mathrm{q}}/\hbar \approx (\epsilon\hat{Z} + \Delta\hat{X})/2$ (Fig. 4-13). In the persistent current basis, the eigenstates of the Pauli operator $\hat{Z}$, denoted $|\pm z\rangle$, correspond to clockwise and counterclockwise circulating currents

$$I \equiv \langle \pm z | \, \hat{I} \, | \pm z \rangle = \langle \pm z | \, I_{\mathrm{p}} \hat{Z} \, | \pm z \rangle = \pm I_{\mathrm{p}} \tag{4.31}$$

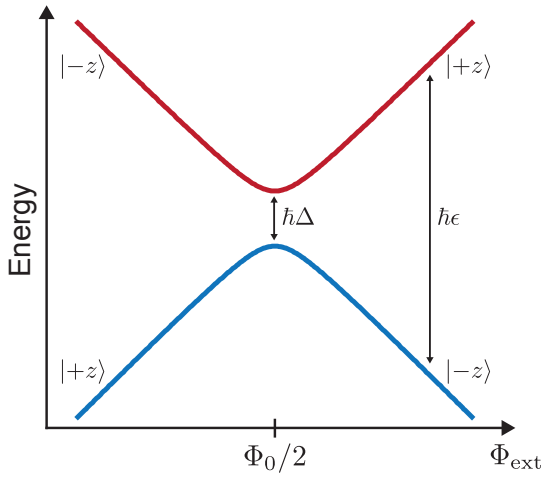

Figure 4-13: Plot of the energies of the ground (blue) and first-excited (red) states of a flux qubit as a function of the external flux Φ_{ext} through the qubit loop. At the degeneracy point ($\Phi_{\text{ext}} = \Phi_0/2$), the ground and excited states are separated in energy by $\hbar\Delta$. When biased away from degeneracy, the qubit states are approximately persistent current states $|\pm z\rangle$.

where $\hat{I}$ is the current operator and I_{p} is magnitude of the qubit persistent current. The interaction term from Eq. (4.25) can be expressed as

$$H_{\text{int}} = \tilde{M} I_{\text{p}}^{\text{A}} I_{\text{p}}^{\text{B}} \hat{Z}^{(\text{A})} \hat{Z}^{(\text{B})} \tag{4.32}$$

which takes the form $H_{\text{int}} = J\hat{Z}^{(\text{A})}\hat{Z}^{(\text{B})}$, where the coupling strength J is given by

$$\hbar J = \tilde{M} I_{\text{p}}^{\text{A}} I_{\text{p}}^{\text{B}} \tag{4.33}$$

A simple intuitive picture for this expression emerges when the qubits are biased such that $\epsilon \gg \Delta$. In this regime, qubit energy eigenstates are approximately equal to the persistent current states $|\pm z\rangle$ with energy eigenvalues $\pm\hbar\epsilon/2 = I_{\text{p}}(\Phi_{\text{ext}} - \Phi_0/2)$, where Φ_{ext} is the external magnetic flux through the qubit loop and Φ_0 is the magnetic flux quantum. Here, the $\hat{Z}\hat{Z}$ interaction is longitudinal with respect to the energy eigenbasis, and the coupling can be understood by considering the effect of the persistent current in one qubit loop on the flux through the other qubit loop. For example, Qubit A induces a state-dependent offset $\delta\Phi_{\text{B}} = \pm\tilde{M} I_{\text{p}}^{\text{A}}$ in the flux through

Qubit B and thus a state-dependent frequency shift of

$$\delta\omega_{01}^{(B)} \approx \pm\epsilon\delta\Phi_{\mathrm{B}} = \pm 2J. \tag{4.34}$$

Note that the coupling measurements reported in the main text were performed in the $\Delta \gg \epsilon$ regime, where the $\hat{Z}\hat{Z}$ interaction is transverse with respect to the energy eigenbasis. In this case, the coupling manifests as an avoided crossing between the $|01\rangle$ and $|10\rangle$ states, which are shifted from their bare energies by $\pm\hbar J$.

4.3.3 Mediated Coupling

Now that we have considered the case of two directly-coupled flux qubits, let's next consider the case of two qubits coupled via a mutual inductance $\tilde{M}$ to an intermediate loop of inductance L (Fig. 4-14). Returning to the longitudinal coupling picture ($\epsilon \gg \Delta$), the persistent current in Qubit A will induce a state-dependent offset flux $\delta\Phi_{\mathrm{C}} = \pm\tilde{M}I_{\mathrm{p}}^{\mathrm{A}}$ in the coupler loop, which changes the current circulating in the loop by $\delta\langle I^{\mathrm{C}}\rangle = \delta\Phi_{\mathrm{C}}/L$ and thus induces an offset of

$$\delta\Phi_{\mathrm{B}} = \delta\Phi_{\mathrm{C}}\frac{\tilde{M}}{L} = \frac{\tilde{M}^2}{L}I_{\mathrm{p}}^{\mathrm{A}} \tag{4.35}$$

in the flux through Qubit B. Note that this expression takes the same form as for the directly-coupled qubits, but with the substitution $\tilde{M} \rightarrow \tilde{M}^2/L \equiv M_{\mathrm{eff}}$. Then, in analogy to Eq. (4.33), the coupling strength is given by

$$J = \frac{\tilde{M}^2}{L}I_{\mathrm{p}}^{\mathrm{A}}I_{\mathrm{p}}^{\mathrm{B}} = M_{\mathrm{eff}}I_{\mathrm{p}}^{\mathrm{A}}I_{\mathrm{p}}^{\mathrm{B}}. \tag{4.36}$$

Finally, let's consider the case where the intermediate loop is replaced with an rf-SQUID coupler (Fig. 4-15). Here, we will assume that the transition frequency between the coupler ground- and first-excited state is much larger than the qubit frequencies, and the coupler is consequently always operated in its ground state. In general, the coupler ground state energy E_0 varies with applied flux f_{C}, as illustrated

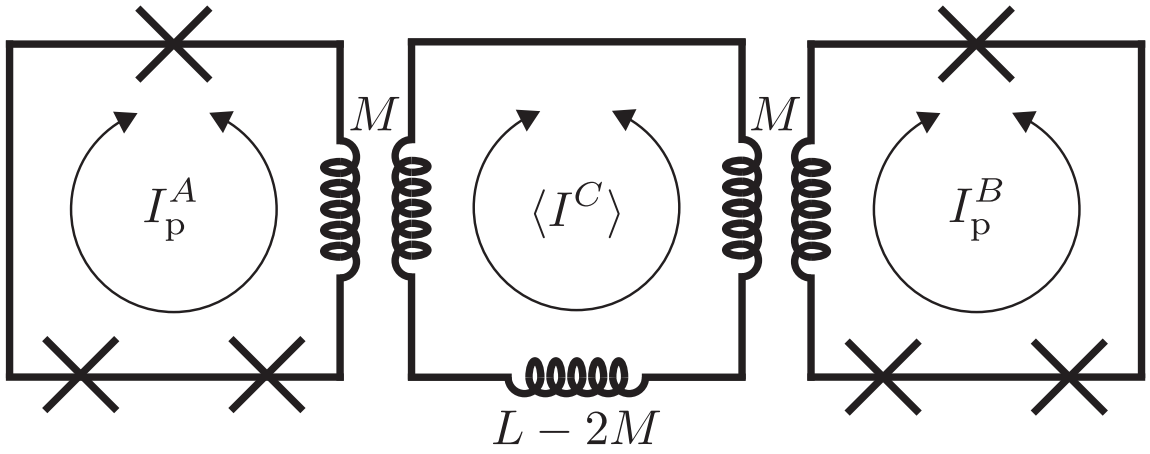

Figure 4-14: Circuit schematic for two flux qubits with persistent currents $I_{\mathrm{p}}^{\mathrm{A,B}}$ which each couple through a mutual inductance $\tilde{M}$ to an intermediate loop of inductance L.

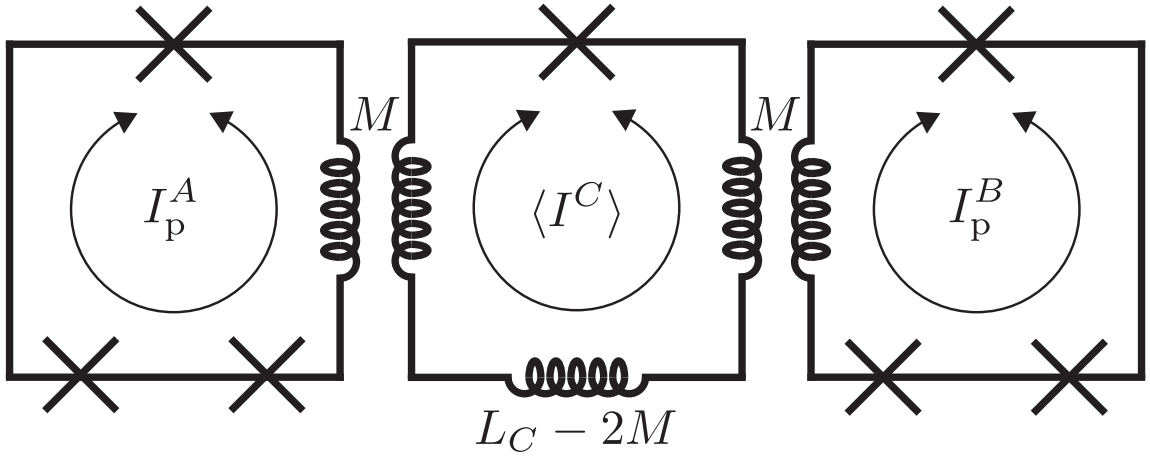

Figure 4-15: Schematic for a circuit similar to Fig. 4-14, but with the intermediate loop replaced with an rf-SQUID coupler.

in Figure 4-16c. For the coupler parameters considered in this work, the circulating current in the coupler loop is approximately equal to the slope of coupler energy with respect to flux, $\langle I^{\mathrm{C}} \rangle \approx \partial E_0^{\mathrm{C}} / \partial \Phi_{\mathrm{C}}$, as illustrated in Figure 4-16d, where we compare this quantity with the expectation value of the current operator $\langle g | \hat{I} | g \rangle$ for the coupler ground sate $|g\rangle$.

We then define the "quantum inductance" for the coupler—as in Ref. [190, 224,

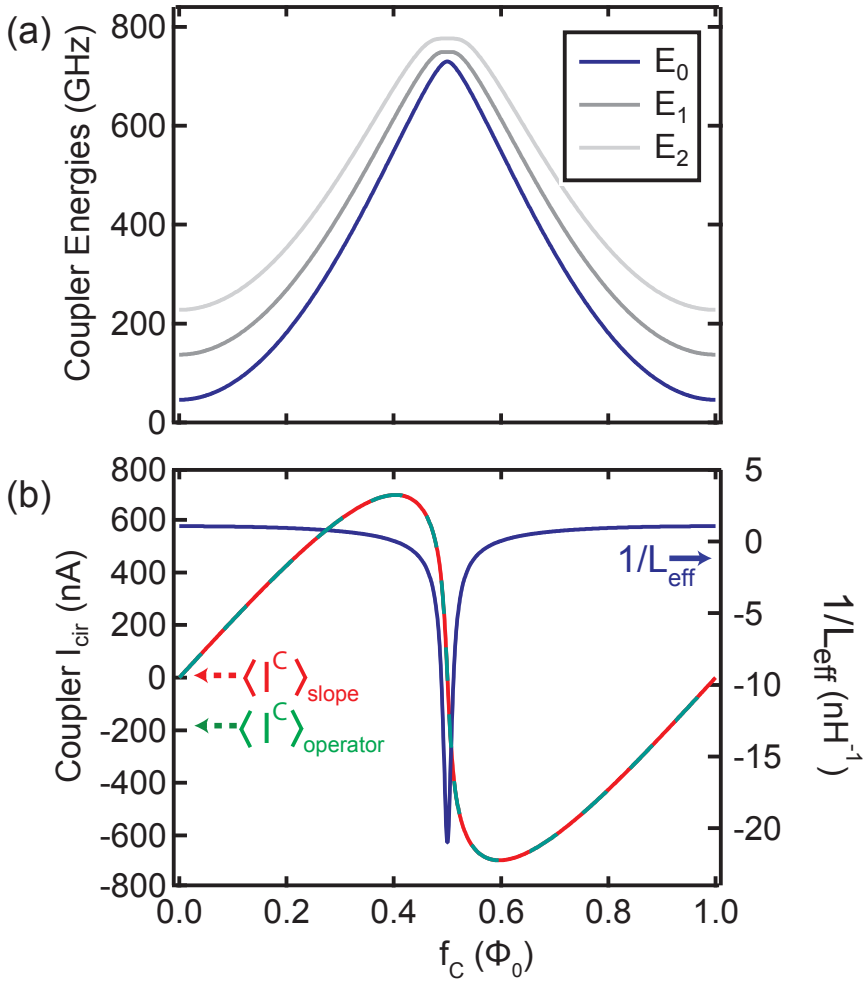

Figure 4-16: **(a)** Illustration of the energies of the ground (blue) and first-excited (grey) states of an rf-SQUID coupler, as a function of the external flux Φ_c through the coupler loop. **(b)** Left axis: comparison of the coupler circulating current, calculated using the slope of the ground state energy (red) and using and using the current operator (green). Right axis: effective inductance of the coupler vs. Φ_c.

436] and in analogy to the "quantum capacitance" described in the charge qubit [128, 224, 421] and semi-conducting qubit [103, 146, 162, 212, 269, 348] literature—as

$$\frac{1}{L_{\text{eff}}} \equiv \frac{\partial \langle I^{\text{C}} \rangle}{\partial \Phi_{\text{C}}} \approx \frac{\partial^2 E_0^{(\text{C})}}{\partial \Phi_{\text{C}}^2} \tag{4.37}$$

Note that unlike a physical inductance, this quantum inductance can take both positive and negative values. Following the same logic as above, we can now express the

coupling strength as

$$J = \frac{\tilde{M}^2}{L_{\text{eff}}} I_{\text{p}}^{\text{A}} I_{\text{p}}^{\text{B}} \tag{4.38}$$

Given a set of qubit and coupler parameters, it is straightforward to calculate J using equation (4.38). We determine L_{eff} by numerically diagonalizing the coupler Hamiltonian to solve for its ground state energy E_0 as a function of Φ_{C}. We separately determine I_{p} by numerically solving for the energy eigenstates $|\psi_j\rangle$ of the qubit Hamiltonian, from which we calculate the matrix elements of the current operator, $\langle\psi_j|\,\hat{I}\,|\psi_k\rangle$, expressed in the energy eigenbasis. When the qubit is biased on degeneracy ($\epsilon = 0$), the I_{p} is given by the off-diagonal matrix elements.

Note that Eq. (4.38) is the same expression for coupling strength used by D-Wave in Ref. [188, 190], with the coupler susceptibility χ defined as the inverse of the effective inductance. However, their approach differs in that instead of diagnolizing the coupler Hamiltonian to solve for χ, D-Wave chooses to approximate χ as the first-order (linear) susceptibility, which can be expressed using a simple analytic formula. This approach works sufficiently well for the coupler parameters of existing D-Wave devices, but the linear approximation breaks down for larger coupler susceptibilities and coupling strengths, as discussed in Ref. [228].

4.3.4 Qubit Flux Offset Due to the Coupler

The semi-classical model can also explain the shifts in qubit parameters due to their interaction with the coupler. For concreteness and to follow the presentation of the main text, we will focus on Qubit B. First, we consider the effect of the coupler on the qubit flux bias. This effect explains the dependence of the qubit frequency on the coupler bias shown in Fig. 4-5c.

As shown in Fig. 4-16d, the circulating current in the coupler loop $\langle I^{\text{C}}\rangle$ varies with the coupler bias Φ_{C}. This circulating current couples into the qubit loop through the mutual inductance M, and therefore threads a flux

$$\delta\Phi_{\text{B}} = \tilde{M}\langle I^{\text{C}}\rangle \tag{4.39}$$

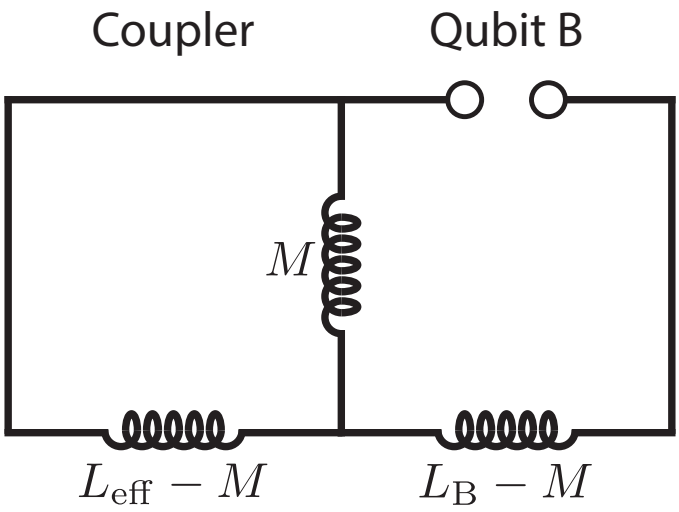

Figure 4-17: Circuit schematic used to model the loading of the qubit inductance due to the coupler $L_{\rm eff}$. The loaded qubit inductance $L_{\rm B}^{\rm loaded}$ is calculated by summing the total impedance of the qubit and coupler circuit, as seen from the small Josephson junction of Qubit B.

through the qubit loop. For a flux qubit described by the Hamiltonian $H_{\rm q}/\hbar \approx (\epsilon\hat{Z} + \Delta\hat{X})/2$, this flux offset corresponds to a shift in ϵ of

$$\delta\epsilon = \frac{2}{\hbar} I_{\rm p} \delta\Phi_{\rm B} = \frac{2}{\hbar} \tilde{M} I_{\rm p} \langle I^{\rm C} \rangle. \tag{4.40}$$

4.3.5 Inductive Loading Model

The coupler also affects the value of Δ, the qubit frequency when biased at its degeneracy point, as shown for Qubit B in Fig. 4-8a,b. This effect can be modeled semi-classically as inductive loading of the qubit inductance by the effective inductance of the coupler.

A circuit schematic for the inductive loading model is shown in Fig. 4-17.[3] Here, we consider the impedance looking out from the Josephson junction, to calculate

[3]Note that a general treatment would also include the effective inductance of Qubit A, $L_{\rm eff}^{\rm (A)}$, but for the device parameters presented here, $L_{\rm eff}^{\rm (A)} \gg L_{\rm eff}^{\rm (C)}$ and therefore has a negligible effect on Qubit B.

loaded qubit inductance

$$L_{\rm B}^{\rm loaded} = L_{\rm B} - M + \left(\frac{1}{L_{\rm eff} - M} + \frac{1}{M}\right)^{-1} = L_{\rm B} - \frac{M^2}{L_{\rm eff}}. \tag{4.41}$$

Note that this expression for the loaded inductance is the same as the renormalized inductance derived in Eq. (4.30). To calculate the semi-classical theory curves for $\Delta_{\rm B}$ versus $f_{\rm C}$ (Fig. 4-8a,b), we first simulate the coupler to determine $L_{\rm eff}(f_{\rm C})$ (Fig. 4-16d). Then, for each value of $f_{\rm C}$, we determine $\Delta_{\rm B}$ by simulating the qubit energy levels using $L_{\rm B}^{\rm loaded}$ for the qubit loop inductance.

4.4 Modeling the Effect of Flux Noise On Qubit Coherence

4.4.1 Definition of Noise Spectral Density

In this work, as in Ref. [480], we choose to characterize noise by the symmetric power spectral density (PSD)

$$S_\lambda(\omega) = \int_{-\infty}^{\infty} \exp(-i\omega\tau)\, \frac{1}{2}\langle \hat{\lambda}(0)\hat{\lambda}(\tau) + \hat{\lambda}(\tau)\hat{\lambda}(0)\rangle\, d\tau \tag{4.42}$$

where $\hat{\lambda}$ is an operator representing a fluctuating parameter λ. The two dominant noise mechanisms for the coupled qubit system presented here are flux noise in the qubit loop and the coupler loop, $\lambda_i = \Phi_{\rm B}, \Phi_{\rm C}$. For $1/f$-like noise, the noise amplitude A_λ is given by[4]

$$S_\lambda(\omega) = A_\lambda^2 \left(\frac{2\pi \times 1{\rm Hz}}{\omega}\right)^\gamma \tag{4.43}$$

where $\gamma \sim 1$.

[4]Note that this definition for $S_\lambda(\omega)$ differs by a factor of 2π from the expression used in Ref. [85], but for the case of $\gamma = 1$ the two definitions of A_λ are equivalent. Also note that the definition of $S_\lambda(\omega)$ here is double-sided, and thus differs by a factor of 2 from the single-sided spectral density used in Ref. [401].

4.4.2 Energy Relaxation Due to $1/f^{\gamma}$ Flux Noise

We have analyzed the data for T_1 of our qubit-coupler system using the Fermi's golden rule model presented in Ref. [480],

$$\frac{1}{T_1} = \sum_{\lambda} 2 \frac{|\langle e| \hat{D}_{\lambda} |g\rangle|^2}{\hbar^2} S_{\lambda}(\omega) \tag{4.44}$$

where the sum is taken over decay mechanisms, $S_{\lambda}(\omega)$ is the power spectral density of the noise responsible for each decay mechanism, and the operator $\hat{D}_{\lambda}$ is the transition dipole moment which couples our system to each noise source.

For the coupled system considered here, T_1 can be decomposed into contributions from the qubit, T_1^{Q}, and the coupler, T_1^{C}, where

$$\frac{1}{T_1} = \frac{1}{T_1^{\mathrm{Q}}} + \frac{1}{T_1^{\mathrm{C}}} \tag{4.45}$$

The qubit contribution dominates away from coupler degeneracy, and both processes contribute when the system is biased near coupler degeneracy.

In our analysis, we assume that the coupler is flux noise limited on its degeneracy, and its decay rate is thus given by

$$\frac{1}{T_1^{\mathrm{C}}} = 2 \frac{|\langle e| \hat{I}^{\mathrm{C}} |g\rangle|^2}{\hbar^2} S_{\Phi_{\mathrm{C}}}(\omega) \tag{4.46}$$

where $|g\rangle$ and $|e\rangle$ are the ground and first excited state of the coupled system

$$\hat{H} = \hat{H}^{\mathrm{Q}} + \hat{H}^{\mathrm{C}} + M \hat{I}^{\mathrm{Q}} \hat{I}^{\mathrm{C}} \tag{4.47}$$

The quantum operators $\hat{H}^{\mathrm{C}}$ and $\hat{I}^{\mathrm{C}}$ ($\hat{H}^{\mathrm{Q}}$ and $\hat{I}^{\mathrm{Q}}$) are the Hamiltonian and loop current operator of the bare coupler (qubit) respectively, and the exact value of the matrix element $\langle e| \hat{I}^{\mathrm{C}} |g\rangle$ can thus be calculated from the device parameters listed in Table 4.1 and the full quantum model of the bare qubit and coupler. The amplitude and exponent of the flux noise power spectral density in our coupler loop are then

chosen to fit the measured values of T_1, T_2^{Ramsey}, and T_2^{Echo} on coupler degeneracy.

4.4.3 First Order Sensitivity to Flux Noise

The sensitivity κ_λ of the qubit freqency to a parameter λ determines the effect of fluctuations in λ on qubit dephasing. In the two-level approximation of the flux qubit, the qubit transition frequency is given by $\omega_{01} \approx \sqrt{\epsilon^2 + \Delta^2}$, and, to first order,

$$\kappa_\lambda \equiv \frac{\partial \omega_{01}}{\partial \lambda} \tag{4.48}$$

$$\approx \frac{\partial \omega_{01}}{\partial \epsilon}\frac{\partial \epsilon}{\partial \lambda} + \frac{\partial \omega_{01}}{\partial \Delta}\frac{\partial \Delta}{\partial \lambda} \tag{4.49}$$

$$= \frac{\epsilon}{\omega_{01}}\kappa_{\epsilon,\lambda} + \frac{\Delta}{\omega_{01}}\kappa_{\Delta,\lambda} \tag{4.50}$$

where $\kappa_{\epsilon,\lambda} \equiv \partial\epsilon/\partial\lambda$ and $\kappa_{\Delta,\lambda} \equiv \partial\Delta/\partial\lambda$.

In the measurements presented in Fig. 4-8, we characterized the coherence of Qubit B when biased near its degeneracy point ($\epsilon_{\text{B}} = 0$). At this bias point, $\kappa_{\epsilon_{\text{B}},\Phi_{\text{B}}}$ and $\kappa_{\epsilon_{\text{B}},\Phi_{\text{C}}}$ are zero. Since Δ_{B} depends only weakly on Φ_{B}, the dominant first-order noise mechanism is $\kappa_{\Delta_{\text{B}},\Phi_{\text{C}}}$, the sensitivity of Δ_{B} to the coupler flux.

4.4.4 Decoherence Due to $1/f^\gamma$ Flux Noise

Here, we consider the effect of $1/f$-like flux noise, as defined in Eq. (4.43), on qubit coherence. In general, this type of noise causes phase decay of the form $\exp[-\chi_N(t)]$, where [85]

$$\chi_N(\tau) = \frac{1}{2\pi}\tau^2 \sum_\lambda \kappa_\lambda^2 \int_0^\infty \mathrm{d}\omega S_\lambda(\omega) g_N(\omega, \tau) \tag{4.51}$$

where τ is the free evolution time and g_N is a filter function which depends on the qubit pulse sequence. For the Ramsey ($N = 0$) and Hanh echo sequences ($N = 1$)

considered in this work

$$g_0(\omega,\tau) \equiv g_0(\omega\tau) = \left(\frac{\sin(\omega\tau/2)}{(\omega\tau/2)}\right)^2 \tag{4.52}$$

$$g_1(\omega,\tau) \equiv g_1(\omega\tau) = \left(\frac{\sin(\omega\tau/4)}{(\omega\tau/4)}\right)^2 \sin^2(\omega\tau/4) \tag{4.53}$$

Substituting equation (4.43) into equation (4.51) and making the additional substitution $\omega\tau \to z$ gives

$$\chi_N(\tau) = \frac{(2\pi \times 1\text{ Hz})^\gamma}{2\pi}\tau^{1+\gamma}\sum_\lambda \kappa_\lambda^2 A_\lambda^2 \int_0^\infty \frac{\mathrm{d}z}{z^\gamma} g_N(z) \tag{4.54}$$

where we have assumed that the fluctuations in each parameter λ share a common noise exponent γ.

We define the $1/e$ dephasing rates $\Gamma_{N,\lambda}$, for each dephasing channel as

$$\Gamma_{N,\lambda} = \left[(2\pi)^{\gamma-1}\kappa_\lambda^2 A_\lambda^2 \int_0^\infty \frac{\mathrm{d}z}{z^\gamma} g_N(z)\right]^{1/(1+\gamma)} \equiv \left[\kappa_\lambda A_\lambda \eta_N^{1/2}\right]^{2/(1+\gamma)} \tag{4.55}$$

where the numerical factors η_0, η_1 depend on the noise exponent γ and the Ramsey and echo filter functions and are defined as

$$\eta_N = (2\pi)^{\gamma-1}\int_0^\infty \frac{\mathrm{d}z}{z^\gamma} g_N(z). \tag{4.56}$$

As discussed in Ref. [85], for the case of $\gamma = 1$, these factors are given by

$$\eta_0 \approx \ln\left(\frac{1}{\omega_{\text{low}} t}\right) \tag{4.57}$$

$$\eta_1 = \ln(2) \tag{4.58}$$

where ω_{low} is the lower cutoff frequency set by the total time of all experimental iterations and t is the typical free evolution time during a single experimental iteration. Note that η_1 is completely independent of the cutoff frequency, thus avoiding any ambiguity in choosing ω_{low} and t when analyzing echo experiments, while η_0 varies

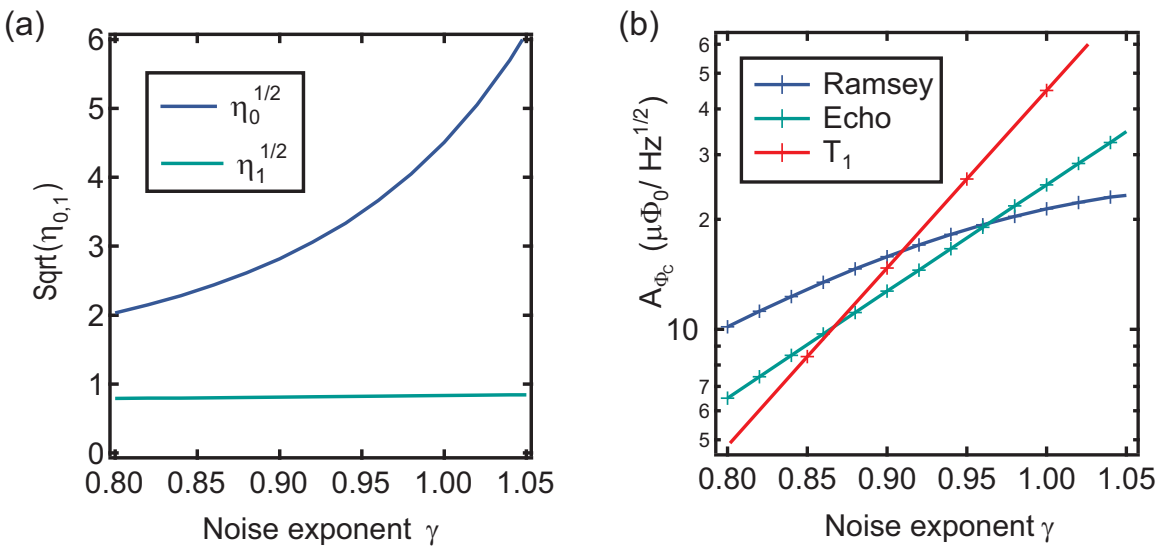

Figure 4-18: Flux noise analysis. **(a)** $\sqrt{\eta_{0,1}}$ vs γ, determined through numerical integration. When calculating η_0, we have assumed $\omega_{\rm low}/2\pi = 3$ mHz and $t = 200$ ns. **(b)** Estimated coupler flux noise amplitude based measured Ramsey, Echo, and T_1 times, as a function of γ.

only weakly with $\omega_{\rm low}t$ for realistic measurement settings.

For $\gamma \neq 1$, we determine the numerical factors through numerical integration of Eq. (4.56), as discussed in Ref. [401]. For the Ramsey sequence,

$$\eta_0 = (2\pi)^{\gamma-1} \int_{\omega_{\rm low}t}^{\infty} \frac{\mathrm{d}z}{z^\gamma} \left(\frac{\sin(z/2)}{z/2} \right)^2 \tag{4.59}$$

and for the Echo sequence,

$$\eta_1 = (2\pi)^{\gamma-1} \int_{0}^{\infty} \frac{\mathrm{d}z}{z^\gamma} \left(\frac{\sin(z/4)}{z/4} \right)^2 \sin^2(z/4) \tag{4.60}$$

Fig. 4-18a shows $\sqrt{\eta_{0,1}}$ as a function of γ for $\omega_{\rm low}/2\pi = 3$ mHz and $\tau = 200$ ns.

4.4.5 Estimating the Flux Noise Amplitude in the Coupler Loop

We now combine the results of the previous sections with our qubit coherence measurements to estimate the flux noise amplitude and exponent in the coupler loop.

We first consider the Ramsey and Echo results presented in Fig. 4-8e,f. We define the total $1/e$ decay rates for Ramsey and Echo experiments as $\Gamma_0 \equiv 1/T_2^{\text{Ramsey}}$ and $\Gamma_1 \equiv 1/T_2^{\text{Echo}}$, respectively. We separate the decay rates into two contributions: Γ_{N,Φ_C} due to flux noise in the coupler loop and $\Gamma_{N,\text{other}}$, which includes the effect of T_1 as well as any additional dephasing.

When the coupler is biased far from degeneracy, Γ_{N,Φ_C} is negligible, and thus $\Gamma_N = \Gamma_{N,\text{other}}$. For simplicity, we model $\Gamma_{N,\text{other}}$ as exponential decay.[5] For arbitrary coupler bias, the total phase decay takes the form

$$\exp[-\Gamma_{N,\text{other}}\tau - (\Gamma_{N,\Phi_\text{C}}\tau)^{1+\gamma}] \tag{4.61}$$

Thus, we can determine Γ_{N,Φ_C} from the measured values of Γ_N and $\Gamma_{N,\text{other}}$ through the relation

$$\Gamma_{N,\Phi_\text{C}} = \Gamma_N \left(1 - \frac{\Gamma_{N,\text{other}}}{\Gamma_N}\right)^{1/(1+\gamma)} \tag{4.62}$$

Finally, from Eq. (4.55) the spectral density of flux noise in the coupler is given by

$$A_{\Phi_\text{C}} = \kappa_{\Phi_\text{C}}^{-1}\eta_N^{-1/2}(\Gamma_{N,\Phi_\text{C}})^{(1+\gamma)/2}, \tag{4.63}$$

where $\kappa_{\Phi_\text{C}} \approx \kappa_{\Delta_B,\Phi_\text{C}}$ is experimentally determined from the slope of Δ_B vs Φ_C (Fig. 4-8a,b).

In Fig. 4-18b we plot the value of A_{Φ_C} that fits best to our Ramsey and Echo measurements using Eq. 4.63, and to our T_1 measurements using Eq. (4.46), for different values of γ. Although we are unable to choose values of A_{Φ_C} and γ that fit perfectly with all three measurements, they are roughly bounded within the triangular region between the three curves in Fig. 4-18b, where $10\ \mu\Phi_0/\sqrt{\text{Hz}} < A_{\Phi_\text{C}} < 19\ \mu\Phi_0/\sqrt{\text{Hz}}$ and $0.86 < \gamma < 0.96$. For concreteness, when plotting theory curves in the main text we choose $\gamma = 0.91$ and $A_{\Phi_\text{C}} = 15\ \mu\Phi_0/\sqrt{\text{Hz}}$, which results in reasonably good agreement with all three measurements.

[5] In reality, when biased away from coupler degeneracy, the qubit dephasing is somewhat non-exponential. However, it is difficult to quantify the non-exponential decay using existing data, and any non-exponential corrections to $\Gamma_{N,\text{other}}$ would only have a small impact on our estimation of A_{Φ_C}.

This estimate for the flux noise in the coupler loop is substantially larger than the value previously reported for flux qubits made with the same fabrication process, where we measured a flux noise amplitude of 1.4 $\mu\Phi_0/\sqrt{\text{Hz}}$ [480]. The most significant difference between the coupler loop and the low-noise qubit loops is the loop size; the coupler loop is 20 times larger in area. Therefore, these results motivate future efforts to study the dependence of flux noise on loop size beyond the scope of this work and previous efforts [263]. Such measurements would help to inform architectural choices for optimizing coherence and coupling in next-generation quantum annealers.

4.5 Outlook

Taken together, this study represents an important step toward designing coupled multi-qubit systems with improved coherence. We have demonstrated tunable coupling between flux qubits with substantially lower persistent currents than existing commercial devices, thereby reducing the qubit sensitivity to flux noise in their respective loops. This approach requires an increased coupler susceptibility, which increases the qubits' sensitivity to flux noise in the coupler loop. We have examined this effect by measuring qubit coherence across the full range of coupler biases, using standard measurement techniques borrowed from the gate-based quantum computing community, which have yet to be applied to commercial quantum annealers. Looking forward, our approach can be extended to achieve larger coupling strength, symmetric bipolar coupling, and $\hat{\sigma}_{\text{x}}\hat{\sigma}_{\text{x}}$ interactions [238, 398], while maintaining low persistent currents. Our results provide new insights into the available design space and suggest the type of systems-level analysis that will be necessary when designing quantum annealers with improved coherence.

Part III

Quantum Algorithms

Chapter 5

The Gate Model

In Part II, we worked through the mathematical formalism of quantum bits and considered a hardware paradigm for realizing these mathematical abstractions using superconducting circuits. These are the raw materials of a quantum computer, but they are not computers themselves. How do we orchestrate these circuits and wavefunctions into something that looks like a computer? In this part, we will begin to put together the pieces and show how the circuits in Part II become the programmable building blocks of a universal computational device. Before we get there, however, we will need to introduce another set of conceptual tools, tools which take the physics of Part II and put them to use.

5.1 Universal Computation

What is a quantum computer? The term 'quantum computer' consists of two words; we dedicated the entirety of Part II to the first word, but so far we have said little of the second. So, before we get to quantum computers, let's spend a few moments on this word. What is a computer? Well, a computer is a device that runs computations—given a string of data as input, a computer performs a series of operations which transforms this input state into a new output state. Normally, this transformation corresponds to the performance of a useful task, and the output of the computation

thus provides the solution to that task.

For example, say we wish to find the answer to the math problem $3 + 5$. To solve this problem with a computer, we need to provide the numbers 3 and 5 as inputs, and we need a device which is capable of performing the arithmetic operation of addition. Inserting the two numbers into our adding machine, the computer will output a new number some time later: 8. Having built this adding machine, we can now insert different sets of numbers as inputs and hope that we get a different output—if we now insert 7 and 14, we should hope that we get the number 21 as output, not 8. However, while the answer to an addition problem obviously depends on the two numbers being added, the *algorithm* for performing addition does not depend on the input. This should be familiar from elementary school arithmetic: given two numbers of arbitrary size, we can add them together by aligning the addends vertically and adding the columns from right to left, carrying an extra digit to the next column when the sum exceeds 9. Following this simple set of rules, we have an algorithm for performing any addition problem we might like.

Emboldened by the success of our adding machine, we might then go about constructing more computers to solve different tasks—a subtraction machine, a multiplication machine, a division machine. Following this to the natural conclusion, we would arrive at a world flooded with specialized computers, each engineered to implement one algorithm and one algorithm only. Our desks and shelves would be very cluttered. This is not the world we live in, and we owe this fact to one of the fundamental laws of the classical theory of computation: starting from a fundamental set of operations, it is possible to construct a device which can run any possible algorithm. We call such a device a *universal computer*, also known as a Turing machine after the British mathematician Alan Turing, who proved the existence of such a device in 1936 [445]. Turing's notion of universal computation became the foundation of modern computer science. It is the reason we have laptops and smartphones and supercomputers, devices which can perform addition *and* division *and* word processing to write theses.

Mathematically, we can articulate the task of a universal computer as such: given

a Boolean string of arbitrary length as an input (that is, a sequence of 0's and 1's which encodes the input data), construct a device capable of performing any Boolean function on that string (that is, any arbitrary algorithm we might wish to perform with our computer). To accomplish this task, we can decompose the space of general Boolean functions into a set of smaller logical operations which act on pairs of bits; these fundamental operations can then be strung together in different combinations to perform different functions suited to different tasks.

In classical computation, these elementary logical operations have familiar names: AND, OR, NOT, XOR. Each of these operations has a corresponding truth table which specifies what that operation does when it acts on one or two input bits. For a pair of input bits x and y, we can write the truth tables for a few of these operations as

NOT :

x	$\overline{x}$
0	1
1	0

(5.1)

AND :

x	y	$x \cdot y$
0	0	0
0	1	0
1	0	0
1	1	1

(5.2)

OR :

x	y	$x + y$
0	0	1
0	1	1
1	0	1
1	1	0

(5.3)

XOR :

x	y	$x \oplus y$
0	0	0
0	1	1
1	0	1
1	1	0

(5.4)

If it is surprising to the reader that all possible classical algorithms can be constructed out of these few simple building blocks, they will be doubly surprised to find that this set of operations is, in fact, overkill. As it turns out, the entire space of Boolean

functions can be recreated by repeated applications of a single logical operation, the NAND gate

$$\text{NAND}: \quad \begin{array}{|c|c|c|} \hline x & y & \overline{x \cdot y} \\ \hline 0 & 0 & 1 \\ 0 & 1 & 1 \\ 1 & 0 & 1 \\ 1 & 1 & 0 \\ \hline \end{array} \tag{5.5}$$

If the name didn't already give it away, we can think of the NAND gate as simply an AND gate followed by a NOT applied to its output bit, and we can combine the truth tables of these two operations from Eqs. (5.1) and (5.2) to arrive at the one in Eq. (5.5). Curiously, however, the inverse is also true: given only the NAND gate, it is possible to recreate the truth tables of any other logical gate, *provided you can duplicate its output bit.* This final point, trivial in classical computation, will take on a new significance in quantum computing, where the laws of physics forbid such duplication [472].

5.2 Quantum Gates

Let's combine the brief sketch of classical computation above with the tools we developed in Part II. A computer, we just showed, can be though of as a device which transforms an input data string into an output string which encodes the solution of the algorithm. The action of this algorithm can, in turn, be decomposed into the collective action of a set of fundamental operations acting on individual bits and pairs of bits. Recalling the mathematical tools we developed in Chapter 2, we see that quantum mechanics offers us a nice mathematical analogue to the discrete logic gates of classical computation: unitary matrices. Indeed, a unitary operation is a sort of quantum algorithm: just as a classical algorithm takes a string of input bits and deterministically transforms them into a new output string, a unitary operation performs a deterministic transformation of a quantum wavefunction, coherently transforming it from one wavefunction into another. The space of unitary matrices is also, in a

real sense, computationally complete—for a system composed of n qubits, the space of n-qubit unitaries contains the full set of possible rotations which can occur given the application of an n-qubit Hamiltonian for some time. Following this argument further, we quickly arrive at a working definition for a universal *quantum* computer: if a universal classical computer is a device capable of performing any Boolean function on an input string consisting of n classical bits, a universal quantum computer is a device capable of performing any unitary operation on an input wavefunction consisting of n *qubits*.

How do we generate a general n-qubit unitary rotation? Just as classical algorithms can be decomposed into a small set of fundamental logic gates, we can build a general n-qubit unitary matrix out of a small set of single- and two-qubit *quantum logic gates*. What do these gates look like? As a first example, let's consider three familiar unitary operators: the Pauli matrices

$$\mathsf{X} = \begin{bmatrix} 0 & 1 \\ 1 & 0 \end{bmatrix} = \text{—}\boxed{\mathsf{X}}\text{—} \tag{5.6}$$

$$\mathsf{Y} = \begin{bmatrix} 0 & -i \\ i & 0 \end{bmatrix} = \text{—}\boxed{\mathsf{Y}}\text{—} \tag{5.7}$$

$$\mathsf{Z} = \begin{bmatrix} 1 & 0 \\ 0 & -1 \end{bmatrix} = \text{—}\boxed{\mathsf{Z}}\text{—} \tag{5.8}$$

In the equations above, we show three equivalent ways to refer to a quantum logic gate. The first is the name of the gate, usually typeset in sanserif in analogy to the notation for classical logic gates. The second is the unitary matrix which describes the gate—this is the quantum version of a truth table in classical logic, and it contains a complete description of what the gate will do when applied to any general quantum wavefunction.

The third notation in the equations above is known as the 'circuit representation' of the gate, and it is used to schematically represent the application of this gate in a quantum algorithm. As an example, we could write down a simple algorithm built

out of these three operations, placing them into a musical staff like so

$$|\psi_0\rangle \text{ —}\boxed{\mathsf{X}}\text{—}\boxed{\mathsf{Z}}\text{—}\boxed{\mathsf{Y}}\text{— } |\psi\rangle \tag{5.9}$$

Expressed in this form, we refer to the number of sequential gate operations as the *depth* of the circuit (in this case, three) and the number of qubits involved in the circuit as its *width* (here, one). By convention, we read this algorithm from left to right: starting with the input state $|\psi_0\rangle$, we first apply an X-gate, then a Z-gate, and finally a Y-gate, which results in the new state $|\psi\rangle$. Mathematically, we could calculate the action of this series of gates by applying the corresponding unitary matrices to the initial wavefunction, multiplying each square matrix with the initial state vector, starting with the rightmost and going left

$$|\psi\rangle = \mathsf{Y}\,\mathsf{Z}\,\mathsf{X}\,|\psi_0\rangle \tag{5.10}$$

$$= \begin{bmatrix} 0 & -i \\ i & 0 \end{bmatrix} \begin{bmatrix} 1 & 0 \\ 0 & -1 \end{bmatrix} \begin{bmatrix} 0 & 1 \\ 1 & 0 \end{bmatrix} |\psi_0\rangle \tag{5.11}$$

To determine what this algorithm does the initial state, we can multiply the unitary matrices corresponding to each gate together and look at the combined unitary operation they produce

$$\hat{U} = \mathsf{Y}\,\mathsf{Z}\,\mathsf{X} \tag{5.12}$$

$$= \begin{bmatrix} 0 & -i \\ i & 0 \end{bmatrix} \begin{bmatrix} 1 & 0 \\ 0 & -1 \end{bmatrix} \begin{bmatrix} 0 & 1 \\ 1 & 0 \end{bmatrix} \tag{5.13}$$

$$= \begin{bmatrix} i & 0 \\ 0 & i \end{bmatrix} \tag{5.14}$$

From this, we can see that the circuit in Eq. (6.21) represents an algorithm for applying a global phase of i to the initial wavefunction.

This is not a particularly interesting algorithm, and it is easy to see that the Pauli matrices alone will never produce a particularly sophisticated computation, let alone universal quantum computation. To see this, notice that these three operations

correspond to application of single-qubit Hamiltonians proportional to each of the three Pauli matrices respectively, applied for a total rotation angle $\theta = \pi$ (as we showed back in Section 2.2). For an input state of either $|0\rangle$ or $|1\rangle$, these operations will simply shuttle the state back and forth between the poles of the Bloch sphere, toggling it between the two computational states just like a classical bit.

So, what are we missing? Recalling our discussion of the two hallmarks of quantum mechanics from Chapter 2, we see that we are missing both of them: coherent superposition and entanglement. Let's start with superposition. In order to realize a general unitary operation, it is clear that we must be able to generate coherent superpositions out of arbitrary input states. To do this, let's pick a unitary operation which generates coherent superposition states, even when the initial state is not in one

$$\mathsf{H} = \frac{1}{\sqrt{2}} \begin{bmatrix} 1 & 1 \\ 1 & -1 \end{bmatrix} = \text{—}\boxed{\mathsf{H}}\text{—} \tag{5.15}$$

This gate is ubiquitous in quantum computing and is known as the *Hadamard gate*, since its matrix description is equivalent to the 2×2 Hadamard matrix from classical mathematics. In the Bloch sphere picture, the Hadamard gate corresponds to a rotation of angle π around a diagonal axis in the xz-plane, and it thus rotates each of the computational states at the poles into equal superpositions on the equator

$$\mathsf{H}\,|0\rangle = \frac{1}{\sqrt{2}}\left(|0\rangle + |1\rangle\right) \tag{5.16}$$

$$\mathsf{H}\,|1\rangle = \frac{1}{\sqrt{2}}\left(|0\rangle - |1\rangle\right) \tag{5.17}$$

Now that we have a gate which gives us coherent superpositions, let's find one that gives us entanglement. Looking at the gates we've considered so far, it's immediately clear that single-qubit gates alone will never give us entanglement. Indeed, as we showed in Section 2.6, entanglement arises as a natural consequence of two qubits evolving according to a general two-qubit Hamiltonian. In general, these Hamiltonians cannot be broken into sums of single-qubit Hamiltonians, and they thus give rise to unitary operations which cannot be broken into products of single-qubit unitaries.

So, if we want entanglement, we need a gate which cannot be written as the product of single-qubit gates—we need a two-qubit gate.

As a first two-qubit gate, let's pick perhaps the most famous example in the literature: the controlled NOT gate, CNOT for short

$$\mathsf{CNOT} = \begin{bmatrix} 1 & 0 & 0 & 0 \\ 0 & 1 & 0 & 0 \\ 0 & 0 & 0 & 1 \\ 0 & 0 & 1 & 0 \end{bmatrix} = \tag{5.18}$$

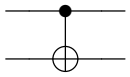

Looking at the unitary matrix above, it easy to see where this gate gets its name: in the upper left 2×2 block of the matrix, we see the single-qubit identity matrix; in the lower right, we see the single-qubit X-gate. So, applying this operation to a two-qubit product state $|xy\rangle$ where $x, y \in \{0, 1\}$, we find that this operation does nothing when the first qubit is in $|0\rangle$

$$\mathsf{CNOT}\,|00\rangle = |00\rangle \tag{5.19}$$

$$\mathsf{CNOT}\,|01\rangle = |01\rangle \tag{5.20}$$

but it applies an X-gate to the second qubit when the first is in $|1\rangle$, flipping its state just like the classical NOT gate from Eq. (5.1)

$$\mathsf{CNOT}\,|10\rangle = |11\rangle \tag{5.21}$$

$$\mathsf{CNOT}\,|11\rangle = |10\rangle \tag{5.22}$$

Noting the correspondence between the quantum X-gate and the classical NOT, we see that this gate could just as accurately have been called a 'controlled X' or CX-gate, and it is common to come across this alternative name and its corresponding circuit representation in the literature

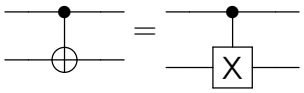

(5.23)

In either case, the interpretation of this circuit element is the same: depending on the state of the upper qubit (in general, the one whose line contains the black dot, also known as the 'control'), apply a single-qubit operation to the lower qubit (in general, the one whose line contains the $\oplus$ symbol or an explicit gate diagram, also known as the 'target').

While it is easy to see that the CNOT cannot be expressed as a product of single-qubit gates, so far it hasn't generated any entanglement—starting with the four two-qubit computational states in Eqs. (5.19)–(5.22), we arrive at same four product states. But what happens when we combine the CNOT with a single-qubit Hadamard gate? Consider the following simple two-qubit circuit applied to the four computational states

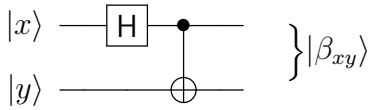

(5.24)

What happens to the computational states when they pass through this circuit? Working through the math explicitly, we find that the two qubits have been transformed into one of the four Bell states, depending on which of the four computational states they started in

$$|\beta_{00}\rangle = \frac{1}{\sqrt{2}}\left(|00\rangle + |11\rangle\right) \tag{5.25}$$

$$|\beta_{01}\rangle = \frac{1}{\sqrt{2}}\left(|01\rangle + |10\rangle\right) \tag{5.26}$$

$$|\beta_{10}\rangle = \frac{1}{\sqrt{2}}\left(|00\rangle - |11\rangle\right) \tag{5.27}$$

$$|\beta_{11}\rangle = \frac{1}{\sqrt{2}}\left(|01\rangle - |10\rangle\right) \tag{5.28}$$

These are entangled states—indeed, as we showed back in Section 2.7, they are *maximally* entangled two-qubit states.

How did the CNOT-gate generate entanglement this time around? Looking at the circuit in Eq. (5.24), things start to make intuitive sense. Prior to applying the CNOT, the Hadamard gate rotated the control qubit into an equal superposition of $|0\rangle$ and $|1\rangle$. Then, when the CNOT is applied, the control qubit gives the target qubit conflicting

instructions, *simultaneously*: in the portion of the superposition corresponding to $|0\rangle$, nothing happens to the second qubit; in the portion corresponding to $|1\rangle$, it flips. So, if we measure the first qubit and collapse the superposition which the Hadamard gate created, we would find ourselves in one of two different universes:

1. When the first qubit randomly collapses to $|0\rangle$, we are in a universe where the CNOT did nothing, and we will find the second qubit in its initial state.

2. When the first qubit randomly collapses to $|1\rangle$, we are instead in a universe where the CNOT flipped the second qubit, and we will find it in the state orthogonal to its initial.

In this sense, the circuit in Eq. (5.24) offers us yet another interpretation of quantum entanglement. This circuit is ubiquitous, and it is widely used as an algorithmic building block for preparing Bell states.

To return to the opening theme of this section: do we now have an universal quantum gate set? We showed that the gates H and CNOT can generate coherent superposition and entanglement, but can they be used to build any arbitrary n-qubit unitary? Well, almost! In our haste to rush towards the two flashiest hallmarks of quantum mechanics, we have accidentally neglected the implicit third: complex phases. Looking at the unitary matrices for H and CNOT in Eqs. (5.15) and (5.18), we notice that these operations are entirely real. As such, while they clearly generate distinctly quantum mechanical states, these states will only occupy a portion of the possible Hilbert space. For example, you can easily convince yourself that, using only combinations of H and CNOT, it is impossible to prepare the cardinal states $|+i\rangle$ or $|-i\rangle$.

To remedy this, we need to add at least one more gate to our gate set. As it turns out, not just any complex gate will do, but the following single-qubit gate is sufficient

$$\mathsf{T} = \begin{bmatrix} 1 & 0 \\ 0 & e^{i\pi/4} \end{bmatrix} = \text{—}\boxed{\mathsf{T}}\text{—} \tag{5.29}$$

This operation—known simply as the T-gate—applies a relative phase of $\phi = \pi/4$

to the $|1\rangle$-state, which is equivalent to a rotation around the z-axis of the Bloch sphere (up to a global phase). Combining the T-gate with H, we easily see that we can now generate all six cardinal states of the Bloch sphere. What is perhaps much more surprising is that, given only these two discrete gates, we can now generate any *arbitrary* single-qubit rotation, producing the continuous space of possible states on the single-qubit Bloch sphere. The proof of this fact, known as the Solovay-Kitaev theorem [112, 245], is one of the foundational theorems of quantum computation. It comes, however, with an unsurprising catch: we never said *how many* of these gates we need to reproduce an arbitrary rotation. According the the Solovay-Kitaev theorem, any single-qubit rotation can be approximated to an error ϵ using $\mathcal{O}(\log^c(1/\epsilon))$ $(c > 0)$ gates drawn from the set of $\{\mathsf{H}, \mathsf{T}\}$. Thus, while perfect reproduction of an arbitrary rotation would require an infinite sequence of these two gates, in many cases a desired rotation can be generated to good precision using an experimentally-tractable number of operations.

This, in turns out, is all we need to form a universal quantum gate set $\mathcal{G}$: a set of single-qubit gates which can prepare any state on the surface of the Bloch sphere, and one two-qubit gate to generate entanglement between qubits

$$\mathcal{G} = \{\mathsf{H}, \mathsf{T}, \mathsf{CNOT}\} \tag{5.30}$$

Thus, we have arrived at the bare minimum number of quantum operations required to construct a universal quantum computer capable of running any quantum algorithm.

5.3 Native Gate Sets and Circuit Compilation

Now that we've arrived at a universal gate set, the question invariably arises: Okay, how do we realize these operations in practice? In Chapter 6, we will begin to answer this question from an experimental standpoint and show how we calibrate physical gates on a superconducting quantum processor. Before we get there, however, we should spend a few moments on one remaining technical point.

In the previous section, we showed that a universal quantum computer can be constructed out of only H-, T-, and CNOT-gates. This was a purely theoretical argument, based only on the mathematical properties of their unitary matrices. However, when it comes time to build a device which implements these gates, they will no longer be abstract mathematical objects: they will be microwave pulses, magnetic flux biases, interactions between physical electrical circuits. And, as we glimpsed in our discussion of single and coupled superconducting qubits in Chapters 3 and 4, the space of possible operations and Hamiltonians a device can implement is constrained by the particular physics of a given hardware platform. So, what happens if our device cannot implement the universal gate set we found in the previous section?

We call the set of physical operations which a given hardware platform is capable of implementing *the native gate set* of a device. In order for a hardware platform to achieve universal quantum computation, this native gate set must also be universal, but not all native gate sets need to be the same. In some hardware platforms, certain operations will be forbidden by the physics of the device, while other operations are more flexible.

For example, as we will see in Chapter 6, superconducting transmon qubits have a native gate set which looks quite different from the one we found in the previous section, and it includes the gates

$$\mathcal{G}' = \{\mathsf{X}_\theta, \mathsf{Y}_\theta, \mathsf{Z}_\theta, \mathsf{Ph}_\theta, \mathsf{CZ}\} \tag{5.31}$$

where the gates $\mathsf{X}_\theta, \mathsf{Y}_\theta, \mathsf{Z}_\theta$ are the continuous-angle rotations around the three Pauli axes we found back in Eqs. (2.62), (2.63), and (2.64)

$$\mathsf{X}_\theta = \begin{bmatrix} \cos(\theta/2) & -i\sin(\theta/2) \\ -i\sin(\theta/2) & \cos(\theta/2) \end{bmatrix} = \text{—}\boxed{\mathsf{X}_\theta}\text{—} \tag{5.32}$$

$$\mathsf{Y}_\theta = \begin{bmatrix} \cos(\theta/2) & -\sin(\theta/2) \\ sin(\theta/2) & \cos(\theta/2) \end{bmatrix} = \text{—}\boxed{\mathsf{Y}_\theta}\text{—} \tag{5.33}$$

$$\mathsf{Z}_\theta = \begin{bmatrix} e^{-i\theta/2} & 0 \\ 0 & e^{i\theta/2} \end{bmatrix} = \text{—}\boxed{\mathsf{Z}_\theta}\text{—} \tag{5.34}$$

the single-qubit gate Ph_θ applies an overall global phase θ to one of the qubits

$$\mathsf{Ph}_\theta = e^{i\theta}\begin{bmatrix}1 & 0\\ 0 & 1\end{bmatrix} = \text{—}\boxed{\mathsf{Ph}_\theta}\text{—} \tag{5.35}$$

and the two-qubit gate CZ is a controlled phase gate, which applies a Z-gate depending on the state of the control

$$\mathsf{CZ} = \begin{bmatrix}1 & 0 & 0 & 0\\ 0 & 1 & 0 & 0\\ 0 & 0 & 1 & 0\\ 0 & 0 & 0 & -1\end{bmatrix} = \tag{5.36}$$

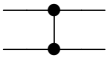

As an aside, notice that the circuit representation of the CZ is symmetric and—unlike the CNOT—it isn't readily apparent which qubit is the control and which the target. While this might seem strange at first, it is consistent with the symmetry of the unitary matrix, which does not distinguish the roles of the two qubits. Indeed, the two qubits are *both* the targets *and* the controls: when the two qubits are both in $|1\rangle$, a π-phase is applied to their joint state, otherwise, nothing occurs. As such, it is perfectly valid to think of either qubit as target or control, and we can write this operation in several different, equivalent ways

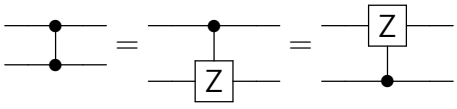

(5.37)

While the transmon gate set $\mathcal{G}'$ contains none of the gates in our theoretical gate set $\mathcal{G}$, it is clear that it too is universal: the continuous single-qubit gates $\mathsf{X}_\theta, \mathsf{Y}_\theta, \mathsf{Z}_\theta$, and Ph_θ can trivially rotate any given single-qubit pure state to any point on the surface of the Bloch sphere—indeed, with much less effort than the discrete gates H and T—and the two-qubit CZ gate is there to provide entanglement. Indeed, since the gate set $\mathcal{G}'$ is universal, we should be able to recreate all the gates in $\mathcal{G}$ using only the native ones in $\mathcal{G}'$. With a little math, we can convince ourselves that the

following relationships do just that

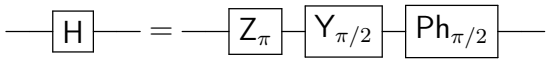

(5.38)

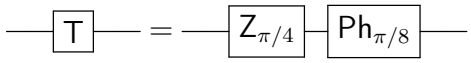

(5.39)

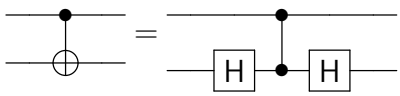

(5.40)

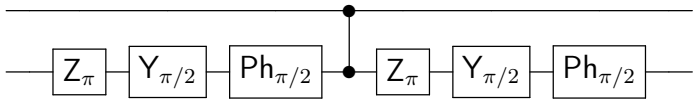

(5.41)

This process, in which a series of gates are broken down and translated into an equivalent sequence of native gates, is known as *circuit compilation*. We will return to this concept extensively in Chapter 7 when we run the Density Matrix Exponentiation algorithm on a small superconducting transmon device, and we will see that efficient circuit compilation is one of the most important steps in running a quantum algorithm on physical hardware. In general, circuit compilation attempts to optimize over two related criteria:

1. Express a given n-qubit unitary using the fewest number of native gates possible.
2. Express a given n-qubit unitary using the highest-fidelity native gates available.

In practice, as we will see, this compilation is decidedly nontrivial, and it requires deep knowledge of the device being used. Indeed, as it turns out, this optimization problem is NP-hard for some quantum circuits [68].

5.4 Case Study: The SWAP Test

For the remainder of this chapter, let's pull together some of the pieces we have discussed so far and consider a simple example of a quantum algorithm, known as the SWAP test. As we will see, this algorithm has a couple nice features which will illuminate the power of discrete gate operations to perform a computational task.

The goal of the SWAP test is to efficiently calculate the purity of an unknown quantum state ρ. Recall from Section 2.8 that the purity γ of a quantum state is defined as the trace of its density matrix squared

$$\gamma \equiv \text{Tr}\left[\rho^2\right] \tag{5.42}$$

As we discussed previously purity γ is bounded between 1 and $1/d$, where $d = 2^n$ is the dimension of the n-qubit density matrix ρ: when $\gamma = 1$, the system is in a pure state; when $\rho = 1/d$, it is in a completely mixed state. For a single qubit, the former corresponds to a point on the surface of the Bloch sphere; the latter, to the point at the center of the sphere.

From the definition in Eq. (5.42), it is easy to see that we can brute force this calculation: given many copies of our unknown state ρ, we can perform a series of measurements which reconstruct the entirety of the density matrix, element by element, and then manually calculate the trace of that matrix squared. This is theoretically possible, but practcially impossible for all but the smallest quantum states. As we'll discuss later in Chapter 8, there exists a robust protocol for reconstructing the density matrix of an unknown qunatum state, know as *quantum state tomography*. The catch, however, is that state tomography requires on order as many measurements as there are elements of the given density matrix. As we showed back in Chapter 2, the density matrix of a multi-qubit system scales exponentially with the number of constituent qubits, making the tomographic reconstruction of even a few tens of qubits astronomically expensive.

In order to *efficiently* calculate the purity of an unknown state ρ, we need to somehow beat this exponential and perform this calculation using resources which scale polynomially with the dimension of the Hilbert space. Looking at the definition of purity in Eq. (5.42) again, we can convince ourselves that such a thing ought to be possible. After all, while calculating the purity using state tomography may be exponentially expensive, it is also exponentially *wasteful*: having performed $\mathcal{O}(2^n)$ measurements to reconstruct the density matrix in all its specificity using state

tomography, Eq. (5.42) then crunches that massive matrix down into one number, spitting out a single value γ regardless of the size of the underlying quantum state. So, can we bypass the density matrix ρ entirely and calculate γ directly?

The SWAP test does exactly this, but there is no free lunch. While the SWAP test calculates γ exponentially faster than the corresponding tomographic method, it sacrifices almost every other piece of information about the state ρ in the process. Having obtained a value of γ, we are no longer able to say which specific state ρ it was derived from—all we can say is that the state of our system belongs to one of the infinite number of states which exist on a shell of some radius in the Bloch sphere, all of which having the same value of γ. Nonetheless, the SWAP test can be a useful 'quantum trick' (as discussed in Section 8.2) for validating the coherence of a large quantum state and convincing yourself that the state of your processor is indeed coherent. The SWAP test is also a submodule of some other quantum algorithms—such the entanglement polytope protocol [459]—which require that the initial state of the algorithm be pure in order for the output to have meaning.

The SWAP test relies on the following mathematical observation

$$\mathrm{Tr}\left[\rho^2\right] = \mathrm{Tr}\left[(\rho \otimes \rho)\,\mathsf{SWAP}\right] \tag{5.43}$$

On the left side of the equation, we have our expression for the purity γ. On the right side, we have an expectation value: specifically, we have the expectation value of a product state $\rho \otimes \rho$ with the SWAP operator, where this operator is defined as the unitary matrix which literally exchanges the states of two quantum systems with each other

$$\mathsf{SWAP} := \sum_{ij}^{d} |ij\rangle \langle ji| \tag{5.44}$$

From this, we can give a physical interpretation to the mathematical fact in Eq. (5.43): the purity of an arbitrary n-qubit quantum state ρ is equal to the expectation value of swapping two copies of that state with each other. The task, then, is to prepare two copies of ρ and directly measure the expectation value of the SWAP operator,

revealing the purity of the underlying state.

5.4.1 Measuring the Purity of a Single Qubit

As a concrete example, let's first consider the SWAP test applied to a single-qubit state. If ρ is the state of a single qubit ($d = 2$), the SWAP operator between two copies of ρ is a 4×4 matrix of the form

$$\mathsf{SWAP} = \begin{bmatrix} 1 & 0 & 0 & 0 \\ 0 & 0 & 1 & 0 \\ 0 & 1 & 0 & 0 \\ 0 & 0 & 0 & 1 \end{bmatrix} \tag{5.45}$$

This matrix should be familiar—indeed, it is exactly the unitary matrix we considered back in Section 2.6 Eq. 2.235 when we considered the general dynamics of two-qubit systems and the emergence of entanglement. We will return to this operation again in Chapter 7, where it forms the backbone of the Density Matrix Exponentiation algorithm.

How do we calculate the expectation value of this operator on a given quantum state? Looking at the matrix in Eq. (5.45), we see that the eigenstates of the SWAP operator are the four single-triplet states

$$|\psi_{\text{trip1}}\rangle = |00\rangle \tag{5.46}$$

$$|\psi_{\text{trip2}}\rangle = \frac{1}{\sqrt{2}}\left(|01\rangle + |10\rangle\right) \tag{5.47}$$

$$|\psi_{\text{trip3}}\rangle = |11\rangle \tag{5.48}$$

$$|\psi_{\text{singl}}\rangle = \frac{1}{\sqrt{2}}\left(|01\rangle - |10\rangle\right) \tag{5.49}$$

where the three triplet states have eigenvalue $+1$ (even parity) and the lone singlet state has eigenvalue -1 (odd parity). These eigenstates, like all eigenstates of a unitary matrix, form a complete basis of states for representing a general wavefunction of equal dimension. To measure the expectation value in Eq. (5.43), we thus need to take our initial state $\rho \otimes \rho$ and project it into the basis of singlet-triplet states,

recording the probability p of the state collapsing into each eigenstate and weighting that probability by the corresponding eigenvalue

$$\mathrm{Tr}\left[(\rho \otimes \rho)\,\mathsf{SWAP}\right] = p_{\mathrm{trip1}} + p_{\mathrm{trip2}} + p_{\mathrm{trip3}} - p_{\mathrm{singl}} \tag{5.50}$$

In practice, however, a quantum computer does not have access to direct measurements in an arbitrary basis, only to the computational basis $|00\rangle, |01\rangle, |10\rangle, |11\rangle$—that is, projecting each qubit in either $|0\rangle$ or $|1\rangle$ and reporting the resulting n-digit bit string. So, if we want to project our state into a particular basis—here, the single-triplet basis—we need to rotate the desired basis states *into* the computational basis, such that the resulting bit strings now correspond to projections in the desired basis.

How do we perform this rotation? Looking at the single-triplet states in Eqs. (5.46)–(5.49), we see that these states are intimately related to the four Bell states

$$|\beta_{00}\rangle = \frac{1}{\sqrt{2}}\left(|00\rangle + |11\rangle\right) \tag{5.51}$$

$$|\beta_{01}\rangle = \frac{1}{\sqrt{2}}\left(|01\rangle + |10\rangle\right) \tag{5.52}$$

$$|\beta_{10}\rangle = \frac{1}{\sqrt{2}}\left(|00\rangle - |11\rangle\right) \tag{5.53}$$

$$|\beta_{11}\rangle = \frac{1}{\sqrt{2}}\left(|01\rangle - |10\rangle\right) \tag{5.54}$$

Taking the expectation value of each of these states with SWAP, we see the Bell basis has the exact same parity properties as the singlet-triplet: $|\beta_0 0\rangle, |\beta_0 1\rangle, |\beta_1 0\rangle$ have even parity (i.e. they are unchanged after exchanging the two underlying single-qubit states) and $|\beta_1 1\rangle$ has odd parity (it picks up a minus sign when we exchange its single-qubit states). Indeed, since the Bell basis and the single-triplet basis are equivalent up to a rotation in the even parity manifold, the sum of the eigenvalue-weighted probabilities in these two bases will be equivalent

$$p_{\mathrm{trip1}} + p_{\mathrm{trip2}} + p_{\mathrm{trip3}} - p_{\mathrm{singl}} = p_{\beta 00} + p_{\beta 10} + p_{\beta 01} - p_{\beta 11} \tag{5.55}$$

So, recalling the motivating equation from Eq. (5.43), our task is now to rotate

our state $\rho \otimes \rho$ from the Bell basis into the computational basis and record the corresponding measurement outcomes to estimate the expection value of SWAP. As it turns out, this chapter has already provided us with all the tools we need to do exactly that rotation. In Eq. (5.24), we showed a quantum circuit for generating each of the four Bell states from each of the four computational states. Our task is now the inverse: given the four Bell states, rotate them into the computational basis. This task is now trivial—we simply need to run the circuit from Eq. (5.24) *backwards*

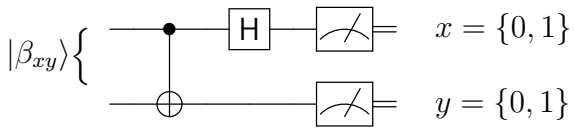

(5.56)

This circuit is commonly known as a Bell measurement: when the input state on the left-hand side of the circuit is equal to one of the four Bell states, measurement of the two qubits at the end of the circuit will deterministically yield a single bit-string which uniquely identifies which Bell state the system was in.

For the SWAP test, however, the input state will *not* be in one of the Bell states, but rather in a product state $\rho \otimes \rho$. As such the Bell measurement will not yield a single bit string, but rather a distribution of bit strings corresponding to the projection of the product state into the Bell basis. Collecting the resulting bit strings and calculating the relative probability of their occurrence, we can estimate the expection value of SWAP as

$$\mathrm{Tr}\left[(\rho \otimes \rho)\,\mathsf{SWAP}\right] = \tilde{p}_{00} + \tilde{p}_{01} + \tilde{p}_{10} - \tilde{p}_{11} \tag{5.57}$$

where $\tilde{p}_{00}, \tilde{p}_{01}, \tilde{p}_{10}, \tilde{p}_{11}$ are the relative probabilities of the four two-qubit measurement outcomes after performing the Bell measurement from Eq. (5.56).

Since there are only two unique eigenvalues, Eq. (5.57) is equivalent to simply recording the probability of being in an even or odd parity state

$$\mathrm{Tr}\left[(\rho \otimes \rho)\,\mathsf{SWAP}\right] = p_{\text{even}} - p_{\text{odd}} \tag{5.58}$$

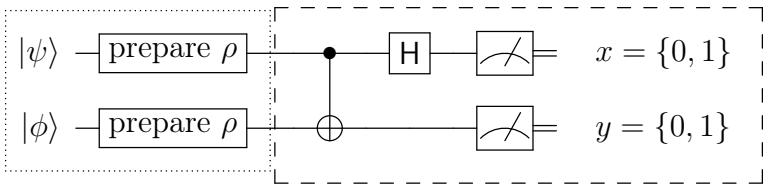

Figure 5-1: The protocol for a single run of the SWAP test on two qubits. The operations in the dotted box prepare the two qubits in the the product state $\rho \otimes \rho$ using some sequence of single-qubit rotations, and the operations in the dashed box perform a Bell measurement as described in Eq. (5.56). By running the circuit many times, recording the parity extracted from measurement outcomes x and y, and summing the estimated probabilities in post-processing according to Eq. (5.58), the algorithm returns an estimate of the purity of state ρ.

which we can determine in classical post-processing by taking the logical AND of the output bits of the Bell Measurement

$$1 - 2(x \wedge y) = \begin{cases} +1, & \text{even parity} \\ -1, & \text{odd parity} \end{cases} \tag{5.59}$$

where x and y are the bits recorded in single-shot measurements of the first and second qubits from Eq. (5.56) respectively, and $\wedge$ is the classical AND operator whose truth table we showed in Eq. (5.2). From here, we can perform repeated Bell measurements on fresh copies of the state $\rho \otimes \rho$, gradually building up an estimate of the probability of being in an even or odd parity state.

Combining these insights, the protocol for performing a SWAP test on two qubits is as follows:

1. Initialize two qubits in the state of interest ρ.

2. Perform a Bell measurement on the two-qubit product state $\rho \otimes \rho$, recording the parity from the two outputs bits x and y by Eq. (5.59).

3. Repeat the circuit many times, gradually building up an estimate for probability of $\rho \otimes \rho$ being in an even parity state (p_{even}) or an odd parity state (p_{odd}).

4. In classical post-processing, subtract the two probabilities according to Eq. (5.58) to get an estimate for the purity of state ρ.

Expressing this as a quantum circuit, we arrive at the two-qubit algorithm for the SWAP test in Fig. 5-1.

5.4.2 Measuring the Purity of an n-Qubit State

For a single qubit—where tomographic reconstruction of the density matrix is still relatively cheap—calculating the purity with the SWAP test is a bit of an overkill, and it is easy enough to measure all the elements of the density matrix ρ and brute force calculate the purity in Eq. (5.42). The real power of the SWAP test, however, comes when we extend the technique to n-qubit states, where state tomography quickly becomes computationally prohibitive.

For concreteness, let's consider the three-qubit state ρ_{ABC}, where the subscripts A, B, C will denote the three physical qubits which compose ρ_{ABC}. The extension to arbitrary multi-qubit states will readily follow from there. To perform a SWAP test on this three-qubit state, we apply our fundamental relationship from Eq. (5.43)

$$\mathrm{Tr}\left[\rho_{ABC}^2\right] = \mathrm{Tr}\left[\left(\rho_{A_1B_1C_1} \otimes \rho_{A_2B_2C_2}\right) \mathsf{SWAP}_{A_1B_1C_1:A_2B_2C_2}\right] \tag{5.60}$$

where ρ_{ABC} is now an 8×8 three-qubit density matrix, the subscripts 1 and 2 keep track of our two copies of ρ_{ABC}, and the SWAP operator is the 64×64 matrix which swaps the qubits in the first copy of ρ with the qubits in the second copy

$$\mathsf{SWAP}_{A_1B_1C_1:A_2B_2C_2} := \sum_{\substack{A_1B_1C_1 \\ A_2B_2C_2}}^{d=2} |A_1B_1C_1A_2B_2C_2\rangle \langle A_2B_2C_2A_1B_1C_1| \tag{5.61}$$

Crucially, we recognize that the global SWAP operator in Eq. (5.61) can be decomposed into the product of local SWAP operators acting only on pairs of qubits

$$\mathsf{SWAP}_{A_1B_1C_1:A_2B_2C_2} = \mathsf{SWAP}_{A_1:A_2} \otimes \mathsf{SWAP}_{B_1:B_2} \otimes \mathsf{SWAP}_{C_1:C_2} \tag{5.62}$$

where each of the SWAP operators on the right-hand side of the equation is the

familiar 4×4 matrix

$$\mathsf{SWAP}_{A_1:A_2} = \sum_{A_1 A_2}^{d=2} |A_1 A_2\rangle \langle A_2 A_1| = \begin{bmatrix} 1 & 0 & 0 & 0 \\ 0 & 0 & 1 & 0 \\ 0 & 1 & 0 & 0 \\ 0 & 0 & 0 & 1 \end{bmatrix} \tag{5.63}$$

The relationship in Eq. (5.62) is extremely powerful, because it tells us that we can implement the global SWAP operation using only local operations on pairs of qubits. Indeed, since each of the two-qubit SWAP operations on the right-hand side of the equation is exactly the same operation we just addressed in the previous section, we can use our routine for the 2-qubit SWAP test as a subroutine of the general $2n$-qubit SWAP test.

From Eq. (5.62), we see that the eigenstates of the global SWAP operator are tensor products of the eigenstates of the local SWAP operators. As such, measuring the expectation value of the global SWAP operator simply requires rotation of the local SWAP eigenstates into the computational basis. That is, we simply perform Bell measurements between pairs of qubits, as illustrated in Fig. 5-2. After performing a Bell measurement on each of the constituent pairs of qubits in the two copies of ρ_{ABC}, the expectation value of the global SWAP operator can be found by recording the probability of being in an even or odd parity state

$$\mathrm{Tr}\left[(\rho_{A_1B_1C_1} \otimes \rho_{A_2B_2C_2})\, \mathsf{SWAP}_{A_1B_1C_1:A_2B_2C_2}\right] = P_{\text{even}} - P_{\text{odd}} \tag{5.64}$$

Here, "even" and "odd" refer to the global state parity, which—following from the SWAP decomposition in Eq. (5.62)—is the product of the local parity measured in each of the Bell measurements

$$\prod_{j=\{A,B,C,\ldots\}}^{n} 1 - 2(x_j \wedge y_j) = \begin{cases} +1, & \text{even global parity} \\ -1, & \text{odd global parity} \end{cases} \tag{5.65}$$

where x_j and y_j are the bits measured at the output of the Bell measurement between

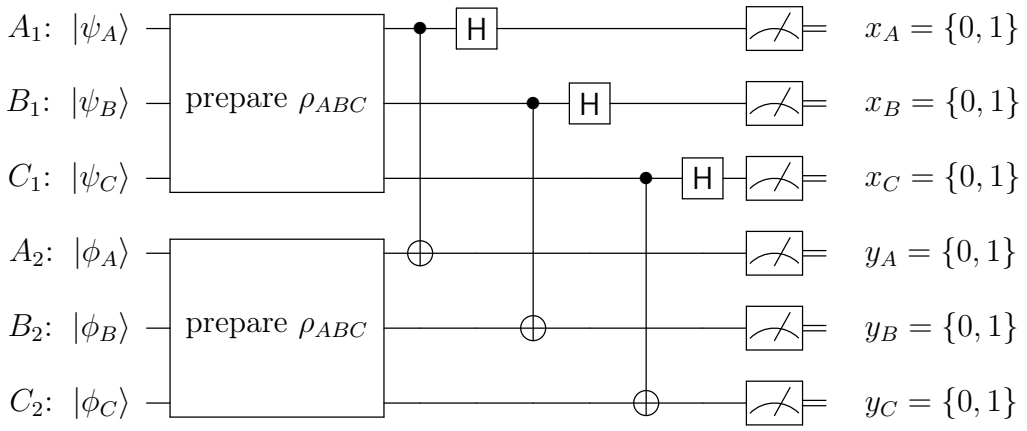

Figure 5-2: An example of the general protocol for a single run of the SWAP test on $2n$ qubits ($n = 3$ shown). At the end of each run, $2n$ bits are recorded and converted to a global parity measurement using Eq. (5.65). The circuit is repeated many times to build up an estimate of the probability of measuring even or odd parity, which in turn gives us an estimate of the purity of ρ.

qubits j_1 and j_2 ($j \in \{A, B, C, \dots\}$), as shown in the measurement outcome of each qubit in Fig. 5-2.

Pulling everything together, the protocol for performing a SWAP test on n qubits is as follows

1. Initialize two sets of n qubits in the state of interest ρ.

2. Perform a Bell measurement on each of the n pairs of constituent qubits, recording a total of $2n$ classical bits after measurement of each qubit.

3. In classical processing, the $2n$ bits are converted into a global parity measurement using Eq. (5.65).

4. Repeated steps 1 through 3 many times, building up an estimate of the probability of the state having even or odd global parity.

5. In classical post-processing, subtract the two probabilities to get an estimate for the purity of state ρ.

Since each run of the general SWAP test only requires a total of $\mathcal{O}(2n)$ measurements, we can see that measuring state purity with the SWAP test is exponentially faster than brute-force state tomography, which requires $\mathcal{O}(2^n)$ measurements.

5.4.3 Experiment: Measuring Purity Loss in a Superconducting Qubit

Having outlined the theoretical foundation of the SWAP test, let's consider what running this algorithm looks like in practice. As a proof of principle, we can run the SWAP test on a small superconducting quantum processor and look at how the purity extracted from the SWAP test compares to the value extracted from brute force tomography. For this experiment, we use a pair of capacitively-coupled flux-tunable transmon qubits in a linear array (for full device details, see Chapters 7 and 10, which report results from the same device).

As we know, the purity of a physical quantum bit will change in time as the qubit undergoes T_1 and T_2 processes: in the latter process, the qubit's purity will decay as the state is drawn from the surface of the Bloch sphere to the center; in the former, the qubit will lose purity as it passes through the volume of the Bloch sphere, followed by an asymptotic recovery in purity as it decays to its ground state $|0\rangle$. In Fig. 5-3, we show simulation results for a single qubit evolving under the influence of amplitude damping and dephasing channels, plotting both the state of the qubit on the Bloch sphere in time, as well as the corresponding purity of the state.

Let's test this on physical hardware. To perform this measurement, we make making a small modification to the two-qubit SWAP test from Fig. 5-1: after preparing the state ρ on both qubits, we will wait a variable length of time t before performing the Bell state. During this time, the qubits will each experience T_1 and T_2 processes, and the SWAP test will record the average purity of the two states as they evolve in time. This measurement will correspond to the quantum circuit shown in Fig. 5-4, where the Hadamard and CNOT gates are compiled into the native transmon gate set using the decompositions from Eqs. (5.38) and (5.41). Pulling the pieces together, our experiment proceeds as follows:

1. Initialize two physical transmon qubits in a common state of interest ρ using single-qubit rotations.

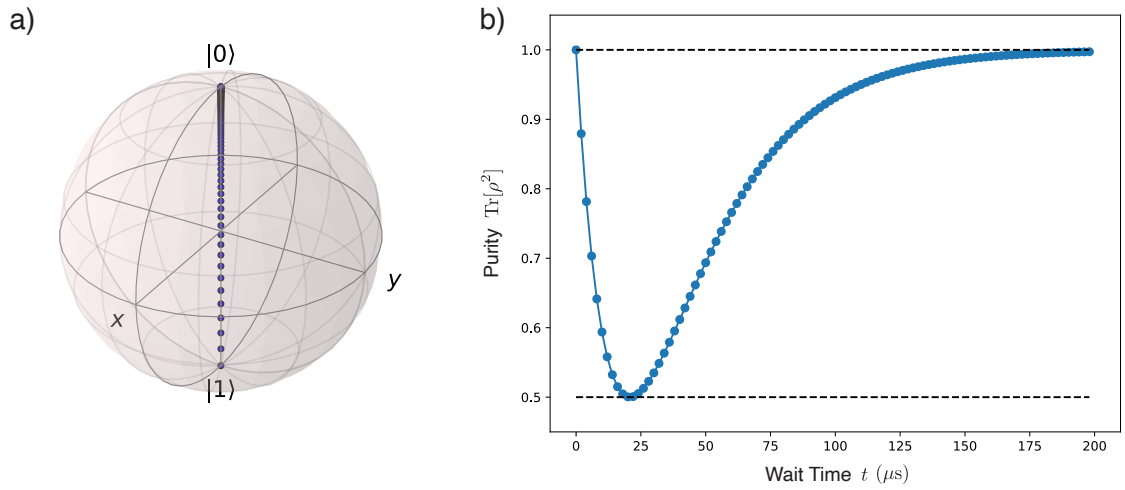

Figure 5-3: Simulation of a single qubit evolving under the influence of amplitude damping and dephasing channels, for an arbitrary choice of coherence times $T_1 = T_2 = 30\mu$s. **(a)** The state of the qubit, sampled at discrete times and plotted as a series of points on the Bloch sphere. When the qubit is initialized in $|1\rangle$, the amplitude damping channel pulls the qubit state through the volume of the Bloch sphere, exponentially decaying to the $|0\rangle$-state. **(b)** The purity of the qubit $\gamma = \mathrm{Tr}[\rho^2]$ calculated at each discrete time in (a). At $t = 0$, the qubit begins in a maximally pure state ($\gamma = 1$, upper dashed line); the qubit then decays to a maximally mixed state at the center of the Bloch sphere, where its purity reaches the theoretical minimum for a single-qubit state ($\gamma = 1/2$, lower dashed line); as the qubit state passes through the center of the Bloch sphere and exponentially decays to the $|0\rangle$-state, its purity gradually recovers and asymptotes back to its maximum ($\gamma = 1$).

2. Wait for time t.

3. Perform a Bell measurement on the two-qubit product state $\rho \otimes \rho$, recording the parity from the two outputs bits.

4. Repeat the circuit many times, gradually building up an estimate for probability of $\rho \otimes \rho$ being in an even parity state (p_{even}) or an odd parity state (p_{odd}).

5. In classical post-processing, subtract the two probabilities to get an estimate for the purity of state ρ.

6. Increase the waiting time t and repeat steps 1 through 5, resulting in an estimate of the purity at the new time.

7. Repeat for several values of t, sampled between $t = 0$ and some later time where

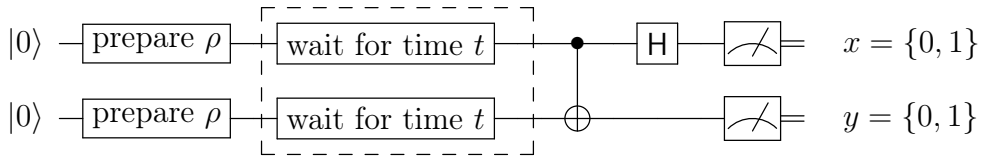

Figure 5-4: A modified version of the standard two-qubit SWAP test in Eq. (5.43). By running the SWAP test many times for several values of the waiting time t, we expect to see the purity of the qubit decay due to amplitude damping and dephasing environment-induced dephasing.

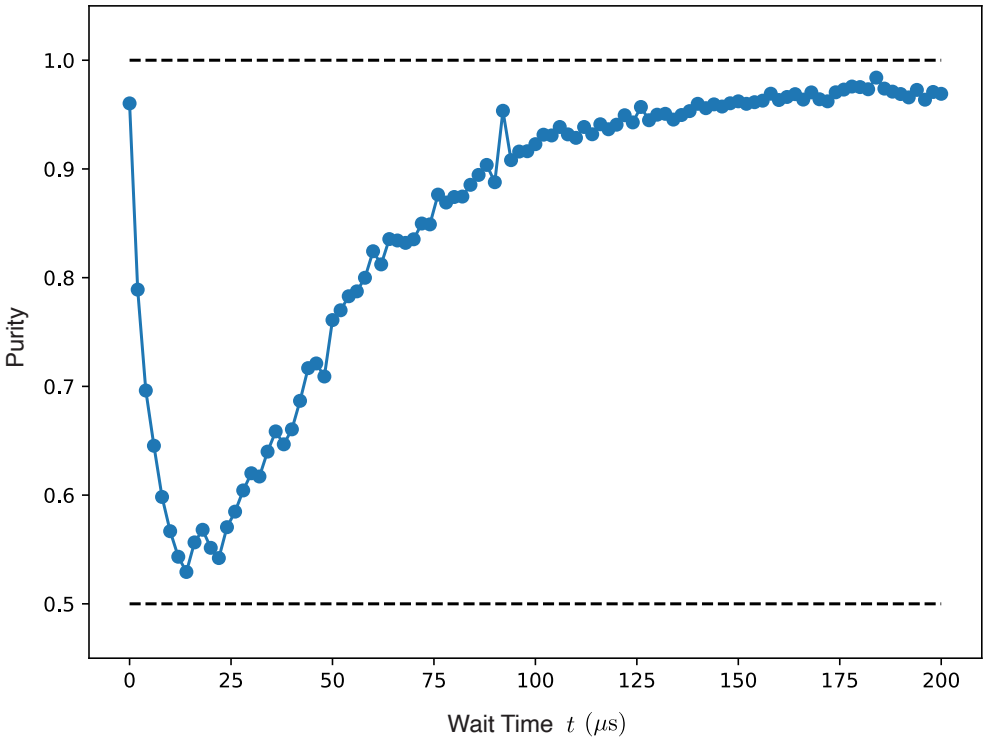

Figure 5-5: Experimental results of the SWAP test applied to two superconducting transmon qubits, each initialized in the $|1\rangle$-state. Running the circuit from Fig. 5-4 for the initial two-qubit state $\rho \otimes \rho = |11\rangle\langle 11|$, we see that the reported single-qubit purity decays in much the same way as predicted in our simulation from Fig. 5-3.

the two qubit states have largely decayed $t \gg T_2$.

In Fig. 5-5, we show the results of running this experiment on a pair of transmon

qubits, where the two qubits are initialized as two copies of the same state $\rho = |1\rangle\langle 1|$

$$\rho \otimes \rho = |1\rangle\langle 1| \otimes |1\rangle\langle 1| = |11\rangle\langle 11| \tag{5.66}$$

Allowing the two qubits to decay over the course of 200μs and plotting the results of the SWAP test at a number of discrete times, we see that the purity of the underlying single-qubit states decays near the theoretical maximum at $t = 0$ to near its minimum at $t \sim 20\mu$s, after which it exponentially decays back to pure state. Note that the purity in Fig. 5-5 begins slightly lower than the theoretical maximum ($\gamma = 1$, upper dashed line) and decays to slightly above the theoretical minimum ($\gamma = 1$, upper dashed line). While the exact cause of this deviation was not investigated in this experiment, this deviation between theory and experiment is consistent which the presence of state-preparation and measurement (SPAM) errors, where the qubits are not prepared exactly in the $|1\rangle$-state at the start of the experiment (due, for example, to some significant thermal population prior to the preparation pulse). We will return to errors of this form in greater detail in Part IV.

How do the results of the SWAP test compare to the value of the purity we would have extracted from state tomography of the underlying single- and two-qubit states over time? In Fig. 5-6, we plot exactly that. Here, the blue data points correspond to the results of the SWAP test, exactly as in Fig. 5-5. In orange, we overlay the two-qubit purity recorded from two-qubit state tomography of both qubits at each discrete delay time. Since the two-qubit purity has a minimum of $\gamma = 1/d = 1/4$, we can compare it to the single-qubit purity reported by the SWAP test by taking its square root at each time (plotted in green), which qualitatively follows the value reported by the SWAP test.

As a final comparison, we can compare the single-qubit purity calculated by the SWAP test with the actual single-qubit purity of each of the constituent qubits. To do this, we can take the two-qubit 4×4 density matrix found using two-qubit state tomography at each discrete time, trace out each of the underlying qubits to get their respective single-qubit 2×2 density matrices, and then calculate the purity of each

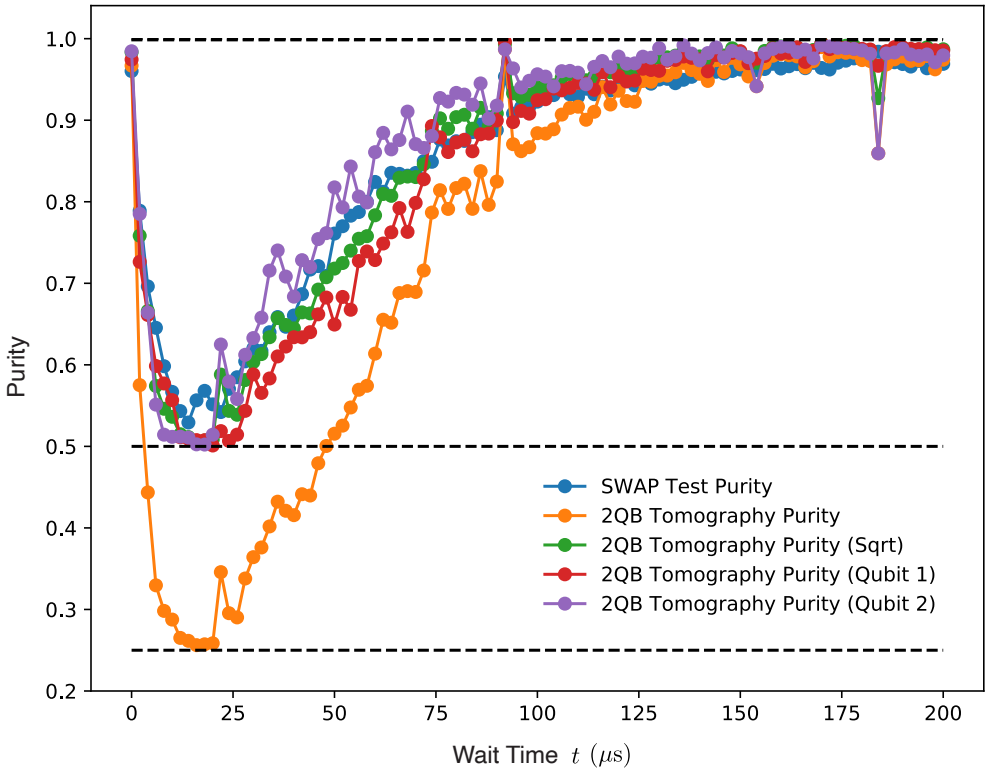

Figure 5-6: Experimental comparison of the purity calculated using the SWAP test (blue, same data set as Fig. 5-5) and the value calculated brute force using state tomography. In orange, we overlay the purity calculated from two-qubit state tomography of the pair of qubits at each time step; since, the two-qubit purity has a minimum of $\gamma = 1/d = 1/4$, we can compare it to the single-qubit purity reported by the SWAP test by taking the square root at each time (plotted in green). In red and purple, we plot the single-qubit purity of each qubit, calculated by tracing their respective single-qubit density matrices from the two-qubit tomography results.

individual qubit from their respective density matrices. In Fig. 5-6, we plot the single-qubit purity calculated from the single-qubit density matrices of each qubit at each discrete delay time, shown in red and purple, respectively. Comparing the red and purple curves, we see that the two qubits decay at slightly different rates—consistent with the two qubits having slightly different coherence times—and the purity recorded by the SWAP test falls between the two. Indeed, when the two copies of ρ required for the SWAP test begin to deviate from one another—such that one qubit is in state ρ and the other in a different state σ—the SWAP test no longer reports the purity,

but rather the *fidelity* between the two imperfect copies

$$\mathcal{F}(\rho, \sigma) = \mathrm{Tr}\left[\rho\,\sigma\right] \tag{5.67}$$

$$= \mathrm{Tr}\left[(\rho \otimes \sigma)\,\mathsf{SWAP}\right] \tag{5.68}$$

In this sense, the SWAP test is a simple example of a basic *quantum characterization* protocol, efficiently extracting some information about the input state. Indeed, we will return to such techniques in greater detail in Part IV of this thesis.

Chapter 6

Calibrating a Universal Gate Set

In Chapter 5, we considered the theoretical foundations of quantum algorithms composed of discrete gate operations, and we showed how to construct a general multi-qubit algorithm out of a small universal gate set composed of only single- and two-qubit operations. In this chapter, we will walk through the steps required to calibrate a universal gate set on a device consisting of coupled superconducting transmon qubits. Building on the device physics of superconducting qubits we built up in Chapter 3, this chapter will outline a set of techniques for calibrating microwave single-qubit gates, as well as a two-qubit CZ gate using local magnetic flux biases. These techniques will then form the foundation of the algorithmic study in Chapter 7, where we utilize these gate operations to perform a deep quantum algorithm, Density Matrix Exponentiation.

This chapter is based on the gate calibration techniques my colleagues and I employed during the Density Matrix Exponentiation [247] and Lindblad tomography [399] experiments reported in Chapters 7 and 10, and I gratefully acknowledge my colleagues Alex Greene and Morten Kjaergaard for their contributions to the calibration protocol reported in this chapter. Portions of the background material outlining the principles of single- and two-qubit gates in superconducting qubits are adapted from Ref. [257].

6.1 Single-Qubit Microwave Gates

In Chapter 5, we showed that any multi-qubit algorithm can be synthesized out of a gate set consisting of the following single- and two-qubit operations

$$\mathcal{G}' = \{\mathsf{X}_\theta, \mathsf{Y}_\theta, \mathsf{Z}_\theta, \mathsf{Ph}_\theta, \mathsf{CZ}\}. \tag{6.1}$$

These quantum operators are mathematical abstractions: taking the matrix representation of each gate, we can show that combinations of these operations allow us to rotate any multi-qubit wavefunction $|\psi\rangle$ into any other wavefunction $|\phi\rangle$ of equal dimension. Thus, these operations form the building blocks of a universal quantum computer, a device capable of performing any desired n-qubit unitary operation. That is, in theory. While the mathematical soundness of this observation is indisputable, quantum computers are not simply theoretical abstractions which live on paper or in a Python notebook. Quantum computers are pieces of hardware—assemblages of wiring and control electronics percision engineered to bring these abstraction to life. Thus, our challenge as quantum engineers is to take the universal gate set in Eq. (6.1) and realize it in physical hardware. The performance of our quantum processor will then depend on the success of our translation, our ability to give these matrices electrical and magnetic flesh.

In this section, we will start by considering the single-qubit gates in Eq. (6.1) and show how to generate these operations with high-fidelity in an architecture of superconducting transmon qubits. This discussion will build naturally on our discussion of the transmon circuit from Section 3.3, showing how such circuits are affected by the introduction of a microwave drive signal. Following a brief outline of the physics at play, we will then walk through the calibration protocol we deploy to calibrate these operations with high fidelity in the laboratory.

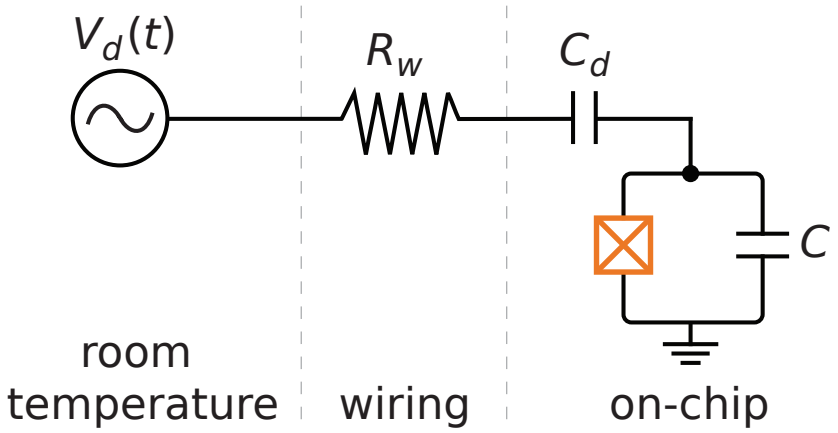

Figure 6-1: Circuit schematic of a microwave drive line coupled to a superconducting transmon qubit. The microwave source produces a time-dependent voltage $V_d(t)$ which travels along a feed line with impedance R_w and capacitively coupled to one of the circuit nodes with capacitance C_d. Figure reproduced from Ref. [257].

6.1.1 Realizing X and Y Gates Using Capacitive Coupling

Consider a single superconducting qubit coupled to a microwave source, as sketched in Fig. 6-1. As we did in Chapter 3, we can start by writing the classical Hamiltonian of this circuit in terms of the charge and flux at each node of the circuit. For simplicity, we can start by treating the qubit as a generic LC-oscillator as in Eq. (3.31). Making this simplification, the combined Hamiltonian of the qubit and drive line is given by

$$H = \frac{1}{2C_\Sigma}\tilde{q}(t)^2 + \frac{1}{2L}\Phi^2 + \frac{C_d}{C_\Sigma}V_d(t)\,\tilde{q} \tag{6.2}$$

where C_d is the capacitance between the qubit and the drive line, $C_\Sigma = C + C_d$ is the total capacitance to ground, and $\tilde{q} = C_\Sigma\dot{\Phi} - C_d V_d(t)$ is the renormalized charge variable of the circuit. Having written the classical Hamiltonian of the circuit, we can now promote the classical electrical variables $\tilde{q}, \Phi$ to quantum mechanical operators $\hat{q}, \hat{\Phi}$ and arrive at the Hamiltonian operator for the combined circuit

$$\hat{H} = \frac{1}{2C_\Sigma}\hat{q}(t)^2 + \frac{1}{2L}\hat{\Phi}^2 + \frac{C_d}{C_\Sigma}V_d(t)\,\hat{q}. \tag{6.3}$$

Drawing on Eqs. (3.134) and (3.136) from Chapter 3, we can perform a basis transformation and rewrite this Hamiltonian in terms of the creation and annihilation operators of the harmonic oscillator

$$\hat{\Phi} = \sqrt{\frac{\hbar Z_0}{2}}(\hat{a}^\dagger + \hat{a}) \tag{6.4}$$

$$\hat{q} = i\sqrt{\frac{\hbar}{2Z_0}}(\hat{a}^\dagger - \hat{a}) \tag{6.5}$$

where $Z_0 = \sqrt{L/C}$ is the impedance of the circuit to ground. Plugging these relations into Eq. (6.3), we arrive at the Hamiltonian

$$\hat{H} = \omega\left(\hat{a}^\dagger\hat{a} + \frac{1}{2}\right) + \frac{C_d}{C_\Sigma}V_d(t)\, i\sqrt{\frac{\hbar}{2Z_0}}(\hat{a}^\dagger - \hat{a}) \tag{6.6}$$

where $\omega = 1/\sqrt{LC}$ is the fundamental frequency of the LC oscillator. Now, since we are using the LC circuit as a stand-in for a generic qubit circuit, we can finally truncate this Hamiltonian such that it only includes the lowest two levels of the oscillator. This truncation is equivalent to the operator substitution

$$\hat{a} \quad \rightarrow \quad \hat{\sigma}_- = \begin{bmatrix} 0 & 0 \\ 1 & 0 \end{bmatrix} \tag{6.7}$$

$$\hat{a}^\dagger \quad \rightarrow \quad \hat{\sigma}_+ = \begin{bmatrix} 0 & 1 \\ 0 & 0 \end{bmatrix}. \tag{6.8}$$

Substituting these 2×2 operators into the Hamiltonian in Eq. (6.6) and dropping the constant offset in the qubit Hamiltonian, we arrive at a form of the Hamiltonian in terms of the familiar Pauli operators

$$\hat{H} = -\frac{\omega_q}{2}\,\hat{Z} + \Omega V_d(t)\,\hat{Y} \tag{6.9}$$

where $\Omega = (C_d/C_\Sigma)\sqrt{\hbar/2Z_0}$ and $\omega_q = (E_1 - E_0)/\hbar$ is the transition frequency of the qubit.

Looking at the right-hand side of Eq. (6.9), we can see that the Hamiltonian breaks nicely into two parts: the first term is simply the bare qubit Hamiltonian H_0; the second, a perturbation H_d due to the introduction of the drive line. Rewriting H_d in the rotating frame of the qubit, this latter term takes on the form

$$\widetilde{H}_d = \Omega V_d(t) \left(\cos(\omega_q t)\,\hat{Y} - \sin(\omega_q t)\,\hat{X}\right). \tag{6.10}$$

In general, we can write the time-dependent voltage in the form

$$V_d(t) = V_0 s(t)\sin(\omega_d t + \phi) \tag{6.11}$$

$$= V_0 s(t)\left(\cos(\phi)\sin(\omega_d t) + \sin(\phi)\cos(\omega_d t)\right) \tag{6.12}$$

where the amplitude V_0 has units of voltage, $s(t)$ is a dimensionless envelope function, and the oscillating part of the voltage can be rewritten in terms of the *in-phase* component $\mathcal{I}$ and *out-of-phase* (or *quadrature*) component $\mathcal{Q}$ of the signal

$$\mathcal{I} = \cos(\phi) \tag{6.13}$$

$$\mathcal{Q} = \sin(\phi). \tag{6.14}$$

Writing Eq. (6.12) in terms of $\mathcal{I}$ and $\mathcal{Q}$ and plugging this expression back into the Hamiltonian in Eq. (6.10), we can rewrite the drive Hamiltonian in the rotating frame as

$$\widetilde{H}_d = \Omega V_0 s(t)\left(\mathcal{I}\sin(\omega_d t) + \mathcal{Q}\cos(\omega_d t)\right) \times \left(\cos(\omega_q t)\,\hat{Y} - \sin(\omega_q t)\,\hat{X}\right). \tag{6.15}$$

Multiplying everything out and taking the rotating wave approximation (i.e., dropping the terms which oscillate at frequency $\omega_q + \omega_d$), we finally arrive at a compact

expression for the drive Hamiltonian

$$\widetilde{H}_d = -\frac{\Omega}{2} V_0 s(t) \begin{bmatrix} 0 & e^{i(\delta\omega\, t+\phi)} \\ e^{-i(\delta\omega\, t+\phi)} & 0 \end{bmatrix} \tag{6.16}$$

where $\delta\omega = \omega_q - \omega_d$ is the detuning between the qubit and drive frequencies.

The relation we arrived at in Eq. (6.16) is extremely powerful. To see why, consider the case where the drive frequency is resonant with the qubit frequency and $\delta\omega = 0$

$$\widetilde{H}_d = -\frac{\Omega}{2} V_0 s(t) \left(\mathcal{I}\hat{X} + \mathcal{Q}\hat{Y} \right). \tag{6.17}$$

From this equation, we see that the introduction of a microwave drive capacitively coupled to our qubit allows us to implement X- or Y-rotations of the qubit state, depending on the phase of the drive signal:

$\boldsymbol{\phi = 0}$: When the drive is applied *in-phase*, the drive Hamiltonian will be proportional to $\hat{X}$, and the qubit state will rotate around the x-axis of the Bloch sphere.

$\boldsymbol{\phi = \pi/2}$: When the drive is applied *in quadrature*, the drive Hamiltonian will be proportional to $\hat{X}$, and the qubit state will instead rotate around the y-axis of the Bloch sphere.

Thus, by choosing the phase of the drive signal between $\phi = 0$ and $\phi = 2\pi$, we can harness the drive Hamiltonian in Eq. (6.17) to generate rotations around an arbitrary axis in the xy-plane of the Bloch sphere

To see how the Hamiltonian in Eq. (6.17) can be harnessed to perform discrete gate operations, we can exponentiate this Hamiltonian to arrive at the corresponding unitary operator

$$\hat{U}_d(t) = \exp\left(\frac{i}{2} \Omega V_0 \int_0^t s(t')\, dt' \, \left[\mathcal{I}\hat{X} + \mathcal{Q}\hat{Y} \right] \right). \tag{6.18}$$

Looking at this unitary operator, we see we now have all the ingredients we need to generate arbitrary X and Y gates. As we just argued, the axis of rotation will be set by the phase of the drive signal ϕ, allowing us to choose whether to perform an X

gate or a Y—or indeed, some arbitrary combination of the two. As for the angle of rotation around this axis, we can see that this is determined by the remaining factors in the exponent, which we can group into an angle

$$\Theta(t) = -\Omega V_0 \int_0^t s(t')\, dt'. \tag{6.19}$$

Looking at this angle, we see that it depends only on the design parameters of the device—i.e., the capacitive coupling to the drive line and the impedance of the circuit—and the amplitude V_0 and envelope $s(t)$ of the drive pulse. Thus, by plugging in the fixed design parameters of the circuit and solving Eq. (6.19) for a desired rotation angle Θ, we can easily find the amplitude and envelope of the pulse required to perform the desired gate operation. From there, we can program the desired pulse shape using an arbitrary waveform generator (AWG) at the input of the drive line, mixing together the desired weighting of $\mathcal{I}$ and $\mathcal{Q}$ to execute the desired rotation.

6.1.2 'Virtual' Z Gates

So far, we have shown how to perform arbitrary X and Y gates using a microwave drive line coupled to the qubit circuit. What about Z gates? As it turns out, we already have all the tools we need to perform arbitrary Z rotations, without introducing any additional control hardware. As we just showed, the only difference between a physical X and Y gate comes from the choice of phase ϕ in the applied microwave signal: offsetting all our pulses by a phase $\phi + \pi/2$, we would effectively turn all of our X gates to Y gates and vice versa (with a change of sign). Recalling our introduction to the Pauli operators in Chapter 2, we'll remember that there is a mathematical operator which performs the exact same exchange of $\hat{X}$ and $\hat{Y}$: the $\hat{Z}$ operator! In this sense, the phase degree of freedom in our microwave drive allows us to encode the action of a Z gate without actually applying a dedicated physical gate. This technique, first shown in Ref. [300], is commonly referred to as a 'virtual' Z gate.

To see how the virtual Z gate works in practice, consider a simple quantum circuit

containing a collection of X, Y, and Z gates of arbitrary angle:

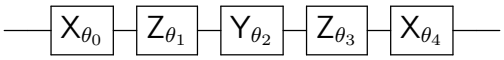

(6.20)

Written as such, this circuit has a depth of five, and it thus requires five physical single-qubit gates to perform the action of this sequence. However, following the argument above, we can absorb each of the Z gates in the circuit above into the X or Y gate which follows it, modifying the phase of pulse accordingly and producing leaving us with an equivalent circuit

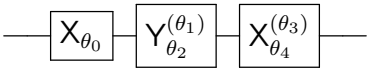

(6.21)

What is the difference between the operations X_{θ_4} and $\mathsf{X}^{(\theta_3)}_{\theta_4}$? Both gates correspond to microwave pulses generated using the $\mathcal{I}$ channel of the AWG, with envelopes calculated such that a total rotation angle of θ_4 is performed. However, we have added an additional phase offset of θ_3 to the latter pulse, absorbing the action of the Z rotation which proceeded it. In the process, we have reduced the depth of our circuit from five to three, reducing the number of physical operations we need to perform to implement the exact same unitary operation.

In many ways, the absorption of the virtual Z gates is similar in spirit to the idea of circuit compilation we considered in Chapter 5, with a key difference. In circuit compilation, non-native gates are realized through combinations of a limited number of pre-defined gates in your native gate set, provided that gate set is universal. In the case of these virtual gates, however, the presence of a Z gate physically alters the native gates surrounding it, modifying the action of those gates. As such, we can draw upon both virtual gates *and* circuit compilation to dramatically reduce the number of physical gates we need to calibrate to one. To see this, we can use the following result from Ref. [301], which shows that any general single-qubit rotation can be generated using only discrete $\mathsf{X}_{\frac{\pi}{2}}$ gates and continuous-angle Z gates

$$\hat{U}(\theta,\phi,\lambda) = \mathsf{Z}_{\phi-\frac{\pi}{2}}\,\mathsf{X}_{\frac{\pi}{2}}\,\mathsf{Z}_{\pi-\theta}\,\mathsf{X}_{\frac{\pi}{2}}\,\mathsf{Z}_{\lambda-\frac{\pi}{2}}. \tag{6.22}$$

Thus, drawing on the device physics we have sketched in this chapter so far, we see that it is possible to generate a universal set of single-qubit rotations using only a single gate calibration: all we have to do is calibrate a single $\mathsf{X}_{\frac{\pi}{2}}$ gate, and every possible single-qubit rotation will follow from the correct choice of virtual Z gates surrounding it.

6.1.3 Accounting for Higher Levels Using DRAG

Before we proceed to an example calibration routine for a physical transmon device, we need to return to a point we brushed under the rug in Section 6.1.1. In our derivation of the driven Hamiltonian which gives rise to our X and Y gates, we conveniently truncated our Hamiltonian to a 2×2 matrix, treating our qubit as a perfect two-level system. As we showed in Chapter 3, this is a highly idealized picture of a physical superconducting qubit—in reality, our circuit has an infinite ladder of higher-energy states, just like an LC oscillator. Now, unlike an LC oscillator, the addition of a Josephson junction adds some anharmonicity to this level structure, and in principle this allows us to uniquely address the lowest two states, treating these two levels as the computational states of a quantum bit.

In reality, however, these higher levels continue to play a part, and we must account for the presence of these higher levels when we attempt to drive transitions between our qubit states, particularly in the case of weakly anharmonic qubits such as the transmon. To see why these higher transitions continue to play a part, consider a microwave drive signal of the form in Eq. (6.17), where the pulse envelope $s(t)$ is a Gaussian function in time. Since our qubits have finite T_1 and T_2 times, we want to make our pulses as short as possible so we can perform as many gate operations as possible before our qubits decay—for a given rotation angle, this corresponds to reducing the width of the envelope $s(t)$ and increasing its amplitude such that the time integral of the pulse remains constant, as we can see in Eq. (6.19). Here, however, we encounter a tradeoff. While reducing the width of the envelope $s(t)$ means we can now perform more gates within the limited coherence time of our qubit, reducing the width of the envelope in time *increases* its width in frequency. Taking the Fourier

transform of a narrow Gaussian envelope $s(t)$, we will find that our pulse now includes a broad spectrum of frequency components, including components which are resonant with the higher transitions of our qubit. As we make our pulse shorter and shorter, the amplitude of these additional frequency components will increase, and we will find that our gate excites not only transitions between $|0\rangle$ and $|1\rangle$ but also between $|1\rangle$ and $|2\rangle$, $|2\rangle$ and $|3\rangle$, and higher and higher up the ladder.

This sort of leakage to states outside the computational basis is exactly what we were hoping to avoid by moving away the LC oscillator. Fortunately, however, there are techniques to mitigate this effect, allowing us to achieve short single-qubit gates with minimal leakage to higher levels. Among these techniques, one of the simplest and most ubiquitous in superconducting qubits is known as Derivative Reduction by Adiabatic Gate, or DRAG for short [113, 152, 320, 321]. The idea behind DRAG is simple: while you output a gate with envelope $s(t)$ on either the $\mathcal{I}$ or $\mathcal{Q}$ ports of your AWG, simultaneously output a signal proportional to the *derivative* of this pulse on the other port of the AWG

$$s(t) \text{ on } \mathcal{I} \quad \rightarrow \quad s' = \begin{cases} s(t) & \text{on } \mathcal{I} \\ \frac{\lambda}{\alpha}\dot{s}(t) & \text{on } \mathcal{Q} \end{cases} \tag{6.23}$$

and vice versa for a pulse on $\mathcal{Q}$, where α is the anharmonicity of the qubit and λ is a dimensionless scaling parameter which we can tune during the calibration of our gate. As we will show in the following section, proper implementation of DRAG is essential to tuning up high fidelity single-qubit gates, and it will occupy a considerable portion of our calibration routine.

6.2 Single-Qubit Gate Calibration Protocol

In this section, we will apply the principles we discussed in the previous section and walk through the steps for calibrating high-fidelity single-qubit gates on a transmon qubit, considering each of the calibration techniques performed in the laboratory. In

the process, we will deliberately commit a profound faux pas. When data is taken in the laboratory, the plots which are recorded often bear the inscrutable names of the specific instruments and variables which were swept to take the data. When data is presented in formal settings—such as a publication, a conference presentation, or a dissertation—it is usually imperative to translate these names into more generally acceptable scientific language. For example, the voltage recorded by the digitizer of a field programmable gate array (FPGA) might be relabeled as '$|1\rangle$-state population', since that is what the signal coming into the digitizer is a proxy for. In this section of the thesis, and this section only, we have chosen to leave the figures unaltered and report them exactly as they are recorded by our measurement software during the calibration process. In this way, we hope to emphasize the constant process of translation which is required during gate calibration, oscillating between the language of instruments and the language of qubits. In the caption of each figure, an explanation is provided to orient the reader and instruct them how to interpret the plot as an experimentalist would in the laboratory.

6.2.1 Finding the Sweet Spot: Roughly

For fixed-frequency transmons of the form we first considered in Section 3.3, the energy spectrum is set entirely by the electrical parameters which are hard-coded into the device during fabrication, such as the physical size of the capacitor paddles and the thickness of the oxide layer in the Josephson junction. In flux-tunable transmons of the form we will consider for the remainder of this thesis, we can tune the energy spectrum of our qubit *in situ* by applying a magnetic flux bias through its DC-SQUID loop, giving us a continuous range of bias parameters at which to implement our single-qubit gates. While this continuous degree of freedom will prove enormously useful for implementing two-qubit gates later in this chapter, when it comes to performing single-qubit gates, we typically choose one bias point in particular: the *sweet spot* corresponding to the maximum frequency of the transmon versus flux. At this point, the first derivative of frequency with respect to magnetic flux equals zero, and the qubit is thus first-order insensitive to small changes in the magnetic flux at this

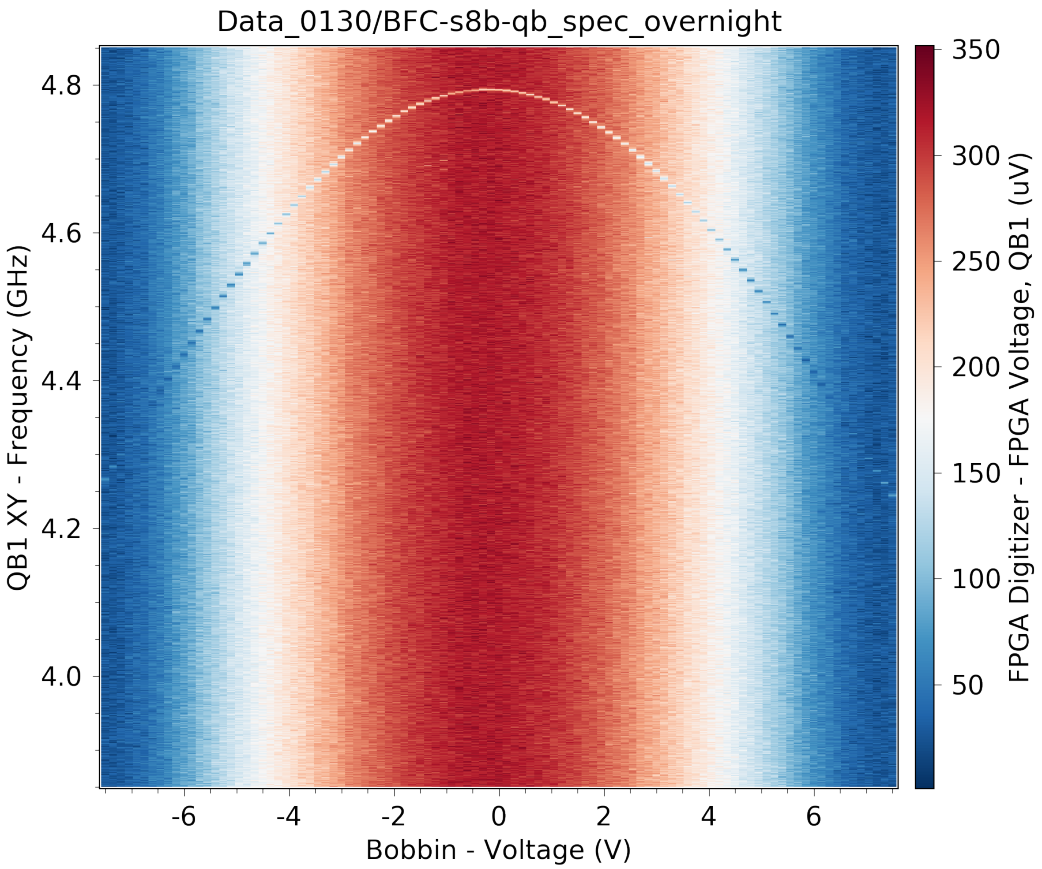

Figure 6-2: Rough qubit spectroscopy of a tunable transmon for a range of magnetic flux biases. Here, the x-axis corresponds to the voltage applied through a bobbin of wire positioned over the qubit chip—as the voltage changes, so too does the current through the bobbin wire, which in turn induces a variable magnetic flux perpendicular to the qubit circuit, biasing the transmon. At each value of the flux bias, the frequency of the drive signal is swept (y-axis) and the signal through the transmission line is recorded by an FPGA digitizer at room temperature (z-axis colormap); when the drive signal is resonant with the transition frequency of the qubit, the frequency of the readout resonator coupled to the qubit shifts and a peak is recorded by the digitizer. Watching this peak move as a function of the applied flux bias, we trace out the upside-down parabola characteristic of the transmon spectrum. The highest point of this parabola, where the first derivative with repect to flux is zero, is commonly referred to as the sweet spot of the qubit, and this point is typically chosen as the operating point for single-qubit gates.

point, reducing the impact of flux noise in the environment. As such, single-qubit gates performed at this symmetry point will generally incur smaller incoherent errors due to qubit dephasing during the duration of the gate operation, resulting in higher fidelity operations.

To find the sweet spot of a tunable transmon, we perform qubit spectroscopy, varying the frequency of a microwave tone and observing the signal through the transmission line to which the qubit is coupled. When the drive signal is resonant with a qubit transition, the qubit will be incoherently driven into a mixed state, shifting the frequency of the readout resonator between it and the transmission line, resulting in a spectroscopy peak at that generator frequency [257]. Performing qubit spectroscopy at a set of discrete flux bias points, we can gradually map out the spectrum of the qubit versus flux and look for the symmetry point where the qubit frequency is maximum. Having found the approximate bias point corresponding to the maximum frequency of the qubit, we record this flux bias and the frequency of the qubit at this point. This will give us an approximate set of coordinates at which to start calibrating our single-qubit gates, coordinates which will be fine-tuned later in the calbration protocol.

6.2.2 Calibrating a π-Pulse Using Rabi Oscillations

Having found the approximate bias point of the sweet spot and the frequency of the qubit at this bias point, we can begin to calibrate π-pulse. To do this, we start by sending down a pulse on the $\mathcal{I}$ port of our AWG, where the frequency of the pulse is set by the transition rough frequency found in spectroscopy and the shape of the envelope is determined by three parameters: the functional form of the envelope, the width of the envelope, and the amplitude of the pulse. Having chosen a functional form of the pulse—typically Gaussian or cosinusoidal, such that the signal is well localized in time—the task is to find the right combination of pulse width and amplitude such that enough power is sent to the qubit to excite it to its $|1\rangle$-state, executing a π-pulse.

To do this, we can choose a pulse width (typically as short as possible while also ensuring that its spectral overlap with the higher energy transitions of the qubit is small) and sweep the amplitude of the pulse, recording the Rabi oscillations which result, as in Fig. 6-3. Sweeping the amplitude of the drive, we record the pulse amplitude at which the signal achieves half of a full oscillation such that the qubit is successfully rotated to the $|1\rangle$-state. Together, this amplitude and the chosen pulse

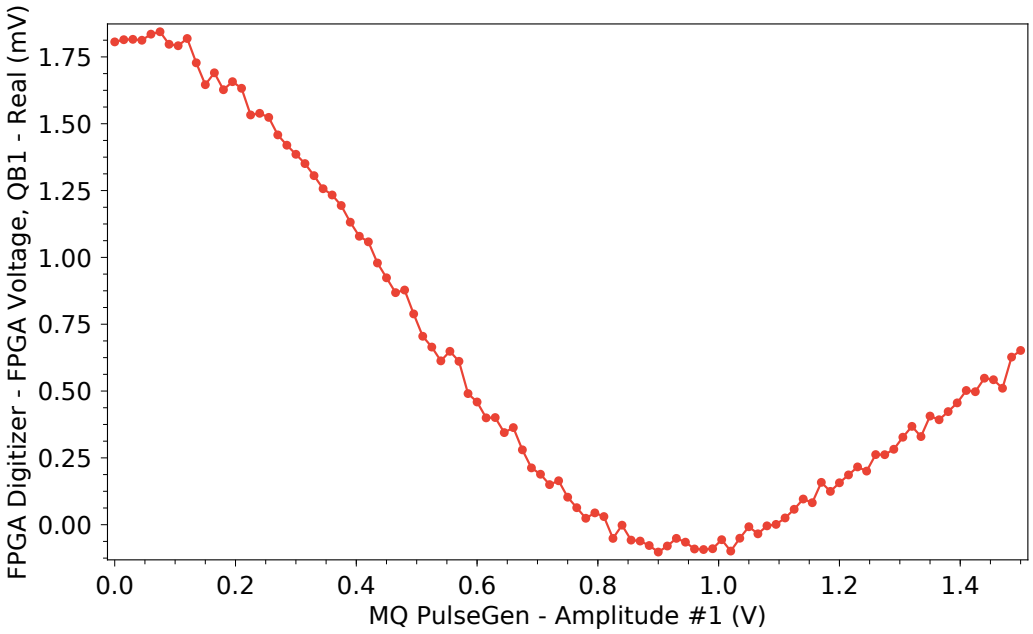

Figure 6-3: Measurement of Rabi oscillations in a tunable transmon qubit biased at its sweetspot and driven using a 30ns cosinusoidal pulse at a frequency of 4.79GHz, varying the amplitude of the signal. The observed oscillation in the magnitude of the signal recorded by the digitizer is a proxy for the state of the qubit as it coherently rotates around the medidian of its Bloch sphere from $|0\rangle$ (digitizer signal: $\sim$ 1.75mV) to $|1\rangle$ ($\sim$ 0mV) and back again. Sweeping the amplitude of the drive, we record the pulse amplitude at which the signal successfully rotates the qubit to the $|1\rangle$-state (here, $\sim$ 0.95V). Together, this amplitude and the chosen pulse width are the approximate parameters of our π-pulse.

width are the approximate parameters of our π-pulse, and we can use these values to proceed to a more precise calibration of the single-qubit gate parameters.

6.2.3 Finding the Sweet Spot: Finely

Once we have a preliminary π-pulse from our Rabi measurement, we can use this pulse to start fine-tuning its parameters more precisely, starting with the location of the bias point we found in qubit spectroscopy. In qubit spectroscopy, our ability to report a precise frequency and magnetic flux corresponding to the sweet spot is limited by the linewidth of our spectroscopy peak, which can be several megahertz wide depending on the drive power of the spectroscopy tone. Imprecise measurement of the sweet spot bias point and frequency will lead to errors in the single-qubit

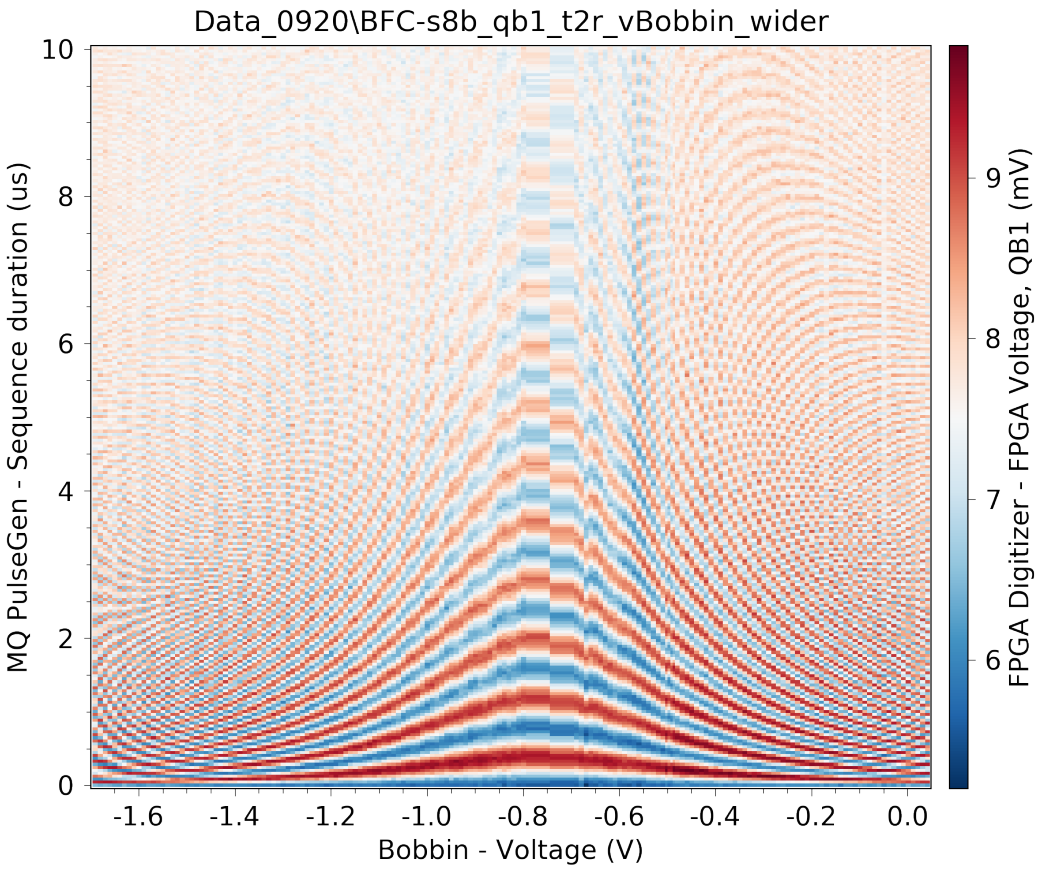

Figure 6-4: Detuned Ramsey measurements taken at a small range of flux bias points around the rough sweet spot we found in spectroscopy (x-axis). Setting the drive frequency slightly above the maximum qubit frequency we found in spectroscopy and sweeping the delay time between the two $\pi/2$-pulses of the Ramsey measurement (y-axis), we record oscillations in the qubit state population (z-axis colormap) equal to the detuning frequency between the qubit transition and the drive. Recording the symmetry point of the chevron where the detuning frequency is minimum (~ -0.75V), we arrive at a more precise value of the sweet spot flux bias point.

gates we perform at this point, in two different ways: if the frequency of the drive is inaccurate, the single-qubit gates will contain coherent errors Z errors due to the detuning in the drive; if the flux bias point is inaccurate, the qubit will not be biased on its sweet spot and will thus be more susceptible to flux noise, leading to incoherent errors during the gate.

To resolve the bias parameters of the pulse more accurately, we can use our rough π-pulse to interferometrically resolve the sweet spot using a series of detuned Ramsey measurements in the following way:

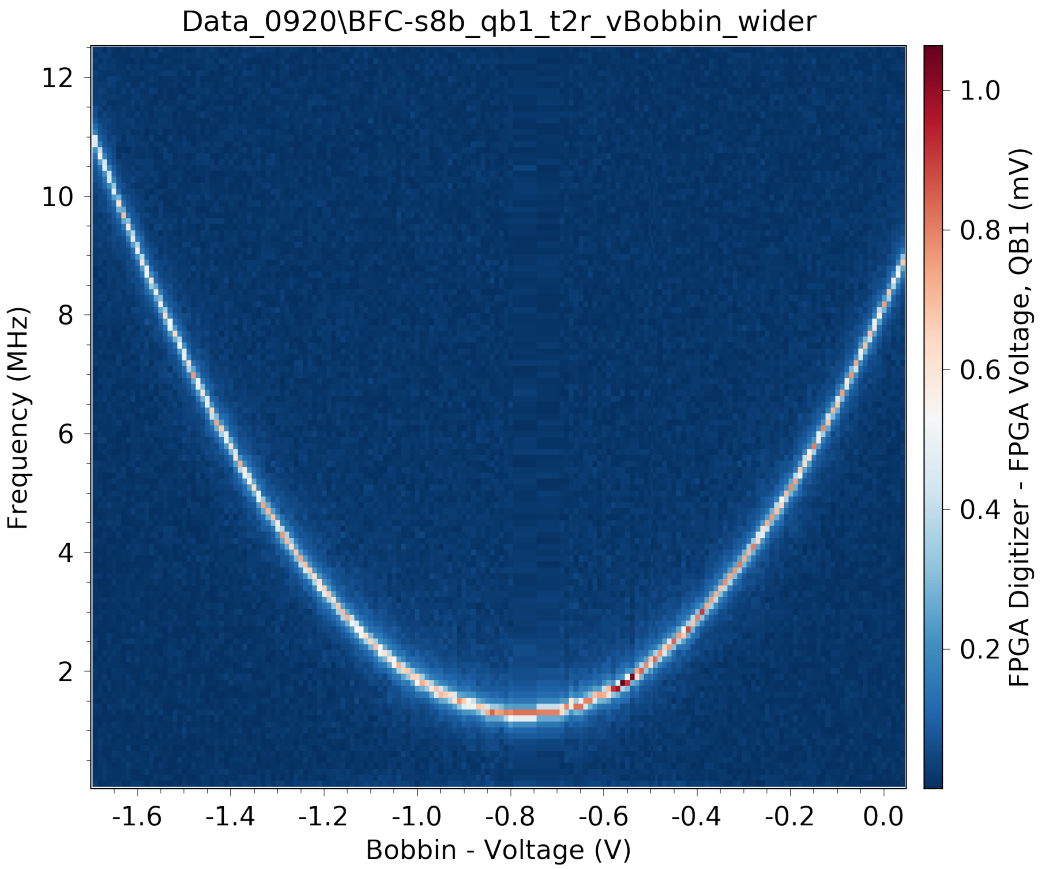

Figure 6-5: The fast Fourier transform (FFT) of each vertical trace in Fig. 6-4. Taking the FFT of each Ramsey measurement results in a peak at the oscillation frequency of the detuned Ramsey measurement (y-axis), mapping out the detuning between the drive frequency (which is fixed) and the qubit frequency (which changes as a function of the flux bias) and allowing us to interferometrically resolve changes in the qubit frequency smaller than the linewidth of our spectroscopy measurement. Recording the minimum detuning frequency and subtracting it from the frequency of the drive, we arrive at a precise measurement of the qubit transition frequency at the sweet spot.

1. Taking the π-pulse we found in our Rabi measurement, we halve the drive amplitude to obtain a $\pi/2$-pulse, allowing us to rotate the qubit state onto the equator of its Bloch sphere.

2. Setting our drive frequency to a value slightly *above* the maximum qubit frequency, we perform a standard Ramsey measurement, applying two $\pi/2$-pulses to the qubit and sweeping the delay time between the two pulses. During this time delay, the qubit state will precess along the equator of the Bloch sphere

at a frequency equal to the detuning between the qubit frequency and the drive frequency, leading to oscillations in the qubit state population as a function of delay time.

3. Repeating step 2 for a small range of flux biases around the sweet spot we found in spectroscopy, the frequency of the Ramsey measurements will decrease as the the qubit comes closer to resonance with the drive, forming a chevron pattern around the sweet spot, as in Fig. 6-4. Recording the symmetry point of the chevron, we arrive at a more precise value of the sweet spot flux bias.

4. Finally, taking the FFT of the oscillating Ramsey trace at each flux bias, we obtain a peak at the detuning frequency between drive pulse and the qubit transition. Looking at the FFT of the chevron pattern we observed in step 3, we can now precisely resolve the qubit transition frequency to greater accuracy than in our original spectroscopy measurement. Recording the frequency of the FFT peak at the sweet spot and subtracting this value from the frequency of our drive tone, we arrive at a more accurate value of the qubit frequency at the sweet spot

6.2.4 DRAG Calibration

So far, we have dialed in the parameters of a single π-pulse. For this pulse to reliably serve as an X-gate in a deep quantum algorithm, we need to test its performance in a sequence of tens, hundreds, and thousands of repeated gates. Indeed, as we perform sequences of many gates, we will become increasingly sensitive to small imperfections in the gate, and, when these errors are coherent, they can constructively build up after many applications of the gate. To calibrate away these small errors, we need to run a set of diagnostics to amplify these errors and tune them away.

In Section 6.1.3, we saw how the presence of higher levels in the transmon can lead to leakage out of the computational subspace and to coherent errors in the qubit rotation. To mitigate this effect with the DRAG protocol from Eq. (6.23), we need to find the right value of the coefficient λ which effectively cancels out the coherent

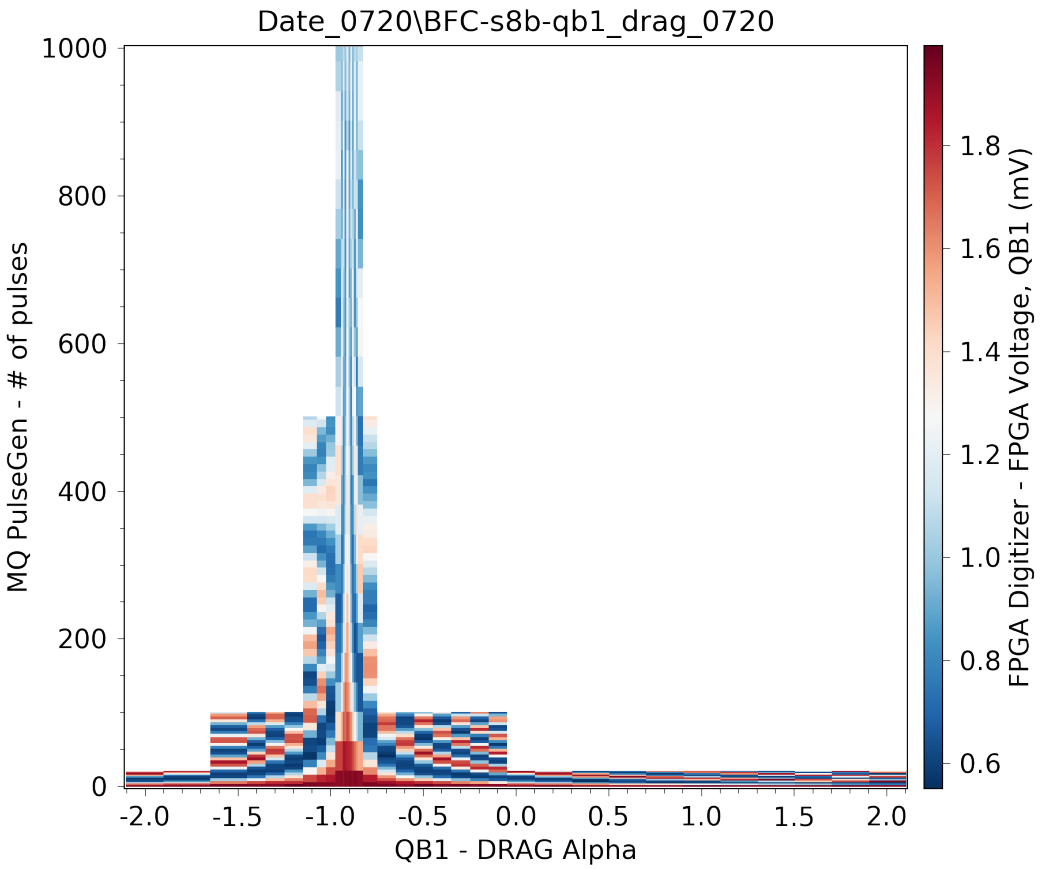

Figure 6-6: DRAG calibration of single-qubit gates. Varying the DRAG coefficient (x-axis), pairs of X-gates are applied to the qubit (y-axis) and the population of the $|0\rangle$-state is recorded (z-axis colormap, higher $|0\rangle$ population in red). When the DRAG coefficient is suboptimal, coherent over-/under-rotations in the X-gate result in oscillation in the $|0\rangle$-state population after multiple pairs of gates. When the coefficient is optimal, the DRAG protocol actively cancels the coherent errors in each gate and the qubit will monotonically decay to an incoherent mixed state as the duration of the gate sequence approaches the coherence time T_2. Recording the symmetry point of the resulting chevron—at which point the coherent oscillations disappear—we obtain the optimal DRAG parameter for our single-qubit gate. For samples of vertical traces at a few different DRAG coefficients, see Figs. 6-7 and 6-8.

over-rotations and leakage.

To calibrate the optimal DRAG parameters, we perform the following measurement: sweeping the strength of the DRAG coefficient, we perform an even number of π-pulses and measure the probability of the qubit being in the $|0\rangle$-state at the end of

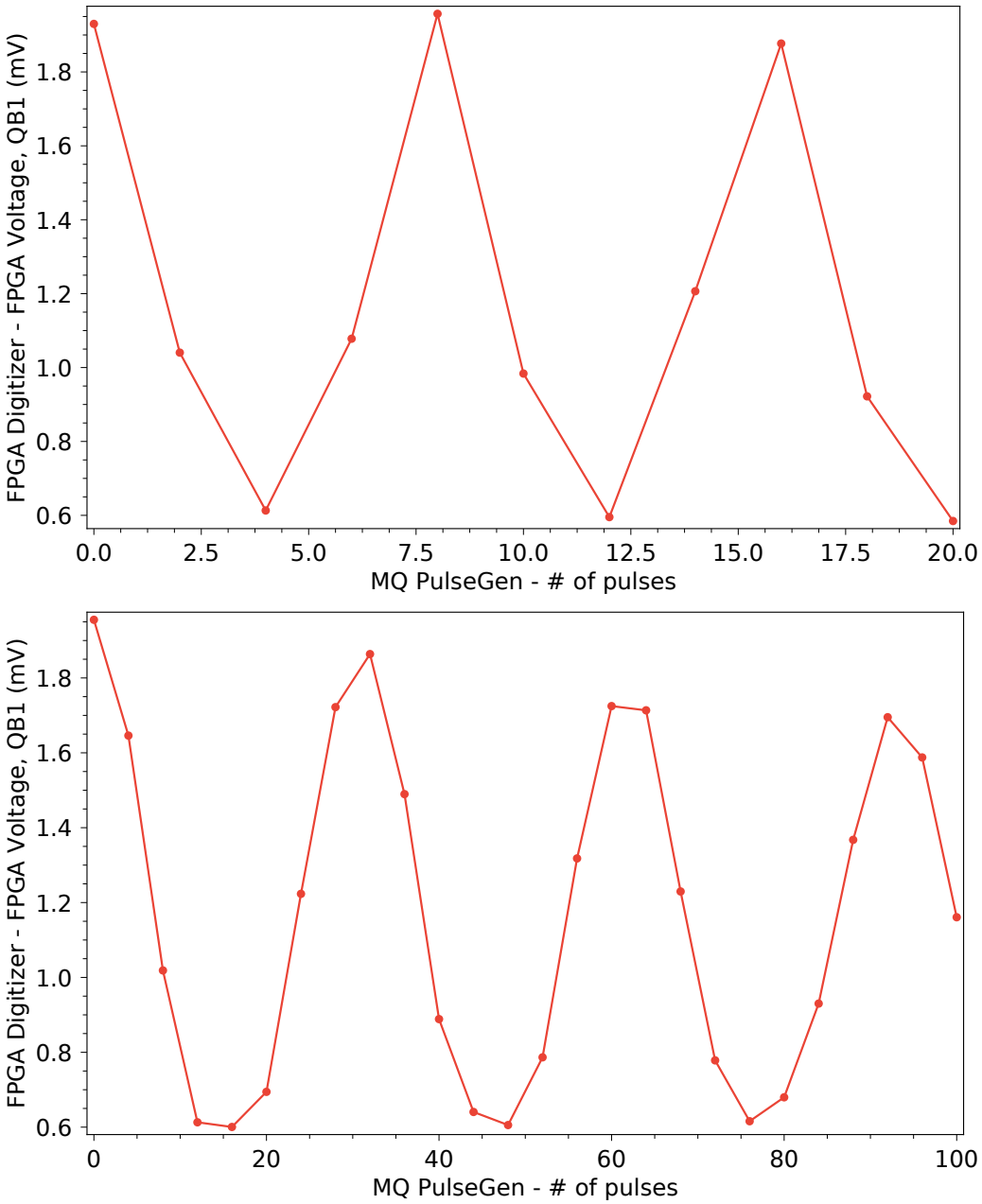

Figure 6-7: Suboptimal sequences of the DRAG calibration in Fig. 6-6, taken for the coefficients $\lambda = 1.4$ (top) and $\lambda = -1.5$ (bottom). When the DRAG coefficient is suboptimal, the coherent errors in X-gate will constructively interfere, rotating the qubit close to the $|1\rangle$-state after several applications of the gate (4 gates in the top trace, 18 in the bottom).

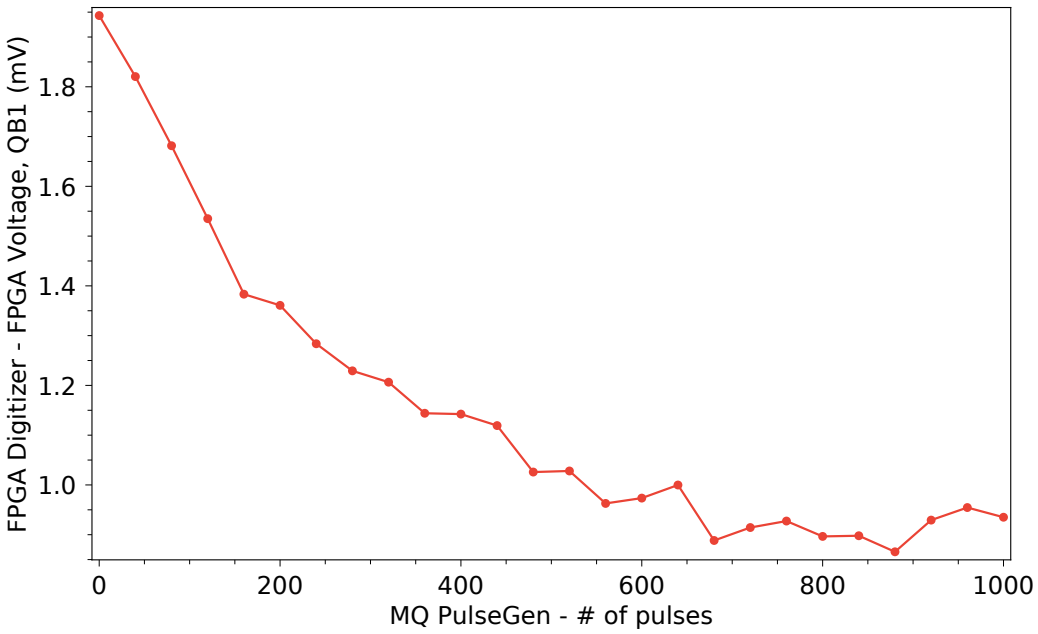

Figure 6-8: Optimal sequence of the DRAG calibration in Fig. 6-6, taken for the coefficients $\lambda = -0.9$. When the DRAG parameter is optimal, the coherent errors in each X-gate is actively cancelled and the qubit monotonically decays to a mixed state even after hundreds of gates. For 1000 applications of the X-gate, the total duration of the sequence is $T = 1000$ gates $\times$ 30 ns/gate $= 30\,\mu$s $\approx T_2$, and the gate is limited by incoherent errors due to finite coherence of the qubit.

the sequence, as such:

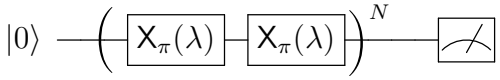

(6.24)

Now, for a perfect π-pulse, all of the X-gates will cancel and the qubit will remain in $|0\rangle$ for all values of n. However, when the DRAG coefficient of our π-pulse is incorrect, the coherent errors in each X-gates will constructively add up, leading to oscillations in the $|0\rangle$-state population due to the over/under-rotation of each gate (Fig. 6-7). When the DRAG parameter is optimal, these oscillations will disappear and the $|0\rangle$-state population will monotonically decay to 50% due to pure dephasing of the qubit during the duration of the gate sequence (Fig. 6-8). Varying the DRAG coefficient and increasing the number of π-pulses in the sequence (limited the width of the microwave pulse and T_2 of the qubit), we obtain a chevron pattern as in Fig. 6-6, where the center of the chevron corresponds to the optimal DRAG parameter.

6.2.5 Fine-Tuning the Pulse Amplitude With a π-Train

Finally, now that we have calibrated the DRAG parameters and are able to reliably perform sequences of tens and hundred of single-qubit rotations, we can perform one additional calibration step to ensure we are driving the qubit at the correct pulse amplitude. Previously, we found the pulse amplitude roughly using a standard Rabi measurement, reading off the approximate pulse amplitude at which the qubit population of the $|1\rangle$-state is maximized.

To fine-tune this value and ensure that we are driving the qubit at the optimal pulse amplitude, we can perform a variant of a Rabi measurement colloquially referred to as a *π-train measurement*. This measurement, similar to the DRAG calibration technique we considered above, relies on the application of multiple gates in series, looking at the constructive build-up of coherent errors and finding the parameters at which these errors disappear. As in a Rabi measurement, we perform a π-pulse and sweep the amplitude of the pulse, recording the point at which the population of the $|1\rangle$-state is maximized. Having recorded this point, we then add pairs of π-pulses to the sequence, as in the circuit

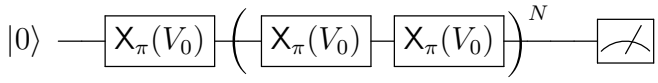

(6.25)

As we increase the odd number of π-pulses applied to the qubit, the frequency of the Rabi measurement as a function of pulse amplitude will increase proportionally. Increasing the number of additional pairs N and sweeping a Rabi measurement over a full period from $V = 0$ to $V = 2V_0$, we see that this makes intuitive sense:

$N = 0$: Performing a single π-pulses and sweeping a Rabi measurement over a full period, the $|1\rangle$-state population will be maximized at a single amplitude, V_0.

$N = 1$: Performing three total π-pulses, rotations will constructively add up and the $|1\rangle$-state population will be maximized at three different amplitudes, $V_0/3$, V_0, and $5V_0/3$.

$N \in \mathbb{Z}$: Performing a general odd number of π-pulses $2N+1$, the $|1\rangle$-state population

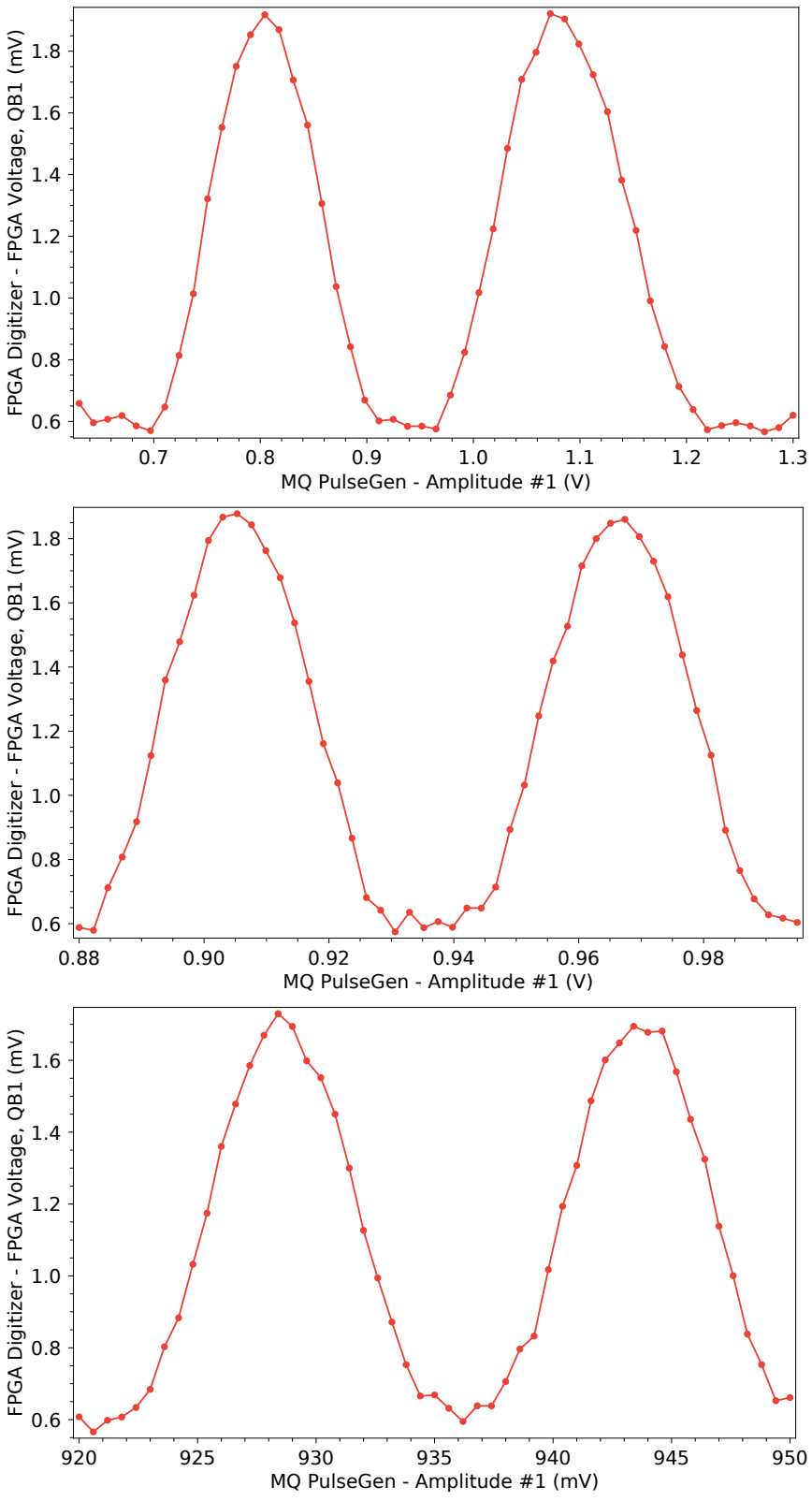
FPGA Digitizer - FPGA Voltage, QB1 (mV)
1.8
1.6
1.4
1.2
1.0
0.8
0.6
0.7
0.8
0.9
1.0
1.1
1.2
1.3
MQ PulseGen - Amplitude #1 (V)
FPGA Digitizer - FPGA Voltage, QB1 (mV)
1.8
1.6
1.4
1.2
1.0
0.8
0.6
0.88
0.90
0.92
0.94
0.96
0.98
MQ PulseGen - Amplitude #1 (V)
FPGA Digitizer - FPGA Voltage, QB1 (mV)
1.6
1.4
1.2
1.0
0.8
0.6
920
925
930
935
940
945
950
MQ PulseGen - Amplitude #1 (mV)

Figure 6-9

will be maximized at $2N + 1$ different amplitudes

$$V = \frac{n\, V_0}{2N + 1} \tag{6.26}$$

where n is the set of odd integers between 1 and $4N + 1$.

Thus, as we increase the number of additional pulse pairs N, the frequency of the of the Rabi measurement increases and the width of the Rabi peak at the amplitude V_0 *decreases*, allowing us to more precisely read off the amplitude V_0 corresponding to a single π-pulse. In practice, this leads to an iterative measurement of the form in Fig.where we iteratively increase the number of π-pulses and decrease the range of the measurement around V_0, updating the value of V_0 each time we add more pulses and increase our amplitude resolution.

6.3 Two-Qubit CZ Gates

So far, we have discussed how to calibrate all of the single-qubit gates in the universal gate set we considered in Eq. (6.1). This leaves us with only a single remaining gate to complete our universal gate set: the two-qubit CZ gate. As it turns out, this is the hardest gate to calibrate in the entire gate set and, at present, two-qubit gate performance remains one of the main roadblocks on the path towards large-scale quantum computation.

Fortunately, however, this is also the gate which gives us the greatest flexibility in

Figure 6-9: Iterative π-train measurements, corresponding to $N = 3$ (top, 7 pulses total), $N = 15$ (middle, 31 pulses), and $N = 62$ (bottom, 125 pulses). Starting with the rough π-pulse amplitude V_0 obtained from the standard Rabi measurement ($N = 0$) in Fig. 6-3, we increase the number of additional pairs of pulses N and decrease the range of amplitudes scanned around V_0, updating the amplitude more precisely as the resolution of the measurement increases. Note the x-axis of each plot: for $N = 62$ in the bottom plot, the period of the Rabi measurement has decreased by two orders of magnitude in comparison to the standard Rabi oscillation in Fig. 6-3, allowing us to dial in the amplitude of a single X-gate to much greater accuracy.

its implementation—as we discussed in Chapter 5, we only need one two-qubit gate to complete our gate set, and we are free to pick any operation which is capable of entangling a pair of qubits. As such, there are multiple viable techniques for implementing two-qubit gates in superconducting qubits—such as flux-activated iSWAP gate and the microwave-activated cross-resonance (CR) gate—each with their own characteristic benefits and drawbacks.

In this section, we will briefly focus on a single two-qubit gate implementation: the flux-activated CZ gate between tunable transmon qubits. In our discussion of DRAG in Section 6.1.3, we considered how the higher levels of our superconducting qubits can lead to errors in our single-qubit gates. Here, however, we will show how these higher levels can be harnessed to implement a two-qubit entangling operation in the coupled qubit subspace.

To see how the CZ gate works, let's start by considering two transmon qubits A and B capacitively coupled to each other with coupling strength g. Truncating the coupled two-qubit system to the lowest three levels, the Hamiltonian is approximately given by

$$\hat{H} = \begin{bmatrix} E_{00} & 0 & 0 & 0 & 0 & 0 \\ 0 & E_{01} & g & 0 & 0 & 0 \\ 0 & g & E_{10} & 0 & 0 & 0 \\ 0 & 0 & 0 & E_{11} & \sqrt{2}g & \sqrt{2}g \\ 0 & 0 & 0 & \sqrt{2}g & E_{02} & 0 \\ 0 & 0 & 0 & \sqrt{2}g & 0 & E_{20} \end{bmatrix} \tag{6.27}$$

where the six indices correspond to the $|00\rangle, |01\rangle, |10\rangle, |11\rangle, |02\rangle, |20\rangle$ states, respectively, and the diagonal elements are sums of the single-qubit energies

$$E_{nm} = E_n^A(\Phi_A) + E_m^B(\Phi_B) \tag{6.28}$$

where $E_n^A(\Phi_A)$ is the flux-dependent energy of the nth level of qubit A. Diagonalizing this Hamiltonian and plotting the lowest six energy eigenstates of the coupled two-qubit versus the magnetic flux through qubit A, we find an energy spectrum of the form plotted in Fig. 6-10.

Looking at this energy spectrum, notice that the off-diagonal coupling terms in

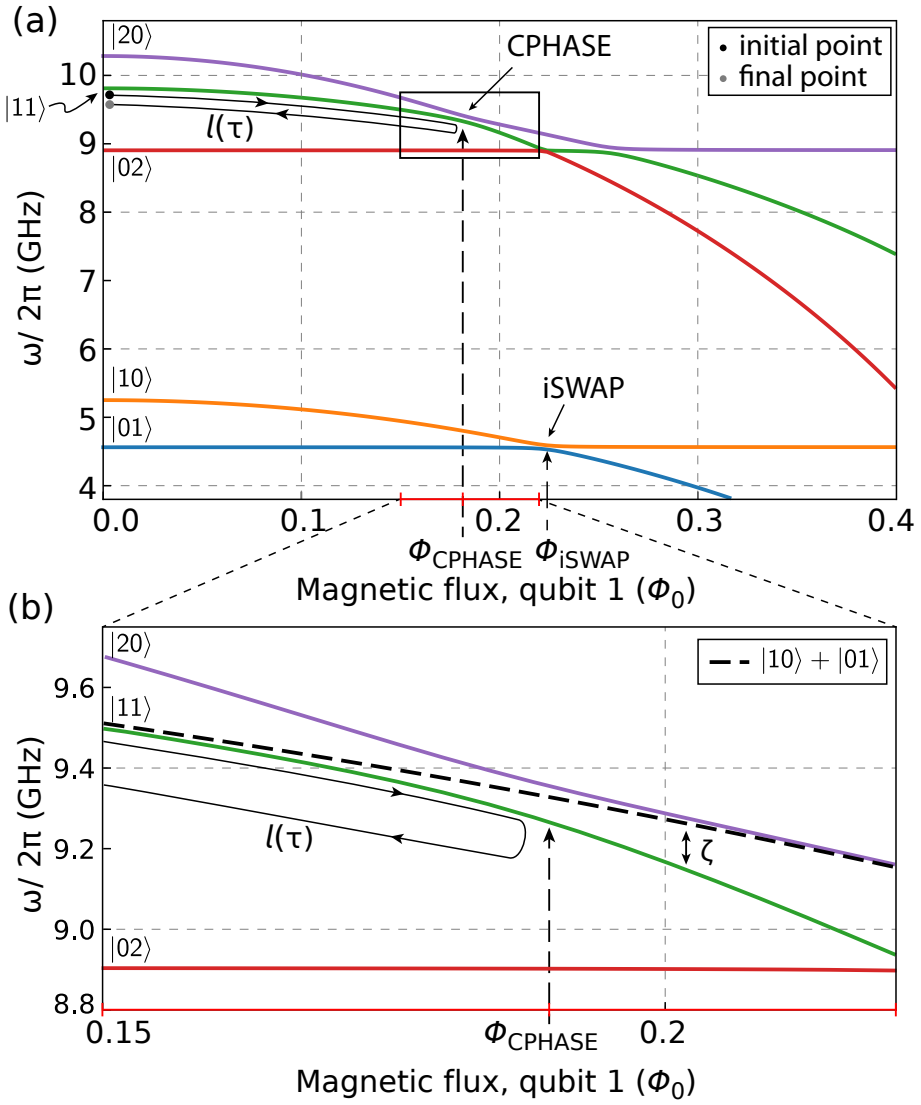

Figure 6-10: The energy spectrum of two capacitively coupled flux-tunable transmon qubits, plotted as a function of the magnetic flux through the higher-energy qubit (here labeled 'qubit 1'). **(a)** Broad plot of the five lowest transition frequencies. The avoided crossing between the states $|20\rangle$ and $|11\rangle$ (emphasized in the black box) is utilized to accrue the necessary state-dependent frequency shift to perform a CZ gate. **(b)** Zoomed plot of the $|02\rangle$, $|11\rangle$, and $|20\rangle$ states in (a), focusing on the avoided crossing between $|20\rangle$ and $|11\rangle$. The path $\ell(\tau)$ illustrates the flux trajectory of duration τ which biases the system from the sweet spot, into the avoided crossing, and back again, implementing the CZ gate. Figure reproduced from Ref. [257].

the two qubit-Hamiltonian give rise to avoided level-crossings between the single-qubit energy eigenstates when they are brought into resonance, just as we saw in Chapter 4 when we characterized ZZ-coupling between coupled flux qubits. These

avoided crossings are the key to implementing a two-qubit CZ gate. To see how, imagine we evolved this system in time as follows:

1. Starting from the initial operating point of the two qubits (i.e., the magnetic flux biases at which we calibrated the single-qubit gates above), we slowly apply a flux bias through one of the qubits such that the $|11\rangle$-state is brought near resonance with the higher excited state $|20\rangle$.

2. Once the system is brought near resonance with $|20\rangle$, we wait some time and allow the system to idle in the avoided crossing, causing the computational states to each accrue some phase θ.

3. Finally, we slowly turn off the magnetic flux bias through the qubit, detuning the $|11\rangle$-state away from $|20\rangle$, returning the system back to its operating point for single-qubit gates.

Together, these three steps form a trajectory ℓ which takes some total time τ to complete. In Fig. 6-10, we can see what this trajectory looks like superposed on top of the coupled two-qubit spectrum. Performing this evolution and allowing each computational state to accrue some phase θ, this excursion results in a unitary operation of the form

$$\hat{U}(\ell) = \begin{bmatrix} 1 & 0 & 0 & 0 \\ 0 & e^{i\theta_{01}(\ell)} & 0 & 0 \\ 0 & 0 & e^{i\theta_{10}(\ell)} & 0 \\ 0 & 0 & 0 & e^{i\theta_{11}(\ell)} \end{bmatrix} \tag{6.29}$$

where the phases θ_{ij} are found by integrating the flux-dependent transition frequencies ω_{ij} over the trajectory $\ell(t)$ for its full duration τ

$$\theta_{ij}(\ell(\tau)) = \int_0^\tau \omega_{ij}[\ell(t)]\, dt. \tag{6.30}$$

Now, if it weren't for the coupling between the qubits, the phase accrued by the $|11\rangle$-state would be exactly equal to the sum of the phases accrued by the $|01\rangle$ and $|10\rangle$ states (since $\omega_{11} = \omega_{01} + \omega_{10}$ for two uncoupled qubits), and the resulting unitary $U(\ell)$ would be separable into the product of single-qubit unitaries. As we showed back

in Chapter 2, such a unitary would not produce entanglement, and it would therefore fail to generate a useful two-qubit gate. Fortunately, however, this is not the case. Diagonalizing the Hamiltonian in Eq. (6.27), we find that the coupling between the qubits results in a repulsion of the $|11\rangle$-state due to the presence of the $|20\rangle$-state, shifting the transition frequency of $|11\rangle$ away from the bare sum of the single-qubit transitions

$$\zeta = \omega_{11} - (\omega_{01} + \omega_{10}) \neq 0. \tag{6.31}$$

This nonzero ζ is exactly what we need to engineer a CZ gate. Recall from Chapter 5 that a CZ gate corresponds to the unitary matrix

$$\mathsf{CZ} = \begin{bmatrix} 1 & 0 & 0 & 0 \\ 0 & 1 & 0 & 0 \\ 0 & 0 & 1 & 0 \\ 0 & 0 & 0 & -1 \end{bmatrix}. \tag{6.32}$$

From this unitary matrix, we see that the CZ gate applies a conditional phase of π to the $|11\rangle$-state relative to the other three computational states. Looking back at the unitary in Eq. (6.35) which arises due to the adiabatic flux trajectory ℓ, we see that we can produce a CZ gate in the following way. First, let's choose a trajectory ℓ_π such that the time integral of ζ along the path integrates to π

$$\int_0^\tau \zeta(\ell_\pi(t))\, dt = \pi. \tag{6.33}$$

From Eqs. (6.30) and (6.31), we see that the left-hand side of this equation is equivalent to the difference in phases θ_{ij} between the computational states

$$\theta_{11}(\ell_\pi) - (\theta_{01}(\ell_\pi) + \theta_{10}(\ell_\pi)) = \pi. \tag{6.34}$$

Plugging $\theta_{11}(\ell)$ into the unitary in Eq. (6.35), we arrive at an expression for the

unitary operation performed after the excursion ℓ_π

$$\hat{U}(\ell_\pi) = \begin{bmatrix} 1 & 0 & 0 & 0 \\ 0 & e^{i\theta_{01}(\ell_\pi)} & 0 & 0 \\ 0 & 0 & e^{i\theta_{10}(\ell_\pi)} & 0 \\ 0 & 0 & 0 & e^{i(\pi+\theta_{01}(\ell_\pi)+\theta_{10}(\ell_\pi))} \end{bmatrix}. \tag{6.35}$$

Comparing the unitary above to the unitary of the CZ gate in Eq. (6.32), we see that these two operators are equivalent up to the single-qubit phases $\theta_{01}(\ell_\pi), \theta_{10}(\ell_\pi)$. Thus, having found a trajectory ℓ_π which achieves the condition in Eq. (6.33), we can simply apply virtual Z gates to each qubit and rotate away the single-qubit phases $\theta_{01}(\ell_\pi), \theta_{10}(\ell_\pi)$ such that only the π phase shift on the $|11\rangle$ state remains, implementing the CZ gate. We will return to this gate in detail in Chapter 7, where we will discuss how to perform and characterize this gate in the context of a real quantum algorithm.

Chapter 7

Density Matrix Exponentiation

In Chapter 5, we considered the broad outline of quantum algorithms. In that discussion, we drew a sharp line between *quantum data* (quantum states which are fed as input into a circuit) and *quantum algorithms* (the series of quantum processes and gates which form the circuit itself). While the distinction between data and algorithm is useful for orienting oneself, it is in fact artificial. As it turns out, there is a fundamental parity between the data which is fed into an algorithm and the set of instructions which determines the operation of the algorithm itself. In the classical theory of computation, this property is know as *homoiconicity*: a set of bits can serve as either the string on which an algorithm acts, or as the instruction set which defines the algorithm itself.

In theory, the principle of homoiconicity should hold for all forms of computation, classical and quantum. In the case of quantum computation, this would mean that the data encoded in a quantum state could interchangeably serve as the input of

This chapter is based in large part on original work reported in Ref. [247], and I gratefully acknowledge all of my coauthors for their contributions to this work, with particular acknowledgment to Morten Kjaergaard, Mollie Schwartz, Alex Greene, Christopher McNally, Mike O'Keeffe, Kevin Obenland, Milad Marvian, Iman Marvian, and William Oliver.

I would also like to acknowledge that in August 2019, during the final stages of the experiment reported in this work, I became aware that Ref. [281]—the original theory work on which much of this experiment was based—was funded in part by the sex offender, human trafficker, and eugenicist Jeffrey Epstein. I humbly acknowledge the survivors of Epstein's crimes, and I acknowledge my failure to recognize and respond to this association sooner.

a quantum algorithm or as the instruction set which defines the algorithm itself. In practice, however, a fundamental asymmetry emerges. In all demonstrations of quantum computation to date, the instruction set which specifies the sequence of gates in a quantum algorithm is defined using *classical data*—for example, a Python driver which sequences a set of microwave pulses to implement a desired multi-qubit algorithm composed of physical gates—while the algorithm itself acts on *quantum data*.

In this work, we consider an algorithm which restores the parity between data and instruction set in a quantum processor, restoring homoiconicity in physical quantum computation. This algorithm, known as Density Matrix Exponentiation (DME) takes two quantum states as input—a data state σ and an instruction state ρ. Starting from a deterministic set of gate operations, DME then executes a unitary operation on the state σ which is defined entirely by the density matrix of the state ρ. In this sense, it is the state ρ—not the circuit diagram of DME itself—which serves as the true instruction set of the algorithm, in absolute parity with the data state σ on which it acts.

In the following work, we develop a hardware-efficient version of DME which runs of a two-qubit transmon device. We demonstrate how—using a single set of classically-defined gates—the operation executed on the data qubit changes as we change the initial state of the instruction qubit. In the process, we study the trade-off between errors which arise from imperfections in the device—such as decoherence and coherent gate errors, which degrade algorithmic performance at longer circuit depths—and errors which arise due to the Trotter-like structure of DME itself, errors which asymptotically decrease as the number of Trotter steps increases.

7.1 Data, Instructions, and Homoiconicity

The equivalence between the instructions used to define programs and the input data on which the instructions operate is a basic principle of classical computer architectures and programming [446]. Replacing classical data with quantum states enables

fundamentally new computational capabilities with scaling advantages for many applications [309, 420], and numerous models have been proposed for realizing quantum computation [122, 138, 373]. However, within each of these models, the quantum data are transformed by a set of gates that are compiled using solely classical information. Conventional quantum computing models thus break the instruction-data symmetry: classical instructions and quantum data are not directly interchangeable. In this work, we use a density matrix exponentiation protocol [281] to execute quantum instructions on quantum data. In this approach, a fixed sequence of classically-defined gates performs an operation that uniquely depends on an auxiliary quantum instruction state. Our demonstration relies on a 99.7% fidelity controlled-phase gate, which enables an algorithmic fidelity surpassing 90% at circuit depths exceeding 70. The utilization of quantum instructions obviates the need for costly tomographic state reconstruction and recompilation, thereby enabling exponential speedup for a broad range of algorithms, including quantum principal component analysis [281], the measurement of entanglement spectra [354], and universal quantum emulation [294].

In classical programmable computers, instructions are specified in the same medium as the data they process (Fig. 7-1) such that programs can can be treated interchangeably with data. This property, known as homoiconicity [312], is a hardware-level property of all classical computers based on the von Neumann architecture [453] as well as of higher-level programming languages like Lisp, Julia, and Wolfram.

In all previous experimentally-realized quantum computational systems—see, for example, the systems studied in Ref. [22, 39, 192]—the relation between instructions and data is fundamentally different. Quantum programs generally comprise a classically-defined list of gates (the instructions) that are applied to a quantum processor (the data) using intermediary control hardware (Fig. 7-2). This programming architecture is thus non-homoiconic: the instructions are manifestly classical, whereas the data are quantum mechanical. Furthermore, if an algorithm requires instructions derived from the present quantum state of the processor, that information must first be extracted from the quantum system (incurring exponential overhead [177]), classically processed and compiled, and then appended to the classical instruction list [19,

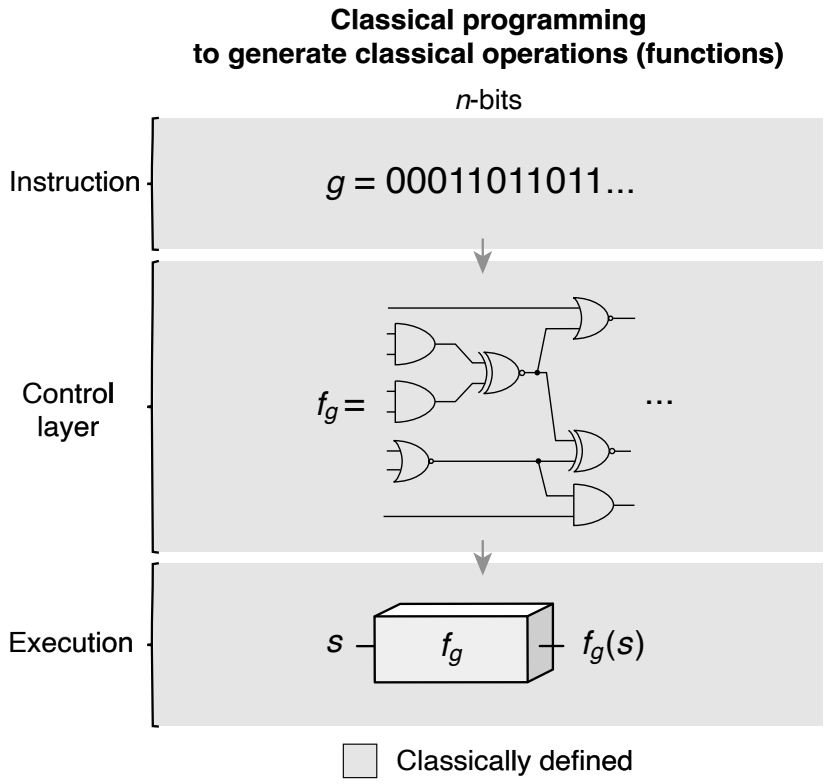

Figure 7-1: Schematic representation of a classical instruction set for classical computing. Here, instructions are defined by a classical bit string g_n which uniquely determines a Boolean-logic function f_{g_n} comprising single-bit and two-bit gates. The control layer executes the resulting circuit on data bits s_n to produce the output $f_{g_n}(s_n)$. [247]

87, 208, 341, 374, 378, 451]. Such a costly reconstruction process would create significant bottlenecks in quantum algorithms at scale [69, 365].

In this work, we demonstrate the use of quantum instructions to implement a quantum program—a unitary operation whose parameters are given by the properties of a quantum state [331, 483, 484]—on a superconducting quantum processor. Our approach is based on density matrix exponentiation (DME), a protocol originally introduced in the context of quantum machine learning [281]. DME is executed by a series of repeated classical control pulses (Fig. 7-3), which, in contrast to conventional quantum programs (Fig. 7-2), carry no information about the instruction set. Rather, the instructions are encoded in the instruction qubits (density matrix ρ), which determine the unitary operations performed on the data qubits (density matrix

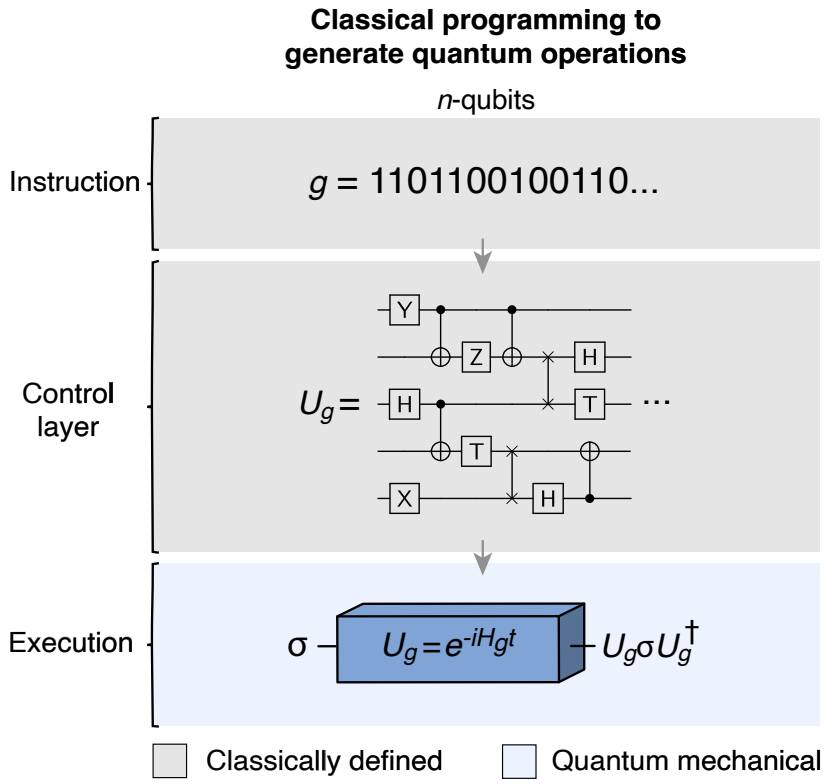

Figure 7-2: Schematic representation of a classical instruction set for conventional quantum computing. Here, the instruction set which encodes a quantum circuit is generated using classical resources: instructions are defined by a classical bit string g_n that uniquely determines a unitary operation U_{g_n} comprising single-qubit and two-qubit gates. The control layer uses solely classical hardware to generate the gate sequence and applies it to the quantum hardware (data qubits σ_n) to execute the unitary evolution $U = \exp(-iH_{g_n}t)$, where H_{g_n} is the quantum circuit Hamiltonian, to produce the output $U_{g_n}\sigma_n U_{g_n}^{\dagger}$. [247]

σ). Thus, both instructions and data are stored in quantum states [331], and together they constitute a quantum computing analogue of homoiconicity. We apply DME to a system comprising two superconducting qubits: a data qubit prepared in state σ, and an instruction qubit prepared in state ρ. In this case, DME implements a unitary rotation on the data qubit about an axis parallel to instruction state. At this scale, the quantum instruction state and its resulting unitary operation are easily predicted and straightforward to reconstruct. However, extending the number of instruction qubits to the so-called 'supremacy regime' [22], in which a classically-specified sequence of gates can produce a quantum state that is too complex to predict and too

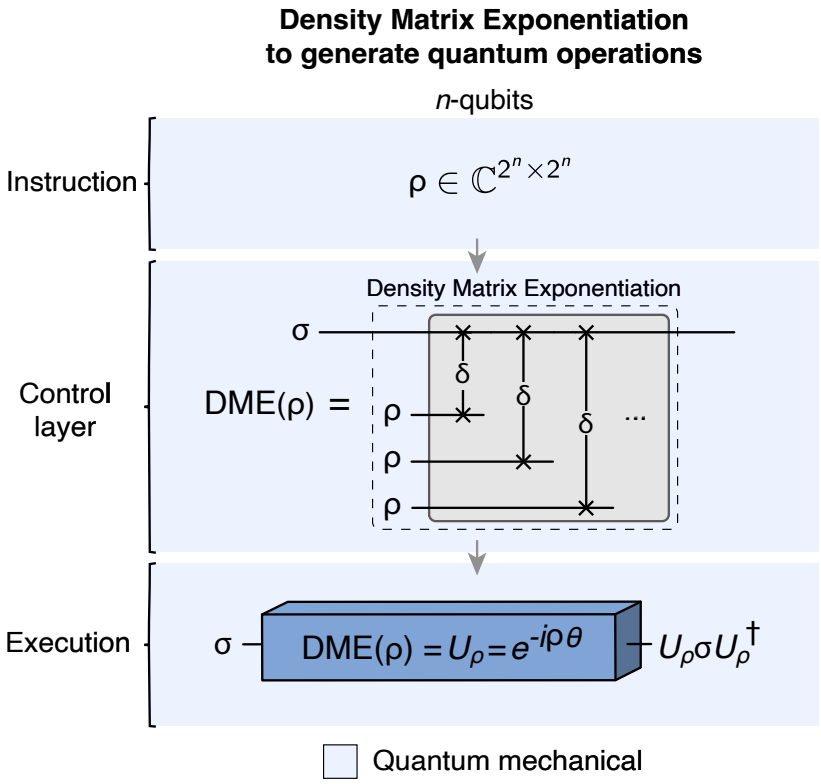

Figure 7-3: Schematic representation of a *quantum* instruction set for quantum computing using the density matrix exponentiation (DME) algorithm. Here, the instruction set which encodes the desired quantum circuit is stored in a set of instruction qubits ρ_n. The control layer uses classical hardware to generate N partial SWAP operations over a small, classically chosen rotation angle $\delta = \theta/N$, where θ is an algorithm-dependent angle. These classically defined operations (grey region) contain no information about the operation implemented on the data qubits (σ_n). Using a Trotterization approach, the partial SWAP operations are repeatedly applied to the quantum hardware (blue region)—data qubits σ_n and identically prepared copies of the instruction qubits ρ_n – to execute the unitary operation $U = \exp(-i\rho_n\theta) \equiv \exp(-iH_{g_n}t)$, for appropriately chosen g_n. The output $U_{\rho_n}\sigma_n U_{\rho_n}^\dagger$ is equivalent to $U_{g_n}\sigma_n U_{g_n}^\dagger$ to within an error $\mathcal{O}(\theta^2/N)$ for appropriately chosen ρ_n. [247]

large to tomographically reconstruct, leads to a remarkable programming and operational framework: while it would be completely impractical to ascertain the quantum instructions stored in an unknown state ρ, one can nonetheless use these instructions to execute a quantum program (as defined above). Programs based on quantum instructions implemented with DME enable a class of efficient algorithms addressing both quantum computation (using ρ to manipulate σ) and quantum metrology (using σ to study ρ). The afforded quantum advantage generally stems from the fact

that DME directly implements unitary operations $e^{-i\rho\theta}$ at the quantum hardware layer, obviating the need for tomographic reconstruction of the instruction state ρ on which these applications are based [177, 242, 281]. One example is private quantum software execution, whereby the action of an unknown (private) unitary U on an arbitrary quantum state may be efficiently emulated using a relatively small set of known input-output relations $\{\rho_{\text{in}}\} \overset{U}{\mapsto} \{\rho_{\text{out}}\}$ [294], far fewer than would be required to compromise the security of U via its tomographic reconstruction. Quantum instructions also enable quantum advantage for quantum semi-definite programming [71] and sample-optimal Hamiltonian simulation [242]. In addition, quantum phase estimation executed using DME can extract with error ϵ the dominant eigenvalues and eigenvectors of ρ—principal component analysis—using only $\mathcal{O}(\theta^2/\epsilon)$ copies of ρ [242, 281]. Even when ρ is a large entangled state, DME can efficiently reveal its entanglement spectrum, a form of reduced-complexity benchmarking [354].

7.2 The DME Protocol

Conceptually, DME implements the unitary operation

$$U = e^{-i\rho\theta} \tag{7.1}$$

on the data qubit(s) according to the instruction state ρ and an algorithm-dependent angle θ. If the data and instruction states are single-qubit pure states σ and ρ, DME rotates σ by an angle θ about an axis defined by the Bloch vector of ρ. More generally, σ and ρ are multi-qubit states, and they need not be pure states. The protocol that implements DME partitions U into a sequence of N steps (Fig. 7-4), each comprising a "partial SWAP" operation [396]

$$\delta\text{SWAP} \equiv e^{-i\text{SWAP}\delta} \tag{7.2}$$

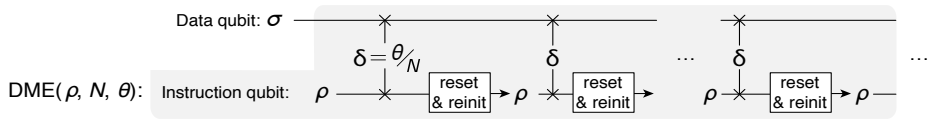

Figure 7-4: Circuit diagram of the Density Matrix Exponentiation (DME) algorithm using active reset and re-initialization to re-prepare the instruction state ρ after each δSWAP operation. [247]

that is applied to σ and ρ [281]. The protocol relies on the relation:

$$\begin{aligned} \mathrm{Tr}_\rho \left[e^{-i\mathsf{SWAP}\delta} \sigma \otimes \rho e^{i\mathsf{SWAP}\delta} \right] &= \sigma - i\delta[\rho, \sigma] + \mathcal{O}(\delta^2) \\ &= e^{-i\rho\delta} \sigma e^{i\rho\delta} + \mathcal{O}(\delta^2). \end{aligned} \tag{7.3}$$

That is, σ undergoes unitary evolution of the form $e^{-i\rho\delta}$ (to first order in δ; see Section 7.12), rotating by a small angle $\delta = \theta/N$. By the reciprocity of SWAP operations, ρ undergoes a complementary unitary evolution about σ, leaving it in a state that differs from the original quantum instruction. As a result, the instruction qubits must be refreshed at each step to provide a new, identical copy of the instruction state ρ. Repeating these steps N times (Fig. 7-4) approximately yields the desired operator

$$\mathsf{DME}(\rho, N, \theta) \rightarrow e^{-i\rho\theta} + \mathcal{O}\left(\frac{\theta^2}{N}\right) \tag{7.4}$$

a result that is closely related to the Trotterization of non-commuting Hamiltonians to perform quantum simulations [280]. Similar to dividing a quantum simulation into smaller steps to reduce errors stemming from the Trotter approximation, partitioning DME into more steps (increasing N), with a smaller partial SWAP angle δ per step, reduces the DME discretization error. The trade-off for increased precision is a need for more copies of the quantum instructions.

There are three general approaches to supplying the N copies of the instruction state ρ needed to execute DME:

1. Teleport copies of the quantum instructions from a third party to the qubits comprising ρ

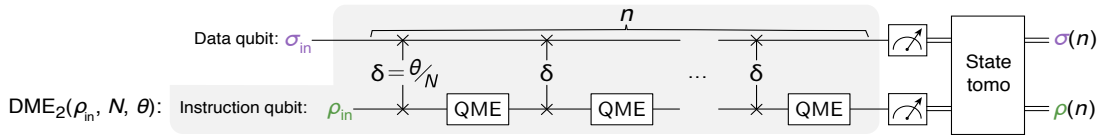

Figure 7-5: An alternative implementation of Density Matrix Exponentiation, which we term DME_2. In DME_2, quantum measurement emulation (QME) is used to approximately reinitialize the instruction qubit to ρ_{in} without active reset and repreparation. The substep parameter n is stepped from 0 to N. In the experiment, we perform n rounds of $\delta\mathsf{SWAP} + \mathsf{QME}$, measure the two-qubit density matrix, and trace over each subsystem to extract the individual data and instruction qubit density matrices ($\sigma(n)$ and $\rho(n)$ respectively). [247]

2. Identically prepare the instructions on N copies of ρ (hardware parallelization, Fig. 7-3)

3. Identically prepare the same set of qubits comprising ρ after each $\delta\mathsf{SWAP}$ (sequential preparation in time, Fig. 7-4)

In this work, we choose option 3: we refresh the same instruction qubit to avoid the need for teleportation or large numbers of instruction qubits, and to allow us to easily vary N.

7.3 Generating N Copies of ρ Using Emulated Measurement

The most obvious approach for using one qubit to generate N copies of ρ (Fig. 7-4) is to use measurement-conditioned active feedback to reset the instruction qubit to its ground state and then re-prepare the instruction state ρ [289]. However, due to measurement infidelity and the decoherence that occurs during the relatively long duration of the requisite measurement, feedback, and preparation steps, the conventional active-reset approach would introduce an unacceptable level of errors on current quantum processors. Here, to minimize such errors and achieve the largest possible circuit depths with our qubits, we instead introduce an alternative approach (Fig. 7-5)

called quantum measurement emulation (QME) that approximately reinitializes the instruction qubit in the time required for a single qubit gate.

QME is a probabilistic operation that mimics an ensemble averaged qubit measurement. For intuition, note that for a sufficiently small angle δ, the states of the two qubits are only slightly altered after a δSWAP operation. In this case, a projective measurement of the instruction qubit in the eigenbasis of ρ would reset the instruction qubit to its original state with high probability. Similarly, an unconditioned ensemble averaged measurement of many such identically prepared states (i.e. a measure-and-forget approach) would reproduce the original ρ with only a slight depolarization. QME mimics this well-known result without actually performing a measurement by imposing a dephasing channel corresponding to the axis of ρ. The QME operation (Fig. 7-5) randomly applies either an identity gate ($\mathbb{1}$) or a π-rotation in the instruction qubit eigenbasis, according to a Bernoulli process with probability $p = 0.5$:

$$-\boxed{\mathsf{QME}_\nu}- = \begin{cases} \mathbb{1} & \text{with } p = 0.5 \\ \mathsf{R}_\nu(\pi) & \text{with } 1-p = 0.5 \end{cases} \tag{7.5}$$

where ν is a normalized vector parallel to the original instruction state. For instruction states aligned with the axes of the Bloch sphere, QME represents a probabilistic application of a Pauli gate. We incorporate QME into our circuit by interleaving δSWAP and QME operations (Fig. 7-5). The QME operations are randomized within each instantiation of the circuit, and in the same spirit as randomized compiling [458], the outcomes of multiple such randomized instantiations are averaged to mimic a single circuit with an active reset of ρ.

The QME-enabled reset of ρ is approximate due to depolarization, which introduces an additional error term to the DME protocol. For our two-qubit demonstration with QME, denoted DME_2, the unitary operation is

$$\mathsf{DME}_2(\rho, N, \theta) \;\; \rightarrow \;\; e^{-i\rho\theta} + \underbrace{\mathcal{O}(\tfrac{\theta^2}{N})}_{\text{discretization}} + \underbrace{\mathcal{O}(\tfrac{\theta^2}{N})}_{\mathsf{QME}}. \tag{7.6}$$

Despite the added error term, QME effectively supplies the requisite copies of ρ with

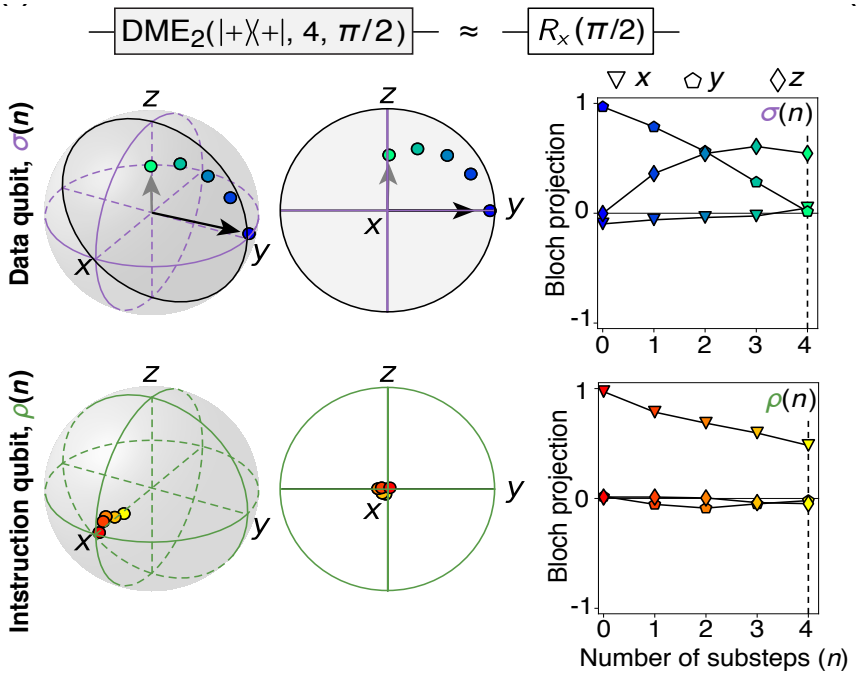

Figure 7-6: Demonstration of quantum instructions using DME. Substeps of $\mathsf{DME}_2(|+\rangle\langle+|, 4, \pi/2)$, corresponding to $\mathsf{R}_X(\pi/2)$ on the target qubit at the final step ($n = N$). Black lines are guides to the eye. [247]

less error than would be incurred with an active feedback approach in our system. Furthermore, its use here is not fundamental to our demonstration. An implementation of arbitrary, unknown quantum instructions could be performed using states from large quantum processors or by state-teleportation, and the underlying physics would be the same as those in this proof-of-principle experiment.

7.4 Implementing the DME$_2$ Algorithm

We implement DME$_2$ using two frequency-tunable superconducting asymmetric transmon qubits [211, 255] in an 'xmon' layout [33], operating with single-qubit gate fidelities exceeding 99.9% and a two-qubit controlled phase gate with 99.7% fidelity (see Section 7.5). In Figures 7-6 and 7-7, we interrupt the algorithm after $n \leq N$ steps and perform state tomography (see Section 7.9) to visualize the evolution of the data-qubit and instruction-qubit. We use an initial state $\sigma_{\text{in}} = |+i\rangle\langle+i|$ for the data qubit, and we introduce the notation $\mathsf{DME}_2(\rho_{\text{in}}, N, \theta)$ to indicate the initial instruction state

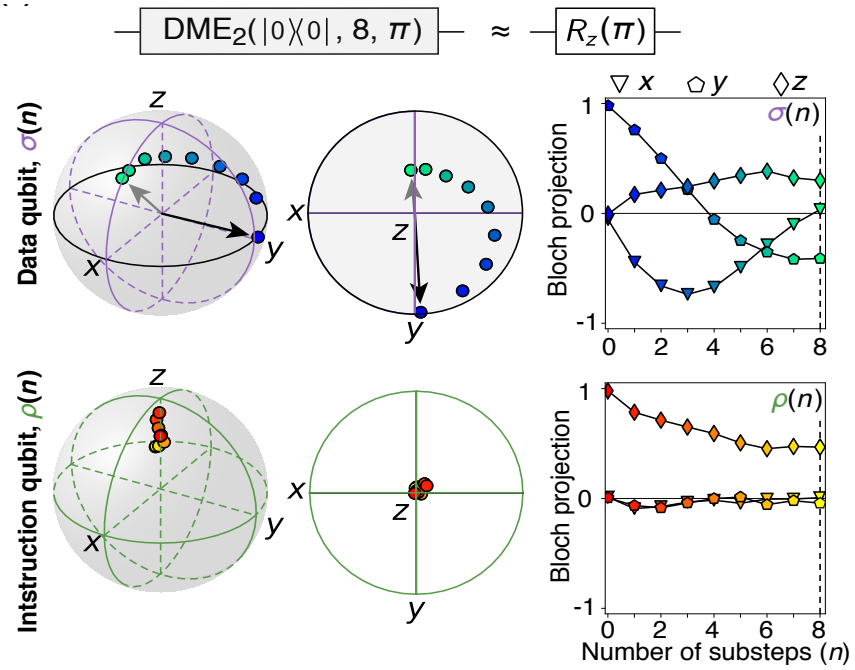

Figure 7-7: Demonstration of quantum instructions using DME. Substeps of $\mathsf{DME}_2(|0\rangle\langle 0|, 8, \pi)$, corresponding to $\mathsf{R}_Z(\pi)$ on the target qubit at $n = N$. [247]

ρ_{in}, total number of steps N, and the phase rotation θ.

Figure 7-6 shows an implementation of $\mathsf{DME}_2(|+\rangle\langle +|, 4, \pi/2)$. Since ρ is x-polarized, this instruction encodes the operation $\mathsf{R}_X(\pi/2)$, a $\pi/2$ rotation about the x axis. Figure 7-7 shows an implementation of $\mathsf{DME}_2(|0\rangle\langle 0|, 8, \pi)$, encoding the instruction $\mathsf{R}_Z(\pi)$, a π rotation about the z axis. In both cases, σ undergoes a rotation about an axis defined by ρ_{in}, which is visible in the step-by-step tomographic reconstruction of the data qubit state $\sigma(n)$. QME maintains the polarization direction of the instruction qubit state $\rho(n)$, albeit with gradual depolarization consistent with the effects of the simulated measurement. The classically defined δSWAP operations are identical in these two cases; it's the change in the instruction state ρ_{in} that causes a different operation on the data qubit. Thus, the implemented quantum program (here, a single-qubit operation) is uniquely determined by the state of another quantum system, a demonstration of quantum instructions.

We next assess DME_2 in the context of an imperfect quantum processor with noise-induced errors in addition to discretization (finite N) errors (Fig. 7-8). Here, we fix target state $\sigma_{\text{in}} = |0\rangle\langle 0|$ and instruction state $\rho_{\text{in}} = |+i\rangle\langle +i|$, and vary total

steps N. This allows us to probe the interplay between discretization error (which decreases with N) and noise-induced errors (which increases with N). We use two angles, $\theta = \pi$ and $\theta = \pi/2$, to elucidate the effects of changing the overall angle. For each experiment, we perform the full algorithm $\mathsf{DME}_2(\rho_{\text{in}}, N, \theta)$ with many QME randomizations, tomographically reconstruct the final density matrix $\sigma(N)$, and calculate its fidelity to an ideal rotation with no discretization or processor error, as given by

$$\sigma_{\text{ideal}} \;=\; e^{-i\rho_{\text{in}}\theta}\sigma_{\text{in}}e^{i\rho_{\text{in}}\theta} \tag{7.7}$$

The state σ_{ideal} can equivalently be thought of as a perfect unitary rotation, or as DME when implemented on an error-free processor with an infinite number of copies of the quantum instructions.

There are two sources of error we must consider in understanding the output of the DME_2 protocol: the approximate nature of the algorithm and imperfections in the quantum processor. To understand the discretization error, we calculate σ_{DME_2}, the outcome of a simulation of the DME_2 circuit (including discretization error) with perfect gates. We sample every possible combination of QME gates for a DME_2 circuit of length N and simulate the application of each circuit to the experimentally-measured $\rho_{\text{in}} \otimes \sigma_{\text{in}}$ (thus accounting for state-preparation errors). The fidelity $F_s(\sigma_{\mathsf{DME}_2}, \sigma_{\text{ideal}})$ quantifies the error due solely to the approximate nature of DME_2 (Fig. 7-8b, dashed lines). Fig. 7-8c shows the fidelity of the measured state $\sigma(N)$ to the ideal algorithm performance, $F_s(\sigma, \sigma_{\mathsf{DME}_2})$. To circuit depth 73, this fidelity exceeds 0.90.

We next account for the effects of imperfections in the physical processor by building a model of DME_2 performance in the presence of processor noise. To the DME_2 circuit with perfect gates we add amplitude-damping and dephasing channels with coherence parameters consistent with independent measurements (see Section 7.11). The fidelity between the model including decoherence effects and σ_{ideal} is plotted in Fig. 7-8b (solid lines), and shows good agreement with experimental data, indicating we are mostly limited by decoherence effects and not by coherent errors in the gates.

Both the simulated and experimental curves reveal an interplay between finite N

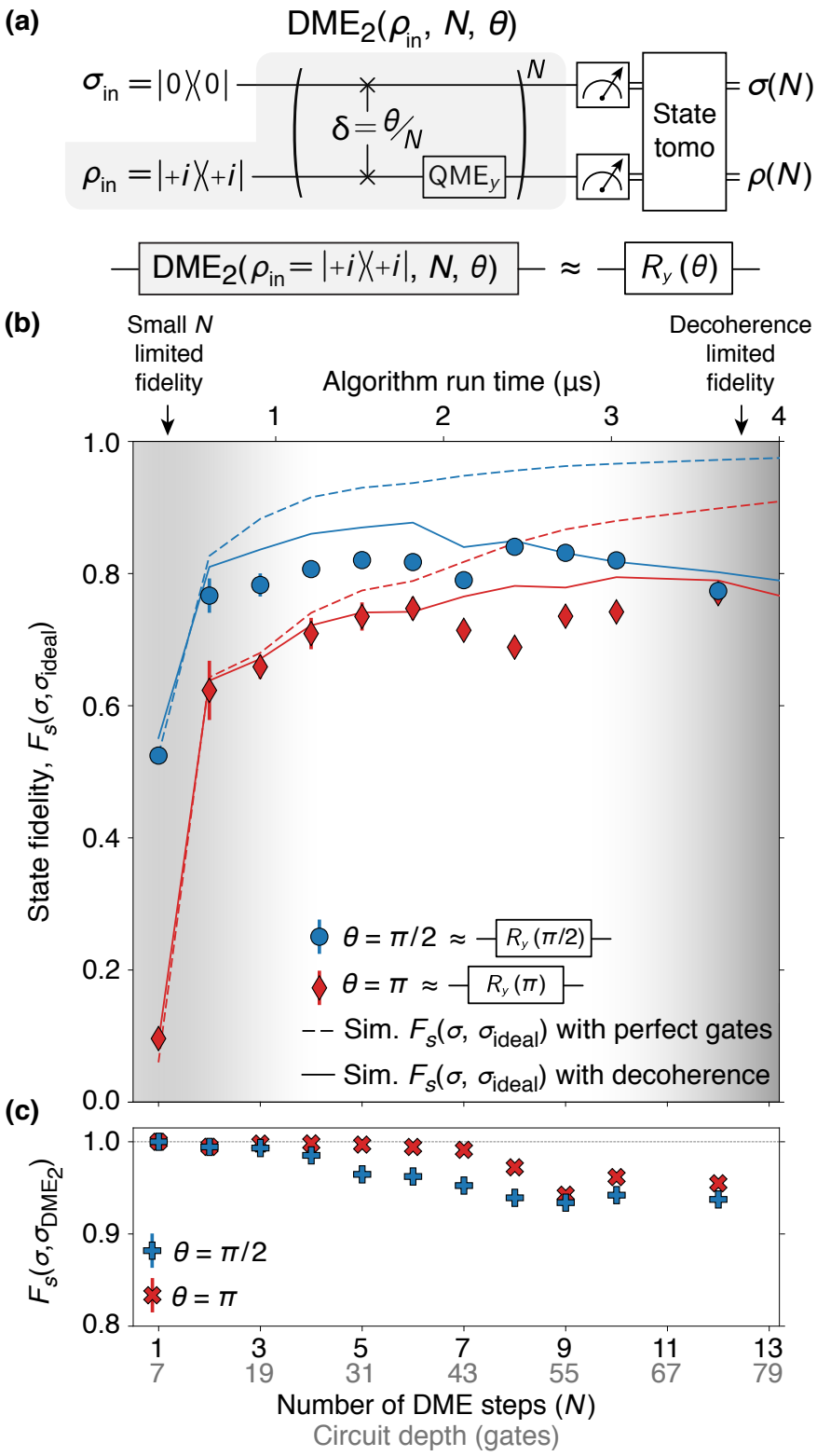
(a)
DME2(ρin, N, θ)
σin = |0⟩⟨0|
ρin = |+i⟩⟨+i|
δ = θ/N
N
QMEy
State tomo
σ(N)
ρ(N)
DME2(ρin = |+i⟩⟨+i|, N, θ)
≈
Ry (θ)
(b)
Small N limited fidelity
Algorithm run time (μs)
Decoherence limited fidelity
State fidelity, Fs(σ, σideal)
θ = π/2 ≈ Ry (π/2)
θ = π ≈ Ry (π)
Sim. Fs(σ, σideal) with perfect gates
Sim. Fs(σ, σideal) with decoherence
(c)
Fs(σ, σDME2)
θ = π/2
θ = π
Number of DME steps (N)
Circuit depth (gates)

Figure 7-8

error and processor error. At small N, the error is dominated by the approximate nature of DME_2 as given in Eq. (7.6). The error is greater for larger θ, consistent with error scaling as $\mathcal{O}(\theta^2/N)$. For large N, the discretization error improves and the processor's performance is instead limited by finite gate fidelity; here, the curves for $\theta = \pi$ and $\theta = \pi/2$ begin to converge. The algorithm is at its most accurate for intermediate N, where discretization error is relatively low and the circuit is sufficiently free of compounding physical errors. This trade-off (improved performance with increasing circuit depth, until gate fidelities become limiting) is a generic property of Trotterized quantum algorithms on noisy processors in the absence of error-correction protocols [376].

To assess the error-budget of the quantum instruction execution independent of its operation on the target quantum state, we perform quantum process tomography. We experimentally reconstruct the process map of the channel implemented by DME_2 (denoted $\chi(\rho_{\text{in}}, N, \theta)$) for a set of instruction states given by the cardinal points on the Bloch sphere. For each ρ_{in}, we sweep N to find the optimal point N_{opt}, defined as that which has the highest process fidelity (see Section 7.9) to the pure rotation $U_{\text{ideal}} = e^{-i\rho_{\text{in}}\theta}$. The mean N_{opt} for $\theta = \pi/2$ is 4, at circuit depth 25; for $\theta = \pi$ this increases to 8, at circuit depth 49.

Figure 7-8: Algorithm performance as a function of N. **(a)** Circuit schematic for $\mathsf{DME}_2(|+i\rangle\langle+i|, N, \theta)$. Data qubit is initialized in $\sigma_{\text{in}} = |0\rangle\langle 0|$. **(b)** State fidelity (F_s) of the data qubit state σ to the ideal state $\sigma_{\text{ideal}} = e^{-i\rho_{\text{in}}\theta}\sigma_{\text{in}}e^{i\rho_{\text{in}}\theta}$ as a function of total DME steps (N). The instruction qubit is initialized to the $|+i\rangle\langle+i|$–state, resulting in an ideal operation $e^{-i\rho_{\text{in}}\theta} = R_y(\theta)$. The x-axis shows the number of $\delta\mathsf{SWAP} + \mathsf{QME}$ steps N (bottom, black), circuit depth (bottom, gray), and active circuit clock time (top). Data for $\theta = \pi$ ($\pi/2$) are shown with red/$\diamond$ (blue/$\circ$) markers. Dashed lines is the state fidelity between σ_{ideal} and a simulated output of the $\mathsf{DME}_2(|+i\rangle\langle+i|, N, \theta)$ circuit, assuming perfect gates. The increasing fidelity with increasing N is a reflection of a reduction of the discretization error scaling as $\mathcal{O}(\theta^2/N)$. Solid lines are the same simulation as shown in dashed lines, but with amplitude damping and depolarizing channels included in the circuit to model the effect of decoherence. **(c)** State fidelity of σ to a simulated output of the $\mathsf{DME}_2(|+i\rangle\langle+i|, N, \theta)$ circuit with perfect gates (denoted $\sigma_{\mathsf{DME}_2}(N)$). Error bars are determined from bootstrap analysis (see Section 7.10). [247]

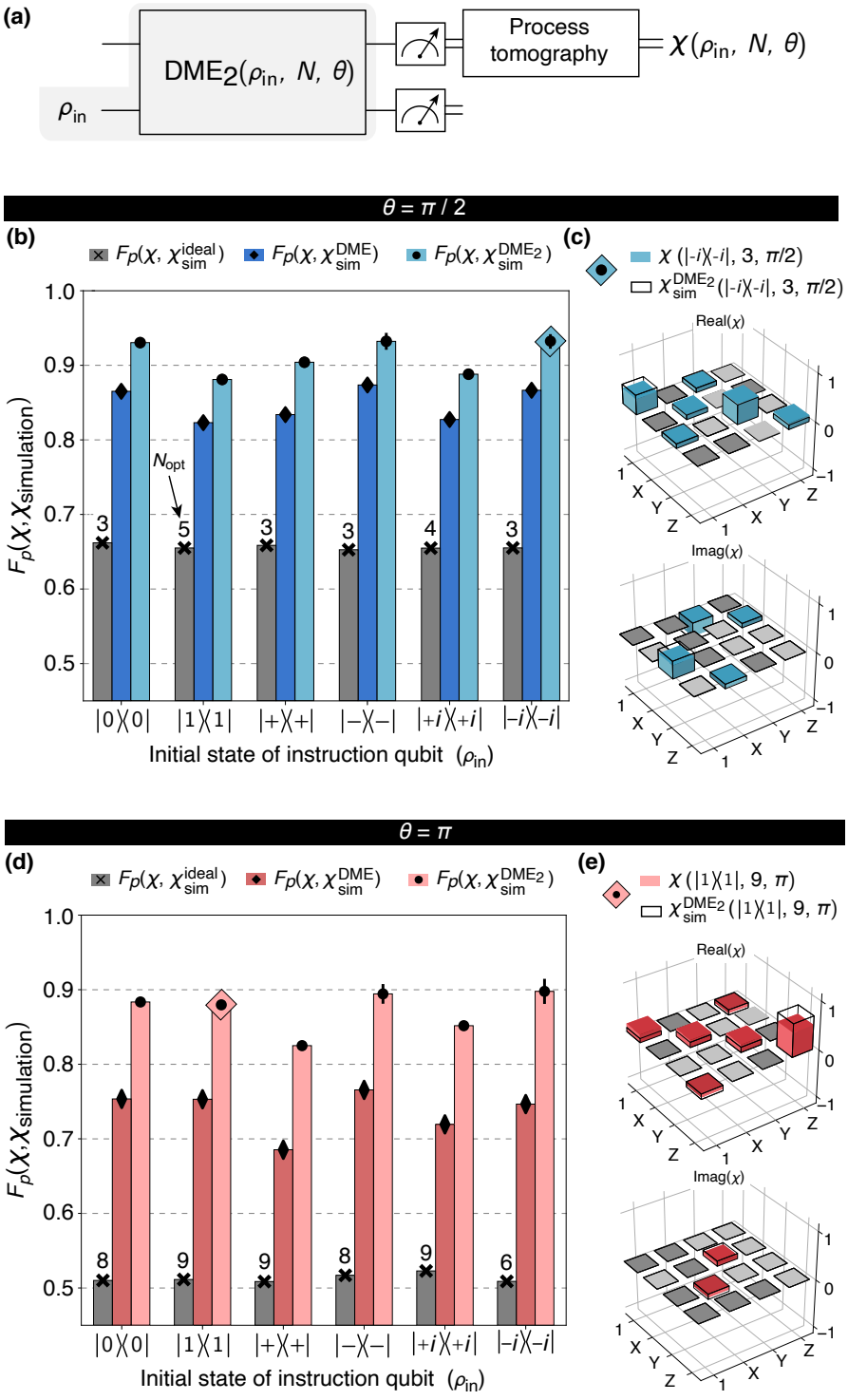
(a)
DME2(ρin, N, θ)
ρin
Process tomography
χ(ρin, N, θ)
θ = π / 2
(b)
Fp(χ, χideal sim)
Fp(χ, χDME sim)
Fp(χ, χDME2 sim)
Fp(χ,χsimulation)
Nopt
3
5
3
3
4
3
|0⟩⟨0|
|1⟩⟨1|
|+⟩⟨+|
|−⟩⟨−|
|+i⟩⟨+i|
|−i⟩⟨−i|
Initial state of instruction qubit (ρin)
(c)
χ (|-i⟩⟨-i|, 3, π/2)
χDME2 sim(|-i⟩⟨-i|, 3, π/2)
Real(χ)
Imag(χ)
θ = π
(d)
8
9
9
8
9
6
(e)
χ (|1⟩⟨1|, 9, π)
χDME2 sim(|1⟩⟨1|, 9, π)

Figure 7-9

In Fig. 7-9 we plot the process fidelity at N_{opt} to several theoretical processes to elucidate the error budget in DME_2. The fidelity to χ_{ideal}, corresponding to the perfect rotation U_{ideal}, is plotted in grey. $F_p(\chi, \chi_{\text{ideal}})$ is greater for $\theta = \pi/2$ than for $\theta = \pi$, as expected from the $\mathcal{O}(\theta^2/N)$ scaling of the discretization error, and is consistent for all cardinal settings of the instruction state. This process fidelity reflects the combination of errors arising from the Trotterized nature of density matrix exponentiation and the errors from imperfect gates and the approximate nature of QME.

We next compare our QME-enabled algorithm to the original DME proposal requiring N copies of ρ_{in}. We label this theoretical process χ_{DME} and calculate the fidelity $F_p(\chi, \chi_{\mathsf{DME}})$, shown in dark blue/red. This fidelity combines the physical errors arising from our imperfect gates and the error from using QME to emulate the re-preparation of ρ_{in}. The difference between $F_p(\chi, \chi_{\mathsf{DME}})$ and $F_p(\chi, \chi_{\text{ideal}})$ is a reflection of finite N error in the underlying DME algorithm.

Finally, we plot the fidelity between our measured process and χ_{DME_2}, a simulated

---

Figure 7-9: Benchmarking algorithmic fidelity of DME_2. **(a)** Circuit schematic. Single-qubit process tomography is performed for a set of six instruction states ρ_{in} representing cardinal points of the Bloch sphere. **(b,d)** Process fidelities between measured process maps and simulated processses, for varying instruction state and overall angle in DME_2. Grey ($\times$ marker) denotes the fidelity $F_p(\chi, \chi_{\text{ideal}})$ between the measured process map χ and the ideal process χ_{ideal}, e.g a rotation of angle θ around the axis given by the Bloch vector of ρ_{in}. The data are presented at $N = N_{\text{opt}}$, determined as the step-number at which the fidelity to χ_{ideal} is maximized; N_{opt} is indicated by the number above each bar. Dark blue/red ($\diamond$ marker) indicates the fidelity $F_p(\chi, \chi_{\mathsf{DME}})$ between the measured process map and a simulated implementation of the DME circuit assuming active reset and reinitialization of the instruction qubit (evaluated at $N = N_{\text{opt}}$). Light blue/red ($\circ$ marker) shows the fidelity $F_p(\chi, \chi_{\mathsf{DME}_2})$ between the measured process map and a simulation of DME_2 with perfect gates and no decoherence using QME to approximately reinitialize the instruction qubit at each step. Error bars are calculated using bootstrap analysis (see Section 7.10). The process map for the point enclosed by a blue/red diamond is shown in (c,e). **(c,e)** Representative process matrices for χ shown in blue and red for $\theta = \pi/2$ and $\theta = \pi$ respectively, evaluated at N_{opt}. Colored process matrix elements indicate points with magnitude $\chi_{ij} > 0.02$; other elements are grey for clarity of scale. Black wire frames denote a process matrix from a simulated implementation of χ_{DME_2} assuming perfect gate operation and no decoherence. [247]

version of the DME_2 algorithm, shown in light blue/red. This fidelity compares the experimental implementation of DME_2 to a classical simulation of DME_2 using perfect operations and is therefore the most direct metric for the performance of our processor. The theoretical χ_{DME_2} is calculated by sampling all QME randomizations and averaging their effect. The average process fidelity $F_p(\chi, \chi_{\mathsf{DME}_2})$ over all instruction settings is 0.91 for $\theta = \pi/2$ and 0.87 for $\theta = \pi$; this algorithmic fidelity is overall reduced for $\theta = \pi$ because N_{opt} occurs at deeper circuit depth.

7.5 Device Parameters

The quantum processor used in this work consists of three asymmetric xmon-style qubits in a linear chain [33, 211, 256]. We use the two leftmost qubits in this protocol; the third is detuned and idles in its ground state. Figure 7-10a shows a schematic of the readout- and control-setup used to control the qubits. Figure 7-10b shows a scanning electron micrograph of a device identical to the one used in this work. In Table 7.1 we summarize the parameters of the two qubits used for the experiments in this work. The measured lifetime T_1 and Ramsey coherence time $T_{2\text{R}}$ exhibit temporal fluctuations, consistent with other reports [81, 250].

For a qubit undergoing frequency modulation (e.g., to implement the CZ gate), frequency-dependent T_1 (and $T_{2\text{R}}$) variations mean that the static coherence times do not necessarily set the relevant limiting time-scale for the qubits [250]. To account for the frequency-dependent variations in coherence as the target qubit undergoes the CZ trajectory, we employ an *effective* T_1 ($T_{2\text{R}}$) parameter, denoted $\widetilde{T}_1$ ($\widetilde{T}_{2\text{R}}$). These effective coherence times take into account any frequency-dependent variations of coherence as the qubit frequency undergoes the trajectory to enact a CZ gate. The effective coherence times are used in simulations of the device performance during

Figure 7-10: **(a)** Schematic of readout- and control-wiring used for these experiments. The microwave line of qubit 3 is used to drive single-qubit gates on qubit 2. **(b)** SEM image of identically fabricated device to the processor used in this work. [247]

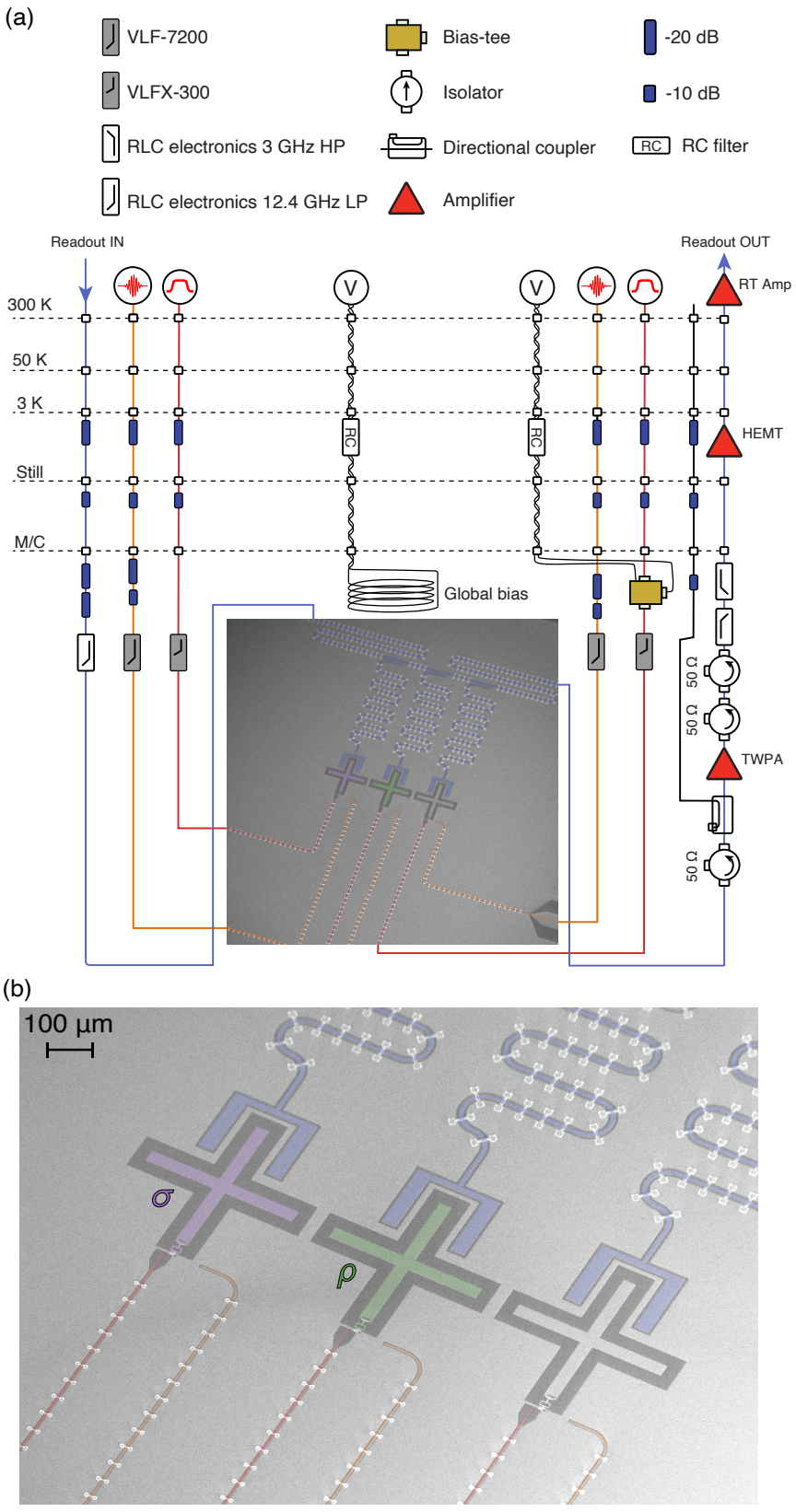
(a)
VLF-7200
VLFX-300
RLC electronics 3 GHz HP
RLC electronics 12.4 GHz LP
Bias-tee
Isolator
Directional coupler
Amplifier
-20 dB
-10 dB
RC
RC filter
Readout IN
Readout OUT
300 K
50 K
3 K
Still
M/C
RT Amp
HEMT
TWPA
Global bias
50 Ω
50 Ω
50 Ω
(b)
100 µm
σ
ρ

Figure 7-10

Parameter	Qubit 1 (σ, target)	Qubit 2 (ρ, instruction)
Idling frequency, $\omega_i/2\pi$	4.748 GHz	4.225 GHz
Anharmonicity, $\eta/2\pi$	-175 MHz	-190 MHz
Coupling strength, $g/2\pi$	10.6 MHz	
Readout resonator frequency, $f_i/2\pi$	7.251 GHz	7.285 GHz
Junction asymmetry	1:5	1:10
Relaxation time at idling point, T_1	23 μs	39 μs
Coherence time at idling point, $T_{2\mathrm{R}}$	13 μs	25 μs
Effective relaxation time during CZ trajectory, $\widetilde{T}_1$	≈ 17 μs	(same as idling)
Effective coherence time during CZ trajectory, $\widetilde{T}_{2\mathrm{R}}$	≈ 5 μs	(same as idling)
Single-qubit gate time, $t_{1\mathrm{qb}}$	30 ns	30 ns
Two-qubit gate time, t_{CZ}	60 ns	

Table 7.1: Parameters of the two qubits used in this work. See Section 7.5 for the definition of $\widetilde{T}_1$ and $\widetilde{T}_{2\mathrm{R}}$.

two-qubit gates. Since the frequency of qubit 2 is fixed during the CZ gate, its effective coherence times are identical to the idling coherence times.

Figure 7-11 shows an example measurement of $\widetilde{T}_1$. We prepare the state $|10\rangle$ (an eigenstate of CZ), apply n CZ gates in sequence, and measure the probability of staying in the $|10\rangle$ state. The exponential decay is fitted and we find a characteristic number of gates, $n_{\widetilde{T}_1} \approx 264$. The CZ gate-time is 60 ns, and we use a 5 ns spacing between each pulse, leading to an effective decay time $\widetilde{T}_1 = n_{\widetilde{T}_1} \cdot t_{\mathrm{CZ}} \approx 17$ μs.

To measure the effective coherence time $\widetilde{T}_{2\mathrm{R}}$ (Fig. 7-12), we prepare the $|+0\rangle$ state, apply n CZ gates, and apply a final $\mathsf{X}_{\pi/2}$ pulse before measuring. Unlike a standard Ramsey measurement, in which we would idle between the $\mathsf{X}_{\pi/2}$ pulses, here we perform back-to-back CZ gates, effectively aggregating decoherence effects over the full frequency range of the CZ gate. To ensure an oscillatory behavior, a small single-qubit phase error is added ($\phi_{\mathrm{q1}} \neq 0$), equivalent to performing a detuned Ramsey experiment Fitting an exponentially damped sine function gives a characteristic decay number $n_{\widetilde{T}_{2\mathrm{R}}} \approx 76$ CZ gates. We again estimate the effective coherence time as $\widetilde{T}_{2\mathrm{R}} = n_{T_{2\mathrm{R}}} \cdot t_{\mathsf{CZ}} \approx 5$ μs.

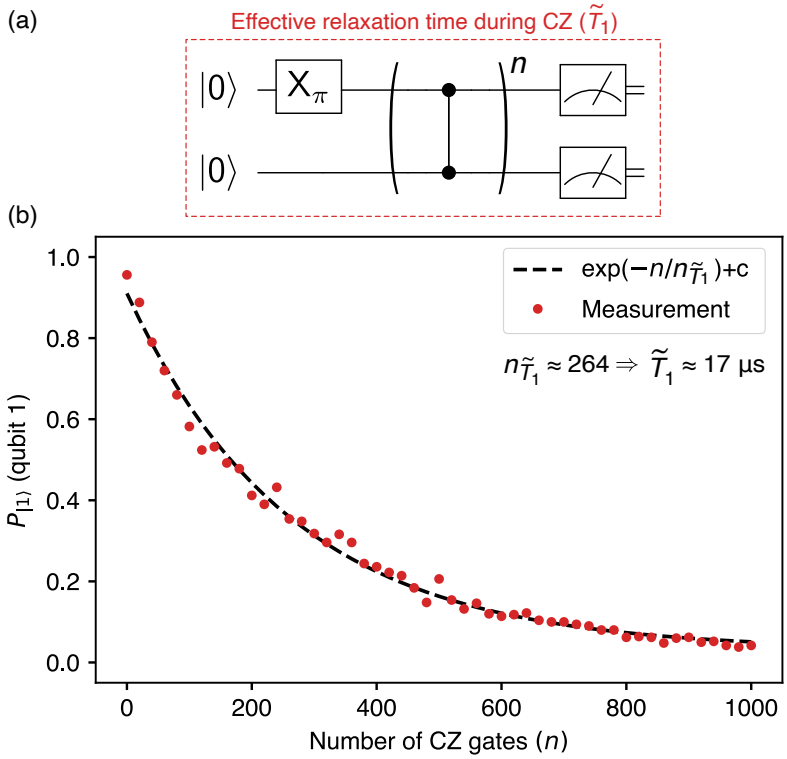

Figure 7-11: **(a)** Measurement circuit to extract effective T_1-like decay time, denoted $\widetilde{T}_1$. **(b)** Probability of measuring qubit 1 in the excited state, as the number of CZ gates is increased. The number $n_{\widetilde{T}_1}$ sets a characteristic gate number, which can be converted into a characteristic time, $\widetilde{T}_1$. [247]

7.6 Gate Characterization

The native gate set of our processor comprises microwave-driven single-qubit x- and y-rotations $\mathsf{R}_X(\phi)$ and $\mathsf{R}_Y(\phi)$, single-qubit virtual-z rotations $\mathsf{R}_Z(\phi)$, and the two-qubit controlled-phase (CZ) gate [258]. In particular, we calibrate a numerically optimized 99.7% fidelity CZ gate [236, 425], using the symmetrized 'NetZero' optimal control waveform that reduces leakage and noise-sensitivity [293, 343, 388].

We use a combination of metrics to quantify the quality of qubit operations during the algorithm. These techniques include single- and two-qubit randomized benchmarking (RB) as well as novel techniques for amplifying and correcting coherent errors.

Figure 7-13 shows single-qubit Clifford randomized benchmarking of the single-

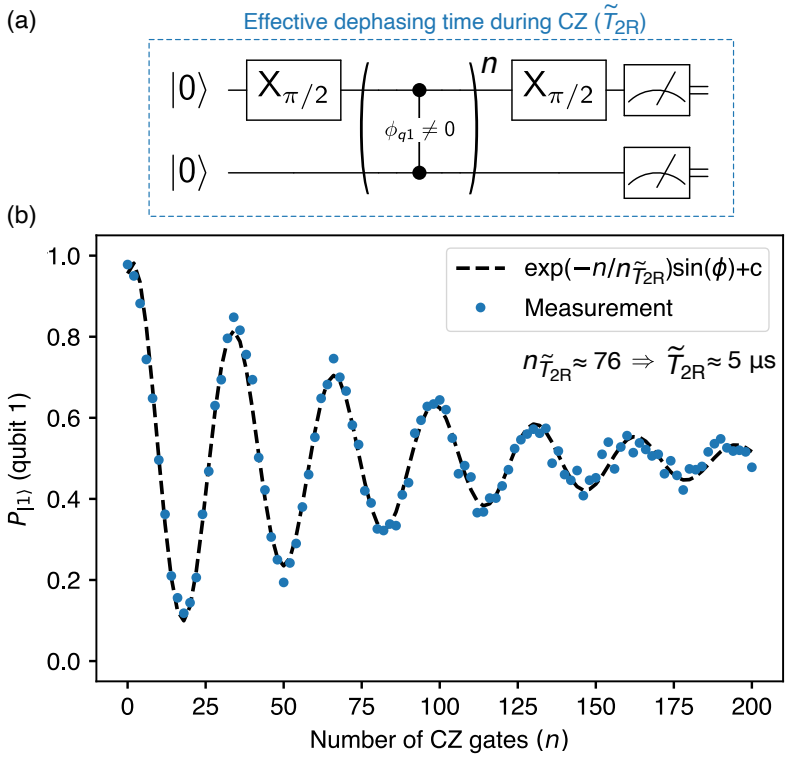

Figure 7-12: **(a)** Measurement circuit to extract effective T_{2R}-like decay time, denoted $\widetilde{T}_{2R}$. We essentially perform a Ramsey measurement but interleave CZ gates. **(b)** Probability of measuring qubit 1 in the excited state, as the number of CZ gates is increased. The number $n_{\widetilde{T}_{2R}}$ gives the effective coherence time $\widetilde{T}_{2R} \approx 5\mu$s. [247]

qubit operations on both qubit 1 (panel b) and 2 (panel c). Each trace averages 25 randomizations of the RB circuit [35]. The reference curves (circuit diagram in panel a, grey dashed box) are fit to a function of the form

$$f(m) = Ap^m + B \tag{7.8}$$

For the one qubit Clifford reference curve we denote p by p_r. The average error per Clifford gate $\mathcal{C}$ can be calculated as

$$\epsilon_r = \frac{1}{2}(1 - p_r) \tag{7.9}$$

The error associated with a specific single-qubit gate is extracted by performing interleaved randomized benchmarking (IRB). We fit the IRB data (circuit diagram

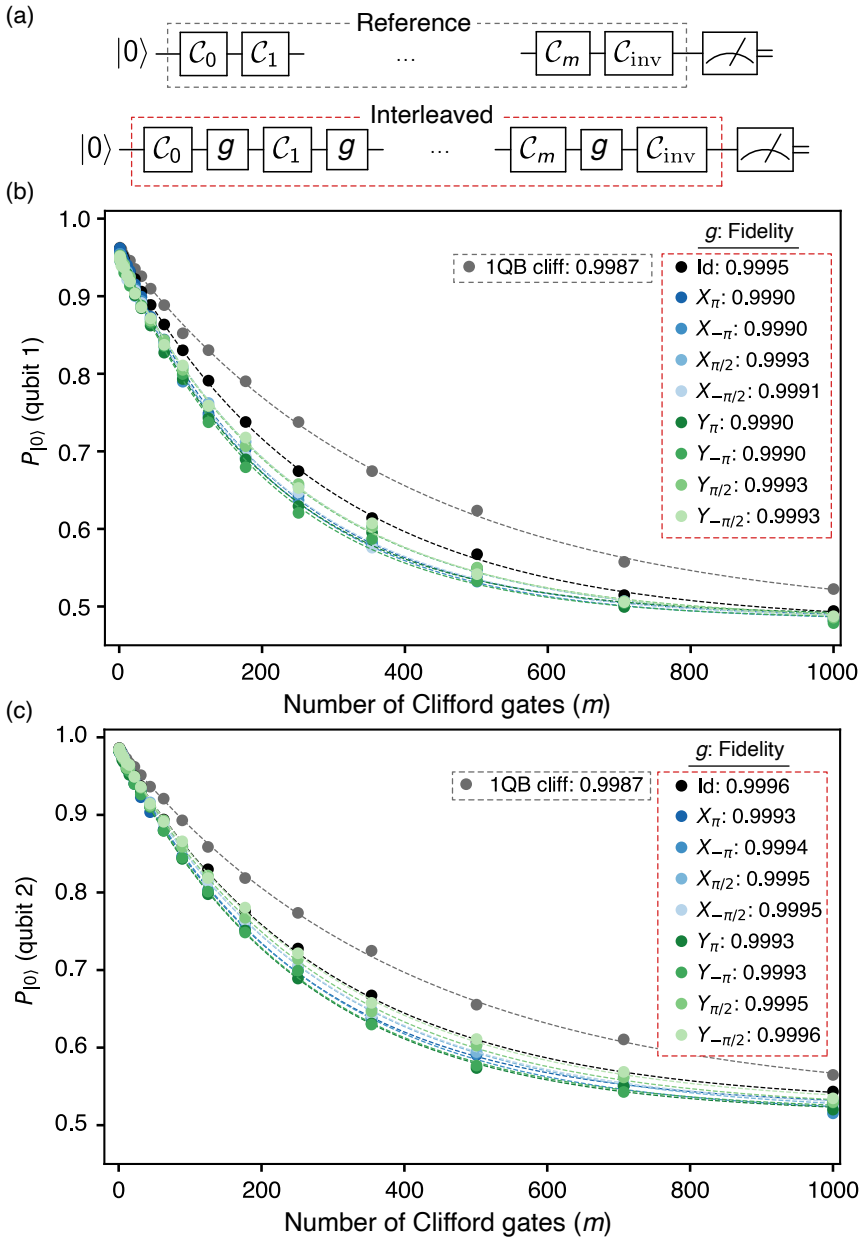

Figure 7-13: **(a)** Circuit diagrams for measuring the reference curve (gray dashed box) and interleaved curve for a single qubit gate g (red dashed box) relevant for Clifford randomized benchmarking for a single qubit. **(b,c)** Results for reference (gray) and interleaved (varying colors, for each gate) randomized benchmarking for qubit 1 and 2, respectively. [247]

in panel a, red dashed box) for the relevant gate (denoted g) to Eq. (7.8) (where p_g denotes the p value for gate g). The normalized error rate for the one-qubit Clifford

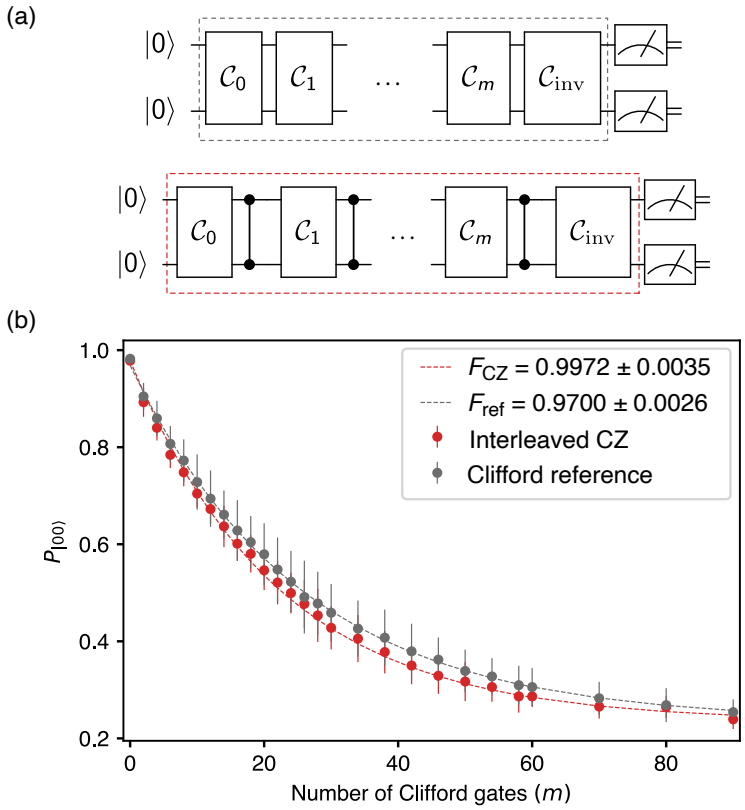

Figure 7-14: **(a)** Gate sequences for measuring the two-qubit Clifford reference (gray dashed box) and interleaved CZ (red dashed box) RB numbers. **(b)** Example decay curve of $P_{|00\rangle}$ as the number of two-qubit Clifford gates (m) is increased. Each datapoint is averaged over $k = 48$ randomizations of the choice of Clifford gates. Error bars are 1σ standard deviations at each point from the 48 measurements, and fitting is performed using forward propagation of points weighted by their error bars.

reference is given by [91]

$$\epsilon_g = \frac{1}{2}(1 - p_g/p_{\text{r}}) \tag{7.10}$$

Using this procedure we find an average Clifford gate fidelity ($F_{\text{r}} = 1 - \epsilon_{\text{r}}$) of 0.9987 for qubit 1 and 0.9987 for qubit 2. The average gate fidelity (i.e. $\bar{F} = \langle 1 - \epsilon \rangle_g$) over all single-qubit gates is 0.9991 for qubit 1 and 0.9994 for qubit 2.

In Fig. 7-14, we assess the two-qubit gate fidelity using randomized benchmarking. The protocol is identical to the single-qubit case, except we measure the probability of being in the $|00\rangle$ state after the sequence [35]. We use 48 randomizations for both reference and interleaved measurements (circuits shown in panel a). In panel b we show the result of the RB and IRB measurements. The error bars are 1σ

standard deviations of the output distribution of the 48 random circuits. The fit is again performed using Eq. (7.8), and error margins are extracted using forward-propagation of weights based on the standard deviation at each m to ensure accurate error bounds. This is achieved using the `absolute_sigma` option of the Python `scipy.optimize.curve_fit` function. The two-qubit Clifford reference error rate is calculated similarly to Eq. (7.9) (with p being the two-qubit Clifford reference value, denoted $p_{2\mathrm{r}}$), but the error per Clifford is modified to

$$\epsilon_{2\mathrm{r}} = \frac{3}{4}(1 - p_{2\mathrm{r}}) \tag{7.11}$$

Then, ϵ_{CZ} is found by performing IRB and fitting the interleaved data to get p_{CZ} and normalizing to the 2QB reference error. Doing so, we find a CZ gate fidelity

$$F_{\mathsf{CZ}} = 1 - \epsilon_{\mathsf{CZ}} = 0.9972 \pm 0.0035 \tag{7.12}$$

To achieve last-mile improvements in fidelity we use numerical optimization techniques to fine-tune parameters of the NetZero waveform, with the RB decay curve as a cost function [236, 388].

7.7 Coherent Error Reduction

As practitioners of quantum computing have explored more complex circuits at greater depth and with more underlying structure, it has become evident that RB is a limited metric for the performance of a gate (see, for example, Ref. [371, 455, 457] and references therein). In particular, small coherent errors can cause disproportionately deleterious effects in algorithms with a repetitive structure (such as Trotterized algorithms), and RB is ill suited to characterize such small coherent errors because it is designed to randomize over them.

To minimize the effects of coherent errors in the CZ gate, we implement a calibration technique which relies on process tomography of long strings of CZ gates

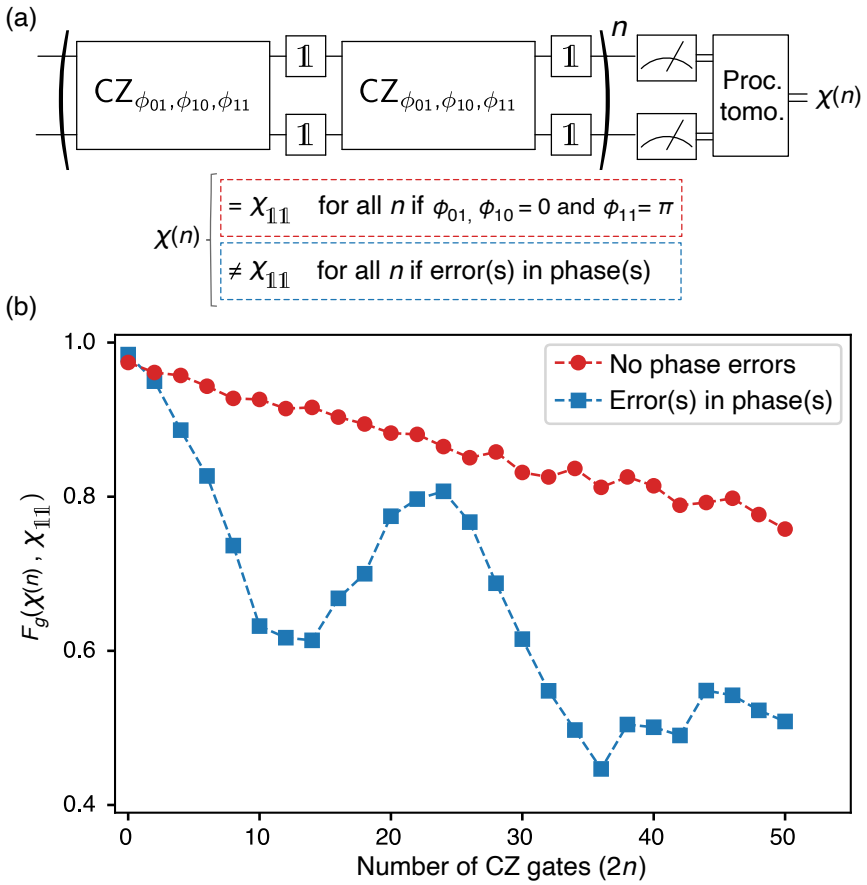

Figure 7-15: **(a)** Gate sequence used to perform process tomography of a sequence of an even number of CZ gates, to get the chi-matrix $\chi(n)$, used to compare with the identity process map to infer coherent errors. The gate-sequence will nominally implement $\chi_{\mathbb{1}\mathbb{1}}$ up to overall system decoherence (visible as the overall decrease of both the linear and oscillating measurements) if there are no phase errors in the $\mathsf{CZ}_{\phi_{01},\phi_{10},\phi_{11}}$ gate. **(b)** The gate fidelity $F_g(\chi(n), \chi_{\mathbb{1}\mathbb{1}})$ as the number of CZ gates $(2n)$ is increased. With no phase errors in the CZ gate, F_g decreases monotonically. With a phase error in the CZ gate F_g will oscillate, with the period indicating the scale of the phase error. [247]

(Fig. 7-15). The general controlled-phase gate (denoted $\mathsf{CZ}_{\phi_{01},\phi_{10},\phi_{11}}$) is given by

$$\mathsf{CZ}_{\phi_{01},\phi_{10},\phi_{11}} = \begin{bmatrix} 1 & 0 & 0 & 0 \\ 0 & e^{-i\phi_{01}} & 0 & 0 \\ 0 & 0 & e^{-i\phi_{10}} & 0 \\ 0 & 0 & 0 & e^{-i\phi_{11}} \end{bmatrix} \tag{7.13}$$

If $\phi_{01} = \phi_{10} = 0$ and $\phi_{11} = \pi$, this produces the target CZ gate. However, for small deviations from these parameters it is still possible to achieve $\gtrsim 0.99$ randomized

benchmarking fidelities. Since small phase deviations can compound to form larger errors—specifically in algorithms with a repeating pattern like DME or quantum error correction protocols—we have developed other calibration strategies to detect and correct such errors.

Our amplification protocol consists of a circuit with two back-to-back blocks of $\mathsf{CZ}_{\phi_{01},\phi_{10},\phi_{11}}$ followed by identity gates on both qubits designed to mimic the presence of single-qubit gates, as shown in Fig. 7-15a. If the CZ gate contains no phase errors, this sequence produces an identity operation, irrespective of the number (n) of such two-CZ blocks applied. We perform two-qubit process tomography to extract the process matrix $\chi(n)$. We compare $\chi(n)$ to the process map of a two-qubit identity operation ($\chi_{\mathbb{1}\mathbb{1}}$) via the gate fidelity $F_g(\chi(n), \chi_{\mathbb{1}\mathbb{1}})$ which is related to the process fidelity (defined in Section 7.9) according to

$$F_g(\chi, \chi') = \frac{dF_p(\chi, \chi') + 1}{d + 1} \tag{7.14}$$

where d is the dimensionality of the Hilbert space ($d = 4$ in the case of a two-qubit gate).

Figure 7-15b shows the gate fidelity of a circuit optimized to remove phase errors from the CZ gate (red circles), and one in which a CZ-gate *with* phase errors is used (blue squares). In the optimized case, the monotonic gate fidelity decay stems only from decoherence effects. However, in the presence of a coherent phase error, the gate fidelity oscillates with n. In this specific example, after roughly 25 CZ gates, the phase-error has effectively rotated by 2π, corresponding to an approximate per-step error of $2\pi/25 \approx 0.08\pi$ in one of the phases.

The evolution of the process maps is useful both practically (for achieving higher performance gates) and scientifically (for understanding the limitations of RB). By examining the details of the process maps, we are able to infer in which of the parameters ϕ_{01}, ϕ_{10}, or ϕ_{11} the error appeared in, and we correct accordingly. This minor correction typically does not change the fidelity as measured with RB (except in the case of particularly egregious phase errors). From Fig. 7-15b it is also clear that

process tomography of a single CZ instance does not reveal the coherent error: the first datapoint for the sequence with phase errors has nearly identical fidelity to the optimized gate. Both of these facts are consistent with a growing understanding that RB may not be the optimal approach to identifying and correcting coherent errors in single- and multi-qubit gates. Finally, the identity gates are inserted between the CZ gates to mimic as closely as possible the generic optimal gate sequence of a two-qubit algorithm without exploiting any specific structure of an algorithm.

7.8 Compilation

We implement δSWAP using single-qubit gates and the entangling CZ gate. δSWAP has an optimal decomposition [449]

$\delta\mathsf{SWAP} =$ 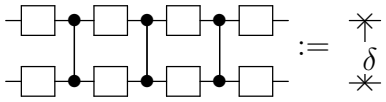 $:=$ (7.15)

where each  represents a general single-qubit gate that depends on the value of δ and  is the CZ gate. The open-source software package `Cirq` [100] is used to determine the appropriate single-qubit gate parameters for a given δSWAP. Our δSWAP construction allows us to rely solely on high-fidelity gates whose performance can be validated and efficiently optimized.

A conceptually transparent approach to generating a δSWAP uses the decomposition

$\delta\mathsf{SWAP} :=$ 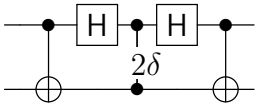 (7.16)

where

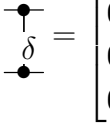 $= \begin{bmatrix} 1 & 0 & 0 & 0 \\ 0 & 1 & 0 & 0 \\ 0 & 0 & 1 & 0 \\ 0 & 0 & 0 & e^{-i\delta} \end{bmatrix} := \mathsf{CZ}_\delta$ (7.17)

is a partial CZ gate and  is the CNOT gate with qubit 2 as the target. The CZ_δ

gate can in turn be compiled using an additional decomposition

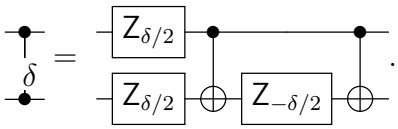

(7.18)

However, such an approach would introduce two CZ gates for each CZ_δ gate, adding significant circuit depth overhead.

We use a more generalized and gate-efficient approach, relying on the fact that any two-qubit gate can generically be decomposed into a circuit with the structure [333, 449]

$U_{\mathrm{2QB}} =$

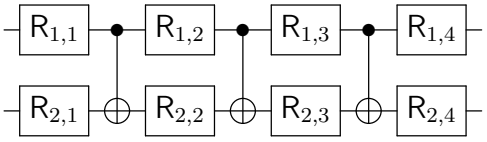

(7.19)

Here $\mathsf{R}_{i,j}$ is a single-qubit gate acting on qubit i at moment j in the circuit.

By using the identity

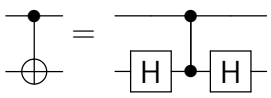

(7.20)

and absorbing the Hadamard gates (H) into the neighboring single-qubit gates, the circuit in Eq. (7.19) becomes identical to the circuit in Eq. (7.15).

We use the open-source software `Cirq` [100] to determine the settings of the single-qubit gates for each value of δ. The single-qubit rotations around the x, y axes are decomposed according to $\mathsf{R}_Z(-\varphi)\mathsf{R}_X(\theta)\mathsf{R}_Z(\varphi)$ (the `PhasedXPowGate` in `Cirq`) and the R_Z rotations are performed virtually [300]. The δSWAP is implemented using the `SwapPowGate` function in `Cirq` (the `SwapPowGate` has a factor of 2 difference, relative to our definition of δSWAP). Thus, we are able to compose a unique composite gate sequence for each δSWAP relying only on high-fidelity single- and two-qubit gates.

Figure 7-16 shows the full compilation protocol. To construct the full $\mathsf{DME}(\rho, N, \theta)$ circuit, we append N copies of the compiled δSWAP gate using $\delta = \theta/N$, interleaving the requisite QME_ν on qubit 2 (the instruction qubit, ρ) to emulate the effect of measurements. Rows 1 and 2 show the generic structure and gate decomposition of our implementation of DME_2. The final layer of single-qubit gates in the δSWAP at

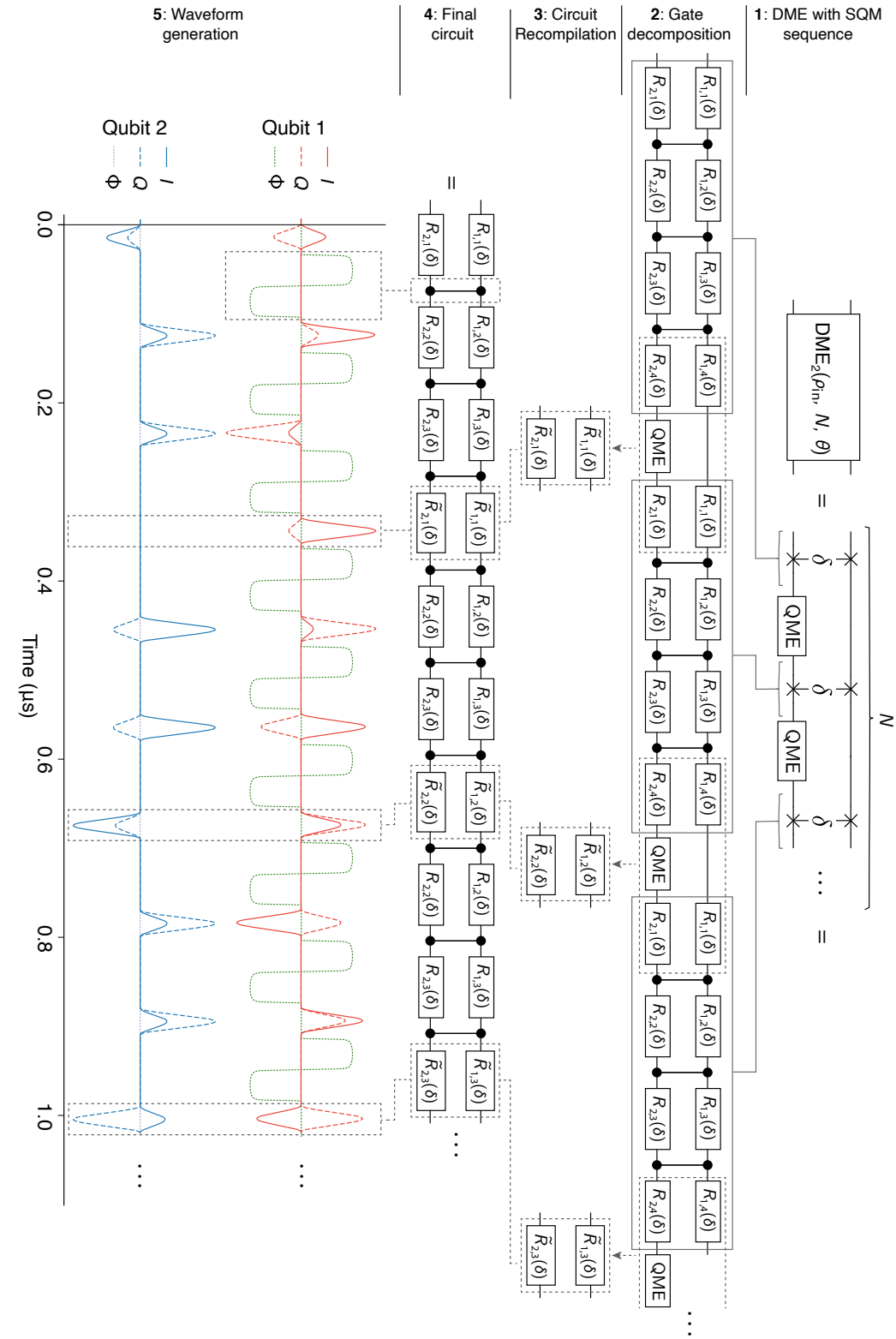
1: DME with SQM sequence
2: Gate decomposition
3: Circuit Recompilation
4: Final circuit
5: Waveform generation
DME2(ρin, N, θ)
QME
δ
N
Qubit 1
Qubit 2
I
Q
Φ
Time (μs)
0.0
0.2
0.4
0.6
0.8
1.0

Figure 7-16

step n can be recompiled together with the QME_ν and the first layer of single-qubit gates in the δSWAP at step $n+1$. We use Cirq to slice out these three layers (Row 2) of single-qubit gates, recompile them into a single layer (Row 3), and reinsert them (Row 4). Finally, in Row 5 we show an example waveform output from our signal generation software, implementing the first $n = 3$ steps in a $N = 5$ DME_2 program.

Our compilation relies upon a restricted set of gates that are readily characterized and numerically optimized. The final compiled circuit has a regular structure (each CZ is followed by exactly one layer of single-qubit gates), amenable to generic tuneup protocols for reducing coherent error buildup. These features enable it to achieve high algorithmic fidelity at significant circuit depth.

7.9 State and Process Tomography

Quantum state tomography is performed by taking advantage of independent single-shot readout of all four computational states $\{00, 01, 10, 11\}$. We first calibrate the measurement operators by building a matrix $\bar{\bar{\beta}}$ that maps the two-qubit Pauli matrices $\hat{\sigma}_{\mathbb{1}\mathbb{1}}, \hat{\sigma}_{\mathbb{1}Z}, \hat{\sigma}_{Z\mathbb{1}}$, and $\hat{\sigma}_{ZZ}$ onto the measurement probabilities p_{ij}

$$\vec{\mathrm{p}} = \bar{\bar{\beta}}\vec{\sigma} \tag{7.21}$$

Figure 7-16: Details of δSWAP and DME compilation. **Row 1:** The density matrix exponentiation algorithm implemented using partial SWAP operations and the simulated quantum measurement (QME) gate. **Row 2:** Decomposing each δSWAP according to Eq. (7.19). Each substep at this step requires 8 layers of gates (7 for δSWAP decomposition and 1 for QME). **Row 3:** The three layers of single-qubit gates stemming from the the end of the δSWAP of step n, followed by QME, and the first layer of single-qubit gates in δSWAP of step $n+1$ can be recompiled into a single layer. **Row 4:** The recompiled gates are reinserted into the algorithm result in the optimal structure of exactly one CZ gate, followed by a single layer of single-qubit gates. **Row 5:** Example waveform output to the I, Q (x, y) ports and the flux tuning pulse (labeled Φ) implementing the 'NetZero' waveform used to implement the CZ gate [293, 388]. [247]

where

$$\vec{\mathrm{p}} \equiv \begin{bmatrix} \mathrm{p}_{00} \\ \mathrm{p}_{01} \\ \mathrm{p}_{10} \\ \mathrm{p}_{11} \end{bmatrix} \quad \text{and} \quad \vec{\sigma} \equiv \begin{bmatrix} \hat{\sigma}_{\mathbb{1}\mathbb{1}} \\ \hat{\sigma}_{\mathbb{1}Z} \\ \hat{\sigma}_{Z\mathbb{1}} \\ \hat{\sigma}_{ZZ} \end{bmatrix} \tag{7.22}$$

The $\bar{\bar{\beta}}$ matrix is calibrated using techniques drawn from Ref. [93]; a full motivation and derivation of the technique can be found there. For a measurement of $\vec{\mathrm{p}}$ with perfect fidelity and no qubit decay during measurements, all components of $\bar{\bar{\beta}}$ have amplitude 0.25; deviations from this amplitude correspond to a calibration of such measurement errors. We begin by calibrating the single-qubit $\bar{\bar{\beta}}$ matrices namely,

$$\begin{bmatrix} \mathrm{p}_0 \\ \mathrm{p}_1 \end{bmatrix} = \begin{bmatrix} \beta_{\mathbb{1}}^0 & \beta_{\mathrm{Z}}^0 \\ \beta_{\mathbb{1}}^1 & \beta_{\mathrm{Z}}^1 \end{bmatrix} \begin{bmatrix} \hat{\sigma}_{\mathbb{1}} \\ \hat{\sigma}_Z \end{bmatrix} \tag{7.23}$$

by fitting Rabi oscillations in p_0 and p_1 for each qubit. Because the two-qubit probability vector $\vec{\mathrm{p}}$ is generated from correlations between single-qubit measurements, the two-qubit $\bar{\bar{\beta}}$ matrix is given by the tensor product of the single-qubit matrices, e.g., $\bar{\bar{\beta}} = \bar{\bar{\beta}}_1 \otimes \bar{\bar{\beta}}_2$.

An arbitrary 4×4 matrix, including a two-qubit density matrix ρ, may be mapped onto the Pauli basis according to

$$\rho = \sum_{i,j=\{\mathbb{1},X,Y,Z\}} c_{ij} \hat{\sigma}_{ij} \tag{7.24}$$

The general 4×4 matrix of this form has sixteen degrees of freedom; trace normalization of a physical density matrix reduces this to fifteen. The native readout gives us access to the components of ρ contained in $\hat{\sigma}_Z$. We gain information about the other components by performing one of nine pre-measurement rotations drawn from

$$\mathsf{R} = \mathsf{R}_1 \otimes \mathsf{R}_2 \tag{7.25}$$

where

$$\mathsf{R}_{1,2} = \begin{cases} \mathsf{R}_Y(-\frac{\pi}{2}) & \text{mapping} \quad \hat{\sigma}_X \mapsto \hat{\sigma}_Z \\ \mathsf{R}_X(\frac{\pi}{2}) & \text{mapping} \quad \hat{\sigma}_Y \mapsto \hat{\sigma}_Z \\ \mathbb{1} & \text{mapping} \quad \hat{\sigma}_Z \mapsto \hat{\sigma}_Z \end{cases} \tag{7.26}$$

For data in Figs. 7-6 and 7-7 (7-8 and 7-9) we perform 2000 (500) single-shot measurements for each tomographic rotation in order to ensure accurate estimates of $\vec{\mathrm{p}}$. Each of the nine rotation-and-measurement pairings provides four linearly independent measurements of a form similar to Eq. (7.21), for a total of thirty-six equations that over-specify fifteen degrees of freedom. We perform maximum-likelihood estimation [30] to derive the positive semi-definite Hermitian matrix that is most consistent with our combined measurement results.

Single-qubit density matrices in Figs. 7-6–7-8 are extracted by performing partial traces over the two-qubit density matrix calculated using the approach described above; the data in Fig. 7-9 are drawn from single-qubit tomography performed on the target qubit using a similar protocol.

Single-qubit quantum process tomography, as presented in Fig. 7-9, is performed using standard techniques [333]. The target qubit is sequentially prepared in four input states

$$\sigma_{\text{in}} = \{|0\rangle\langle 0|, |1\rangle\langle 1|, |+\rangle\langle +|, |i\rangle\langle i|\} \tag{7.27}$$

which span the single-qubit Hilbert space. These prepared states are then passed through the process $\mathsf{DME}_2(\rho_{\text{in}}, N, \theta)$ and single-qubit state tomography is performed to extract the set of mappings $\{\sigma_{\text{in}} \xmapsto{\mathsf{DME}_2(\rho_{\text{in}},N,\theta)} \sigma(N)\}$. Linear combinations of these mappings provide the process map χ that reveals the effect of the quantum channel on an arbitrary input density matrix. We then employ techniques developed in Ref. [252] to efficiently project χ onto the closest completely positive and trace-preserving (CPTP) mapping χ_{CPTP}, ensuring physicality of the process.

7.10 Bootstrap Error Analysis

We employ bootstrapping techniques to derive the uncertainty bounds in Figs. 7-8 and 7-9. In principle, one could simply take a sample of many QME randomizations and calculate the mean and uncertainty within that dataset. However, those error bars are not representative of the error in the DME_2 protocol—rather, they represent the uncertainty of a protocol in which only a single QME randomization is used to perform DME_2. As a result, these error bars are unphysically large, particularly at small N where the protocol chooses from one of only a few paths that have very different outcomes.

The true uncertainty of the DME_2 protocol is captured by: first, accumulating enough QME samples to ensure sufficient randomizations; then, building density/process matrices from the average outcome of all these randomizations; and finally, repeating this process many times with different randomizations to estimate the uncertainty. This is precisely what bootstrapping accomplishes [131].

The following describes the protocol for extracting boostrapped averages and uncertainties for Fig. 7-8. For each data point representing a unique setting of $\mathsf{DME}_2(\rho_{\text{in}}, N, \theta)$, we employ the following protocol:

1. For a given instantiation of the QME gates, execute $\mathsf{DME}_2(\rho_{\text{in}}, N, \theta)$ and perform two-qubit state tomography.

2. For r_{QME} different instantiations of QME gates, repeat step 1 to accumulate the experimental density matrices from which bootstrapped samples will be drawn.

3. Using sample-with-replacement, select n_{samp} samples from the r_{QME} datasets and average the density matrices together. This represents a single bootstrapped density matrix.

4. Perform a partial trace over the instruction qubit to extract the reduced density matrix of the target system.

5. Calculate the state fidelity to the states of interest, where fidelity is calculated as [470]

$$F_s(\sigma, \sigma') = \mathrm{Tr}\left(\sqrt{\sqrt{\sigma'}\sigma\sqrt{\sigma'}}\right)^2 \tag{7.28}$$

6. Repeat steps 3–5 a total of N_{samp} times to extract mean fidelities and 1σ uncertainties.

The bootstrapping protocol for generating process maps and process fidelities in Fig. 7-9 is similar to that used for state tomography, but we lay it out here explicitly for completeness.

1. For a given instantiation of the QME gates, prepare the target input states $\{\sigma_{\mathrm{in}}\}$, apply $\mathsf{DME}_2(\rho_{\mathrm{in}}, N, \theta)$, and perform single-qubit state tomography to generate the mappings $\{\sigma_{\mathrm{in}} \mapsto \sigma(N)\}$ required for process tomography.

2. For r_{QME} different instantiations of QME gates, repeat step 1 to produce a set of $4 \times r_{\mathsf{QME}}$ single-qubit density matrices.

3. For each of the four σ_{in}, select an independent sample-with-replacement of n_{samp} σ_{out} instances and average together, leaving four averaged mappings $\{\sigma_{\mathrm{in}} \mapsto \sigma_{\mathrm{out}}\}$.

4. Calculate the process matrix using the averaged mappings $\sigma_{\mathrm{in}} \mapsto \sigma(N)$. This represents a single bootstrapped process matrix.

5. Calculate the process fidelity to the process of interest, where the process fidelity between two χ-matrices is given by [332]

$$F_p(\chi, \chi') \;=\; \mathrm{Tr}\left(\sqrt{\sqrt{\chi'}\chi\sqrt{\chi'}}\right)^2 \tag{7.29}$$

6. Repeat steps 3–5 a total of N_{samp} times to extract mean fidelities and 1σ uncertainties.

In Fig. 7-8 we collect $r_{\mathsf{QME}} = 295$ circuit randomizations; in Fig. 7-9 we collect $r_{\mathsf{QME}} = 105$ circuit randomizations. In both cases we use $n_{\mathrm{samp}} = 100$ and $N_{\mathrm{samp}} = 50$.

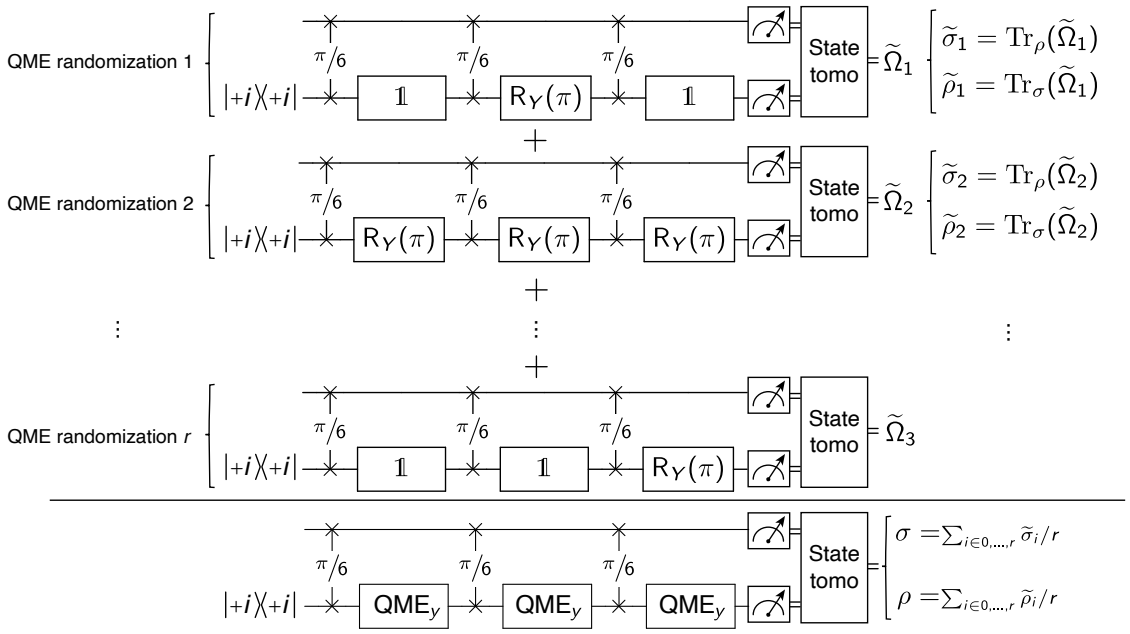

Figure 7-17: Schematic definition of experimental execution of a DME protocol using QME operations (i.e. DME_2). [247]

The number of QME randomizations used for process tomography was limited by experimental time due to the significant additional experimental overhead required for process tomography in comparison to state tomography, as well as the fact that in Fig. 7-9 we characterize processes for six settings of ρ. The bootstrap sample size n_{samp} and number of bootstrap samples N_{samp} are chosen somewhat arbitrarily, as in all bootstrapping implementations, but are designed to ensure that each bootstrapped sample approaches a central limit with respect to the underlying QME randomization. A graphical representation of the convergence under QME randomizations is shown in Fig. 7-18; more details are provided in Section 7.12.

7.11 Circuit Simulation with Noise

In order to show the qualitative consistency between the data in Fig. 7-8 and a model of coherence-limited implementation of the DME_2 protocol, we simulate the randomized DME_2 circuits with added decoherence. We input a DME_2 circuit generated by Cirq to a software tool that adds decoherence (amplitude damping and dephas-

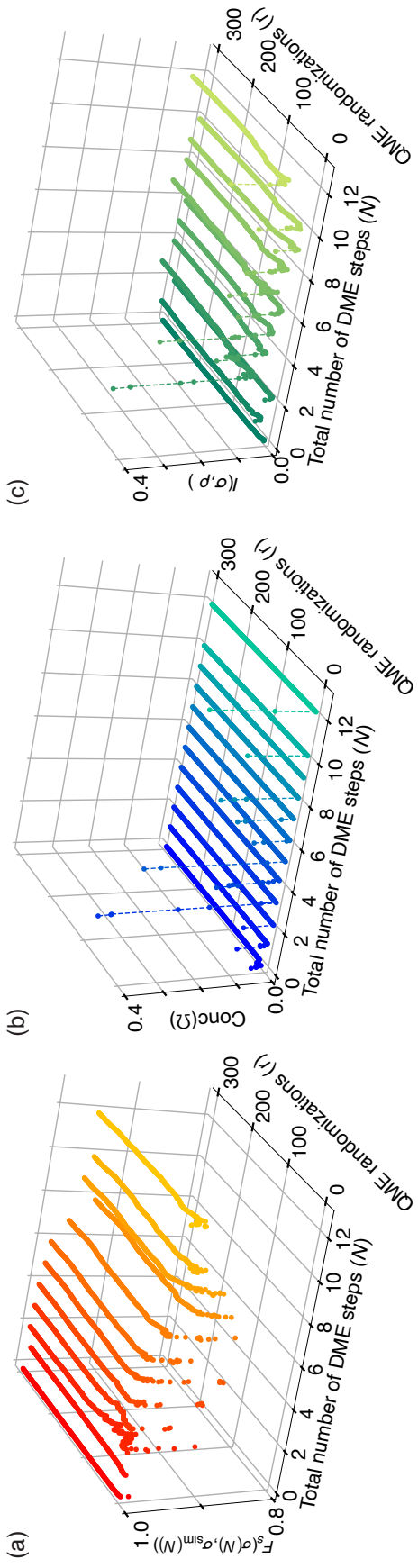

Figure 7-18: **(a)** The state fidelity between the measured output state and the result of ideal gates implementing DME, as the number of QME randomizations are increased, as defined in Fig. 7-17. **(b)** Concurrence in the two-qubit density matrix Ω (the combined state of the system), for increasing number of QME randomizations. **(c)** The mutual information between the two subsystems σ and ρ, as more randomizations of QME are used. [247]

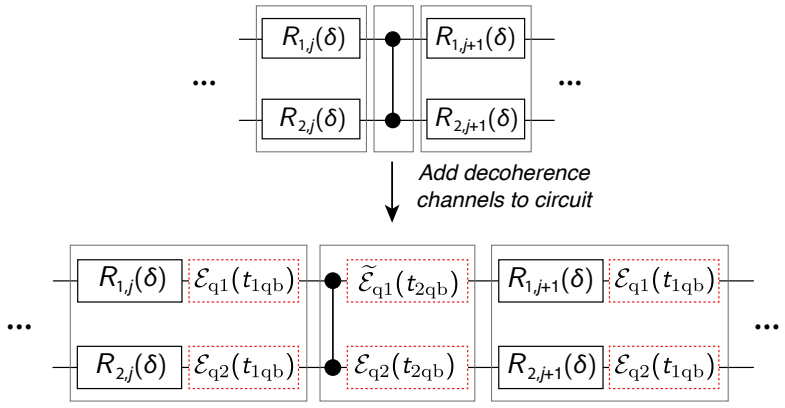

Figure 7-19: Instrumenting the DME_2 circuit for simulation of decoherence-induced errors. [247]

ing) channels corresponding to the identity for duration(s) of the preceding one- or two-qubit gate. An example of this procedure is shown in Fig. 7-19.

The channel $\mathcal{E}$ that composes amplitude damping and dephasing is given by

$$\mathcal{E}_{qk}(t_{1qb}) : \rho_{qk} \mapsto \sum_{\substack{i=1,2 \\ j=1,2,3}} A_{i,\Gamma_1}(t_{1qb}) D_{j,\Gamma_\phi}(t_{1qb}) \rho_{qk} D^\dagger_{j,\Gamma_\phi}(t_{1qb}) A^\dagger_{i,\Gamma_1}(t_{1qb}) \tag{7.30}$$

where $A_{i,\Gamma_1}(t)$ is the amplitude damping process (with $\Gamma_1 = 1/T_1$), and $D_{j,\Gamma_\phi}(t)$ is the dephasing process ($\Gamma_\phi = 1/T_{2R} - 1/2T_1$), $\Gamma_{1,qk}$ and $\Gamma_{\phi,qk}$ are the appropriate coherence parameters for qubit k, and t is the time of the preceding single- or two-qubit gate on that qubit. The amplitude damping and dephasing Krauss operators

are given by

$$A_{1,\Gamma_1}(t) = \begin{bmatrix} 1 & 0 \\ 0 & e^{-\Gamma_{1,\mathrm{q}k}t/2} \end{bmatrix} \tag{7.31}$$

$$A_{2,\Gamma_1}(t) = \begin{bmatrix} 0 & \sqrt{1-e^{-\Gamma_{1,\mathrm{q}k}t}} \\ 0 & 0 \end{bmatrix} \tag{7.32}$$

$$D_{1,\Gamma_\phi}(t) = \begin{bmatrix} e^{-\Gamma_{\phi,\mathrm{q}k}t/2} & 0 \\ 0 & e^{-\Gamma_{\phi,\mathrm{q}k}t/2} \end{bmatrix} \tag{7.33}$$

$$D_{2,\Gamma_\phi}(t) = \begin{bmatrix} \sqrt{1-e^{-\Gamma_{\phi,\mathrm{q}k}t}} & 0 \\ 0 & 0 \end{bmatrix} \tag{7.34}$$

$$D_{3,\Gamma_\phi}(t) = \begin{bmatrix} 0 & 0 \\ 0 & \sqrt{1-e^{-\Gamma_{\phi,\mathrm{q}k}t}} \end{bmatrix} \tag{7.35}$$

The channel $\widetilde{\mathcal{E}}$ is defined similarly to $\mathcal{E}$, but decoherence rates in the process definitions are replaced with their *effective* coherence parameters. The channel $\widetilde{\mathcal{E}}$ thus accounts for the modified coherence properties as qubit 1 undergoes the CZ trajectory (see Figs. 7-11 and 7-12).

Each instrumented circuit yields an QME-dependent density matrix representing the simulated finite-coherence circuit output for that QME realization. These density matrices are averaged over all 2^N QME realizations (for a DME_2 circuit with N steps), thus producing the noisy simulated two-qubit DME_2 output state, denoted 'Sim. $F_s(\sigma, \sigma_{\mathrm{ideal}})$ with decoherence' and plotted as a solid line in Fig. 7-8b.

For the simulations presented, we used parameters $T_1 = 20$ μs, $T_{2\mathrm{R}} = 10$ μs for both qubits, and effective coherence times for qubit 1 of $\widetilde{T}_1 = 10$ μs and $\widetilde{T}_{2\mathrm{R}} = 5$ μs during the channel $\widetilde{\mathcal{E}}$. These parameters are qualitatively consistent with, but overall reduced from, the measured parameters in Table 7.1. This difference may indicate additional coherent errors not captured by this model (e.g., from residual ZZ-interaction or leakage out of the computational subspace).

7.12 Algorithmic Error in DME_N

In this section we show that the algorithmic error in $\mathsf{DME}_N(\rho, N, \theta)$ (the version of DME in which the instruction state is refreshed with a new, perfect copy after each Trotter step) may be modeled as an amplitude damping channel and derive its scaling with the parameters of the algorithm. We do so first for a specific instruction state and then generalize to an arbitrary instruction. Throughout, we use $\hat{\sigma}_i$ to indicate the corresponding Pauli matrix.

Suppose that we have instruction and target qubits initially in states ρ and σ, respectively, and apply the operation $e^{-i\mathsf{SWAP}\delta}$ to the joint state $\rho \otimes \sigma$. We will first consider the special case in which $\rho = |0\rangle\langle 0|$ and then show how this generalizes to an arbitrary state. The effect of the $\delta\mathsf{SWAP}$ on the target qubit is given by the quantum channel

$$\mathcal{E}^{\rho=|0\rangle\langle 0|}_{\delta\mathsf{SWAP}}(\sigma) = \mathrm{Tr}_\rho\left(e^{-i\mathsf{SWAP}\delta}\Big[\sigma \otimes |0\rangle\langle 0|\Big]e^{i\mathsf{SWAP}\delta}\right) \tag{7.36}$$

Next, we use the fact that

$$e^{i\mathsf{SWAP}\delta} = \cos(\delta)\hat{\sigma}_{\mathbb{1}\mathbb{1}} + i\sin(\delta)\mathsf{SWAP} \tag{7.37}$$

which follows from the fact that $\mathsf{SWAP}^2 = \hat{\sigma}_{\mathbb{1}\mathbb{1}}$ where $\hat{\sigma}_{\mathbb{1}\mathbb{1}}$ is the two-qubit identity matrix. Using this together with the identity $\mathrm{Tr}_\rho\left(\mathsf{SWAP}(X \otimes Y)\right) = YX$ (where Tr_ρ is a partial trace over the second subsystem), we find

$$\mathcal{E}^{\rho=|0\rangle\langle 0|}_{\delta\mathsf{SWAP}}(\sigma) = \cos^2(\delta)\sigma + i\cos(\delta)\sin(\delta)[\sigma, |0\rangle\langle 0|] + \sin^2(\delta)\,|0\rangle\langle 0| \tag{7.38}$$

Using the matrix representation of σ in the $\{|0\rangle, |1\rangle\}$ basis, we find that σ transforms as

$$\begin{bmatrix} \sigma'_{00} & \sigma'_{01} \\ \sigma'_{10} & \sigma'_{11} \end{bmatrix} = \begin{bmatrix} \sigma_{00} + \sigma_{11}\sin^2(\delta) & \cos\delta e^{-i\delta}\sigma_{01} \\ \cos\delta e^{+i\delta}\sigma_{10} & \sigma_{11}\cos^2(\delta) \end{bmatrix} \tag{7.39}$$

where $\sigma_{ij} = \langle i|\sigma|j\rangle$ as measured in the $\{|0\rangle, |1\rangle\}$ basis. The channel that implements this transformation has a simple interpretation as the composition of a rotation and

an amplitude decay.

Let

$$\mathcal{U}_\delta^{\rho=|0\rangle\langle 0|}(\cdot) = e^{-i\delta|0\rangle\langle 0|}(\cdot)e^{i\delta|0\rangle\langle 0|} = e^{-i\frac{\delta}{2}\hat{\sigma}_Z}(\cdot)e^{+i\frac{\delta}{2}\hat{\sigma}_Z} \tag{7.40}$$

be the superoperator corresponding to the unitary $e^{-i\delta|0\rangle\langle 0|}$, or equivalently, the superoperator corresponding to the rotation by angle δ around the z-axis. Also, let $\mathcal{A}_p$ be the amplitude damping channel described by the Kraus decomposition

$$\mathcal{A}_p(\sigma) = A_1\sigma A_1^\dagger + A_2\sigma A_2^\dagger \tag{7.41}$$

where

$$A_1 = \begin{bmatrix} 1 & 0 \\ 0 & \sqrt{1-p} \end{bmatrix} \quad , \quad A_2 = \begin{bmatrix} 0 & \sqrt{p} \\ 0 & 0 \end{bmatrix}. \tag{7.42}$$

This amplitude damping channel describes the process in which the system in state $|1\rangle$ decays to state $|0\rangle$ with probability p. It can be shown that the amplitude damping channel satisfies the condition

$$\mathcal{A}_p \circ \mathcal{U}_\delta = \mathcal{U}_\delta \circ \mathcal{A}_p \tag{7.43}$$

for all $\theta \in [0, 2\pi)$. This equality implies that the action of this channel is invariant under rotations around z axis.

Then, using Eq. (7.39) one can show that

$$\mathcal{E}_{\delta\mathsf{SWAP}}^{\rho=|0\rangle\langle 0|}(\sigma) = \mathcal{A}_{\sin^2(\delta)} \circ \mathcal{U}_\delta(\sigma) = \mathcal{U}_\delta \circ \mathcal{A}_{\sin^2(\delta)}(\sigma). \tag{7.44}$$

The overall effect of one Trotter step of DME_N can therefore be understood as the following: (i) applying the unitary $e^{-i\delta|0\rangle\langle 0|}$ to the system σ, followed by (ii) applying the amplitude damping channel $\mathcal{A}_{\sin^2\delta}$ to the system σ. Note that because of the condition in Eq. (7.43), by flipping the order of steps (i) and (ii) we get exactly the same final state.

Now suppose we repeat the above operation N times. That is we prepare the instruction qubit in state $\rho = |0\rangle\langle 0|$, couple it to σ via the unitary $e^{-i\mathsf{SWAP}\delta}$, then

discard the instruction qubit and prepare it again in state $|0\rangle\langle 0|$, repeating the above procedure with N different copies of ρ. Then, using Eq. (7.43) one can show that, given an initial state σ, the final state of the target system will be

$$\left[\mathcal{E}_{\delta\mathsf{SWAP}}^{\rho=|0\rangle\langle 0|}\right]^N(\sigma) = \left[\mathcal{A}_{\sin^2(\delta)} \circ \mathcal{U}_\delta\right]^N(\sigma) = \mathcal{A}_{\sin^2(\delta)}^N \circ \mathcal{U}_{N\delta}(\sigma). \tag{7.45}$$

Since amplitude damping channels are closed under composition, we see that

$$\mathcal{A}_{\sin^2(\delta)}^N = \mathcal{A}_{1-\cos^{2N}(\delta)}. \tag{7.46}$$

Therefore, the overall effect on the target system is equivalent to applying the perfect unitary $e^{-iN\delta|0\rangle\langle 0|}$ and then applying the amplitude damping channel $\mathcal{A}_{1-\cos^{2N}(\delta)}$.

Now, suppose that in the above procedure, instead of preparing the state $|0\rangle\langle 0|$ we prepare the instruction qubit in state $|\phi\rangle\langle\phi| = V|0\rangle\langle 0|V^\dagger$, where V is an arbitrary unitary. Then, using the fact that $\mathsf{SWAP}(V \otimes V') = (V' \otimes V)\mathsf{SWAP}$, one can show that the overall effect of this transformation on the target system can be described as a unitary rotation $e^{-iN\delta|\phi\rangle\langle\phi|}$ followed by an amplitude damping channel in the basis defined by state $|\phi\rangle$ and its orthogonal state.

To translate explicitly to the language earlier in this chapter, let $\delta = \theta/N$ and $\rho = |\phi\rangle\langle\phi|$, and use the above procedure to implement the unitary $e^{-i\rho\theta}$ on the target system σ, using N copies of the instruction state ρ. From Eq. (7.46) we find that the overall error in this procedure is determined by the probability $p_N = 1 - \cos^{2N}(\delta)$. Then, for $\delta \in (0, 2\pi]$ and $N \gg 1$ we have

$$p_N = 1 - \cos^{2N}\left(\frac{\theta}{N}\right) \approx 1 - e^{-\frac{\theta^2}{N}} \approx \frac{\theta^2}{N}, \quad \text{for large } N. \tag{7.47}$$

In the limit of large N, this corresponds to an algorithmic error for the DME_N algorithm of $\mathcal{O}(\theta^2/N)$.

7.13 Algorithmic Error Due to QME

Here we provide an intuitive picture for the quantum measurement emulation (QME) operation as well as a formal proof of the modified algorithmic error bound in Eq. (7.6).

We will build the intuition for this section by returning to the concrete example from Section 7.12, i.e., the instruction qubit prepared in $\rho = |0\rangle\langle 0|$. We will also suppose that the target qubit is prepared in an orthogonal state, say, $\sigma = |+i\rangle\langle +i|$ (which is an eigenstate of the Pauli matrix $\hat{\sigma}_Y$). Since δSWAP is a symmetric operation by the logic in Section 7.12 the state of ρ following a small δSWAP interaction is given by a rotation about the y-axis followed by an amplitude damping channel (which we will neglect for the moment). In this case, the state of the instruction qubit becomes

$$\rho' = \begin{bmatrix} \cos^2(\delta) & -\cos(\delta)\sin(\delta) \\ -\cos(\delta)\sin(\delta) & \sin^2(\delta) \end{bmatrix}. \tag{7.48}$$

The trace distance between ρ and ρ' is of order $|\delta|$. However, if we measure and forget the state of the instruction qubit in the basis of its original polarization (i.e., the z-basis), the coherent off-diagonal components of the density matrix are dephased and we are left with

$$\rho'' = \begin{bmatrix} \cos^2(\delta) & 0 \\ 0 & \sin^2(\delta) \end{bmatrix}. \tag{7.49}$$

The trace distance between ρ'' and ρ is of order δ^2. Because DME operates in the $\delta \ll 1$ regime, we have $\delta^2 \ll \delta$. Measuring and forgetting therefore leaves the instruction qubit in a slightly perturbed state that is closer to that of the initial state ρ.

The intuition developed for $\rho = |0\rangle\langle 0|$ extends naturally to an arbitrary initial state $\rho = |\nu_\parallel\rangle\langle\nu_\parallel|$, in a basis defined by $\nu = \{|\nu_\parallel\rangle, |\nu_\perp\rangle\}$. A small arbitrary rotation will result in the state

$$\rho' = \cos^2(\beta)\,|\nu_\parallel\rangle\langle\nu_\parallel| + \sin^2(\beta)\,|\nu_\perp\rangle\langle\nu_\perp| + \cos(\beta)\sin(\beta)\left(e^{i\phi}\,|\nu_\parallel\rangle\langle\nu_\perp| + e^{-i\phi}\,|\nu_\perp\rangle\langle\nu_\parallel|\right), \tag{7.50}$$

where β and ϕ generically paramterize the rotation. A measurement in the basis ν

dephases the off-diagonal elements in this basis, leaving

$$\rho'' = \cos^2(\beta) \left|\nu_\parallel\right\rangle\!\left\langle\nu_\parallel\right| + \sin^2(\beta) \left|\nu_\perp\right\rangle\!\left\langle\nu_\perp\right|, \tag{7.51}$$

which is closer than ρ' to ρ by a factor of $|\beta|$.

Performing a physical measurement along an arbitrary axis ν generically would require (i) rotating ν onto the z-axis, (ii) performing a projective readout, and $iii)$ rotating back to the original axis. All of these steps require finite clock time: single-qubit gates typically require tens of nanoseconds to complete, with measurements requiring hundred of nanoseconds to perform. We would like to avoid this significant experimental overhead while still maintaining the ability to partially restore the instruction qubit to its initial state. Instead of physically performing the measurement, we can apply the unitaries $\{\hat{\sigma}_\mathbb{1}, \hat{\sigma}_\nu\}$ with equal probabilities, where $\hat{\sigma}_\nu = \hat{n}_\parallel \cdot (\hat{\sigma}_X, \hat{\sigma}_Y, \hat{\sigma}_Z)$ and $\hat{n}_\parallel$ is a unit vector parallel to ρ. Such protocols may be equivalently thought of as an approach to turning a coherent error into an incoherent error along a known axis. This protocol is the quantum measurement emulation (QME) operation.

When averaged over many iterations, the randomized QME operation dephases the system in the ν basis, just as in Eq. (7.50)–(7.51). Assuming the instruction qubit is initially in state ρ', it turns out that the resulting state is the same for measurement and random gate application, i.e.,

$$\frac{\left|\nu_\parallel\right\rangle\!\left\langle\nu_\parallel\right| \rho' \left|\nu_\parallel\right\rangle\!\left\langle\nu_\parallel\right| + \left|\nu_\perp\right\rangle\!\left\langle\nu_\perp\right| \rho' \left|\nu_\perp\right\rangle\!\left\langle\nu_\perp\right|}{2} = \frac{\hat{\sigma}_\mathbb{1}\rho'\hat{\sigma}_\mathbb{1} + \hat{\sigma}_\nu\rho'\hat{\sigma}_\nu}{2} = \frac{1}{2\pi}\int_0^{2\pi} d\gamma\, e^{-i\gamma\hat{\sigma}_\nu}\rho' e^{i\gamma\hat{\sigma}_\nu}\,. \tag{7.52}$$

These three terms represent respectively measuring and forgetting, random gate application, and phase randomization. Their equivalence can be understood more formally from the standpoint of the stochastic master equation, to which Ref. [218] provides an accessible introduction. This approach is also related to the Quantum Zeno Effect, in which persistent measurement along an axis of interest "pins" the qubit state to that axis by continuously dephasing any rotations away from it [216].

Finally, we calculate the additional error introduced to the DME algorithm by the

use of QME. For this, we return to the specific case where $\rho = |0\rangle\langle 0|$ (though this also generalizes to arbitrary ρ). As in Section 7.12, we apply the unitary $e^{-i\mathsf{SWAP}\delta}$ to the joint state $\sigma \otimes |0\rangle\langle 0|$ and then randomly apply one of the unitaries $\{\hat{\sigma}_{\mathbb{1}}, \hat{\sigma}_Z\}$ to the instruction qubit. Then, it can be shown that the total state of instruction and target qubit is given by

$$\begin{aligned}&\frac{1}{2}\Big(e^{-i\mathsf{SWAP}\delta}\Big[\sigma \otimes |0\rangle\langle 0|\Big]e^{i\mathsf{SWAP}\delta} + (\hat{\sigma}_{\mathbb{1}} \otimes \hat{\sigma}_Z)e^{-i\mathsf{SWAP}\delta}\Big[\sigma \otimes |0\rangle\langle 0|\Big]e^{i\mathsf{SWAP}\delta}(\hat{\sigma}_{\mathbb{1}} \otimes \hat{\sigma}_Z)\Big)\\ &= \underbrace{\mathcal{E}^{\rho=|0\rangle\langle 0|}_{\delta\mathsf{SWAP}}(\sigma) \otimes |0\rangle\langle 0|}_{\mathsf{DME}} - \underbrace{\sin^2(\delta)\,\langle 1|\sigma|1\rangle\,\Big[\,|0\rangle\langle 0| \otimes \hat{\sigma}_Z\Big]}_{\mathsf{QME\ error}}\,,\end{aligned} \tag{7.53}$$

where $\mathcal{E}^{\rho=|0\rangle\langle 0|}_{\delta\mathsf{SWAP}}(\sigma)$ is the quantum channel defined in Eq. (7.44). Note that the first term, $\mathcal{E}^{\rho=|0\rangle\langle 0|}_{\delta\mathsf{SWAP}}(\sigma) \otimes |0\rangle\langle 0|$ is exactly the desired state which can be used for the next round of DME. On the other hand, the second term $\sin^2(\delta)\,\langle 1|\sigma|1\rangle\,\Big[\,|0\rangle\langle 0| \otimes \hat{\sigma}_Z\,\Big]$ can be treated as an error. To find the contribution of this term in the total error, we use the fact that the trace-norm is nonincreasing under any trace-preserving quantum operation $\mathcal{F}$: $\|\mathcal{F}(X)\|_{\mathrm{tr}} \leq \|X\|_{\mathrm{tr}}$, where $\|\cdot\|_{\mathrm{tr}}$ is trace norm, i.e., sum of the absolute value of the eigenvalues of the operator.

For the second term in Eq. (7.53) we have

$$\Big\|\sin^2(\delta)\,\langle 1|\sigma|1\rangle\,\Big[\,|0\rangle\langle 0| \otimes \hat{\sigma}_Z\Big]\Big\|_{\mathrm{tr}} = 2\sin^2(\delta)\,\langle 1|\sigma|1\rangle \leq 2\sin^2(\delta). \tag{7.54}$$

Therefore, the additional error introduced by each application of QME is bounded by $2\sin^2(\delta)$.

Repeating this process N times, and using the triangle inequality for the trace norm, we find that the distance between the final total system state and the state produced by DME is bounded by $2N\sin^2(\delta)$. Choosing $\delta = \theta/N$, we find that the overall additional error introduced by the use of QME is bounded by

$$2N\sin^2(\delta) = 2N\sin^2\left(\frac{\theta}{N}\right) \leq \frac{2\theta^2}{N}\,. \tag{7.55}$$

The right hand side of Eq. (7.55) is the QME-induced error contribution.

7.14 Quantifying the Impact of Finite QME Randomizations

To properly implement the probabilistic nature of the QME operation we instantiate each DME_2 circuit a number of times. Consider as an example the $N = 3$ version of the DME_2 circuit from Fig. 7-8

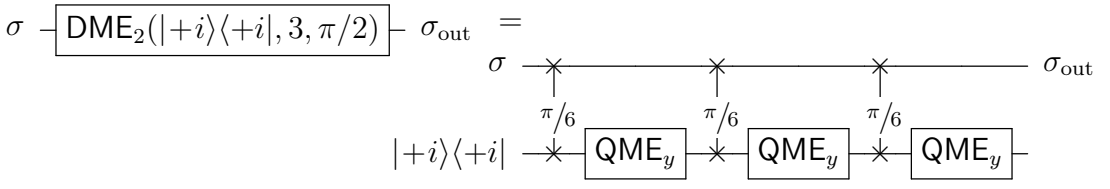

(7.56)

In this case, each QME presents a random choice between applying $\mathsf{R}_Y(\pi)$ or $\mathbb{1}$ at each occurence. For an N-step DME_2, there are 2^N configurations of QME gates. In the experiment it is infeasible to sample all 2^N realizations, so instead we sample a smaller number, denoted r. The circuits below show $r = 3$ random example realizations of the circuit:

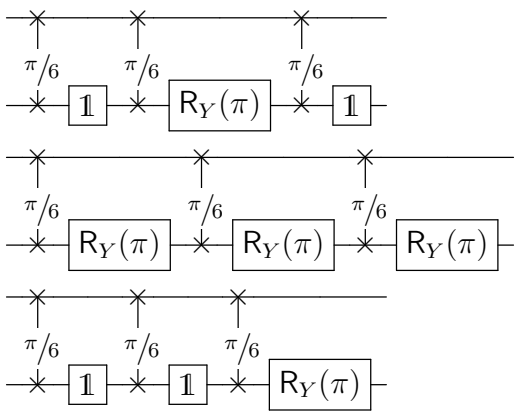

(7.57)

(7.58)

(7.59)

In the experiment, a total of r_{QME} of circuits are executed, providing a sample from which we can extract average properties. The generic process for extracting average properties over r instantiations is sketched in Fig. 7-17.

From the datasets obtained in our experiment, we can also explore algorithmic behavior as the randomizations of QME increase toward the central limit. In Fig. 7-18 we plot three relevant figures of merit as a function of r and N for the $\theta = \pi$ dataset of Fig. 7-8. Figure 7-18a shows the evolution of the state fidelity of the output state as a function of r. For all values of N we observe that after approximately $\sim$50 randomizations, the effect of introducing more circuits with random choices of QME gates does not significantly alter the result. Figure 7-18b shows the concurrence of the two-qubit density matrix, a measurement of bipartite entanglement in the system [474]. After just a few randomizations $r > 10$, concurrence goes to zero, indicating that (quantum) correlations have been suppressed, as expected. There may also be classical correlations between the σ and ρ subsystems. Figure 7-18c we therefore plot the mutual information $I(\sigma, \rho)$ between each subsystem, where

$$I_\Omega(\sigma, \rho) = S(\mathrm{Tr}_\sigma(\Omega)) + S(\mathrm{Tr}_\rho(\Omega)) - S(\Omega) \tag{7.60}$$

is the mutual information and $S(\Omega) = -\mathrm{Tr}\,(\Omega \ln \Omega)$ is the von Neumann entropy of the density matrix Ω. Here we again observe that after $r > 10$ any correlations between the subsystems are effectively removed.

7.15 Outlook

By executing a quantum program whose instructions are stored in a quantum state, we have established the first experimental approach to instilling homoiconicity in quantum computing. The DME_2 algorithm used here to generate quantum instructions takes advantage of a 99.7% fidelity controlled-phase gate combined with a novel simulated quantum measurement technique. We achieve output state fidelities exceeding 0.9 even at circuit depth of 73 sequential gates and process fidelities close to 0.9 independent of the instruction setting.

Our realization of quantum instructions represents a new approach to quantum computer programming. It uses a fixed set of classical pulses that serve as a program

"scaffolding" and an auxiliary quantum state to encode the program instructions. Intuitively, since the classical scaffolding is always the same, it must be the quantum states that uniquely determine the quantum instructions. While we used pure states to form the quantum instructions in DME_2, the general DME algorithm generalizes to mixed states and efficiently extends to multi-qubit systems, requiring only the ability to perform controlled versions of the SWAP operation between pairs of target and instruction qubits [155, 242, 294, 354]. Because it bypasses costly and unscalable tomography and recompilation requirements, DME and related algorithms enable exponential speedup for a range of applications spanning quantum state metrology [281], guaranteed private quantum software [294], efficient measurement of large-scale entangled quantum systems [354], and quantum machine learning [51].

Part IV

Quantum Characterization

Chapter 8

Characterizing Quantum Processors

In Part II of this thesis, we reviewed the mathematical formalism for describing the evolution of single- and multi-qubit systems under the influence of a general Hamiltonian operator and the Schrödinger equation. This picture, in which qubits evolve along the surfaces of their respective Bloch spheres and entangle with one another to form large and correlated nonclassical states, was then leveraged in Part III to construct quantum algorithms composed of discrete single- and two-qubit logical gates. However, as we also saw in Part III, the formalism of unitary operators and coherent evolution fails to capture many errors which arise in quantum processors, and this model quickly breaks down when we try to run algorithms on physical quantum hardware.

This breakdown, of course, is not indicative of any fundamental flaw in quantum mechanics. To the best of our knowledge, the Schrödinger equation provides a complete description of quantum mechanics at all scales of matter. This suggests that, if we were able to write down the wavefunction of the entire universe at a particular moment in time and the Hamiltonian capturing all the forces at play between each constituent quantum bit across all of space, we could perfectly describe the quantum

The seven categories of QCVV outlined in this chapter, as well as many of the references associated with each category, are based on correspondences with Dr. Robin Blume-Kohout, and I gratefully acknowledge his generous contributions to the structure and framing of this chapter.

mechanical state of the universe at any future moment. The problem, of course, is that we *cannot* write down either of these mathematical objects: the exponential scaling of quantum mechanics forbids this, rendering a complete classical description of even the most modest wavefunctions absolutely intractable.

So too with our quantum bits in the laboratory. If we could provide a full quantum mechanical description of the entirety of our laboratory apparatus—of the superconducting circuits which encode our quantum bits, of the aluminum film and silicon substrate they are fabricated out of, of the dilution refrigerator and microwave electronics which house and probe them, of the humans who toil in the laboratory and measure them—we would find that there are no errors, so to speak, just quantum information coherently sloshing around throughout the entirety of the device, generating entanglement across all scales of matter. This, of course, hardly makes for a useful computer. If we want to engineer programmable and controllable quantum systems, we need to establish some sense of order, erect firm borders around our qubits so that the information they encode stays exactly where we want it, moves exactly how we want it. We need, in other words, to impose our mathematical abstraction upon physical reality and assure ourselves that the two line up. And when they fail to do so, we need robust metrics for determining the degree of mismatch and the severity of the ensuing errors.

In this chapter, we will discuss a number of different techniques and formalisms for articulating what is going on at the interface between mathematical abstraction and physical reality. Together, this body of research is typically known as Quantum Characterization, Verification, and Validation—QCVV for short. Starting from the premise that complete classical knowledge of a large quantum mechanical system is impossible, these techniques can be understood as different attempts to simplify the problem, to take an intelligent cut through Hilbert space which tells us something interesting, albeit partial, about the full quantum mechanical system. In this pursuit, we quickly find that there are no absolute, final answers—only variously interesting, well-posed, and complementary questions. Looking back over four decades of research, we find that these techniques roughly break down into seven distinct archetypes, each

of which focuses on a different *type of question* we might ask our quantum processor.

8.1 Ad Hoc Methods: Rabi, Ramsey, T_1, T_2

This category is the oldest of the seven, and many of the techniques included here trace their lineage to long before the advent of quantum computing. Here, we are interested in measuring physical properties our systems which correspond to familiar physical units, such as time or frequency. These techniques, while still widely in use as rough heuristics to validate the prospective performance of quantum bits, largely fall in the domain of physics experiments rather than that of computational benchmarks. As such, they are often best deployed in systems which are still too experimental to be considered useful quantum bits. Examples of commonly used ad hoc methods include:

Rabi oscillation: A continuous drive is applied to the quantum system, resonant with the transition frequency between two energy eigenstates of the system. Sweeping either the duration or amplitude of the drive, the system coherently rotates along the median of its Bloch sphere, coherently oscillating back and forth between the poles $|0\rangle$ and $|1\rangle$. Measuring the probability of the state being in either $|0\rangle$ or $|1\rangle$ at discrete values of the drive duration (or drive power), the system will trace out a sinusoid corresponding to the projection of the oscillation onto the z-axis of the Bloch sphere, as we showed in Eq. 3.37. The successful demonstration of coherent Rabi oscillations is often one of the first tests to verify if a new hardware modality can be operated as a quantum bit, and Rabi measurements are commonly used to calibrate the pulse power and duration required to perform a single π-pulse.

T_1 **measurement:** A single π-pulse is applied to the system—coherently rotating it from the ground state $|0\rangle$ to the excited state $|1\rangle$—and a variable time delay is swept prior to measuring the system. When we measure the system at discrete times, the probability of measuring the system in $|1\rangle$ will exponentially decay as

a function of the time delay, corresponding to the qubit spontaneously losing an excitation to its environment, decaying through the center of the Bloch sphere from one pole to the other. The characteristic $1/e$ time of this decay is known as the T_1 time, which provides a rough heuristic for the timescale in which the qubit will randomly experience a bit flip.

Ramsey oscillation: A $\pi/2$-pulse coherently rotates the system from the ground state $|0\rangle$ to the equator of the Bloch sphere; after a variable delay time, a second $\pi/2$-pulse is applied and the system is immediately measured. Depending on the detuning between the drive signal and the qubit frequency, the system will precess along the equator of the Bloch sphere during the variable time delay, changing which state the system is rotated into after the second $\pi/2$-pulse. Measuring the state of the system as a function of the variable time delay, the system will trace out a sinusoid whose frequency is equal to the detuning between the qubit frequency and drive. Ramsey measurements are commonly used to verify successful preparation of coherent superposition states, and Ramsey interferometry—where the drive frequency is adjusted until the frequency of oscillation goes to zero—is a powerful tool for precisely measuring the qubit frequency.

T_2, Echo, and CPMG measurements: Performing a Ramsey measurement on a physical quantum system, the oscillation will be bounded by an exponentially decaying envelope which corresponds to the qubit spiralling into the center of the Bloch sphere as it gradually decoheres. The characteristic $1/e$ time of this decay is known as the T_2 time (or, in some works, the T_2^* or T_2^{Ramsey} times), which provides a rough heuristic for the timescale in which the qubit will randomly lose phase information to the environment. The Ramsey sequence can also be modified by applying one or more *pi*-pulses in the middle of the time delay (known as a *Hahn echo sequence* in the case of $n = 1$ π-pulses, or a *CPMG sequence* in the case of $n > 1$); by increasing the number of *pi*-pulses during the evolution, the sequence intrinsically refocuses and filters out lower-frequency

noise, allowing detailed characterization of the qubit's sensitivity to different frequency components of the noise environment.

8.2 Quantum Tricks

Techniques in this category attempt to demonstrate that a processor can do something distinctly 'quantum': something which would distinguish it, unambiguously, from a classical computer. This category is founded on the belief that the defining characteristic of a quantum processor is its degree of 'quantum-ness,' whether or not that behavior has any bearing on the performance of an actual computation. This category includes protocols for efficiently demonstrating and quantifying quantum entanglement [135, 172, 205, 311, 459], coherence and purity [275, 286], or state teleportation [40]. Unlike the tomographic protocols discussed in detail below, these techniques emphasize efficiently over completeness, attempting to extract a single number (such as concurrence or purity) instead of a complete description of the entire quantum mechanical state. While these techniques offer useful methods for studying the behavior of controllable quantum systems at scale, like the ad hoc methods above, they largely fall in the domain of physics experiments rather than that of computational benchmarks.

8.3 State Tomography and Its Applications

As we saw in Chapter 2, the two most distinctive features of quantum mechanics—coherent superposition of orthogonal classical states and entanglement between systems—emerge as natural consequences of the variety of quantum mechanical states which arise from evolution under the Schrödinger equation. Taking this key insight as a starting point, techniques in this category attempt to measure and reconstruct the quantum states which are created on a quantum processor, proving that the processor managed to create something distinctly quantum mechanical and providing tools for quantifying the processor's success in producing a desired state.

Recall that a general quantum mechanical state ρ is not directly measurable: if we perform a single measurement of the state, it will randomly collapse into either the $+1$ or -1 eigenstate of our measurement basis, producing a single classical bit of information. How then do we distinguish between all the possible states of the Bloch sphere?

Here, the foundational technique is *quantum state tomography* [5, 92, 150, 178, 207, 220, 322, 394, 452, 462, 464, 487]. As we showed in Chapter 2 in our derivation of the Bloch sphere picture, the single-qubit Pauli matrices form a orthonormal basis for describing any general single-qubit state ρ. As such, we can expand the matrix ρ into a sum of Pauli matrices, weighted by the expectation value of the state with each Pauli operator

$$\rho = \frac{\mathrm{Tr}[\hat{I}\rho]\hat{I} + \mathrm{Tr}[\hat{X}\rho]\hat{X} + \mathrm{Tr}[\hat{Y}\rho]\hat{Y} + \mathrm{Tr}[\hat{Z}\rho]\hat{Z}}{2} \tag{8.1}$$

where the expectation value $\mathrm{Tr}[\hat{I}\rho]$ is unity for all physical density matrices, by conservation of probability. As for the other three expectation values, in the Bloch sphere picture, these can be thought of as the projections of the point $\rho(x, y, z)$ onto each of the three orthogonal axes. The goal of state tomography is to piece together these projections, reconstructing Hilbert space from an orthogonal set of slices (*tomos* in ancient Greek, from which *tomography* takes its name).

While the state ρ cannot be directly measured, its shadows along the three axes of the Bloch sphere can. Recall that the expectation value $\mathrm{Tr}[\hat{A}\rho]$ is interpreted as the average value of the observable $\hat{A}$: while a single measurement of $\hat{A}$ will collapse the state into a discrete outcome $+1$ or -1, the average of many measurements of $\hat{A}$ will converge to the true expectation value. As such, all we need to do is perform many measurements of the state ρ along each of the three Pauli axes, take the average outcome of each, and plug the resulting values into Eq. (8.1) to reconstruct the full matrix representation of the state ρ.

In most hardware modalities, experimentalists do not have direct access to measurement along arbitrary axes of the Bloch sphere, only to measurement along the

fixed axis which defines the qubit bases ($\hat{Z}$ by convention). Thus, rather than measure the expectation values $\mathrm{Tr}[\hat{X}\rho]$ and $\mathrm{Tr}[\hat{X}\rho]$ directly, a $\pi/2$-pulse around either $\hat{Y}$ or $\hat{X}$ is applied to the qubit prior to measurement, rotating the Bloch sphere such that the effective measurement axis is either $\hat{X}$ or $\hat{Y}$ respectively.

While state tomography provides an elegant protocol for completely reconstructing the density matrix of an unknown state ρ, the completeness of this reconstruction comes at an exponential price: for a general n-qubit state, the number of axes along which the state must be measured scales as 3^n in order to capture all the products of Pauli components required to construct a general multi-qubit density matrix (as we saw earlier in Section 2.6). Nonetheless, state tomography has become a ubiquitous technique for characterizing and verifying the states produced on small quantum processors, and a number of variants have emerged which attempt to approximately reconstruct quantum states more efficiently than brute force tomography of the full Hilbert space [4, 67, 107, 140, 171, 266, 272, 413, 437].

8.4 Process Tomography and Its Variants

This category of techniques is intimately related to state tomography, but it substantially reframes the question. Instead of aiming to characterize the interesting quantum mechanical states created on a quantum processor, these techniques seek to characterize the *processes* which created those interesting states in the first place. In some sense, this question goes deeper than the one posed by state tomography: while the set of possible states give us a window into the unusual phenomena of quantum mechanics, these states are ultimately just consequences of the action of quantum *operators*—unitary operators in the case of discrete gates; Hamiltonians in the case of general dynamics. As we saw in Part III, these operators are the building block of quantum algorithms; if quantum states are the data at the input and output of an algorithm, quantum processes are the algorithm itself. Thus, if we want to characterize the action of a quantum algorithm, regardless of the data we feed it, we need to understand the structure of the operators modifying the state of the system during

the computation.

Here, the foundational technique is *quantum process tomography* [94, 96, 144, 209, 239, 244, 282, 335, 357, 402, 433, 466]. Like state tomography, process tomography pieces together slices through Hilbert space to reassemble an unknown matrix of interest. However, whereas state tomography pieces together an unknown $2^n \times 2^n$ density matrix, process tomography pieces together an unknown *process matrix*. In the case of unitary dynamics, this matrix will be equivalent to the $2^n \times 2^n$ unitary rotation matrices we studied in Chapter 2. In most practical cases, however, the unitary representation at least partially breaks down, and we require a more flexible—and indeed more expensive—formalism for describing the evolution of a system in the presence of noise. In Chapter 9, we will discuss a number of equivalent formalisms for representing a general quantum process. Here, we will sketch the main consideration undergirding each of these representations and the general protocol for extracting these mathematical objects from measurement.

Imagine you have a multi-qubit state ρ. Taking this state as an input, you then run a quantum algorithm on ρ, at the end of which you wind up with some new quantum state $\Lambda(\rho)$. Both ρ and $\Lambda(\rho)$ are density matrices with dimension $2^n \times 2^n$, where the latter density matrix is some function of the former—that is, like all algorithms, the state of the output $\Lambda(\rho)$ depends on the state of the input ρ. Mathematically, we can write the relationship between the input and output states as some sum of operators $\{K_i\}$ acting on the initial state ρ

$$\Lambda(\rho) = \sum_i K_i \rho K_i^\dagger. \tag{8.2}$$

The states ρ and $\Lambda(\rho)$ are easily knowable from state tomography, but how can we reconstruct the set of operators $\{K_i\}$ responsible for the journey between the two? It is easy to see that this set of operators is not unique. For example, if the input and output states of our algorithms correspond to the qubit states $|1\rangle$ and $|0\rangle$, there are multiple ways that the former could have turned into the latter. To name only a few:

1. Perhaps a π-pulse was applied around the $\hat{X}$-axis ($\hat{U}_X(\pi)$), rotaing the qubit

from one pole to the other along the circumference of the yz-plane;

2. or, perhaps a π-pulse was applied around the $\hat{Y}$-axis ($\hat{U}_Y(\pi)$), rotaing the qubit instead along the circumference of the xz-plane;

3. or, perhaps a π-pulse was applied around some other equatorial axis;

4. still yet, perhaps the evolution wasn't unitary at all, and the state was pulled through the Bloch sphere due to a T_1 process.

How do we distinguish between each of these processes if they all turn the state $|1\rangle$ into $|0\rangle$?

The answer, of course, is to run the process on more input states. After all, while all of the processes above will turn the state $|1\rangle$ into $|0\rangle$, they don't perform the same for all input states: if we had instead inputted the state $|+\rangle$, we would find that all of the processes above would lead to very different final states. This is the key insight of process tomography: process tomography is the technique by which a set of known quantum states are inputted into an unknown black box, and the input-output relationship is systematically interrogated until the full mathematical description of the box is determined.

Like state tomography, this reconstruction doesn't come cheap. The price we must pay to reconstruct a general quantum process scales as the product of two exponentials: just like in state tomography, we must once again perform an exponential number of basis measurements to reconstruct each output state ($\sim \mathcal{O}(2^n)$), but we must now also cycle over an exponential number of *input states* (also $\sim \mathcal{O}(2^n)$) to ensure that we have a complete basis set of inputs and outputs (overall number of measurements $\sim \mathcal{O}(2^{2n})$). Nonetheless, as we demonstrated in Part III, full process reconstruction is perfectly feasible for small systems of one or two qubits, and it has become a ubiquitous technique for characterizing single- and two-qubit gates.

Like state tomography, process tomography has also spawned an array of variants [17, 45, 233, 308, 387, 461]. In Chapter 10, we will return to the most notable of these variants, known as *gate set tomography* [56, 57, 167, 303]. This category also

attempts at more efficient partial gate characterization [134, 148, 283, 342, 437, 489], Pauli channel tomography [186, 187, 395], phase estimation [243], and spectral tomography [198]. Finally, while process tomography is traditionally associated with the characterization of discrete quantum processes—black boxes which translate a single input to a single output—this category also includes techniques for reconstructing quantum dynamics, including the reconstruction of Hamiltonian [80, 102, 120, 166, 206, 406] and Lindblad operators [43, 44, 399, 407, 488], the latter of which we will return to in great detail throughout the following chapters.

8.5 Model Verification

While the preceding categories of QCVV fall squarely in the domain of physics, the following categories become somewhat more abstract and computation-centric. Model verification attempts to generalize beyond the scope of both state and process characterization: instead of asking how well a given quantum processor prepared some particular quantum state or implemented some particular quantum process, we instead ask, *How well does this processor perform on a variety of tasks we might ask it to do?* Or, more specifically, *Can we build a model which predicts the performance of our processor, regardless of what task we choose to run on it?*

This branch of QCVV has the closest ties to quantum error correction: given the error threshold of a particular correction protocol as a model, we must then verify that a processor satisfies this threshold, allowing the correction protocol to succeed [34, 104, 110, 175, 176, 210, 217, 226, 288, 336, 385, 400, 412, 430, 442, 444, 456]. Here, we see that the boundaries between the different categories of QCVV are not rigid: in addition to more model-centric characterization techniques like cycle benchmarking [136] and Pauli noise estimation [186, 187, 395], many of techniques we considered in the process characterization category—such as gate set tomography and some forms of process tomography—can also be applied towards model verification.

8.6 Holistic Benchmarking

This category is the complement to model verification. Whereas model verification aims to capture the performance of a vast range of applications from the error rates of individual components, benchmarking aims to run a limited set of representative applications on a processor and use their success as a proxy for the performance of the processor. This category of QCVV is founded on the belief that while a universal quantum computer can run any arbitrary algorithm, in practice there are only a limited number of interesting tasks we would actually want to run on a processor, and the performance of these applications cannot be effectively predicted using a reductionist model for the errors of their components. At the moment, it remains unclear which of these two categories of techniques will provide the best metric for measuring the performance of real algorithms on large-scale quantum processors, and as such the two are currently used in parallel to complement each other.

Examples of holistic benchmarks include tests of actual algorithms on physical processors [121, 126, 142, 199, 267, 278, 299, 304, 310, 377, 477, 482], quantum volume metrics [52, 108], cross-entropy benchmarking (XEB) [22], demonstrations of quantum error correction [34, 92, 106, 164, 253, 326, 375, 476], and volumetric benchmarking [59, 370].

8.7 Supremacy

This final category is unique among the seven. While all the other categories offer various methods for comparing aspects of quantum systems to a particular quantum mechanical model or another quantum processor, supremacy metrics attempt to directly compare the performance of a quantum processor to the best possible *classical* processor [6, 109, 193]. In this respect, while supremacy metrics often overlap with holistic benchmarking techniques in practice, their primary motivations are completely different. As an example, we can compare cross-entropy benchmarking—the characterization technique most famously used in claims of supremacy [22]—to an-

other holist benchmark such as quantum volume. While the quantum volume aims to provide a purely quantum mechanical metric for comparing one quantum computer to another, cross-entropy benchmarking seeks to benchmark the relative performance of a quantum computer and a classical computer on the same task.

Techniques motivated by demonstration of supremacy include random circuit sampling [22, 327], quantum chemistry and QAOA algorithms [139, 403], boson sampling [270, 284], instantaneous quantum polynomial (IQP) circuits [73], and analog simulation [154, 181]. Among the different characterization paradigms, this paradigm is the most dependent on the current state of quantum and classical algorithm research: as new and more efficient quantum algorithms are discovered, and as new classical algorithms are found which outperform their quantum counterparts, the threshold for claims of supremacy must adjust accordingly.

Chapter 9

Quantum Processes, Dynamics, Markovianity

In Chapter 8, we sorted the tangled task of characterizing quantum systems into a rough zoology of seven categories. Over the next several chapters, we will focus in detail on one category of characterization techniques: the characterization of quantum processes. In this chapter, we will review a few of the mathematical formalisms for representing both discrete quantum processes (such as the Kraus and χ-matrix representations) as well as continuous quantum dynamics in the presence of loss, as described by the Lindblad master equation. These mathematical preliminaries will then set the stage for the characterization technique presented in Chapter 10: Lindblad tomography.

9.1 Quantum Processes and Physicality Constraints

Imagine you have a collection of qubits which are prepared in an arbitrary quantum state described by the density matrix ρ. Then, something happens to your qubits, and at a later time you discover that they are now in a new state described by the density matrix $\Lambda(\rho)$. Now, anything could have happened to the qubits—perhaps you ran some intentional operations on the qubit in the interim, an algorithm for example,

or maybe your qubit encountered some noise and lost information to its environment. Regardless of what happened to the qubits in their journey from state ρ to state $\Lambda(\rho)$, we want to be able to describe the *quantum process* which transformed them from one state to another.

In more formal mathematical language, we can say that a quantum process is a linear map on density matrices $\rho \to \Lambda(\rho)$ which takes an arbitrary initial state $\rho \in \mathcal{H}$ in some Hilbert space $\mathcal{H}$ and outputs another state $\Lambda(\rho) \in \mathcal{H}$ [167]. Put another way, the quantum process doesn't just describe the particular input-output relationship $\rho \to \Lambda(\rho)$ but instead models what would happen to any arbitrary initial state subjected to the same series of events. In this way, the quantum process describes not only the particular transformation $\rho \to \Lambda(\rho)$ we observed, but also what would have happened if we prepared a completely different state σ and watched it transform $\sigma \to \Lambda(\sigma)$.

As we will see, we have a great deal of flexibility when it comes to describing a given quantum process, and there are many valid representations we can use to do so. However, while it would be tempting to just write down any matrix which performs the transformation $\rho \to \Lambda(\rho)$ and call it a quantum process, if we're not careful, we could wind up with a process that transforms certain input states into nonsensical output states. Indeed, the laws of quantum mechanics tell us that there are two basic constraints which a quantum process must satisfy in order to actually exist in the real world:

Complete Positivity (CP): For any initial state ρ, the final state after applying the quantum process $\Lambda(\rho)$ must have nonnegative probabilities for measuring any physical observable. For example, if you find that the probability of measuring one of your qubits in the $|0\rangle$-state after applying the map is -50%, something has gone horribly wrong.

Trace Preservation (TP): The total probability of measuring the system in all of its eigenstates must be conserved. In other words, the trace of the density matrix ρ before applying the map must be equal to the trace of $\Lambda(\rho)$ after

applying the map. For example, if ρ is a single-qubit state corresponding to a 50/50 superposition of $|0\rangle$ and $|1\rangle$, you shouldn't find that $\Lambda(\rho)$ has a 90% probability of being measured in $|0\rangle$ and a 45% probability of being measured in $|1\rangle$, since the total probability of the state in either eigenstate is now 135%.[1]

Taken together, a quantum process which satisfies both Complete Positivity and Trace Preservation is known as a CPTP map.

9.2 Process Map Representations and Metrics

Given a general quantum process $\rho \to \Lambda(\rho)$, there are several different representations with which to express the process. In this section, we'll discuss three of the most common representations: Kraus operators, the process matrix (also known as the χ-matrix), and the Pauli Transfer Matrix.

9.2.1 Kraus Operators

A general CP map for the process $\rho \to \Lambda(\rho)$ can be written as

$$\Lambda(\rho) = \sum_{i=1}^{N} K_i \rho K_i^\dagger \tag{9.1}$$

where $N \leq d^2$, $d = 2^n$ is the dimension of the Hilbert space for n qubits, and the set of matrices $\{K_i\}$ are known as the *Kraus operators*. Note that while the Kraus operators have the same dimension as unitary operators—that is, they are $d \times d$ matrices—they need not be unitary, Hermitian, or invertible. In general, equations of the form in Eq. (9.1) are known as the *operator-sum representation* of a quantum process.

Since Kraus operators act on quantum states like normal operators (as opposed to superoperators, as we will soon see), they are often the easiest the interpret by quick

[1] Interestingly, this constraint can be relaxed if the process contains leakage errors outside the computational subspace—in which case the total probability would go down, since there is some population in states outside the scope of $\Lambda(\rho)$—but in general the total probability shouldn't increase [167].

inspection and basic intuition. For example, consider a quantum process described by the following two Kraus operators K_0 and K_1:

$$K_0 = \begin{bmatrix} 1 & 0 \\ 0 & \sqrt{1-p} \end{bmatrix} \tag{9.2}$$

$$K_1 = \begin{bmatrix} 0 & \sqrt{p} \\ 0 & 0 \end{bmatrix}. \tag{9.3}$$

Looking at these operators, we can easily interpret their action on a quantum state: K_1 transforms the $|1\rangle$-state to $|0\rangle$ with probability p, while K_0 leaves the $|0\rangle$-state unchanged and reduces the amplitude of $|1\rangle$. From this, we can quickly see that these Kraus operators describe spontaneous emission, also known as an *amplitude damping channel*. When you measure T_1 of a qubit, this is the channel you are observing, and the decay time T_1 can be used to directly calculate the probability p in the operators above.

However, while Kraus operators are easy to interpret, the fact that you need to keep track of numerous operators to describe a single physical channel can be inconvenient and often makes them less straightforward to analyze numerically. As previously stated, you need as many as d^2 Kraus operators to describe a single channel. While amplitude damping requires far fewer than the maximum number of operators (only two, as we just saw), other single-qubit channels require all four Kraus operators.

For example, the *depolarizing channel* is a process which transforms a quantum state into a completely mixed state with probability p. It can be described by four Kraus operators, which correspond to random rotations around all the Bloch sphere

axes with probability p:

$$K_0 = \sqrt{1 - \frac{3}{4}p}\,\mathbb{1} = \begin{bmatrix} \sqrt{1-\frac{3}{4}p} & 0 \\ 0 & \sqrt{1-\frac{3}{4}p} \end{bmatrix} \tag{9.4}$$

$$K_1 = \frac{p}{\sqrt{2}}\mathsf{X} = \begin{bmatrix} 0 & \frac{1}{\sqrt{2}}p \\ \frac{1}{\sqrt{2}}p & 0 \end{bmatrix} \tag{9.5}$$

$$K_2 = \frac{p}{\sqrt{2}}\mathsf{Y} = \begin{bmatrix} 0 & \frac{-i}{\sqrt{2}}p \\ \frac{i}{\sqrt{2}}p & 0 \end{bmatrix} \tag{9.6}$$

$$K_3 = \frac{p}{\sqrt{2}}\mathsf{Z} = \begin{bmatrix} \frac{1}{\sqrt{2}}p & 0 \\ 0 & \frac{-1}{\sqrt{2}}p \end{bmatrix} \tag{9.7}$$

As we will see in the following section, the χ-matrix is much less verbose—all quantum channels are described using a single $d^2 \times d^2$ matrix, though the interpretation of this matrix will be somewhat less straightforward.

9.2.2 The χ-Matrix

Let's consider an alternative, though no less valid, way of describing our quantum process $\rho \to \Lambda(\rho)$. Instead of coming up with a new set of operators for every quantum channel—as we did with the Kraus operators—let's think of all quantum channels as applying the same fixed set of operations, though with varying weights of each operation. This is just like how we can express an arbitrary quantum state ρ as the weighted sum of a fixed set of matrices: the Pauli operators. Indeed, both unitary and Kraus operators can also be written in the Pauli basis, so we can decompose the Kraus operators we saw above as

$$K_i = \sum_{j=1}^{d^2} a_{ij} P_j \tag{9.8}$$

where $P = \frac{1}{\sqrt{2}}\{\mathbb{1}, \mathsf{X}, \mathsf{Y}, \mathsf{Z}\}^{\otimes n}$ is the set of n-qubit Pauli operators and the matrix of coefficients a sets their relative weight in each operator. Plugging in the decomposition from Eq. (9.8) into the operator-sum equation in Eq. (9.1), we get a new expression

for the action of our channel

$$\Lambda(\rho) = \sum_{j,k=1}^{d^2} \chi_{jk} P_j \rho P_k \tag{9.9}$$

where χ is a $d^2 \times d^2$ matrix which contains all the relative weights of the Pauli operators $\chi_{jk} = \sum_i a_{ij} a_{ik}^*$. For obvious reasons, χ is commonly referred to as the χ-matrix, or interchangeably as the *process matrix*. Since P and ρ are independent of the process $\rho \to \Lambda(\rho)$, it is clear from Eq. (9.9) that the matrix χ completely determines the map Λ.

Since the χ-matrix expresses the channel in the Pauli basis, processes such as the depolarizing channel—which, as we saw just saw, already involves a sum over Pauli rotations—are easily expressed in this new formalism

$$\chi = \begin{bmatrix} 1 - 3p/4 & 0 & 0 & 0 \\ 0 & p/4 & 0 & 0 \\ 0 & 0 & p/4 & 0 \\ 0 & 0 & 0 & p/4 \end{bmatrix} \tag{9.10}$$

which clearly maps to the corresponding Kraus operators in Eq. (9.4)–(9.7).

On the other hand, processes which seemed intuitive in the Kraus operator formalism but which don't decompose cleanly into the Pauli basis—such as the amplitude damping channel—become somewhat more opaque and inscrutable when turned into a χ-matrix:

$$\chi = \begin{bmatrix} (1 + \sqrt{1-p})^2 & 0 & 0 & p/2 \\ 0 & p/2 & -ip/2 & 0 \\ 0 & ip/2 & p/2 & 0 \\ p/2 & 0 & 0 & (1 + \sqrt{1-p})^2 \end{bmatrix} \tag{9.11}$$

Nonetheless, the χ-matrix provides a perfectly valid method for representing these processes, and it will reproduce the exact same math as the Kraus representation.

Furthermore, since the χ-matrix is ultimately a matrix of coefficients, it is not an operator in the same sense as the Kraus operators or (as we will see in the next section) the Pauli Transfer Matrix. That is, you cannot simply multiply the χ-matrix by your state ρ to get a new state $\Lambda(\rho)$. Rather, as Eq. (9.9) clearly states, it is the

Pauli matrices which are actually acting on ρ, and χ simply dictates the magnitude of that operation in the grander process.

Again, neither the Kraus nor χ-matrix representation is more correct than the other. However, like a sentence spoken in two different languages, the form best suited for comprehension of its meaning will fall to context. Anecdotally, the Kraus operator formalism is often favored among theorists and pure quantum physicists, who appreciate and take full advantage of its verbosity. Meanwhile, the χ-matrix representation is typically the tool of choice for quantum information experimentalists, since the Pauli decomposition lends itself particularly naturally to characterization protocols such as process tomography, in which Pauli rotations are applied before and after the quantum channel of interest to thoroughly map out the input-output relationship which χ formally describes.

9.2.3 Pauli Transfer Matrices

For a third example of how one can express a general quantum process, we consider the Pauli Transfer Matrix (PTM) formalism. In some sense, the PTM balances the desirable qualities of both Kraus operators and the χ-matrix: like more familiar operators such as unitary matrices or Kraus operators, the PTM is a true operator in the sense that its action can be readily assessed by multiplying it directly with a quantum state; like the χ-matrix, it is always given by a single $d^2 \times d^2$ matrix, and matrices for different process can be readily compared using a simple formula for the process fidelity.

The entries of the Pauli Transfer Matrix R_Λ are given by

$$(R_\Lambda)_{ij} = \frac{1}{d} \operatorname{Tr}\{P_i \Lambda(P_j)\} \tag{9.12}$$

where $\Lambda(P_j)$ can be roughly thought of as the action of the process on a series of states given by the Pauli operators.[2] Unlike χ, the entries of R_Λ are real numbers in

[2]This shouldn't be taken too literally since $\rho = P_j$ is not a physical density matrix, though $\Lambda(P_j)$ is perfectly well defined if you plug $\rho = P_j$ into either Eq. (9.1) or Eq. (9.9).

the interval $[-1, 1]$, and the matrix is not in general symmetric.

The PTM for the depolarizing channel is given by

$$R_\Lambda = \begin{bmatrix} 1 & 0 & 0 & 0 \\ 0 & 1-p & 0 & 0 \\ 0 & 0 & 1-p & 0 \\ 0 & 0 & 0 & 1-p \end{bmatrix} \tag{9.13}$$

and the PTM for the amplitude damping channel is given by

$$R_\Lambda = \begin{bmatrix} 1 & 0 & 0 & 0 \\ 0 & \sqrt{1-p} & 0 & 0 \\ 0 & 0 & \sqrt{1-p} & 0 \\ p & 0 & 0 & 1-p \end{bmatrix}. \tag{9.14}$$

As alluded to above, the PTM formalism provides a natural method for applying a process to a state of interest

$$|\Lambda(\rho)\rangle\rangle = R_\Lambda \, |\rho\rangle\rangle \tag{9.15}$$

where $|\rho\rangle\rangle$ is a $d^2 \times 1$ *vector* containing all the information of the $d \times d$ density *matrix* ρ. The form of Eq. (9.15) should look familiar—it's exactly how you would apply a unitary operator to a state vector $|\psi\rangle$. However, unlike the state vector $|\psi\rangle$, the *operator* vector $|\rho\rangle\rangle$ is not in general a pure state, and it can be thought of as the vectorization of any allowed density matrix ρ. For a given density matrix ρ, the corresponding operator vector $|\rho\rangle\rangle$ is given by

$$|\rho\rangle\rangle = \sum_k \mathrm{Tr}\left[P_k \rho\right] |k\rangle\rangle. \tag{9.16}$$

Since R_Λ can be seen as an operator acting on the higher-dimensional state vector $|\rho\rangle\rangle$, matrices such as R_Λ are commonly referred to as *superoperators*. Conveniently, unlike with χ-matrices, the action of multiple processes applied sequentially can be

represented by simply multiplying their PTM's together

$$R_{\Lambda_1 \circ \Lambda_2} = R_{\Lambda_1} R_{\Lambda_2} \tag{9.17}$$

exactly as one would do with unitary operators.

9.2.4 Process Fidelity

Once you've described your quantum channel using one of the representations above, what do you do with it? For example, if all you want is to simulate the action of the channel on a particular input state, all you need to do is write down the map in one of the formalisms described above and use the corresponding formula—Eq. (9.1) for Kraus operators, Eq. (9.9) for χ-matrices, or Eq. (9.15) for Pauli Transfer Matrices—to find $\Lambda(\rho)$ for your particular input state ρ.

However, the situation will often arise when you want to compare two quantum processes with one another. For example, maybe you just ran process tomography on a gate operation, and you want to figure out how close the experimental operation is to the ideal operation you wanted to implement. How do you compare the measured process to the ideal one, quantifying your degree of success?

The most common metric for calculating the degree of similarity between two quantum processes is known as the *process fidelity*. This metric relies on the χ-matrix formalism and bears a strong similarity to the even more ubiquitous metric for *state fidelity*,

$$F_s(\rho_{\text{meas}}, \rho_{\text{ideal}}) = \text{Tr}\left[\sqrt{\sqrt{\rho_{\text{ideal}}}\,\rho_{\text{meas}}\,\sqrt{\rho_{\text{ideal}}}}\right]^2 \tag{9.18}$$

where ρ_{meas} and ρ_{ideal} are the measured and ideal states, respectively, and F_s is the state fidelity between them. The state fidelity is a real, positive number in the interval $[0, 1]$, where $F_s = 1$ corresponds to the states being equivalent and $F_s = 0$ corresponds to them being orthogonal. For the specific case where the ideal and measured states

are pure, this reduces to the even more iconic form

$$F_s(\rho_{\text{meas}}, \rho_{\text{ideal}}) = \text{Tr}\left[\rho_{\text{meas}}\, \rho_{\text{ideal}}\right]. \tag{9.19}$$

Analogously, we can define the fidelity between two quantum processes as

$$F_p(\chi_{\text{meas}}, \chi_{\text{ideal}}) = \text{Tr}\left[\sqrt{\sqrt{\chi_{\text{ideal}}}\, \chi_{\text{meas}}\, \sqrt{\chi_{\text{ideal}}}}\right]^2 \tag{9.20}$$

where χ_{meas} and χ_{ideal} are respectively the measured and ideal processes in the χ-matrix representation, and F_p is the process fidelity between them. Just like state fidelity, the process fidelity is a real, positive number in the interval $[0, 1]$, where $F_p = 1$ corresponds to the processes being equivalent and $F_p = 0$ corresponds to them being orthogonal. For the specific case where the ideal and measured processes are unitary, this reduces to

$$F_p(U_{\text{meas}}, U_{\text{ideal}}) = \text{Tr}\left[U_{\text{meas}}\, U_{\text{ideal}}\right]. \tag{9.21}$$

9.3 The Lindblad Master Equation

So far in this chapter, we have thought about quantum processes as *discrete* phenomena: a density matrix ρ passes through some black box, and we wish to build a predictive model for the box which describes for whatever new state $\Lambda(\rho)$ it might spit out. Notice that nowhere in the discussion above did a time axis come into play. That is, the formalisms above do not account for the time dynamics at work inside of the box. For example, if it takes 50 microseconds for the box to spit out a new state, then the process map describing this box will only be valid at two times: $t = 0$, when the system is still in state ρ; and $t = 50\mu$s, when the system is in the final state $\Lambda(\rho)$. As for the time $0 < t < 50\mu$s during which the system is in the box, our map can say nothing.

Now, in practice, we often have experimental access to a knob which allows us to probe the box as a function of time—say, by varying the time we allow the system to

evolve before measuring—such that we slice the box into a set of discrete snapshots and write a process map for each slice. We will return to this picture in Chapter 10 in our discussion of Lindblad tomography, but for now just notice that taking discrete snapshots of the process as a function of time simply turns one black box into a concatenation of many smaller boxes—once again, we are unable to say anything about what the system is up to in the middle of those processes, in the times between our discrete time steps.

How do we describe the continuous dynamics of a quantum process? The simple answer, of course, is to write down the Hamiltonian governing the evolution of the system. As we discussed at the beginning of Chapter 8, to the best of our knowledge, the Schrödinger equation is valid at all scales of matter. Were we to write down the wavefunction of the entire universe, we believe that we would find that its evolution to be perfectly unitary, governed by the action of an unfathomably massive Hamiltonian capturing all the forces between every quantum bit across all of space. The problem, of course, is that we do not have access to the universal wavefunction, much less its Hamiltonian. Indeed, we *cannot* have access to either of these mathematical objects, not just because the universe is a very big place, but because the classical description of these operators in the world of paper and pencils and fleshy humans scales *exponentially* with the size of the system.

Abandoning all hope of describing the dynamics of the universal wavefunction, how do we describe the dynamics of a small slice of this wavefunction? For example, how do we describe the evolution of a handful of qubits in a quantum processor? These qubits are, of course, part of the universe, and their evolution will be accounted for somewhere in the universal Hamiltonian. Our task is thus to carve out the sliver of this Hamiltonian which describes the evolution of our small system.

Now, if our processor is in a product state with the rest of the universe and there is no interaction between the processor and the rest of the universe, then the Hamiltonian fragment describing our processor will be, itself, a valid Hamiltonian. In this case, the dynamics of our processor will be completely unitary within the reduced Hilbert space of the device, and we can completely describe the dynamics of

any initial state of the processor ρ using the Schrödinger equation, as we found back in Eq. (2.192)

$$\frac{d\rho}{dt} = -\frac{i}{\hbar}\left[\hat{H}, \rho\right] \tag{9.22}$$

where the Hamiltonian $\hat{H}$ spans the reduced Hilbert space of the processor. In this picture, the evolution of the processor will be entirely, and all of the information contained in the system.

This is a highly idealized picture. In practice, our processor is never perfectly isolated from the rest of the universe: as the universal wavefunction evolves, information will be exchanged between the processor and the rest of the environment, and entanglement will spread beyond the confines of our processor. When this happens, the unitary evolution of the universal Hamiltonian will no longer be unitary from the perspective of our subsystem. Instead, it will appear that information is leaking out of the processor, causing the processor to randomly decohere over time. This phenomenon should be familiar: this is exactly what happens to our qubits during a T_1 or T_2 process.

These processes are not unitary, so they cannot be described by plugging a reduced Hamiltonian into the Schrödinger equation. And yet, as we just saw in Section 9.2, we can construct operators which capture the discrete evolution of one density matrix to another, whether or not the underlying process is unitary. Can we do the same for continuous dynamics? Can we find dynamic operators which, when plugged into the suitable differential equation and solved at discrete times, yield the process maps we found in Section 9.2, in the same way that the Hamiltonian gives rise to discrete unitary operations?

The answer is yes—in some cases. To model the dynamics of an open quantum system coupled to a larger environment, we can take the Schrödinger equation from Eqs. (2.192) and (9.22) and add some additional terms to the differential equation which attempt to capture the non-unitary part of the dynamics. Doing so, we arrive at a new differential equation, commonly referred to as the *Lindblad master equation*,

or equivalently the *master equation in Lindblad form*

$$\frac{d\rho}{dt} = -\frac{i}{\hbar}\left[\hat{H}, \rho\right] + \sum_{i=1}^{d^2-1} \gamma_i \left(\hat{L}_i \rho \hat{L}_i^\dagger - \frac{1}{2}\left\{ \hat{L}_i^\dagger \hat{L}_i, \rho \right\} \right) \tag{9.23}$$

where $\{A, B\} \equiv AB + BA$ is the *anticommutator*, d is the dimension of the Hilbert space of the reduced system, $\hat{H}$ is the Hamiltonian in this reduced Hilbert, the operators $\{\hat{L}_i\}$ represent the coupling of the system to the environment, and the positive coefficents $\gamma_i > 0$ are the decay rates which set the timescales of these couplings. As we can see, the first term in Eq. (9.23) is simply the Schrödinger equation: this term captures the coherent part of the dynamics. As for the remaining terms, these are clearly governed by the action of the operators $\{\hat{L}_i\}$, which are commonly known as the *jump operators* of the system. Unlike the Hamiltonian $\hat{H}$, which must be a Hermitian matrix, the set of jump operators need not be Hermitian: in general, the set of matrices $\{\hat{L}_i\}$ simply needs to form a complete orthonormal basis of Hilbert-Schmidt operators in the system's Hilbert space, with the constraint that the square of each jump operator $\hat{L}_i^2$ is proportional to the identity. Unbound from the constraint of Hermiticity, this differential equation in no longer confined to the production of unitary evolution and can now account for decay into the environment.

As an example, let's consider a T_1 process, where a single qubit randomly loses an excitation into the environment via spontaneous emission. For a single qubit, we can describe this phenomenon using a single jump operator proportional to the lowering operator σ_-

$$\hat{L} = \sigma_- \equiv \begin{bmatrix} 0 & 1 \\ 0 & 0 \end{bmatrix}. \tag{9.24}$$

For the simplicity of the following example, let's set the Hamiltonian governing the qubit's coherent evolution proportional to the Pauli $\hat{Z}$ operator, corresponding to rotation around the z-axis of the Bloch sphere at a frequency corresponding to the energy difference $\hbar\omega$ between the two qubit states $|0\rangle$ and $|1\rangle$

$$\hat{H} = -\frac{\hbar\omega}{2}\hat{Z} = \begin{bmatrix} -\frac{1}{2}\hbar\omega & 0 \\ 0 & \frac{1}{2}\hbar\omega \end{bmatrix}. \tag{9.25}$$

Plugging this jump operator into the master equation in Eq. (9.23) with a decay rate γ, the differential equation describing this process becomes

$$\frac{d\rho}{dt} = -\frac{i}{\hbar}\left[\hat{H}, \rho\right] + \frac{\gamma}{2}\left(2\sigma_-\rho\sigma_+ - \sigma_+\sigma_-\rho - \rho\sigma_+\sigma_-\right). \tag{9.26}$$

To solve this differential equation, it is useful to make a change of variables and rewrite this equation in the rotating frame of the qubit's coherent evolution

$$\tilde{\rho}(t) \equiv e^{i\hat{H}t}\rho(t)e^{-i\hat{H}t}. \tag{9.27}$$

Making this substitution, the first term in Eq. (9.26) conveniently drops out and we are left with the terms describing the incoherent evolution

$$\frac{d\tilde{\rho}}{dt} = \frac{\gamma}{2}\left(2\tilde{\sigma}_-\tilde{\rho}\tilde{\sigma}_+ - \tilde{\sigma}_+\tilde{\sigma}_-\tilde{\rho} - \tilde{\rho}\tilde{\sigma}_+\tilde{\sigma}_-\right) \tag{9.28}$$

where the jump operator is now written in the rotating frame of the qubit

$$\tilde{\sigma}_- \equiv e^{i\hat{H}t}\sigma_- e^{-i\hat{H}t} = e^{-i\omega t}\sigma_- \tag{9.29}$$

$$\tilde{\sigma}_+ \equiv e^{i\hat{H}t}\sigma_+ e^{-i\hat{H}t} = e^{+i\omega t}\sigma_+ \tag{9.30}$$

Plugging Eqs. (9.29) and (9.30) into Eq. (9.28), we arrive at the final equation of motion

$$\frac{d\tilde{\rho}}{dt} = \frac{\gamma}{2}\left(2\sigma_-\tilde{\rho}\sigma_+ - \sigma_+\sigma_-\tilde{\rho} - \tilde{\rho}\sigma_+\sigma_-\right). \tag{9.31}$$

We can solve this equation of motion by decomposing the state $\tilde{\rho}$ into its coordinates $(\lambda_x, \lambda_y, \lambda_z)$ in the volume of the Bloch sphere

$$\lambda_x = \lambda_x(0)e^{-\frac{\gamma}{2}t} \tag{9.32}$$

$$\lambda_y = \lambda_y(0)e^{-\frac{\gamma}{2}t} \tag{9.33}$$

$$\lambda_z = \lambda_z(0)e^{-\gamma t} + 1 + e^{-\gamma t} \tag{9.34}$$

As a final substitution, let us define the probability p of an emission occurring during

an elapsed time t in terms of the decay rate γ as

$$p \equiv 1 - \exp\left[-\gamma t\right]. \tag{9.35}$$

Doing this, we can easily confirm that the evolution described by the Bloch vector equations in Eqs. (9.32)–(9.34) is equivalent to the quantum process representation

$$\tilde{\rho}(t) = \Lambda(\tilde{\rho}(0)) \equiv K_0 \tilde{\rho} K_0^\dagger + K_1 \tilde{\rho} K_1^\dagger \tag{9.36}$$

where

$$K_0 = \begin{bmatrix} 1 & 0 \\ 0 & \sqrt{1-p} \end{bmatrix} \tag{9.37}$$

$$K_1 = \begin{bmatrix} 0 & \sqrt{p} \\ 0 & 0 \end{bmatrix}. \tag{9.38}$$

These operators should be familiar: they are exactly the Kraus operators for amplitude damping we defined in Eqs. (9.2) and (9.3). Thus, we have shown that just as the solution to the Schroödinger equation produces the unitary operators describing coherent evolution at discrete times, the solution of the Lindblad master equation produces process maps describing more general evolution at discrete times.

9.4 Markovianity

In the previous section, we showed the continuous time dynamics of a quantum system under the Lindblad master equation can be evaluated at discrete time to yield the process maps we explored earlier in this chapter. However, unlike the relationship between the set of possible Hamiltonian operators and possible unitary operators, this mapping is not one-to-one. In coherent evolution under the Schroödinger equation, every Hamiltonian produces a set of discrete unitary operations, and every unitary operator can be expressed as the discrete action of a Hamiltonian at some time. The same is not true for general quantum dynamics. While every set of jump opera-

tors will produce a set of process maps when evaluated at discrete times, not every quantum process which has an operator-sum representation can be written down as a corresponding master equation.

Indeed, while the operator-sum representation of a quantum process is completely general and provides a complete mapping between all initial and final density matrices, the set of processes which can be described by a master equation is much more limited. Indeed, as we can see from the master equation in Eq. (9.23), this differential equation can only account for processes where information leaks out of the system of interest—that is, processes which are well described by a decay rate γ—such as the exponential loss of excitations during a T_1 process or phase information during a T_2 process. Such processes can be described as Markov chains since the probability of a schochastic error happening at time t is independent of whatever happened to the system at an earlier time $t - \epsilon$. In this sense, the errors occurring in the system over time are uncorrelated, and it is common to say that such a system is 'memoryless': at any given time, the environment acting on our system has no prior memory of the system at an earlier time which might alter its action on the system. Fittingly, processes of this kind are generally known as *Markovian dynamics*.

While the class of Markovian processes includes many of the most ubiquitous errors which occur in experimental quantum processors—such as T_1 and T_2 decay—there exist errors that are *not* Markovian in nature and thus cannot be described by a master equation. As an example, consider the toy system of two qubits we examined back in Section 2.6. Again, let's consider two qubits A and B, one of which is prepared in $|0\rangle$ and the other in $|1\rangle$ such that their combined product state is given by

$$\rho_{AB}(t=0) = |01\rangle\langle 01|_{AB} \tag{9.39}$$

$$= \begin{bmatrix} 0 & 0 & 0 & 0 \\ 0 & 1 & 0 & 0 \\ 0 & 0 & 0 & 0 \\ 0 & 0 & 0 & 0 \end{bmatrix}_{AB} \tag{9.40}$$

Let's then evolve the two qubits according to the Hamiltonian from Eq. (2.231)

$$\hat{H}_{AB} = \hbar\omega(\hat{I}\otimes\hat{I} + \hat{X}\otimes\hat{X} + \hat{Y}\otimes\hat{Y} + \hat{Z}\otimes\hat{Z}). \tag{9.41}$$

What happens to the two qubits during this evolution? As in Section 2.6, let's consider a few key moments during the evolution of the two qubits, each separated by an elapsed time $T = \pi/(8\omega)$:

$t = 0$: The two qubits begin in a product state of $|0\rangle_A$ and $|1\rangle_B$, as we defined in Eq. (9.70).

$t = T$: As the qubits interact with each other, they gradually becomes entangled with each other. At $t = T$, the two qubits have evolved into a maximally entangled state, as we showed in Eq. (2.246)

$$\rho_{AB}(t=T) = \frac{1}{2}(|01\rangle_{AB} - i\,|10\rangle_{AB})(\langle 01|_{AB} + i\,\langle 10|_{AB}) \tag{9.42}$$

$$= \frac{1}{2}\begin{bmatrix} 0 & 0 & 0 & 0 \\ 0 & 1 & i & 0 \\ 0 & -i & 1 & 0 \\ 0 & 0 & 0 & 0 \end{bmatrix}_{AB} \tag{9.43}$$

$t = 2T$: The entangled state continues to evolve, and the qubits gradually disentangle from each other. At $t = 2T$, the two qubits have evolved back into a product state, though now with their initial states swapped, as we showed in Eq. (2.237)

$$\rho_{AB}(t=2T) = |10\rangle\langle 10|_{AB} \tag{9.44}$$

$$= \begin{bmatrix} 0 & 0 & 0 & 0 \\ 0 & 0 & 0 & 0 \\ 0 & 0 & 1 & 0 \\ 0 & 0 & 0 & 0 \end{bmatrix}_{AB} \tag{9.45}$$

$t = 3T$: Having swapped states, the qubits continue to evolve and once again become

entangled with each other, but now into the state we found back in Eq. (2.248)

$$\rho_{AB}(t = 3T) = \frac{1}{2}(|10\rangle_{AB} - i\,|01\rangle_{AB})(\langle 10|_{AB} + i\,\langle 01|_{AB}) \tag{9.46}$$

$$= \frac{1}{2}\begin{bmatrix} 0 & 0 & 0 & 0 \\ 0 & 1 & -i & 0 \\ 0 & i & 1 & 0 \\ 0 & 0 & 0 & 0 \end{bmatrix}_{AB} \tag{9.47}$$

$\boldsymbol{t = 4T}$**:** The qubits once again disentangle, and at $t = 4T$ they return to the product state they started in back at $t = 0$, as we can see from Eq. (2.238)

$$\rho_{AB}(t = 4T) = |01\rangle\langle 01|_{AB} \tag{9.48}$$

$$= \begin{bmatrix} 0 & 0 & 0 & 0 \\ 0 & 1 & 0 & 0 \\ 0 & 0 & 0 & 0 \\ 0 & 0 & 0 & 0 \end{bmatrix}_{AB} \tag{9.49}$$

$\boldsymbol{t \geq 4T}$**:** Having returned to their initial state, we can treat $t = 4T$ as the new $t = 0$, and we can easily see that the evolution above will repeat ad infinitum, with the qubits returning to their initial state every multiple of $4T$.

Looking at the evolution of the two qubits over the interval $0 \leq t \leq 4T$, it's clear to see that the dynamics of the two qubit system are entirely unitary, by definition; after all, we arrived at these states through simple application of the Schrödinger equation using the Hamiltonian in Eq. (2.231), so the evolution of the system can be completely described without the need of the master equation.

What happens if we play this same story back, but we only look at one of the two qubits? That is, at each time step in the evolution, let's take the partial trace of the resulting two-qubit state such that we are left with only the single-qubit state of qubit A. In this toy model, we are effectively treating qubit B as the environment which couples to qubit A, and we now wish to model the dynamics of qubit A in the presence of this coupling.

Once again, let's consider the moments in the evolution discussed above, but now

from qubit A's point of view:

$t = 0$: Qubit A begins in the $|0\rangle$-state, as we can clearly see from the partial trace of the product state in Eq. (9.70)

$$\rho_A(t=0) = \mathrm{Tr}_B[\rho_{AB}(t=0)] \tag{9.50}$$
$$= |0\rangle\langle 0|_A \tag{9.51}$$
$$= \begin{bmatrix} 1 & 0 \\ 0 & 0 \end{bmatrix}_A \tag{9.52}$$

$t = T$: As time evolves, the state of qubit A decoheres from a pure state on the surface of the Bloch sphere to an incoherent mixture at its center. At $t = T$, qubit A is in a maximally mixed state, as we can see from taking the partial state of the two-qubit state in Eq. (9.42)

$$\rho_A(t=T) = \mathrm{Tr}_B[\rho_{AB}(t=T)] \tag{9.53}$$
$$= \frac{1}{2}\begin{bmatrix} 1 & 0 \\ 0 & 1 \end{bmatrix}_A . \tag{9.54}$$

$t = 2T$: The entangled state continues to evolve, and the qubits gradually disentangle from each other. At $t = 2T$, the two qubits have evolved back into a product state, though now with their initial states swapped, as we can see from taking the partial state of Eq. (9.44)

$$\rho_A(t=2T) = \mathrm{Tr}_B[\rho_{AB}(t=2T)] \tag{9.55}$$
$$= |1\rangle\langle 1|_A \tag{9.56}$$
$$= \begin{bmatrix} 0 & 0 \\ 0 & 1 \end{bmatrix}_A \tag{9.57}$$

$t = 3T$: Having passed through the Bloch sphere and traveled from one pole to the other, the state of qubit A turns around and again begines to decohere back into the volume of the Bloch sphere. At $t = 3T$, qubit A is once again in a

maximally mixed state, as we can see from the partial trace of Eq. (9.46)

$$\rho_A(t = 3T) = \mathrm{Tr}_B[\rho_{AB}(t = 3T)] \tag{9.58}$$

$$= \frac{1}{2}\begin{bmatrix} 1 & 0 \\ 0 & 1 \end{bmatrix}_A \tag{9.59}$$

$\boldsymbol{t = 4T}$**:** Finally, qubit A completes its journey back and forth along the pole of the Bloch sphere, returning to its initial state at $t = 0$

$$\rho_A(t = 4T) = \mathrm{Tr}_B[\rho_{AB}(t = 4T)] \tag{9.60}$$

$$= |0\rangle\langle 0|_A \tag{9.61}$$

$$= \begin{bmatrix} 1 & 0 \\ 0 & 0 \end{bmatrix}_A \tag{9.62}$$

How do we account for what happens to qubit A over the interval $0 \leq t \leq 4T$? From the two-qubit picture, the story is completely straightforward: as the two qubits evolve, they periodically become entangled with each other; as we saw back in Section 2.8, when we try to separate two qubits which are entangled with each other, each will appear to be a mixed state; thus, the evolution of qubit A from pure state to mixed state and back and forth is simply an artifact of the coherent evolution of the underlying two-qubit state. Case closed.

But what happens if we show qubit A to someone without telling them about qubit B? What would they make of qubit A's journey? Focusing only on the single-qubit picture above, something very strange is happening:

$\boldsymbol{0 \leq t \leq T}$**:** During this interval, qubit A appears to be spontaneously decohering, as if under the influence of a depolarizing channel. From this, we might conclude that the qubit has lost simply lost its phase information to the environment, and we would attempt to find jump operators which account for this loss.

$\boldsymbol{T \leq t \leq 2T}$**:** Having lost its phase information to the environment in the previous interval, qubit A appears to receive a new phase from the environment, evolving

from a completely mixed state into a new pure state. Looking at the combined interval $0 \leq t \leq 2T$, this suddenly looks more like an amplitude damping channel than a depolarizing channel, except that the polarity of the channel is all wrong. Instead of losing an excitation to the environment, qubit A appears to have *gained* one from the environment. Moreover, if we finely sample the evolution of the system during this combined interval, we would find that the qubit's path through the Bloch sphere is not an exponential decay—as we would expect from either depolarizing or amplitude dampling channels—but rather a sinusoid. Clearly none of the jump operators we have found in this chapter can account for that.

$2T \leq t \leq 4T$: Having completed half a period of this sinuosoid, we find that qubit A once again reteats along the pole of the Bloch sphere, as if it is losing the excitation it just gained back into the environment. This loss is short-lived: if we continue the clock and observe the state for $t \geq 4T$, we find that the environment returns the excitation again, swapping it back and forth with qubit A for the rest of time.

The evolution of qubit A described above cannot be described by any single-qubit master equation. We call processes of this form *non-Markovian*. Unlike the environment in a Markovian process, the environment in the system above (that is, qubit B) clearly has a memory of where qubit A was at every given point in time—having passed through the center of the Bloch sphere twice (once at $t = T$ and then again at $t = 3T$), the environment knows whether it should send qubit A to $|1\rangle$ or $|0\rangle$. This phenomenon clearly violates the requirements of a Markov chain: when the environment sees a state sitting at the center of the Bloch sphere, it should do the exact same thing to that state *regardless of where it came from*.

9.5 Detecting Non-Markovianity

We will return to the picture of non-Markovian errors above extensively in Chapter 10. Before we get there, however, we will briefly consider a technique for detecting the presence of non-Markovian errors in a physical system. While this technique is only one of a number of proposed measures for non-Markovianity in the literature [379, 450], the method described below will be prove particularly useful in the following demonstration of Lindblad tomography, where we will use it to validate whether or not the Markovian model holds for an observed quantum evolution and, thus, whether or not we can describe the channel using the Lindblad master equation.

In order to detect the presence of a non-Markovian process, we must first define the limits of what can happen under a Markovian process given the action of the master equation. To start, let's look at the form of the master equation in Eq. (9.23)

$$\frac{d\rho}{dt} = -\frac{i}{\hbar}\left[\hat{H}, \rho\right] + \sum_{i=1}^{d^2-1} \gamma_i \left(\hat{L}_i \rho \hat{L}_i^\dagger - \frac{1}{2}\left\{\hat{L}_i^\dagger \hat{L}_i, \rho\right\}\right). \tag{9.63}$$

Picking an arbitrary Hamiltonian $\hat{H}$ and set of jump operators $\{\hat{L}_i\}$ with positive decay rates γ_i, let's imagine evolving two different initial states ρ_1 and ρ_2 under this equation. In particular, let's look at the distance between these two states on the Bloch sphere and see how it changes over the course of the evolution. To simplify this, let's first look at the master equation in the case of unitary evolution only ($\{\hat{L}_i\} = 0$) and then in the case of Markovian evolution in the absence of coherent evolution ($\hat{H} = 0$):

Unitary evolution: Starting with two states ρ_1 and ρ_2 located somewhere on the surface or within the volume of the Bloch sphere, the distance between these two states will remain *constant* for all time. As an example, consider the two

initial single-qubit states

$$\rho_1 = |1\rangle\langle 1| \tag{9.64}$$

$$\rho_2 = |+\rangle\langle +| \tag{9.65}$$

which are each rotated under the influence of a Hamiltonian

$$\hat{H} = \hbar\omega\hat{Z}. \tag{9.66}$$

Looking at these two states over the course of their evolution, we can take the trace distance of the two states as a function of time, where the trace distance D between the two states is defined as

$$D = |\rho_1(t) - \rho_2(t)|/2 \tag{9.67}$$

and

$$|M| \equiv \mathrm{Tr}\left[\sqrt{M^\dagger M}\right] \tag{9.68}$$

In the Bloch sphere picture, the trace distance can be easily visualized as the geometric distance between the coordinates defining the two states. From this definition, it is easy to see that the trace distance between our example states ρ_1 and ρ_2 must remain constant. Since ρ_1 is an eigenstate of the example Hamiltonian above, its position will not change in time. Meanwhile, the Hamiltonian will cause ρ_2 to rotate around the equator of the Bloch sphere, always maintaining a fixed distance from the stationary state of ρ_1 at the pole. Indeed, it is easy to see that this must be true for *any* pair of initial states ρ_1 and ρ_2 and any possible Hamiltonian $\hat{H}$ since, as we showed back in Chapter 2, unitary rotations during Hamiltonian evolution correspond to rotations of the Bloch sphere itself: rotate the sphere however you wish, and the relative distance between any two points on the sphere must remain constant.

Markovian evolution: Let's now take the same two initial states as in the unitary

example but instead look at their evolution under a set of jump operators in the master equation. As a concrete example, let's consider the jump operator corresponding to an amplitude damping channel, as we showed in Eq. (9.24):

$$\hat{L} = \sigma_- \equiv \begin{bmatrix} 0 & 1 \\ 0 & 0 \end{bmatrix}. \tag{9.69}$$

Plugging our two states into the master equation and evolving them according to this operator with decay rate γ, we see that both states will exponentially decay towards the $|0\rangle$-state of the Bloch sphere. Indeed, this is exactly what happens during T_1 decay: regardless of the initial state of the qubit, the qubit will gradually decay to $|0\rangle$ via the shortest path through the Bloch sphere. Thus, we can see that the action of this non-unitary process causes the trace distance between any pair of initial states—no matter how far away they are initially—to *monotonically decrease* over time, as they are all compelled towards the same final state. It is easy to convince oneself that this feature is a natural consequence of any process which can be modelled as a Markov chain: if the process has no memory of the initial state, then the steady state of any Markovian process must be independent of the initial state, causing all states to converge to the same final state. Thus, the monotonic decrease in trace distance will hold true for any valid set of jump operators in the master equation.

Non-Markovian processes violate this condition. While processes governed by the master equation require that the trace distance between any two initial states must remain constant (in the case of unitary evolution) or decrease monotonically in time (in the case of Markovian evolution), the trace distance between two states evolving under non-Markovian dynamics can *increase* in time. Returing to our example of non-Markovian evolution from above, we can see this is indeed possible. As we saw, when qubit A is initially prepared in the $|0\rangle$-state, it will oscillate between the poles of the Bloch sphere, periodically passing through the center of the sphere when it becomes maximally entangled with qubit B.

Now, what would have happened if we instead prepared qubit A in the $|1\rangle$-state

and ran it through the exact same process? That is, let's just change the state of qubit A but leave the initial state of qubit B and the underlying two-qubit Hamiltonian unchanged. In this case, the initial two-qubit state of qubits A and B at $t = 0$ is now

$$\rho_{AB}(t=0) = |11\rangle\langle 11|_{AB} \tag{9.70}$$

$$= \begin{bmatrix} 0 & 0 & 0 & 0 \\ 0 & 0 & 0 & 0 \\ 0 & 0 & 0 & 0 \\ 0 & 0 & 0 & 1 \end{bmatrix}_{AB} . \tag{9.71}$$

What happens when we evolve this state according to the Hamiltonian in Eq. (9.41), tracing out qubit A as before? Well, *nothing happens*. Indeed, the initial state of the two qubits is now an eigenstate of the Hamiltonian, so the state of qubit A will remain constant in time.

Comparing these two different initial states of qubit A

$$\rho_1(t=0) = |0\rangle\langle 0|_A \tag{9.72}$$

$$\rho_2(t=0) = |1\rangle\langle 1|_A \tag{9.73}$$

and evolving each according to the same interaction with qubit B, we see that these two states clearly violate the trace distance condition required for evolution under the master equation: during the interval $0 \leq t \leq 2T$, the trace distance between the two states will decrease as $\rho_1(t)$ oscillates towards the $|1\rangle$-state where $\rho_2(t)$ is frozen in time; then, during the interval $2T \leq t \leq 4T$, $\rho_1(t)$ oscillates away from $\rho_2(t)$ and back towards the $|0\rangle$-state, causing the trace distance between the two states to *increase*. Thus, even if we don't know the state of qubit B or the underlying multi-qubit Hamiltonian governing the evolution of qubit A and its environment, the relative behavior of these two different initial states clearly alerts us to a violation of the master equation, indicating that the dynamics of qubit A cannot be captures by a single-qubit Hamiltonian or set of jump operators.

Recognizing this particular property of non-Markovian dynamics, the group of

Breuer, Laine, and Piilo proposed a method for characterizing the presence of non-Markovian dynamics by comparing the trace distance between pairs of states in an open quantum system [74]. In this method, a pair of states $\rho_1(t)$ and $\rho_2(t)$ are passed through a common process and the trace distance between them $D(\rho_1(t), \rho_2(t))$ is measured. Comparing the trace distance as a function of time, the degree of non-Markovian behavior in the environment N_{markov} is found by maximizing the integral

$$N_{\text{markov}} = \max_{\rho_1(0),\rho_2(0)} \int_{\sigma>0} \sigma(t, \rho_1(0), \rho_2(0))dt \tag{9.74}$$

where $\sigma(t, \rho_1(0), \rho_2(0)) = \frac{d}{dt}D(\rho_1(t), \rho_2(t))$. That is, the Breuer metric integrates the derivative of the trace distance between a pair of states over all time intervals where the derivative is positive (i.e., trace distance increasing), quantifying the degree to which the trace distance increases during application of the channel. Thus, the larger the value of N_{markov}, the more non-Markovian the channel. Indeed, we will apply this metric to a physical quantum processor in Chapter 10 and show that it successfully accounts for non-Markovian dynamics in the system, and we will discuss its limitations when employed in noisy experimental systems.

Chapter 10

Lindblad Tomography

In our taxonomy of QCVV in Chapter 8, we noted that one of the major categories of techniques concerns the characterization of quantum processes: processes which translate one quantum state into another quantum, either via time evolution or application of a quantum algorithm composed of discrete gates. In Chapter 9, we focused on this category of techniques in more detail and discussed the mathematical formalism of process maps, Lindblad operators, and Markovianity—tools which are vital in the characterization of operations in physical quantum system in the presense of errors.

In this chapter, we will outline and present the first experimental results of a novel characterization protocol for tomographically reconstructing the mathematical objects discussed in Chapter 9 from experimental data. This technique, which we call *Lindblad tomography*, provides a robust framework for finding the most likely underlying Hamiltonian and Lindbladian of a physical multi-qubit system from an ensemble of time domain measurements. In this way, Lindblad tomography can be thought of as an extension of standard process tomography: where process tomog-

This chapter is based in large part on original work reported in Ref. [399], and I gratefully acknowledge all of my coauthors for their contributions to this work, with particular acknowledgment to Johannes Borregaard, Morten Kjaergaard, Alex Greene, Joseph Barreto, Matthias Christandl, and William Oliver.

raphy provides a protocol for reconstructing a quantum process at a discrete time, Linbdlad tomography pieces together the processes found at a series of discrete time steps to recover the dynamic operators from which these processes arise. Along the way, we will discuss how this technique accounts for state preparation and measurement (SPAM) errors which might interfere with our interpretation of data, and we will pair our characterization with the Markovianity metric discussed in Section 9.5 to vaildate whether or not the observed evolution can be fit to operators in the master equation representation.

10.1 A New Tool in the QCVV Toolbox

As we discussed in Chapter 8, there currently exists a broad toolbox of quantum characterization, verification, and validation (QCVV) techniques for experimentalists to draw from. Indeed, opening up a quantum engineer's toolbox and pulling out the most common techniques, we would find that this toolbox contains standard T_1/T_2 measurements, randomized benchmarking (RB) [133, 287], and state/process tomography [346], to name only a few. These techniques each ask fundamentally different questions from each other, and as such each has its own set of strengths and weaknesses [132].

For example, as we have seen in Part III, randomized benchmarking provides an approach for assessing the average fidelity of quantum gate operations independent of state preparation and measurement (SPAM) errors, and it has consequently become a standard measure of performance for experimental quantum devices. However, the average fidelity alone does not provide much information about the actual noise processes at play in the device, and such details are crucial to more fully modeling quantum device and developing tailored error mitigation and correction techniques [424, 442–444, 479].

State and process tomography, on the other hand, provide more detailed information about discrete moments in a qubit's evolution, such as the qubit state at a particular time or the quantum process corresponding to a gate operation of a fixed

duration. However, these tomographic protocols are extremely sensitive to imperfections in state preparation and measurement errors—errors, that is, in the preparation of known states at the beginning of the tomographic protocol and accurate readout along different measurement axes at the end—and caution must be exercised in order to consistently interpret the results of tomography in the presence of these SPAM errors [307]. Building on traditional tomographic protocols, a number of theoretical and experimental works have demonstrated self-consistent characterization of SPAM errors in process tomography and gate characterization [240, 302, 303, 307]. Common to many of these techniques is the use of maximum likelihood estimation (MLE), which provides a robust and flexible estimation procedure capable of handling overcomplete data and constrained problems. While such techniques offer a promising step forward, the characterization of a discrete moment in a qubit's evolution is not always sufficient, and one often requires detailed knowledge about how the noise environment and crosstalk between qubits dynamically influence evolution in time [82].

In this chapter, we discuss a new technique for characterizing the dynamics of a multi-qubit system from an ensemble of time-domain measurements, which we call Lindblad tomography (LT). Mathematically, the goal of LT is to estimate the most likely Hamiltonian, quantum jump operators, and corresponding decay rates which describe the evolution of a multi-qubit system in time. Throughout this chapter, we will refer to this task as extracting the *Lindbladian* of the channel. This task is, in some sense, an expansion of the goal of process tomography: process tomography reconstructs a process map at a single time step; Lindblad tomography aims to reconstruct the underlying dynamic operators which give rise to the process maps for continuous times. Applying this technique, one could use LT to characterize the noise processes experienced by a qubit during free evolution—such as T_1- and T_2-processes, which, as we've discussed, can be formally described as amplitude damping and dephasing channels respectively. Similarly, LT could also be used to evaluate and diagnose a deliberately engineered channel, such as a tailored Hamiltonian implemented on an analogue quantum simulator [182] or a quantum annealing system, similar to what we explored in Chapters 3 and 4.

However, as we discussed in Chapter 9, the relationship between the process map and master equation formalisms is not one-to-one: unlike in coherent evolution, where every unitary operator arises from solution of the Schrödinger equation given some Hamiltonian at some discrete time, not every process map corresponds to a set of jump operators and decay rates in the master equation formalism. As such, our ability to extract the Lindbladian using LT rests on a fundamental assumption: **the evolution of the quantum system is Markovian and well described by a *time-independent* master equation.** That is, since non-Markovian dynamics cannot be captured by Lindblad operators in the master equation, our ability to extract these operators is contingent on the Markovianity of the channel we are attempting to characterize. As such, verification of the Markovian assumption prior to extracting the Lindbladian is vital, as we will see shortly.

10.2 Lindblad Tomography Protocol

From an experimental standpoint, LT can be thought of as a hybrid of three distinct tools which are ubiquitious in the laboratory:

Process tomography: Like standard process tomography, Lindblad tomography cycles over a set of initial qubit states and measurement axes to reconstruct an instantaneous process map at each discrete time step.

T_1 and T_2 measurement: Unlike standard process tomography, Lindblad tomography is also a time-domain measurement, much like standard T_1 and T_2 characterization. Indeed, like a T_1 or T_2, LT sweeps the duration of a quantum channel and records how information moves between the qubits and their environment in time.

Classical optimization: After collecting a series of discrete tomographic slices as a function of time, we run the data through a classical maximum likelihood algorithm to back out the underlying Hamiltonian and Lindblad operators.

Formally, we can describe the measurement protocol for performing LT using the quantum circuit in Fig. 10-1a. Walking through this circuit from left to right, we can see that this circuit consists of three primary steps:

1. The qubit is initialized in a state ρ_0 close to its ground state and one of six single-qubit gates $\mathsf{R}_s = \{\mathbb{1}, \mathsf{X}_\pi, \mathsf{Y}_{\pm\frac{\pi}{2}}, \mathsf{X}_{\mp\frac{\pi}{2}}\}$ is applied, initializing the qubit as close as possible to each of the six cardinal states of the Bloch sphere ($|0\rangle$, $|1\rangle$, $|\pm\rangle$, $|\pm i\rangle$), respectively.

2. The idling channel $\tilde{\mathbb{1}}(t)$ is swept as a function of time, corresponding to a variable time delay between state preparation and measurement during which no experimental controls are performed on the qubit. In the absence of any noise, the idling channel would correspond to the identity channel $\mathbb{1}(t)$.

3. One of three single-qubit gates $\mathsf{R}_b = \{\mathbb{1}, \mathsf{Y}_{-\frac{\pi}{2}}, \mathsf{X}_{\frac{\pi}{2}}\}$ is applied prior to measurement, corresponding to measurement in the Pauli z-, x-, and y-bases.

These steps are then repeated for all combinations of initial state, channel duration, and measurement basis, and the results are saved in classical memory for analysis.

Looking at the circuit diagram in Fig. 10-1a, subsets of pre- and post-pulses should be immediately familiar. Looking at the highlighted sequence of pale green gates—where a X_π gate is applied prior to the variable time delay and the state is measured in the z-basis—we see that this sequence is identical to a standard T_1 measurement. Looking at the highlighted sequence of purple gates—where a $\mathsf{Y}_{\frac{\pi}{2}}$ gate is applied prior to the variable time delay and the state is measured in the x-basis—we see that this sequence is identical to a standard T_2 measurement. This observation gives us a nice physical intuition for what LT is doing: by cycling over the full set of pre- and post-pulses and sweeping a variable time delay between them, LT is effectively piecing together all possible combinations of T_1 and T_2 measurements to tomographically reconstruct the full quantum loss channel.

Once all the measurements have been performed and all the data has been collected, the entire data set is passed through a series of computations for analysis, as illustrated in Fig. 10-1b. This analysis framework consists of three main components:

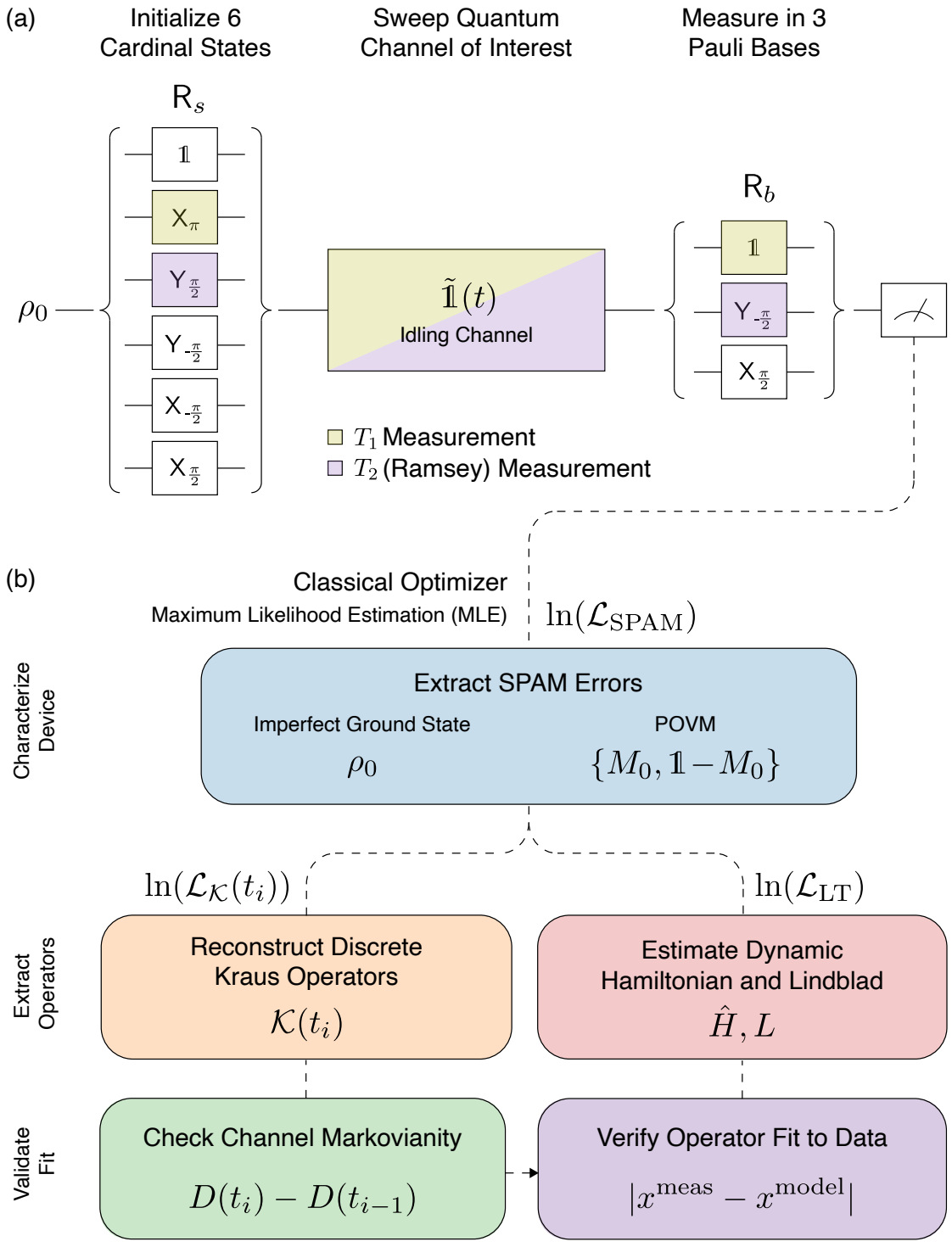
(a)
Initialize 6 Cardinal States
Sweep Quantum Channel of Interest
Measure in 3 Pauli Bases
R_s
R_b
ρ_0
$\tilde{\mathbb{1}}(t)$
Idling Channel
T_1 Measurement
T_2 (Ramsey) Measurement
(b)
Classical Optimizer
Maximum Likelihood Estimation (MLE)
$\ln(\mathcal{L}_{\mathrm{SPAM}})$
Characterize Device
Extract SPAM Errors
Imperfect Ground State
ρ_0
POVM
$\{M_0, \mathbb{1} - M_0\}$
$\ln(\mathcal{L}_{\mathcal{K}}(t_i))$
$\ln(\mathcal{L}_{\mathrm{LT}})$
Extract Operators
Reconstruct Discrete Kraus Operators
$\mathcal{K}(t_i)$
Estimate Dynamic Hamiltonian and Lindblad
$\hat{H}, L$
Validate Fit
Check Channel Markovianity
$D(t_i) - D(t_{i-1})$
Verify Operator Fit to Data
$|x^{\mathrm{meas}} - x^{\mathrm{model}}|$

Figure 10-1

Characterize Device: The data corresponding to the zero-duration channel $\tilde{\mathbb{1}}(t = 0)$ is fed into an MLE routine to determine the matrix elements of the initial density matrix ρ_0 and the positive operator-valued measures (POVMs) representing the imperfect measurement apparatus.

Extract Operators: Using the SPAM parameters found in the previous step, we independently estimate the Kraus operators which capture each discrete time (orange bubble in Fig. 10-1b) and the Hamiltonian and Lindblad operators which capture continuous time evolution (red bubble).

Validate Fit: Finally, we compare the results of the Kraus and Lindblad extractions in the previous step—running the former through a Markovianity metric and the latter through a standard error analysis—to determine whether the Markovian assumption holds.

Over the next few sections, we will walk through each of these analysis steps in detail and discuss how we perform the corresponding calculations. After that, we will look at the result of a first experimental demonstration of this technique on a pair of coupled superconducting transmon qubits, and we will show what Lindblad tomography reveals about the underlying physics of the device.

Figure 10-1: Single-qubit Lindblad tomography (LT) protocol. **(a)** The sequence of measurements required for single-qubit LT. The qubit is prepared in its imperfect ground state ρ_0 and one of six single-qubit pre-pulses R_s is applied to rotate the qubit as close as possible to each cardinal state of the Bloch sphere; free evolution of the quantum system is swept; and one of three post-pulses R_b is applied to rotate the measurement axis into each Pauli basis. **(b)** Analysis protocol for LT. Results from all combinations of pre-/post-pulses and channel durations are passed to a classical optimizer based on maximum likelihood estimation (MLE). SPAM errors due to imperfect ground state preparation and measurement infidelity are extracted from data at $t = 0$, and the results are used to separately estimate: (left path) the Kraus operators $\mathcal{K}(t_i)$ for each discrete channel duration t_i and channel Markovianity using the trace distance D between pairs of states; (right path) the Hamiltonian $\hat{H}$ and Lindblad matrix L for continuous time t, where the operator fit to data is evaluated using the average error between the measurement outcomes predicted by the operators (x^{model}) and data (x^{meas}).

10.3 Extracting SPAM Errors

As we discussed earlier, accurate interpretation of quantum tomography results requires thorough understanding of the SPAM errors at play in the device being characterized. This makes intuitive sense: if process tomography relies on a set of well-understood input states and orthogonal measurement axes in order to piece together the input-output relationship of the process, we better be able to reliably prepare those input states and accurately measure along the necessary axes. To confirm that this is indeed the case, we must first characterize the SPAM errors in our device and compensate for them accordingly. In the derivation which follows, we will consider the protocol for characterizing a single-qubit state, and we will then discuss how this protocol naturally extends to multi-qubit systems.

To reconstruct the most likely SPAM errors in our device, we start by defining a simple maximum likelihood function

$$\mathcal{L}_{\text{SPAM}} = (p_0)^f \times (p_1)^{\bar{f}}. \tag{10.1}$$

Here, p_0 and p_1 are the probabilities of measuring the qubit in the $|0\rangle$- and $|1\rangle$-states, respectively, and f and $\bar{f}$ are the number of recorded measurements of the qubit in either $|0\rangle$ and $|1\rangle$ after a series of many repeated measurements. Now, experimentally we do not have direct access to the underlying probabilities p_0 and p_1, just as we do not have access to the quantum mechanical wavefunction. However, we do have access to f and $\bar{f}$ since these are just the number of random outcomes we get when we measure our qubit in the z-basis. Using only these recorded outcomes and the equation in Eq. (10.1), we can numerically estimate the most likely underlying probabilities: given the measurement outcomes f and $\bar{f}$, the most likely underlying probabilities can be found by numerically maximizing the function $\mathcal{L}_{\text{SPAM}}$ with respect to p_0 and p_1.

Now, these probabilities alone do not tell us anything about our SPAM errors. But we know that these probabilities come from somewhere: namely, from the expectation

value of a quantum state ρ with some measurement operator M, exactly as we showed back in Chapter 2. Let us then redefine these probabilities as

$$p_0 \equiv \mathrm{Tr}[\rho_0 M_0] \tag{10.2}$$

$$p_1 \equiv \mathrm{Tr}[\rho_0 M_1] \tag{10.3}$$

where ρ_0 is a general single-qubit density matrix corresponding to the (potentially imperfect) initial state of our protocol

$$\rho_0 = \begin{bmatrix} a & b \\ b^* & 1-a \end{bmatrix} \tag{10.4}$$

and the operators M_0 and M_1 are the positive operator-valued measures (POVMs) corresponding to (again, potentially imperfect) measurement of the states $|0\rangle$ and $|1\rangle$, respectively

$$M_0 = \begin{bmatrix} m_0 & m_1 \\ m_1^* & m_2 \end{bmatrix} \tag{10.5}$$

$$M_1 = \mathbb{1} - M_0. \tag{10.6}$$

In the absence of SPAM errors, the initial state ρ_0 will correspond to the ground state of the qubit and the POVMs will correspond to accurate measurement of the states $|0\rangle$ and $|1\rangle$

$$\rho_0 = \begin{bmatrix} 1 & 0 \\ 0 & 0 \end{bmatrix} \tag{10.7}$$

$$M_0 = \begin{bmatrix} 1 & 0 \\ 0 & 0 \end{bmatrix} \tag{10.8}$$

$$M_1 = \begin{bmatrix} 0 & 0 \\ 0 & 1 \end{bmatrix}. \tag{10.9}$$

To quantify the deviation of our device from this ideal, let's plug the probabilities

in Eqs. (10.2) and (10.3) into the maximum likelihood function in Eq. (10.1)

$$\mathcal{L}_{\text{SPAM}} = \text{Tr}[\rho_0 M_0]^f \times \text{Tr}[\rho_0 M_1]^{\bar{f}}. \tag{10.10}$$

Now, we're getting somewhere! Looking at this equation, we can now say that given the measurement outcomes f and $\bar{f}$, the most likely SPAM parameters can be found by numerically maximizing the function $\mathcal{L}_{\text{SPAM}}$ with respect to the unknown matrix elements of the density matrix in Eq. (10.4) and the POVM in Eq. (10.5).

We can say this, but we would be wrong. Looking at Eq. (10.10), we can see that this function is sorely underdetermined: given the two measurement outcomes f and $\bar{f}$, it is impossible to accurately reconstruct the five independent matrix elements we need to determine our initial state and POVMs. Thankfully, however, LT naturally gives us a lot of data to play with. Looking back at the measurement protocol in Fig. 10-1a, we see that we actually have 18 different sets of results to work with when $\tilde{\mathbb{1}}(t=0)$, corresponding to all of the different combinations of pre- and post-pulses in our tomography sequence.

So let's add these sequences to our maximum likelihood equation. Looking at Eq. (10.10), we can expand this equation into a product over all combinations of initial states $s \in \{|0\rangle, |1\rangle, |+\rangle, |-\rangle, |+i\rangle, |-i\rangle\}$ and measurement axes $b \in \{z, x, y\}$

$$\mathcal{L}_{\text{SPAM}} = \prod_{b,s} \left(\text{Tr}[\rho_s M_b]^{f(s,b)} \times \text{Tr}[\rho_s (\mathbb{1} - M_b)]^{\bar{f}(s,b)} \right) \tag{10.11}$$

where ρ_s is the rotated ground state generated from application of one of the six pre-rotations R_s

$$\rho_s = \mathsf{R}_s \rho_0 \mathsf{R}_s^\dagger, \tag{10.12}$$

M_b is the POVM corresponding to measuring $|0\rangle$ in Pauli basis b

$$M_b = \mathsf{R}_b M_0 \mathsf{R}_b^\dagger, \tag{10.13}$$

and the scalars $f(s,b)$ and $\bar{f}(s,b)$ are the number of recorded measurement outcomes

'0' and '1' recorded during repeated measurements of state ρ_s in measurement basis b. Looking at Eq. (10.11), we see that this maximum likelihood function is now overdetermined, and we can now maximize this function over the full set of rotations to find the unknown matrix elements of ρ_0 and M_0, fully capturing the SPAM errors of the device. To make this function easier to optimize over, it is convenient to take the natural logarithm of the likelihood function and turn in to a log-likelihood function

$$\ln(\mathcal{L}_{\text{SPAM}}) = \sum_{b,s} \left(f(s,b) \ln(\text{Tr}[\rho_s M_b]) \times \bar{f}(s,b) \, \text{Tr}[\rho_s (\mathbb{1} - M_b)] \right). \tag{10.14}$$

Having taken the logarithm of $\mathcal{L}_{\text{SPAM}}$, our task is now to minimize $\ln(\mathcal{L}_{\text{SPAM}})$ with respect to the unknown SPAM parameters, which in practice is a better behaved optimization problem.

Now, in general, we have carefully avoided one thorny issue. Looking at either Eq. (10.11) or (10.14), we have made a tacit assumption that the rotations R_s and R_b are the unitary matrices we believe they are. However, these rotations correspond to physical gate operations, and the fiducial gates required to initialize the cardinal states and rotate the measurement basis cannot be assumed to be error free. In order to fully characterize these operations, one would therefore have to parameterize these gates as arbitrary rotation matrices and estimate them together with the POVM and initial state parameters, in much the same way as in gate set tomography [240]. However, in Lindblad tomography, we significantly simplify the analysis by excluding the effects of imperfect rotation from our estimation. Here, our motivation is twofold. First, we note that, for many NISQ-era devices across hardware modalities, errors due to imperfect measurement and ground state preparation exceed single-qubit gate errors. Second, since our ultimate goal is to characterize the idling channel over several multiples of the qubit's T_1 and T_2 times (tens of microseconds for superconducting qubits, in comparison to tens of nanoseconds to implement a single-qubit gate), the channel errors are naturally amplified relative to the errors in the fiducial gates, regardless of their intrinsic magnitude (in much the same way as in GST and RB). Furthermore, while ignoring the contribution of these errors typically introduces the

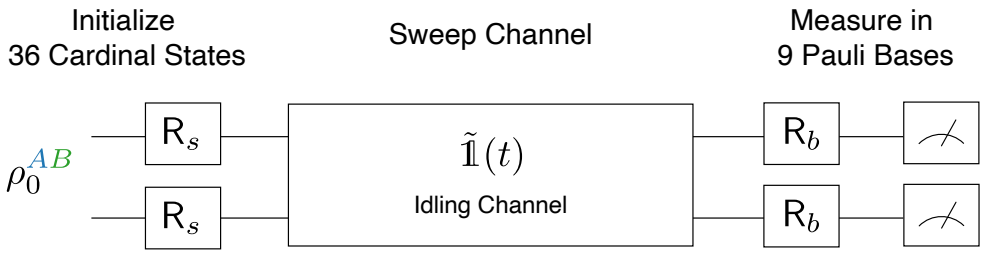

Figure 10-2: Two-qubit Lindblad tomography measurement protocol. The two qubits A and B are initialized into their shared ground state ρ_0^{AB} and prepared in each of 36 combinations of cardinal states; the channel of interest is swept; the qubits are rotated into each of nine combinations of Pauli bases and measured. The full set of measurement results are passed through the same classical optimizer as in the single-qubit protocol, SPAM errors are extracted, and the instantaneous process maps and dynamic operators are estimated using MLE.

issue of gauge freedom, we note that errors in the idling channel are first-order gauge invariant (FOGI), and the contribution of errors in the fiducial gates can be safely ignored in this scenario [58, 60, 330]. We also note that randomized benchmarking, which is not influenced by SPAM errors, can be performed prior to LT to obtain an independent estimate of the rotation pulse errors, as we will disuss later in this chapter in our presentation of experimental results.

Finally, we note that this technique for characterizing SPAM naturally extends to multi-qubit systems, as does the rest of LT. For two qubits A and B, we can represent the initial state as a general two-qubit density matrix ρ_0^{AB}, and we characterize the measurement apparatus using four 4×4 POVM matrices $\{M_{00}, M_{01}, M_{10}, M_{11}\}$, corresponding to measurement of the states $|00\rangle$, $|01\rangle$, $|10\rangle$, and $|11\rangle$, respectively. To determine the matrix elements of the initial state and the POVMs, we maximize a log-likelihood function analogous to Eq. (10.14), but now containing four terms for each combination of pre- and post-rotation (corresponding to measurement of each of the four two-qubit computational states) and summing over the full set of two-qubit pre- and post-pulses shown in Fig. 10-2.

10.4 Reconstructing the Kraus Operators at Discrete Times

Having characterized the SPAM errors for our device, we can now proceed to characterize the quantum channel of interest. Now, before we estimate the Lindbladian of the channel for continuous time t, we will first separately extract the instantaneous evolution maps of the channel at each discrete time step t_i, as in standard process tomography. As we will see, while this extraction is independent of the Lindblad estimation itself, the extraction of the instantaneous process maps will provide a means to separately confirm the the validity of the time-independent Markovian model.

As we showed in Chapter 9, any quantum operation can be described by a set of Kraus operators such that the final state is related to the initial state as

$$\rho = \sum_j \mathcal{K}_j \rho_0 \mathcal{K}_j^\dagger \tag{10.15}$$

where the Kraus operators $\{\mathcal{K}_j\}$ satisfy the condition $\sum_j \mathcal{K}_j^\dagger \mathcal{K}_j = \mathbb{1}$ for a trace-preserving process. However, as we also discussed in our comparison of the different process representations in Chapter 9, note that the Kraus operators are only unique up to a unitary transformation: a quantum channel can be described by two different but equivalent sets of Kraus operators $\{\mathcal{K}_j\}$ and $\{\mathcal{K}'_k\}$, which will be related through a unitary matrix U such that $\mathcal{K}_j = \sum_k U_{jk} \mathcal{K}'_k$. To avoid this ambiguity, it is often helpful to resort to a process matrix representation of the channel χ, which is unique in a specified operator basis. However, since the process matrix can be readily calculated from the Kraus operators and vice versa, one can choose either description without loss of generality. In this demonstration, we chose to estimate the Kraus operators, however we note that we also used the same MLE approach to estimate the process matrix but found a slower convergence of the optimization compared to the Kraus estimation. We believe this is likely due to the unitary freedom in fixing the elements of the Kraus matrices. In what follows, we will therefore describe the estimation of

the Kraus operators.

To find the most likely Kraus operators which describe quantum channel at each discrete time step t_i, our task is once again to minimize a log-likelihood function based on the outcomes of repeated measurements f and $\bar{f}$. For the Kraus estimation, this function takes on a similar form to the one we used for the SPAM estimation in Eq. (10.14). Here, however, we are no longer constrained to the subset of data where $\tilde{\mathbb{1}}(t = 0)$, and our likelihood function now accounts for the state of the system at eachdiscrete time step $t_i \in [t_1, t_2, \ldots, t_N]$

$$\ln(\mathcal{L}_{\mathcal{K}}(t_i)) = \sum_{b,s} f(s,b,i) \ln\left(\mathrm{Tr}\left[\rho_s(t_i) M_b\right]\right) + \bar{f}(s,b,i) \ln\left(\mathrm{Tr}\left[\rho_s(t_i)(\mathbb{1} - M_b)\right]\right) \tag{10.16}$$

where the state $\rho_s(t_i)$ is now the discrete time evolution of the initial state ρ_s at time t_i under the evolution of the Kraus operators

$$\rho_s(t_i) = \sum_j \mathcal{K}_j(t_i) \rho_s \mathcal{K}_j^\dagger(t_i) \tag{10.17}$$

and the initial state ρ_s and POVM M_b are the matrices we already found during the SPAM estimation. Thus, given the measurement outcomes at each discrete time step $f(s,b,i)$ and $\bar{f}(s,b,i)$, the most likely process maps which describe the action of the channel at each time step can be found by minimizing the function $\ln(\mathcal{L}_{\mathcal{K}}(t_i))$ in Eq. (10.16) with respect to the matrix elememnts of the unknown Kraus operators $\{\mathcal{K}_j(t_i)\}$. As with the SPAM characterization, this protocol generalizes naturally to multi-qubit systems, where the dimension and number of the unknown Kraus operators scales with the size of the system.

10.5 Qualitatively Validating the Markovian Model

Having obtained the Kraus operators for each discrete time step of the channel, we can use this information to provide qualitative insight into whether or not the

measured quantum channel can be fit to a Markovian model (left path in Fig. 10-1b). To accomplish this, we will implement the measure proposed in Ref. [74], which quantifies the backflow of information from the environment characteristic of non-Markovian error [279, 485]. This measure is particularly suitable for the purposes of validating Lindblad tomography because it considers the noise process over time, in contrast to instantaneous measures such as the one proposed in Ref. [471]. We note that other non-Markovianity measures exist that also consider the noise process over time and that may provide complementary information about the nature of non-Markovianity [380]. However, for the purpose of simply assessing the validity of the Markovianity assumption of LT, the measure of Ref. [74] is sufficient.

As we previously discussed in Section 9.5, the measure of Breuer et al. [74] exploits the following fact: for any quantum process which can be captured by a time-dependent master equation of the form

$$\dot{\rho}(t) = -\frac{i}{\hbar}[\hat{H}(t), \rho(t)] + \sum_i \gamma_i(t) \left(\hat{L}_i(t)\rho(t)\hat{L}_i^\dagger(t) - \frac{1}{2}\{\hat{L}_i^\dagger(t)\hat{L}_i(t), \rho(t)\} \right) \tag{10.18}$$

with positive decay rates $\gamma_i(t) > 0$, the trace distance $D(\rho_1(0), \rho_2(0))$ between two initial states $\rho_1(0), \rho_2(0)$ can only decrease. Here, $\hat{H}(t)$ and $\{\hat{L}_i(t)\}$ are the time-dependent Hamiltonian and jump operators of the process.

Since non-Markovian processes cannot be captured by a time-dependent master equation of the form in Eq. (10.18), an increasing trace distance between two states under the evolution of a common channel signifies violation of Eq. (10.18) and thus the presence of non-Markovian errors. Based on this observation, the measure N_{markov} is suggested in Ref. [74] as

$$N_{\text{markov}} = \max_{\rho_1(0),\rho_2(0)} \int_{\sigma>0} \sigma(t, \rho_1(0), \rho_2(0))dt \tag{10.19}$$

where $\sigma(t, \rho_1(0), \rho_2(0)) = \frac{d}{dt}D(\rho_1(t), \rho_2(t))$. In other words, we integrate the derivative of the trace distance between a pair of states over all time intervals where the derivative is positive (i.e., trace distance increasing). Thus, the larger the value of

N_{markov}, the more non-Markovian the channel. However, we note that the quantitative value of N_{markov} can be ambiguous, since the value is unbounded and extremely sensitive to experimental noise in individual data points. As such, rather than treat N_{markov} as a quantitative metric, we instead treat it as a qualitative metric, plotting the trace distance as a function of the channel duration and looking for sustained periods of increasing trace distance. We then complement this observation with a rigorous quantitative analysis of the error between the operator predictions and data, as discussed further in Section 10.7

10.6 Extracting the Lindbladian

So far, we have shown how to extract the Kraus operator description of the channel at each discrete time step, and we have used this information to assess the Markovianity of the channel. Now, if the channel is Markovian, we can proceed to the main thrust of Lindblad tomography: the tomographic reconstruction of the Lindblad operators describing the channel for continuous time t (right path in Fig. 10-1b). If, on the other hand, the channel is non-Markovian, one will be unable to find a set of operators which describe the data, since non-Markovian processes cannot be fit to a master equation. However, note that the Markovianity measure employed in Section 10.5 only tells if the process can be captured by a general master equation with a time-dependent Lindbladian, and it does not guarantee that the assumption of a time-*independent* Lindbladian is fulfilled. As such, comparison between the Markovinaity metric and the fit of the extracted Lindbladian allows us to qualitatively distinguish between three possibilities:

1. **The channel is Markovian and described by a time-independent Lindbladian.** In this case, the extracted operators fit the data and the Markovianity measure will show a monotonically decreasing trace distance between pairs of states.

2. **The channel is non-Markovian.** In this case, the extracted operators poorly

fit the data and the Markovianity measure will show clear periods of increasing trace distance.

3. **The channel is Markovian but not described by a time-independent Lindbladian.** In this case, the extracted operators poorly fit the data while the Markovianity measure shows a monotonically decreasing trace distance between pairs of states. The appearance of this phenomenon may also indicate failure in the MLE optimization itself, and additional analysis is required to confirm that the poor fit is physically meaningful.

For a time-independent Lindbladian, the master equation from Eq. (10.18) simplifies to

$$\dot{\rho} = -\frac{i}{\hbar}[\hat{H}, \rho] + \sum_{i=1}^{d^2-1} \gamma_i (\hat{L}_i \rho \hat{L}_i^\dagger - \frac{1}{2}\{\hat{L}_i^\dagger \hat{L}_i, \rho\}). \tag{10.20}$$

Choosing an operator basis $\{\sigma_i\}$ consisting of a Hilbert-Schmidt orthogonal set of traceless Hermitian operators in dimension d (which can be constructed from tensor products of single-qubit Pauli matrices and the identity), the master equation can be rewritten as

$$\dot{\rho} = -\frac{i}{\hbar}[\hat{H}, \rho] + \sum_{i,j=1}^{d^2-1} L_{ij} (\sigma_i \rho \sigma_j^\dagger - \frac{1}{2}\{\sigma_j^\dagger \sigma_i, \rho\}) \tag{10.21}$$

where L_{ij} is a Hermitian and positive semidefinite matrix capturing the incoherent evolution, commonly referred to as *the Lindblad matrix*.

Similar to the relationship between the process matrix χ and the Kraus operators discussed in Section 10.4, the Lindblad matrix is unique while the jump operators have a unitary freedom: the Lindblad equation in Eq. (10.20) is invariant under a unitary transformation of the jump operators and decay rates. In particular, a new set of jump operators and decay rates $\{\sqrt{\gamma_i'}\hat{L}_i'\}$ can be constructed from the set $\{\sqrt{\gamma_j}\hat{L}_j\}$ as $\sqrt{\gamma_i'}\hat{L}_i' = \sum_j U_{ij}\sqrt{\gamma_j}\hat{L}_j$, where U is a unitary matrix. Since the Lindblad matrix can readily be obtained from the decay rates and jump operators (and vice versa), one can choose either representation without loss of generality. In the following analysis, we choose to directly estimate the Lindblad matrix, and we derive the jump operators by diagonalizing this matrix. Specifically, a (unique) set of jump operators can be

obtained by diagonalizing the Lindblad matrix as

$$\hat{L}_i = \sum_{j=1}^{d^2-1} U_{ij}\sigma_j \tag{10.22}$$

where U is a unitary matrix such that $L = U\mathbb{D}U^\dagger$, where $\mathbb{D} = \text{diag}(\gamma_1, \gamma_2, \ldots, \gamma_{d-1})$ is a diagonal matrix with the decay rates.

To estimate the most likely Hamiltonian and Lindblad matrix which describe the continuous action of the quantum channel for all time t, we once again construct a log-likelihood function. However, unlike the MLE function for extracting the Kraus operators in Eq. (10.16), we must now account not only for all combinations of initial states and measurement axes, *but also for all channel durations.* We therefore seek to maximize a log-likelihood function over all time steps t_i

$$\ln(\mathcal{L}_{\text{LT}}) = \sum_{i=1}^{N} \ln(\mathcal{L}(t_i)) \tag{10.23}$$

where the likelihood function at each discrete time $\ln(\mathcal{L}(t_i))$ is defined as in Eq. (10.16)

$$\ln(\mathcal{L}_{\mathcal{K}}(t_i)) = \sum_{b,s} f(s,b,i) \ln\left(\text{Tr}\left[\rho_s(t_i)M_b\right]\right) + \bar{f}(s,b,i) \ln\left(\text{Tr}\left[\rho_s(t_i)(\mathbb{1} - M_b)\right]\right), \tag{10.24}$$

except that we no longer write the state $\rho_s(t_i)$ as the discrete evolution of the initial state ρ_s using the Kraus operators $\rho_s(t_i) = \sum_i \mathcal{K}_i \rho_s \mathcal{K}_i^\dagger$. Instead, we now find $\rho_s(t_i)$ by numerically solving the master equation in Eq. (10.21) for each guess at the elements of the Hamiltonian and the Lindblad matrices, where we evaluate the master equation at each time step t_i by numerical exponentiation of the Lindbladian. As with the SPAM and Kraus estimation, a Cholesky decomposition is used to ensure that the Lindblad matrix is positive semidefinite.

10.7 Error and χ^2 Analysis

Once the most likely Lindbladian has been extracted, we evaluate the results of the optimization by calculating the error between the predictions of the operators and data. For each time step, the error for a given set of initial state and measurement axis is computed as

$$\text{error}(t_i) = \left| x_i^{\text{meas}} - x_i^{\text{model}} \right| \tag{10.25}$$

where x_i^{meas} is the measurement probability obtained in experiment at time step t_i and x_i^{model} is the corresponding estimate from the outcome of the MLE routine. The error is then averaged over time steps, and the average error for a given combination of initial state and measurement axis is reported.

In addition, the p-value of the operator fit can be similarly calculated using a χ^2 analysis of the extracted operators and data. In statistics, the χ^2 test quantifies how likely it is that the data could have been produced by an assumed model known as the null hypothesis. In LT, our null hypothesis is the assumption that the data is well fit by a time-independent Markovian master equation. The χ^2 value is then computed as

$$\chi^2(t_i) = \sum_{j=1}^{k} \frac{(x_{i,j}^{\text{meas}} - x_{i,j}^{\text{model}})^2}{x_{i,j}^{\text{model}}} \tag{10.26}$$

with the same definitions of x^{meas} and x^{model} as in Eq. (10.25). However, unlike in the error calculation, we must also sum over the the total number of categories $k = 2^n$ that the n-qubit data can fall into: 2 for the single-qubit data ('0' or '1'), 4 for the two-qubit data ('00', '01', '10', or '11').

Under the null hypothesis, the deviation between x_i^{observed} and x_i^{expected} is normally distributed due to the central limit theorem, and it is well known that (given a large enough sample size) the χ^2 statistic follows the χ^2-distribution with $k-1$ degrees of freedom [101]. Intuitively, the larger the value of χ^2, the greater the discrepancy

between the observed and expected values. For any value of χ^2, the χ^2-distribution can then be used to compute the probability that a value at least as extreme might have been obtained, which is known as the p-value. If one finds a particularly small p-value, then one should consider rejecting the null hypothesis on the grounds that the assumed model is not very likely to have actually produced the observed data. Whether one accepts or rejects the null hypothesis is determined by a threshold p-value (commonly denoted as α), which is chosen in advance of analyzing the data. This threshold is set arbitrarily and simply expresses how conservative one would like to be when deciding to reject the null hypothesis, trading off false positives for false negatives as the threshold is set lower and lower. In our case, we will refrain from choosing a specific α and let the data speak for itself, noting that higher p-values indicate data that is more compatible with a Markovian assumption, while lower values suggest deviation between the Markovian model and data.

In the experimental demonstration of Lindblad tomography which follows, we compute the average error and p-value over time, for each combination of initial state and measurement basis. The p-value is computed from the χ^2 distribution with one degree of freedom to account for the two different measurement outcomes (three independent degrees of freedom for the two-qubit data, $k-1$ in general). Since the different outcomes are not inherently included in the calculation of the error, we also average over the different outcome types when calculating error. Since we are calculating the error between two probabilities, the error is bounded between 0 and 1. The p-value is inherently bounded between 0 (bad fit) and 1 (exact fit). Under the null hypothesis, the p-values should actually be uniformly distributed due to statistical error, and so an average p-value of around 0.5 indicates very close agreement with the null-hypothesis. We emphasize that in all cases, whenever the expected probabilities are small, the relative error and the p-value will both suffer even if the fit is qualitatively quite good.

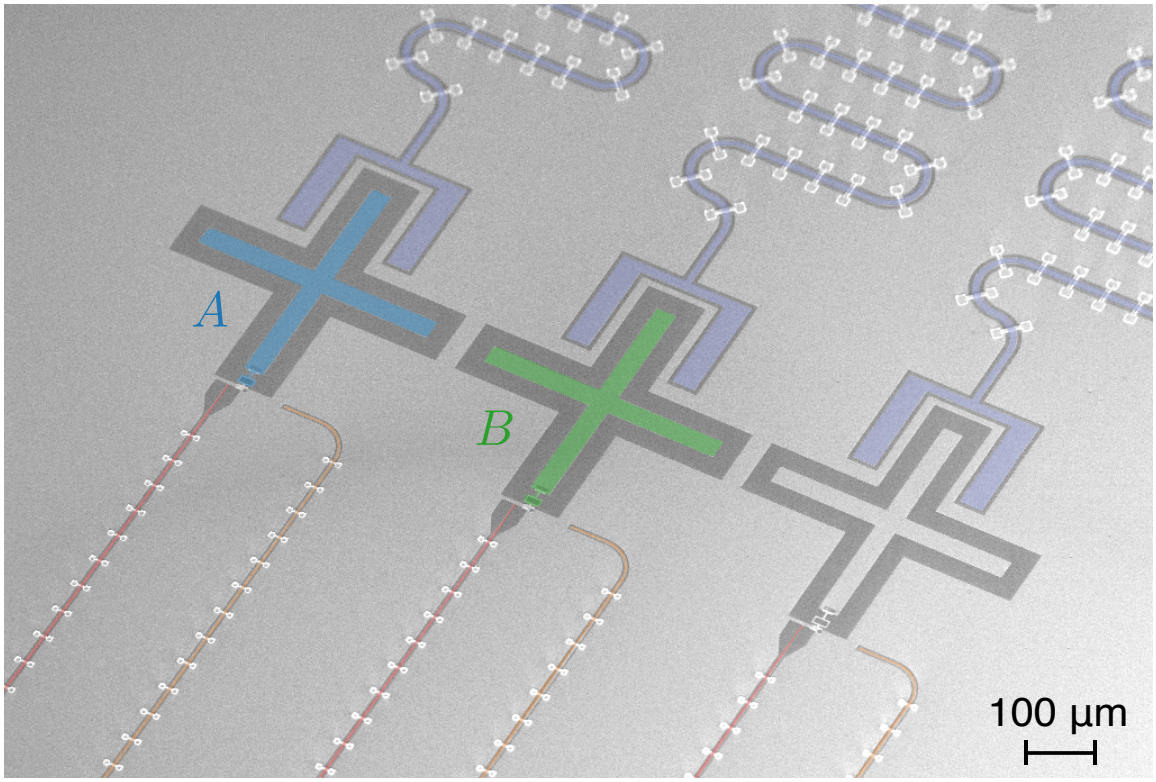

Figure 10-3: SEM image of an identically fabricated copy of the device characterized in this work, consisting of three capacitively coupled superconducting flux-tunable transmon qubits arranged in a linear chain. For this initial proof-of-principle demonstration of single- and two-qubit Lindblad tomography, we chose to consider only the left and middle qubits of the chain, which we label qubits A and B, respectively. The rightmost qubit is far detuned to its frequency minimum and left to idle in its ground state for the duration of the characterization protocol.

10.8 Experimental Demonstration of Lindblad Tomography

So far, our discussion of Lindblad tomography has been entirely theoretical. For the remainder of this chapter, we will discuss what happens when you apply this protocol to a physical device in the laboratory. As a first demonstration of Lindblad tomography, we implemented this protocol on the same three-qubit device we studied extensively in Part III, which consists of three capacitively coupled superconducting flux-tunable transmon qubits arranged in a linear chain (Fig. 10-3). For this initial proof-of-principle demonstration of single- and two-qubit Lindblad tomography, we

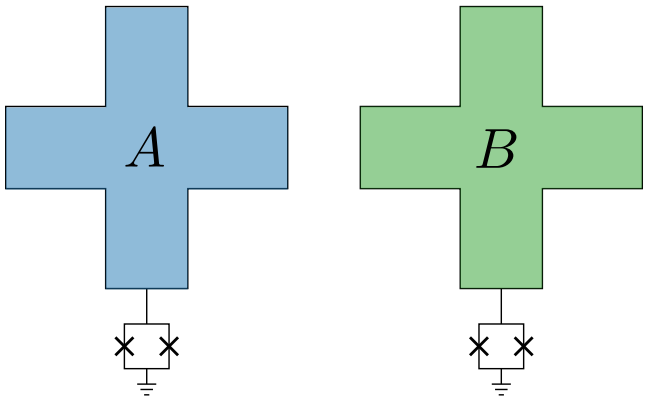

Figure 10-4: Schematic of the two coupled transmon qubits characterized in this experiment, corresponding to the left and middle qubits in the three-qubit chain in Fig. 10-3.

Parameter	Qubit A	Qubit B
Idling Frequency, $\omega_i/2\pi$	4.744GHz	4.222GHz
Anharmonicity, $\eta/2\pi$	-175MHz	-190MHz
Coupling Strength, $g/2\pi$	12MHz	
Junction Asymmetry	1:5	1:10
Single-qubit Gate Time	30ns	30ns
Readout Resonator Frequency, $\omega_r/2\pi$	7.252GHz	7.285GHz
Energy Relaxation Time, T_1	26μs	35μs
Ramsey Decay Time, T_2	25μs	24μs

Table 10.1: Device parameters for the two qubits characterized in this work. Reported values of T_1 and T_2 are found by fitting the raw data from the corresponding subsets of the single-qubit LT sequence (highlighted gates in Fig. 10-1a, no pulses applied to the neighboring qubits) and recording the decay time of the fit, consistent with standard experimental convention. LT generalizes this technique by extracting the decay channel from the full set of initial states, measurement axes, and channel durations.

chose to consider only the left and middle qubits of the chain, which we label qubit A and B, respectively. The rightmost qubit is far detuned to its frequency minimum and left to idle in its ground state for the duration of the characterization protocol. Significant device parameters for qubits A and B are noted in Table 10.1. For many of the figures which follow, we will schematically represent the two coupled transmon qubits A and B in cartoon form, as in Fig. 10-4.

10.8.1 SPAM Characterization

Running Lindblad tomography on this device, our first task is to extract the SPAM errors, as discussed in Section 10.3. We do this two ways: first, estimating the SPAM errors for each qubit individually using the data collected from single-qubit LT, and then for the combined two-qubit system using two-qubit LT. In both cases, the maximization of the log-likelihood function was performed using MATLAB's built-in function `fmincon`, which is a gradient-based numerical optimizer for constrained nonlinear problems. To avoid a situation where optimizer gets stuck in local minima, multiple starting points were tried to find a good approximation of the global minimum, which we accomplished by sampling random POVMs and initial states as starting points. For both estimations, we sampled over 10^4 different starting points. To constrain the space of the search, we restricted the search space of the optimization to be within some deviation of perfect POVMs and zero temperature thermal initial state, varying this allowed deviation until a global minimum was found. In particular, we found that restricting the initial thermal population of the $|1\rangle$-state to be smaller than 5% resulted in the most successful results, a constraint which is consistent with estimation of the effective device temperature for the two transmon qubits in a dilution refrigerator at a base temperature of 11mK [223].

For the single-qubit estimation of qubit A, we used data where the neighboring qubit B was kept in the ground state and measured in the z-basis such that no pulses were applied to qubit B during the measurement (and vice versa for estimation of qubit B). The POVMs found from the maximization are

$$M_0^A = \begin{bmatrix} 0.870 & 0.00 + 0.015i \\ 0.00 - 0.015i & 0.168 \end{bmatrix} \tag{10.27}$$

$$M_0^B = \begin{bmatrix} 0.880 & -0.004 - 0.031i \\ -0.004 + 0.031i & 0.165 \end{bmatrix} \tag{10.28}$$

indicating that there are significant measurement errors on the order of 10–20%. The

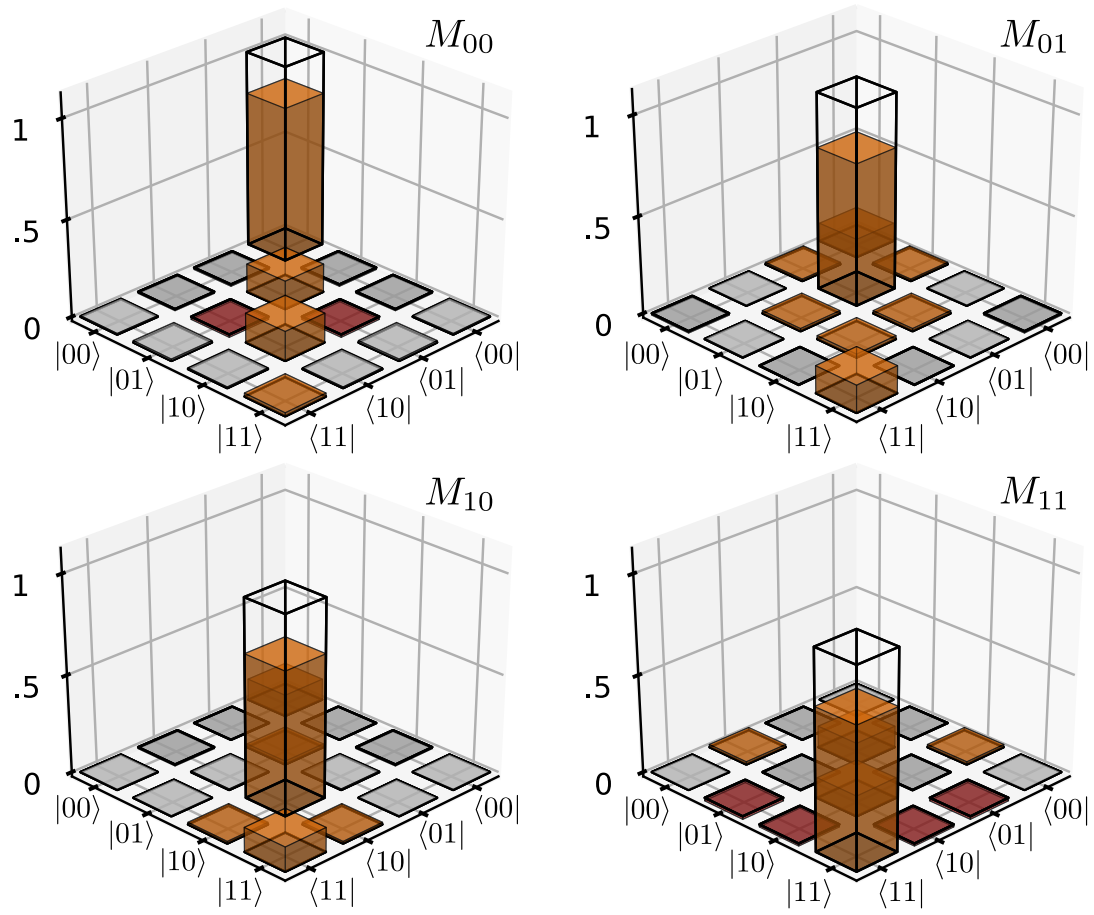

Figure 10-5: Extracted two-qubit POVMs, corresponding to imperfect measurement of the states $|00\rangle$, $|01\rangle$, $|10\rangle$, and $|11\rangle$, respectively (negative values shown in red, perfect POVMs shown in wireframe, imaginary parts and elements smaller than 10^{-2} omitted for visual clarity).

estimated initial states are

$$\rho_0^A = \begin{bmatrix} 0.999 & -0.002 - 0.005i \\ -0.002 + 0.005i & 0.001 \end{bmatrix} \tag{10.29}$$

$$\rho_0^B = \begin{bmatrix} 0.998 & 0.009 - 0.04i \\ 0.009 + 0.04i & 0.002 \end{bmatrix}. \tag{10.30}$$

For the combined two-qubit system, we found the following POVM elements (illus-

trated in Fig. 10-5)

$$M_{00} = \begin{bmatrix} 0.7920 & -0.010 - 0.019i & -0.008 + 0.010i & 0.006 - 0.002i \\ -0.010 + 0.019i & 0.146 & -0.014 + 0.000i & 0.010 - 0.004i \\ -0.080 - 0.010i & -0.014 + 0.000i & 0.151 & 0.006 - 0.007i \\ 0.006 + 0.002i & -0.010 + 0.004i & 0.006 + 0.007i & 0.018 \end{bmatrix} \tag{10.31}$$

$$M_{01} = \begin{bmatrix} 0.095 & 0.010 + 0.014i & 0.002 + 0.002i & -0.009 + 0.002i \\ 0.010 - 0.014i & 0.726 & 0.014 + 0.002i & 0.003 + 0.004i \\ 0.002 - 0.002i & 0.014 - 0.002i & 0.018 & -0.004 - 0.002i \\ -0.009 - 0.002i & 0.003 - 0.004i & -0.004 + 0.002i & 0.130 \end{bmatrix} \tag{10.32}$$

$$M_{10} = \begin{bmatrix} 0.110 & 0.00 + 0.002i & -0.008 - 0.009i & 0.002 - 0.003i \\ 0.000 - 0.002i & 0.017 & 0.006 - 0.010i & 0.002 - 0.001i \\ -0.008 + 0.009i & 0.006 + 0.010i & 0.727 & 0.011 - 0.001i \\ 0.002 + 0.003i & 0.002 + 0.001i & 0.011 + 0.001i & 0.124 \end{bmatrix} \tag{10.33}$$

$$M_{11} = \begin{bmatrix} 0.002 & 0.000 + 0.003i & 0.014 - 0.003i & 0.001 + 0.003i \\ 0.000 - 0.003i & 0.111 & -0.005 + 0.007i & -0.015 + 0.001i \\ 0.013 + 0.003i & -0.005 - 0.007i & 0.104 & -0.013 + 0.010i \\ 0.001 - 0.003i & -0.015 - 0.001i & -0.013 - 0.010i & 0.718 \end{bmatrix} \tag{10.34}$$

and an initial two-qubit state (illustrated in Fig. 10-6)

$$\rho_0^{AB} = \begin{bmatrix} 0.992 & -0.001 + 0.000i & 0.000 + 0.000i & 0.000 - 0.001i \\ -0.001 + 0.000i & 0.004 & 0.001 - 0.002i & 0.000 + 0.003i \\ 0.000 + 0.000i & 0.001 + 0.002i & 0.001 & -0.001 + 0.000i \\ 0.000 + 0.001i & -0.003i & -0.001 + 0.000i & 0.003 \end{bmatrix}. \tag{10.35}$$

As we discussed in Section 10.3, in general we would need to account for imperfections in the single-qubit gates used to initialize our state and rotate our measurement axis. However, as we note, Lindblad tomography is resilient to errors in the single-qubit fiducial gates R_s and R_b required for state preparation and measurement axis rotation, and we can safely exclude these errors from our model. Nonetheless, we can in-

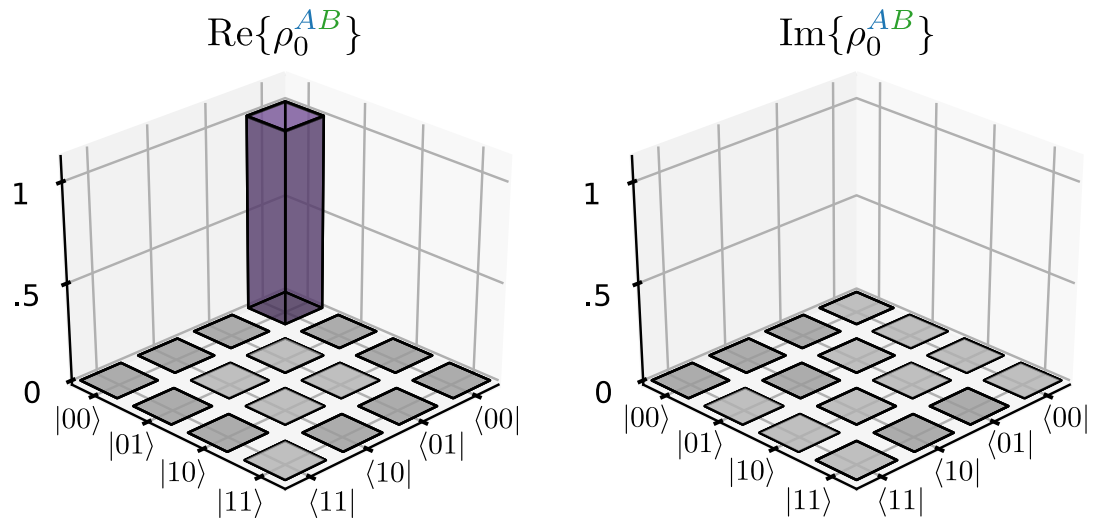

Figure 10-6: Skyscraper plots of the imperfect two-qubit ground state ρ_0^{AB} extracted during two-qubit LT (ideal ground state shown in wireframe, elements smaller than 10^{-2} omitted for visual clarity).

dependently characterize these rotations by performing Interleaved Clifford Randomized Benchmarking (IRB) on the full set of single-qubit gates $\mathsf{R} \in \{\mathbb{1}, \mathsf{X}_{\pi}, \mathsf{Y}_{\pm\frac{\pi}{2}}, \mathsf{X}_{\mp\frac{\pi}{2}}\}$ required to run Lindblad tomography on each qubit. For each of these operations, we record fidelities in excess of 99.9%—over an order of magnitude greater than the fidelity observed for state initialization or measurement—indicating that errors in the single-qubit rotations have negligible impact on state-initialization and POVM estimation in comparison to imperfect thermalization and measurement error.

Having extracted the SPAM parameters of our device, we can briefly pause to analyze these prelminary results and see what they tell us about our device. Looking at the extracted initial states in Eq. (10.29) and (10.30), we note that the initial single-qubit states are very similar to thermal states of the form

$$\rho_{\text{thermal}} = a\,|0\rangle\langle 0| + (1-a)\,|1\rangle\langle 1| \tag{10.36}$$

where $a \in [0, 1]$. Minimizing the trace distance $D(\rho_{\text{thermal}}, \rho_0)$ between the estimated initial states and a thermal state with respect to the thermal parameter a, we find minimal trace distances $D(\rho_{\text{thermal}}, \rho_0^A) = 0.01$ $(D(\rho_{\text{thermal}}, \rho_0^B) = 0.04)$ for $a = 0.999$

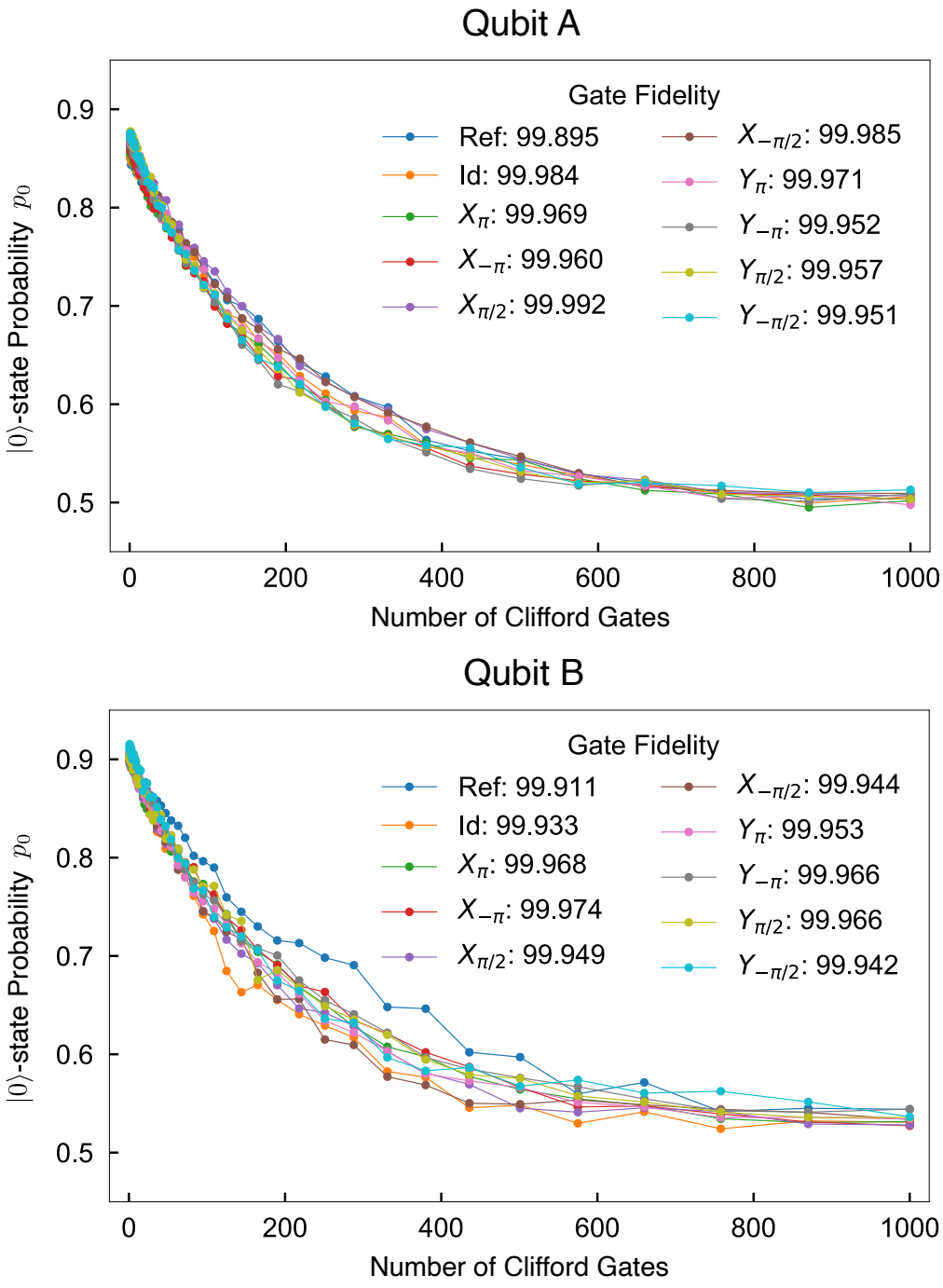

Figure 10-7: Single-qubit reference and interleaved Clifford randomized benchmarking. Characterization of nine single-qubit gates performed on qubit A and B, with Clifford reference fidelity ('Ref') and interleaved gate fidelities recorded in the legend. This set includes all the gates required for state preparation (R_s) and measurement axis rotation (R_b), and each of these gates exceeds an interleaved RB fidelity of 99.9%.

($a = 0.998$). This result is thus consistent with the observation that the imperfect ground state of a superconducting qubit at finite temperature can be approximated as a thermal state of an anharmonic oscillator [257].

Now, traditionally the SPAM errors for a single qubit in a multi-qubit device would be found by characterizing the qubit while all its neighbors are left in their ground states. This would imply that, to use the device characterized here as an example, the manipulation and readout of qubit B should have no effect on the POVM and initial state of qubit A. The extent to which this holds can be tested by comparing the estimated single-qubit POVMs and initial states for both qubits with the joint two-qubit POVM and initial state estimated using full two-qubit LT. The deviation between the estimated single- and two-qubit POVMs can be quantified as the trace distance $D(M_{xy}, M_x \otimes M_y)$, where M_x (M_y) are the estimated single qubit POVMs for qubit A (B), M_{xy} is a two-qubit POVM, and $x, y \in \{0, 1\}$. Doing so, we find a trace distance of 0.04 for $xy = 00, 01, 10$ and 0.05 for $xy = 11$. As for the deviation between the single- and two-qubit initial states, the trace distance between the estimated initial two-qubit state ρ_0^{AB} and the product state $\rho_0^A \otimes \rho_0^B$ constructed from the single-qubit estimates is found to be $D(\rho_0^{AB}, \rho_0^A \otimes \rho_0^B) = 0.05$. Comparing the initial two-qubit state ρ_0^{AB} to a product of single-qubit thermal states (see above), we find a trace distance of 0.01 for thermal populations $a = 0.998$ (qubit A) and $a = 0.994$ (qubit B).

10.8.2 Single-Qubit Kraus and Lindblad Extraction

Having characterized the SPAM errors for both the single- and two-qubit channels, we can now proceed to tomographically reconstruct the channel. To start, we will consider the results of single-qubit LT applied to qubit A, reconstructing the single-qubit idling channel of qubit A using both the Kraus and Lindblad formalisms. To perform the Kraus and Lindblad optimizations, we maximized their respective log-likelihood function using MATLAB's built-in functions `fmincon` and `fminsearch`. For the Kraus optimization, `fmincon` was used in order to enforce the constraint of a trace-preserving map and, as with the SPAM characterization, the interior-point

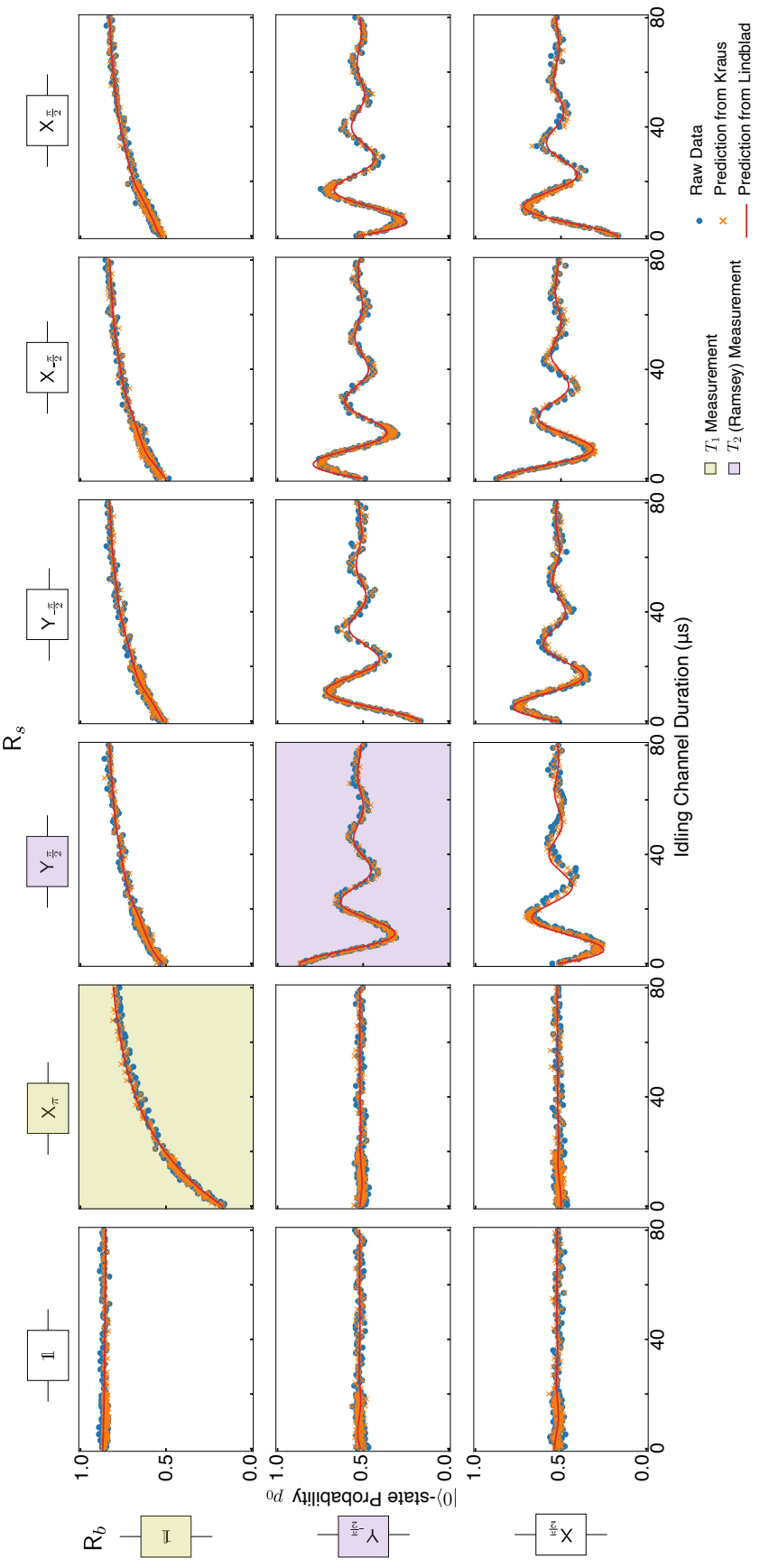

Figure 10-8: Single-qubit LT results for the full set of initial states and measurement bases, performed on qubit A while qubit B is its ground state. The purple T_2 plot is the same used in Fig. 10-10. We emphasize that, while standard T_1 and T_2 metrics are determined by simply fitting the measurement results of a single set of pre- and post-pulses (pale green or purple, respectively), the Kraus operators (orange) and Lindbladian (red) here are determined from the full set of 18 measurement sequences (36 initial states $\times$ 9 measurement bases = 324 sequences for two-qubit LT).

algorithm was used. As an initial point of the optimization, we used Kraus operators corresponding to an identity channel to estimate the Kraus operators of the first time step, where the evolution from the initial state is presumed to be small. The resulting estimate was then used as starting point for the next time step and this procedure was iterated for the whole time series. As for the Lindblad estimation, all physically constraints of the evolution could be ensured by employing a Cholesky decomposition of the Lindblad matrix and using the Hermiticity of the Hamiltonian to reduce the number of free parameters. The optimization therefore allowed for an unconstrained optimizer, and we used the `fminsearch` optimizer of MATLAB, which uses the gradient-free simplex search method of Ref. [259]. As initial starting point for the optimization, we used the Lindblad matrix corresponding to pure dephasing and (zero-temperature) amplitude damping for the single qubit Lindblad estimation.

In Fig. 10-8, we show the results of extracting the single-qubit Kraus operators and most likely Lindbladian for qubit A of our superconducting transmon device, superposed over the raw data obtained at each time step for all eighteen combinations of pre- and post-rotation. Here, blue dots show the raw measurement probability p_0, averaged from 1000 single-shot measurements of the final state $\rho_s(t_i)$; orange $\times$'s show the predicted outcome of an imperfect measurement M_b of the state $\rho_s(t_i)$, estimated by applying the extracted Kraus operators to the extracted imperfect initial state ρ_s as in Eq. (10.17); and the solid red line traces out the predicted measurement results for the continuous evolution of qubit A over all times t, as predicted by the most likely Hamiltonian and Lindblad matrices. As such, the red line and orange $\times$'s not only capture the channel noise but also account for the estimated SPAM errors of our device.

Performing this optimization over all eighteen sets of pre- and post-pulses and all time steps, we find that the mostly likely jump operators for the single-qubit noise

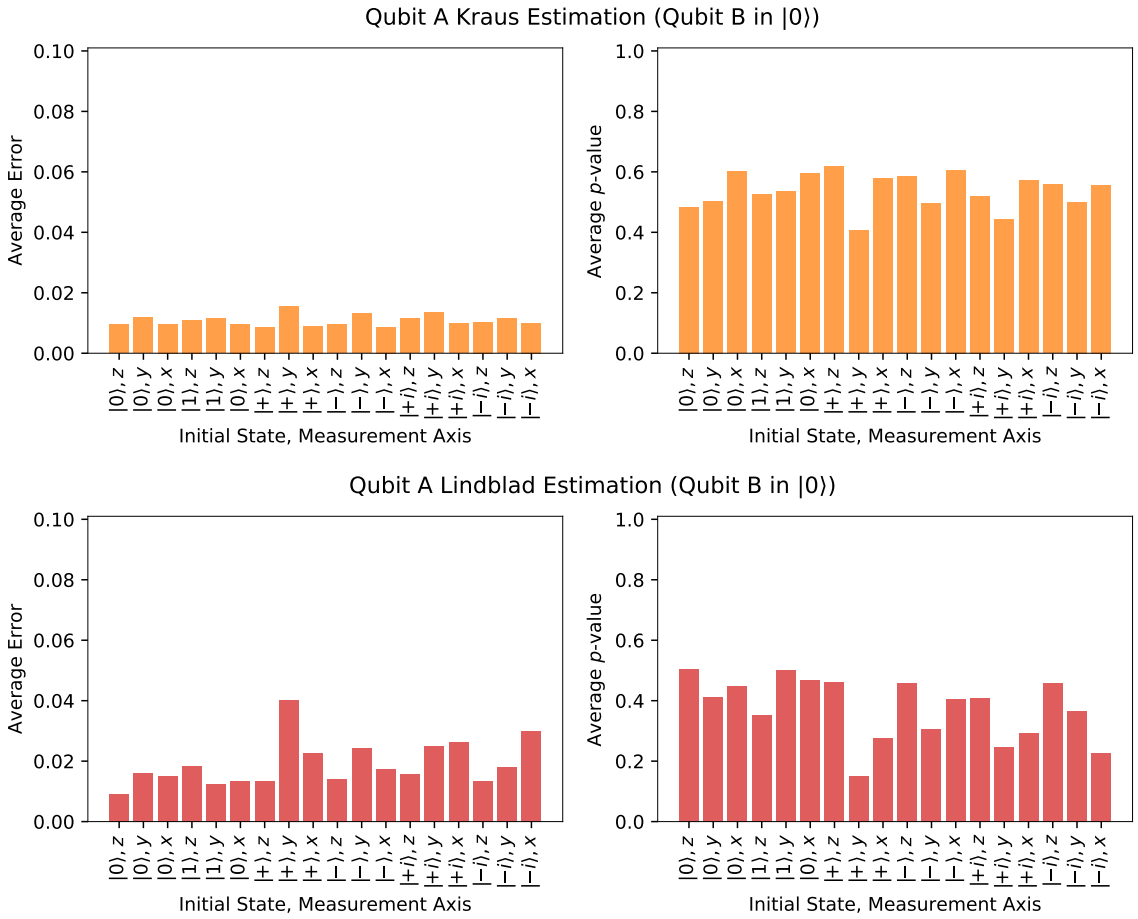

Figure 10-9: Error analysis of the extracted single-qubit Kraus (orange) and Lindblad (red) operators for qubit A when qubit B is in $|0\rangle$. The error and p-value between the data and the estimated operators are calculated for each time step, initial state, and measurement axis of qubit A, and the results are averaged over the first $20\mu s$.

channel of qubit A are

$$\hat{L}_1 = \begin{bmatrix} -0.551 - 0.052i & 0.030 - 0.622i \\ 0.030 - 0.010i & 0.551 + 0.052i \end{bmatrix} \tag{10.37}$$

$$\hat{L}_2 = \begin{bmatrix} 0.438 - 0.019i & 0.144 + 0.757i \\ 0.144 - 0.042i & -0.438 + 0.019i \end{bmatrix} \tag{10.38}$$

with decay rates $\gamma_1 = 0.029$ MHz and $\gamma_2 = 0.037$ MHz, respectively. Looking at the corresponding red traces in Fig. 10-8, we note that these operators generally fit the data well, and the average error and p-values of all the extracted operators are shown in Fig. 10-9.

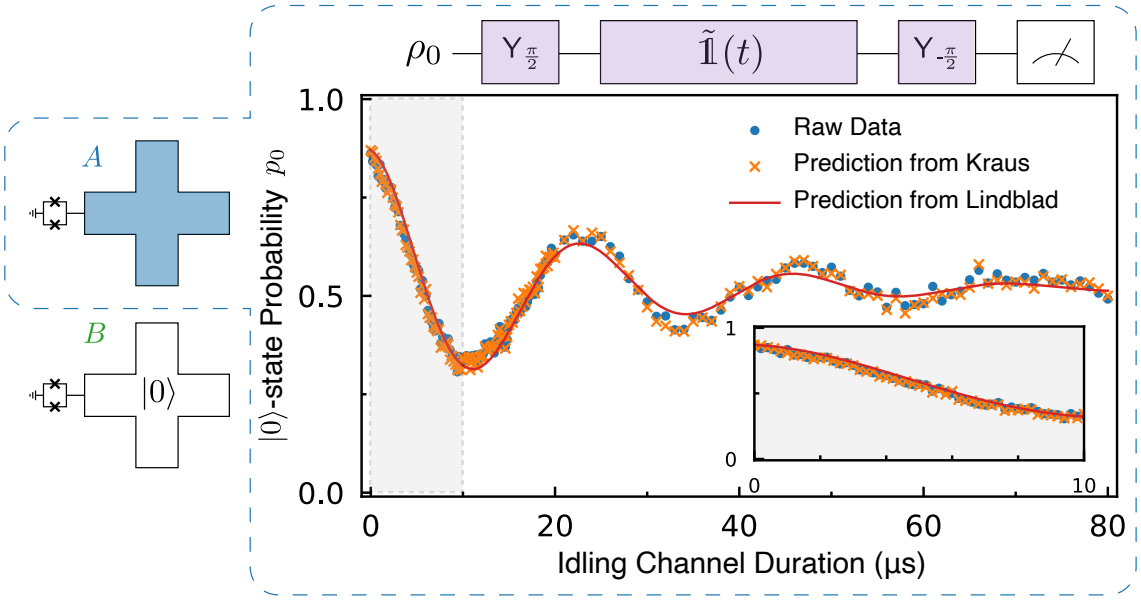

Figure 10-10: Lindblad tomography applied to the idling channel of a single superconducting transmon qubit. Data and analysis results for the LT sequence corresponding to a T_2 Ramsey measurement (purple gates in Fig. 10-1a), when the neighboring qubit is prepared near its ground state $|0\rangle$. Blue points are p_0 of the state $\rho_s(t_i)$, averaged from 1000 single-shot measurements (discussed in Section 10.3, fitted value of T_2 recorded in Table 10.1, shot noise $1/\sqrt{N} \sim 3\%$). Orange $\times$'s are predicted measurement outcomes obtained from applying the Kraus operators estimated at each discrete time t_i to the extracted initial state ρ_0 given an imperfect measurement M_0 (technique discussed in Section 10.4). Red line traces the predicted outcomes for continuous time t, based on the most likely time-independent Lindblad and Hamiltonian operators (technique discussed in Section 10.6, average error $= 2.25 \times 10^{-2}$). Results for the first 10μs are enlarged for clarity in inset.

However, looking at the full set of measurements, we note that there is some small disagreement between the Lindblad fits (red) and the data (blue) for sequences corresponding to T_2-type measurements. For example, we observe that the Lindblad fit slightly underestimates the decay time for the dataset when qubit A is prepared in $|+\rangle$ and measured in the x-basis (purple highlighted plot in Fig. 10-8). However, looking at this measurement in the context of the full matrix of pre- and post-pulses, we note small temporal fluctuations in the channel over the course of the data aquisition period, and we see that the Lindblad fit consequently overestimates the decay time of some traces relative to others. Since LT finds the single time-independent Lindblad operator which best describes *all* combinations of pre- and post-pulses, spurious

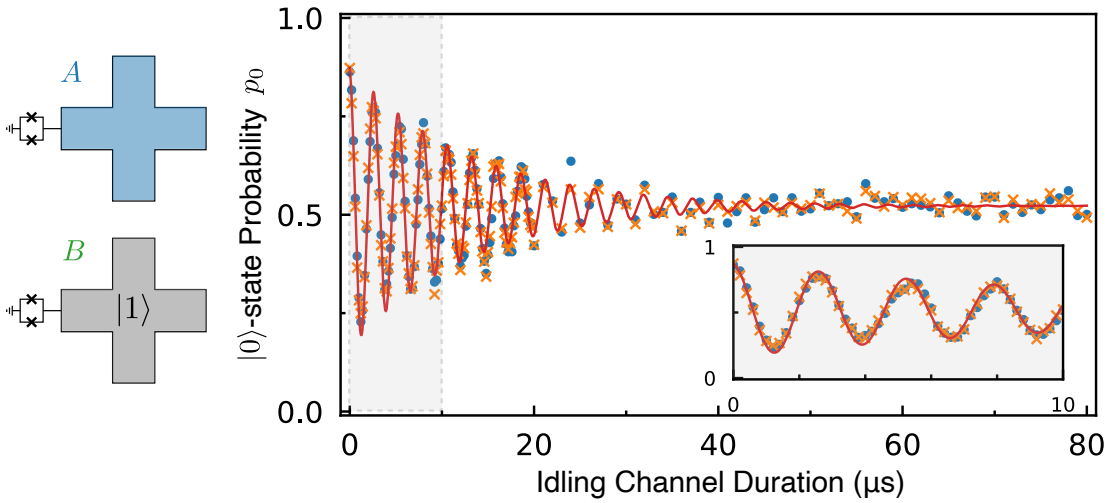

Figure 10-11: The same measurement as depicted in Fig. 10-10, now taken when the neighboring qubit is near its excited state $|1\rangle$ (most likely Lindbladian in red, average error $= 2.29 \times 10^{-2}$). The always-on ZZ-coupling between the two transmon qubits induces a state-dependent frequency shift when the neighbor is excited, which manifests here as a faster oscillation frequency.

temporal fluctuation in the channel during a small set of measurements constitutes a partial violation of the time-independent assumption of LT, and this fluctuation will affect the fit of the other datasets.

What happens when we change the state of qubit B? In the plots in Fig. 10-8, we chose to leave qubit B in its ground state during the tomography of A. In principle, this should not matter—if the two qubits are uncoupled from each other, then their combined Hamiltonian should be separable, and the evolution of qubit A should have no dependence of whatever we do to qubit B in the meantime. So let's test this. What happens when we alter the state of qubit B and repeat our characterization of A? To get some intuition for how this affects our characterization, let's just focus on one of the eighteen plots in Fig. 10-8, corresponding to a standard T_2 measurement of qubit A (purple hightlighted plot). In Fig. 10-10, we focus in on this plot, highlighting the state of qubit B during this measurement sequence. For this sequence, we find that the most likely Lindblad operators have an average error of 2.25×10^{-2} to data.

In Fig. 10-11, we show what happens when we repeat this exact same measurement, now putting qubit B into its $|1\rangle$-state while we characterize qubit A. One look

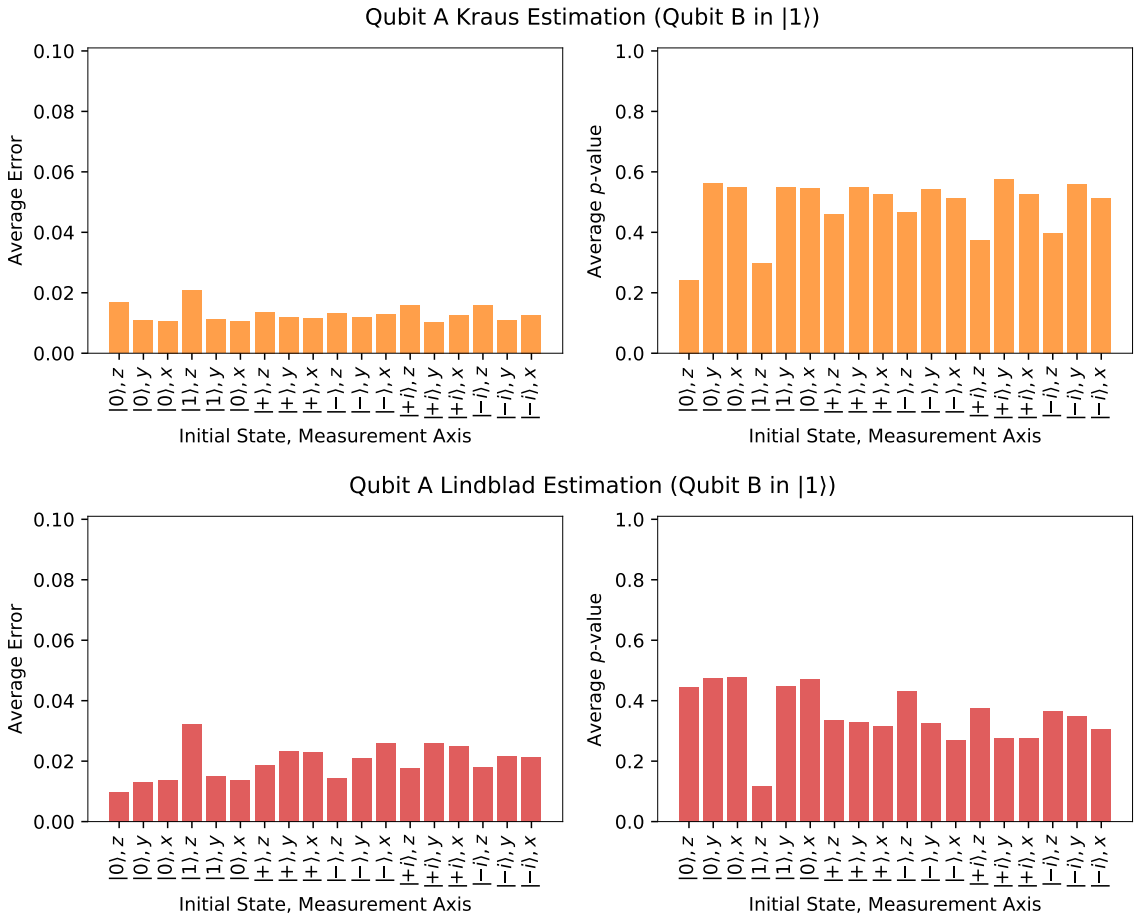

Figure 10-12: Error analysis of the extracted single-qubit Kraus (orange) and Lindblad (red) operators for qubit A when qubit B is in $|0\rangle$. The error and p-value between the data and the estimated operators are calculated for each time step, initial state, and measurement axis of qubit A, and the results are averaged over the first $20\mu s$.

at the raw data in this plot (blue), and it is immediately clear that the state of qubit B has a significant impact on the evolution of qubit A—the two qubits are not separable. Nonetheless, we can run LT on this data set and the other 17 combinations of pre- and post-pulses, extracting the most likely Kraus (orange) and Lindblad (red) operators which describe this evolution. Calculating the error of these operators to data (Fig 10-12), we find error values comparable to what we found when qubit B was in $|0\rangle$ (average Lindblad error $= 2.29 \times 10^{-2}$). Thus, while qubit B is clearly altering the state of A, the evolution of A remains well-described by a set of single-qubit jump operators.

What happens when we can repeat this measurement one more time, but now

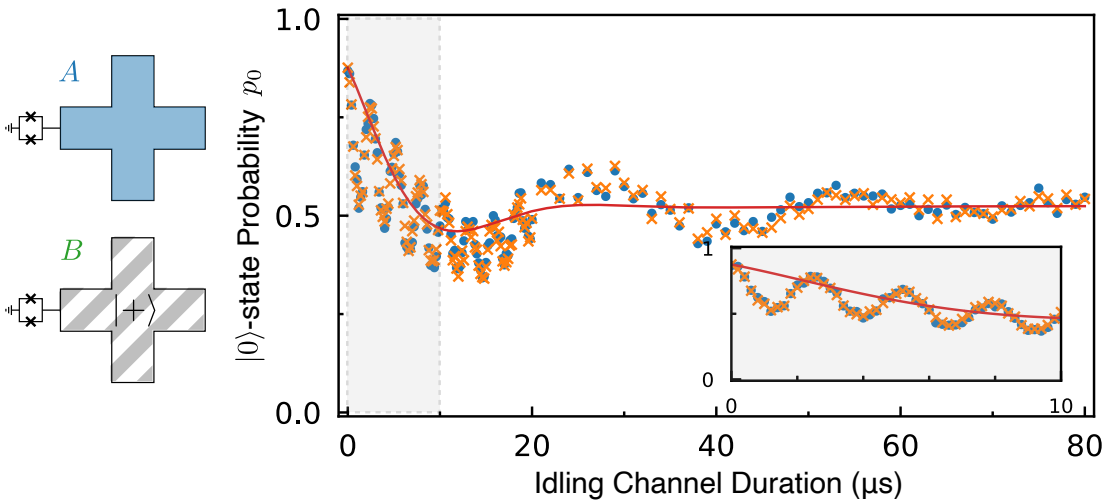

Figure 10-13: The same measurement as depicted in Figs. 10-10 and 10-11, now taken when the neighboring qubit is in a superposition state $|+\rangle$. In this basis, the always-on ZZ-coupling is an entangling operation, and the data is poorly predicted by the most likely single-qubit Lindbladian (red, average error $= 6.91 \times 10^{-2}$), a hallmark of non-Markovian evolution.

putting qubit B into the superposition state $|+\rangle$ during the characterization of A? Looking at the results of this measurement in Fig. 10-13, we see that once again the state of qubit B has modified the evolution of qubit A. And yet, running this data set through LT along with the other pre- and post-pulses, we find something remarkably different happens when we try to estimate the most likely Lindbladian. Looking at the red trace in Fig. 10-13, we see that the extracted Lindbladian fits the data extremely poorly, failing to capture the high-frequency oscillations observed in data (average Lindblad error $= 6.91 \times 10^{-2}$). This failure to fit the data is emphasized in the error analysis of the Lindblad operator for the remaining seventeen plots (Fig 10-14, bottom): while the estimated Lindbladian succeeds in fitting many of the constituent tomographic sequences (such as the sequences corresponding to T_1 measurements), the estimated Lindbladian systematically fails to fit the T_2-like sequences, resulting in notably higher error values and lower p-values.

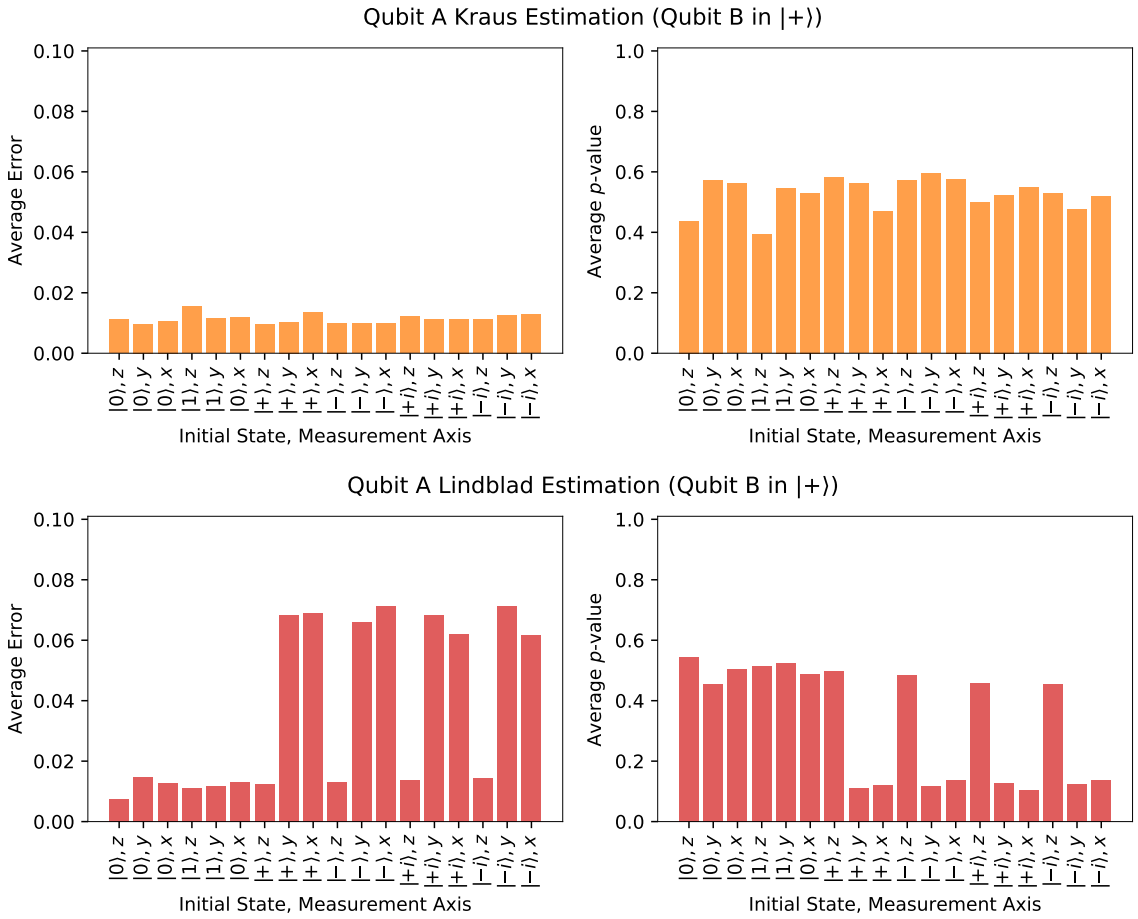

Figure 10-14: Error analysis of the extracted single-qubit Kraus (orange) and Lindblad (red) operators for qubit A when qubit B is in $|0\rangle$. The error and p-value between the data and the estimated operators are calculated for each time step, initial state, and measurement axis of qubit A, and the results are averaged over the first $20\mu s$. Note that now that qubit B is prepared in a superposition state, we observe dramatically worse Lindblad fits (i.e., larger errors and lower p-values) for the sequences corresponding to T_2-like measurements of qubit A, consistent with the poor Lindblad fit shown in Fig. 10-13. Meanwhile, the sequences corresponding to T_1-like measurements of qubit A (which are blind to the entanglement with qubit B) show comparatively good fits to data even when qubit B is in $|+\rangle$.

10.8.3 Single-Qubit Markovianity Check

To make sense of the Lindblad fits in Figs. 10-10, 10-11, and 10-13, we now consider the results of these data sets when we apply the Markovianity check we discussed in Section 9.5. Armed with the estimated Kraus operators for the single-qubit idling channels of qubit A, we perform the optimization in Eq. (10.19) over all of the initial

states of the LT protocol and calculate the measure N_{markov}.

In Fig. 10-15, we graphically illustrate N_{markov}—given here by the total area in red—for each of the configurations of qubit B shown in Figs. 10-10, 10-11, and 10-13. Notably, when qubit B is initialized in the state $|+\rangle$, the idling channel of qubit A registers clear periods of increasing trace distance (Fig. 10-15c). This behavior disappears when qubit B is initialized in either the $|0\rangle$- or $|1\rangle$-state (Fig. 10-15a,b, respectively): in these cases, increases in the trace distance appear to arise from isolated statistical fluctuations in the data, with the trace distance otherwise monotonically decreasing over the channel duration.

Comparing the poor Lindblad fit from Fig. 10-13 with the corresponding results of the Markovianity metric in Fig. 10-15c, we see that the failure of our fit is *not* the fault of the optimizer—a failure, that is, to find the right Lindbladian to fit the data. Instead, as we have discussed in Section 10.5 and 9.5, the Markovianity metric is alerting us to the presence of non-Markovian errors, errors which cannot be fit to *any* Lindbladian.

However, to see why these errors only appear when qubit B is prepared in $|+\rangle$ and not when it is prepared in $|0\rangle$ or $|1\rangle$, we need to interrogate more fully what qubit A and qubit B are doing to one another during their free evolution. Single-qubit results alone will not answer this, so let's run LT on the full two-qubit system and see what is really going on here.

10.8.4 Two-Qubit operator extraction and Markovianity

As we showed in Section 10.3, the estimation of the two-qubit Kraus and Lindblad operators follows from a straightforward generalization of the single-qubit LT protocol, as shown in Fig. 10-2. To characterize qubit A and B together, we must prepare the two qubits in each of the 36 combinations of single-qubit cardinal states and measure them in each of the 9 combinations of single-qubit Pauli bases, leading to a total of 324 different time-domain sequences we must optimize over to extract the most likely operators. Indeed, looking at the enormous jump in the number of required measurements for two-qubit LT in comparison to single-qubit LT, it is easy to see that

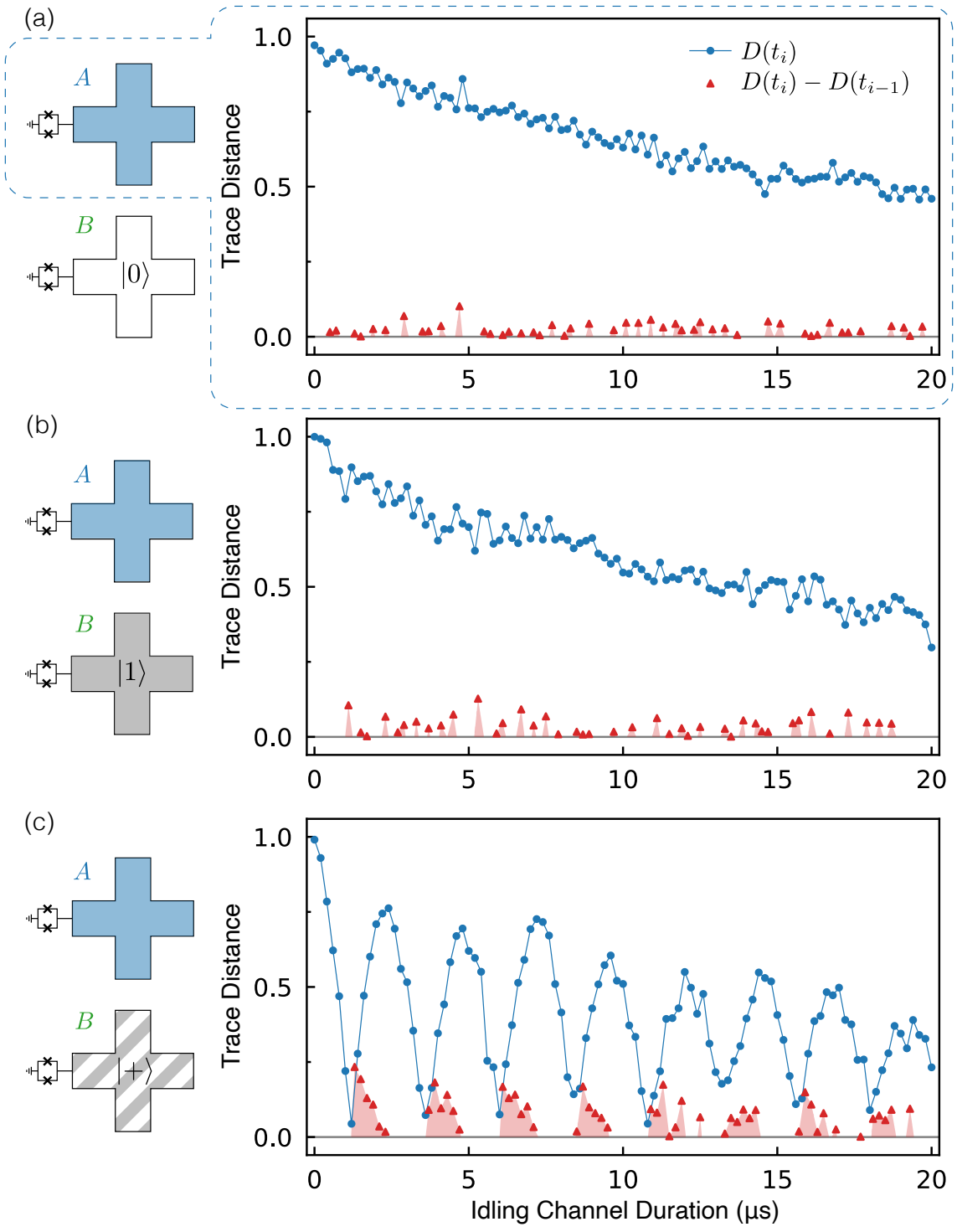
(a)
A
B
|0⟩
(b)
A
B
|1⟩
(c)
A
B
|+⟩
Trace Distance
1.0
0.5
0.0
0
5
10
15
20
$D(t_i)$
$D(t_i) - D(t_{i-1})$
Idling Channel Duration (μs)

Figure 10-15

the resources required characterize an n-qubit system scales exponentially with the number of qubits—exactly as in process or gate set tomography—requiring 6^n initial states and 3^n measurement axes to fully reconstruct the dynamics of the system.

However, while full characterization of an arbitrarily large quantum processor with Lindblad tomography would prove physically impossible, two qubits are well within the realm of experimental practicality. Indeed, in Fig. 10-16, we show a subset of the results obtained for running LT on both qubit A and B, extracting the operators which best describe the two-qubit dynamics of the combined system. As in Figs. 10-10, 10-11, and 10-13, raw data are reported in blue, predictions from extracted Kraus operators in orange, and predictions from the mostly-likely Hamiltonian and Lindblad operators in red. Crucially, these four plots represent only four of the 324 tomographic sequences which go into the extraction of the operators, and the results of the two-qubit Kraus and Lindblad operators in these plots represent the consensus across all 324 tomographic sequences.

Having extracted the two-qubit operators, we can revisit the poor Lindblad fit we observed in Fig. 10-13. What happens when we repeat this exact same measurement, putting both qubit A and B in their $|+\rangle$-states and measuring them in the x-basis, but now reconstructing the combined two-qubit idling channel of their combined evolution? In Fig. 10-17, we show exactly that. Here, we apply an identical set of pre- and post-rotations as in Fig. 10-13, but now reporting the results of the most

---

Figure 10-15: Markovianity of the single-qubit idling channel. **(a–c)** Qualitatively comparing the measured Markovianity of qubit A's idling channel when qubit B is prepared in $|0\rangle$, $|1\rangle$, or $|+\rangle$ respectively. We find the two initial states of qubit A which together yield the largest value of N_{markov}, and we plot the trace distance D between these two states at each time t_i (blue points), as well as the difference in trace distance between sequential times (red triangles, values less than 0 omitted for visual clarity, since they do not contribute to N_{markov}). Summing the area under the red points amounts to the discrete version of Eq. (10.19), with sustained periods increasing trace distance indicating the presence of non-Markovian errors. When qubit B is prepared in $|+\rangle$ as in (c), we observe clear periods of increasing trace distance, suggesting the greatest presence of non-Markovian errors.

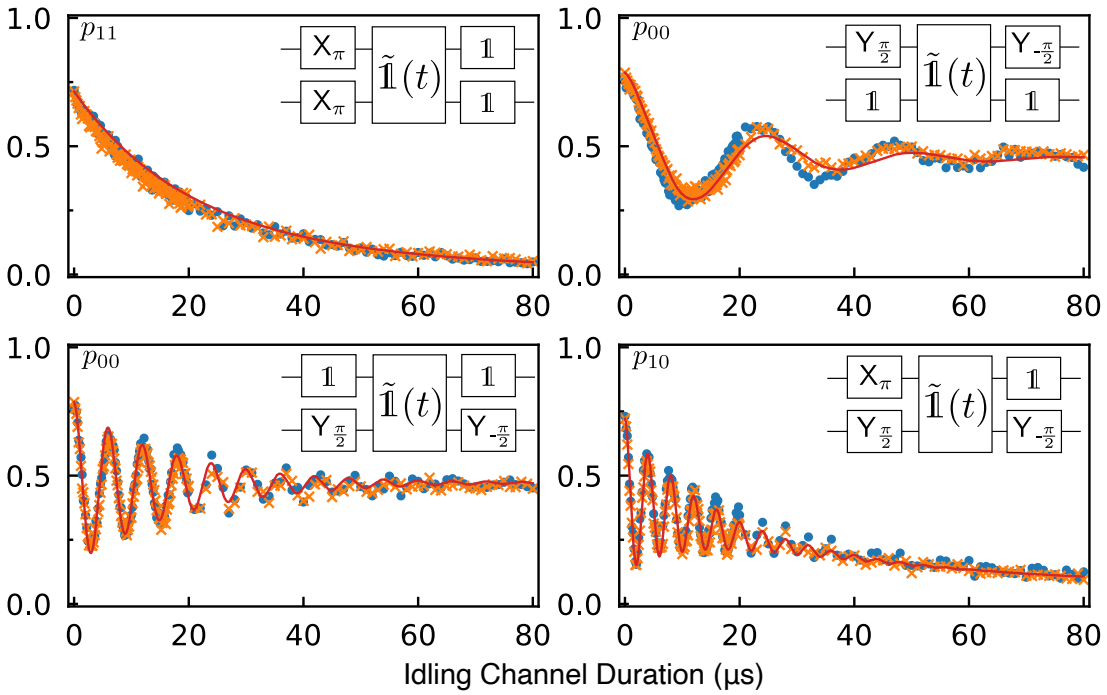

Figure 10-16: Two-qubit Lindblad tomography results for four of the 324 tomographic sequences characterized in two-qubit LT. Raw data are reported in blue, predictions from extracted two-qubit Kraus operators in orange, and predictions from the mostly-likely two-qubit Hamiltonian and Lindblad operators in red. Here, the most likely Kraus and Lindblad operators represent the consensus across all 324 tomographic sequences.

likely two-qubit Kraus and Lindblad operators which describe their joint evolution.

Looking at the fit of the two-qubit Lindbladian in Fig. 10-17, we see that estimated operators now fit the data significantly better than in Fig. 10-13 (average error = 2.15×10^{-2} for the two-qubit operators, in comparison to 6.91×10^{-2} for the single). This is not a fluke: in Figs. 10-18 and 10-19, we report the error of the Kraus and Lindblad extractions over all 324 tomographic sequences. Unlike in Fig. 10-14, we do not see systematically higher fitting errors for any subset of the LT sequences, indicating that the extracted operators fit all sequences with good success. Moreover, when we run the full set of two-qubit data through the Markovianity check, we find that no pair of two-qubit initial states demonstrates the oscillating trace distance seen so clearly in Fig. 10-15c. Looking at Fig. 10-20, where we show the pair of two-qubit states which yield the highest value of N_{markov}, we see that their relative trace

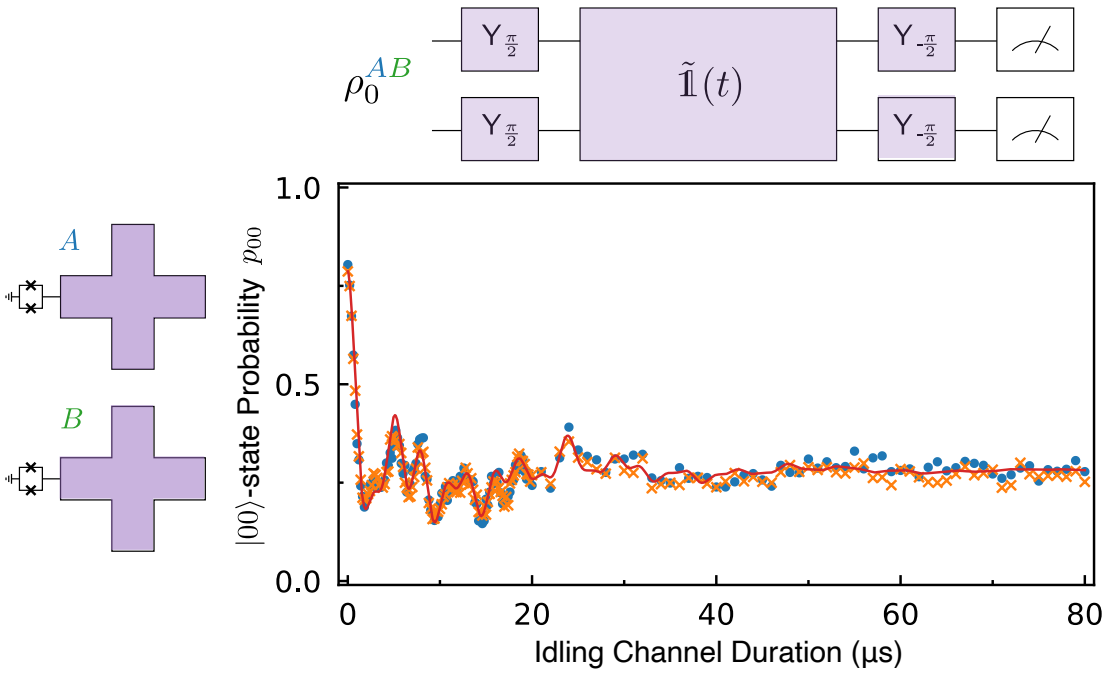

Figure 10-17: The same measurement as depicted in Fig. 10-13, but now interrogated using two-qubit LT. While the pulse sequence is identical to the one performed in the single-qubit characterization in Fig. 10-13, the data is now well-predicted by the most likely two-qubit Lindbladian (average error = 2.15×10^{-2}); this observation, paired with the result of the Markovianity metric shown in Fig. 10-20, suggests that the channel is Markovian in the two-qubit frame.

distance decreases monotonically in time during the two qubits' evolution. Comparing the error analysis in Fig.10-19 with the Markovianity check in Fig. 10-20, we conclude that the error is largely Markovian in the two-qubit picture.

10.8.5 Investigating the Non-Markovianity

How do we make sense of this result? How is it that the idling channel of qubit A was non-Markovian for certain states of qubit B, but Markovian when we account for qubit B in the full two-qubit picture. To get some intuition for what is going on in our device, we can look at the actual two-qubit operators which yielded the successful fits in Figs. 10-16 and 10-17. Running LT on the full set of two-qubit data, we estimate

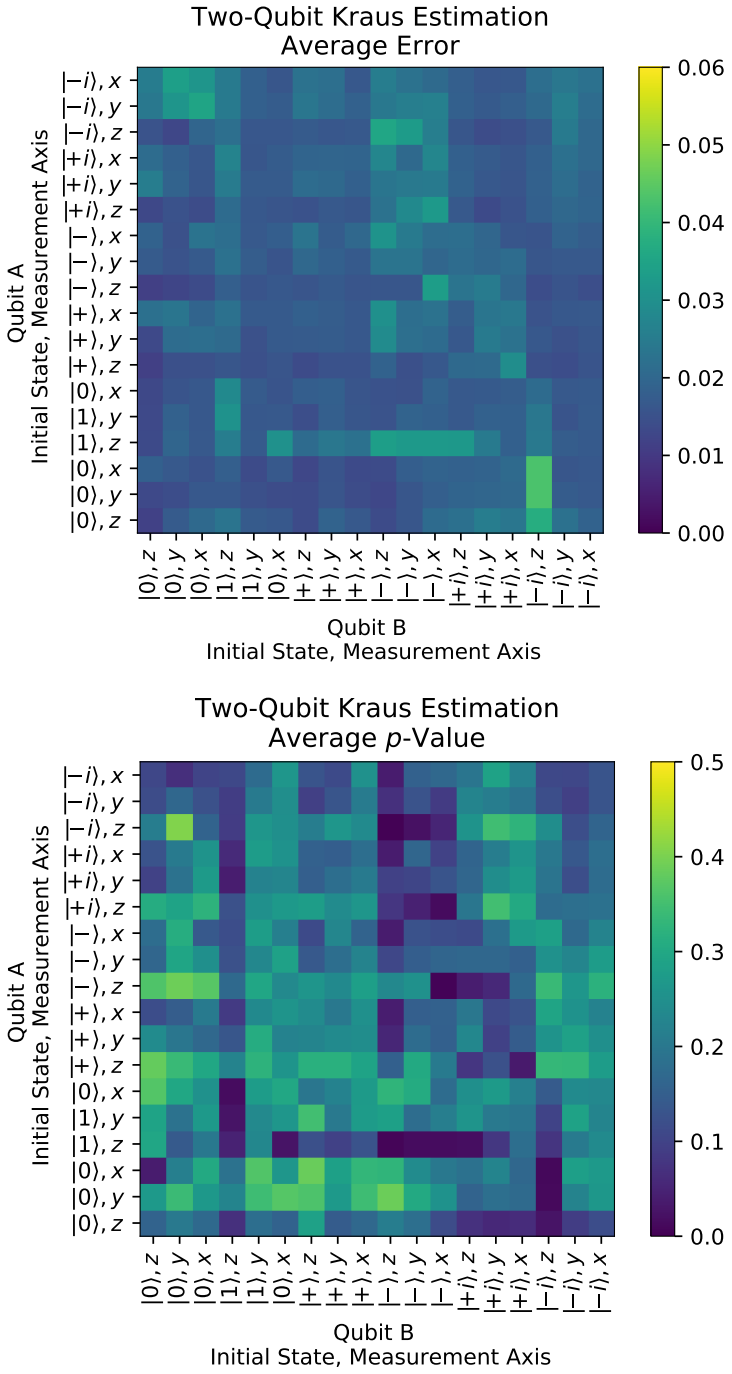

Figure 10-18: Analyzing the Kraus extraction of the two-qubit idling channel. The error and p-value between the data and the Lindblad estimation are calculated for each time step and qubit configuration (qubit A on y-axis, B on x-axis), and the results are averaged over the first $20\mu s$.

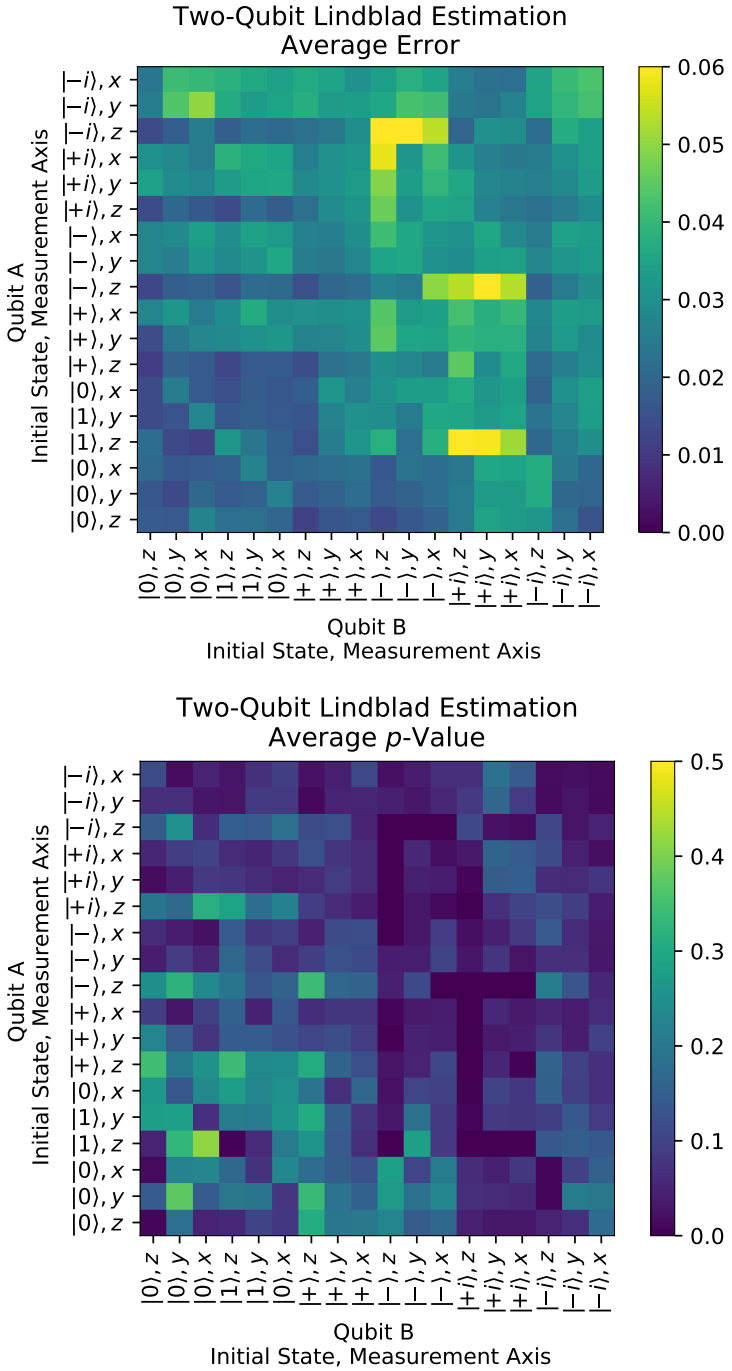

Figure 10-19: Analyzing the Kraus extraction of the two-qubit idling channel. The error and p-value between the data and the Lindblad estimation are calculated for each time step and qubit configuration (qubit A on y-axis, B on x-axis), and the results are averaged over the first $20\mu s$. Note that, unlike in Fig. 10-14, we do not see systematically higher fitting errors for any subset of the LT sequences, indicating that the extracted operators fit all sequences with good success.

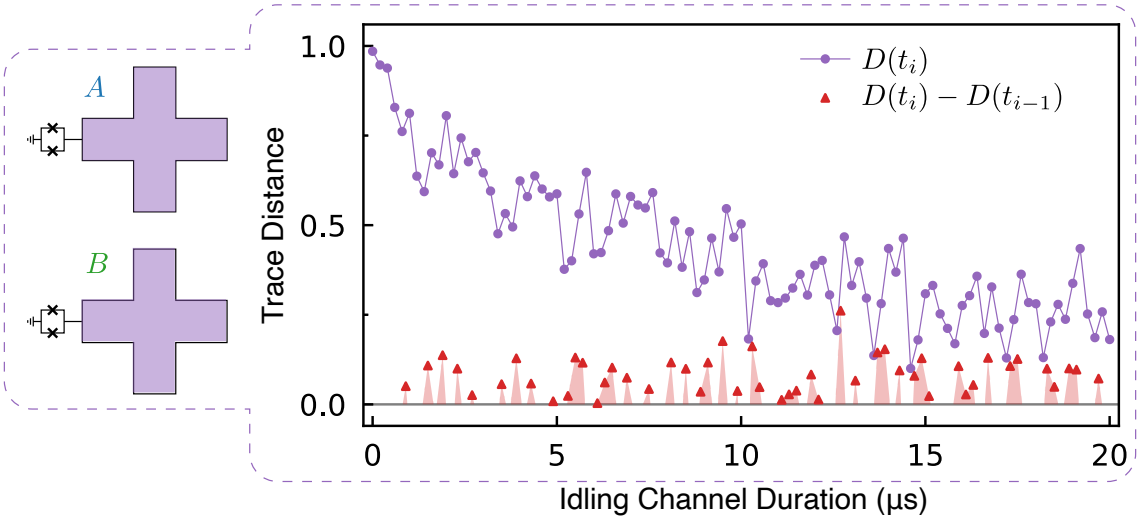

Figure 10-20: Markovianity of the two-qubit idling channel. Here, we find the pair of two-qubit initial states of qubits A and B which together yield the largest value of N_{markov}, and we plot the trace distance D between these two states at each time t_i (blue points), as well as the difference in trace distance between sequential times (red triangles, values less than 0 omitted for visual clarity, since they do not contribute to N_{markov}). Summing the area under the red points amounts to the discrete version of Eq. (10.19), with sustained periods increasing trace distance indicating the presence of non-Markovian errors. Unlike in Fig. 10-15c, we find that none of the two-qubit sequences display the clear oscillations we observed in the single-qubit frame, indicating the channel errors are largely Markovian in the two-qubit frame.

the following two-qubit Hamiltonian

$$\hat{H}_e = \hbar \begin{bmatrix} -0.001 & 0.008 + 0.024i & 0.004 - 0.003i & 0.001 + 0.015i \\ 0.008 - 0.024i & -1.035 & 0.000 + 0.098i & -0.019 + 0.004i \\ 0.004 + 0.003i & 0.000 - 0.098i & -0.258 & -0.009 + 0.000i \\ 0.001 - 0.015i & -0.019 + 0.004i & -0.009 + 0.000 & 1.323 \end{bmatrix} \tag{10.39}$$

with angular frequencies in units of $2\pi \times$ MHz, relative to the laboratory frame of the driving pulses used for single-qubit rotations. Were these pulses chosen to be resonant with the qubit frequencies, we would expect the diagonal elements of the Hamiltonian to be zero.

From the Hamiltonian extracted in Eq. (10.39), we see that there is a frequency detuning of $\Delta\omega_A/2\pi = 0.258/2\pi$ MHz $= 41.1$kHz for qubit A and $\Delta\omega_B/2\pi = 1.04/2\pi$ MHz $= 165$kHz for qubit B, which give rise to the oscillations seen in Fig. 10-

10a (qubit A) and in the bottom left figure of Fig. 10-16. However, we notice that this Hamiltonian is clearly not separable: looking at the frequency of the $|11\rangle$-state, we see that it is not equal to the sum of the individual excitation frequencies. This is consistent with a Hamiltonian of the form

$$\hat{H} = \hat{H}_A + \hat{H}_B + \hat{H}_{zz} \tag{10.40}$$

where $\hat{H}_A$ and $\hat{H}_B$ are the single-qubit Hamiltonians of qubits A and B respectively and $\hat{H}_{zz}$ is an interaction term of the form

$$\hat{H}_{zz}/\hbar = \omega_{zz} \, |11\rangle\langle 11| = \frac{\omega_{zz}}{4}(ZZ - ZI - IZ + II) \tag{10.41}$$

where $\omega_{zz} = \omega_{11} - \omega_{01} - \omega_{10}$ is the strength of the ZZ-interaction.

The presence of this ZZ-interaction is well understood from the physics of coupled transmon qubits. For two transmon qubits interacting via a fixed capacitance, the resulting dispersive repulsion of the $|20\rangle$- and $|02\rangle$-states shifts the frequency of the $|11\rangle$-state and gives rise to a ubiquitous "always-on" ZZ-interaction in the computational subspace of the form in Eq. (10.41) [153]. Consequently, when the two qubits are far detuned from each other—as they are in this experiment—this interaction results in an effective two-qubit Hamiltonian of the form [337]

$$\hat{H}/\hbar = \omega_A \, |10\rangle\langle 10| + \omega_B \, |01\rangle\langle 01| + (\omega_A + \omega_B + \omega_{zz}) \, |11\rangle\langle 11| \tag{10.42}$$

where ω_A, ω_B are the $|0\rangle \rightarrow |1\rangle$ transition frequencies of qubits A and B, respectively. Thus, when one of the qubits is prepared in either $|0\rangle$ or $|1\rangle$, this interaction is manifest as a state-dependent frequency shift. Indeed, this is exactly what we observed in Figs. 10-10 and 10-11: comparing these two measurements, we see that the Ramsey frequency of qubit A increases when we excited qubit B from $|0\rangle$ to $|1\rangle$, indicating that the detuning between our drive frequency and the qubit transion frequency has increased; since the drive frequency was constant between the two measurements, we conclude that the qubit frequency itself changed as a result of the excitation of qubit

B, exactly as we would expect from a nonzero ω_{zz}.

Looking at the diagonal elements of the extracted Hamiltonian in Eq. (10.39), we estimate the frequency shift from the ZZ-coupling to be

$$\omega_{zz}/2\pi = (1.32 - (-0.26 - 1.04))/2\pi \text{ MHz} = 416\text{kHz}, \tag{10.43}$$

which is consistent with the difference in oscillation frequency seen in Figs. 10-10 and 10-11. As a check, we can compare this to the value of ω_{zz} we would expect from device parameters using the relation [337]

$$\omega_{zz} = \frac{2g^2}{\Delta - \eta_B} + \frac{2g^2}{-\Delta - \eta_A} \tag{10.44}$$

where η_A, η_B are the anharmonicity of qubits A and B, respectively; g is the coupling strength between the two qubits; and $\Delta = \omega_i^A - \omega_i^B$ is the frequency detuning between them. Substituting in the parameters for our device from Table 10.1, we estimate a state-dependent frequency shift $\omega_{zz}/2\pi = 425$kHz, consistent with the value found from the Hamiltonian extraction using LT.

However, something very different happens when the two qubits are prepared in an initial state $|{+}{+}\rangle$. Taking this state and evolving it according to the Hamiltonian in Eq. (10.42), we find that the ZZ-interaction turns into an entangling operation in this basis: as the two qubits evolve, they will change from a product state into an entangled state and back again. This should sound very familiar. Indeed, this is exactly the picture that we used to introduce the notion of non-Markovianity back in Section 10.5. If we take a pair of qubits which are periodically entangling with one another and only consider the evolution of one of the qubits, the coupling will swap information between the qubit we are measuring and its neighbor. This is precisely what happens when we perform single-qubit LT on qubit A. By effectively tracing qubit B out of the two-qubit idling channel, we have turned qubit B into an environment with memory, and the periodic entanglement between the two qubits manifests as a non-Markovian error in the single-qubit picture (Fig. 10-15c). However, if the evolution of *both* qubits is considered, as in the two-qubit Kraus estimation,

the always-on interaction is revealed to be unitary and this non-Markovian behavior disappears (Fig. 10-20).

10.8.6 Interpreting the Jump Operators

Having estimated the unitary part of the idling channel—and shown how it accounts for the appearance of non-Markovian errors in the single-qubit frame—we finally turn to the extracted two-qubit jump operators and their decay rates, operators which reveal the mechanisms by which information is lost to the environment during the channel. Running two-qubit LT on both qubit A and B, we estimate the following jump operators for the two-qubit system

$$\hat{L}_1 = \begin{bmatrix} 0.501 = 0.001i & 0.000 + 0.001i & -0.0002 + 0.002i & -0.002 + 0.000i \\ 0.000 - 0.001i & 0.499 - 0.001i & -0.001 + 0.001i & -0.002 + 0.002i \\ -0.001 - 0.001i & 0.001 - 0.001i & -0.499 & 0.000 + 0.001i \\ 0.002 + 0.000i & -0.001 - 0.001i & 0.000 + 0.000i & -0.501 + 0.000i \end{bmatrix} \tag{10.45}$$

$$\hat{L}_2 = \begin{bmatrix} 0.448 - 0.001i & 0.109 + 0.246i & 0.001 - 0.002i & 0.002 - 0.002i \\ 0.061 - 0.125i & -0.451 + 0.002i & -0.001 + 0.002i & 0.002 + 0.005i \\ -0.003 - 0.002i & -0.003 + 0.001i & 0.454 + 0.001i & 0.109 + 0.249i \\ -0.004 + 0.001i & 0.000 + 0.002i & 0.064 - 0.131i & -0.451 - 0.002i \end{bmatrix} \tag{10.46}$$

$$\hat{L}_3 = \begin{bmatrix} -0.072 + 0.161i & 0.639 - 0.031i & -0.003 - 0.001i & 0.007 + 0.00i \\ 0.114 + 0.039i & 0.072 - 0.161i & -0.001 + 0.001i & -0.005 - 0.001i \\ 0.002 + 0.003i & 0.001 + 0.002i & -0.071 + 0.162i & 0.655 - 0.044i \\ 0.002 - 0.003i & -0.001 - 0.002i & 0.134 + 0.035i & 0.071 - 0.163i \end{bmatrix} \tag{10.47}$$

$$\hat{L}_4 = \begin{bmatrix} 0.004 + 0.000i & -0.001 - 0.003i & 0.000 - 0.703i & -0.003 + 0.00i \\ 0.000 - 0.001i & 0.000 - 0.002i & -0.004 - 0.002i & 0.000 - 0.703i \\ 0.001 + 0.078i & 0.002 + 0.001i & 0.000 + 0.002i & -0.002 - 0.003i \\ 0.000 - 0.001i & -0.001 + 0.079i & 0.000 - 0.001i & -0.004 + 0.000i \end{bmatrix} \tag{10.48}$$

where the corresponding decay rates were found to be $\gamma_1 = 0.071$ MHz, $\gamma_2 = 0.097$ MHz, $\gamma_3 = 0.042$ MHz, and $\gamma_4 = 0.055$ MHz.

How do we interpret the structure of these jump operators? Motivated by our understanding of the dominant error mechanisms for superconducting qubits, we can compare the extracted operators above to products of single-qubit amplitude damping and dephasing processes (i.e., T_1 and T_2 processes, respectively), which correspond to jump operators of the form

$$\hat{L}_{d,1} \propto \sigma_z \otimes \hat{I} \tag{10.49}$$

$$\hat{L}_{d,2} \propto \hat{I} \otimes \sigma_z \tag{10.50}$$

$$\hat{L}_{-,1} \propto \sigma_- \otimes \hat{I} \tag{10.51}$$

$$\hat{L}_{-,2} \propto \hat{I} \otimes \sigma_- \tag{10.52}$$

$$\hat{L}_{+,1} \propto \sigma_+ \otimes \hat{I} \tag{10.53}$$

$$\hat{L}_{+,2} \propto \hat{I} \otimes \sigma_+ \tag{10.54}$$

where the operators σ_z and $\sigma_- = |0\rangle\langle 1|, \sigma_+ = \sigma_-^\dagger$ correspond to dephasing and amplitude damping to a thermal state at finite temperature, respectively.

To investigate whether traditional T_1 and T_2 models accurately describe the evolution of our qubits, we run a separate maximum likelihood optimization of the Lindbladian, this time constraining the jump operators to be of the form in Eqs. (10.49)–(10.54) and leaving only the rates (γ) and Hamiltonian ($\hat{H}$) as free parameters. We will refer to this as the *restricted* optimization, while the previous optimization over general jump operators is referred to as the *free* optimization. We compare the output of this restricted optimization by calculating the diamond norm distance between the two Liouvillian superoperators

$$\delta(t) = \|\Phi(\mathbb{L}_{\text{free}}, t) - \Phi(\mathbb{L}_{\text{restricted}}, t)\|_\diamond \tag{10.55}$$

where $\mathbb{L}_{\text{free}}$ ($\mathbb{L}_{\text{restricted}}$) is the Liouvillian superoperator corresponding to the free (restricted) optimization and $\Phi(\mathbb{L}, t)$ is the Choi-matrix representation of $e^{\mathbb{L}t}$. For a diamond norm distance δ, the minimum error probability when trying to distinguish between the two channels for each measurement shot is $(1 - \delta/2)/2$ [46]. For $t \leq 80$

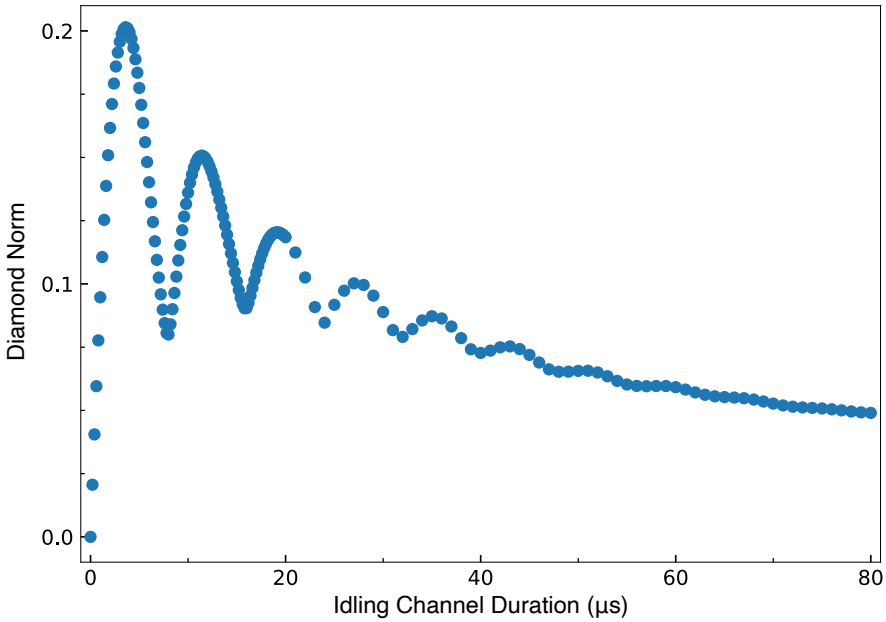

Figure 10-21: Deviation between the estimated Liouvillian of the restricted and free optimization. The deviation is calculated as the diamond norm of the difference between the two superoperators, as in Eq. (10.55).

μs, we find that $\delta(t) \leq 0.2$; evaluating the asymptotic limit, we find that $\delta(\infty) = 0.06$, indicating that the two evolutions result in similar steady states (Fig. 10-21).

From this analysis, we conclude that the extracted jump operators from the unrestricted optimization are largely consistent with single-qubit amplitude damping and dephasing channels, confirming that standard T_1 and T_2 models describe the data reasonably well. However, the deviation from the single-qubit model is significant and consistent with the observed always-on interaction between the qubits, which can lead to two qubit decay channels. Further investigation is necessary to pinpoint the physical mechanisms responsible for these errors, a promising direction for future work.

We also compare the steady state of the two-qubit Lindbladian found in the free optimization (ρ_{ss}^{AB}) to the initial two-qubit state (ρ_0^{AB}) from the SPAM estimation. Calculating the trace distance between these two states, we find a distance $D(\rho_{\text{ss}}^{AB}, \rho_0^{AB}) = 0.09$, indicating a slight deviation between the two. This is unexpected since the superconducting qubits are initialized by waiting many multiples

of T_1—letting them relax to the steady state of the idling channel—and one would therefore have expected the steady state to be identical to the initial state. We note, however, that the deviation is relatively small and may originate from the fact that we only fit to data up to 80μs ($\sim 2T_1$ for qubits A and B, as shown in Table 10.1) and the qubits have not fully relaxed.

10.9 Outlook and Discussion

In the work reported in this chapter, we have presented a technique for extracting the time-independent Hamiltonian, jump operators, and corresponding decay rates of an experimental quantum channel, which we refer to as Lindblad tomography (LT). As we have seen, this technique combines aspects of state/process tomography and time-domain T_1/T_2 measurement with Hamiltonian, Lindblad, and SPAM error estimation based on maximum likelihood (MLE). Lindblad tomography provides detailed information about the errors and noise environment of physical quantum devices and can be used to identify sources of qubit-qubit crosstalk.

While much of this proof-of-principal study focused primarily on noise processes which arise due to the presence of neighboring qubits, Lindblad tomography is by no means limited to error sources found in this work. On the contrary, since LT is agnostic to the structure of the noise environment prior to measurement, this framework can be naturally applied to study a broad range of noise sources which impact the idling channel—such as coupling to coherent two-level systems (TLSs) [251], dephasing due to photons in readout resonators [411], and interaction with quasiparticles [415] in superconducting systems—all of which may leave traces in the extracted Lindbladian and result in varying degrees of non-Markovian error. In addition, LT could prove to be a useful framework for investigating changes in the noise environment over time [82, 369], as well as a valuable tool for validating new quantum control and error correction techniques.

As noted in the introduction, we conclude by reiterating that the number of measurements required for Lindblad tomography scales exponentially with the number

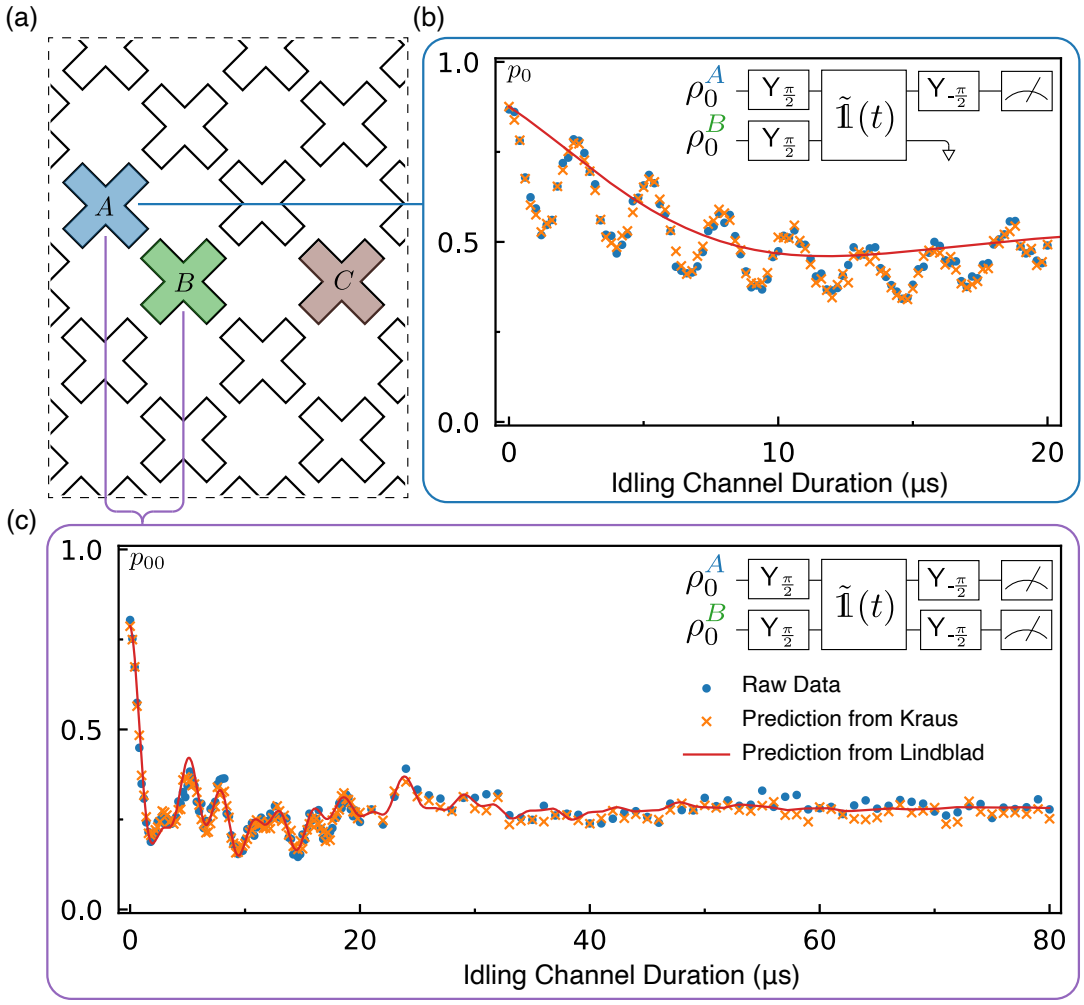

Figure 10-22: Outlook: applying Lindblad tomography to a large superconducting quantum processor. **(a)** Schematic of a large quantum processor, where the two qubits studied in this work are thought of as neighboring qubits (A and B) in a large two-dimensional grid of N qubits. In addition to studying nearest-neighbor interactions, LT can be performed just as easily on distant qubits (for example, A and C) to study nonlocal crosstalk. A general protocol for evaluating the presence of non-Markovian errors might proceed as follows: **(b)** First, we perform single-qubit LT on each qubit in the grid (a task which scales $\mathcal{O}(N)$) and evaluate the quality of each Lindblad fit. We look for qubits which exhibit a poor single-qubit Lindblad fit and compare the fit with the result of the Markovianity metric. When these two metrics are in agreement, we conclude that the evolution is non-Markovian in the single-qubit frame. **(c)** We then perform two-qubit LT on each pair of qubits in the grid (a task which scales $\mathcal{O}(N^2)$) and evaluate the quality of each Lindblad fit. Comparing (b) and (c) in concert with their repective Markovianity checks, we hone in on the neighboring qubit which is the source of the non-Markovian error and work to mitigate it.

of qubits, as with standard process tomography or GST. Thus, full characterization of a large quantum processor using LT remains experimentally impractical. However, since crosstalk between qubits is almost entirely two-body, characterization of all combinations of two-qubit patches on a large quantum processor using LT will nevertheless provide valuable insights into the collective noise environment of the full processor, and these measurements can be used to bootstrap higher-order errors [165, 277]. As the number of two-qubit patches only scales as $\sim N^2$ for an N-qubit device (regardless of hardware platform), characterization of direct two-qubit crosstalk with Lindblad tomography can therefore, in principle, be done efficiently. Furthermore, for devices where it is reasonable to assume that crosstalk is restricted to pairs of qubits within a certain maximal separation (as may well be the case for devices with equally spaced qubits, as in a lattice of superconducting qubits), the number of pairs to be characterized would only scale as $\mathcal{O}(N)$, though investigating the validity of this approach remains the subject of future work. As research scales to larger and more complex systems and the possible sources of crosstalk and unintentional qubit entanglement inevitably increases, we are confident that repeated Lindblad tomography of single- and two-qubit patches will provide an important step towards modeling the dynamics of large-scale quantum processors.

Part V

Quantum Supremacy

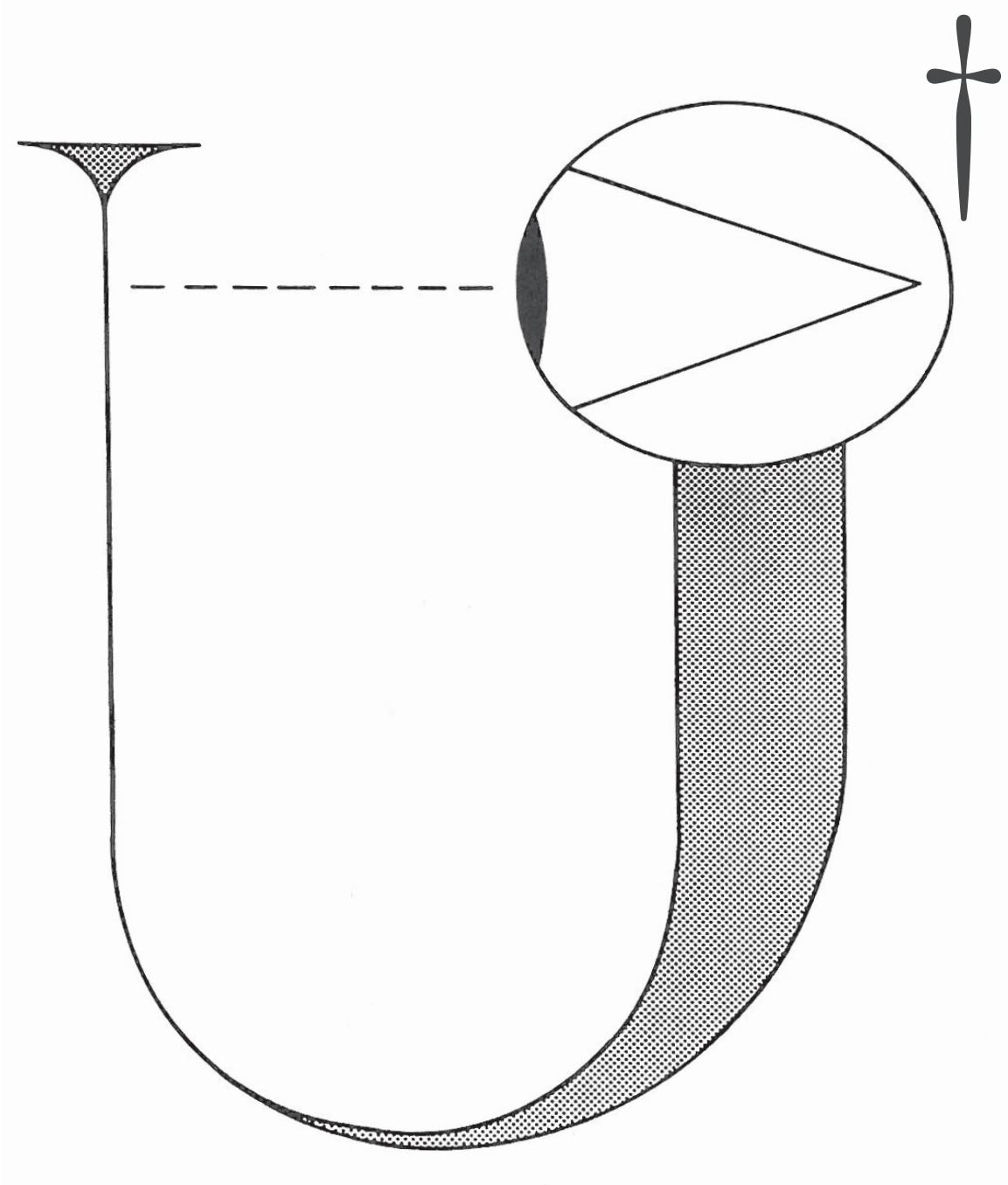

Chapter 11

Preface

In Chapter 1, I compared the structure of this dissertation to that of a randomized benchmarking sequence, where Part V serves as the inversion gate of the circuit, bending the document back upon itself. Standing now at the symmetry point of this document, a few words of preface are in order before the fold.

The following essay was written in the fall of 2021, during the long and grueling thaw after two years of the COVID-19 pandemic. While many of the texts and phenomena considered in the essay predate the pandemic, of all the work in this thesis, this piece bears the clearest influence of that period. It was a period, some may remember, when the world caught fire. In the midst of the blaze, I learned how to read again. Through reading, I came to understand that the fire this time was no aberration, that the flames were a long time coming. So, like many scholars in so many disciplines, I decided it was time to confront the fire in my own work. This task would not have been possible without the support, feedback, and care of all the collaborators who helped me sort through the kindling: I am profoundly grateful to Stefan Helmreich for his mentorship during the writing of this essay; to Julia Menzel and Cristopher Moore for their feedback on early drafts of this work; to Sarah Fleming for her careful edits and nourishing conversation throughout the writing process; and to all of the anonymous colleagues I passed copies to during its development. Reflecting on this work almost a year later, at a moment when our

collective memory of the pandemic slips into an anxious amnesia, the essay already feels dated in some respects. Time moves strangely these days. And time can do so much.

The essay in the following chapter offers a sustained mediation on the structural role of language in the physical sciences, but close readers may note that it also offers a quieter reflection on time. Here, I will point out that the essay was also written shortly after the completion of the Lindblad tomography manuscript reported in Chapter 10, and both works concern, in their own ways, the rigorous characterization of time. Putting these two bodies of work side by side in this thesis, it is immediately clear that they play—as Wittgenstein and Lyotard would put it [285]—very different language games. But when I first began drafting the essay which would become *Cutting the Ground Loop* and I tried to imagine the reader who would encounter it, I imagined the essay as if it were a chapter of a quantum computing thesis, immediately following a chapter on Lindblad tomography. I imagined a curious science student stumbling upon it by chance, as I had once stumbled upon Wheeler's "Information, Physics, Quantum" and his portentous Universe-circuit [468]. In that sense, the following chapter was in fact the first one to be written explicitly for this thesis. Perhaps, then, this final chapter is the real thesis after all, and all the chapters which precede it are my earnest attempts to invert the critique, to dig through my past and find some beauty in the science which might rise to the critique, salvage the enterprise. In this task, at least, I believe I have succeeded.

And so, I arrive at the end of this dissertation convinced that the research presented in this final chapter is inseparable from the body of technical work which precedes it. I caution readers who attempt to encounter one at the expense of the other. Here, I dimly imagine two different readers holding this volume: one, a quantum engineer who reads everything but this final chapter; the other, a student of language and science studies who skips the technical chapters and turns straight to this final one. I fear these two readers would emerge from their respective encounters with this dissertation as irreconcilable mirror images of each other—one rotated clockwise, the other counterclockwise. These readers would have little to say to one

another, at a time when our ability to talk to one another is so vital. So I ask much of the reader. I ask the reader for their patience and, above all, for their trust. In turn, I place my trust in you. We are learning a new language together, and our first conversations will be clumsy. That's okay; we still have time.

To the reader who accepts my trust and works their way through the entirety of this dissertation in kind, engaging rigorously with both the science and the critique, traversing the tangled loop to its completion: welcome back. We have much work to do together.

—September 2022

Cutting the Ground Loop

Chapter 12

Cutting the Ground Loop

12.1 Introduction

For many scientists in the accelerating field of quantum computing, it is difficult to imagine writing a research manuscript, dissertation, or grant proposal in 2021 without prominently citing the 2019 *Nature* paper of Arute et al. on random sampling with an intermediate-scale quantum processor, code-named Sycamore [22].[1] In that work, the researchers at Google Quantum AI demonstrated successful preparation of random quantum states spanning 53 quantum bits (qubits), corresponding to a computational state-space of dimension 2^{53}. That is, the prepared quantum mechanical states of the processor can be mathematically described by a matrix of numbers spanning 2^{53} (approximately 10^{16}, or ten million billion) entries wide and tall, with each entry encoding a piece of information about the state. Since the measurement outcomes of a quantum state are by their nature probabilistic, measurement of each of the 53 qubits results in a characteristic probability distribution of possible bit-strings (a list of 53 zeroes and ones). For a subset of prepared states, the corresponding output

[1] While I will frequently refer to this manuscript using the last name of the first author on the paper, this is not to single out Dr. Arute in particular for praise or blame. With the exception of the final two authors—Google Engineering Director Hartmut Neven and John Martinis of the University of California, Santa Barbara, who co-led the experiment—the seventy-seven authors are listed in alphabetical order by last name.

Figure 12-1: Cover of the October 2019 issue of the journal *Nature* announcing the first experimental demonstration of quantum supremacy.

bit-strings were then compared to the results of physics simulations performed on a selection of industrial supercomputers and cloud computing platforms. However, for a separate subset of quantum states prepared using a more complicated set of operations, the authors found they were unable to generate comparable simulation results using the Summit supercomputer, currently the most powerful computer in the world. To do so, the authors estimated, would take ten thousand years of processing time.

The October 2019 paper of Arute et al. landed like a clap of thunder upon the quantum computing community, if not the academic and popular science community at large. As of October 2021, the paper has garnered over two thousand scholarly citations and 865,000 views. Aggregating from 341,661 tracked articles of similar age

across a portfolio of journals, the data science firm Altmetric LLP currently ranks the article the third highest in "online attention"—a metric which combines academic citation, online manuscript views, press coverage, and social media references [21]. Why the fanfare? Granted, the successful calibration and operation of 53 qubits represented a significant engineering milestone in the field of quantum computing hardware, and this alone was enough to attract the attention of many superconducting quantum hardware engineers. But the *New York Times*? No, the electric reception had everything to do with the achievement promised in the title of the article, "Quantum supremacy using a programmable superconducting processor." The front cover of the October issue of *Nature* was even more succinct, cutting all but the first two words:

QUANTUM SUPREMACY

Classical supercomputer outperformed by quantum chip for the first time

This essay is a record of a few key moments in the history of those two words, how they were first coupled, what they have meant together and apart, and the debates that have arisen over the consequences of their union. It is a reflection on the origin of a specific technical term with a specific history, but it is also a meditation on language itself, how the words we use do the things that they do. To perform this task, I have elected to consider a term from my own area of research. I have done this not because I believe quantum computing is necessarily exceptional in its baggage or its sins but because I take to heart historian of science Donna Haraway's wise dictum that we must not undertake studies of activities in which we do not have a stake. As a scientist in the thorny field of experimental quantum information science, I am entangled with quantum supremacy and I am implicated by what it means. The problem, as I will attempt to illustrate over the course of this essay, is that we are stuck in a dangerous loop. The solution, I argue, is not simply to replace the words we use with new ones, though indeed we must do that too. Quantum supremacy is a fraught and hazardous term which has no place in our language or in our practice,

but it is also a glitch which reveals something deeper and more sinister about the enterprise of our scientific labor in the era of mass incarceration and resurgent white nationalism. It is an opportunity for reflection and for action. If we truly wish to do something about it, I believe we must start by attending to the invisible and powerful circuits of matter and meaning we have woven in our work. In doing so, we might yet learn how to sever these short circuits and build new connections in their place.

12.2 Emergence of a Hazardous Concept

The term 'quantum supremacy' is a young one, even with respect to the relatively adolescent discipline of quantum mechanics (itself a mere century old). First coined in 2012 by the California Institute of Technology physicist John Preskill in his article "Quantum computing and the entanglement frontier," quantum supremacy refers to the then-theorized potential of quantum computers to solve certain problems otherwise intractable on even the largest classical computer [364].[2] Here, the term 'classical computer' refers to any computational device which processes information using binary bits (zeroes and ones), such as a laptop, smartphone, abacus, or vast industrial supercomputing cluster. The outline of the argument is relatively straightforward: since quantum systems occupy an exponentially increasing number of computational states in Hilbert space (2^n states for n qubits, so on order 2^{53} for a mere handful of 53 qubits), at a certain point no computer relying on classical bits will be able to encode this vast state within the physical limits of space or time (the number of atoms in the observable universe or the time elapsed since the big bang, for example). Quantum systems, on the other hand, have no trouble winding this vast amount of information within the tight folds of their state space. If this property of quantum mechanics can be properly controlled and harnessed for information processing, quantum computers won't just be faster and more powerful than all other computers which came before. They will stand supreme over them.

[2]Interestingly, the no-less loaded term "entanglement *frontier*" thankfully never gained comparable traction, though the resonance between frontier and supremacy will be relevant later in this essay.

It bears saying that 'quantum supremacy' isn't just an object of scientific inquiry; it is also a series of words. The emergence of a technical term can tell us a great deal about the times in which it first appeared. For example, the historian Leo Marx once famously noted how the word 'technology'—despite its Grecian artifice—is a neologism that first appeared only in the nineteenth century. In the midst of the massive cultural and economic upheaval of the second industrial revolution—a period where machines such as the steam engine and the telegraph were radically restructuring human perception of space and time—the word 'technology' entered the vernacular to fill a conceptual void [298]. In much the same way, 'quantum supremacy' is the verbal manifestation of a critical moment in the history of quantum information science. While the potential for quantum computers to efficiently solve certain classically intractable problems had been speculated since at least the publication of mathematician Peter Shor's algorithm for prime factorization in 1994, the lag between theory and engineering has been significant. Even today, no physical quantum computer has managed to run Shor's algorithm for any but the most trivial elementary school arithemtic problems.[3]

As the technical hurdles required to build a quantum computer became more apparent with each passing decade, so too did the promise of running a useful quantum algorithm become more distant. Quantum computing was in a rut. It needed a change of perspective. While the task of running a *useful* task exponentially quickly on a quantum computer proved too onerous in the short term, surely one could cook up *something* for a quantum computer to do which a classical computer could not. In 2012, this vague spectral 'something' was given a name: *quantum supremacy*. While much effort has been put into defining what quantum supremacy *is* and how it can be achieved, it is equally important to draw attention to what it *is not*. Unlike Peter Shor's factorization protocol or any of the subsequent theoretical algorithms that followed in its wake, quantum supremacy isn't an application. Crucially, neither is it a mathematical proof or theorem. While the exponential computational speedup of a

[3]In 2001, a research group at IBM succeeded in running Shor's algorithm on a small NMR system of 7 qubits, the culmination of which was the factorization of the number 15 into 5×3 [448]. Subsequent demonstrations in the decades since have proved similarly modest.

quantum computer has long been speculated, there remains no theoretical guarantee that this enhancement is absolute. For every quantum 'killer app' promising unparalleled computational advantage—such as prime factorization or quantum simulation of chemistry processes—there may exist a yet undiscovered classical algorithm capable of performing the same task even faster.

If quantum supremacy isn't an algorithm or a theorem, what is it? Here, it is worth paying close attention to John Preskill's first usage of the term, which I quote at length for context:

> We fervently wish for controlled quantum systems that are large yet exhibit profoundly quantum behavior. The reason we find this quest irresistible can be stated succinctly:
>
> *Classical systems cannot in general simulate quantum systems efficiently.*
>
> We cannot yet prove this claim, either mathematically or experimentally, but we have reason to believe it is true; arguably, it is one of the most interesting distinctions ever made between quantum and classical. It means that well controlled large quantum systems may "surpass understanding," behaving in ways we find surprising and delightful.
>
> We therefore hope to hasten the onset of the era of ***quantum supremacy***, when we will be able to perform tasks with controlled quantum systems going beyond what can be achieved with ordinary digital computers. To realize that dream, we must overcome the formidable enemy of decoherence, which makes typical large quantum systems behave classically. [364]

The choice of words here is significant: quantum supremacy is defined as, variously, a "quest," a "claim," a "belief," an "era," and a "dream." Note also that the excerpt above contains no equations or citations, nor do any of the first three pages in the paper it is quoted from. Granted, this is partly a question of genre—Preskill's comments arrived not in a peer-reviewed journal article but in the transcription of a rapporteur talk he had delivered one year prior at the twenty-fifth Solvay Conference on Physics in Brussels, arguably the most prestigious conference in all of physics. There is an interesting parallel here with physicist Richard Feynman's off-the-cuff comment, delivered in a keynote talk at the inaugural conference on Physics and Computation at the Massachusetts Institute of Technology (MIT) in 1981, that "nature isn't classical,

dammit, and if you want to make a simulation of nature, you'd better make it quantum mechanical." [141, p. 486][4] Feynman's remark is widely considered to be the first intimation of what we today call a quantum computer; indeed, Feynman's keynote address is the first citation in the 2019 *Nature* paper of Arute et al.

Paying close attention to Preskill's choice of words, we might note that his remarks have more stylistically in common with a religious sermon on the eve of a crusade than a pedagogical scientific lecture. It is particularly interesting to note the repeated use of the intimate and mysterious pronoun "*we*" ("we fervently wish," "we cannot yet prove," "we hope to hasten," "we must overcome"). While the rhetorical "we" is used conventionally in many scientific publications as short-hand for *we-the-coauthors-of-this-manuscript*, Preskill's implied "we" works not as a collective authorial pronoun, but as a device for engaging the audience and implicating them in the conversation. This immediately begs the question, to whom is Preskill addressing his remarks? The physical bodies in attendance at the Solvay conference? The rebellious professional cohort of "quantum informationists" referenced a paragraph earlier in his introduction? The anonymous reader of the published remarks? You? Me?

In the decade since delivering his remarks, Preskill's indefinite "we" has ossified into what we today recognize as the quantum computing community. While our ranks are drawn from different disciplines—quantum theory, electrical engineering, atomic physics, experimental condensed matter, material science, chemistry, classical computer science—the aspirational spirit of Preskill's address has served as a binding narrative to unite a disparate array of technical vernaculars and practices. Like Shakespeare's Henry V, rousing the troops on Saint Crispin's day—*we few, we happy few*—Preskill is giving his audience a pep talk. The dark days are upon us. The "formidable enemy" of experimental noise and decoherence is at our gates and in our laboratories. Let all who heed the call gather under a common banner. Though our methods may differ, let us unite in common cause and venture forth, arm in arm, towards the dawn of a new era: *the era of quantum supremacy.*

[4]Incidentally, John Preskill is the Richard P. Feynman Professor of Theoretical Physics at Caltech, where Feynman famously taught.

12.3 The Supremacy Feud

On October 23, 2019, "Quantum supremacy using a programmable superconducting processor" appeared in the prestigious journal *Nature* as if from out of the blue. The orchestrated surprise of the paper's release was unusual and significant. Within the physics community, it is considered customary to upload a preprint of all research manuscripts to an open-access online repository known as the arXiv prior to submitting the work for peer review. In this manner, authors have the opportunity to openly invite feedback on their work during the peer review process and, more importantly, to publicly stake their claim lest they get 'scooped' during the lengthy and unpredictable review process. However, in cases of extraordinary scientific impact, the arXiv submission is avoided entirely and a manuscript will be submitted to the final journal in total secrecy, with reviewers cautioned to keep the existence of the work confidential until final approval and publication. Such was the case for the February 2016 publication in *Physical Review Letters* reporting the first experimental observation of gravitational waves at the Laser Interferometer Gravitational-Wave Observatory (LIGO) in September 2015; three of the authors of that work went on to win the Nobel Prize in Physics for the result [8].

The supremacy result was met with controversy even before the article hit newsstands. While the official publication of the article in *Nature* likely came as a complete surprise to many readers, a few members of the superconducting quantum computing community became aware of the result a full month prior due to an embarrassing online leak of the final manuscript.[5] As it turned out, this twist of fate gave the Google team's competitors a head start to mount a reply. On October 21, two days *before* the official publication of the result in *Nature*, researchers in a competing quantum computing team at IBM posted a scathing rebuttal to the results of Arute et al [347].[6] At

[5]Ironically, the leak was the result not of a hacker, but of a clerical error on the website of one of the author's employer, the National Aeronautics and Space Administration (NASA).

[6]Since the IBM rebuttal was posted prior to its official release in *Nature*, the leaked Google manuscript is anachronistically cited as: "E. G. Rieffel and al. Quantum supremacy using a programmable superconducting processor. *NASA AMES Research Center Technical Report NASA/TP-2019-220319*, 2019."

issue was the very question of what 'supremacy' actually meant in the context of the Google team's experiment. For the authors of the paper, the comparison was clear: in 200 seconds, they had performed a computational task on a quantum processor which would have taken the world's largest classical supercomputer ten thousand years to imitate. Of course, the scientists couldn't afford to wait the ten millennia required to actually test this comparison; instead, they extrapolated this number from the runtimes of a series of smaller physics simulations performed on the Summit supercomputer. Since the scaling of these simulations with the size of the quantum system is well understood, all that remained was to connect the dots and project what the effective runtime would be for a simulation of the full system.

While no one disputed the mathematical soundness of this extrapolation, the researchers at IBM argued that the quantum-classical comparison in the paper was fundamentally inaccurate. While it may be true that the particular classical simulation considered in the paper would take thousands of years to converge, the team at Google had not chosen the *best* possible classical algorithm for comparison: had they instead performed a classical computing trick involving offloading a portion of their simulation data to secondary storage during the computation, the IBM authors estimated that full simulation of the 54-qubit device would require only 2.5 days of computing time on Summit. This then begs the question: does a speedup of 200 seconds on a quantum computer versus 2.5 days on the world's most powerful classical computer constitute proof of quantum supremacy? Recall again that 'supremacy' is not a mathematical theorem or threshold which can be either upheld or violated. So if it's not a fixed value or quantity, who arbitrates what is or is not quantum supremacy?

The answer to this riddle will come as little surprise to historians of science: people do. While the preemptive attack on their result likely came as an embarrassment and frustration to many of the scientists and executives at Google, history will likely remember them as the winners of the ensuing debate. After a series of back and forth blows on Twitter and via each company's PR team, most outside researchers were willing to concede that Google had succeeded in their claim for a number of reasons,

temporal, environmental, and epistemological. Yes, most of us conceded, 2.5 days is certainly a lot shorter than ten thousand years, but it's still three orders of magnitude longer than the 200 seconds ($3.\overline{33}$ minutes or 2.31×10^{-3} days) it look to run on the quantum processor. The quantum computer beat the classical in either case; is that not quantum supremacy? Add to that equation the enormous power consumption of the warehouse-scale Summit compared to the tiny room-sized Sycamore, plus the fact that the IBM team in their haste had not actually run the simulation they proposed, and most modest witnesses—to borrow historian Steven Shapin and Simon Schaffer's expression, by way of Donna Haraway, for the arbiter of scientific experiment [183, 418, p. 65]—were willing to turn the other cheek. Besides, time was on Google's side. After all, since the trick proposed by the IBM researchers did nothing to obviate the fundamental exponential scaling of quantum mechanics, the addition of only a few more qubits to the processor would have quickly foiled the secondary storage technique and rendered the simulation once again classically intractable on any human scale. Perhaps no supremacy today, but tomorrow and tomorrow and tomorrow.

While many scientists remember well the Google-IBM supremacy feud of October 2019, the noise of that spectacle likely obscured from memory another event which occurred in the hours after the publication of Google's result. Like the Google-IBM feud, this event also concerned the nature of the 'supremacy' in 'quantum supremacy'; it occurred, however, not in the realm of scientific debate and corporate intrigue but in the realm of politics and social media. In the immediate fanfare following the posting of Arute et al. in *Nature*, Ivanka Trump—advisor to and daughter of then United States president Donald J. Trump—took to Twitter and Instagram to announce her enthusiasm for the result. The post led with a photo of Ivanka and her father in the Oval Office, alongside then White House Deputy Chief of Staff for Policy Coordination Christopher Liddell and Deputy U.S. Chief Technology Officer Michael Kratsios. The photo had been taken the previous December to commemorate the signing of the National Quantum Initiative (NQI) Act, the largest infusion of national research funding into quantum information science (QIS) in US history. Donald Trump, seated, holds the leather bound bill towards the camera while his daughter and advisors stand

Figure 12-2: October 2019 Instagram post by Ivanka Trump congratulating her father and the Google corporation for their "collaboration" in achieving quantum supremacy. The accompanying photograph, taken at the signing of the National Quantum Initiative (NQI) Act in December 2018, features (left to right) White House Deputy Chief of Staff for Policy Coordination Christopher Liddell, Deputy U.S. Chief Technology Officer Michael Kratsios, President Donald J. Trump, and Director of the Office of Economic Initiatives and Entrepreneurship Ivanka Trump.

beaming beside him; even in the small Twitter thumbnail, it is easy to make out his enormous sawtooth signature in the center of the white blotch of paper. "It's official! [explosion emoji]," Ivanka writes,

> The USA has achieved quantum supremacy! [US flag emoji] In collaboration w/ the Trump Admin & UC Santa Barbara, @Google quantum computer Sycamore has completed a calculation in 3 min 20 sec that would take about 10,000 years for a classical comp.
>
> #QIS is a critical industry of the future. That's why @POTUS signed the National Quantum Initiative Act- record level funding for quantum R&D- into law 2018. We're proud to have contributed to this major milestone, quantum supremacy, and usher in the next gen of quantum tech in America! [439]

Tweets, like books and scientific manuscripts, are texts. They are collections of words which do things, and we can take them apart to analyze what they are do-

ing and how they are doing it. The post opens with a declaration, "The USA has achieved quantum supremacy," punctuated on either side by an emoji of a cartoon explosion on the left, often used to signify surprise or excitement, and of the United States flag on the right. This statement will likely make many scientists uncomfortable. Few would have batted an eye at the similarly structured sentence, *"Scientists at the Google Quantum AI lab have demonstrated quantum supremacy."* This statement reads as self evident: the scientists—in this case the authors of the paper—did the experiment and got the result. Ivanka Trump's modification of this statement is significant. Rather than attribute the achievement of quantum supremacy to a group of researchers, she frames quantum supremacy as first and foremost a *national* accomplishment. This statement is echoed in the next sentence, where she congratulates the "collaboration" between the Google corporation (the employer of the majority of scientists on the paper), the University of California at Santa Barbara (where a portion of the Sycamore processor was fabricated), and the presidential administration of Donald Trump.

The word "collaboration" is worth sitting with here. When scientists speak of collaboration, they usually refer to a partnership between researchers who would otherwise be considered to belong to separate research groups or institutions. In this way, one might speak of a collaboration between theorists at a center for mathematical physics in Copenhagen and experimentalists at a large research university in Cambridge, Massachusetts. Few scientists would consider themselves to be in collaboration with their government sponsors; for many, government patronage is to be regarded as necessary for but separate to the actual task of science. Science, or so the story goes, is not political. This relationship of necessity/separateness between scientists and their national benefactors is codified in a block of stock text which authors are required to include in the acknowledgments section at the end of every manuscript which received government funding. In the manuscript of *Arute et al.* this appears in the form of the boilerplate disclaimer:

> The views and conclusions contained herein are those of the authors and should not be interpreted as necessarily representing the official policies

> or endorsements, either expressed or implied, of AFRL [the Air Force Research Laboratory] or the US government. [22]

Ivanka Trump's tweet complicates this statement by upending any pretense of scientific and political separateness. For her, the achievement of quantum supremacy indeed represents the official policy and endorsement, expressed *and* implied, of the United States government. Whatever the individual nationalities of the scientists who worked on the project, the achievement of quantum supremacy was above all an American accomplishment, backed by American capital on American soil. The era of quantum supremacy was here, and it had borders.

12.4 Ancilla in the Forum

The broader social and political connotations of quantum supremacy were apparent long before Ivanka Trump made the connection explicit. In May 2017, less than a year after Donald Trump rode to power on a wave of white supremacist rehetoric, Univerity of Potsdam professor of complexity science Karoline Wiesner posted a short article to the arXiv titled "The careless use of language in quantum information." [469] In the article, Wiesner points out that the field of quantum computing has something of a language problem on its hands and notes two concrete examples. The first regards the term *ancilla qubit*, a ubiquitous phrase in the field of quantum error correction to denote quantum bits which temporarily store information during an algorithm, but do not themselves contribute directly to the computation. The term is not without motivation—the Merriam-Webster dictionary defines 'ancilla' as "an aid in achieving or mastering something difficult," with is indeed how these computational objects are employed by both theorists and hardware designers [18]. However, as Wiesner notes, the etymology of 'ancilla' tells a different story. While it is not uncommon for ancient words to warp and shift phonemes over the millennia, nucleating a variety of divergent meanings in a vast web of vernaculars, the English word 'ancilla' is visually identical to the Latin. Indeed, since modern English employs the Latin alphabet, the word would have been as legible to Virgil and Cicero as it is to today's quantum

computing scientists, and the core meaning of the word would have traveled across space and time intact. With one crucial exception. For the Romans, an ancilla was not a *what* but a *who*, or more percisely a *she*: "maid-servant, female slave." [318]

Wiesner's second example, of course, was *quantum supremacy*. Rather than point to classical sources for reference, the article draws upon a more modern political example for comparison. Wiesner's commentary here is strikingly restrained, consisting of only short, declarative statements of fact:

> The English word 'supremacy' denotes the quality or state of having more power, authority, or status than anyone or anything else. These days the word is closely associated with the politics of 'white supremacy' in the apartheid regime of South Africa between 1948 and 1991, known for its institutionalised racial segregation and discrimination. The term 'quantum supremacy' was coined in 2012. It overtly refers to a value system of unequal human rights. Scientific articles and workshops using this term are increasing quickly in number.

Wiesner goes on to note that while John Preskill issued an open invitation for an alternative term as early as the very year in which he coined it [367], that call was largely ignored. The article concludes with a simple invitation for reflection on what all this might mean for practicing scientists who employ terms without considering their deeper connotations. "The association with slavery, misogyny, and racial segregation in these examples is certainly not intended," Wiesner writes, "but it is careless. Language is powerful. The choice of terminology in science is no exception. We as a scientific community have to think about what we want to stand for and how this is reflected in the way we communicate."

Wiesner's article did not go unnoticed. Within hours of its posting, the article was picked up by the community-run manuscript aggregator and discussion forum SciRate [105]. Scrolling through the comments thread today and scanning the list of responders, the thread reads like a roll call of the quantum information theory community, with many of its most cited scholars weighing in, Preskill himself included. While I am uninterested in calling out particular scientists here,[7] it is worth pointing

[7]When quoting comments on the SciRate forum, I have chosen to omit the names of the forum posters. Instead, I refer to each by a pseudonym composed of their total citation number and h-

to the dominant trends which emerged in the thread, trends which reflect many of the responses in the broader quantum computing community at large. Some responded with exasperation. "With 'supremacy' I can at least see where the argument is coming from, even if I don't find it particularly convincing," wrote scientist `H25-2500`. "But the 'ancilla' example is nonsensical. Firstly, 'ancilla' was not 'invented recently for the field of quantum information'. More importantly, it has never had the meaning, or even connotation, of 'female slave' in English." The poster proceeded to provide a list of dictionary and encyclopedia entries to support their claim—including a surreal digression about the shared origin of 'testify' and 'testicle'—before ultimately concluding that "unless you're still writing papers in Latin, you can safely continue to use 'ancilla' without offending anyone."

Another responder, `H38-7000`, concurred with the sentiment, though they reiterated it in less bombastic terms:

> I get that these words may remind us of something bad, but it doesn't follow that they cause any actual bad effects. For example, they don't strengthen white supremacist groups (as far as I can tell) or make racial minorities feel unwelcome (as far as I can tell). Words have multiple meanings, sometimes with varying levels of offensiveness. But we don't stop talking about rapeseed oil, or the polynomial hierarchy, or dictatorship tests or colonizing the gut, simply because part of those phrases are also involved in bad things that people do.

These two comments are significant and point to a larger trend in how many scientists evaluate and justify the words they use: rather than think about language as a collection of historical objects that structure our encounter with the world, words are evaluated based on their capacity to inflict direct harm or offend individual people, though the metric by which this harm or offense would be evaluated is never specified. Weighing the terms 'ancilla' and 'supremacy' according to this murky criteria, both authors retreat to vague generalizations about how neither has witnessed or can imagine either term causing offense: *"you can safely continue to use 'ancilla' without*

index—a widely recognized metric for citation impact—as a crude proxy to draw attention to the perceived stature of the scholars who participated in the thread. For example, `H38-7000` is a scientist with an h-index of 38 (i.e., 38 of their publications have at least 38 citations each) and approximately 7000 total citations.

*offending **anyone**"*; *"they don't strengthen white supremacist groups [...] or make racial minorities feel unwelcome **(as far as I can tell)**."*

Not all voices who weighed in were so certain. In one of the few personal reflections on the thread, `H52-12000` noted that the question of personal offense was somewhat besides the point:

> it is not even about being directly offensive to other people, i simply can't get myself to say 'quantum supremacy', it suggests some superiority involving human beings (the whole field of QC hitting other people over the head with their 'quantum-supreme experiments'). I mean how do you read a popular science article with the title 'Scientists are about to achieve quantum supremacy' versus the title 'Future experiments are about to exhibit a quantum advantage'. Ancilla seems a different matter, partially because its meaning as a female servant is not so well-known and it is just a technical term like slave bosons or so.

This impulse to turn the camera around and ask what these words might say about the authors themselves—as opposed to what they might do to the members of some imagined external audience—is echoed by another poster, `H38-6500`, who writes: "'Quantum supremacy' feels so bad precisely because we use 'quantum' as a synonym for our peer group. That makes the analogy to the repugnant 'white supremacy' particularly close, unfortunately." While clearly neither of these authors would consider themselves 'quantum *supremacists*,' the sheer thought that they might mistakenly be construed as such seems sufficiently alarming to warrant jettisoning the term altogether.

While both Karoline Wiesner's original article and the SciRate thread it catalyzed have likely faded from the memories of many scientists,[8] debate over the term 'quantum supremacy' would resume in force during the 2019 publication frenzy of the Google result. These debates reached a climax in December of that year with the publication of a correspondence in *Nature* titled "Instead of 'supremacy' use 'quantum advantage'." In addition to the three lead authors of the letter—Carmen Palacios-

[8] At the time of writing, Wiesner's piece has only 6 documented citations, in comparison to 246 for the document containing Preskill's original coining of the term. Some might argue that this comparison is unfair, since Wiesner's piece was not a work of scientific research and was never peer-reviewed. Neither, it must be said, was Preskill's.

Berraquero, CEO and co-founder of the quantum computing start-up Nu Quantum; Leonie Mueck, former *Nature* editor and Chief Product Officer of the quantum software start-up Riverlane; and Divya M. Persaud, composer and doctoral scholar in planetary science at University College London—the letter was backed by thirteen signatories representing an international cohort of researchers from across the physics community. Shortly thereafter, a slightly modified version of the *Nature* correspondence appeared as an open letter on a dedicated website titled Responsibility in Quantum Science, the text of which I quote here in full:

> Inherently violent language subtly pervades science, including in space exploration, computing and genetics. For example, terms around human and robotic spaceflight, such as "conquest," "colonization," and "settlement" evoke the "terra nullius" arguments of settler colonialism and must be contextualized within the ongoing issues of neo-colonialism. Such language is now creeping into the field of quantum computing. We call for the community to drop the term 'quantum supremacy' and to use 'quantum advantage' instead.
>
> The calculation speed of quantum computers surpasses that of even the fastest supercomputers – hence the 'supremacy' tag. The community claims that this is a technical term with a specified meaning. Critics argue that it is misleading because quantum computers in general do not reign over their classical counterparts, although they could eventually outcompete them in solving specific problems.
>
> Any technical justification for the 'supremacy' descriptor could get swamped as it enters the public arena after the intense media coverage of the past few months. The term has implications of violence, neo-colonialism and racism through its association with "white supremacy". In our view, it is irresponsible to override the historical context of such words, which risk sustaining divisions in race, gender and class. Instead, quantum computing should be an open arena and an inspiration for a new generation of scientists. [344]

After the letter, the website includes a form for readers to record their contact information and sign on in support—as of late 2021, the letter has gathered over a hundred and fifty signatures. None of the authors on the original SciRate thread appear as signatories.

While the open letter generated a fair share of word of mouth around laboratories and coffee machines at the time of its publication, the reception from many scientists

was ambivalent, if not outright apathetic. Among those who took the letter seriously, the general response was perhaps best characterized in an essay by University of Texas at Austin computer scientist Scott Aaronson, posted on his popular quantum computing blog *Shtetl-Optimized*. In the post, titled "Quantum Dominance, Hegemony, and Superiority," Aaronson weighs in on the supremacy discourse and responds directly to the letter's call to replace 'quantum supremacy' with 'quantum advantage' [3]. Although Aaronson expresses sympathy for the sentiment of the letter—in response to a direct email from Mueck, he writes that "as the father of a math-loving 6-year-old girl, I understood and shared her concerns"—he equivocates over whether the community would be able to find a suitable replacement for the term. Reflecting on 'quantum advantage,' Aaronson wonders "couldn't that term, too, remind vulnerable people about the unfair advantages that some groups have over others? Indeed, while 'advantage' is certainly subtler than 'supremacy,' couldn't that make it all the more insidious, and therefore dangerous?" Unsatisfied, Aaronson runs through a list of proposed alternatives—'quantum ascendancy' (too cultish), 'quantum inimitability' (too hard to pronounce), 'quantum eclipse' (too cute)—before finally concluding that the search for an alternative term remains "an open problem."

Besides, Aaronson wonders, what are the implications of retracting 'supremacy' in the first place? Here, he gives voice to the collective handwringing of many scientists by invoking a classic slippery slope argument: "once we've ceded an open-ended veto over technical terms that remind anyone of anything bad, where does it stop? How do we ever certify a word as kosher? At what point do we all get to stop arguing and laugh together?" Aaronson proceeds to rattle off a list of physics terms which might end up on the chopping block for their evocation of violence or denial of a "multiplicity of perspectives and cultures"—'annihilation operators,' 'unitary matrices,' 'bra/ket notation,' 'daggers,' and of course 'ancilla.' This "obsession" over the implications of language, Aaronson argues, is not only a distraction, it perpetrates real harm by (unintentionally) antagonizing well-meaning scientists:

> In this context, the trouble with obsessing over terms like 'quantum supremacy' is not merely that it diverts attention, while contributing nothing to fight-

> ing the world's actual racism and sexism. The trouble is that the obsessions are actually harmful. For they make academics—along with progressive activists—look silly. They make people think that we must not have meant it when we talked about the existential urgency of climate change and the world's other crises. They pump oxygen into right-wing echo chambers.
>
> But it's worse than ridiculous, because of the message that I fear is received by many outside the activists' bubble. When you say stuff like '[quantum] supremacy is for racists,' what's heard might be something more like:
>
> > "Watch your back, you disgusting supremacist. Yes, you. You claim that you mentor women and minorities, donate to good causes, try hard to confront the demons in your own character? Ha! None of that counts for anything with us. You'll never be with-it enough to be our ally, so don't bother trying. We'll see to it that you're never safe, not even in the most abstruse and apolitical fields. We'll comb through your words—even words like 'ancilla qubit'—looking for any that we can cast as offensive by our opaque and ever-shifting standards. And once we find some, we'll have it within our power to end your career, and you'll be reduced to groveling that we don't. Remember those popular kids who bullied you in second grade, giving you nightmares of social ostracism that persist to this day? We plan to achieve what even those bullies couldn't: to shame you with the full backing of the modern world's moral code. See, we're the good guys of this story. It's goodness itself that's branding you as racist scum."

Confronted by this grotesque specter of jeering elementary school anxiety, Aaronson offers a staggering rebuttal. "Yeah 'quantum supremacy' is not a term I would've coined, and it's certainly not a hill I'd choose to die on," but perhaps, he argues, there is a ring of truth to the word after all. If scientists are caught in a double-bind, trapped between their commitment to accurate technical language on the one hand and their earnest desire to combat "actual racism and sexism" on the other, what if we instead chose to lean into the term and own it? Here, Aaronson recalls a revelation he had in the aftermath of Donald Trump's election:

> The thinking was: even as white supremacy was making its horrific resurgence in the US and around the world, here we were, physicists and computer scientists and mathematicians of varied skin tones and accents and genders, coming together to pursue a different and better kind of

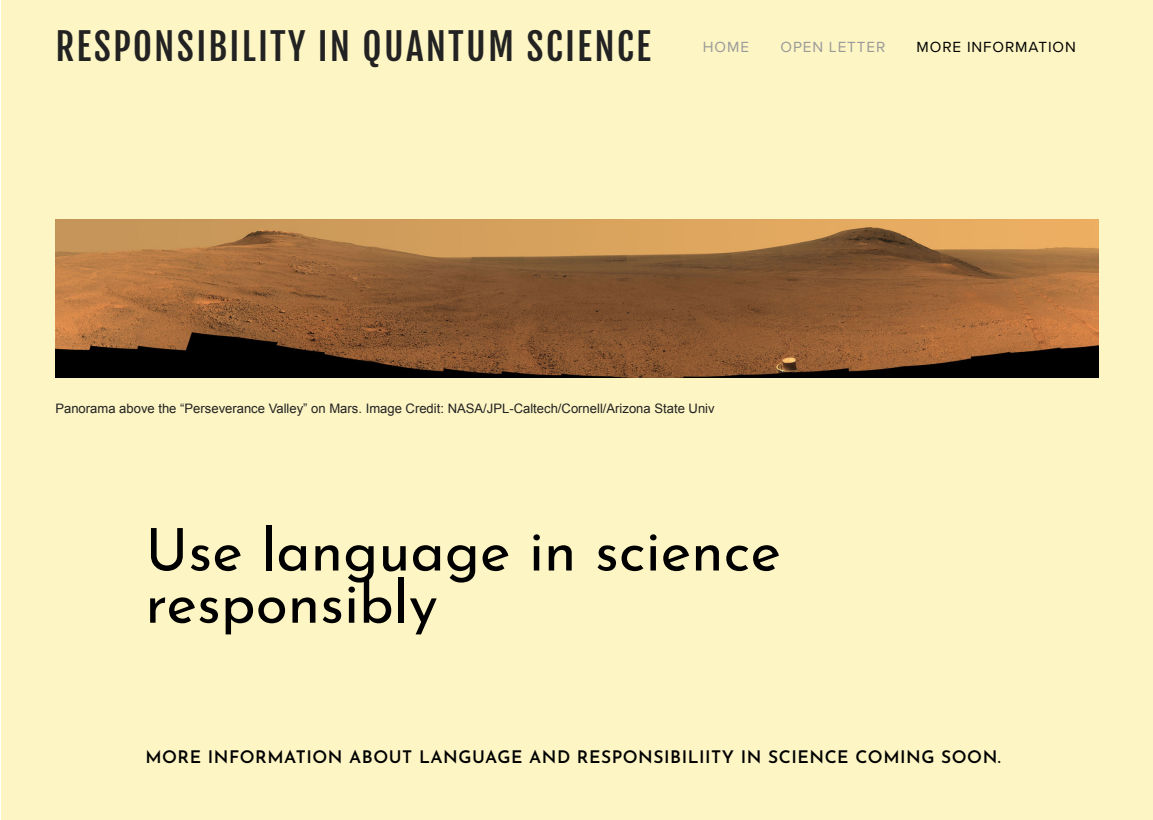

Figure 12-3: Screen capture of the More Information tab on the website for Responsibility in Quantum Science, as of late 2021 [317].

> supremacy—a small reflection of the better world that we still believed was possible. You might say that we were **reclaiming** the word "supremacy"—which, after all, just means a state of being supreme—for something non-sexist and non-racist and inclusive and good.

Aaronson concludes the article by imagining a utopian future where "my colleagues and I still use the term 'quantum supremacy' whenever we care to, and none of us have been cancelled or ostracized for it;" a future where "quantum computing researchers now have bigger fish to fry than arguments over words——like moving beyond quantum supremacy to the first useful quantum simulations, as well as the race for scalability and fault-tolerance." A future, that is, where words are words and science is science.

In researching this essay, I returned to the website of Responsibility in Quantum Science to see if there had ever been a response to Aaronson's piece or to the similar arguments which appeared around the same time. At the top of group's webpage, next to the tab titled 'Open Letter,' there is a button labeled 'More Information.'

Clicking on the tab leads visitors to a barren orange webpage adorned with a long panorama image of Perseverance Valley on Mars and the text [317]:

Use language in science responsibly

MORE INFORMATION ABOUT LANGUAGE AND RESPONSIBILIITY IN SCIENCE COMING SOON.

The webpage has not been updated in two years.

12.5 Supremacy is (Not) a Metaphor

Physics is an enormously useful analytical framework. Drawing upon a common set of mathematical and empirical practices, physics has provided self-consistent descriptions of phenomena across a vast range of scales, from the cosmological (such as the motion of galaxies and the properties of supermassive black holes) to the subatomic (quarks, leptons, and the constituent stuff of matter). Emboldened by their successful accounts of the natural world, many physicists have ventured beyond the traditional boundaries of their craft and applied physical methods to areas of interest in the social science and humanities. For example, Franz Boas, the German-American scholar widely credited for founding modern anthropology in the early twentieth century, originally received his doctorate in physics on the optical properties of water. At their best, these interdisciplinary ventures have promoted new avenues of communication among scholars in a range of disciplines and fostered capacious new ways of viewing the world. Here, I am personally indebted to the examples set by the physicists Karen Barad and Chanda Prescod-Weinstein—two scholars who have powerfully mobilized their backgrounds in theoretical particle physics to critique the discipline of physics from within, bringing it into conversation with theories of gender performativity [32], critical race [359], and postcolonialism [31].

At their worst, however, these ventures have given physicists license to displace and subordinate entire bodies of preceding scholarship, re-deriving them from 'first principles' and re-orienting them according to a narrow set of physical laws. Here,

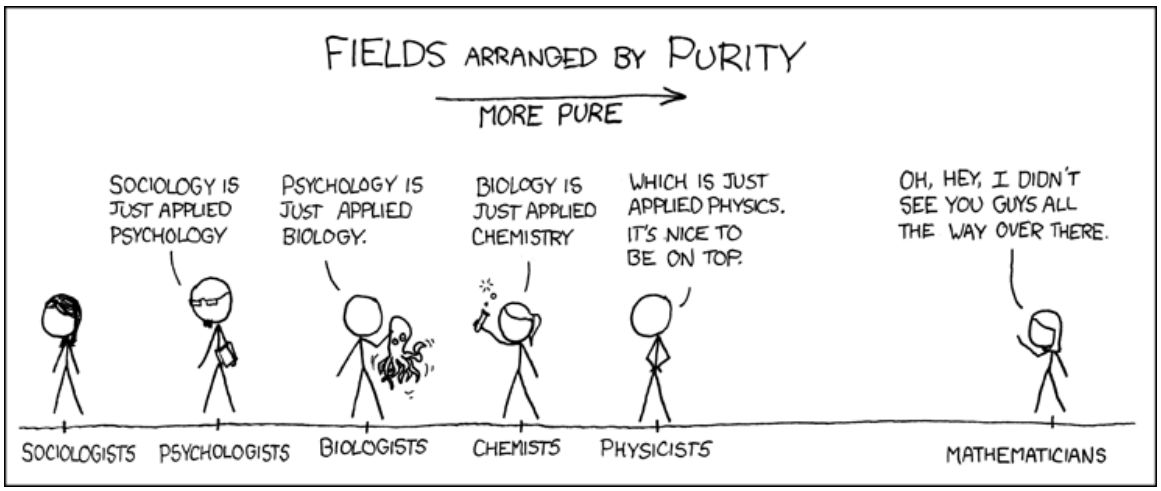

Figure 12-4: A June 2008 webcomic by American cartoonist Randall Munroe from his popular website XKCD. Avatars representing a collection of disciplines are arranged in order of their ascending "purity," with physics and math at the top of the hierarchy. In Munroe's hallmark style, a hidden message appears when viewers hover their mouse over the graphic: "On the other hand, physicists like to say physics is to math as sex is to masturbation." [323]

I am reminded of a popular webcomic by the cartoonist Randall Munroe which circulated widely during my earliest high school physics classes. In the comic, avatars representing a range of disciplines are ordered according to their relative "purity"—sociology, then psychology, then biology, then chemistry—with a physicist near the right hand side proclaiming "It's nice to be on top." [323] After a long blank space, a mathematician even further to the right comments, "Oh, hey, I didn't see you guys all the way over there." While the joke, of course, is that physicists haughtily perceive themselves to occupy the top of a hierarchy of knowledge—a position they jockey with mathematicians over—this hierarchy is far from imaginary. Indeed, it has a material impact on the conditions of our education and our research: it is no coincidence that, in high school, I was required to take biology in ninth grade, chemistry in tenth grade, and physics in eleventh grade; in college, these same three departments were housed in three separate buildings arranged in the exact same order along one side of a long quad [225].

This phenomenon, far from representing some architectural or curricular anomaly, constitutes what historian of science Peter Galison has called the "physicalized archi-

tecture of knowledge." [151, p. 785] The fact that we observe these pattern in the world around us does not make them natural; rather, it reminds us that humans build structures which reflect the dominant beliefs and values of the culture in which they are built. In the case of science, these structures frequently replicate the same linear geometry Munroe depicts in his comic, with physics at the apex.[9] In this way, Galison notes, it struck the architect of an eight-story physics complex in Liverpool as perfectly natural to place the offices of the theoretical physicists on the top floor:

> Usually a theoretical physicist will require services, a blackboard and in some cases a bed to lie on to help his deliberations... [W]e have put him in an 'ivory tower' overlooking the city in the vain hope that the view over Liverpool may inspire him. [151, p. 787]

I belabor this point in order to draw attention to a fact that will be important later in this essay: the conceptual and the material are not separable. Rather, they are mutually constitutive, giving shape to one another in a feedback loop.[10] A society which believes in a hierarchy of knowledge builds towers to house the keepers of this knowledge; the tower becomes material proof of the hierarchy and reinforces the beliefs of its occupants; departments expand, grants are awarded, new towers are built, et cetera, et cetera, ad infinitum. Like chicken and egg, the beginning of the loop is often obscured—we are usually entering it *in media res*.

Standing in this penthouse suite (metaphorically, physically), surveying the landscape of knowledge, it should come as little surprise that, in all the commentary on language written by physicists in the preceding sections, none of the writers paused to consult a linguist. While the authors on the SciRate forum would likely have objected to a forum of anthropologists debating the nuances of quantum electrodynamics, these

[9] Significantly, while the relative order of these disciplines appears consistently across a range of architectural plans, Galison notes that the orientation is often flipped with physics housed at the base and chemistry, microbiology, and physiology housed progressively up the tower. In much the same way, many high school science curricula require physics in the ninth grade and biology in the eleventh. Here, physics is interpolated between two dual functions, both as "the top" of a hierarchy (as in Munroe's comic) and as its foundation.

[10] This concept should be familiar to physicists in its resemblance to the relationship between the electric and magnetic fields of a propagating photon, each giving rise to the other. In this way, one can think of the conceptual and the material as governed by a set of coupled differential equations. Of course, unlike Maxwell's equations in a vacuum, there is no analytic solution here.

same scholars appear to have no issue commenting on what language does or does not do. Moreover, they do so with great authority. Had any of these authors taken a moment to conduct a literature review—as each would no doubt have instructed their students to do prior to embarking on a scientific research project—they would have quickly discovered that they had been scooped decades earlier. To arrive at this realization, of course, would have required them to leave their tower.

The question is not a new one: *what do we do when the same word appears in multiple dissimilar contexts?* As it happens, this very question was famously raised the same year that Preskill coined 'quantum supremacy.' In 2012, the Indigenous studies scholars Eve Tuck (Unangax, enrolled Aleut) and Wayne Yang coauthored an article for the inaugural issue of the journal *Decolonization: Indigeneity, Education & Society* titled "Decolonization is not a metaphor." Over the course of the essay, Tuck and Yang craft a powerful and enduring critique of the ways in which the term *decolonization* has been appropriated outside the context of Indigenous activism. "Our goal in this article," Tuck and Yang write,

> is to remind readers what is unsettling about decolonization. Decolonization brings about the repatriation of Indigenous land and life; it is not a metaphor for other things we want to do to improve our societies and schools. The easy adoption of decolonizing discourse by educational advocacy and scholarship, evidenced by the increasing number of calls to "decolonize our schools," or use "decolonizing methods," or, "decolonize student thinking", turns decolonization into a metaphor. [441, p. 1]

This "metaphorization of decolonization," Tuck and Yang argue, allows educators to commit a tactical evasion: by turning *decolonization* into a general panacea for a range of civil rights and social justice ills, one pays lip service to a progressive agenda while draining the term of its specificity. In this way, one can abstractly use the term *decolonization* to absolve themselves of guilt, while at the very same time ignoring the specific demands of Indigenous communities—"the repatriation of Indigenous land and life" in the settler-colonial nations of (what we now call) North America, full stop.

While the contents of the two sets of arguments differ in many meaningful ways, there are a number of formal similarities between the work of Tuck and Yang and

the debates we observe above regarding quantum supremacy. For one, both lines of argument involve explicating the difference between multiple terms which contain the same keyword. In the case of Tuck and Yang, this means comparing the terms 'decolonize stolen land' and 'decolonize education' and showing that *decolonize* means something different in each case. In the case of the scientists in the preceding sections, many of their arguments similarly boil down to how the *supremacy* in 'quantum supremacy' differs from in 'white supremacy.' Tuck and Yang then take this a step further and argue that not all deployments of *decolonize* are equally valid. Rather, there is one usage which is real ('decolonize stolen land') and many usages which are merely pale metaphors ('decolonize education,' 'decolonize the mind,' 'decolonize schools'). These metaphorical deployments of *decolonize* then do harm to the real usage by thinning its meaning. In this way, the statement "decolonization is not a metaphor" works to sweep aside these distracting deployments so that we might instead focus on its true, non-metaphorical meaning.

A very similar argument simmers beneath much of the discourse involving quantum supremacy. Indeed, one can easily imagine an essay titled "Supremacy is not a metaphor," in which the authors compare 'quantum supremacy' to 'white supremacy' and show how the metaphorical usages of *supremacy* distract from the real one. The issue is that there isn't just one hypothetical essay titled "Supremacy is not a metaphor." There are two, and they say opposite things:

1. The first essay would take up the call of Responsibility in Quantum Science and argue that 'white supremacy' is the real form of supremacy which demands our immediate action and attention. 'Quantum supremacy,' on the other hand, is merely a hollow corporate rebranding of this original meaning. In this way, 'quantum supremacy' distracts from the frightening political implications of *supremacy* and "override[s] the historical context" of the word [344]. The solution, then, is to untether quantum computing from the word 'supremacy' altogether, a task which can be accomplished simply by changing the word to 'quantum advantage.'

2. The second essay would follow the argument of scientists such as Scott Aaronson. 'Quantum supremacy,' the authors would argue, is of course the real supremacy, in that it is grounded in mathematics and scientific empiricism. 'White supremacy,' on the other hand, is the delusion of racists with no understanding of science. Here, 'white supremacy' is the distraction from 'quantum supremacy,' dividing well-meaning scientists and preventing them from realizing their shared calling. The solution, then, is to embrace the mantle of 'quantum supremacy' and pursue "a different and better kind of supremacy" grounded in the laws of nature, not politics [3].

Like a riddle, the author of each essay stands before us, each guarding the door to a supremacy. Behind one of these two doors, they tell us, is the real supremacy. Behind the other, the metaphor. One guard speaks the truth, the other lies. Which door do we choose?

Both, and neither. 'Quantum supremacy' and 'white supremacy' are both metaphors. They are also both real. This is not a trivial solution; indeed it is not a solution at all. Rather, it is an observation that the riddle is ill-defined, and it is the opening of a sideways pathway towards a deeper understanding of how language works. Just as the tower of physics at the beginning of this section is both a metaphor for the imagined hierarchy of knowledge *and* a literal building which actualizes this metaphor, 'supremacy' operates in a feedback loop of material and belief. For shorthand, we can say that *supremacy is (not) a metaphor*, interpolating between the two meanings by simultaneously reading and omitting the parenthetical. This is not a new concept, and in the next section I will attempt to derive this statement. For this derivation, I will rely not on math or formal logic but on a history of ideas. In this task, the goal is not to uncover some deep and indisputable kernel of truth which validates this argument. Rather, I am interested in deriving how I have arrived at my own understanding of language, which thinkers I have been in conversation with, and which contours of thought have guided and compelled my own.

12.6 Derivation in Oak, Turmeric, Matsutake

In this section, I will trace a brief history of twentieth century language studies, focusing in particular on three historical moments: the early-century development of *semiology* by structural linguists, the mid-century move towards *semiotics* by post-structuralist philosophers, and the late-century intervention of *material-semiotics* by feminist scholars of science. In tracing these three moments sequentially, my goal is neither genealogical (implying that one movement birthed the next) nor teleological (positioning each moment as a chapter in the book of history, pointing towards some grand future conclusion). Instead, I point to these three moments because each emerged from—and responded to—a particular set of historical and political considerations over the past century. This timeline should be familiar to physicists. It is also the timeline of modern quantum theory.

In 1915, seven years before the observation of quantized spin by the German physicists Otto Stern and Walther Gerlach, the Swiss linguists Charles Bally and Albert Sechehaye published a series of posthumous lecture notes by their professor, Ferdinand de Saussure, titled *Course in General Linguistics* (*Cours de linguistique générale*).[11] Over the course of the lectures, delivered at the University of Geneva between 1906 and 1911, Saussure articulated a new framework of study in the field of linguistics, which he termed *semiology*. Saussure's question was a deceptively complex one: how do words arrive at their meaning? Phrased another way, what is the relationship between a word and the thing to which it refers? Are they the same thing? For Saussure, the answer was a definitive no. To make this question more tractable, he introduced a set of three technical terms which linguists could use to distinguish between the separate and interrelated parts of language: the *signifier*, the *signified*, and the *sign*.[12]

[11] Physicists may notice a passing similarity between Saussure's *Course in General Linguistics* and one of the foundational texts of modern physics, *The Feynman Lectures on Physics*. Like Saussure's text, Richard Feynman's lectures were collated and assembled with the help of two coauthors, Robert B. Leighton and Matthew Sands. Like Bally and Sechehaye, Leighton and Sands' contributions to that work are largely forgotten. Saussure and Feynman's, on the other hand, are not.

[12] Throughout this section, I will use the following typographic convention to distinguish between these three terms: the signifier will be cast in sanserif (tree), the signified will be written without

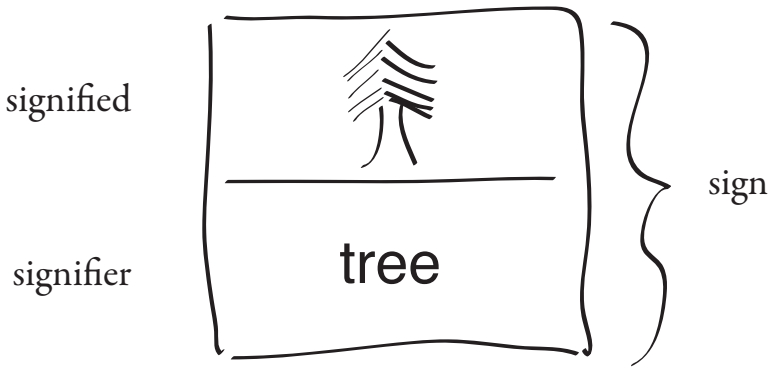

Figure 12-5: The structuralist model of signification. The sound-image tree (the signifier) is coupled to a physical tree in the real world (the signified), and together the two form the sign of 'tree.' Adapted from Ref. [114].

For a concrete example of how to use these terms, I will employ the same example which Saussure offers in his original text: what is the relationship between the word tree and the wooden leafy organism I see outside my window? It is clear to see that these are not the same thing:

1. The former is a name, or more accurately, a "sound-image" [114, p. 66]—when spoken, it is a collection of syllables materialized in sound; in text, a visual arrangement of ink blotches or pixels in the shape of letters. Together, Saussure calls the sound-image tree a *signifier*.

2. The latter is a thing in the world—something that offers shade in the summer, loses its leaves in the fall, and can be harvested for firewood in the winter.[13] Saussure call this the *signified*. Importantly, the signified doesn't have to be a physical object (a tree, a horse, a building) but can be a concept as well (truth, justice, love).

modifiers (tree), and the sign will be enclosed in single quotes ('tree').

[13]This description is of course imperfect and implies a particular set of biological and geographic assumption: not all species of trees lose their leaves in colder weather, and not all climates get cold enough for such a biological mechanism to activate in the first place, yet we would still call them all trees. That said, the contingency of language in the face of anthropogenic climate change warrants closer attention.

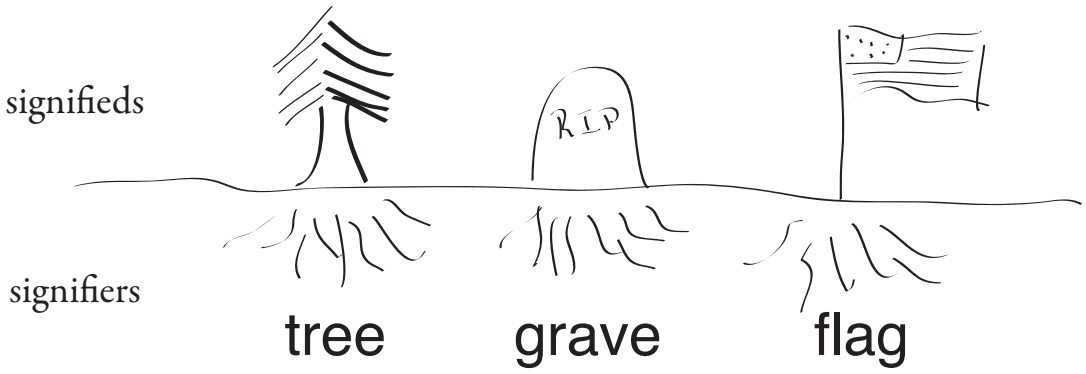

Figure 12-6: A visual metaphor for the structuralist model of language. Each sign is an independent tree in the forest of language, with the signified extending above ground and the signifier below.

While the signifier and the signified are two separate things, "the two elements," Saussure writes, "are intimately united, and each recalls the other." [114, p. 66] This feedback loop or "speaking-circuit," in which the pixels tree signify a physical tree and vice versa, is called the *sign* (*semîon* in Greek, from which *semiology* takes its name). The sign is thus the fundamental building block of meaning; it is the site at which the realm of things and the realm of utterances meet in a dynamic process of *signification*.

It is perhaps not coincidental that Saussure chose a tree as the emblem for his new framework of language. Indeed, the tree is a useful visualization for how Saussure conceptualizes language on a deeper level. Trees extend primarily in one dimension: up and down. Language, for Saussure, does much the same thing. For text to be intelligible, the letters must be read in a particular spatial order—the choice is of course arbitrary (left to right in English or French, right to left in Arabic or Hebrew), but a choice must be made and followed. So too with spoken language: insofar as language is auditory, it unfolds in the time-domain with one syllable following the other. Collectively, Saussure groups these phenomena under a fundamental principle of language, which he calls "the linear nature of the signifier." [114, p. 70] This linearity is not simply a temporal-spatial relationship during the duration of utterance; it is

also a historical relationship. Words, like trees, have roots. In some cases, a word may change significantly over the centuries: for example, the modern English word 'alcohol' comes from the medieval Arabic 'al-kuḥl,' which originally referred to a chemical solution for transmuting the mineral stibnite into elemental antimony, a process which was used for synthesizing cosmetic eye shadow. [36] In others, such as the aforementioned 'ancilla,' the meaning has shifted in the transmission from Latin into English, though the signifier itself has not. In this way, one might say that some words spread out as they grow up, like beech trees, and others grow straight up, like cypress. Regardless of species, all inevitably grow upwards with the passage of time.

In the century following its original transcription by Bally and Sechehaye, semiology underwent a series of profound critiques and revisions by scholars in a range of disciplines. Collectively, this vast expansion of Saussure's model of signification coalesced under a new name, *semiotics*. One of the most influential of these revisions began in the middle of the twentieth century with a group of thinkers who variously assumed the label of *poststructuralist*.[14] In contrast to the 'structuralists'—the linguists who closely associated themselves with the work of Saussure and the field of Structural Linguistics he posthumously inaugurated—the poststructuralists took exception with the clear boundary between the signifier (which exists in language) and the signified (which exists in the real world). This critique was largely motivated by two historical factors which Sassure could not have predicted at the time of his death in 1913, one technological and one political. On the technological side, the middle decades of the twentieth century saw an explosion in the transmission of popular culture, with film, radio, and television becoming ubiquitous in many European and American households. If Saussure had been entirely comfortable drawing a line between the sound-image tree and a tree in the garden, cultural critics of the mid-century were forced to contend with a new range of concepts which appeared to

[14]While poststructuralism is often associated with a particular current of mid-century French critique, the term has been variously attached to thinkers in a range of languages up to an including the present day. While not all embraced the label, a partial list of poststructuralist scholars would include literary theorist Roland Barthes, philosopher Jacques Derrida, historian Michel Foucault, gender theorist Judith Butler, cultural theorist Jean Baudrillard, and feminist scholar Luce Irigaray, to name only a few.

resist this easy binary. How would Saussure have classified the image of a tree in a photograph or a television show? Certainly it is not a real tree but a representation of one filtered through the optical media of a camera. In what way, then, is it different from the sound-image tree, which is itself a representation rendered in the abstract media of sound or image? Is the photograph of a tree a signifier or a signified? What does this mean for the real tree in my yard, itself an oblique and imperfect impression of light on my cornea?

The second factor, of course, was fascism. Writing in the aftermath of World War II, the poststructuralists were part of a larger cultural postmortem of what had gone so monstrously wrong in the 1930s and '40s. How had it happened that Europe—cradle of the Enlightenment, self-proclaimed bastion of science and technology—had descended into totalitarian madness and built the crematoria as its apotheosis? How had the same nation produced both Albert Einstein and Adolf Hitler? While many turned meekly to the economics of the post–World War I depression for answers, the poststructuralists turned to language. Picking up the tools Saussure had left decades earlier, these writers attempted to diagnose the mechanisms of signification at work in fascist political speeches and mass propaganda. To do so, however, the tools required modification. For the poststructuralists, Saussure's unproblematic separation of the realm of language and the realm of objects became symptomatic of a deeper philosophical malady at the heart of Western intellectual life. There was something disturbing about the immaculate unity of the sign, something authoritarian. If there was a true one-to-one correspondence between the signifier and signified of 'tree'—that is, if I believe that the sound-image tree uniquely connects me to an object in the real world—one might argue, as the Nazis did, that the sound-image Aryan indeed connects to a real state of genetic perfection and Jew to real debasement. Lest we isolate fascism to Europe: so too of white and black in the United States under Jim Crow. Saussure's metaphor was prophetic. Trees, like words, can be beautiful. They can provide shelter—shade in the summer, firewood in the winter. They can also be used to lynch a body.

The poststructuralist intervention took many divergent forms, but a useful entry

point can be found in the work of the French literary critic Roland Barthes and his 1957 book *Mythologies*. In that work, Barthes proposes a framework for analyzing how mythology functions as a type of speech. Barthes' model of mythology, as we will see, is remarkably general and can be applied as easily to a piece of fascist propaganda as to an advertisement for household detergent [38]. In articulating this model, Barthes addressed the two historical factors above by offering two substantial modifications to Saussure's model of signification. The first was to radically expand the domain of the signifier. For Saussure, the signifier was either a sound or a collection of letters on a page; for Barthes, it could be almost anything that carries meaning:

> We shall therefore take *language*, *discourse*, *speech*, etc., to mean any significant unit or synthesis, whether verbal or visual; a photograph will be a kind of speech for us in the same way as a newspaper article; **even objects will become speech, if they mean something.** This generic way of conceiving language is in fact justified by the very history of writing: long before the invention of our alphabet, objects like the Inca quipu, or drawings, as in pictographs, have been accepted as speech. [37, p. 219]

In this way, Barthes succinctly resolves the puzzle of the photographed tree by exploding the boundaries of language. Here, Barthes and many of the poststructuralists parted ways with traditional linguists by insisting that the photograph of a tree is as much an object of language as the lexical sound-image tree. Not only that, a physical tree can itself function as a piece of language by becoming a signifier for something else: for example, an oak tree becomes a signifer when it is planted in the memory of a loved one, who then becomes the signified.

Barthes' second modification to Saussure's model follows naturally from this collapse of the clear boundary between the signifier and the signified. For Saussure, signification happens only once—signifier and signified meet and are consummated in a singular sign. For Barthes and the poststructuralists, signification happens over and over again, and these processes can nest within each other. This can be seen clearly in the example of the memorial tree. On the first level, the sound-image tree couples to the physical oak tree to form the sign 'tree.' This sign then becomes the signifier of a second level of signification, where it now refers to the memory of a loved

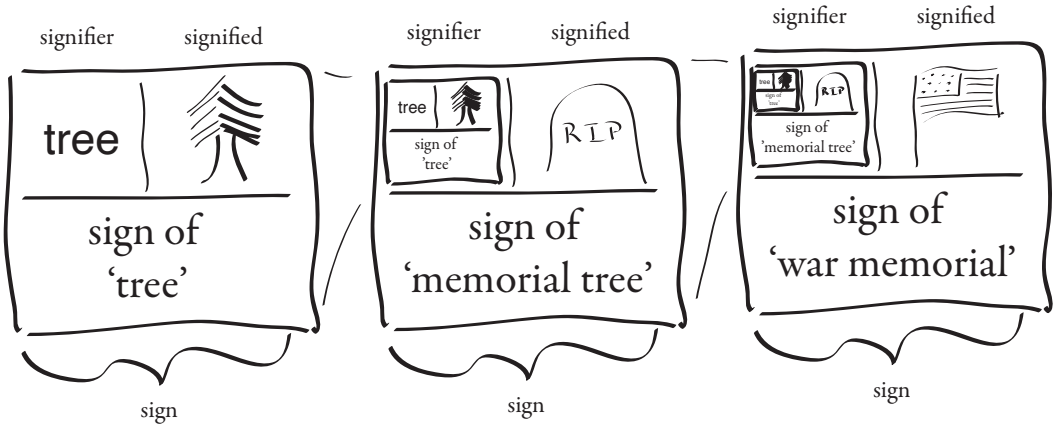

Figure 12-7: The poststructuralist chain of signification. The sign of 'tree' becomes the signifier in a second layer of signification, signifying the death of a loved one in the myth of 'a memorial tree.' The sign of the memorial tree might then become the signifier in yet another layer of language, perhaps signifying the struggle of a nation in 'a war memorial.' Adapted from Ref. [37].

one. Barthes calls this process a "second-order semiological system" [37, p. 223]:

1. On the first level, we have what Saussure calls language. Sound-image (signifier) and object (signified) meet and co-create a meaning (a sign).

2. On the second level, we have what Barthes calls the "metalanguage" of *myth* [37, p. 224]. Here, the sign formed on the first level becomes the signifer for something else which exists beyond the raw materiality of the original signified.

For Barthes, myth is not a pejorative label—it is not a statement about what is true or false, but about how language operates. Some myths, like the association of a tree with a deceased loved one, are comforting and compassionate. However, if we ignore the mythic layer and focus only on the first level of language, Barthes argues that readers and critics fall victim to a grand deception. When I see the word tree, I might think I see a real tree somewhere out in the real world, preserved in some pure state of nature. But in doing so, I ignore how the tree has been "decorated" by its context:

> A tree is a tree. Yes, of course. But a tree as expressed by [mid-century French poet and musician] Minou Drouet is no longer quite a tree, it is a

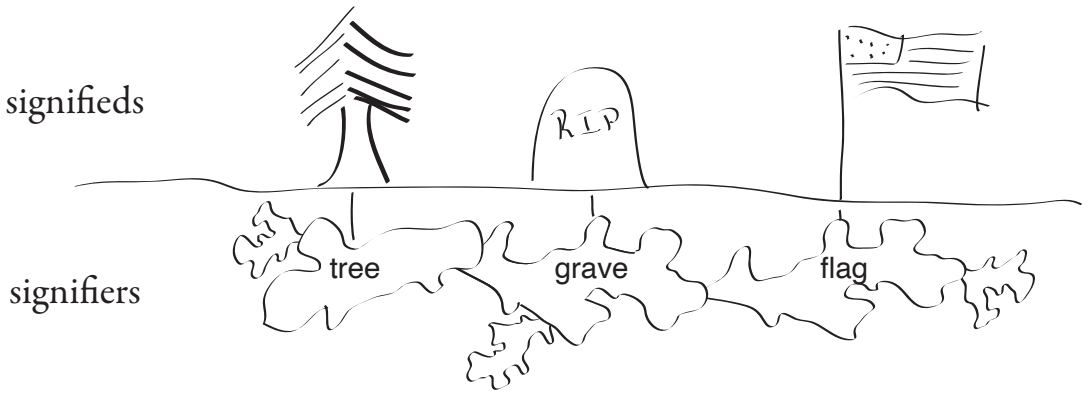

Figure 12-8: The rhizomatic model of language, as proposed by Deleuze and Guattari. Unlike the structuralist model, where every sign stands independently, individual signifieds emerge from an interconnected horizontal root network of signifiers beneath the surface. The horizontal expanse of roots serves as a visual metaphor for Barthes' chain of signification.

> tree which is decorated, adapted to a certain type of consumption, laden with literary self-indulgence, revolt, images, in short with a type of social *usage* which is added to pure matter. [37, p. 218]

The invisible metalanguage of myth works to naturalize these human decorations and convince the reader that, well, that's just how trees are. In this way, the sign of 'Aryan' or of 'White' no longer refers to some pure state of biological reality, but has been devoured by a human myth to signify racial supremacy. The moment we collapse these two levels, as was the case in Nazi Germany or Jim Crow America, we mistake the myth for reality.

While Roland Barthes restricts his model to second-order signification, radical poststructuralists such as the philosopher Jacques Derrida would later extend Barthes' framework to nth-order and argue that the limit as n goes to infinity does not exist [118]. They would point out, to use the example above, that 'biological reality' is not the final referent of race but is itself a part of a perpetually nested chain of signification in which scientific observations are given meaning. Thus, if language for Saussure is a forest of trees—a collection of monolithic objects, each separable for the others—language for the poststructuralists is something tangled, labyrinthine,

and infinitely relational. Here, we can borrow a similarly horticultural visualization coined by the poststructuralist philosophers Gilles Deleuze and Félix Guattari: the *rhizome* [115]. Where tress extend up and down along a single axis, rhizomes such as ginger and turmeric propagate in an orthogonal dimension, parallel to the plane of the ground. Moreover, while a tree is visible in its singularity—one massive trunk extending grandly into the air—a rhizome is subterranean and multiple: each node in a rhizome can spout its own small bud above the surface and, if separated from the rest of the root network, contains all the genetic information needed to replicate itself indefinitely. Like signifiers in the poststructuralist chain of signification—words, images, and objects connecting to one another in layer upon layer of meaning-making—the appearance of individual sprouts above ground disguises the vast interconnected network of relation stretching out beneath the surface. In this way, the rhizome maintains, as the great Martinican poet and critic Édouard Glissant once put it, "the idea of rootedness but challenges that of the totalitarian root." [163, p. 11]

For all its mind-bending complexity and abstraction, the poststructuralist method has proved extremely useful for diagnosing a range of phenomena in a number of disciplines. As a concrete example, we might look to the work of philosopher Judith Butler—widely recognized as one of the founding thinkers of queer theory—who famously adapted poststructuralist methods to the study of gender. In doing so, Butler showed how gender, much like language, is not natural, but instead takes shape through a dynamic and arbitrary semiotic process [83, 84]. For other tasks, however, the poststructuralist method proved lacking. By endlessly deferring the final signified, many poststructuralists privileged language over matter, with the material world vanishing somewhere in an endless hall of mirrors. While this move worked for many literary theorists and artists—particularly those who embraced poststructuralism's aesthetic descendant, *postmodernism* [221, 285]—it was less effective in addressing the concerns of scholars in the sciences. By the late twentieth century, it was clear that language alone could not account for the reproducible peaks of a laboratory spectrogram or the lost limbs of a civilian in Vietnam, though it had a part to play in both. The task, then, was to reconcile the world of language and of matter without

ignoring the former or denying the latter.

Again, this work has taken many forms in many disciplines. Here, I want to focus on a particularly heterogeneous body of scholarship undertaken by feminist scholars of science, technology, and society (STS)—a body of scholarship which has immeasurably influenced my project in this essay.[15] Where the poststructuralists reduced matter to language, feminist STS scholars have insisted that both have a significant part to play in the construction of meaning, a process which the historian of science Donna Haraway famously called *material-semiotic* [184, p. 588]. Once again, the material-semiotic move was an expressly political one: how do feminists resist science as an apparatus of militarism (the invention of weapons and tools of war), capitalism (the extraction and exploitation of labor), colonialism (the subordination of indigenous communities and theft of native land), and patriarchy (the elevation of a gendered set of normative ideals) without abandoning objectivity altogether [184, p. 578]? Where the postmodernists appeared eerily at ease abandoning any notion of reality, Haraway and her colleagues refused to choose between science on the one hand and their commitment to dismantling systems of oppression on the other.

For scholars of feminist STS, this choice—like the separation of language and matter itself—represents a false binary. To see this, one has to understand the vantage from which they are seeing in the first place. They have to pay attention to the eyes they are seeing with, the tongue they are speaking with, and the body those parts are plugged into. Insofar as they are human practices, language and science don't happen in the aether. They are encountered at the body: an imagine created in the reflection of light on a cornea, or a word formed at the interface of lip and tooth. As such, Haraway demanded that scientists practice "embodied objectivity," objectivity which is aware of the position—material, historical, political, social, racial, sexual—from which judgements and observations are made [184, p. 581]. Take, for

[15]The list of thinkers here is too vast to name in full and spans a range of professional disciplines (history of science, philosophy, anthropology, as well as the physical sciences) and a range of feminist practices (including queer, trans, and nonbinary feminisms), though a partial list would include historian of science Donna Haraway, philosopher and physicist Karen Barad, queer and disability theorist Mel Chen, post-colonial historian of botany Banu Subramaniam, theoretical cosmologist Chanda Prescod Weinstein, and anthropologist Anna Tsing.

example, the image from a satellite or from a scanning electron microscope (SEM). These images may be breathtaking and wondrous, stimulating the imagination, but they are also just that: images. Like the photograph of a tree, they are also the process of multiple layers of mediation and signification. This is not to say they are not real, but it is to say that they are partial and contingent. Both are performed using extremely sophisticated and expensive instruments, which depend on specific historical-political conditions of educational and financial resources. In both cases, data had to be processed for the image to appear at all, and the choice of analysis function can radically alter the image. These eyes are not unique. Rather, they reveal a fundamental condition of all eyes, organic and mechanical:

> The "eyes" made available in modern technological sciences shatter any idea of passive vision; these prosthetic devices show us that all eyes, including our own organic ones, are active perceptual systems, building on translations and specific ways of seeing, that is, ways of life. There is no unmediated photograph or passive camera obscura in scientific accounts of bodies and machines; there are only highly specific visual possibilities, each with a wonderfully detailed, active, partial way of organizing worlds. [184, p. 583]

To ignore this—to think the microscope and the satellite are transparent windows into the world, offering unlimited access at all scales of matter—is to perpetrate a "god trick," to fool yourself into believing you are "seeing everything from nowhere." [184, p. 581]

To visualize this network of embodied language, matter, and circumstance, we can turn to a final ecological metaphor provided by the anthropologist Anna Tsing: the mushroom. In her 2015 book, *The Mushroom at the End of the World: On the Possibility of Life in Capitalist Ruins*, Tsing documents almost a decade of fieldwork interviewing scientists, traders, and migrant workers involved in the cultivation of matsutake, a particularly rare and valuable species of mushroom prized as a delicacy in Japan. [440] Like the sprouts of a rhizome root network, individual mushrooms emerge from vast fungal bodies extending weblike underground. In scale, both spatial and temporal, these webs of mycelium can far exceed those of the rhizome: the world's largest living organism, the jovially named "Humongous

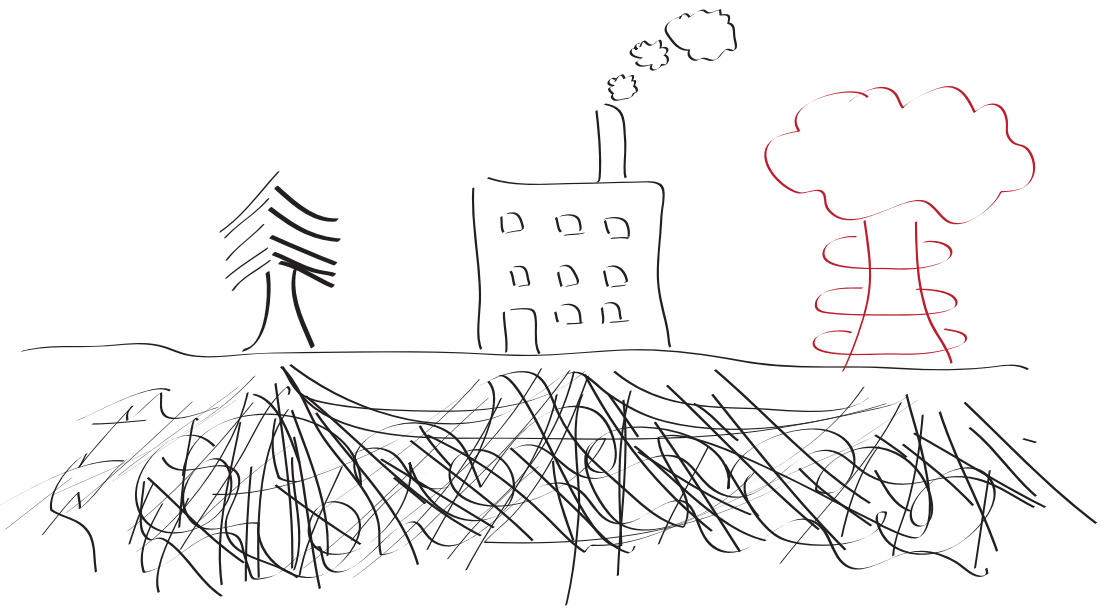

Figure 12-9: The mycelium network of material-semiotics, inspired by the work of Anna Tsing [440]. The subterranean root network of the rhizome is replaced with a vast and diffuse network of fungal fibers, tangling together the realms of the natural, the industrial, and the catastrophic.

Fungus," covers almost nine square kilometers in Oregon's Malheur National Forest; it is over 2,400 years old. Moreover, unlike Saussure's tree or the poststructuralist rhizome, the mushroom defies the Western binary of Man (a creature of thoughts and intentions) and Nature (a passive backdrop lush with resources, waiting to be harnessed). Trees and rhizomes can be planted and arranged in meticulous parks or plantations, tamed to the whims of human hands; mushrooms, particularly the elusive matsutake, cannot. Rather, humans must seek out these precious delicacies in unexpected places, leading to a massive underground economy of migrant workers and traders spread across numerous continents, invisible to most consumers. In turn, the mushroom feeds off the leftover detritus of human industrialization, thriving in sites of modern environmental devastation and ruin: a messy kitchen, an abandoned factory or logging site, even the irradiated blast radius of an atomic bombing. If the tree and rhizome were vestiges of a romantic agrarian ideal, Tsing's mushroom is tuned to the reality of human-induced climate disaster, revealing the inescapable

symbiosis between the human and non-human. Thus, the network of global finance, labor, and industry tangles with the non-human fungal network of the mushroom. Language and matter: neither separable, always intertwined, the one feeding off the other.

12.7 The Zeugmatic Short

If the relevance of the preceding section to the conversation about quantum supremacy is not immediately clear, suffice it to say that people have been thinking about language for at least as long as they have been thinking about quantum mechanics. As scientists, we would do well to attend to this century of intellectual labor before making off-hand proclamations about what language does and does not do. Indeed, with a little humility, we would quickly see that the past century has provided an abundance of tools for making these semantic riddles tractable. So, equipped with these tools, let us return to the question we concluded a previous section with: is quantum supremacy a metaphor, or is white supremacy? Which one is real?

From a material-semiotic perspective, it is clear that this is another false binary: they are both metaphors, and they are both real. They are both metaphors in the sense that each is a sign in a chain of signification—after all, what is a metaphor if not a piece of language which signifies another piece of language? Moreover, both quantum supremacy and white supremacy are myths in Barthes' sense of the word. If quantum mechanics is a language which connects technical terms (signifiers) to material phenomena (signifieds), then quantum supremacy operates as at the level of metalanguage, using details from quantum mechanics (for example, the vastness of Hilbert space) as signifiers for computational power. In much the same way, the biological condition of whiteness operates as a signifier in the myth of racial supremacy. Here, of course, we see that the second-order model is dangerously insufficient: 'the biological condition of whiteness' is not fundamental but is itself a multi-order process of signification which draws on phenomena both physical (a deficiency of the pigment melanin) and social (legal segregation) as signifiers in the myth of race. Indeed, race

is a material-semiotic object, emerging out of a complex network of physical, social, and historical considerations.

So too with quantum mechanics. As philosopher of science Karen Barad notes in their 2007 book *Meeting the Universe Halfway*, the 'pure physics' of quantum theory is not the ground floor of reality, but itself emerges from a material-semiotic process. Here, Barad famously points to the 1922 experiment of Otto Stern and Walther Gerlach, widely remembered as the first direct measurement of quantized electron spin, the primordial quantum bit. When the polarized silver atoms failed to leave a visible mark on the detector at the end of the experiment, Stern's breath—suffused with sulfur from his habit of smoking cheap cigars—unexpectedly converted the silver to jet black silver sulfide, rendering the bifurcated pattern visible to the human eye. For Barad, Stern's cigar becomes an integral part of the laboratory apparatus, revealing something about the porous boundary between the laboratory and the social world outside. Barad's language here is extremely precise:

> Apparatuses are not static laboratory setups but a dynamic set of open-ended practices, iteratively refined and reconfigured. As the revised diagram of the Stern-Gerlach apparatus indicates, a cigar is among the significant materials that are relevant to the operation and success of the experiment[...] Not any cigar will do. Indeed, the cigar is a "condensation"—a "nodal point," as it were—of the workings of other apparatuses, including class, nationalism, economics, and gender, all of which are a part of this Stern-Gerlach apparatus. **Which is not to say that all relevant factors figure in the same way or with the same weight. The precise nature of this configuration (i.e., the specific practices) matters.** Nor is it to suggest that social factors determine the outcome of scientific investigations. Indeed, it would be a mistake to understand the presence of the cigar in the diagram as a symbol of the fact that the experimenter's intrinsic identity (e.g., his gender and class) is a determining factor in the outcome of the experiment. This reading would be mistaken in several important ways: it misunderstands the nature of gender, class, individuals, practices, materiality, agency, and casuality. [...] The point is, rather, that in this case, material practices that contributed to the production of gendered individuals also contributed to the materialization of this specific scientific result ("gender-and-science-in-the-making"): "objects" and "subjects" are coproduced through specific material-discursive practices. [32, p. 167]

The contingency of the Stern-Gerlach experiment on a cheap cigar—a rhizomatic "nodal point" connecting the semiotic practices in the laboratory with the 'external' world of gender and race—does not invalidate the results of the experiment. The quantization of electron spin is real. But so too is the gender disparity in the sciences. So too are the effects of racist police brutality. Science, gender, and race are real. The issue is that these realities are not separable—they are intertwined and emerge together. "The social and the scientific," Barad writes, "are co-constituted. They are made together—but neither is just made up." [32, p. 168] Both the social and the scientific matter, in the dual senses of 'matter': they are both concepts which matter (in the sense that they are both significant), and they both inscribed in matter (they leave material traces on bodies).

Quantum supremacy and white supremacy both matter. Each emerges from a material-semiotic process, but this does not mean they are the same thing. This is crucial. To confuse this point would be to naturalize race on the one hand and reduce science to social construction on the other. Details matter. When we consider the interplay of the social and the material in the emergence of phenomena, we must take Barad's point above that not all of these "relevant factors figure in the same way or with the same weight. The precise nature of this configuration (i.e., the specific practices) matters." [32, p. 167] In mathematical terms, not all coefficients in a Fourier expansion are equal; it depends on the function. In poststructuralist terms, not all nodes in a rhizome are in equal proximity to one another; it depends on the myth. So too with the material-semiotic. The relative orientation of actors (human and non-human) in space (geography), time (history), and language (a chain of signification) matters. Like sinews of a massive fungal body, some fibers tangle and merge many times over, while others spread far from one another, connected imperceptibly via the diffuse and vast network of strands between them.

Studying the relative position of 'quantum supremacy' and 'white supremacy' in the material-semiotic web, we arrive again at the elephant in the room: they share the same nine final letters. This matters, but how it matters also matters. Is the 'supremacy' in 'quantum supremacy' the same as in 'white supremacy'? Or, more to

the point, how does 'supremacy' connect 'quantum' and 'white' without collapsing the distinction between them? Again, this is precisely the question at the heart of Eve Tuck and Wayne Yang's 2012 essay "Decolonization is Not a Metaphor," and it is useful to consider how scholars grappled with the consequences of Tuck and Yang's powerful argument. How, we might ask, is the 'decolonization' in 'decolonizing Indigenous tribal land' both the same and different from in 'decolonizing the mind'? How do we prevent 'decolonization' from becoming "an empty signifier to be filled by any track towards liberation" [441, p. 7]—depleted of its urgent call for the repatriation of tribal lands—without demanding that some of these tracks are real and others are merely metaphorical?

Here, we can consider one possible model offered by the anthropologist Stefan Helmreich. In his 2020 essay, "Not a Metaphor," Helmreich responds to Tuck and Yang's provocation by considering the rhetorical device of *zeugma*: "the use of a word to modify or govern two or more words usually in such a manner that it applies to each in a different sense." [195, p. 446] In explaining how zeugma works, the literary theorist Gillian Beer offers an example from Charles Dickens' 1836 novel *The Pickwick Papers* [41, p. 298]:

> *Miss Bolo rose from the table considerably agitated, and went straight home, in a flood of tears and a Sedan chair.*

Dickens is playfully toying with the word 'in' by using it in two different senses: to be '*in* tears' (an emotional state) and '*in* a chair' (physically seated). He only uses the word 'in' once, but the reader's interpretation of that word oscillates as it inflects the tears and the chair differently. In this way, Helmreich notes, the word "vibrates between two meanings, one literal, the other figurative, destabilizing what was thought to be literal in the first place." [195, p. 449] Indeed, while one might be tempted to distinguish between the metaphorical usage of 'in' ('in tears') and the real ('in a chair'), zeugma unsettles this distinction by revealing that both are materizalized in language, though differently. Helmreich notes a deep resonance with Donna Haraway's call for situated meanings. "The uneasy laughter generated by many examples of zeugma," Helmreich writes,

> indicates the affective valence of language, and, more, emphasizes the politics of situated meanings—and in ways that resonate with Tuck and Yang's call for an attentiveness to the politics of metaphor. As Haraway has lately put it, 'It matters what matters we use to think other matters with; it matters what stories we tell to tell other stories with; it matters what knots knot knots, what thoughts think thoughts, what descriptions describe descriptions, what ties tie ties.' It matters what metaphors motivate what metaphors. It matters what concepts are yoked together by zeugma, and how. [195, p. 449]

In this way, the word 'decolonizing' in '*decolonizing* Indigenous tribal land' and '*decolonizing* the mind' operates zeugmatically. It is the same word, but its meaning oscillates and vibrates depending on which phrase it appears in—on its situation. By attending to the zeugmatic function of language, Helmreich argues, we can honor Tuck and Yang's critique of the situated politics of metaphor—the co-opting of decolonization discourse in ways that distract from focused anti-colonial action—while also attending to metaphorical and figurative function of all language, as poststructuralism and material-semiotics point us to.

'Quantum supremacy' and 'white supremacy' are similarly yoked together by zeugma. Like Dickens' 'in,' like Tuck and Yang's 'decolonization,' 'supremacy' is zeugmatically inflected by its proximity to either 'quantum' or 'white,' and the word means something different in each term. We must attend to that difference, but we must also attend to the fact that it is the same word. In this sense, we must undertake a critique which is the inverse of Tuck and Yang's. For Tuck and Yang, the issue lay in the false sense of equivalency between various forms of 'decolonization,' and their goal was to show that the same word can mean different things in different contexts. If the quotations from scientists in the early sections of this essay are any indication, it would appear that 'supremacy' suffers from the opposite problem: for many scientists, even the ones who acknowledge the need to change their language, there is an underlying belief that 'supremacy' means something different in 'quantum supremacy' than in 'white supremacy.' This is false. Zeugma, after all, is a relationship of simultaneous similarity (the same word) and difference (multiple contextual meanings), and we would be misled if we focused only on the difference to the exclusion of the

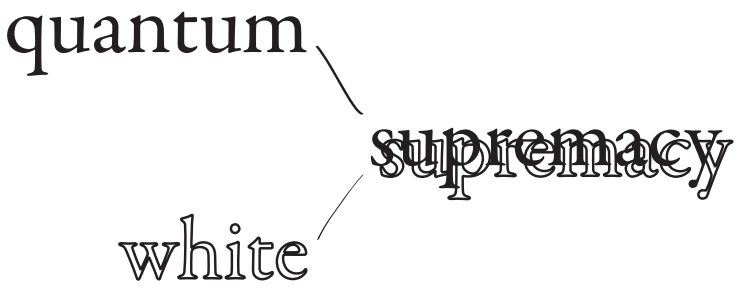

Figure 12-10: The zeugmatic short. 'Supremacy' operates as a semiotic tether between 'quantum' and 'white,' altered by its proximity to each and reciprocally altering each.

similarity. We must also attend to the fact that zeugma operates in both directions: if 'supremacy' changes meaning depending on its proximity to either 'quantum' or 'white,' both words are reciprocally inflected by their proximity to the aspiration of 'supremacy.' In this way, the rhetorical device of zeugma functions something like an electrical short circuit, tethering together two distinct pieces of circuitry in such a way that current travels invisibly between them, altering the operation of each, sometimes catastrophically.

Probing the zeugmatic short circuit, what do 'quantum supremacy' and 'white supremacy' have in common? How do both 'quantum' and 'white' each take shape under the guiding influence of 'supremacy'? In both cases, as I showed earlier in this section, 'supremacy' is a myth, in the sense of higher-order signification. More specifically, both 'quantum supremacy' and 'white supremacy' are *myths of power*. 'Quantum supremacy' asks us to imagine a class of devices (quantum computers) which dominates all others (classical computers). In much the same way, 'white supremacy' posits one race of humans above all others. So too of 'national supremacy' (the domination of one geopolitical community over all others, as in the myth of American exceptionalism) and 'intellectual supremacy' (the domination of one academic discipline, as in the physics hierarchy). Supremacy—'quantum,' 'white,' or otherwise—is a god trick. To believe you have access to power above all others is to imagine yourself divine. This is not a coincidence, it is baked into the etymology of the word itself.

The Oxford English Dictionary traces the first usage of the modern English word 'supremacy' to the Acts of Supremacy passed by the Parliament of England in the sixteenth century [429]. These acts legally established the English monarchs as the head of the Church of England, bypassing the authority of the pope. In this way, 'supremacy' legally yoked together the realms of the human (politics and statecraft) and the divine (arbitration over theological matters) in the hands of a single ruler. Like monarch-priests surveying the entirety of creation, when we compare quantum computers to classical computers and argue that the former can accomplish tasks which would require the age of the universe to perform on the latter, we are imagining that we have eyes which can comprehend all the atoms in the universe or multiple big bangs. We are confusing mathematical eyes with our own profoundly finite organic ones, ignoring the murky process of translation between them.

This process of translation is neither transparent nor innocent, and it requires constant maintenance. In the case of white supremacy, American history and law are scarred with repeated attempts to impress the domain of the supreme onto the domain of the human. Here, we can refer to the work of American legal scholar Dorothy Roberts and her 2011 book *Fatal Invention*. In the opening chapter, "The Invention of Race," Roberts documents how the American social construct of racial supremacy—a construct which emerged in the colonial period to legitimize the enslavement of abducted Africans and their descendants, as well as the feudal plantation economy they powered—was instantiated in law throughout the nineteenth and twentieth centuries, perpetuating the vantage point of white supremacy long after the legal emancipation of Black citizens in 1863. As an example, Roberts cites the 1857 Supreme Court case of Dred Scott, a case that cemented centuries of racist social precedent in law by affirming the legal subordination of Black Americans, both enslaved and free, to white Americans. The court's decision in the case of Dred Scott not only provided legal precedent for over a century of segregation, disenfranchisement, and terrorism; it set in motion a surreal cycle of court cases over what it meant to be white in the first place. In the decades surrounding the turn of the twentieth century, the horrific Black-white binary of American law was tested by an influx of immigrants from Asia

and Eastern Europe—some of whom legally petitioned to be counted as 'white' in American law. As Roberts notes:

> Determining which groups of immigrants met the whiteness test for naturalization became a vital legal issue for almost a century. Between 1878 and 1952, state and federal judges issued decisions in fifty-two racial prerequisite cases, including two argued before the U.S. Supreme Court in the 1920s. In these cases, judges ruled that Chinese, Japanese, Koreans, Filipinos, Hawaiians, Afghanis, Native Americans, and anyone of mixed ancestry were not white. Arabs, Syrians, and Asian Indians were considered white by some judges and not by others. Armenians were more successful at claiming whiteness, despite their geographic origins east of the Bosporus Strait, which separates Europe from Asia. [382, p. 15]

Since the condition of whiteness has no final signified in either biology or geography, the flawed logic of white supremacy must be constantly reassessed and reformulated in order to appear coherent. The poet and literary theorist Fred Moten has compared this process to the maintenance of the Ptolemaic model of the solar system: starting from the flawed premise that the earth was at the center of the universe, Ptolemy and his followers produced an increasingly elaborate model of orbitals and epicycles to conform their model to astronomical observation, a model which was entirely obviated by the adoption of the heliocentric model of the solar system. "It's amazing," Moten notes,

> how much brilliant intellectual work these guys had to do so that they could stay wrong. It's like that particular cosmology was trying to maintain a kind of cascade failure—every time you shored up one thing, another one would break, but you kept having to do it. You kept having to fix it and it became more and more and more and more elaborate. Epicycles of epicycles. So there's this kind of weird thing where, on the one hand it's kind of stupid because there's a much simpler and easier way to understand the universe, and on the other hand there's something brilliant and ingenious about it because look at all that beautiful weird filigree work you had to do. In a slightly—I wouldn't use the word beautiful or anything—but I would say that the maintenance of racism is similar. It's really fucking stupid, but there's a certain amount of impressive intellectual work that has been done in order to maintain it. [319]

Ptolemy's god trick was to imagine earthly eyes in the center of the cosmos, a supreme vantage point around which all of creation pivots. This vantage point, like the priv-

ileged position of whiteness in American law, is untenable without constant maintenance. A similar sort of iterative, epicyclic logic is at work in claims of quantum supremacy. As we saw earlier in the Google-IBM feud which followed the publication of Arute et al., proof of quantum supremacy can be elusive and contentious. Did the quantum computer do something which would take the best classical computer ten thousand years to complete, or two and a half days? Does it matter? Again, despite the perception that quantum supremacy is a fundamental feature of quantum mechanics, the term itself has no final referent in either mathematical proof or formal logic. Instead, the term 'quantum supremacy,' like 'white supremacy,' works to naturalize a baggy set of convictions grounded variously in science (quantum supremacy as a set of empirical observations), social identity (quantum supremacy as the shared aspiration of a professional community), and commerce (quantum supremacy as a feature distinguishing the product of one corporation from another). When these convictions are threatened—as when the IBM scientists countered the claims of the Google paper—the term must mutate to accommodate the challenge. While these mutations and corrections may appear self-consistent, they obscure and gild the same cascade failure endemic to all claims of supremacy.

12.8 Ground Loops

In the earlier sections of this essay, we saw how much of the controversy about the term 'quantum supremacy' revolved around the question of whether or not the word might offend individual people. By now, it should be clear that this was the wrong question to ask, or at least an extremely incomplete one. Language is not an inert object, a collection of stones cast at individual people, causing individual harm. Language is a network of relation, a web pointing to other pieces of language. Language tangles with matter and gives rise to phenomena; it doesn't just describe phenomena that already exist in the world. So when we talk about what 'quantum supremacy' does or doesn't do, the question isn't simply whether or not the word might unintentionally remind someone of a different type of supremacy. The question is, how does the aspiration

of supremacy short-circuit quantum computing to other systems of power? How does quantum supremacy mimic and naturalize some of the same noxious patterns we find in, for example, racial supremacy?

This is not to say that quantum supremacy isn't offensive. It is, for all the reasons that scientists might anticipate, but also for other reasons which may not seem immediately connected to issues of race, gender, and power. Foremost, I am *angered* by quantum supremacy, by the careless language that circulates in the quantum computing community and the systems of power it traffics with. I am also offended by quantum supremacy, but I am offended by it in much the same way that I am offended by most high-profile scientific results. I am offended by what it makes legible and what it obscures. When my colleagues and I encountered the media frenzy around the quantum supremacy result in 2019, what struck some of us most was how little the acclaim had to do with our day-to-day life in the laboratory. While major news outlets fantasized about what quantum supremacy might mean for the future of technology and commerce, hardly any attention was paid to the work that produced that result. As a feat of engineering, the experiment of Arute et al. is a technical masterwork. It is also, as Chanda Prescod-Weinstein would point out, the product of years of intellectual and physical labor by scientists, engineers, technicians, custodial staff members, administrative assistants, cafeteria dining staff, child-rearing spouses and domestic workers, et al.—the vast majority of whom go uncredited in the final manuscript, let alone in the glossy news articles announcing the result [362]. This will hardly strike most scientists as strange—authorship and acknowledgements are strictly reserved for individuals who contributed to the scientific content of the work, though this is hardly a rigorous distinction.[16] It is, however, symptomatic of a

[16]In their official guidelines on submitted research manuscripts [353], the American Physical Society (APS) specifies that the acknowledgement section at the end of a manuscript can be used to "recognize named individuals who contributed scientifically to the research of the paper; cite the funding agencies that provided financial support for the work; and note the affiliation of institutions in the byline. Acknowledgments to people precede those of financial support." However, on the other hand, "acknowledgments may not recognize those who helped in preparing the paper; editors who handled the peer review of the paper; those who contributed general encouragement (family, friends); or those who provided services that were not directly part of the research. Acknowledgements may not include a dedication or a memorial."

larger problem. 'Quantum supremacy' is the *product* of labor, and it is also a *product* in the capitalist sense: it's a computational resource that can be sold to consumers; it's a buzzword appearing on corporate advertising and press releases to enhance a company mythology; it's a scientific result which generates revenue for the for-profit journal which published the result. Products, as Karl Marx once noted, have a way of concealing the labor that goes into their creation such that they appear miraculous. In this way, the "mystical character" of quantum supremacy operates as a commodity fetish [296, p. 319], obfuscating a profoundly unequal system of production, not unlike how the mystique of white supremacy masked and normalized the monstrous workings of the feudal plantation economy.

What would the story of quantum supremacy look like if it were told by the laborers who made the result possible? Indeed, if quantum computing research is a war against "the formidable enemy of decoherence," as John Preskill put it in his original address on quantum supremacy [364], it should come as little surprise that the history of that war is told by generals and heads of state, not by the soldiers on the front lines. What do things look like in the trenches? Well, not so glamorous. Quantum computing research, like most scientific labor, is quite often repetitive and mundane, filled with tasks that will never appear in a journal publication. Since quantum processors are extremely sensitive devices, the successful execution of an experiment requires a delicate balance of environmental considerations, and this balance requires constant maintenance. For example, in experimental quantum computing using superconducting circuits, devices are encased in a dilution refrigerator and cooled to a fraction of a degree above absolute zero—tens of millikelvin, two orders of magnitude colder than the darkest vacuum of outer space. Maintenance of this temperature requires a particular set of thermodynamic conditions—to say nothing of the economic and institutional conditions required to purchase such an apparatus in the first place—and the slightest change in the pressure or flow of cryogens throughout the system can render a device inoperable. When the conditions are just right and an experiment is finally performed, the technicians or graduate students responsible for successful maintenance of these conditions may go uncredited in the final research manuscript.

Among the forms of invisible labor undertaken in a quantum computing lab, one of the most frustrating and fascinating is the hunt for ground loops. Ground loops occupy a strange liminal space in the scientific imagination. On the one hand, the concept of a ground loop is simple—so simple, in fact, that it hardly warrants mention in an academic research publication. On the other hand, it is so technical that most physics students will go the entirety of their undergraduate and graduate careers without ever encountering the concept in a class or textbook. Like many of the laboratory gremlins that occupy an experimentalist's time, it instead occupies the realm of lab folklore and myth. To date, the only textbook description I can find for a ground loop appears in a highly technical volume on experiment design by Philip C. D. Hobbs, a self-employed engineering consultant who runs a firm called ElectroOptical Innovations, titled *Building Electro-Optical Systems: Making It All Work*. Hobbs' aspiration in writing the book is encapsulated in an epigraph by Richard Feynman at the start of the textbook, excerpted from his 1996 Nobel Prize lecture:

> We have a habit in writing articles published in scientific journals to make the work as finished as possible, to cover up all the tracks, to not worry about the blind alleys or describe how you had the wrong idea first, and so on. So there isn't any place to publish, in a dignified manner, what you actually *did* in order to get to do the work. [202, p. vi]

Hobbs relishes in these covered up tracks and blind alleys, compiling nearly a thousand pages of technical details required to successfully operate an electo-optical physics experiment. In doing so, Hobbs imagines his work as a survival guide for beleaguered graduate students. "This book," as he frames it on his company website,

> is an attempt to provide a systematic and accessible presentation of the practical lore of electro-optical instrument design and construction: in other words, it's the book I needed as a graduate student, but couldn't find.
>
> It's intended in the first instance for use by oppressed graduate students in physics and electrical engineering, who have to get their apparatus working long enough to take some data before they can graduate. When they do, they'll find that real-world design work has much the same harassed and overextended flavor, so in the second instance, it's intended as a self-teaching guide and professional reference for working electro-optical

designers. [203]

Hobbs' section on ground loops is short, only about one page long [202, p. 621]. A ground loop, he writes, occurs when an experimental setup is connected to electrical ground at multiple points, such that the entire setup forms a closed loop. To understand the implications of this loop, we must say a few more words about what electrical ground means and does.

The concept of ground is crucial in electrical engineering.[17] Normally, when we think about a simple electrical circuit, we imagine a loop of wire connecting a voltage source (say, a 1.5-volt battery) to a load (such as a small light bulb). As long as the loop remains intact, the voltage difference across the battery will push electrons along the loop, powering the light bulb. If this loop is broken, the electrons can no longer circulate and the light bulb turns off. This is how a light switch works: when you toggle the switch, a piece of metal behind the switch flicks into position and completes the loop, powering the light; toggle it again, and the metal pulls out of position, breaking the loop and turning the light off. This circuit evidently requires two lengths of wire, one to connect the light bulb to the positive terminal of the battery, and another to connect it to the negative terminal. Together, the battery, light bulb, and the two strands of wire connecting them form a closed loop. Now, we might ask: what is the difference between the closed loop we just described and an open loop, consisting of only a single wire connecting the bulb to one terminal of the battery? Surely the circuit is still connected—after all, the remaining terminal of the battery is connected to the bulb by air. Air, like metal in a wire, conducts electricity, which is how we get lightning. The issue, of course, is that air has a much larger resistance than metal, so it conducts electricity more poorly; in order to power the light bulb via the air, we would require a battery with a voltage massive enough to ionize the air, forcing current through. Impractical (and dangerous), for sure, but we will note that the difference between an open circuit and a closed circuit is not binary; it too is a question of material and of proximity, of medium and of force.

As above, so below. While the notion of plugging a circuit into the air might

[17] For an excellent and accessible introduction to electrical ground, see Ref. [349].

sound fanciful, the same logic applied to the ground is absolutely practical. Taking our open circuit and plugging the loose ends deep into the soil, we would find it takes only a hundred or so volts (the voltage of a standard power outlet) to illuminate our light bulb. While dirt, sand, and stone are generally poor conductors, the resistance of a wire scales inversely with the width of its cross-section; the thicker the wire, the lower the resistance. A strand of 20-gauge speaker wire has a cross-sectional diameter of about a millimeter; the diameter of the planet Earth is almost 13,000 kilometers at the equator. Thus, from an electrical standpoint, the earth can be thought of as an enormous wire, a vast and mobile reservoir of electric charge. When we plug both ends of our open circuit into the earth—perhaps by attaching it to a metallic water pipe traveling beneath the building—the battery pulls electrons out of the earth on one side and pushes them back into the planet on the other. The ground completes the circuit. Moreover, since all points on the earth's surface are electrically connected to each other with low resistance, the planetary surface can be approximated as a plane of constant voltage. Since electrical properties depend only on *relative* voltage—the difference in voltage between two points, as opposed to the *absolute* voltage of any one point—electrical engineers are free to define the constant voltage of the earth as 'zero.' Planetary ground thus provides a common reference plane for all other electrical systems: the ground wire in one home will have the same voltage as the ground wire in its neighbor, which will be at the same voltage as in a home on the other side of the planet.[18]

Most consumer and industrial electronics are grounded—that is, they are connected to a conducting rod dug into the planetary surface, usually by way of a third

[18]The image of electrical ground as an infinite reservoir or absolute reference plane is, of course, another form of god trick. From a situated position, we would necessarily ask, *where is the literal ground of electrical ground?* One need only look at history to understand the urgency of this question. In the nineteenth century, the American telegraph industry laid vast lengths of cable between the Atlantic and Pacific coasts, enabling fast communication across the United States. Rather than spend money on two massive lengths of wire per telegraph circuit, the telegraph system employed electrical ground to complete the circuit, mobilizing the soil of continental America as part of the communication network. The role of the telegraph system in the colonization of the American continent—a project of violently seizing Indigenous land in the name of agriculture and industry—is not coincidental. Electrical ground is often sacred ground and stolen ground, appropriated and made 'productive' by the forces of colonization.

prong on their power cable. This is particularly true for precision microwave electronics, which generate oscillating electromagnetic signals in the radio frequency (RF) spectrum and play an important role in modern telecommunications technologies, such as Wi-Fi and 5G. In RF devices, electrical ground provides a boundary condition for signals traveling down wave-guides, like the coaxial cable plugging an internet router into the wall. The stability and invariance of electrical ground anchors these waves such that they travel with a precise frequency, amplitude, and phase—the parameters which encode communications signals. Building on decades of electrical engineering technology developed throughout the past century, many quantum computing platforms rely on RF instruments to control the quantum states of the processor. This is particularly true for processors based on superconducting qubits, such as the Sycamore device used in the work of Arute et al. A single superconducting qubit is usually connected to one or two coaxial cables—one to drive the qubit between quantum states using a microwave pulse, and often one to position the qubit on its energy landscape using magnetic flux. Each of these cables—dozens in total to control a 54-qubit device such as Sycamore—is routed up through the dilution refrigerator, through a series of electrical isolators and attenuators, and out to a box of control electronics at room temperature, where the signals are finally grounded. The stability of signals passed through these cables is paramount; any noise on the line or spurious electrical current, and the fragile quantum state in the processor will rapidly decohere, losing its ability to run any computation.

Ideally, all of these cables will be electrically connected at a single point, the ground. In this way, the electrical signals fan out from a common point like branches from a tree trunk, a single reference point. In practice, however, these cables often make contact at unintended places. For example, the metallic connectors of a tight bundle of coax cables might touch each other when plugged into the refrigerator. While the point of contact might be almost imperceptible—as small as a few millimeters of metal touching each other—this is enough to electrically short the two cables together, allowing current to pass through with hardly any resistance. When this happens, the cables are now connected at two points, once at ground and once at the

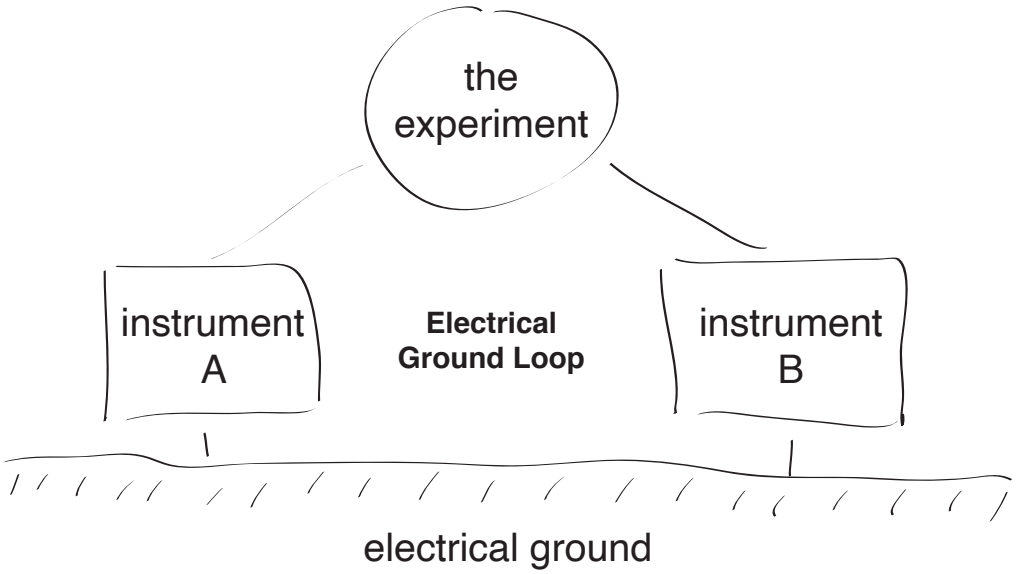

Figure 12-11: An electrical ground loop. Two instruments, each connected to electrical ground, are accidentally shorted together when plugged into a common experiment, forming a closed electrical circuit. The area enclosed by this loop is then susceptible to stray magnetic flux, inducing spurious electrical currents which pour noise into the experimental apparatus.

unintended contact. They form a closed loop of wire, a *ground loop*. This loop completes an electric circuit. Unlike the circuit of a battery and light bulb, the ground loop should carry no electric current. Since the wires are grounded, and electrical ground has approximately constant voltage, all points along the ground loop should have equal electrical potential, meaning there is no electrostatic force to push current along the wire.

The Faraday-Maxwell equation—one of the four foundational equations of electromagnetism, collectively attributed to the nineteenth-century Scottish physicist and mathematician James Clerk Maxwell[19]—states that a temporally varying magnetic

[19]The Faraday-Maxwell Equation, often referred to as Faraday's Law of Induction after the nineteenth-century English physicist Michael Faraday, can be written in differential form as

$$\frac{\partial \mathbf{B}}{\partial t} = -\nabla \times \mathbf{E}$$

where the left-hand side of the equation is the time derivative of the magnetic field vector $\mathbf{B}$ (the

field will induce a spatially varying electric field, and vice versa. This means that if you take a bar magnet and pull it back and forth through a closed loop of wire, the changing magnetic flux of the magnet passing through the loop will generate a circulating electric field along the circumference of the wire. The force generated by this electric field will pull electrons around the loop, producing an electric current. If there is a light bulb on the loop and the magnet is strong enough or moving fast enough, the bulb will illuminate. So it is with ground loops. While an ideal ground loop carries no current, current can be induced in the loop via an oscillating magnetic field in the environment, and contemporary engineering has provided plenty of these. The modern American power outlet provides an alternating electric current at a rate of 60Hz (i.e., it changes direction 120 times per second). As a result, all electronics radiate a small electromagnetic field oscillating at this rate. While the strength of this field is low—perhaps only a few milligauss—the magnetic flux is proportional to the enclosed area of the loop, and even a small field can generate a measurable current in a large enough loop with low enough resistance. For a pair of cables connecting a large dilution refrigerator to a rack of control electronics, this loop can be several meters in diameter, resulting in an induced current large to override the carefully calibrated signals being sent to the quantum processor. In this way, the noisy hum of the ground loop as it is threaded by ambient magnetic fields is enough to rapidly dephase your qubits, irretrievably scrambling your quantum state, rendering computation impossible.

While the mechanism that causes ground loops in relatively simple—the general sketch relies on little more than an undergraduate electromagnetism background—the mitigation of their effect is slow and arduous. After cooling down your quantum processor—a process which can take several days—and observing an abnormally large amount of noise in the device, the task is to meticulously hunt down these unintended points of contact along the measurement chain, isolating them and breaking the loop. In a standard experimental setup, there can be dozens of coax lines crisscrossing

rate at which the magnetic field changes in time) and the right-hand side is the curl of the electric field vector **E** (the vorticity of the electric field, as in a closed loop).

across a laboratory, and the slightest brush of exposed metal between two can form a ground loop. Sometimes the contact is less obvious—perhaps the outer shield of a cable makes contact with the massive steel frame supporting the refrigerator, which in turn connects to electrical ground via its contact with one of the pumps or compressors circulating the cryogens. Since the transit of electric current is invisible to the human eye, it is impossible to locate a ground loop by sight. Instead, you need to systematically isolate a pair of possible connections, testing their electric connection with a multimeter and remeasuring the qubits to see if the noise level has changed, repeating this process over and over again until the errant contact is found. If it isn't, an entire measurement setup will be disassembled and put back together, cable by cable, instrument by instrument, until perfect isolation is assured. If the qubit noise still does not change, then perhaps the issue wasn't a ground loop at all. A ground loop is just one of many possible sources of noise in the qubit environment. The hunt for other sources can be similarly arduous.

Two separate instruments, plugged deep into the ground like trees in soil; their tendrils brush, exchanging invisible current, pulled from the expanse of dirt, through root, bark, leaves, metal, and back into the endless ground, completing the circle. We cock our heads. Déjà vu. Replace the instruments with signs, 'quantum' on one end of the yard, 'white' on the other. Their limbs stretch far and wide. As each bends towards supremacy, their branches kiss—an invisible spark is exchanged, a short circuit is formed. The arc of 'quantum'-'supremacy'-'white' stretches across the yard like a rainbow, like an upside-down smile, terminating in ground. An arc is a strand until it hits the ground. Then it becomes a loop—a loop through what? Following the trunk of each tree down, down underground into the soil, wood shatters into a spiderweb of decay, skeins of fungus tangling with root until the line between the one and the other blurs beyond recognition. The web pulsates, grows, recoils, burrows beneath the yard, waiting in sleepless slumber, knotting the loop.

Quantum supremacy is (not) a metaphor. It's a ground loop. Above ground, the zeugmatic short of 'supremacy' connects 'quantum' and 'white' at a point of fatal contact. Below ground, the two signs are sustained and given meaning through a

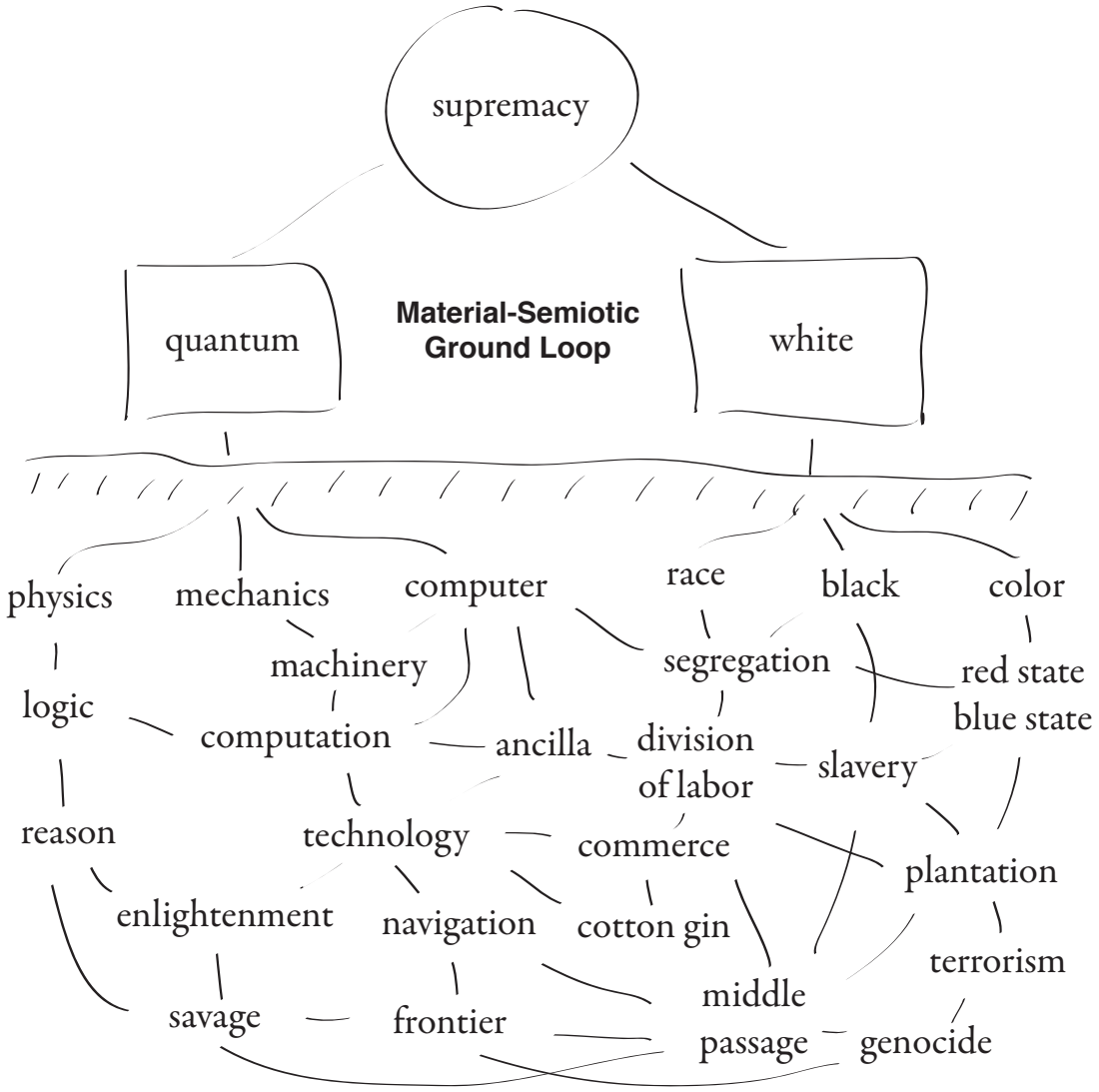

Figure 12-12: A material-semiotic ground loop. Two signs, 'quantum' and 'white,' are zeugmatically shorted to one another via 'supremacy.' In turn, each sign is given meaning through its chain of relation in the vast signifying network of material-semiotics, connecting 'quantum' and 'white' through subterranean means and forming a closed circuit of signification.

vast chain of signification, a common ground. Weaving through this diffuse network, the chains touch an innumerable number of times, shuttling meaning between the two distant trees. Somewhere underground, a loop is formed. The existence of this loop is not a trivial solution, a hand-wavy argument that everything touches everything underground, shorting every word and thing to every other word and thing in equal measure. Position and proximity, as Haraway and Barad remind us, matter. The manner in which 'quantum' and 'white' make contact underground matters—it defines the resistance of the pathway underground, the extent to which the loop conducts. Electrical ground, despite the approximations of scientists and engineers, is not a perfect conductor, a plane of constant voltage. The material composition of the ground at each point—whether it is damp soil or dry sand, for example—matters. So too with material-semiotic ground. Teasing out the degree to which two signs connect to one another (and via how many links) is a matter of generations of arduous work. Again, this work is often unrecognized.

I will not attempt to re-derive the underground material-semiotic connection between 'quantum' and 'white.' Instead, I refer to history, to data, and to those who came before me, uncovering the web strand by subterranean strand. This web is also a sort of bibliography, a citational ground plane connecting ideas, thinkers, and resources to one another across space and time, revealing new forms of proximity that cut across both. Like all bibliographies, it is always incomplete, always a work in progress. For our task here, it includes:

- the work of Jamaican writer and cultural theorist Sylvia Wynter, whose analysis of the origins of Western modernity traces a foundational connection between the invention of 'logic' and 'reason' (the bedrock of Western scientific empiricism) and the Spanish colonization of Central America in the sixteenth century (i.e. the arbitrary and enduring distinction between 'rational' Europeans and 'savage' Indigenous peoples, justifying atrocities against the latter). [478]

- the work of cosmologist Chanda Prescod-Weinstein, who notes how fundamental astronomy research has historically relied on the privileged vantage point of

massive telescopes built on Indigenous tribal land, such as the Thirty Meter Telescope (TMT) on the sacred Native Hawaiian land of Maunakea. [361]

- Prescod-Weinstein's critique of the affective labor foisted onto Black and femme faculty in the sciences, who are disproportionately expected to serve as diversity educators for their peers and therapists for their students—labor which is underpaid and illegible to tenure committees, often coming at the expense of research time. [362]

- demographic data published by the American Physical Society (APS), the largest professional organization of physicists: in 2018, only 3% of bachelor's degrees in physics in the United States were awarded to Black or African American students, while Black people of college age (18–24) made up 14.24% of the US population; this is a decline from two decades earlier, in 1998, when 5% of physics degrees went to Black or African American students, while their relative proportion of the population has remained roughly constant (13.95%). [29]

- the work of political scientist and Black studies scholar Cedric Robinson on *racial-capitalism*, studying how the European invention of race preceded the invention of capitalism in the sixteenth century—i.e., that capitalism first emerged atop a deeply radicalized substratum of intra-European labor, in concert with the emerging technoscientific enterprise of 'New World' colonization—rendering the labor hierarchies of modern capitalism inseparable from the unequal valuation of racialized bodies. [386]

- the interdisciplinary work of Karen Barad, particularly their recent work on nuclear coloniality, exploring how US nuclear testing has relied on the horrific colonial exploitation of the Marshall Islands, polluting the ocean with radioactive fallout and poisoning generations of Indigenous islanders. [31]

- the recent work of Indigenous science studies scholar Eli Nelson on the early history of American institutions of science and engineering, showing how these

institutions emerged to directly aid the American project of land theft and genocide against Native Americans. [23]

- the work of Ruha Benjamin and her critique of the "New Jim Code," where modern systems of algorithmic surveillance and categorization—systems enabled by advances in science and engineering—re-encode racist value systems and perpetuate systems of racial supremacy. [47]

- Karoline Wiesner's critique of the term 'ancilla' in quantum computing, which draws a semantic connection between the division of computational labor in a quantum processor and earlier systems of compulsory, gendered slave labor. [469]

- John Preskill's concurrent coining of the terms 'quantum supremacy' and 'entanglement frontier,' two terms which (unintentionally) call our attention to zeugmatic overlap between the scientific and colonial imaginations. [364]

Taken as a whole, we can think of this system as a *material-semiotic ground loop*—a closed signifying circuit formed in language and in matter, conducting noise like a massive hidden antenna.

Crucially, the metaphor of a ground loop is classical, not quantum mechanical. The noise in a ground loop can be explained entirely using classical electromagnetism; it has no quantum coherence, which is precisely why it frustrates attempts at quantum computation. Throughout this essay, I have avoided invoking any metaphors which explicitly reference quantum mechanics, even when such metaphors might have been extremely useful: Barad's notion of "the entanglement of matter and meaning" is a succinct articulation of the way in which quantum theory resonates with material-semiotics [32]; similarly, their model of comparing two concepts through "diffractive analysis"—observing the points of constructive and destructive interference like fringes in a double-slit experiment (mapping points of similarity, difference, and all the shades in between)—is a compelling visualization of the comparison between 'quantum supremacy' and 'white supremacy,' and has much in common with the zeugmatic analysis employed above [32, p. 34].

I have avoided these metaphors, because quantum computing has turned quantum mechanics into a product. I don't want us to be blinded by its mystique. Instead, I want us to look past the commodity fetish and notice the classical labor which makes quantum phenomena possible in the laboratory. Here, the metaphor of ground loops is useful. It is not without irony that scientists—obsessed as we are with isolating our experiments, mercilessly hunting down any possible points of electrical or mechanical connection to the outside environment—have been so naïve when it comes to noticing the invisible connections in our language, short-circuiting our aspirations to systems of power we claim to despise. The two tasks have much in common. In both cases, the labor of tracking down these connections is painful and thankless. The days spent searching for ground loops in an experimental system will never be recorded in a final journal article; they are separate from the 'real science,' from the product we are trying to sell. Instead, this work retreats into the realm of lab folklore, of bitter hushed conversations around a coffee machine. So too with the ground loops in our language. This is semantics, we are told, not science—a task best left to the polite company of tenured forum posters and bloggers, or to underpaid graduate students and DEI faculty hires. When such connections are found, they are treated as aberrations, errors to be quietly mitigated so that the task of science proceeds undaunted. Unfortunately, errors can tell us a great deal about how systems work in the first place.

12.9 Glitch in the System, or, The Black Cat Seen Twice

The record skips.

For many scientists in the accelerating field of quantum computing, it is difficult to imagine writing a research manuscript, dissertation, or grant proposal in 2021 without prominently citing the 2019 *Nature* paper of Arute et al. At the same time, however, it has become difficult to imagine using the term 'quantum supremacy' in

any of those same documents. Words, like most things, go in and out of style. For all the controversy and euphoria surrounding its 2019 demonstration, the term 'quantum supremacy' has waned somewhat in the years following the publication of Arute et al. Between its first appearance in 2012 and December 2021, 172 research publications have been posted to the arXiv containing the term 'quantum supremacy.' Of those, 77 were posted following the October 2019 publication of the Google manuscript—a rate of occurrence which is only slightly greater than in the four years prior to its publication. To put these numbers in perspective, they can be compared to the number of articles which cited Arute et al. during that same period. According to the citation aggregator Web of Science, 1,308 publications have cited the manuscript of Arute et al. as of December 2021, making it the single most cited quantum computing paper of the last decade—a feat which is all the more remarkable given that it was published in the final months of that decade. The discrepancy between these two numbers should give us pause. From the citation count alone, it should be overwhelmingly clear that the result of Arute et al. continues to serve a foundational role in the internal identity of the quantum computing community. But if the words 'quantum supremacy' aren't being used, how do scientists articulate what the result means to them? What's being said, and what isn't?

From one vantage, it would appear that scientists have taken to heart the call of Responsibility in Quantum Science. Running the same arXiv search for all occurrences of 'quantum advantage' since the publication of Arute et al. and overlaying the results with 'quantum supremacy,' we find that almost five times more articles appear using 'advantage' (360 articles) than 'supremacy' (77 articles). While it is tempting to credit this discrepancy to the intervention of Palacios-Berraquero, Mueck, and Persaud, the story is complicated the moment we zoom out. Scanning the arXiv for all occurrences of 'quantum advantage' and 'quantum supremacy' over their entire respective histories, we find that 'advantage' already dramatically outnumbered 'supremacy' at the time of the Google result. Moreover, while rate of occurrences for 'supremacy' has remained roughly constant since 2015, the number of occurrences of 'advantage' has increased exponentially—literally. At face value, the large discrep-

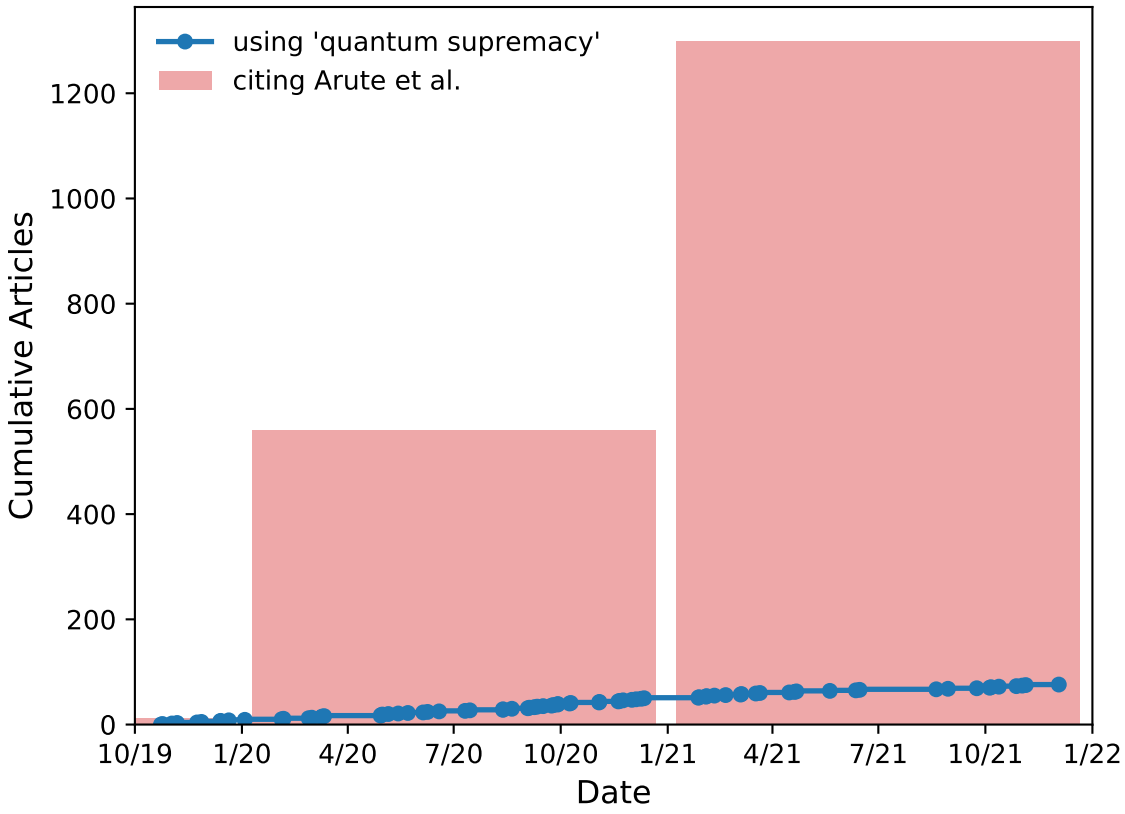

Figure 12-13: Graph of the cumulative number of articles posted to the arXiv containing the term 'quantum supremacy' since the October 2019 publication of Arute et al., overlaid atop a histogram of the cumulative number of articles citing Arute et al. in 2019 (13 articles), 2020 (546), and 2021 (740). (Keyword occurrence data obtained from arXiv.org; citation data obtained from Web Of Science)

ancy between these two numbers would seem to paint a success story: an offensive term failed to gain traction in our vocabulary, while a milder and less offensive term has accelerated in usage. Perhaps, then, 'quantum supremacy' was simply a mistaken term after all, a linguistic error which scientists have successfully corrected. The ground loop is separated, the experiment is run, the result is published.

The needle finds its groove, the song remains the same.

I suggest we sit with the error. Errors, like noisy ground loops, can teach you a lot about how a system is intended to operate. This should be familiar to any computer scientist or coder. When a piece of code runs smoothly, the machinery of a programming language will run invisibly in the background, parsing the instructions silently before outputting the result. Make a mistake, and the machinery immediately

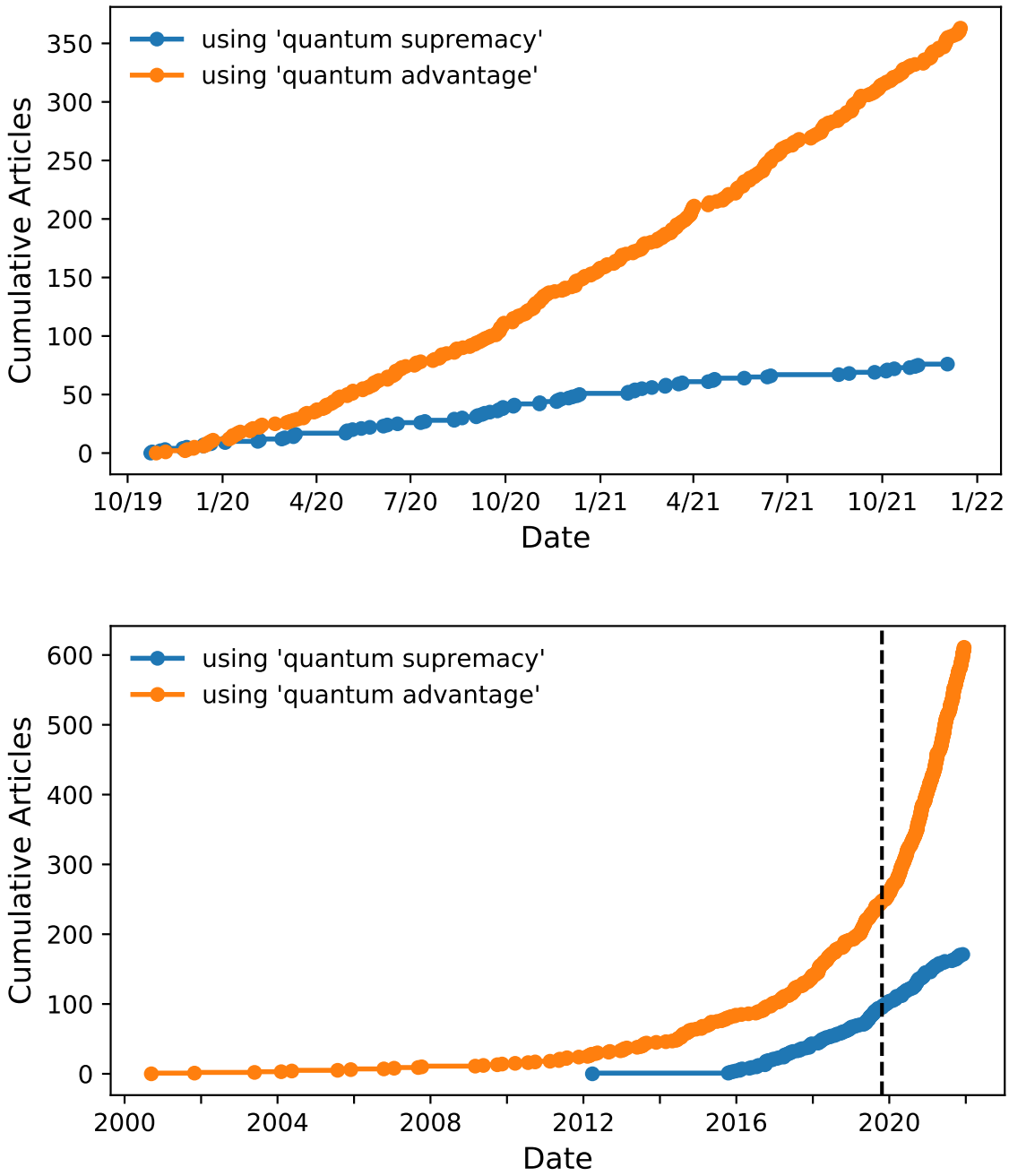

Figure 12-14: (top) Graph comparing the cumulative number of articles posted to the arXiv containing the terms 'quantum supremacy' versus 'quantum advantage' since the October 2019 publication of Arute et al. (bottom) The same graph, plotted over the entirety of their respective histories. The vertical dashed line indicates the publication date of Arute et al. (Data obtained from arXiv.org)

becomes visible—the gears seize, grinding to a cacophonous halt. Mistype the name of a variable somewhere in the code or bungle the syntax of a logical operation, and

a sequence of error messages will likely pop up the moment you try to run it. These error messages not only alert the programmer to the presence of a mistake somewhere in the script, they offer a window into how the computer tried and failed to parse the code. Decipher the error message, retrace the cascade of failures back to the source, and you gradually learn what it means to write 'good code,' code which is legible to the machine, which speaks its language. Again, we return to language. The machine's language is also our language, albeit defamiliarized. Programming languages, like all languages, are inseparable from the people who write them, who are in turn inseparable from the material-semiotic systems they are writing from within. In this way, coding errors not only reveal what machines might consider 'normal,' they also trace the contours of the normative systems those machines are operating in.

This point is central to the recent work of sociologist Ruha Benjamin. In her book *Race After Technology*, Benjamin shows how modern tech glitches can offer a glimpse into deeper systems of racial inequity, systems which lurk invisibly beneath the surface of society, running silently in the background. Silently, that is, until there's a break in the facade. Here, Benjamin draws a compelling parallel to the way *déjà vu* functions in Lana and Lilly Wachowski's 1999 science fiction film *The Matrix*. In the dystopian future of the film, mankind has been imprisoned by sentient machines and their bodies have been turned into biological batteries, a vast energy source for their mechanical captors; to pacify their prey, the machines construct a massive virtual reality simulation of the late twentieth century for the human minds to play in, tricking them into believing they are free. The provocative conceit of the film is that the world around us might not be real, but rather an elaborate computer simulation we have been fooled into believing is real.[20] After all, since the simulation is designed to be indistinguishable from reality, we are unable to tell the difference between the two.

[20]In the decades following the release of *The Matrix*, the metaphorical function of the titular simulation has been read through a number of different lenses, perhaps most notably as a queer and trans allegory. In this reading, the simulation becomes a stand-in for the invisible coercive power of heterosexual and cisgender norms, a delusion which some of us have awakened from and now fugitively navigate within. For a recent trans critique of this reading, see [95, pp. 52–55].

Until there's a glitch. At a pivotal moment in the film, a black cat crosses the path of the protagonist, Neo; seconds later, a black cat crosses his path again. *Woah, déjà vu.* Neo's companions turn in alarm, the music becomes tense. Déjà vu, we are told, is not simply a spurious recursion in memory, a trivial lapse in our individual perceptual faculties. Instead, the double encounter with the cat is evidence of a material alteration in the fabric of the simulation—code being modified and overwritten by the machine taskmasters—affecting all its occupants. The encounter with the cat(s) proves fatal—within moments, agents of the simulation descend upon their location, and a violent encounter ensues. The glitch has consequences. Indeed, the glitch of déjà vu, Benjamin writes, "is not an insignificant 'mistake' to be patched over, but rather serves as a signal of something foundational about the structure of the world meant to pacify humans. It draws attention to the construction and reconstruction of the program and functions as an indication that those seeking freedom should be ready to spring into action." [47, p. 85] Like the skip of a phonograph needle, reminding the listener that the band isn't actually in the room with them, the error reveals the simulation.

These glitches, Benjamin argues, aren't simply the stuff of science fiction. They are all around us, and they offer glimpses into a dystopia which is absolutely material, absolutely present. As an example, Benjamin points to a 2017 viral video posted by Chukwuemeka Afigbo, a Nigerian program manager at Facebook [9]. In the video, Afigbo records an individual holding their hand under an automatic soap dispenser—the machine quickly whirs to action, a stream of suds is deposited into the cupped hand. Afigbo then invites a second person to give the machine a try—they wave their hand under the dispenser for ten seconds, but the dispenser remains silent. The individual then grabs a white piece of paper towel and holds it over their outstretched palm—the dispenser immediately springs to life. For many physicists, the mystery of the glitched soap dispenser will be clear, perhaps even comical. The automated dispenser likely relies on a small infrared light source: when an object is placed within the beam, some amount of light is reflected back and captured by an adjacent detector, at which point the soap is dispensed. Of course, since ambient light already contains

some amount of infrared radiation, the detector must be calibrated to avoid misfiring. The engineers who design the device must impose a threshold for the amount of reflected light required to trigger it: if the threshold is too low, the dispenser will discharge soap constantly; too high, and only a mirror will reflect back enough light to activate it. Between these two extremes, a judgement had to be made. A line had to be drawn. As Afigbo's video shows, the white skin of the first person reflected enough infrared light to satisfy the sensor; the Black skin of the second did not.

The physical mechanisms of infrared light and epidermal melanin are well understood, but they alone are insufficient to explain this particular encounter between machine and body [360]. While physics might lead us to explain away the issue—to conclude that this is just how infrared sensors work—this impulse obscures from view a series of simpler and more pressing questions. The calibration of the sensor may have been arbitrary, but it certainly wasn't random. Before the product was mass produced, the soap dispenser surely went through numerous rounds of testing, fine-tuning the threshold to minimize the amount of wasted soap and maximize the number of satisfied users. The fact that the dispenser failed to recognize Black skin is significant, but it doesn't necessarily point us to deliberate and intentional animus on the part of the designers. It doesn't have to. Rather, it suggests something much simpler and more insidious about the conditions in which most technology is developed: none of the engineers were Black. If they had been, the dispenser would likely never have made it to market in this form; the sensor would have been found to be faulty during development and it would have been recalibrated, if not replaced with a different mechanism altogether. In this way, Benjamin writes, "the discriminatory soap dispenser offers a window onto a wider social terrain," exposing the material impact of a lack of racial diversity in engineering, and silently replicating a longstanding vocabulary of racial hygiene [47, p. 67]. The automated soap dispenser is far from an individual anomaly, and it must be situated within a broader matrix of technology and social relation, a matrix which defines who is visible, who is invisible, and when:

> For instance, we might reflect upon the fact that the infrared technology of an automated soap dispenser treats certain skin tones as normative

> and upon the reason why this technology renders Black people invisible when they hope to be seen, while other technologies, for example facial recognition for police surveillance, make them hypervisible when they seek privacy. When we draw different technologies into the same frame, the distinction between "trivial" and "consequential" breaks down and we can begin to understand how Blackness can be both marginal and focal to tech development. [47, p. 68]

Much like the deep space telescope or scanning electron microscope, the infrared soap dispenser and facial recognition software are apparatuses of vision, windows onto the world. Indeed, as Haraway would remind us, they are never transparent, always contingent, encoding and replicating a partial vision of the world. The question then becomes, who calibrates that partial vision? Who is the window designed for?

Let's take the metaphor of déjà vu a step further, since it too concerns vision, what we see or don't see. Like a black cat crossing our path, we receive a *New York Times* alert announcing that scientists at Google have demonstrated quantum supremacy. Months later, another crosses our path, this time with the news that white supremacists have stormed the United States capitol. We double take.

> ***Neo:*** *Woah, déjà vu.*
> ***Trinity:*** *What did you just say?*
> ***Neo:*** *Nothing, uh, just had a little... déjà vu.*
> ***Trinity:*** *What did you see?*
> ***Neo:*** *A black cat went past us... and then another that looked just like it.*
> ***Trinity:*** *How much like it, was it the same cat?*
> ***Neo:*** *Might have been, I'm not sure.* [454, 1:19:05]

We're seeing double. Was it the same cat, or a coincidence, a trick of the light? Might have been. How can we be sure? We turn to our colleagues and ask if they can validate our observation, if they saw what we just saw. They look at us askance, *what cat?* We cautiously present our findings. *Was it a real cat,* they ask, *or a metaphorical one?* We laugh it off, but the recursion haunts us, like the fog of a half-remembered dream. Cross-eyed, we return to lab. There are experiments to run, discoveries to be made, papers to publish. Somewhere deep in the refrigerator, Schrödinger's metaphor purrs.

The loop of the ground loop is also the loop of déjà vu. Like the black cat, like the

glitched soap dispenser, the zeugmatic slippage of 'supremacy' alerts us to something terribly amiss in the fabric of our reality. If 'quantum supremacy' is a glitch, what does it reveal about our reality? What does it bring into focus, and what does it expose in the margins? Again, we return to the text. When a prominent quantum information scientist posted on SciRate that 'quantum supremacy' does not "make racial minorities feel unwelcome (as far as I can tell)," the void enclosed in that parenthetical spoke volumes [105]. There was no one in the forum to disagree. Again, this is not a question of individual actors saying the wrong at the wrong time; it's about the material and social conditions which made such an utterance possible and sensible in the first place. Those parentheses are a window onto the warped landscape in which 'quantum supremacy' emerged, the salted terrain which has nurtured and sustained it. It's a window into history, into the myths we tell each other.

In 1927, twenty-nine scientists convened in Brussels to attend a conference endowed by the Belgian industrialist Ernest Solvay. The group photograph from that meeting is legendary among physicists, and the list of attendees reads like the index of an introductory physics textbook. Albert Einstein sits front row center, flanked on all sides by the architects of modern quantum theory: Erwin Schrödinger, Wolfgang Pauli, Werner Heisenberg, Paul Dirac, Louis de Broglie, Max Born, Niels Bohr, Max Planck, Marie Curie, Hendrik Lorentz. Over half of the participants are Nobel Prize winners. In 2011, an illustrious cohort of scientists once again convened in Brussels, this time to celebrate the centennial of the Solvay Conference. Much had changed about the world in the intervening years; some things had not. When John Preskill took the lectern at the twenty-fifth Solvay Conference and unveiled 'quantum supremacy' for the first time, he did so to an audience that remained overwhelmingly male, overwhelmingly white. We need not speculate whether or not an audience member raised any objections to Preskill's choice of words: in 2013, the organizers of the Solvay conference published a compiled volume of the proceedings of the conference, complete with transcriptions of the Q&A session following each talk. No objections were raised [366]. Like the faulty soap dispenser, 'quantum supremacy' made it to market with extraordinarily narrow oversight. Indeed, one look at the

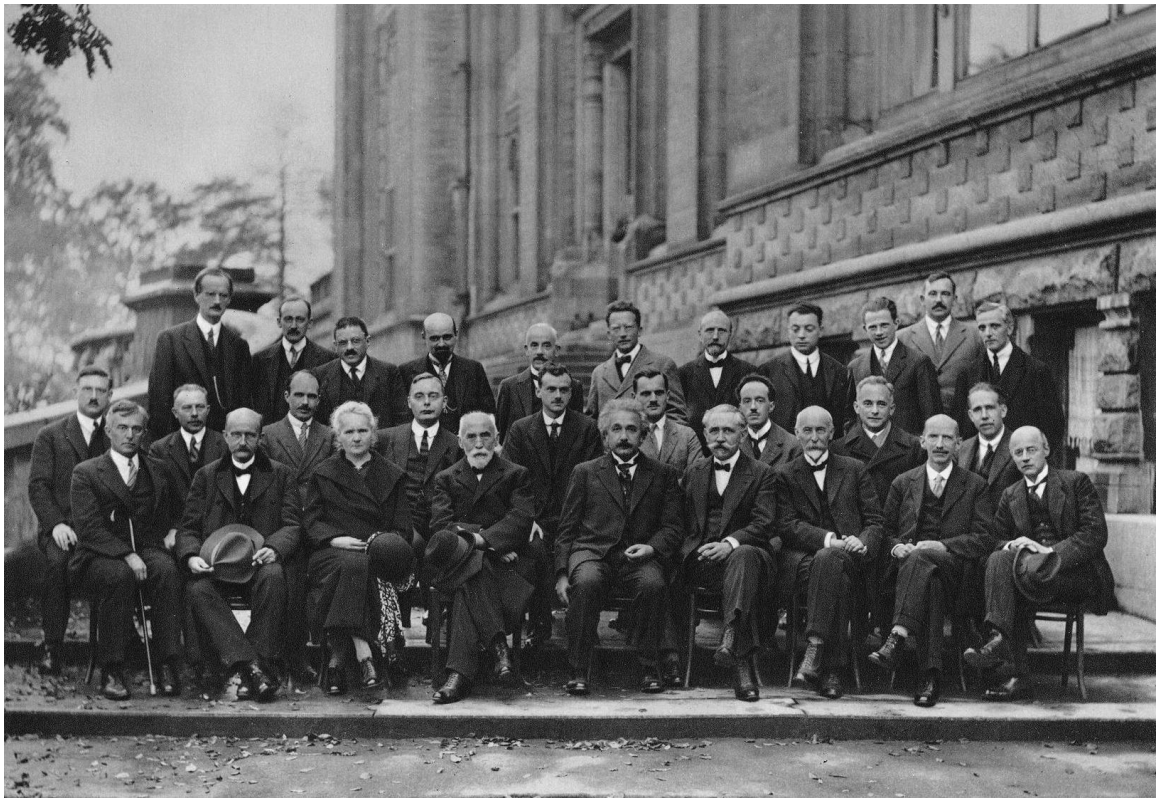

Figure 12-15: Group photograph of the attendees at the fifth Solvay Conference on Physics in Brussels, October 1927. Many of the scientists assembled are considered founders of modern quantum theory, including Erwin Schrödinger, Wolfgang Pauli, Werner Heisenberg, Paul Dirac, Louis de Broglie, Max Born, Niels Bohr, Max Planck, Marie Curie, Hendrik Lorentz, and Albert Einstein.

group photograph from the conference—superposed with the legendary image of Einstein, Heisenberg, Schrödinger et al. at the same conference eighty-four years prior, a cascade of infrared reflected back and forth across the century—and the mystery of Preskill's *"we"* becomes eerily clear. This is who 'quantum supremacy' was designed for.

What then of 'quantum advantage'? In early October 2019, shortly after the leaked manuscript of Arute et al. began circulating online, *Quanta Magazine* published a column by Preskill titled "Why I Called It 'Quantum Supremacy'." In the piece, Preskill walks readers through the scientific context of the Google result, focusing only briefly on the controversy brewing around the term itself. In doing so, Preskill meditates on why 'quantum advantage'—a term which, we have seen, was

Figure 12-16: Group photograph of the attendees at the twenty-fifth Solvay Conference on Physics in Brussels, October 2011.

already accelerating in prominence at the time—is the wrong word for the job:

> In 2012, I proposed the term "quantum supremacy" to describe the point where quantum computers can do things that classical computers can't, regardless of whether those tasks are useful. With that new term, I wanted to emphasize that this is a privileged time in the history of our planet, when information technologies based on principles of quantum physics are ascendant.
>
> The words "quantum supremacy"—if not the concept—proved to be controversial for two reasons. One is that supremacy, through its association with white supremacy, evokes a repugnant political stance. The other reason is that the word exacerbates the already overhyped reporting on the status of quantum technology. I anticipated the second objection, but failed to foresee the first. In any case, the term caught on, and it has been embraced with particular zeal by the Google AI Quantum team.
>
> I considered but rejected several other possibilities, deciding that quantum supremacy best captured the point I wanted to convey. One alternative is "quantum advantage," which is also now widely used. But to me, "advantage" lacks the punch of "supremacy." In a race, a horse has an advantage if it wins by a nose. In contrast, the speed of a quantum computer vastly

> exceeds that of classical computers, for certain tasks. At least, that's true in principle. [368]

As we've seen, this point was quickly echoed by Scott Aaronson, who concurred with Preskill that 'advantage' lacked the right punch:

> See, it's like this. Preskill meant "quantum supremacy" to refer to a momentous event that seemed likely to arrive in a matter of years: namely, the moment when programmable quantum computers would first outpace the ability of the fastest classical supercomputers on earth, running the fastest algorithms known by humans, to simulate what the quantum computers were doing (at least on special, contrived problems). And ... "the historic milestone of quantum advantage"? It just doesn't sound right. Plus, as many others pointed out, the term "quantum advantage" is already used to refer to ... well, quantum *advantages*, which might fall well short of supremacy. [3]

Preskill and Aaronson are exactly right. The problem with 'quantum supremacy' has never been that it was the wrong word for the task at hand. The problem has always been that that it's the *right word*. 'Quantum supremacy' is a glitch in the original sense of the word: *glitsh*, Yiddish for 'to skate,' 'to slip.' It's a slip of the tongue; a Freudian slip, perhaps. It's exactly the word we mean to say, though perhaps not in polite company.

When we switch from 'quantum supremacy' to 'quantum advantage,' we don't sever the ground loop. We bury it underground. Out of sight, down amidst the tangle of mycelium. Scott Aaronson's belief in a "better kind of supremacy" was dangerously naïve, but he was absolutely right about one thing: "while 'advantage' is certainly subtler than 'supremacy,' couldn't that make it all the more insidious, and therefore dangerous?" [3] Despite their best intentions, the authors of Responsibility in Quantum Science misdiagnosed the problem. Quantum computing doesn't simply have a problem with its *signifiers*, with the names we attach to phenomena and what those names may remind people of. Quantum computing has a *sign problem*. The problem is what the name is pointing towards; the problem is the chain of signification wrapped around our wrists. The sound-image quantum supremacy points us to the cascade of myth at the heart of our research, the myth of power which we replicate in

our social and professional formation, in the stories we tell to delight our corporate and government sponsors, in the forms of labor we choose to recognize and choose to make invisible, unpublishable. It is, to permute Preskill's words, the punch which precedes the broken nose; conceal the fist and the shattered cartilage remains. The legacy of white supremacy is worth learning from. The violent regime of racial supremacy never disappeared, not even in the parts of the world inhabited by progressive and well-meaning scientists. It too quietly mutated into invisible 'advantage'—made it easier for some people to get a bank loan, or obtain a tenured faculty position, or dodge murder at the hands of the police, or tell an automated soap dispenser that their body is really there. When we throw out a word and leave a system intact, we suture up the rift in the simulation, but the simulation remains. We're just hiding the error messages.

12.10 3:20

In July of 2021, the team at Google Quantum AI held an online summer symposium live on YouTube, the company's video platform. Less than two years had passed since the publication of Arute et al., but the chasm between the two events felt boundless. In March 2020, five months after the fanfare of the supremacy result, the first outbreak of COVID-19 rolled across the United States like wildfire, ushering in years of intermittent mass lockdown, quarantine, and heightened economic precarity, forcing even the most routine in-person interaction online. At the time of writing, 830,549 people have died of COVID-19 in the US alone, with the total number of cases exceeding 57 million nationally. On May 25, 2020, George Perry Floyd Jr. was murdered in broad daylight by an officer of the Minneapolis Police Department for, allegedly, trying to use a counterfeit $20 bill. George Floyd's murder set in motion the largest series of mass protests in American history. On January 6, 2021, white nationalists stormed the United States Capitol in an attempt to overturn the presidential election in favor of Donald Trump. Few arrests were made.

Arriving in the aftermath of all this, the tone at the Google summer symposium

was remarkably upbeat. The sun was shining at the end of the long first winter of the pandemic, COVID case numbers were on the decline in many states, and the first round of vaccines promised herd immunity in many communities. Sitting in a conference room in Cambridge, Massachusetts, I was not immune to optimism. For the first time in over a year, my labmates and I gathered to watch the livestream over lunch, in person and unmasked. While this optimism was tempered less than a month later with the arrival of the Delta variant and yet another wave of mass infections, the recording of the symposium reads like a snapshot of mid-pandemic hubris: Google scientists strut around their new laboratory complex in Santa Barbara without masks, offering viewers a seductive window through their computer monitors and into the cutting edge future of quantum computing research. The symposium opens with a keynote address by Hartmut Neven, leader of the Quantum AI team and one of the two principal investigators on the work of Arute et al. Over the course of half an hour, Neven—collared shirt unbuttoned to the chest, massive sunglasses glistening high atop his forehead—bounces between an assortment of presentation genres, shifting from technical research talk to shareholder meeting, speculative outlook to recruitment advertisement. The term 'quantum supremacy' doesn't appear a single time. Neven begins his talk by announcing that, in the next two years, the Google team plans to double in size, hiring over a hundred new employees. "We cherish diversity along many dimensions," Neven intones, "and we think it makes our team stronger." [329] As for what 'diversity' means in this context, Neven quickly clarifies:

> One misconception I would like to dispel is, please don't think "Oh, I'm not working in superconducting quantum computing so the Google team is probably not so interested in me." That is not correct. Again: diversity. If you have a background in photonic systems or in ion trap systems, if you have skills in adjacent engineering disciplines such as microwave engineering, chip layout, chip manufacturing techniques, we would like to hear from you.

Toward the end of the keynote address, Neven flashes to a blank blue slide with the words "Prospects for real world impact" emblazoned across it. "Ultimately we have to answer this question," he reflects. "It will cost billions of dollars to build

an error-corrected quantum computer—hey, if you have it, what are you going to do with it? And we owe it to our investors—whether those are taxpayers or Google shareholders—we owe the world a good answer to that." He then transitions to a slide with four columns: "Energy" (using quantum simulation for nuclear fusion research to fight global warming); "Pharmaceuticals" (modelling the quantum mechanics of neuroreceptors for targeted drug development);[21] "Machine Learning" (using quantum speedups in linear algebra to train deep neural networks); "Computer Graphics" (modelling interference patterns in nature for more realistic video game graphics and virtual worlds). "Admittedly these areas are slightly speculative," Neven concedes, "I'm not saying there will be big commercial relevance assured, but these are very worthwhile areas to look at."

Among these outlook slides, one image in particular caught my eye. On the machine learning slide, Neven includes a cartoon graphic of a neural network. On the left side of the graphic are a cluster of points labeled 'image'; these points then connect to a network of dots in the center of the cartoon, orange lines connecting between them like a tangle of fibers; on the right, these lines connect to one of two points, labelled 'Cat' and 'Dog' respectively. The graphic is a common one in machine learning textbooks, and it attempts to illustrate how neural networks process the raw data of a photograph and determine whether it is an image of, say, a dog or a cat. Of course, there is nothing special or particularly lucrative about the task of sorting dogs and cats, so consumers are free to decide which categories they would like to sort photographs into. Indeed, as Ruha Benjamin notes, similar algorithms for predictive policing are already in wide circulation among US law enforcement agencies—these algorithms, trained on data steeped in racial bias, are known to disproportionately mislabel Black defendants as criminals in comparison to white defendants [47, p. 81]. When we talk about satisfying investors, whose investments are we really talking about? What happens when the financial interests of Google shareholders conflict, as they historically have, with those of average American taxpayers? What happens

[21]Here, Neven notably avoids any mention of the ongoing pandemic, instead indulging in a bizarre anecdote about how the soft drink 7 Up originally contained lithium citrate, a mood stabilizer used to treat bipolar disorder.

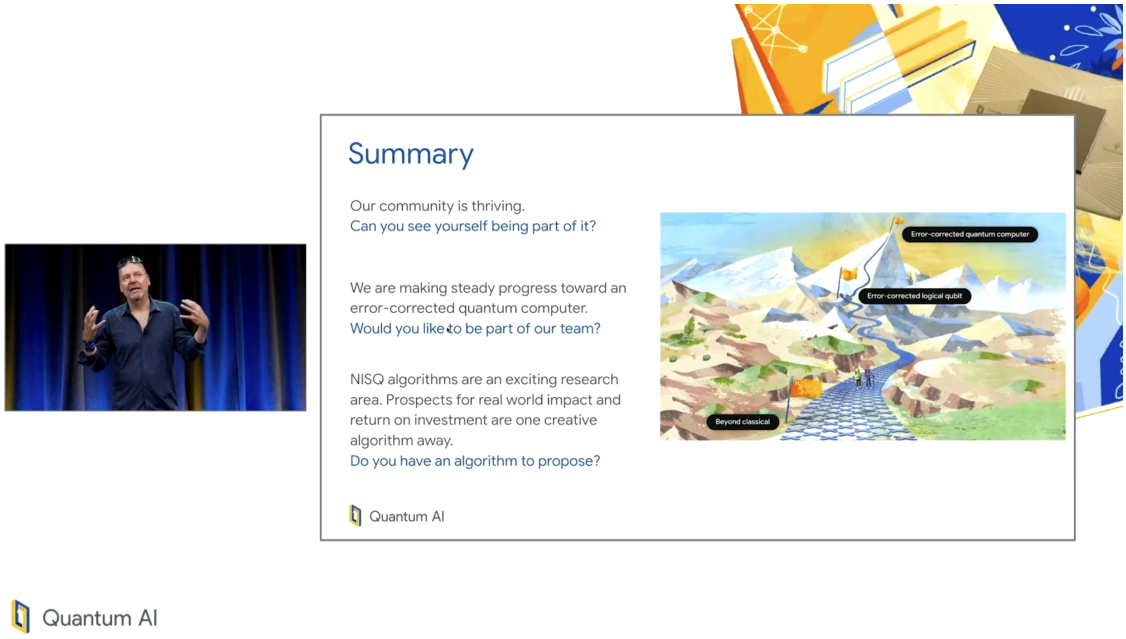

Figure 12-17: Summary slide of the keynote presentation by Hartmut Neven at the Google Quantum Summer Symposium 2021. Image captured from Ref. [329].

when the strategic interests of the American Empire conflict, as they definitionally must, with the existential interests of the the Global South? I stare at the image a moment too long and it becomes fuzzy, the vectors of the bipartite graph blurring into a tangle of Saussurian sycamore, limbs converging to a single point, a final signified. Cat. Dog. Except now the letters are getting mixed up, scrambled in the pixelated video compression of a bad internet connection, and for a moment I think I see new words. White. Black. I stare a beat too long. Aryan. Jew. What are we really building here?

Neven concludes his talk with a summary slide. "Our community is thriving," the first bullet point reads, "Can you see yourself being part of it?" On the right hand side, a stylized illustration shows two hikers venturing up a mountain trail, the path paved with cartoon qubits. The trail is marked with flags corresponding to milestones in the development of a quantum computer, implying that the physical path of the trail is also a metaphorical time axis. In the foreground, the trail is marked with a flag labeled 'beyond classical'—another euphemism for 'quantum supremacy'—which the viewer takes to mean the present moment, or perhaps the near past of 2019. The

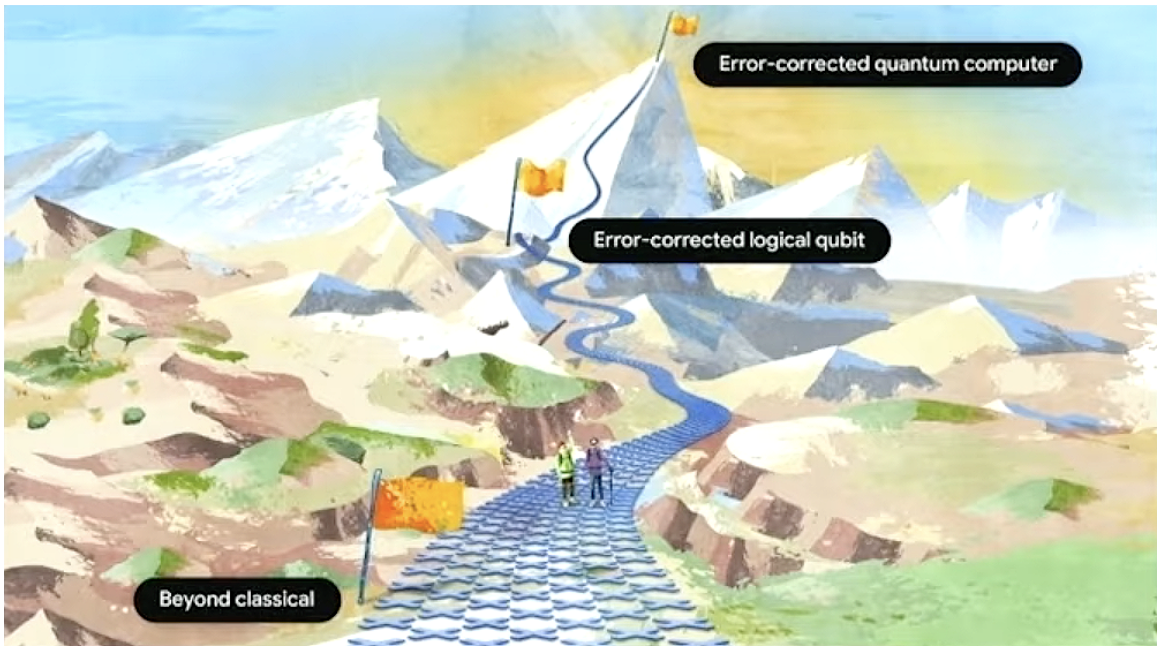

Figure 12-18: Illustration of the road to an error-corrected quantum computer from Hartmut Neven's summary slide, enhanced for visual clarity. Image captured from Ref. [329].

hikers—who we take to be stand-ins for Google engineers—are depicted many yards beyond this point, though it's unclear who is in the present: the hikers, or the viewer trailing behind them outside the picture frame? Perhaps the engineers are in our future while the rest of us are stuck in their past, and Neven's invitation to join the hike is also an invitation to catch up with them. In either case, all eyes point further down the trail, upwards to the summit of the mountain in the distance. Upwards into the future, to the ultimate penthouse view. "There are solid prospects for real-world impact and return on investment," Neven concludes, "and we often say that we are just one creative algorithm away from that." Somewhere in the distance, behind the angular whiteness of the mountain, the warm glow of a new sunrise illuminates the landscape. Impossibly, the mountain casts no shadow on the trail.

"And with this, I would like to hand it over to Emi who will delight us with a poem." The scene changes, and the viewer is instantly teleported to a new room. The next speaker introduces herself as Emtithal Mahmoud, a Sudanese-American poet, activist, scientist by training, and Goodwill Ambassador for the United Na-

tions Refugee Agency. For the symposium, Mahmoud was commissioned to write an inspirational poem, which she tentatively titles "Quantum and Consciousness." The poem runs about seven minutes in length, densely pulling together a collection of quantum computing terms into a narrative of shared struggle and triumph. *"A new milestone:"* she recites, *"as we becomes our own error correction / overcoming each disturbance from an environment that makes a habit of saying no / and not yet / and try again / and why / and how / and why again as we make progress on the proverbial road to discovery.*

> *Can you imagine a world where our understanding of a few systems can change the course of climate change? / helping us forge a path towards a fully decarbonized world / avoiding disaster / where our understanding of how the sun works can help us reverse engineer mechanisms that attempt to shine a light / so to speak / on change itself*
>
> *and this, this is only the beginning / personalized medicine for the healers / new materials for the builders / countless opportunities for those dreamers among us / who want to imagine a world of our own choosing / where we are not limited by the bounds of our bodies / or our societies / or our systems.* [291]

Mahmoud concludes her poem with an address to those who might doubt her vision of a better world. *"This is the moment / the moment where I'm always asked how it is I can wholly believe in something I cannot see / My new favorite answer: have you heard of this thing called quantum? / Yeah, it's everything."*

As I watched the symposium live in that conference room at MIT, surrounded by my colleagues and labmates, the discomfort in the room was palpable. A couple graduate students suppressed giggles when Mahmoud announced the title of her poem, others rolled their eyes—later at the coffee machine, a postdoc railed against the notion of quantum consciousness, insisting that Mahmoud did not fully understand the quantum-classical boundary. Partway through the poem, a visiting researcher from a prestigious collaborating group asked for us to shut the stream off and switch to a different video from the previous year's symposium. In summer 2020, as much of the United States smoldered from the ongoing uprising for racial justice, the organizers of the Google symposium invited Baba Brinkman, a white Canadian rap performer,

to produce a series of freestyles about quantum computing. The performance the researcher excitedly wanted to put on was titled "3:20." [76] The gimmick of the performance was that Brinkman freestyled for three minutes and twenty seconds—the length of time it took the Sycamore processor to perform the quantum supremacy computation—while viewers posted quantum computing terms in the chat window for inspiration in real time. Watching Brinkman scroll through the chat and rattle off phrases like 'color code surface code' and 'quantum money,' the names of many of the participants were immediately familiar from the author lists of high-impact quantum computing papers. *"This is the way that I step up,"* he stumbles, off beat,

> *and maybe even bust words. / Sometimes I have to defrag my brain / with those coupled clusters. / They're unitary. / It's very nice / when I'm spitting this scary rap. / Is it alive or dead? / I don't know. / It's the Schrodinger's cat. / See what I'm saying? / That's the way that the story is told. / I am quantum.*

There is a macabre déjà vu to the performance's title, though this appeared lost on Brinkman and the giddy audience. At the very moment that Brinkman was deliriously counting down two hundred seconds, protesters across the country were counting down over twice that duration in silence, bodies splayed across asphalt in defiant monument. Months prior to the freestyle, the American comedian and social theorist Dave Chappelle released a chilling monologue in solidarity with the protests. In the piece, Chappelle passes the mic to the righteous anger of Black Americans across the country, insisting there is nothing he could say on stage as a celebrity which hadn't already been said by millions of other voices without stages. "Does it matter about celebrity?" Chappelle asks. "No! This is the streets talking for themselves." [89] Chappelle titled the piece *8:46*, the length of time that officer Derek Chauvin knelt on George Floyd's neck.

Sitting in that conference room in July 2021, watching Emtithal Mahmoud recite her poem, I too felt deeply uncomfortable. I quickly realized, not for the first time, that it was for a different reason than many of my colleagues. What made me uncomfortable was not so much the content of Mahmoud's poem—the insinuation, for example, that quantum mechanics and consciousness might have something to

do with one another—but rather the circumstances which surrounded her delivery of it. At the symposium the prior year, Mahmoud had delivered a sobering poem about grief, anti-Black violence, global hunger, and the possibility of re-imagining the world anew through quantum mechanics, though not without ambivalence. *"In those moments,"* she reads, *"quantum mechanics as an escape / or a catch-all cure to all of our problems / seems more appealing than ever before / and I let this notion fill me up / even now."* [290] The tacit shadow of doubt, of the impossibility of easy escape, is never fully dispelled; it hangs over the rest of the piece, haunting the remainder of the gathering. The contrast with Baba Brinkman's piece the following day—an incoherent karaoke of empty quantum signifiers, cloaked in faux Black vernacular affectation—is staggering. In 2021, with Brinkman no longer on the schedule, it felt like the organizers of the event were asking Mahmoud to serve double duty. On the one hand, she was to reprise Brinkman's role as entertainer, to delight the audience with callouts to quantum computing terms and hype them up for the engineering task ahead. On the other, she was to shoulder the burden of Neven's nebulous promise of diversity, to take the stage and speak on behalf of those who hadn't been invited on the hike. To absolve the gathering of the fact that, once again, there were no other Black speakers on the schedule. To become our error correction.

Again, I suggest we sit with the error. Sitting in the metaphorical conference room, we might notice a particular theory of diversity which runs throughout the Google quantum summer symposium series. This theory is perhaps best articulated during a telling moment in the keynote address. Flashing a photograph of the newly completed laboratory campus—walls adorned with vibrant and abstract blotches of color—Neven boasts of the team's artist in residence program, an initiative which strives to create "very pleasant working environments conducive to creative work." [329] Creative work, like coming up with a creative algorithm to justify a multibillion-dollar research boondoggle, to guarantee return on investment. The art on the wall, like Mahmoud's poem, is *ancillary* to this task. Which is to say, it is "an aid in achieving or mastering something difficult," the task of research; aid which, as Karoline Weisner might reminder us, is drenched in a history of gendered, racialized, and compulsory labor.

Creativity in quantum computing, like diversity, is a resource—which is to say, it's a substance to be mined and extracted, fuel for the engine of progress. There is a reason why, in Neven's keynote, he frames diversity as a multi-disciplinary hiring initiative. To pursue their aggressive research timeline, Google Quantum AI requires a hundred new employees in two years. Each year, perhaps a couple dozen people receive doctoral degrees in superconducting quantum computing worldwide. To fill the delta between those two numbers, there is no option but to expand the hiring search to researchers in "adjacent engineering disciplines," disciplines which incidentally suffer from the same lack of racial and gender diversity as physics and engineering at large. There is no generosity in this effort. Google—like IBM, like Amazon, like Microsoft, like MIT—is looking for more workers for the factory. They're looking for labor, for more hands to quietly hunt ground loops.

This is not to say that hiring a diverse workforce is not important. As Ruha Benjamin's example of the automated soap dispenser in the previous section already illustrates, it is absolutely essential. The problem is that—like removing the term 'quantum supremacy' from our vocabulary—it is only the first and most visible step in a much harder process. Many scientists still dream, like Scott Aaronson, of a world where "physicists and computer scientists and mathematicians of varied skin tones and accents and genders com[e] together to pursue a different and better kind of supremacy," overcoming the barriers of language to recognize their shared calling [3]. In this narrative, racism, sexism, homophobia, transphobia, abelism, anti-indigeneity are all roadblocks on a path which already stands in front of us. Remove an offensive term, hire a diverse labor force, and the path itself remains unchanged. We cherish diversity and creativity when they allow us to do the things we already wanted to do in the first place. But what happens when an invited speaker delivers a poem which doesn't delight us, but horrifies us in its reckoning with unspoken atrocity? What happens when an artist fails to make a laboratory more pleasant, exposing instead the brutal reality contained within those walls? What happens when, recalling the prophecy of Aaronson's jeering specter, the "women and minorities" we mentor spurn our pantomime hospitality, call foul on our tax-deductible donations to "good causes,"

lose patience in watching us shadowbox with "the demons in [our] own character"? What happens when the artists, and the poets, and the ground loop hunters see what the leaders of quantum computing evidently cannot: that the path before us is the problem, that it leads us not to a glorious mountaintop, but a crematorium? There is no better supremacy waiting for us at the end of this path. There is only the same supremacy.

During Derek Chauvin's trial in March 2021, body camera footage revealed that the duration of George Floyd's murder had been previously underreported, that Chauvin had in fact knelt on his neck for nine minutes and twenty-nine seconds. George Floyd was unresponsive for the final three minutes and fifty-one seconds [274]. The exact timestamp does nothing to change the outcome, but in the grim accounting of supremacy—of which tasks take minutes, days, millennia—consider the data again. It took our community three minutes and twenty seconds to claim supremacy in a bottle colder and darker than space. It took three minutes and fifty-one seconds for a nation to erect a monument to supremacy on a man's neck.

Hiding the words 'quantum supremacy' doesn't cut the ground loop. Neither does hiring a poet once a year for a public livestream, or recruiting Black bodies, female bodies, queer bodies to do the work you already promised your shareholders. If you really want to cut the ground loop, you have to completely unearth the chain of signification which created the short in the first place, prying it apart fiber by fiber. If you really want to cut the ground loop, you have to hire a diverse workforce and give them the tools to utterly dismantle the systems which made their absence sensible in the first place. The twist of the automated soap dispenser story is important: speculation aside, we'll never know the color of the lead engineer's skin. Perhaps they put their hand under the prototype detector and discovered that it believed them invisible. Perhaps they reported this discovery to their colleagues and their manager, drafted up plans for an ingenious solution. What we do know is this: that discovery did nothing to change the final product. Maybe shareholders reasoned it was too expensive for the company to change course and switch the detector to a different model. Or maybe the detector worked for all the other test subjects, so the

manager assumed it was all in the engineer's head. Or maybe there was a bonus promised to engineers who successfully designed devices that worked the first time, and the engineer bit their tongue to pay rent and keep food on the table. Again, again, this isn't about individuals. It isn't about finding the right actors to heroically intervene and save us from ourselves. It's about systems. It's about dismantling the protocol of racial capitalism which strives at every moment to make such an intervention impossible in the first place. It's about abolition.

12.11 Coda: Cutting the Ground Loop

> *The blues remembers everything the country forgot.*
> *We waited and we watched.*
> *We waited and we watched.* [315]

"What," asks the great prison abolitionist Ruth Wilson Gilmore, "is to be done?" [159]

In her tweet celebrating the Google result, Ivanka Trump wrote that quantum information science is "a critical industry of the future." [439] On this point at least, the two Trumps, John Preskill, Scott Aaronson, Harmut Neven, Emtithal Mahmoud, the signatories of Responsibility in Quantum Computing, and the vast majority of the quantum computing research community appear to be in agreement. Of course, the thing about the future is that it doesn't exist yet. It's appears always out of reach, untethered to the present. As such, it can be tempting to imagine the future as an empty vessel, a chalice waiting to be filled with our wildest hopes and dreams. So it is with quantum computing. As we've seen, for some the future promise of quantum computation is a promise of strategic national dominance; for others, it's an aspirational milestone on the path to scientific enlightenment. Or a lucrative investment opportunity. Or the miraculous solution to climate change. Or a hopeful panacea to cleanse the world of violence and hate. We shape the future to reflect our desires, even if those desires are never entirely our own.

The past isn't so easily persuaded. For all our elaborate theories of time, as physicists, our profession doesn't encourage us to think about the past in any great

specificity. For us, the fruits of the past have already been thoroughly harvested—the theories of those who came before us have already been picked clean, strip-mined and supplanted by better theories, by better experiments with newer and more sophisticated instruments. Our past is a shallow one: the timestamps in our bibliographies are measured in years from the present, a decade or so at most. This is the sliver of usable history we have to work with, the retreating strand of territory that might still yield new results, new publications, new flags to plant in virgin soil. It's the distance between the foreground of Neven's mountain landscape and the hikers less than a mile in the distance, collapsed and foreshortened onto the flat plane of a PowerPoint slide. All eyes point toward the future, to a cartoon mountain looming in the distance, its radiant glow distracting us from the shadows falling in the wrong direction. What happens if we avert our eyes from the path in front of us, shatter the sharp perimeter of the keynote slide? What happens if we turn around? Will we be able to face the history which led us to this point?

If we are truly committed to removing supremacy from our community, we must change our strategy. Here, we have much to learn from the movement for prison abolition. What prison abolitionists like Ruth Wilson Gilmore understand is that the modern criminal justice system cannot be reformed. The American crisis of mass incarceration is not simply an isolated phenomenon, a lone tree bearing poison fruit. It's a mushroom, a symptom of deep and structural decay metastasizing beneath the surface. Which is to say, mass incarceration is not an aberrant error in an otherwise just society—it's the glitch that reveals the machinery of a deeply unjust society, a society whose sense of justice is utterly entangled with the myth of racial supremacy, with the imperatives of commerce and capital. Remove the buildings called prisons, and such a society will rebuild the same structures under a different name. To remove prisons permanently, to *abolish* the system of mass incarceration itself, you must work towards a society where prisons no longer make sense. This is the task of abolition. This is our task as well: to endeavor, not towards a world without the signifier supremacy, but towards a world without 'supremacy.' The task is to abolish the conditions of possibility which gave rise to this gnarled sign in the first place. To do

this, Gilmore tells us, we must change everything. Students of semiotics know this to be true. Language is a fault tolerant system. Remove a single sign from the web of signification, and the vacuum left in its absence will be filled like scar tissue, stitched back together by the countless fibers at its perimeter. To remove supremacy for good, we must weave this web anew, restructure the logic which gave it meaning in the first place. We must rewire the ground itself.

Abolition is a metaphor, but this does not mean it isn't real. Nor does it mean, as Tuck and Yang might warn us, that we are draining the word of the political specificity which anti-prison activists tirelessly work towards. Metaphors, as Barad and Helmreich remind us, can reveal deep connections between seemingly separate things. Handled with care, they can be tools of solidarity. As physicists, our task is not to re-derive what abolition means from first principles, to place ourselves in its center, shape what it looks like in our own image. The work of abolition is happening right now, we just can't see it from our penthouse suite. Outside our tower of intellectual supremacy, the streets are speaking for themselves. Press your ears to the floorboards—the sound is coming from inside the tower as well. If we are committed to abolishing supremacy, we need to start listening. We need to stand in solidarity with the struggle against mass incarceration and police brutality, against anti-Black violence and colonial expansion. We need to recognize that our labor is not separable from these systems, that we have been complicit in their machinery. We must turn our tools against this machine, refuse the projects of national supremacy, technological supremacy, economic supremacy, military supremacy, legal supremacy, racial supremacy, and intellectual supremacy which our benefactors and our employers have in mind for us. We must refuse their service bell.

Refusal is an action. Before we can articulate what must be done, we must also be prepared to say what will *not* be done, what we refuse to do. But refusal is not the same as complaint. Our task is not simply to decry the systems we hope to abolish, hoping that someone else will come along and do something about it. Abolition, Gilmore reminds us, "is not a recitation of catastrophe or a culture of complaint.

> Indeed, catastrophe and complaint, if that's all we do, are the kinds of

> practices that induce in many people who are listening what my friend, the historian Daryl Scott, calls 'contempt and pity.' And abolition is not looking for contempt or pity.[22] [161]

Beyond catastrophe, beyond complaint, abolition is fundamentally a creative practice—creative, not in the ancillary sense of aiding or serving some higher calling, but creativity as the task itself. Creative, as in *creating*: creating systems of social equity, creating networks of mutual aid, creating solidarity across the particularities of individual struggle, creating common struggle. We must create, because our future is not simply one of absence—some hollow vessel waiting to be filled—but of absolute and material presence. Again, Ruth Wilson Gilmore says it best: "abolition, in my view, is not the absence of cops and prisons. It's the *presence* of everything we need to secure that absence. And renew. And rehearse the world." [160]

Rehearse—as in *practice*. How do we practice the world we are working toward, and how do we practice what we preach? Again, this work is already happening. On June 10, 2020, students and researchers across the world participated in #ShutDownSTEM—a movement co-organized in large part by physicist Chanda Prescod-Weinstein and her coalition Particles For Justice. For one day, scientists stopped what they were doing and joined a mass boycott of scientific labor in solidarity with the movement for Black lives, refusing to engage in sponsored research, refusing to grade exams, refusing to peer-review papers, refusing to hunt ground loops. Refusing, that is, to maintain the brutal machinery of scientific progress, to keep the lights on in the tower. One day was not enough to demolish the tower for good, but it was enough to start creating something in its place. It was enough time for us to come together and start talking to each other, to reckon with what we're really doing here. For one day, we took our eyes off the cartoon mountain dangling in the distance and looked back over our shoulders, felt the vertigo of history in our wake. We looked at each other and remembered that we are accountable not just to shareholders and sponsors, advisors and thesis committees, but to each other. What happened on June 10 was a different type of glitch. The system of science stuttered like broken code,

[22]For Gilmore's reference to "contempt and pity," see Ref. [414].

Figure 12-19: Graphic from the website of #ShutDownSTEM, compiling a list of activities to abstain from during the strike on June 10, 2020 [2].

momentarily failed to be productive, and through this rift we caught a glimpse of a different way of being with each other. In the absence of our routine labor, we created presence. We created consciousness. Fiber by fiber, the ground plane split. Together, we started reknotting it anew, differently.

These strands lead us beyond the guarded borders of our discipline. Our task is not simply to invite new people across the border, to gatekeep and discipline a new and diverse workforce to police the borders with us. Our task is to tear these borders down, to follow where these connections take us and allow ourselves to be changed by that journey. To do this, we can start by recognizing that some of the most important experiments in quantum mechanics are being performed right now, not in corporate laboratory facilities, but in community DIY spaces. In 2014, Rasheedah Phillips and Camae Ayewa formed an interdisciplinary creative collective in North Philadelphia called Black Quantum Futurism (BQF). Neither Phillips nor Ayewa are physicists by training—they resist easy disciplinary labels, refuse to acquiesce to their borders. They are artists, activists, community organizers. In a recent bio, Rasheedah Phillips describes herself as "a queer Philadelphia-based housing attorney, parent, interdisciplinary artist, and Black Futurist cultural producer" [352, p. 122]; Camae Ayewa, who also performs under the name Moor Mother,[23] identifies herself as "a musician, poet, visual artist, soundscape artist, and workshop facilitator." [352, p. 120] The goal of the BQF collective, as laid out in the group's first volume on theory and practice, was to explore "the intersections of imagination, futurism, literature, art, creative media, DIY-aesthetics, and activism in marginalized communities." [351, p. 79] With this blueprint, over the past decade Phillips and Ayewa have brought together a group of artists and scholars across creative practices—music, poetry, creative writing, visual arts, Black Studies, anthropology, mysticism—to develop a new body of theory in the struggle against racial supremacy. This work refuses genre constraints and em-

[23]In addition to her work with Black Quantum Futurism, Camae Ayewa co-leads the free jazz collective Irreversible Entanglements and has produced numerous works under the name Moor Mother, including the critically acclaimed albums *Analog Fluids Of Sonic Black Holes* (2019), *Circuit City* (2020), and *Black Encyclopedia of the Air* (2021). The epigraph of this section is taken from the piece "The Blues Remembers Everything The Country Forgot," the second track on her 2020 collaborative album with New York City rapper billy woods, *BRASS*.

braces the connections these borders attempt to sever, "weav[ing] together quantum physics, afrofuturism, and Afrodiasphoric concepts of time, ritual, text, and sound and creating counterhistories and Black quantum womanist futures that challenge exclusionary, mainstream versions of history and future." [352, p. 119]

Critically, while the Black Quantum Futurists draw liberally from the work of traditional quantum physicists, they treat this work with no particular reverence. Unlike the poetry of Emtithal Mahmoud at the Google Quantum AI Symposium, the work of the BQF collective refuses to acknowledge quantum mechanics as the bedrock of the universe, the final signified which grounds their practice in some ultimate reality. It is not "everything" [291]. Instead, they treat quantum physics as one set of tools among many, a bag of metaphors to be arranged horizontally with those provided by poets, abolitionists, and ancestors. In doing so, they reveal deep connections which Western physicists have historically ignored. For example, in his essay for the BQF collective titled "The Implications of Africa-centered Conceptions of Time and Space for Quantitative Theorizing," the Black Studies scholar and professor Nikitah Okembe-RA Imani notes profound connections between modern quantum mechanical theories of causality and Indigenous African cosmologies of time. In drawing this connection, Imani is uninterested in arguing about who 'discovered' quantum mechanics, or in explaining African theories of time from the Western vantage of quantum theory. Instead, he turns the table and interprets quantum theory from the philosophical framework of Indigenous Africans. This turn to Indigenous philosophy is crucial to the BQF project. "The premise of Africa-centered scholarship," Imani writes, "is not merely that it emphasizes the importance of studying Africana phenomena, but also that it attempts to engage that study beginning from Africana philosophical perspectives." [213, pp. 31–32] Engaging rigorously with these alternative philosophical perspectives, Imani demonstrates how many of the most bizarre or counter-intuitive claims of quantum theory are only strange when encountered from the limited perspective of Western philosophy. In some sense, this is another derivation of the material-semiotic connection, showing how our intuition of natural phenomena is everywhere meditated by a set of social, cultural, and historical

Figure 12-20: Black Quantum Futurism (Camae Ayewa, left; Rasheedah Phillips, right) at the Community Future Laboratory, an arts gallery, library, workshop space, and recording studio the collective operated in North Philadelphia from May 2016 to May 2017. Photograph by Kenzi Foto.

positions which structure our limited viewpoint. By starting from a different set of philosophical assumptions, we imagine the web of signification differently, shift the ground beneath our feet.

We can no longer pretend that the viewpoint of quantum computing is innocent or apolitical. The Black Quantum Futurists understand this deeply. In 2021, Rasheedah Phillips and Camae Ayewa received the Collide residency award from CERN, the world's largest center for experimental particle physics. The competitive residency, which CERN hosts every year, "invites artists from across the world to submit proposals for a research-led residency based on interaction with CERN's scientific community. The focus of the residency is to invite artists into the Laboratory to think, discuss, be informed and inspired, and to comprehend the challenges of fundamental research and the big questions that inform physics today." [54] For their application, Phillips and Ayewa proposed a project titled "CPT Symmetry and

Violations." The title is zeugmatic. In high-energy physics, CPT stands for charge, parity, and time: when these three quantities are reversed, the laws of modern physics are symmetric and remain invariant, unchanged. Historically, however, the acronym means something different. "In physics," Phillips and Ayewa write, "CPT Symmetry is a fundamental symmetry of physical laws that holds for all physical phenomena. The acronym also carries another meaning in the phrase 'Colored People's Time.' CPT, in that sense, is often used as a negative stereotype to refer to Black people as being chronically late." [53] Placing these acronyms in resonance reveals another ground loop. Clocks, like quantum computers, are machines which seek to encode and materialize principles of physics. When these machines encounter human bodies, as with Ruha Benjamin's example of the automated soap dispenser, which bodies will be legible within the narrow perspective of the machine's programming, and which will be rendered invisible? Which bodies will be on time and productive, synchronized to the master clock of commerce and progress? Which bodies will be late, unproductive? Which bodies will run out of time, run into trouble, be in the wrong place at the wrong time?

In their essay "Placing Time, Timing Space: Dismantling the Master's Map and Clock," Phillips and Ayewa note the violence we perpetrate when we blindly place our faith in these machines, take the laws which they encode at face value. They shatter the god trick, push back against the notion that "just as we take for granted that a map is a true representation of the territory it is depicting, we assume that clocks can capture the true nature of time and reality or subjective temporal experience.

> Indeed clocks do the opposite—they objectify time and render flat all experiential notions of time. [Philosopher Henri] Bergson's critique on maps could be said of clocks, in that they are merely symbolic moments rather than the moments themselves. For Western society bound to the Master Clock, mechanical and digital clock time become the synchronizing mechanism—instead of the subjective duration of your "now" interacting with other nows. Trauma and dissociation happen in a society that negatively qualifies a departure from or disruption of mechanical clock time.
>
> White men have conquered both time and space and then said they were the same thing, and what that has meant for Black people is the colonization of the temporal space of the future and the future of man in

> the universe. Black Quantum Futurism reappropriates clocks and maps to deconstruct hegemonic Western Spacetimes and dismantle the master's clocks. We create maps that embrace the inherent tensions between space and time and that provide opportunities for reconfiguring of the same. [149, p. 11]

What then of the future? In a recent interview with Arts at CERN, Rasheedah Phillips and Camae Ayewa were asked precisely this question, *How do you envision the future?* "In the future," they reply,

> the past and future are not cut off from the present. Both dimensions influence the whole of our lives, who we are and who we become at any particular point in space-time. In this future, we have dismantled oppressive, hegemonic temporalities and timelines and developed, recovered, and synthesized healthy alternative temporal dynamics in our communities and the world.
>
> We see this work as cyclical, ongoing, dynamic, generative, and generations-long. We project a vision of our shared future(s) where we have actively begun to address how future(s) are made inaccessible to marginalized communities in general and Black people in particular. We have developed positive futurity concepts and sustainable technologies of joy that benefit low-income, vulnerable, and marginalized communities. We see "in the future" an active engagement with temporalities and alternative temporal orientations—to quote [Indigenous Studies scholar Mark] Rifkin, "the new time rebels advocate a radically different approach to temporality." [53]

If quantum computing has any hope of surviving supremacy—that is, if it truly points us towards a sustainable future, a future which is just and equitable for all—it must also become a science of the past. It must look backwards and engage with the past rigorously, critically. Quantum computing must stand accountable to history, reckon with the entanglements of matter and meaning which have structured our language, our practices, and our aspirations. It must also become a witness to the present. Quantum computing must refuse the programs of supremacy which have fed it, stand in solidarity with the struggle for liberation across disciplines, across genres, across borders. And when the numbness finally wears off and the myth shatters, it must provide space to gather and to mourn, to reflect and remember everything our science and our nation and our culture have taught us to forget. To do this, we need to change our language. We need to recognize, as Karoline Wiesner noted in her

original article, that our language has been careless [469]. It has lacked care. This is how we cut the ground loop. We do it with care. We abolish supremacy when we stitch together something stronger in its place—carefully, fiber by fiber, together. Only then can we start talking about the future.

Only then will we realize we've been talking about the future all along.

Bibliography

[1] #SayTheirNames. URL: https://sayevery.name (visited on 08/26/2022).

[2] #ShutDownSTEM. URL: https://www.shutdownstem.com/who (visited on 01/27/2022).

[3] Scott Aaronson. "Quantum Dominance, Hegemony, and Superiority". In: *Shtetl-Optimized* (Dec. 19, 2019). URL: https://scottaaronson.blog/?p=4450 (visited on 12/12/2021).

[4] Scott Aaronson. *Shadow Tomography of Quantum States*. 2017. DOI: 10.48550/ARXIV.1711.01053. URL: https://arxiv.org/abs/1711.01053.

[5] Scott Aaronson. "The learnability of quantum states". In: *Proceedings of the Royal Society A: Mathematical, Physical and Engineering Sciences* 463.2088 (Sept. 2007), pp. 3089–3114. DOI: 10.1098/rspa.2007.0113. URL: https://doi.org/10.1098%2Frspa.2007.0113.

[6] Scott Aaronson and Lijie Chen. *Complexity-Theoretic Foundations of Quantum Supremacy Experiments*. 2016. DOI: 10.48550/ARXIV.1612.05903. URL: https://arxiv.org/abs/1612.05903.

[7] Amira Abbas, Stina Andersson, Abraham Asfaw, Antonio Corcoles, Luciano Bello, Yael Ben-Haim, Mehdi Bozzo-Rey, Sergey Bravyi, Nicholas Bronn, Lauren Capelluto, Almudena Carrera Vazquez, Jack Ceroni, Richard Chen, Albert Frisch, Jay Gambetta, Shelly Garion, Leron Gil, Salvador De La Puente Gonzalez, Francis Harkins, Takashi Imamichi, Pavan Jayasinha, Hwajung Kang, Amir H. Karamlou, Robert Loredo, David McKay, Alberto Maldonado, Antonio Macaluso, Antonio Mezzacapo, Zlatko Minev, Ramis Movassagh, Giacomo Nannicini, Paul Nation, Anna Phan, Marco Pistoia, Arthur Rattew, Joachim Schaefer, Javad Shabani, John Smolin, John Stenger, Kristan Temme, Madeleine Tod, Ellinor Wanzambi, Stephen Wood, and James Wootton. *Learn Quantum Computation Using Qiskit*. 2020. URL: http://community.qiskit.org/textbook.

[8] B. P. Abbott et al. "Observation of Gravitational Waves from a Binary Black Hole Merger". In: *Phys. Rev. Lett.* 116 (6 Feb. 2016), p. 061102. DOI: 10.1103/PhysRevLett.116.061102. URL: https://link.aps.org/doi/10.1103/PhysRevLett.116.061102.

[9] Chukwuemeka Afigbo. *If you have ever had a problem grasping the importance of diversity in tech and its impact on society, watch this video*. Twitter post. Aug. 16, 2017. URL: https://twitter.com/nke_ise/status/897756900753891328?s=20 (visited on 12/15/2021).

[10] Dorit Aharonov and Michael Ben-Or. "Fault-Tolerant Quantum Computation with Constant Error Rate". In: *SIAM Journal on Computing* 38.4 (2008), pp. 1207–1282. DOI: 10.1137/S0097539799359385. eprint: https://doi.org/10.1137/S0097539799359385. URL: https://doi.org/10.1137/S0097539799359385.

[11] Dorit Aharonov, Wim van Dam, Julia Kempe, Zeph Landau, Seth Lloyd, and Oded Regev. *Adiabatic Quantum Computation is Equivalent to Standard Quantum Computation*. 2005. arXiv: quant-ph/0405098 [quant-ph].

[12] Tameem Albash, Itay Hen, Federico M. Spedalieri, and Daniel A. Lidar. "Reexamination of the evidence for entanglement in a quantum annealer". In: *Phys. Rev. A* 92 (6 Dec. 2015), p. 062328. DOI: 10.1103/PhysRevA.92.062328. URL: http://link.aps.org/doi/10.1103/PhysRevA.92.062328.

[13] Antoniya Aleksandrova, Victoria Borish, and William K. Wootters. "Real-vector-space quantum theory with a universal quantum bit". In: *Phys. Rev. A* 87 (5 May 2013), p. 052106. DOI: 10.1103/PhysRevA.87.052106. URL: https://link.aps.org/doi/10.1103/PhysRevA.87.052106.

[14] Panos Aliferis, Daniel Gottesman, and John Preskill. "Quantum Accuracy Threshold for Concatenated Distance-3 Codes". In: *Quantum Info. Comput.* 6.2 (Mar. 2006), pp. 97–165. ISSN: 1533-7146.

[15] M. S. Allman, F. Altomare, J. D. Whittaker, K. Cicak, D. Li, A. Sirois, J. Strong, J. D. Teufel, and R. W. Simmonds. "rf-SQUID-Mediated Coherent Tunable Coupling between a Superconducting Phase Qubit and a Lumped-Element Resonator". In: *Phys. Rev. Lett.* 104 (17 Apr. 2010), p. 177004. DOI: 10.1103/PhysRevLett.104.177004. URL: https://link.aps.org/doi/10.1103/PhysRevLett.104.177004.

[16] M. S. Allman, J. D. Whittaker, M. Castellanos-Beltran, K. Cicak, F. da Silva, M. P. DeFeo, F. Lecocq, A. Sirois, J. D. Teufel, J. Aumentado, and R. W. Simmonds. "Tunable Resonant and Nonresonant Interactions between a Phase Qubit and *LC* Resonator". In: *Phys. Rev. Lett.* 112 (12 Mar. 2014), p. 123601. DOI: 10.1103/PhysRevLett.112.123601. URL: https://link.aps.org/doi/10.1103/PhysRevLett.112.123601.

[17] J. B. Altepeter, D. Branning, E. Jeffrey, T. C. Wei, P. G. Kwiat, R. T. Thew, J. L. O'Brien, M. A. Nielsen, and A. G. White. "Ancilla-Assisted Quantum Process Tomography". In: *Physical Review Letters* 90.19 (May 2003). DOI: 10.1103/physrevlett.90.193601. URL: https://doi.org/10.1103%2Fphysrevlett.90.193601.

[18] *ancilla*. Merriam-Webster. URL: https://www.merriam-webster.com/dictionary/ancilla (visited on 01/27/2022).

[19] Christian Kraglund Andersen, Ants Remm, Stefania Lazar, Sebastian Krinner, Johannes Heinsoo, Jean-Claude Besse, Mihai Gabureac, Andreas Wallraff, and Christopher Eichler. "Entanglement stabilization using ancilla-based parity detection and real-time feedback in superconducting circuits". In: *npj Quantum Information* 5.1 (Aug. 2019). ISSN: 2056-6387. DOI: 10.1038/s41534-019-0185-4.

[20] Markus Ansmann, H. Wang, Radoslaw C. Bialczak, Max Hofheinz, Erik Lucero, M. Neeley, A. D. O'Connell, D. Sank, M. Weides, J. Wenner, A. N. Cleland, and John M. Martinis. "Violation of Bell's inequality in Josephson phase qubits". In: *Nature* 461.7263 (Sept. 2009), pp. 504–506. DOI: 10.1038/nature08363.

[21] *Article metrics for 'Quantum supremacy using a programmable superconducting processor'*. Nature.com. URL: https://www.nature.com/articles/s41586-019-1666-5/metrics (visited on 12/12/2021).

[22] Frank Arute, Kunal Arya, Ryan Babbush, Dave Bacon, Joseph C. Bardin, Rami Barends, Rupak Biswas, Sergio Boixo, Fernando G. S. L. Brandao, David A. Buell, Brian Burkett, Yu Chen, Zijun Chen, Ben Chiaro, Roberto Collins, William Courtney, Andrew Dunsworth, Edward Farhi, Brooks Foxen, Austin Fowler, Craig Gidney, Marissa Giustina, Rob Graff, Keith Guerin, Steve Habegger, Matthew P. Harrigan, Michael J. Hartmann, Alan Ho, Markus Hoffmann, Trent Huang, Travis S. Humble, Sergei V. Isakov, Evan Jeffrey, Zhang Jiang, Dvir Kafri, Kostyantyn Kechedzhi, Julian Kelly, Paul V. Klimov, Sergey Knysh, Alexander Korotkov, Fedor Kostritsa, David Landhuis, Mike Lindmark, Erik Lucero, Dmitry Lyakh, Salvatore Mandrà, Jarrod R. McClean, Matthew McEwen, Anthony Megrant, Xiao Mi, Kristel Michielsen, Masoud Mohseni, Josh Mutus, Ofer Naaman, Matthew Neeley, Charles Neill, Murphy Yuezhen Niu, Eric Ostby, Andre Petukhov, John C. Platt, Chris Quintana, Eleanor G. Rieffel, Pedram Roushan, Nicholas C. Rubin, Daniel Sank, Kevin J. Satzinger, Vadim Smelyanskiy, Kevin J. Sung, Matthew D. Trevithick, Amit Vainsencher, Benjamin Villalonga, Theodore White, Z. Jamie Yao, Ping Yeh, Adam Zalcman, Hartmut Neven, and John M. Martinis. "Quantum supremacy using a programmable superconducting processor". In: *Nature* 574.7779 (2019), pp. 505–510. DOI: 10.1038/s41586-019-1666-5. URL: https://doi.org/10.1038/s41586-019-1666-5.

[23] Kiran Asher, Mel Y. Chen, Kareem Khubchandani, Eli Nelson, and Banu Subramaniam. "Cyborgs Unbound. Feminist STS, Interdisciplinarity, and Graduate Education". In: *Catalyst: Feminism, Theory, Technoscience* 7.1 (2021), pp. 1–34.

[24] S. Ashhab, A. O. Niskanen, K. Harrabi, Y. Nakamura, T. Picot, P. C. de Groot, C. J. P. M. Harmans, J. E. Mooij, and Franco Nori. "Interqubit coupling mediated by a high-excitation-energy quantum object". In: *Phys. Rev. B* 77 (1 Jan. 2008), p. 014510. DOI: 10.1103/PhysRevB.77.014510. URL: http://link.aps.org/doi/10.1103/PhysRevB.77.014510.

[25] Alain Aspect, Jean Dalibard, and Gérard Roger. "Experimental Test of Bell's Inequalities Using Time- Varying Analyzers". In: *Physical Review Letters* 49.25 (Dec. 1982), pp. 1804–1807. DOI: 10.1103/PhysRevLett.49.1804.

[26] Alán Aspuru-Guzik, Anthony D. Dutoi, Peter J. Love, and Martin Head-Gordon. "Simulated Quantum Computation of Molecular Energies". In: *Science* 309.5741 (2005), pp. 1704–1707. DOI: 10.1126/science.1113479. eprint: https://www.science.org/doi/pdf/10.1126/science.1113479. URL: https://www.science.org/doi/abs/10.1126/science.1113479.

[27] aya. *im hole*. Hyperdub, 2021.

[28] aya. *too oh won nein*. self-released, 2020.

[29] *Bachelor's Degrees Earned by African Americans, by Major*. American Physical Society. URL: https://www.aps.org/programs/education/statistics/aamajors.cfm (visited on 12/13/2021).

[30] K. Banaszek, G. M. D'Ariano, M. G. A. Paris, and M. F. Sacchi. "Maximum-likelihood estimation of the density matrix". In: *Phys. Rev. A* 61 (1 Dec. 1999), p. 010304. DOI: 10.1103/PhysRevA.61.010304.

[31] Karen Barad. "After the End of the World. Entangled Nuclear Colonialisms, Matters of Force, and the Material Force of Justice". In: *Theory & Event* 22.3 (2019), pp. 524–550.

[32] Karen Barad. *Meeting the Universe Halfway. Quantum Physics and the Entanglement of Matter and Meaning*. Durham: Duke University Press, 2007.

[33] R. Barends, J. Kelly, A. Megrant, D. Sank, E. Jeffrey, Y. Chen, Y. Yin, B. Chiaro, J. Mutus, C. Neill, P. O'Malley, P. Roushan, J. Wenner, T. C. White, A. N. Cleland, and John M. Martinis. "Coherent Josephson Qubit Suitable for Scalable Quantum Integrated Circuits". In: *Phys. Rev. Lett.* 111.8 (Aug. 2013), p. 080502. DOI: 10.1103/PhysRevLett.111.080502.

[34] R. Barends, J. Kelly, A. Megrant, A. Veitia, D. Sank, E. Jeffrey, T. C. White, J. Mutus, A. G. Fowler, B. Campbell, Y. Chen, Z. Chen, B. Chiaro, A. Dunsworth, C. Neill, P. O'Malley, P. Roushan, A. Vainsencher, J. Wenner, A. N. Korotkov, A. N. Cleland, and John M. Martinis. "Superconducting quantum circuits at the surface code threshold for fault tolerance". In: *Nature* 508.7497 (Apr. 2014), pp. 500–503. DOI: 10.1038/nature13171. URL: https://doi.org/10.1038%2Fnature13171.

[35] R. Barends, J. Kelly, A. Megrant, A. Veitia, D. Sank, E. Jeffrey, T. C. White, J. Mutus, A. G. Fowler, B. Campbell, Y. Chen, Z. Chen, B. Chiaro, A. Dunsworth, C. Neill, P. O'Malley, P. Roushan, A. Vainsencher, J. Wenner, A. N. Korotkov, A. N. Cleland, and John M. Martinis. "Superconducting quantum circuits at the surface code threshold for fault tolerance". In: *Nature* 508.7497 (Apr. 2014), pp. 500–503. ISSN: 0028-0836. DOI: 10.1038/nature13171.

[36] "alcohol". In: *Chambers Dictionary of Etymology*. Ed. by Robert K. Barnhardt. Edinburgh: Chambers, 1988, pp. 22–23.

[37] Roland Barthes. "Myth Today". In: *Mythologies*. Trans. by Richard Howard and Annette Lavers. New York: Hill and Wang, 2012, pp. 215–274.

[38] Roland Barthes. "Saponids and Detergents". In: *Mythologies*. Trans. by Richard Howard and Annette Lavers. New York: Hill and Wang, 2012, pp. 32–34.

[39] Stefanie Barz, Elham Kashefi, Anne Broadbent, Joseph F. Fitzsimons, Anton Zeilinger, and Philip Walther. "Demonstration of Blind Quantum Computing". en. In: *Science* 335.6066 (Jan. 2012), pp. 303–308. ISSN: 0036-8075, 1095-9203. DOI: 10.1126/science.1214707.

[40] M. Baur, A. Fedorov, L. Steffen, S. Filipp, M. P. da Silva, and A. Wallraff. "Benchmarking a Quantum Teleportation Protocol in Superconducting Circuits Using Tomography and an Entanglement Witness". In: *Phys. Rev. Lett.* 108 (4 Jan. 2012), p. 040502. DOI: 10.1103/PhysRevLett.108.040502. URL: https://link.aps.org/doi/10.1103/PhysRevLett.108.040502.

[41] Gillian Beer. "Wave Theory and the Rise of Literary Modernism". In: *Open Fields. Science in Cultural Encounter*. New York: Oxford University Press, 1996.

[42] J. S. Bell. "On the Einstein Podolsky Rosen paradox". In: *Physics Physique Fizika* 1 (3 Nov. 1964), pp. 195–200. DOI: 10.1103/PhysicsPhysiqueFizika.1.195. URL: https://link.aps.org/doi/10.1103/PhysicsPhysiqueFizika.1.195.

[43] Bruno Bellomo, Antonella De Pasquale, Giulia Gualdi, and Ugo Marzolino. "Reconstruction of Markovian master equation parameters through symplectic tomography". In: *Phys. Rev. A* 80 (5 Nov. 2009), p. 052108. DOI: 10.1103/PhysRevA.80.052108. URL: https://link.aps.org/doi/10.1103/PhysRevA.80.052108.

[44] Eitan Ben Av, Yotam Shapira, Nitzan Akerman, and Roee Ozeri. "Direct reconstruction of the quantum-master-equation dynamics of a trapped-ion qubit". In: *Phys. Rev. A* 101 (6 June 2020), p. 062305. DOI: 10.1103/PhysRevA.101.062305. URL: https://link.aps.org/doi/10.1103/PhysRevA.101.062305.

[45] Ariel Bendersky, Fernando Pastawski, and Juan Pablo Paz. "Selective and Efficient Estimation of Parameters for Quantum Process Tomography". In: *Phys. Rev. Lett.* 100 (19 May 2008), p. 190403. DOI: 10.1103/PhysRevLett.100.190403. URL: https://link.aps.org/doi/10.1103/PhysRevLett.100.190403.

[46] Giuliano Benenti and Giuliano Strini. "Computing the distance between quantum channels: usefulness of the Fano representation". In: *Journal of Physics B: Atomic, Molecular and Optical Physics* 43.21 (Oct. 2010), p. 215508. DOI: 10.1088/0953-4075/43/21/215508. URL: https://doi.org/10.1088/0953-4075/43/21/215508.

[47] Ruha Benjamin. *Race After Technology. Abolitionist Tools for the New Jim Code*. Cambridge: Polity Press, 2019.

[48] Charles H. Bennett. "How to Define Complexity in Physics, and Why". In: *Complexity, Entropy, and the Physics of Information. The Proceedings of the 1988 Workshop on Complexity, Entropy, and the Physics of Information Held May–June, 1989 in Sante Fe, New Mexico*. Ed. by Wojciech H. Zurek. Redwood City, CA: Addison-Wesley, 1990, pp. 137–148.

[49] Charles H. Bennett and Gilles Brassard. "Quantum cryptography: Public key distribution and coin tossing". In: *Theoretical Computer Science* 560 (Dec. 2014), pp. 7–11. DOI: 10.1016/j.tcs.2014.05.025. URL: https://doi.org/10.1016%2Fj.tcs.2014.05.025.

[50] Charles H. Bennett, Gilles Brassard, Claude Crépeau, Richard Jozsa, Asher Peres, and William K. Wootters. "Teleporting an unknown quantum state via dual classical and Einstein-Podolsky-Rosen channels". In: *Phys. Rev. Lett.* 70 (13 Mar. 1993), pp. 1895–1899. DOI: 10.1103/PhysRevLett.70.1895. URL: https://link.aps.org/doi/10.1103/PhysRevLett.70.1895.

[51] Jacob Biamonte, Peter Wittek, Nicola Pancotti, Patrick Rebentrost, Nathan Wiebe, and Seth Lloyd. "Quantum machine learning". In: *Nature* 549.7671 (Sept. 2017), pp. 195–202. ISSN: 0028-0836. DOI: 10.1038/nature23474.

[52] Lev Bishop, Sergey Bravyi, Andrew W. Cross, Jay M. Gambetta, John A. Smolin, and March. "Quantum Volume". In: *AQuantum Volume. Technical Report*. 2017.

[53] *Black Quantum Futurism. "Black Diasporan temporalities share many parallels with quantum principles"*. Arts At CERN. 2021. URL: https://arts.cern/article/black-quantum-futurism-black-diasporan-temporalities-share-many-parallels-quantum (visited on 03/26/2021).

[54] *Black Quantum Futurism wins this year's Collide residency award*. CERN. 2021. URL: https://home.cern/news/news/knowledge-sharing/black-quantum-futurism-wins-years-collide-residency-award (visited on 02/16/2021).

[55] Alexandre Blais, Ren-Shou Huang, Andreas Wallraff, S. M. Girvin, and R. J. Schoelkopf. "Cavity quantum electrodynamics for superconducting electrical circuits: An architecture for quantum computation". In: *Phys. Rev. A* 69 (6 June 2004), p. 062320. DOI: 10.1103/PhysRevA.69.062320. URL: http://link.aps.org/doi/10.1103/PhysRevA.69.062320.

[56] Robin Blume-Kohout, John Gamble, Erik Nielsen, Kenneth Rudinger, Jonathan Mizrahi, Kevin Fortier, and Peter Maunz. "Demonstration of qubit operations below a rigorous fault tolerance threshold with gate set tomography". In: *Nature Communications* 8 (Feb. 2017). DOI: 10.1038/ncomms14485.

[57] Robin Blume-Kohout, John King Gamble, Erik Nielsen, Jonathan Mizrahi, Jonathan D. Sterk, and Peter Maunz. *Robust, self-consistent, closed-form tomography of quantum logic gates on a trapped ion qubit*. 2013. DOI: 10.48550/ARXIV.1310.4492. URL: https://arxiv.org/abs/1310.4492.

[58] Robin Blume-Kohout, Erik Nielsen, Kenneth Rudinger, Kevin Young, Mohan Sarovar, and Timothy Proctor. "Idle tomography: Efficient gate characterization for N-qubit processors". In: *APS March Meeting Abstracts*. Vol. 2019. APS Meeting Abstracts. Jan. 2019, P35.006, P35.006.

[59] Robin Blume-Kohout and Kevin C. Young. "A volumetric framework for quantum computer benchmarks". In: *Quantum* 4 (Nov. 2020), p. 362. DOI: 10.22331/q-2020-11-15-362. URL: https://doi.org/10.22331%2Fq-2020-11-15-362.

[60] Robin J Blume-Kohout. "Idle Tomography". In: (Jan. 2019). eprint: https://www.osti.gov/biblio/1581878.

[61] Niels Bohr. *The Philosophical Writings of Niels Bohr. Vol. I: Atomic Theory and the Description of Nature*. Woodbridge, CT: Ox Bow Press, 1963.

[62] Niels Bohr. *The Philosophical Writings of Niels Bohr. Vol. II: Essays, 1933–1957, on Atomic Physics and Human Knowledge*. Woodbridge, CT: Ox Bow Press, 1963.

[63] Niels Bohr. *The Philosophical Writings of Niels Bohr. Vol. III: Essays, 1958–1962, on Atomic Physics and Human Knowledge*. Woodbridge, CT: Ox Bow Press, 1963.

[64] Niels Bohr. *The Philosophical Writings of Niels Bohr. Vol. IV: Causality and Complementarity*. Ed. by Jane Faye and Henry J. Folse. Woodbridge, CT: Ox Bow Press, 1998.

[65] Sergio Boixo, Troels F. Ronnow, Sergei V. Isakov, Zhihui Wang, David Wecker, Daniel A. Lidar, John M. Martinis, and Matthias Troyer. "Evidence for quantum annealing with more than one hundred qubits". In: *Nat Phys* 10.3 (Mar. 2014), pp. 218–224. ISSN: 1745-2473. URL: http://dx.doi.org/10.1038/nphys2900.

[66] Sergio Boixo, Vadim N. Smelyanskiy, Alireza Shabani, Sergei V. Isakov, Mark Dykman, Vasil S. Denchev, Mohammad H. Amin, Anatoly Yu Smirnov, Masoud Mohseni, and Hartmut Neven. "Computational multiqubit tunnelling in programmable quantum annealers". In: *Nature Communications* 7 (Jan. 2016), pp. 10327–. URL: http://dx.doi.org/10.1038/ncomms10327.

[67] Eliot Bolduc, Genevieve Gariepy, and Jonathan Leach. "Direct measurement of large-scale quantum states via expectation values of non-Hermitian matrices". In: *Nature Communications* 7 (Jan. 2016), p. 10439. DOI: 10.1038/ncomms10439.

[68] Adi Botea, Akihiro Kishimoto, and Radu Marinescu. "On the Complexity of Quantum Circuit Compilation". In: *SOCS*. 2018.

[69] Adi Botea, Akihiro Kishimoto, and Radu Marinescu. "On the complexity of quantum circuit compilation". In: *Eleventh Annual Symposium on Combinatorial Search*. 2018.

[70] V. Bouchiat, D. Vion, P. Joyez, D. Esteve, and M. H. Devoret. "Quantum Coherence with a Single Cooper Pair". In: *Physica Scripta* T76.1 (1998), p. 165. DOI: 10.1238/physica.topical.076a00165. URL: https://doi.org/10.1238/physica.topical.076a00165.

[71] Fernando G. S. L. Brandão, Amir Kalev, Tongyang Li, Cedric Yen-Yu Lin, Krysta M. Svore, and Xiaodi Wu. "Quantum SDP Solvers: Large Speed-ups, Optimality, and Applications to Quantum Learning". In: *arXiv:1710.02581* (Apr. 2019).

[72] Siegmund Brandt and Hans Dieter Dahmen. *The Picture Book of Quantum Mechanics*. 3rd ed. New York: Springer, 2001.

[73] Michael J. Bremner, Ashley Montanaro, and Dan J. Shepherd. "Achieving quantum supremacy with sparse and noisy commuting quantum computations". In: *Quantum* 1 (Apr. 2017), p. 8. DOI: 10.22331/q-2017-04-25-8. URL: https://doi.org/10.22331%2Fq-2017-04-25-8.

[74] Heinz-Peter Breuer, Elsi-Mari Laine, and Jyrki Piilo. "Measure for the Degree of Non-Markovian Behavior of Quantum Processes in Open Systems". In: *Phys. Rev. Lett.* 103 (21 Nov. 2009), p. 210401. DOI: 10.1103/PhysRevLett.103.210401. URL: https://link.aps.org/doi/10.1103/PhysRevLett.103.210401.

[75] Alec Maassen van den Brink, A J Berkley, and M Yalowsky. "Mediated tunable coupling of flux qubits". In: *New Journal of Physics* 7.1 (2005), p. 230. URL: http://stacks.iop.org/1367-2630/7/i=1/a=230.

[76] Baba Brinkman. *Freestyle Rap "3:20" by Baba Brinkman (Quantum Summer Symposium 2020)*. filmed July 23, 2020. TensorFlow. 2020. URL: https://youtu.be/oUgG9Z2N7pE (visited on 09/08/2020).

[77] Joseph W. Britton, Brian C. Sawyer, Adam C. Keith, C. -C. Joseph Wang, James K. Freericks, Hermann Uys, Michael J. Biercuk, and John J. Bollinger. "Engineered two-dimensional Ising interactions in a trapped-ion quantum simulator with hundreds of spins". In: *Nature* 484.7395 (2012), pp. 489–492. DOI: 10.1038/nature10981. URL: https://doi.org/10.1038/nature10981.

[78] J. Brooke, D. Bitko, T. F. Rosenbaum, and G. Aeppli. "Quantum Annealing of a Disordered Magnet". In: *Science* 284.5415 (1999), pp. 779–781. ISSN: 0036-8075. DOI: 10.1126/science.284.5415.779.

[79] P. I. Bunyk, E. M. Hoskinson, M. W. Johnson, E. Tolkacheva, F. Altomare, A. J. Berkley, R. Harris, J. P. Hilton, T. Lanting, A. J. Przybysz, and J. Whittaker. "Architectural Considerations in the Design of a Superconducting Quantum Annealing Processor". In: *IEEE Transactions on Applied Superconductivity* 24.4 (Aug. 2014), pp. 1–10. ISSN: 1051-8223. DOI: 10.1109/TASC.2014.2318294.

[80] Daniel Burgarth and Koji Maruyama. "Indirect Hamiltonian identification through a small gateway". In: *New Journal of Physics* 11.10 (Oct. 2009), p. 103019. DOI: 10.1088/1367-2630/11/10/103019. URL: https://doi.org/10.1088%2F1367-2630%2F11%2F10%2F103019.

[81] Jonathan J. Burnett, Andreas Bengtsson, Marco Scigliuzzo, David Niepce, Marina Kudra, Per Delsing, and Jonas Bylander. "Decoherence benchmarking of superconducting qubits". en. In: *npj Quantum Inf* 5.1 (June 2019), pp. 1–8. ISSN: 2056-6387. DOI: 10.1038/s41534-019-0168-5.

[82] Jonathan J. Burnett, Andreas Bengtsson, Marco Scigliuzzo, David Niepce, Marina Kudra, Per Delsing, and Jonas Bylander. "Decoherence benchmarking of superconducting qubits". In: *npj Quantum Information* 5.1 (2019), p. 54. DOI: 10.1038/s41534-019-0168-5. URL: https://doi.org/10.1038/s41534-019-0168-5.

[83] Judith Butler. *Bodies That Matter. On the Discursive Limits of "Sex"*. New York: Routledge, 1993.

[84] Judith Butler. *Gender Trouble. Feminism and the Subversion of Identity*. New York: Routledge, 1990.

[85] Jonas Bylander, Simon Gustavsson, Fei Yan, Fumiki Yoshihara, Khalil Harrabi, George Fitch, David G. Cory, Yasunobu Nakamura, Jaw-Shen Tsai, and William D. Oliver. "Noise spectroscopy through dynamical decoupling with a superconducting flux qubit". In: *Nat Phys* 7.7 (July 2011), pp. 565–570. ISSN: 1745-2473. URL: http://dx.doi.org/10.1038/nphys1994.

[86] Tim Byrnes, Na Young Kim, Kenichiro Kusudo, and Yoshihisa Yamamoto. "Quantum simulation of Fermi-Hubbard models in semiconductor quantum-dot arrays". In: *Phys. Rev. B* 78 (7 Aug. 2008), p. 075320. DOI: 10.1103/PhysRevB.78.075320. URL: https://link.aps.org/doi/10.1103/PhysRevB.78.075320.

[87] P. Campagne-Ibarcq, E. Flurin, N. Roch, D. Darson, P. Morfin, M. Mirrahimi, M. H. Devoret, F. Mallet, and B. Huard. "Persistent Control of a Superconducting Qubit by Stroboscopic Measurement Feedback". In: *Phys. Rev. X* 3 (2 May 2013), p. 021008. DOI: 10.1103/PhysRevX.3.021008.

[88] Fritjof Capra. *The Tao of Physics. An Exploration of the Parallels Between Modern Physics and Eastern Mysticism*. Boulder: Shambhala Publications, 1989.

[89] Dave Chapelle. *8:46*. Netflix. 2020. URL: https://youtu.be/3tR6mKcBbT4 (visited on 06/12/2020).

[90] Yu Chen, C. Neill, P. Roushan, N. Leung, M. Fang, R. Barends, J. Kelly, B. Campbell, Z. Chen, B. Chiaro, A. Dunsworth, E. Jeffrey, A. Megrant, J. Y. Mutus, P. J. J. O'Malley, C. M. Quintana, D. Sank, A. Vainsencher, J. Wenner, T. C. White, Michael R. Geller, A. N. Cleland, and John M. Martinis. "Qubit Architecture with High Coherence and Fast Tunable Coupling". In: *Phys. Rev.*

Lett. 113 (22 Nov. 2014), p. 220502. DOI: 10.1103/PhysRevLett.113.220502. URL: http://link.aps.org/doi/10.1103/PhysRevLett.113.220502.

[91] Zijun Chen. "Metrology of Quantum Control and Measurement in Superconducting Qubits". PhD thesis. University of California, Santa Barbara, Jan. 2018.

[92] Kevin S. Chou, Jacob Z. Blumoff, Christopher S. Wang, Philip C. Reinhold, Christopher J. Axline, Yvonne Y. Gao, L. Frunzio, M. H. Devoret, Liang Jiang, and R. J. Schoelkopf. "Deterministic teleportation of a quantum gate between two logical qubits". In: *Nature* 561.7723 (Sept. 2018), pp. 368–373. DOI: 10.1038/s41586-018-0470-y. URL: https://doi.org/10.1038%2Fs41586-018-0470-y.

[93] J. M. Chow, L. DiCarlo, J. M. Gambetta, A. Nunnenkamp, Lev S. Bishop, L. Frunzio, M. H. Devoret, S. M. Girvin, and R. J. Schoelkopf. "Detecting highly entangled states with a joint qubit readout". In: *Physical Review A* 81.6 (June 2010). ISSN: 1094-1622. DOI: 10.1103/physreva.81.062325.

[94] J. M. Chow, J. M. Gambetta, L. Tornberg, Jens Koch, Lev S. Bishop, A. A. Houck, B. R. Johnson, L. Frunzio, S. M. Girvin, and R. J. Schoelkopf. "Randomized Benchmarking and Process Tomography for Gate Errors in a Solid-State Qubit". In: *Phys. Rev. Lett.* 102 (9 Mar. 2009), p. 090502. DOI: 10.1103/PhysRevLett.102.090502. URL: https://link.aps.org/doi/10.1103/PhysRevLett.102.090502.

[95] Andrea Long Chu. *Females*. London and New York: Verso, 2019.

[96] Isaac L. Chuang and M. A. Nielsen. "Prescription for experimental determination of the dynamics of a quantum black box". In: *Journal of Modern Optics* 44.11-12 (Nov. 1997), pp. 2455–2467. DOI: 10.1080/09500349708231894. URL: https://doi.org/10.1080%2F09500349708231894.

[97] Elysia Crampton Chuquima. *ORCORARA 2010*. PAN, 2020.

[98] Elysia Crampton Chuquima. *Selected Demos & DJ Edits, 2007–2019*. self-released, 2020.

[99] Barry A. Cipra. "The Ising Model Is NP-Complete". In: *SIAM News* 33 (6 2000). URL: https://archive.siam.org/pdf/news/654.pdf.

[100] Cirq-v0.5.0. "A python library for writing, manipulating, and optimizing quantum circuits and running them against quantum computers and simulators." In: *https://github.com/quantumlib/cirq* ().

[101] William G. Cochran. "The χ^2 Test of Goodness of Fit". In: *The Annals of Mathematical Statistics* 23.3 (1952), pp. 315–345. DOI: 10.1214/aoms/1177729380. URL: https://doi.org/10.1214/aoms/1177729380.

[102] Jared H. Cole, Sonia G. Schirmer, Andrew D. Greentree, Cameron J. Wellard, Daniel K. L. Oi, and Lloyd C. L. Hollenberg. "Identifying an experimental two-state Hamiltonian to arbitrary accuracy". In: *Phys. Rev. A* 71 (6 June 2005), p. 062312. DOI: 10.1103/PhysRevA.71.062312. URL: https://link.aps.org/doi/10.1103/PhysRevA.71.062312.

[103] J. I. Colless, A. C. Mahoney, J. M. Hornibrook, A. C. Doherty, H. Lu, A. C. Gossard, and D. J. Reilly. "Dispersive Readout of a Few-Electron Double Quantum Dot with Fast rf Gate Sensors". In: *Phys. Rev. Lett.* 110 (4 Jan. 2013), p. 046805. DOI: 10.1103/PhysRevLett.110.046805. URL: http://link.aps.org/doi/10.1103/PhysRevLett.110.046805.

[104] Joshua Combes, Christopher Ferrie, Chris Cesare, Markus Tiersch, G. J. Milburn, Hans J. Briegel, and Carlton M. Caves. *In-situ characterization of quantum devices with error correction*. 2014. DOI: 10.48550/ARXIV.1405.5656. URL: https://arxiv.org/abs/1405.5656.

[105] *Comments on 'The careless use of language in quantum information'*. SciRate. URL: https://scirate.com/arxiv/1705.06768 (visited on 12/12/2021).

[106] A. Córcoles, Easwar Magesan, Srikanth Srinivasan, Andrew Cross, M Steffen, Jay Gambetta, and Jerry Chow. "Demonstration of a quantum error detection code using a square lattice of four superconducting qubits". In: *Nature communications* 6 (Apr. 2015), p. 6979. DOI: 10.1038/ncomms7979.

[107] Marcus Cramer, Martin B. Plenio, Steven T. Flammia, Rolando Somma, David Gross, Stephen D. Bartlett, Olivier Landon-Cardinal, David Poulin, and Yi-Kai Liu. "Efficient quantum state tomography". In: *Nature Communications* 1.1 (Dec. 2010). DOI: 10.1038/ncomms1147. URL: https://doi.org/10.1038%2Fncomms1147.

[108] Andrew W. Cross, Lev S. Bishop, Sarah Sheldon, Paul D. Nation, and Jay M. Gambetta. "Validating quantum computers using randomized model circuits". In: *Phys. Rev. A* 100 (3 Sept. 2019), p. 032328. DOI: 10.1103/PhysRevA.100.032328. URL: https://link.aps.org/doi/10.1103/PhysRevA.100.032328.

[109] Alexander M. Dalzell, Aram W. Harrow, Dax Enshan Koh, and Rolando L. La Placa. "How many qubits are needed for quantum computational supremacy?" In: *Quantum* 4 (May 2020), p. 264. DOI: 10.22331/q-2020-05-11-264. URL: https://doi.org/10.22331%2Fq-2020-05-11-264.

[110] Andrew S. Darmawan and David Poulin. "Tensor-Network Simulations of the Surface Code under Realistic Noise". In: *Phys. Rev. Lett.* 119 (4 July 2017), p. 040502. DOI: 10.1103/PhysRevLett.119.040502. URL: https://link.aps.org/doi/10.1103/PhysRevLett.119.040502.

[111] Lorraine Daston and Peter Galison. *Objectivity*. Princeton: Zone Books, 2007.

[112] Christopher M. Dawson and Michael A. Nielsen. *The Solovay-Kitaev algorithm*. 2005. DOI: 10.48550/ARXIV.QUANT-PH/0505030. URL: https://arxiv.org/abs/quant-ph/0505030.

[113] Amrit De. *Fast Quantum Control for Weakly Nonlinear Qubits: On Two-Quadrature Adiabatic Gates*. 2015. DOI: 10.48550/ARXIV.1509.07905. URL: https://arxiv.org/abs/1509.07905.

[114] Ferdinand de Saussure. "Nature of the Linguistic Sign". In: *Course in General Linguistics*. New York: McGraw-Hill, 1959.

[115] Gilles Deleuze and Félix Guattari. "Introduction. Rhizome". In: *A Thousand Plateaus. Capitalism and Schizophrenia*. Trans. by Brian Massumi. Minneapolis: University of Minnesota Press, 1987, pp. 3–25.

[116] Vasil S. Denchev, Sergio Boixo, Sergei V. Isakov, Nan Ding, Ryan Babbush, Vadim Smelyanskiy, John Martinis, and Hartmut Neven. "What is the Computational Value of Finite-Range Tunneling?" In: *Phys. Rev. X* 6 (3 Aug. 2016), p. 031015. DOI: 10.1103/PhysRevX.6.031015. URL: http://link.aps.org/doi/10.1103/PhysRevX.6.031015.

[117] X.-L. Deng, D. Porras, and J. I. Cirac. "Quantum phases of interacting phonons in ion traps". In: *Phys. Rev. A* 77 (3 Mar. 2008), p. 033403. DOI: 10.1103/PhysRevA.77.033403. URL: https://link.aps.org/doi/10.1103/PhysRevA.77.033403.

[118] Jacque Derrida. *Of Grammatology*. Trans. by Gayatri Chakravorty Spivak. Baltimore: Johns Hopkins University Press, 1976.

[119] M. H. Devoret. "Quantum Fluctuations in Electrical Circuits". In: *Fluctuations Quantiques/Quantum Fluctuations*. Ed. by S. Reynaud, E. Giacobino, and J. Zinn-Justin. 1997, p. 351.

[120] C. Di Franco, M. Paternostro, and M. S. Kim. "Hamiltonian Tomography in an Access-Limited Setting without State Initialization". In: *Phys. Rev. Lett.* 102 (18 May 2009), p. 187203. DOI: 10.1103/PhysRevLett.102.187203. URL: https://link.aps.org/doi/10.1103/PhysRevLett.102.187203.

[121] L. DiCarlo, J. M. Chow, J. M. Gambetta, Lev S. Bishop, B. R. Johnson, D. I. Schuster, J. Majer, A. Blais, L. Frunzio, S. M. Girvin, and R. J. Schoelkopf. "Demonstration of two-qubit algorithms with a superconducting quantum processor". In: *Nature* 460.7252 (June 2009), pp. 240–244. DOI: 10.1038/nature08121. URL: https://doi.org/10.1038%2Fnature08121.

[122] David P. DiVincenzo. "Quantum gates and circuits". In: *Proc. R. Soc. London A* 454.1969 (Jan. 1998), pp. 261–276. DOI: 10.1098/rspa.1998.0159.

[123] DJ Rashad. *Double Cup*. Hyperdub, 2016.

[124] DJ Rashad. *Just a Taste Vol. I*. Ghettophiles, 2011.

[125] *Do you care deeply about the quality and scalability of your #quantum processor?* Atlantic Quantum. Mar. 2022. URL: https://www.linkedin.com/posts/atlantic-quantum_quantum-activity-6908067054633537536-A12G/ (visited on 07/13/2022).

[126] Yulong Dong and Lin Lin. "Random circuit block-encoded matrix and a proposal of quantum LINPACK benchmark". In: *Physical Review A* 103.6 (June 2021). DOI: 10.1103/physreva.103.062412. URL: https://doi.org/10.1103%2Fphysreva.103.062412.

[127] Jiangfeng Du, Nanyang Xu, Xinhua Peng, Pengfei Wang, Sanfeng Wu, and Dawei Lu. "NMR Implementation of a Molecular Hydrogen Quantum Simulation with Adiabatic State Preparation". In: *Phys. Rev. Lett.* 104 (3 Jan. 2010), p. 030502. DOI: 10.1103/PhysRevLett.104.030502. URL: https://link.aps.org/doi/10.1103/PhysRevLett.104.030502.

[128] T. Duty, G. Johansson, K. Bladh, D. Gunnarsson, C. Wilson, and P. Delsing. "Observation of Quantum Capacitance in the Cooper-Pair Transistor". In: *Phys. Rev. Lett.* 95 (20 Nov. 2005), p. 206807. DOI: 10.1103/PhysRevLett.95.206807. URL: http://link.aps.org/doi/10.1103/PhysRevLett.95.206807.

[129] Sepehr Ebadi, Tout T. Wang, Harry Levine, Alexander Keesling, Giulia Semeghini, Ahmed Omran, Dolev Bluvstein, Rhine Samajdar, Hannes Pichler, Wen Wei Ho, Soonwon Choi, Subir Sachdev, Markus Greiner, Vladan Vuletić, and Mikhail D. Lukin. "Quantum phases of matter on a 256-atom programmable quantum simulator". In: *Nature* 595.7866 (2021), pp. 227–232. DOI: 10.1038/s41586-021-03582-4. URL: https://doi.org/10.1038/s41586-021-03582-4.

[130] *Educational Resources*. Google Quantum AI. 2022. URL: https://quantumai.google/education (visited on 07/18/2022).

[131] B. Efron. "Bootstrap Methods: Another Look at the Jackknife". In: *Ann. Statist.* 7.1 (Jan. 1979), pp. 1–26. DOI: 10.1214/aos/1176344552.

[132] Jens Eisert, Dominik Hangleiter, Nathan Walk, Ingo Roth, Damian Markham, Rhea Parekh, Ulysse Chabaud, and Elham Kashefi. "Quantum certification and benchmarking". In: *Nature Reviews Physics* 2 (2020), pp. 382–390.

[133] Joseph Emerson, Robert Alicki, and Karol Życzkowski. "Scalable noise estimation with random unitary operators". In: *Journal of Optics B: Quantum and Semiclassical Optics* 7.10 (Sept. 2005), S347–S352. DOI: 10.1088/1464-4266/7/10/021. URL: https://doi.org/10.1088%2F1464-4266%2F7%2F10%2F021.

[134] Joseph Emerson, Marcus Silva, Osama Moussa, Colm Ryan, Martin Laforest, Jonathan Baugh, David G. Cory, and Raymond Laflamme. "Symmetrized Characterization of Noisy Quantum Processes". In: *Science* 317.5846 (Sept. 2007), pp. 1893–1896. DOI: 10.1126/science.1145699. URL: https://doi.org/10.1126%2Fscience.1145699.

[135] S. J. van Enk, N. Lütkenhaus, and H. J. Kimble. "Experimental procedures for entanglement verification". In: *Phys. Rev. A* 75 (5 May 2007), p. 052318. DOI: 10.1103/PhysRevA.75.052318. URL: https://link.aps.org/doi/10.1103/PhysRevA.75.052318.

[136] Alexander Erhard, Joel Wallman, Lukas Postler, Michael Meth, Roman Stricker, Esteban Martinez, Philipp Schindler, Thomas Monz, Joseph Emerson, and R. Blatt. "Characterizing large-scale quantum computers via cycle benchmarking". In: *Nature Communications* 10 (Nov. 2019). DOI: 10.1038/s41467-019-13068-7.

[137] Edward Farhi, Jeffrey Goldstone, Sam Gutmann, Joshua Lapan, Andrew Lundgren, and Daniel Preda. "A Quantum Adiabatic Evolution Algorithm Applied to Random Instances of an NP-Complete Problem". In: *Science* 292.5516 (2001), pp. 472–475. ISSN: 0036-8075. DOI: 10.1126/science.1057726. URL: http://science.sciencemag.org/content/292/5516/472.

[138] Edward Farhi, Jeffrey Goldstone, Sam Gutmann, and Michael Sipser. "Quantum Computation by Adiabatic Evolution". In: *arXiv:quant-ph/0001106* (Jan. 2000).

[139] Edward Farhi and Aram W Harrow. *Quantum Supremacy through the Quantum Approximate Optimization Algorithm*. 2016. DOI: 10.48550/ARXIV.1602.07674. URL: https://arxiv.org/abs/1602.07674.

[140] Christopher Ferrie. "Self-Guided Quantum Tomography". In: *Phys. Rev. Lett.* 113 (19 Nov. 2014), p. 190404. DOI: 10.1103/PhysRevLett.113.190404. URL: https://link.aps.org/doi/10.1103/PhysRevLett.113.190404.

[141] Richard P. Feynman. "Simulating Physics with Computers". In: *International Journal of Theoretical Physics* 21.6/7 (1982), pp. 467–488.

[142] C. Figgatt, D. Maslov, K. A. Landsman, N. M. Linke, S. Debnath, and C. Monroe. "Complete 3-Qubit Grover search on a programmable quantum computer". In: *Nature Communications* 8.1 (Dec. 2017). DOI: 10.1038/s41467-017-01904-7. URL: https://doi.org/10.1038%2Fs41467-017-01904-7.

[143] A.B. Finnila, M.A. Gomez, C. Sebenik, C. Stenson, and J.D. Doll. "Quantum annealing: A new method for minimizing multidimensional functions". In: *Chemical Physics Letters* 219.5 (1994), pp. 343–348. ISSN: 0009-2614. DOI: http://dx.doi.org/10.1016/0009-2614(94)00117-0. URL: http://www.sciencedirect.com/science/article/pii/0009261494001170.

[144] Jaromır Fiurá šek and Zden ěk Hradil. "Maximum-likelihood estimation of quantum processes". In: *Phys. Rev. A* 63 (2 Jan. 2001), p. 020101. DOI: 10.1103/PhysRevA.63.020101. URL: https://link.aps.org/doi/10.1103/PhysRevA.63.020101.

[145] *Five Years at the Radiation Laboratory. Originally Presented to Members of the Radiation Laboratory by the Massachusetts Institute of Technology, Cambridge, 1946*. 1991 IEEE MTT-S International Microwave Symposium Edition. Cambridge, MA: Massachusetts Institute of Technology, 1991.

[146] Michael M. Fogler. "Ground-State Energy of the Electron Liquid in Ultrathin Wires". In: *Phys. Rev. Lett.* 94 (5 Feb. 2005), p. 056405. DOI: 10.1103/PhysRevLett.94.056405. URL: http://link.aps.org/doi/10.1103/PhysRevLett.94.056405.

[147] Paul Forman. "Weimar culture, causality, and quantum theory. Adaptation by German physicists and mathematicians to a hostile environment". In: *Historical Studies in the Physical Sciences* 3 (1971), pp. 1–115.

[148] Austin G. Fowler, D. Sank, J. Kelly, R. Barends, and John M. Martinis. *Scalable extraction of error models from the output of error detection circuits*. 2014. DOI: 10.48550/ARXIV.1405.1454. URL: https://arxiv.org/abs/1405.1454.

[149] Black Quantum Futurism. "Placing Time, Timing Space. Dismantling the Master's Map and Clock". In: *Black Quantum Futurism. Theory & Practice Volume II*. Ed. by Rasheedah Phillips. Philadelphia: The Afrofuturist Affair, 2021, pp. 9–13.

[150] W. Gale, E. Guth, and G. T. Trammell. "Determination of the Quantum State by Measurements". In: *Phys. Rev.* 165 (5 Jan. 1968), pp. 1434–1436. DOI: 10.1103/PhysRev.165.1434. URL: https://link.aps.org/doi/10.1103/PhysRev.165.1434.

[151] Peter Galison. "The Trading Zone. Coordinating Action and Belief". In: *Image and Logic. A Material Culture of Microphysics*. Chicago: University of Chicago Press, 1997.

[152] J. M. Gambetta, F. Motzoi, S. T. Merkel, and F. K. Wilhelm. "Analytic control methods for high-fidelity unitary operations in a weakly nonlinear oscillator". In: *Phys. Rev. A* 83 (1 Jan. 2011), p. 012308. DOI: 10.1103/PhysRevA.83.012308. URL: https://link.aps.org/doi/10.1103/PhysRevA.83.012308.

[153] M. Ganzhorn, G. Salis, D. J. Egger, A. Fuhrer, M. Mergenthaler, C. Müller, P. Müller, S. Paredes, M. Pechal, M. Werninghaus, and S. Filipp. "Benchmarking the noise sensitivity of different parametric two-qubit gates in a single superconducting quantum computing platform". In: *Phys. Rev. Research* 2 (3 Sept. 2020), p. 033447. DOI: 10.1103/PhysRevResearch.2.033447. URL: https://link.aps.org/doi/10.1103/PhysRevResearch.2.033447.

[154] Xun Gao, Sheng-Tao Wang, and L.-M. Duan. "Quantum Supremacy for Simulating a Translation-Invariant Ising Spin Model". In: *Phys. Rev. Lett.* 118 (4 Jan. 2017), p. 040502. DOI: 10.1103/PhysRevLett.118.040502. URL: https://link.aps.org/doi/10.1103/PhysRevLett.118.040502.

[155] Yvonne Y. Gao, Brian J. Lester, Kevin S. Chou, Luigi Frunzio, Michel H. Devoret, Liang Jiang, S. M. Girvin, and Robert J. Schoelkopf. "Entanglement of bosonic modes through an engineered exchange interaction". en. In: *Nature* 566.7745 (Feb. 2019), pp. 509–512. ISSN: 1476-4687. DOI: 10.1038/s41586-019-0970-4.

[156] J. J. Garcıa-Ripoll, M. A. Martin-Delgado, and J. I. Cirac. "Implementation of Spin Hamiltonians in Optical Lattices". In: *Phys. Rev. Lett.* 93 (25 Dec. 2004), p. 250405. DOI: 10.1103/PhysRevLett.93.250405. URL: https://link.aps.org/doi/10.1103/PhysRevLett.93.250405.

[157] Murray Gell-Mann and James B. Hartle. "Quantum Mechanics in the Light of Quantum Cosmology". In: *Complexity, Entropy, and the Physics of Information. The Proceedings of the 1988 Workshop on Complexity, Entropy, and the Physics of Information Held May–June, 1989 in Sante Fe, New Mexico*. Ed. by Wojciech H. Zurek. Redwood City, CA: Addison-Wesley, 1990, pp. 425–458.

[158] I. M. Georgescu, S. Ashhab, and Franco Nori. "Quantum simulation". In: *Rev. Mod. Phys.* 86 (1 Mar. 2014), pp. 153–185. DOI: 10.1103/RevModPhys.86.153. URL: https://link.aps.org/doi/10.1103/RevModPhys.86.153.

[159] Ruth Wilson Gilmore. "What Is To Be Done?" In: *American Quarterly* 63.2 (2011), pp. 245–265.

[160] Ruth Wilson Gilmore, Angela Yvonne Davis, Mike Davis, and Keeanga-Yamahtta Taylor. *Abolition, Cultural Freedom, Liberation*. filmed October 2021. Haymarket Books. URL: https://youtu.be/WLO0UuSnPzU (visited on 10/05/2021).

[161] Ruth Wilson Gilmore and Naomi Murakawa. *Covid 19, Decarceration, and Abolition (Full)*. filmed April 2020. Haymarket Books. URL: https://youtu.be/hf3f5i9vJNM (visited on 04/28/2020).

[162] L. I. Glazman, I. M. Ruzin, and B. I. Shklovskii. "Quantum transport and pinning of a one-dimensional Wigner crystal". In: *Phys. Rev. B* 45 (15 Apr. 1992), pp. 8454–8463. DOI: 10.1103/PhysRevB.45.8454. URL: http://link.aps.org/doi/10.1103/PhysRevB.45.8454.

[163] Édouard Glissant. "Errantry, Exile". In: *Poetics of Relation*. Trans. by Betsy Wing. Ann Arbor: The University of Michigan Press, 1997, pp. 11–22.

[164] Ming Gong, Xiao Yuan, Shiyu Wang, Yulin Wu, Youwei Zhao, Chen Zha, Shaowei Li, Zhen Zhang, Qi Zhao, Yunchao Liu, Futian Liang, Jin Lin, Yu Xu, Hui Deng, Hao Rong, He Lu, Simon Benjamin, Cheng-Zhi Peng, Xiongfeng Ma, and Jian-Wei Pan. "Experimental exploration of five-qubit quantum error correcting code with superconducting qubits". In: *National Science Review* 9 (Jan. 2021). DOI: 10.1093/nsr/nwab011.

[165] L. C. G. Govia, G. J. Ribeill, D. Ristè, M. Ware, and H. Krovi. "Bootstrapping quantum process tomography via a perturbative ansatz". In: *Nature Communications* 11.1 (2020), p. 1084. DOI: 10.1038/s41467-020-14873-1. URL: https://doi.org/10.1038/s41467-020-14873-1.

[166] Christopher E Granade, Christopher Ferrie, Nathan Wiebe, and D G Cory. "Robust online Hamiltonian learning". In: *New Journal of Physics* 14.10 (Oct. 2012), p. 103013. DOI: 10.1088/1367-2630/14/10/103013. URL: https://doi.org/10.1088%2F1367-2630%2F14%2F10%2F103013.

[167] Daniel Greenbaum. *Introduction to Quantum Gate Set Tomography*. 2015. DOI: 10.48550/ARXIV.1509.02921. URL: https://arxiv.org/abs/1509.02921.

[168] A. Greene, M. Kjaergaard, M. E. Schwartz, G. O. Samach, A. Bengtsson, M. O'Keeffe, D. K. Kim, M. Marvian, A. Melville, B. M. Niedzielski, A. Vepsalainen, R. Winik, J. Yoder, D. Rosenberg, S. Lloyd, T. P. Orlando, I. Marvian, S. Gustavsson, and W. D. Oliver. *Error mitigation via stabilizer measurement emulation*. 2021. DOI: 10.48550/ARXIV.2102.05767. URL: https://arxiv.org/abs/2102.05767.

[169] Markus Greiner, Olaf Mandel, Tilman Esslinger, Theodor W. Hänsch, and Immanuel Bloch. "Quantum phase transition from a superfluid to a Mott insulator in a gas of ultracold atoms". In: *Nature* 415.6867 (2002), pp. 39–44. DOI: 10.1038/415039a. URL: https://doi.org/10.1038/415039a.

[170] David J. Griffiths. *Introduction to Quantum Mechanics*. 2nd ed. Upper Saddle River, NJ: Pearson Prentice Hall, 2005.

[171] David Gross, Yi-Kai Liu, Steven T. Flammia, Stephen Becker, and Jens Eisert. "Quantum State Tomography via Compressed Sensing". In: *Phys. Rev. Lett.* 105 (15 Oct. 2010), p. 150401. DOI: 10.1103/PhysRevLett.105.150401. URL: https://link.aps.org/doi/10.1103/PhysRevLett.105.150401.

[172] Otfried Gühne and Géza Tóth. "Entanglement detection". In: *Physics Reports* 474.1-6 (Apr. 2009), pp. 1–75. DOI: 10.1016/j.physrep.2009.02.004. URL: https://doi.org/10.1016%2Fj.physrep.2009.02.004.

[173] Simon Gustavsson, Fei Yan, Gianluigi Catelani, Jonas Bylander, Archana Kamal, Jeffrey Birenbaum, David Hover, Danna Rosenberg, Gabriel Samach, Adam P. Sears, Steven J. Weber, Jonilyn L. Yoder, John Clarke, Andrew J. Kerman, Fumiki Yoshihara, Yasunobu Nakamura, Terry P. Orlando, and William D. Oliver. "Suppressing relaxation in superconducting qubits by quasiparticle pumping". In: *Science* (2016). ISSN: 0036-8075. DOI: 10.1126/science.aah5844.

[174] Simon Gustavsson, Fei Yan, Gianluigi Catelani, Jonas Bylander, Archana Kamal, Jeffrey Birenbaum, David Hover, Danna Rosenberg, Gabriel Samach, Adam P. Sears, Steven J. Weber, Jonilyn L. Yoder, John Clarke, Andrew J. Kerman, Fumiki Yoshihara, Yasunobu Nakamura, Terry P. Orlando, and William D. Oliver. "Suppressing relaxation in superconducting qubits by quasiparticle pumping". In: *Science* 354.6319 (2016), pp. 1573–1577. DOI: 10.1126/science.aah5844. eprint: https://www.science.org/doi/pdf/10.1126/science.aah5844. URL: https://www.science.org/doi/abs/10.1126/science.aah5844.

[175] Mauricio Gutiérrez, Conor Smith, Livia Lulushi, Smitha Janardan, and Kenneth R. Brown. "Errors and pseudothresholds for incoherent and coherent noise". In: *Phys. Rev. A* 94 (4 Oct. 2016), p. 042338. DOI: 10.1103/PhysRevA.94.042338. URL: https://link.aps.org/doi/10.1103/PhysRevA.94.042338.

[176] Mauricio Gutiérrez, Lukas Svec, Alexander Vargo, and Kenneth R. Brown. "Approximation of realistic errors by Clifford channels and Pauli measurements". In: *Phys. Rev. A* 87 (3 Mar. 2013), p. 030302. DOI: 10.1103/PhysRevA.87.030302. URL: https://link.aps.org/doi/10.1103/PhysRevA.87.030302.

[177] Jeongwan Haah, Aram W. Harrow, Zhengfeng Ji, Xiaodi Wu, and Nengkun Yu. "Sample-Optimal Tomography of Quantum States". In: *IEEE Transactions on Information Theory* 63.9 (Sept. 2017), pp. 5628–5641. ISSN: 0018-9448, 1557-9654. DOI: 10.1109/TIT.2017.2719044.

[178] H. Häffner, W. Hänsel, C. F. Roos, J. Benhelm, D. Chek-al-kar, M. Chwalla, T. Körber, U. D. Rapol, M. Riebe, P. O. Schmidt, C. Becher, O. Gühne, W. Dür, and R. Blatt. "Scalable multiparticle entanglement of trapped ions". In: *Nature* 438.7068 (Dec. 2005), pp. 643–646. DOI: 10.1038/nature04279. URL: https://doi.org/10.1038%2Fnature04279.

[179] Peter L. Hagelstein, Stephen D. Senturia, and Terry P. Orlando. *Introductory Applied Quantum and Statistical Mechanics*. Hoboken, NJ: Wiley, 2004.

[180] Armand Hammer. *Shrines*. Backwoodz Studioz, 2020.

[181] D Hangleiter, M Kliesch, M Schwarz, and J Eisert. "Direct certification of a class of quantum simulations". In: *Quantum Science and Technology* 2.1 (Feb. 2017), p. 015004. DOI: 10.1088/2058-9565/2/1/015004. URL: https://doi.org/10.1088%2F2058-9565%2F2%2F1%2F015004.

[182] Dominik Hangleiter, Ingo Roth, Jens Eisert, and Pedram Roushan. "Precise Hamiltonian identification of a superconducting quantum processor". In: (2021). arXiv: 2108.08319 [quant-ph].

[183] Donna Haraway. *Modest_ Witness@Second_ Millennium.FemaleMan©Meets_ OncoMouse™. Feminism and Technoscience*. New York: Routledge, 1997.

[184] Donna Haraway. "Situated Knowledges. The Science Question in Feminism and the Privilege of Partial Perspective". In: *Feminist Studies* 14.3 (1988).

[185] Stefano Harney and Fred Moten. *The Undercommons. Fugitive Planning and Black Study*. Wivenhoe: Minor Compositions, 2013. URL: https://www.minorcompositions.info/wp-content/uploads/2013/04/undercommons-web.pdf.

[186] Robin Harper, Steven T. Flammia, and Joel J. Wallman. "Efficient learning of quantum noise". In: *Nature Physics* 16.12 (Aug. 2020), pp. 1184–1188. DOI: 10.1038/s41567-020-0992-8. URL: https://doi.org/10.1038%2Fs41567-020-0992-8.

[187] Robin Harper, Wenjun Yu, and Steven T. Flammia. "Fast Estimation of Sparse Quantum Noise". In: *PRX Quantum* 2 (1 Feb. 2021), p. 010322. DOI: 10.1103/PRXQuantum.2.010322. URL: https://link.aps.org/doi/10.1103/PRXQuantum.2.010322.

[188] R. Harris, A. J. Berkley, M. W. Johnson, P. Bunyk, S. Govorkov, M. C. Thom, S. Uchaikin, A. B. Wilson, J. Chung, E. Holtham, J. D. Biamonte, A. Yu. Smirnov, M. H. S. Amin, and Alec Maassen van den Brink. "Sign- and Magnitude-Tunable Coupler for Superconducting Flux Qubits". In: *Phys. Rev. Lett.* 98 (17 Apr. 2007), p. 177001. DOI: 10.1103/PhysRevLett.98.177001. URL: http://link.aps.org/doi/10.1103/PhysRevLett.98.177001.

[189] R. Harris, J. Johansson, A. J. Berkley, M. W. Johnson, T. Lanting, Siyuan Han, P. Bunyk, E. Ladizinsky, T. Oh, I. Perminov, E. Tolkacheva, S. Uchaikin, E. M. Chapple, C. Enderud, C. Rich, M. Thom, J. Wang, B. Wilson, and G. Rose. "Experimental demonstration of a robust and scalable flux qubit". In: *Phys. Rev. B* 81 (13 Apr. 2010), p. 134510. DOI: 10.1103/PhysRevB.81.134510. URL: http://link.aps.org/doi/10.1103/PhysRevB.81.134510.

[190] R. Harris, T. Lanting, A. J. Berkley, J. Johansson, M. W. Johnson, P. Bunyk, E. Ladizinsky, N. Ladizinsky, T. Oh, and S. Han. "Compound Josephson-junction coupler for flux qubits with minimal crosstalk". In: *Phys. Rev. B* 80 (5 Aug. 2009), p. 052506. DOI: 10.1103/PhysRevB.80.052506. URL: http://link.aps.org/doi/10.1103/PhysRevB.80.052506.

[191] R. Harris, Y. Sato, A. J. Berkley, M. Reis, F. Altomare, M. H. Amin, K. Boothby, P. Bunyk, C. Deng, C. Enderud, S. Huang, E. Hoskinson, M. W. Johnson, E. Ladizinsky, N. Ladizinsky, T. Lanting, R. Li, T. Medina, R. Molavi, R. Neufeld, T. Oh, I. Pavlov, I. Perminov, G. Poulin-Lamarre, C. Rich, A. Smirnov, L. Swenson, N. Tsai, M. Volkmann, J. Whittaker, and J. Yao. "Phase transitions in a programmable quantum spin glass simulator". In: *Science* 361.6398 (2018), pp. 162–165. DOI: 10.1126/science.aat2025. eprint: https://www.science.org/doi/pdf/10.1126/science.aat2025. URL: https://www.science.org/doi/abs/10.1126/science.aat2025.

[192] R. Harris, Y. Sato, A. J. Berkley, M. Reis, F. Altomare, M. H. Amin, K. Boothby, P. Bunyk, C. Deng, C. Enderud, S. Huang, E. Hoskinson, M. W. Johnson, E. Ladizinsky, N. Ladizinsky, T. Lanting, R. Li, T. Medina, R. Molavi, R. Neufeld, T. Oh, I. Pavlov, I. Perminov, G. Poulin-Lamarre, C. Rich, A. Smirnov, L. Swenson, N. Tsai, M. Volkmann, J. Whittaker, and J. Yao. "Phase transitions in a programmable quantum spin glass simulator". en. In: *Science* 361.6398 (July 2018), pp. 162–165. ISSN: 0036-8075, 1095-9203. DOI: 10.1126/science.aat2025.

[193] Aram W. Harrow and Ashley Montanaro. "Quantum computational supremacy". In: *Nature* 549.7671 (Sept. 2017), pp. 203–209. DOI: 10.1038/nature23458. URL: https://doi.org/10.1038%2Fnature23458.

[194] Stefan Helmreich. "Introduction: Arriving at Artificial Life". In: *Silicon Second Nature. Culturing Artificial Life in a Digital World*. Berkeley: University of California Press, 1998, pp. 15–18.

[195] Stefan Helmreich. "Not a Metaphor. A Comment on Evelyn Fox Keller's 'Cognitive Functions of Metaphor in the Natural Sciences'". In: *Interdisciplinary Science Reviews* 45.3 (2020), pp. 446–458.

[196] Stefan Helmreich. *Silicon Second Nature. Culturing Artificial Life in a Digital World*. Berkeley: University of California Press, 1998.

[197] Stefan Helmreich. "Simulation in Santa Fe". In: *Silicon Second Nature. Culturing Artificial Life in a Digital World*. Berkeley: University of California Press, 1998, pp. 28–62.

[198] Jonas Helsen, Francesco Battistel, and Barbara M. Terhal. "Spectral quantum tomography". In: *npj Quantum Information* 5.1 (Sept. 2019). DOI: 10.1038/s41534-019-0189-0. URL: https://doi.org/10.1038%2Fs41534-019-0189-0.

[199] Cornelius Hempel, Christine Maier, Jonathan Romero, Jarrod McClean, Thomas Monz, Heng Shen, Petar Jurcevic, Ben P. Lanyon, Peter Love, Ryan Babbush, Alán Aspuru-Guzik, Rainer Blatt, and Christian F. Roos. "Quantum Chemistry Calculations on a Trapped-Ion Quantum Simulator". In: *Phys. Rev. X* 8 (3 July 2018), p. 031022. DOI: 10.1103/PhysRevX.8.031022. URL: https://link.aps.org/doi/10.1103/PhysRevX.8.031022.

[200] Nick Herbert. "FLASH—A superluminal communicator based upon a new kind of quantum measurement". In: *Found Phys* 12 (1982), pp. 1171–1179. URL: https://doi.org/10.1007/BF00729622.

[201] Rebecca Herzig. *Suffering for Science. Reason and Sacrifice in Modern America*. New Brunswick, NJ: Rutgers University Press, 2005.

[202] Philip C. D. Hobbs. *Building Electro-Optical Systems. Making It All Work*. Hoboken: John Wiley & Sons, 2008.

[203] Philip C. D. Hobbs. *Phil Hobbs' Optics Page*. ElectroOptical Innovations. URL: https://electrooptical.net (visited on 12/13/2021).

[204] Alexander S. Holevo. "Bounds for the quantity of information transmitted by a quantum communication channel". In: *Problemy Perdachi Informatsii* 9.3 (1973), pp. 3–11.

[205] Paweł Horodecki. "Measuring Quantum Entanglement without Prior State Reconstruction". In: *Phys. Rev. Lett.* 90 (16 Apr. 2003), p. 167901. DOI: 10.1103/PhysRevLett.90.167901. URL: https://link.aps.org/doi/10.1103/PhysRevLett.90.167901.

[206] P.-Y. Hou, L. He, F. Wang, X.-Z. Huang, W.-G. Zhang, X.-L. Ouyang, X. Wang, W.-Q. Lian, X.-Y. Chang, and L.-M. Duan. "Experimental Hamiltonian Learning of an 11-Qubit Solid-State Quantum Spin Register". In: *Chinese Physics Letters* 36.10 (Oct. 2019), p. 100303. DOI: 10.1088/0256-307x/36/10/100303. URL: https://doi.org/10.1088%2F0256-307x%2F36%2F10%2F100303.

[207] Z. Hradil. "Quantum-state estimation". In: *Phys. Rev. A* 55 (3 Mar. 1997), R1561–R1564. DOI: 10.1103/PhysRevA.55.R1561. URL: https://link.aps.org/doi/10.1103/PhysRevA.55.R1561.

[208] L Hu, Y Ma, W Cai, X Mu, Y Xu, W Wang, Y Wu, H Wang, YP Song, C-L Zou, et al. "Quantum error correction and universal gate set operation on a binomial bosonic logical qubit". In: *Nature Physics* 15.5 (2019), pp. 503–508.

[209] L. Hu, Y. Ma, W. Cai, X. Mu, Y. Xu, W. Wang, Y. Wu, H. Wang, Y. P. Song, C.-L. Zou, S. M. Girvin, L-M. Duan, and L. Sun. "Quantum error correction and universal gate set operation on a binomial bosonic logical qubit". In: *Nature Physics* 15.5 (Feb. 2019), pp. 503–508. DOI: 10.1038/s41567-018-0414-3. URL: https://doi.org/10.1038%2Fs41567-018-0414-3.

[210] Ming-Xia Huo and Ying Li. "Learning time-dependent noise to reduce logical errors: real time error rate estimation in quantum error correction". In: *New Journal of Physics* 19.12 (Dec. 2017), p. 123032. DOI: 10.1088/1367-2630/aa916e. URL: https://doi.org/10.1088%2F1367-2630%2Faa916e.

[211] M. D. Hutchings, J. B. Hertzberg, Y. Liu, N. T. Bronn, G. A. Keefe, Markus Brink, Jerry M. Chow, and B. L. T. Plourde. "Tunable Superconducting Qubits with Flux-Independent Coherence". In: *Phys. Rev. Applied* 8 (4 Oct. 2017), p. 044003. DOI: 10.1103/PhysRevApplied.8.044003.

[212] S. Ilani, L. A. K. Donev, M. Kindermann, and P. L. McEuen. "Measurement of the quantum capacitance of interacting electrons in carbon nanotubes". In: *Nat Phys* 2.10 (Oct. 2006), pp. 687–691. ISSN: 1745-2473.

[213] Nikitah Okembe-RA Imani. "The Implications of Africa-Centered Conceptions of Time & Space for Quantitative Theorizing. Limitations of Paradigmatically-Bound Philosophical Meta-Assumptions". In: *Black Quantum Futurism. Theory & Practice Volume I*. Ed. by Rasheedah Phillips. Philadelphia: The Afrofuturist Affair, 2015, pp. 31–48.

[214] S.V. Isakov, I.N. Zintchenko, T.F. Rønnow, and M. Troyer. "Optimised simulated annealing for Ising spin glasses". In: *Computer Physics Communications* 192 (2015), pp. 265–271. ISSN: 0010-4655. DOI: http://dx.doi.org/10.1016/j.cpc.2015.02.015. URL: http://www.sciencedirect.com/science/article/pii/S0010465515000727.

[215] Sorin Istrail. "Statistical Mechanics, Three-Dimensionality and NP-Completeness: I. Universality of Intracatability for the Partition Function of the Ising Model across Non-Planar Surfaces (Extended Abstract)". In: *Proceedings of the Thirty-Second Annual ACM Symposium on Theory of Computing*. STOC '00. Portland, Oregon, USA: Association for Computing Machinery, 2000, pp. 87–96. ISBN: 1581131844. DOI: 10.1145/335305.335316. URL: https://doi.org/10.1145/335305.335316.

[216] Wayne M Itano, Daniel J Heinzen, JJ Bollinger, and DJ Wineland. "Quantum zeno effect". In: *Physical Review A* 41.5 (1990), p. 2295.

[217] Pavithran Iyer and David Poulin. "A small quantum computer is needed to optimize fault-tolerant protocols". In: *Quantum Science and Technology* 3.3 (June 2018), p. 030504. DOI: 10.1088/2058-9565/aab73c. URL: https://doi.org/10.1088%2F2058-9565%2Faab73c.

[218] Kurt Jacobs and Daniel A. Steck. "A straightforward introduction to continuous quantum measurement". In: *Contemporary Physics* 47.5 (Sept. 2006), pp. 279–303. ISSN: 1366-5812. DOI: 10.1080/00107510601101934.

[219] D. Jaksch, C. Bruder, J. I. Cirac, C. W. Gardiner, and P. Zoller. "Cold Bosonic Atoms in Optical Lattices". In: *Phys. Rev. Lett.* 81 (15 Oct. 1998), pp. 3108–3111. DOI: 10.1103/PhysRevLett.81.3108. URL: https://link.aps.org/doi/10.1103/PhysRevLett.81.3108.

[220] Daniel F. V. James, Paul G. Kwiat, William J. Munro, and Andrew G. White. "Measurement of qubits". In: *Phys. Rev. A* 64 (5 Oct. 2001), p. 052312. DOI: 10.1103/PhysRevA.64.052312. URL: https://link.aps.org/doi/10.1103/PhysRevA.64.052312.

[221] Fredric Jameson. *Postmodernism. or, The Cultural Logic of Late Capitalism*. Durham: Duke University Press, 1991.

[222] E. Jané, G. Vidal, W. Dür, P. Zoller, and J. I. Cirac. "Simulation of quantum dynamics with quantum optical systems". In: (2002). DOI: 10.48550/ARXIV.QUANT-PH/0207011. URL: https://arxiv.org/abs/quant-ph/0207011.

[223] X. Y. Jin, A. Kamal, A. P. Sears, T. Gudmundsen, D. Hover, J. Miloshi, R. Slattery, F. Yan, J. Yoder, T. P. Orlando, S. Gustavsson, and W. D. Oliver. "Thermal and Residual Excited-State Population in a 3D Transmon Qubit". In: *Phys. Rev. Lett.* 114 (24 June 2015), p. 240501. DOI: 10.1103/PhysRevLett.114.240501. URL: https://link.aps.org/doi/10.1103/PhysRevLett.114.240501.

[224] Göran Johansson, Lars Tornberg, and C. M. Wilson. "Fast quantum limited readout of a superconducting qubit using a slow oscillator". In: *Phys. Rev. B* 74 (10 Sept. 2006), p. 100504. DOI: 10.1103/PhysRevB.74.100504. URL: http://link.aps.org/doi/10.1103/PhysRevB.74.100504.

[225] Eugene J. Johnson and Michael J. Lewis. "Thompson Laboratories". In: *Williams College. The Campus Guide*. New York: Princeton Architectural Press, 2019, pp. 73–75.

[226] Peter D. Johnson, Jonathan Romero, Jonathan Olson, Yudong Cao, and Alán Aspuru-Guzik. *QVECTOR: an algorithm for device-tailored quantum error correction*. 2017. DOI: 10.48550/ARXIV.1711.02249. URL: https://arxiv.org/abs/1711.02249.

[227] Tadashi Kadowaki and Hidetoshi Nishimori. "Quantum annealing in the transverse Ising model". In: *Phys. Rev. E* 58 (5 Nov. 1998), pp. 5355–5363. DOI: 10.1103/PhysRevE.58.5355. URL: http://link.aps.org/doi/10.1103/PhysRevE.58.5355.

[228] Dvir Kafri, Chris Quintana, Yu Chen, Alireza Shabani, John M. Martinis, and Hartmut Neven. "Tunable inductive coupling of superconducting qubits in the strongly nonlinear regime". In: *Phys. Rev. A* 95 (5 May 2017), p. 052333. DOI: 10.1103/PhysRevA.95.052333.

[229] David Kaiser. ""Shut Up and Calculate"". In: *How The Hippies Saved Physics. Science, Counterculture, and the Quantum Revival*. New York: Norton, 2011, pp. 1–23.

[230] David Kaiser. "From FLASH to Quantum Encryption". In: *How The Hippies Saved Physics. Science, Counterculture, and the Quantum Revival*. New York: Norton, 2011, pp. 195–235.

[231] David Kaiser. *How The Hippies Saved Physics. Science, Counterculture, and the Quantum Revival*. New York: Norton, 2011.

[232] David Kaiser. "Introduction". In: *How The Hippies Saved Physics. Science, Counterculture, and the Quantum Revival*. New York: Norton, 2011, pp. xi–xxvi.

[233] Amir Kalev, Robert Kosut, and Ivan Deutsch. "Quantum Tomography Protocols with Positivity are Compressed Sensing Protocols". In: *npj Quantum Information* 1 (Dec. 2015), p. 15018. DOI: 10.1038/npjqi.2015.18.

[234] Helmut G. Katzgraber, Firas Hamze, Zheng Zhu, Andrew J. Ochoa, and H. Munoz-Bauza. "Seeking Quantum Speedup Through Spin Glasses: The Good, the Bad, and the Ugly". In: *Phys. Rev. X* 5 (3 Sept. 2015), p. 031026. DOI: 10.1103/PhysRevX.5.031026. URL: http://link.aps.org/doi/10.1103/PhysRevX.5.031026.

[235] keiyaA. *Forever, Ya Girl*. Forever Recordings, 2020.

[236] J. Kelly, R. Barends, B. Campbell, Y. Chen, Z. Chen, B. Chiaro, A. Dunsworth, A. G. Fowler, I.C. Hoi, E. Jeffrey, A. Megrant, J. Mutus, C. Neill, P. J. J. O Malley, C. Quintana, P. Roushan, D. Sank, A. Vainsencher, J. Wenner, T. C. White, A. N. Cleland, and John M. Martinis. "Optimal Quantum Control Using Randomized Benchmarking". In: *Phys. Rev. Lett.* 112.24 (June 2014), p. 240504. ISSN: 0031-9007. DOI: 10.1103/PhysRevLett.112.240504.

[237] Andrew J. Kerman. *Efficient numerical simulation of complex Josephson quantum circuits*. 2020. DOI: 10.48550/ARXIV.2010.14929. URL: https://arxiv.org/abs/2010.14929.

[238] Andrew J. Kerman and William D. Oliver. "High-Fidelity Quantum Operations on Superconducting Qubits in the Presence of Noise". In: *Phys. Rev. Lett.* 101 (7 Aug. 2008), p. 070501. DOI: 10.1103/PhysRevLett.101.070501. URL: http://link.aps.org/doi/10.1103/PhysRevLett.101.070501.

[239] Dohun Kim, Zhan Shi, C. B. Simmons, D. R. Ward, J. R. Prance, Teck Seng Koh, John King Gamble, D. E. Savage, M. G. Lagally, Mark Friesen, S. N. Coppersmith, and Mark A. Eriksson. "Quantum control and process tomography of a semiconductor quantum dot hybrid qubit". In: *Nature* 511.7507 (July 2014), pp. 70–74. DOI: 10.1038/nature13407. URL: https://doi.org/10.1038%2Fnature13407.

[240] Dohun Kim, D. R. Ward, C. B. Simmons, John King Gamble, Robin Blume-Kohout, Erik Nielsen, D. E. Savage, M. G. Lagally, Mark Friesen, S. N. Coppersmith, and M. A. Eriksson. "Microwave-driven coherent operation of a semiconductor quantum dot charge qubit". In: *Nature Nanotechnology* 10.3 (2015), pp. 243–247. URL: https://doi.org/10.1038/nnano.2014.336.

[241] K Kim, S Korenblit, R Islam, E E Edwards, M-S Chang, C Noh, H Carmichael, G-D Lin, L-M Duan, C C Joseph Wang, J K Freericks, and C Monroe. "Quantum simulation of the transverse Ising model with trapped ions". In: *New Journal of Physics* 13.10 (Oct. 2011), p. 105003. DOI: 10.1088/1367-2630/13/10/105003. URL: https://doi.org/10.1088/1367-2630/13/10/105003.

[242] Shelby Kimmel, Cedric Yen-Yu Lin, Guang Hao Low, Maris Ozols, and Theodore J. Yoder. "Hamiltonian simulation with optimal sample complexity". en. In: *npj Quantum Inf* 3.1 (Mar. 2017), pp. 1–7. ISSN: 2056-6387. DOI: 10.1038/s41534-017-0013-7.

[243] Shelby Kimmel, Guang Hao Low, and Theodore J. Yoder. "Robust calibration of a universal single-qubit gate set via robust phase estimation". In: *Phys. Rev. A* 92 (6 Dec. 2015), p. 062315. DOI: 10.1103/PhysRevA.92.062315. URL: https://link.aps.org/doi/10.1103/PhysRevA.92.062315.

[244] Shelby Kimmel, Marcus P. da Silva, Colm A. Ryan, Blake R. Johnson, and Thomas Ohki. "Robust Extraction of Tomographic Information via Randomized Benchmarking". In: *Phys. Rev. X* 4 (1 Mar. 2014), p. 011050. DOI: 10.1103/PhysRevX.4.011050. URL: https://link.aps.org/doi/10.1103/PhysRevX.4.011050.

[245] A Yu Kitaev. "Quantum computations: algorithms and error correction". In: *Russian Mathematical Surveys* 52.6 (Dec. 1997), pp. 1191–1249. DOI: 10.1070/rm1997v052n06abeh002155. URL: https://doi.org/10.1070/rm1997v052n06abeh002155.

[246] M. Kjaergaard, M. E. Schwartz, A. Greene, G. O. Samach, A. Bengtsson, M. O'Keeffe, C. M. McNally, J. Braumüller, D. K. Kim, P. Krantz, M. Marvian, A. Melville, B. M. Niedzielski, Y. Sung, R. Winik, J. Yoder, D. Rosenberg, K. Obenland, S. Lloyd, T. P. Orlando, I. Marvian, S. Gustavsson, and W. D. Oliver. "Demonstration of Density Matrix Exponentiation Using a Superconducting Quantum Processor". In: *Phys. Rev. X* 12 (1 Jan. 2022), p. 011005. DOI: 10.1103/PhysRevX.12.011005. URL: https://link.aps.org/doi/10.1103/PhysRevX.12.011005.

[247] M. Kjaergaard, M. E. Schwartz, A. Greene, G. O. Samach, A. Bengtsson, M. O'Keeffe, C. M. McNally, J. Braumüller, D. K. Kim, P. Krantz, M. Marvian, A. Melville, B. M. Niedzielski, Y. Sung, R. Winik, J. Yoder, D. Rosenberg, K. Obenland, S. Lloyd, T. P. Orlando, I. Marvian, S. Gustavsson, and W. D. Oliver. "Demonstration of Density Matrix Exponentiation Using a Superconducting Quantum Processor". In: *Phys. Rev. X* 12 (1 Jan. 2022), p. 011005. DOI: 10.1103/PhysRevX.12.011005. URL: https://link.aps.org/doi/10.1103/PhysRevX.12.011005.

[248] Morten Kjaergaard, Mollie E. Schwartz, Jochen Braumüller, Philip Krantz, Joel I.-J. Wang, Simon Gustavsson, and William D. Oliver. "Superconducting Qubits: Current State of Play". In: *Annual Review of Condensed Matter Physics* 11.1 (2020), pp. 369–395. DOI: 10.1146/annurev-conmatphys-031119-050605. eprint: https://doi.org/10.1146/annurev-conmatphys-031119-050605. URL: https://doi.org/10.1146/annurev-conmatphys-031119-050605.

[249] Klein. *Harmattan*. Pentatone, 2021.

[250] P. V. Klimov, J. Kelly, Z. Chen, M. Neeley, A. Megrant, B. Burkett, R. Barends, K. Arya, B. Chiaro, Yu Chen, A. Dunsworth, A. Fowler, B. Foxen, C. Gidney, M. Giustina, R. Graff, T. Huang, E. Jeffrey, Erik Lucero, J. Y. Mutus, O. Naaman, C. Neill, C. Quintana, P. Roushan, Daniel Sank, A. Vainsencher, J. Wenner, T. C. White, S. Boixo, R. Babbush, V. N. Smelyanskiy, H. Neven, and John M. Martinis. "Fluctuations of Energy-Relaxation Times in Superconducting Qubits". In: *Phys. Rev. Lett.* 121.9 (Aug. 2018), p. 090502. DOI: 10.1103/PhysRevLett.121.090502.

[251] P. V. Klimov, J. Kelly, Z. Chen, M. Neeley, A. Megrant, B. Burkett, R. Barends, K. Arya, B. Chiaro, Yu Chen, A. Dunsworth, A. Fowler, B. Foxen, C. Gidney, M. Giustina, R. Graff, T. Huang, E. Jeffrey, Erik Lucero, J. Y. Mutus, O. Naaman, C. Neill, C. Quintana, P. Roushan, Daniel Sank, A. Vainsencher, J. Wenner, T. C. White, S. Boixo, R. Babbush, V. N. Smelyanskiy, H. Neven, and John M. Martinis. "Fluctuations of Energy-Relaxation Times in Superconducting Qubits". In: *Phys. Rev. Lett.* 121 (9 Aug. 2018), p. 090502. DOI: 10.1103/PhysRevLett.121.090502. URL: https://link.aps.org/doi/10.1103/PhysRevLett.121.090502.

[252] George C. Knee, Eliot Bolduc, Jonathan Leach, and Erik M. Gauger. "Quantum process tomography via completely positive and trace-preserving projection". In: *Phys. Rev. A* 98 (6 Dec. 2018), p. 062336. DOI: 10.1103/PhysRevA.98.062336.

[253] E. Knill, R. Laflamme, R. Martinez, and C. Negrevergne. "Benchmarking Quantum Computers: The Five-Qubit Error Correcting Code". In: *Phys. Rev. Lett.* 86 (25 June 2001), pp. 5811–5814. DOI: 10.1103/PhysRevLett.86.5811. URL: https://link.aps.org/doi/10.1103/PhysRevLett.86.5811.

[254] Jens Koch, Terri M. Yu, Jay Gambetta, A. A. Houck, D. I. Schuster, J. Majer, Alexandre Blais, M. H. Devoret, S. M. Girvin, and R. J. Schoelkopf. "Charge-insensitive qubit design derived from the Cooper pair box". In: *Physical Review A* 76.4 (Oct. 2007). DOI: 10.1103/physreva.76.042319. URL: https://doi.org/10.1103%2Fphysreva.76.042319.

[255] Jens Koch, Terri M. Yu, Jay Gambetta, A. A. Houck, D. I. Schuster, J. Majer, Alexandre Blais, M. H. Devoret, S. M. Girvin, and R. J. Schoelkopf. "Charge-insensitive qubit design derived from the Cooper pair box". In: *Phys. Rev. A* 76.4 (Oct. 2007), p. 042319. ISSN: 1050-2947. DOI: 10.1103/PhysRevA.76.042319.

[256] Jens Koch, Terri M. Yu, Jay Gambetta, A. A. Houck, D. I. Schuster, J. Majer, Alexandre Blais, M. H. Devoret, S. M. Girvin, and R. J. Schoelkopf. "Charge-insensitive qubit design derived from the Cooper pair box". In: *Physical Review A* 76.4 (2007), p. 042319. ISSN: 1050-2947. DOI: 10.1103/PhysRevA.76.042319.

[257] P. Krantz, M. Kjaergaard, F. Yan, T. P. Orlando, S. Gustavsson, and W. D. Oliver. "A quantum engineer's guide to superconducting qubits". In: *Applied Physics Reviews* 6.2 (June 2019), p. 021318. DOI: 10.1063/1.5089550. URL: https://doi.org/10.1063%2F1.5089550.

[258] P. Krantz, M. Kjaergaard, F. Yan, T. P. Orlando, S. Gustavsson, and W. D. Oliver. "A quantum engineer's guide to superconducting qubits". In: *App. Phys. Rev.* 6.2 (June 2019), p. 021318. DOI: 10.1063/1.5089550.

[259] J. C. Lagarias, J. A. Reeds, M. H. Wright, and P. E. Wright. "Convergence Properties of the Nelder-Mead Simplex Method in Low Dimensions". In: *SIAM Journal of Optimization* 9.1 (1998), pp. 112–147.

[260] Graham Lambkin. *Solos*. Blank Forms, 2021.

[261] Graham Lambkin and Jason Lescalleet. *Photographs*. Erstwhile Records, 2013.

[262] Christopher G. Langton, ed. *Artificial Life. Proceedings of an Interdisciplinary Workshop on the Synthesis and Simulation of Living Systems*. Redwood City, CA: Addison-Wesley, 1988.

[263] T. Lanting, A. J. Berkley, B. Bumble, P. Bunyk, A. Fung, J. Johansson, A. Kaul, A. Kleinsasser, E. Ladizinsky, F. Maibaum, R. Harris, M. W. Johnson, E. Tolkacheva, and M. H. S. Amin. "Geometrical dependence of the low-frequency noise in superconducting flux qubits". In: *Phys. Rev. B* 79 (6 Feb. 2009), p. 060509. DOI: 10.1103/PhysRevB.79.060509. URL: http://link.aps.org/doi/10.1103/PhysRevB.79.060509.

[264] T. Lanting, A. J. Przybysz, A. Yu. Smirnov, F. M. Spedalieri, M. H. Amin, A. J. Berkley, R. Harris, F. Altomare, S. Boixo, P. Bunyk, N. Dickson, C. Enderud, J. P. Hilton, E. Hoskinson, M. W. Johnson, E. Ladizinsky, N. Ladizinsky, R. Neufeld, T. Oh, I. Perminov, C. Rich, M. C. Thom, E. Tolkacheva, S. Uchaikin, A. B. Wilson, and G. Rose. "Entanglement in a Quantum Annealing Processor". In: *Phys. Rev. X* 4 (2 May 2014), p. 021041. DOI: 10.1103/PhysRevX.4.021041. URL: http://link.aps.org/doi/10.1103/PhysRevX.4.021041.

[265] B. P. Lanyon, C. Hempel, D. Nigg, M. Müller, R. Gerritsma, F. Zähringer, P. Schindler, J. T. Barreiro, M. Rambach, G. Kirchmair, M. Hennrich, P. Zoller, R. Blatt, and C. F. Roos. "Universal Digital Quantum Simulation with Trapped Ions". In: *Science* 334.6052 (2011), pp. 57–61. DOI: 10.1126/science.1208001. eprint: https://www.science.org/doi/pdf/10.1126/science.1208001. URL: https://www.science.org/doi/abs/10.1126/science.1208001.

[266] B. P. Lanyon, C. Maier, M. Holzäpfel, T. Baumgratz, C. Hempel, P. Jurcevic, I. Dhand, A. S. Buyskikh, A. J. Daley, M. Cramer, M. B. Plenio, R. Blatt, and C. F. Roos. "Efficient tomography of a quantum many-body system". In: *Nature Physics* 13.12 (Sept. 2017), pp. 1158–1162. DOI: 10.1038/nphys4244. URL: https://doi.org/10.1038%2Fnphys4244.

[267] B. P. Lanyon, T. J. Weinhold, N. K. Langford, M. Barbieri, D. F. V. James, A. Gilchrist, and A. G. White. "Experimental Demonstration of a Compiled Version of Shor's Algorithm with Quantum Entanglement". In: *Phys. Rev. Lett.* 99 (25 Dec. 2007), p. 250505. DOI: 10.1103/PhysRevLett.99.250505. URL: https://link.aps.org/doi/10.1103/PhysRevLett.99.250505.

[268] B. P. Lanyon, J. D. Whitfield, G. G. Gillett, M. E. Goggin, M. P. Almeida, I. Kassal, J. D. Biamonte, M. Mohseni, B. J. Powell, M. Barbieri, A. Aspuru-Guzik, and A. G. White. "Towards quantum chemistry on a quantum computer". In: *Nature Chemistry* 2.2 (2010), pp. 106–111. DOI: 10.1038/nchem.483. URL: https://doi.org/10.1038/nchem.483.

[269] L. Latessa, A. Pecchia, A. Di Carlo, and P. Lugli. "Negative quantum capacitance of gated carbon nanotubes". In: *Phys. Rev. B* 72 (3 July 2005), p. 035455. DOI: 10.1103/PhysRevB.72.035455. URL: http://link.aps.org/doi/10.1103/PhysRevB.72.035455.

[270] Ludovico Latmiral, Nicolò Spagnolo, and Fabio Sciarrino. "Towards quantum supremacy with lossy scattershot boson sampling". In: *New Journal of Physics* 18.11 (Nov. 2016), p. 113008. DOI: 10.1088/1367-2630/18/11/113008. URL: https://doi.org/10.1088%2F1367-2630%2F18%2F11%2F113008.

[271] Bruno Latour and Steve Woolgar. *Laboratory Life. The Construction of Scientific Facts*. Princeton: Princeton University Press, 1979.

[272] Jong Yeon Lee and Olivier Landon-Cardinal. "Practical variational tomography for critical one-dimensional systems". In: *Phys. Rev. A* 91 (6 June 2015), p. 062128. DOI: 10.1103/PhysRevA.91.062128. URL: https://link.aps.org/doi/10.1103/PhysRevA.91.062128.

[273] K. W. Lehnert, K. Bladh, L. F. Spietz, D. Gunnarsson, D. I. Schuster, P. Delsing, and R. J. Schoelkopf. "Measurement of the Excited-State Lifetime of a Microelectronic Circuit". In: *Phys. Rev. Lett.* 90 (2 Jan. 2003), p. 027002. DOI: 10.1103/PhysRevLett.90.027002. URL: https://link.aps.org/doi/10.1103/PhysRevLett.90.027002.

[274] Eric Levinson and Aaron Cooper. *Derek Chauvin's trial in death of George Floyd begins with showing jurors video of his final moments*. CNN.com. Mar. 30, 2021. URL: https://www.cnn.com/2021/03/29/us/derek-chauvin-george-floyd-trial-start.

[275] Che-Ming Li, Neill Lambert, Yueh-Nan Chen, Guang-Yin Chen, and Franco Nori. "Witnessing Quantum Coherence: from solid-state to biological systems". In: *Scientific reports* 2 (Nov. 2012), p. 885. DOI: 10.1038/srep00885.

[276] Daniel A. Lidar and Haobin Wang. "Calculating the thermal rate constant with exponential speedup on a quantum computer". In: *Phys. Rev. E* 59 (2 Feb. 1999), pp. 2429–2438. DOI: 10.1103/PhysRevE.59.2429. URL: https://link.aps.org/doi/10.1103/PhysRevE.59.2429.

[277] Megan N. Lilly and Travis S. Humble. "Modeling Noisy Quantum Circuits Using Experimental Characterization". In: *arXiv:2001.08653* (2020).

[278] Norbert M. Linke, Dmitri Maslov, Martin Roetteler, Shantanu Debnath, Caroline Figgatt, Kevin A. Landsman, Kenneth Wright, and Christopher Monroe. "Experimental comparison of two quantum computing architectures". In: *Proceedings of the National Academy of Sciences* 114.13 (Mar. 2017), pp. 3305–3310. DOI: 10.1073/pnas.1618020114. URL: https://doi.org/10.1073%2Fpnas.1618020114.

[279] Bi-Heng Liu, Li Li, Yun-Feng Huang, Chuan-Feng Li, Guang-Can Guo, Elsi-Mari Laine, Heinz-Peter Breuer, and Jyrki Piilo. "Experimental control of the transition from Markovian to non-Markovian dynamics of open quantum systems". In: *Nature Physics* 7.12 (2011), pp. 931–934. DOI: 10.1038/nphys2085. URL: https://doi.org/10.1038/nphys2085.

[280] Seth Lloyd. "Universal Quantum Simulators". en. In: *Science* 273.5278 (Aug. 1996), pp. 1073–1078. ISSN: 0036-8075, 1095-9203. DOI: 10.1126/science.273.5278.1073.

[281] Seth Lloyd, Masoud Mohseni, and Patrick Rebentrost. "Quantum principal component analysis". en. In: *Nat. Phys.* 10.9 (Sept. 2014), pp. 631–633. ISSN: 1745-2481. DOI: 10.1038/nphys3029.

[282] Mirko Lobino, Dmitry Korystov, Connor Kupchak, Eden Figueroa, Barry C. Sanders, and A. I. Lvovsky. "Complete Characterization of Quantum-Optical Processes". In: *Science* 322.5901 (2008), pp. 563–566. DOI: 10.1126/science.1162086. eprint: https://www.science.org/doi/pdf/10.1126/science.1162086. URL: https://www.science.org/doi/abs/10.1126/science.1162086.

[283] Cecilia C. López, Ariel Bendersky, Juan Pablo Paz, and David G. Cory. "Progress toward scalable tomography of quantum maps using twirling-based methods and information hierarchies". In: *Phys. Rev. A* 81 (6 June 2010), p. 062113. DOI: 10.1103/PhysRevA.81.062113. URL: https://link.aps.org/doi/10.1103/PhysRevA.81.062113.

[284] A. P. Lund, Michael J. Bremner, and T. C. Ralph. "Quantum sampling problems, BosonSampling and quantum supremacy". In: *npj Quantum Information* 3.1 (Apr. 2017). DOI: 10.1038/s41534-017-0018-2. URL: https://doi.org/10.1038%2Fs41534-017-0018-2.

[285] Jean-François Lyotard. *The Postmodern Condition. A Report on Knowledge*. Trans. by Geoff Bennington and Brian Massumi. Minneapolis: University of Minnesota Press, 1984.

[286] Chiara Macchiavello and Massimiliano F. Sacchi. "Detecting Lower Bounds to Quantum Channel Capacities". In: *Phys. Rev. Lett.* 116 (14 Apr. 2016), p. 140501. DOI: 10.1103/PhysRevLett.116.140501. URL: https://link.aps.org/doi/10.1103/PhysRevLett.116.140501.

[287] Easwar Magesan, J. M. Gambetta, and Joseph Emerson. "Scalable and Robust Randomized Benchmarking of Quantum Processes". In: *Phys. Rev. Lett.* 106 (18 May 2011), p. 180504. DOI: 10.1103/PhysRevLett.106.180504. URL: https://link.aps.org/doi/10.1103/PhysRevLett.106.180504.

[288] Easwar Magesan, Daniel Puzzuoli, Christopher E. Granade, and David G. Cory. "Modeling quantum noise for efficient testing of fault-tolerant circuits". In: *Phys. Rev. A* 87 (1 Jan. 2013), p. 012324. DOI: 10.1103/PhysRevA.87.012324. URL: https://link.aps.org/doi/10.1103/PhysRevA.87.012324.

[289] P. Magnard, P. Kurpiers, B. Royer, T. Walter, J.-C. Besse, S. Gasparinetti, M. Pechal, J. Heinsoo, S. Storz, A. Blais, and A. Wallraff. "Fast and Unconditional All-Microwave Reset of a Superconducting Qubit". In: *Physical Review Letters* 121.6 (Aug. 2018), p. 060502. DOI: 10.1103/PhysRevLett.121.060502.

[290] Emtithal Mahmoud. *Day 1 poem by Emi Mahmoud (Quantum Summer Symposium 2020)*. filmed July 22, 2020. TensorFlow. 2020. URL: https://youtu.be/oUgG9Z2N7pE (visited on 09/03/2020).

[291] Emtithal Mahmoud. *Quantum poetry: Part 1 - Quantum Summer Symposium 2021*. Google Quantum AI. 2021. URL: https://youtu.be/oUgG9Z2N7pE (visited on 07/30/2021).

[292] Salvatore Mandrà, Zheng Zhu, Wenlong Wang, Alejandro Perdomo-Ortiz, and Helmut G. Katzgraber. "Strengths and weaknesses of weak-strong cluster problems: A detailed overview of state-of-the-art classical heuristics versus quantum approaches". In: *Phys. Rev. A* 94 (2 Aug. 2016), p. 022337. DOI: 10.1103/PhysRevA.94.022337. URL: http://link.aps.org/doi/10.1103/PhysRevA.94.022337.

[293] John M. Martinis and Michael R. Geller. "Fast adiabatic qubit gates using only sigmaz control". In: *Physical Review A* 90.2 (Aug. 2014), p. 022307. ISSN: 1050-2947. DOI: 10.1103/PhysRevA.90.022307.

[294] Iman Marvian and Seth Lloyd. "Universal Quantum Emulator". In: *arXiv:1606.02734* (June 2016).

[295] Karl Marx. "The Eighteenth Brumaire of Louis Bonaparte". In: *The Marx-Engels Reader*. Ed. by Robert C. Tucker. New York: W. W. Norton & Company, 1996.

[296] Karl Marx. "The Fetishism of Commodities and the Secret Thereof". In: *The Marx-Engels Reader*. Ed. by Robert C. Tucker. New York: W. W. Norton & Company, 1996.

[297] Karl Marx and Friedrich Engels. *The Communist Manifesto*. Trans. by Samuel Moore. New York: Pocket Books, 1964.

[298] Leo Marx. "Technology. The Emergence of a Hazardous Concept". In: *Technology and Culture* 51.3 (2010), pp. 561–577.

[299] Alexander J. McCaskey, Zachary P. Parks, Jacek Jakowski, Shirley V. Moore, T. Morris, Travis S. Humble, and Raphael C. Pooser. *Quantum Chemistry as a Benchmark for Near-Term Quantum Computers*. 2019. DOI: 10.48550/ARXIV.1905.01534. URL: https://arxiv.org/abs/1905.01534.

[300] David C McKay, Christopher J Wood, Sarah Sheldon, Jerry M Chow, and Jay M Gambetta. "Efficient Z gates for quantum computing". In: *Phys. Rev. A* 96.2 (Aug. 2017), p. 22330. DOI: 10.1103/PhysRevA.96.022330.

[301] David C. McKay, Stefan Filipp, Antonio Mezzacapo, Easwar Magesan, Jerry M. Chow, and Jay M. Gambetta. "Universal Gate for Fixed-Frequency Qubits via a Tunable Bus". In: *Phys. Rev. Applied* 6 (6 Dec. 2016), p. 064007. DOI: 10.1103/PhysRevApplied.6.064007. URL: https://link.aps.org/doi/10.1103/PhysRevApplied.6.064007.

[302] J. Medford, J. Beil, J. M. Taylor, S. D. Bartlett, A. C. Doherty, E. I. Rashba, D. P. DiVincenzo, H. Lu, A. C. Gossard, and C. M. Marcus. "Self-consistent measurement and state tomography of an exchange-only spin qubit". In: *Nature Nanotechnology* 8.9 (2013), pp. 654–659. DOI: 10.1038/nnano.2013.168. URL: https://doi.org/10.1038/nnano.2013.168.

[303] Seth T. Merkel, Jay M. Gambetta, John A. Smolin, Stefano Poletto, Antonio D. Córcoles, Blake R. Johnson, Colm A. Ryan, and Matthias Steffen. "Self-consistent quantum process tomography". In: *Phys. Rev. A* 87 (6 June 2013), p. 062119. DOI: 10.1103/PhysRevA.87.062119. URL: https://link.aps.org/doi/10.1103/PhysRevA.87.062119.

[304] Kristel Michielsen, Madita Nocon, Dennis Willsch, Fengping Jin, Thomas Lippert, and Hans De Raedt. "Benchmarking gate-based quantum computers". In: *Computer Physics Communications* 220 (Nov. 2017), pp. 44–55. DOI: 10.1016/j.cpc.2017.06.011. URL: https://doi.org/10.1016%2Fj.cpc.2017.06.011.

[305] MIKE. *"Disco!"* 10k, 2021.

[306] MIKE. *weight of the world*. 10k, 2020.

[307] D Mogilevtsev, J Řeháček, and Z Hradil. "Self-calibration for self-consistent tomography". In: *New Journal of Physics* 14.9 (Sept. 2012), p. 095001. DOI: 10.1088/1367-2630/14/9/095001. URL: https://doi.org/10.1088%2F1367-2630%2F14%2F9%2F095001.

[308] M. Mohseni and D. A. Lidar. "Direct Characterization of Quantum Dynamics". In: *Phys. Rev. Lett.* 97 (17 Oct. 2006), p. 170501. DOI: 10.1103/PhysRevLett.97.170501. URL: https://link.aps.org/doi/10.1103/PhysRevLett.97.170501.

[309] Ashley Montanaro. "Quantum algorithms: an overview". en. In: *npj Quantum Information* 2.1 (Nov. 2016), p. 15023. ISSN: 2056-6387. DOI: 10.1038/npjqi.2015.23.

[310] Thomas Monz, Daniel Nigg, Esteban A. Martinez, Matthias F. Brandl, Philipp Schindler, Richard Rines, Shannon X. Wang, Isaac L. Chuang, and Rainer Blatt. "Realization of a scalable Shor algorithm". In: *Science* 351.6277 (Mar. 2016), pp. 1068–1070. DOI: 10.1126/science.aad9480. URL: https://doi.org/10.1126%2Fscience.aad9480.

[311] Thomas Monz, Philipp Schindler, Julio T. Barreiro, Michael Chwalla, Daniel Nigg, William A. Coish, Maximilian Harlander, Wolfgang Hänsel, Markus Hennrich, and Rainer Blatt. "14-Qubit Entanglement: Creation and Coherence". In: *Phys. Rev. Lett.* 106 (13 Mar. 2011), p. 130506. DOI: 10.1103/PhysRevLett.106.130506. URL: https://link.aps.org/doi/10.1103/PhysRevLett.106.130506.

[312] C. N. Mooers, L. P. Deutsch, and R. W. Floyd. "Programming Languages for Non-Numeric Processing—1: TRAC, a Text Handling Language". In: *Proceedings of the 1965 20th National Conference*. ACM '65. Cleveland, Ohio, USA: Association for Computing Machinery, 1965, pp. 229–246. ISBN: 9781450374958. DOI: 10.1145/800197.806048.

[313] J. E. Mooij, T. P. Orlando, L. Levitov, Lin Tian, Caspar H. van der Wal, and Seth Lloyd. "Josephson Persistent-Current Qubit". In: *Science* 285.5430 (1999), pp. 1036–1039. DOI: 10.1126/science.285.5430.1036. eprint: https://www.science.org/doi/pdf/10.1126/science.285.5430.1036. URL: https://www.science.org/doi/abs/10.1126/science.285.5430.1036.

[314] J. E. Mooij, T. P. Orlando, L. Levitov, Lin Tian, Caspar H. van der Wal, and Seth Lloyd. "Josephson Persistent-Current Qubit". In: *Science* 285.5430 (1999), pp. 1036–1039. ISSN: 0036-8075. DOI: 10.1126/science.285.5430.1036.

[315] Moor Mother and billy woods. "The Blues Remembers Everything The Country Forgot". In: *BRASS*. featuring Wolf Weston (of Saint Mela). Backwoodz Studioz, 2020.

[316] Christopher Moore and Stephan Mertens. "The Deep Question: P vs. NP". In: *The Nature of Computation*. New York: Oxford University Press, 2011.

[317] *More Information*. Responsibility in Quantum Science. URL: https://www.quantumresponsibility.org/about (visited on 12/12/2021).

[318] "ancilla". In: *Pocket Oxford Latin Dictionary: Latin-English*. Ed. by James Morwood. Oxford University Press, 2012. URL: https://www.oxfordreference.com/view/10.1093/acref/9780191739583.001.0001/b-la-en-00001-0000676.

[319] Fred Moten. *A Conversation with Fred Moten 12/02/18*. filmed December 2018. Woodbine NYC. URL: https://www.youtube.com/watch?v=I6b5N%5C_u7Ebs/ (visited on 12/03/2018).

[320] F. Motzoi, J. M. Gambetta, P. Rebentrost, and F. K. Wilhelm. "Simple Pulses for Elimination of Leakage in Weakly Nonlinear Qubits". In: *Phys. Rev. Lett.* 103 (11 Sept. 2009), p. 110501. DOI: 10.1103/PhysRevLett.103.110501. URL: https://link.aps.org/doi/10.1103/PhysRevLett.103.110501.

[321] F. Motzoi and F. K. Wilhelm. "Improving frequency selection of driven pulses using derivative-based transition suppression". In: *Phys. Rev. A* 88 (6 Dec. 2013), p. 062318. DOI: 10.1103/PhysRevA.88.062318. URL: https://link.aps.org/doi/10.1103/PhysRevA.88.062318.

[322] W. J. Munro, D. F.V. James, A. G. White, and Paul G Kwiat. "Tomography and its role in Quantum Computation". English (US). In: *HP Laboratories Technical Report* 53 (Mar. 2001). ISSN: 1368-6798.

[323] Randall Munroe. *Purity*. XKCD. June 2008. URL: https://xkcd.com/435 (visited on 12/12/2021).

[324] Y. Nakamura, Yu. A. Pashkin, and J. S. Tsai. "Coherent control of macroscopic quantum states in a single-Cooper-pair box". In: *Nature* 398.6730 (Apr. 1999), pp. 786–788. DOI: 10.1038/19718. URL: https://doi.org/10.1038%2F19718.

[325] Yunseong Nam, Jwo-Sy Chen, Neal C. Pisenti, Kenneth Wright, Conor Delaney, Dmitri Maslov, Kenneth R. Brown, Stewart Allen, Jason M. Amini, Joel Apisdorf, Kristin M. Beck, Aleksey Blinov, Vandiver Chaplin, Mika Chmielewski, Coleman Collins, Shantanu Debnath, Kai M. Hudek, Andrew M. Ducore, Matthew Keesan, Sarah M. Kreikemeier, Jonathan Mizrahi, Phil Solomon, Mike Williams, Jaime David Wong-Campos, David Moehring, Christopher Monroe, and Jungsang Kim. "Ground-state energy estimation of the water molecule on a trapped-ion quantum computer". In: *npj Quantum Information* 6.1 (2020), p. 33. DOI: 10.1038/s41534-020-0259-3. URL: https://doi.org/10.1038/s41534-020-0259-3.

[326] V. Negnevitsky, M. Marinelli, K. K. Mehta, H.-Y. Lo, C. Flühmann, and J. P. Home. "Repeated multi-qubit readout and feedback with a mixed-species trapped-ion register". In: *Nature* 563.7732 (Nov. 2018), pp. 527–531. DOI: 10.1038/s41586-018-0668-z. URL: https://doi.org/10.1038%2Fs41586-018-0668-z.

[327] C. Neill, P. Roushan, K. Kechedzhi, S. Boixo, S. V. Isakov, V. Smelyanskiy, A. Megrant, B. Chiaro, A. Dunsworth, K. Arya, R. Barends, B. Burkett, Y. Chen, Z. Chen, A. Fowler, B. Foxen, M. Giustina, R. Graff, E. Jeffrey, T. Huang, J. Kelly, P. Klimov, E. Lucero, J. Mutus, M. Neeley, C. Quintana, D. Sank, A. Vainsencher, J. Wenner, T. C. White, H. Neven, and J. M. Martinis. "A blueprint for demonstrating quantum supremacy with superconducting qubits". In: *Science* 360.6385 (Apr. 2018), pp. 195–199. DOI: 10.1126/science.aao4309. URL: https://doi.org/10.1126%2Fscience.aao4309.

[328] J. A. Nelder and R. Mead. "A Simplex Method for Function Minimization". In: *The Computer Journal* 7.4 (Jan. 1965), pp. 308–313. ISSN: 0010-4620. DOI: 10.1093/comjnl/7.4.308. eprint: https://academic.oup.com/comjnl/article-pdf/7/4/308/1013182/7-4-308.pdf. URL: https://doi.org/10.1093/comjnl/7.4.308.

[329] Hartmut Neven. *Day 1 Keynote - Quantum Summer Symposium 2021*. Google Quantum AI. 2021. URL: https://youtu.be/VGGHG1a98vA (visited on 07/30/2021).

[330] Erik Nielsen. In preparation.

[331] M. A. Nielsen and Isaac L. Chuang. "Programmable Quantum Gate Arrays". In: *Physical Review Letters* 79.2 (July 1997), pp. 321–324. DOI: 10.1103/PhysRevLett.79.321.

[332] Michael A Nielsen. "A simple formula for the average gate fidelity of a quantum dynamical operation". en. In: *Phys. Lett. A* 303.4 (Oct. 2002), pp. 249–252. ISSN: 0375-9601. DOI: 10.1016/S0375-9601(02)01272-0.

[333] Michael A Nielsen and Isaac L Chuang. *Quantum Computation and Quantum Information: 10th Anniversary Edition*. New York, NY, USA: Cambridge University Press, 2011. ISBN: 1-107-00217-6 978-1-107-00217-3.

[334] A. O. Niskanen, K. Harrabi, F. Yoshihara, Y. Nakamura, and J. S. Tsai. "Spectroscopy of three strongly coupled flux qubits". In: *Phys. Rev. B* 74 (22 Dec. 2006), p. 220503. DOI: 10.1103/PhysRevB.74.220503. URL: http://link.aps.org/doi/10.1103/PhysRevB.74.220503.

[335] Jeremy Lloyd O'Brien, G. J. Pryde, A. G. White, Timothy C. Ralph, and David Branning. "Demonstration of an all-optical quantum controlled-NOT gate". In: *Nature* 426 (2003), pp. 264–267.

[336] T. E. O'Brien, B. Tarasinski, and L. DiCarlo. "Density-matrix simulation of small surface codes under current and projected experimental noise". In: *npj Quantum Information* 3.1 (Sept. 2017). DOI: 10.1038/s41534-017-0039-x. URL: https://doi.org/10.1038%2Fs41534-017-0039-x.

[337] P. J. J. O'Malley, J. Kelly, R. Barends, B. Campbell, Y. Chen, Z. Chen, B. Chiaro, A. Dunsworth, A. G. Fowler, I.-C. Hoi, E. Jeffrey, A. Megrant, J. Mutus, C. Neill, C. Quintana, P. Roushan, D. Sank, A. Vainsencher, J. Wenner, T. C. White, A. N. Korotkov, A. N. Cleland, and John M. Martinis. "Qubit Metrology of Ultralow Phase Noise Using Randomized Benchmarking". In: *Phys. Rev. Applied* 3 (4 Apr. 2015), p. 044009. DOI: 10.1103/PhysRevApplied.3.044009. URL: https://link.aps.org/doi/10.1103/PhysRevApplied.3.044009.

[338] Jim O'Rourke. *Bad Timing*. Drag City, 1997.

[339] Jim O'Rourke. *Shutting Down Here*. Portraits GRM, 2020.

[340] Jim O'Rourke. *The Visitor*. Drag City, 2009.

[341] Nissim Ofek, Andrei Petrenko, Reinier Heeres, Philip Reinhold, Zaki Leghtas, Brian Vlastakis, Yehan Liu, Luigi Frunzio, SM Girvin, Liang Jiang, et al. "Extending the lifetime of a quantum bit with error correction in superconducting circuits". In: *Nature* 536.7617 (2016), pp. 441–445.

[342] Ryo Okamoto, Holger F. Hofmann, Shigeki Takeuchi, and Keiji Sasaki. "Demonstration of an Optical Quantum Controlled-NOT Gate without Path Interference". In: *Phys. Rev. Lett.* 95 (21 Nov. 2005), p. 210506. DOI: 10.1103/PhysRevLett.95.210506. URL: https://link.aps.org/doi/10.1103/PhysRevLett.95.210506.

[343] William D. Oliver, Yang Yu, Janice C. Lee, Karl K. Berggren, Leonid S. Levitov, and Terry P. Orlando. "Mach-Zehnder Interferometry in a Strongly Driven Superconducting Qubit". In: *Science* 310.5754 (2005), pp. 1653–1657. ISSN: 0036-8075. DOI: 10.1126/science.1119678.

[344] *Open Letter*. Responsibility in Quantum Science. URL: https://www.quantumresponsibility.org/openletter (visited on 12/12/2021).

[345] T. P. Orlando, J. E. Mooij, L. Tian, et al. "Superconducting persistent-current qubit". In: *Physical Review B* 60(22) (1999), p. 15 398.

[346] Matteo Paris and Jaroslav Rehacek, eds. *Quantum State Estimation*. Springer-Verlag Berlin Heidelberg, 2004. DOI: 10.1007/b98673.

[347] Edwin Pednault, John A. Gunnels, Giacomo Nannicini, Lior Horesh, and Robert Wisnieff. "Leveraging Secondary Storage to Simulate Deep 54-qubit Sycamore Circuits". In: (2019). arXiv: 1910.09534 [quant-ph].

[348] K. D. Petersson, G. Smith, D. Anderson, P. Atkinson, G. A. C. Jones, and D. A. Ritchie. "Charge and Spin State Readout of a Double Quantum Dot Coupled to a Resonator". In: *Nano Letters* 10 (8 2010), p. 2789. DOI: 10.1021/nl100663w.

[349] Charles Petzold. "Seeing Around Corners". In: *Code. The Hidden Language of Computer Hardware and Software*. Redmond: Microsoft Press, 2000, pp. 32–39.

[350] Wolfgang Pfaff, Tim H. Taminiau, Lucio Robledo, Hannes Bernien, Matthew Markham, Daniel J. Twitchen, and Ronald Hanson. "Demonstration of entanglement-by-measurement of solid-state qubits". In: *Nature Physics* 9.1 (Jan. 2013), pp. 29–33. DOI: 10.1038/nphys2444. arXiv: 1206.2031 [quant-ph].

[351] Rasheedah Phillips, ed. *Black Quantum Futurism. Theory & Practice Volume I*. Philadelphia: The Afrofuturist Affair, 2015.

[352] Rasheedah Phillips, ed. *Black Quantum Futurism. Theory & Practice Volume II*. Philadelphia: The Afrofuturist Affair, 2021.

[353] *Physical Review Letters: Information for Authors*. American Physical Society. URL: https://journals.aps.org/prl/authors (visited on 01/20/2022).

[354] Hannes Pichler, Guanyu Zhu, Alireza Seif, Peter Zoller, and Mohammad Hafezi. "Measurement Protocol for the Entanglement Spectrum of Cold Atoms". In: *Phys. Rev. X* 6.4 (Nov. 2016), p. 041033. DOI: 10.1103/PhysRevX.6.041033.

[355] S. H. W. van der Ploeg, A. Izmalkov, Alec Maassen van den Brink, U. Hübner, M. Grajcar, E. Il'ichev, H.-G. Meyer, and A. M. Zagoskin. "Controllable Coupling of Superconducting Flux Qubits". In: *Phys. Rev. Lett.* 98 (5 Feb. 2007), p. 057004. DOI: 10.1103/PhysRevLett.98.057004. URL: https://link.aps.org/doi/10.1103/PhysRevLett.98.057004.

[356] B. L. T. Plourde, J. Zhang, K. B. Whaley, F. K. Wilhelm, T. L. Robertson, T. Hime, S. Linzen, P. A. Reichardt, C.-E. Wu, and John Clarke. "Entangling flux qubits with a bipolar dynamic inductance". In: *Phys. Rev. B* 70 (14 Oct. 2004), p. 140501. DOI: 10.1103/PhysRevB.70.140501. URL: http://link.aps.org/doi/10.1103/PhysRevB.70.140501.

[357] J. F. Poyatos, J. I. Cirac, and P. Zoller. "Complete Characterization of a Quantum Process: The Two-Bit Quantum Gate". In: *Phys. Rev. Lett.* 78 (2 Jan. 1997), pp. 390–393. DOI: 10.1103/PhysRevLett.78.390. URL: https://link.aps.org/doi/10.1103/PhysRevLett.78.390.

[358] Chanda Prescod-Weinstein. "Dark Matter Isn't Dark". In: *The Disordered Cosmos. A Journey Into Dark Matter, Spacetime, and Dreams Deferred*. New York: Bold Type Books, 2021, pp. 29–44.

[359] Chanda Prescod-Weinstein. *The Disordered Cosmos. A Journey Into Dark Matter, Spacetime, and Dreams Deferred*. New York: Bold Type Books, 2021.

[360] Chanda Prescod-Weinstein. "The Physics of Melanin". In: *The Disordered Cosmos. A Journey Into Dark Matter, Spacetime, and Dreams Deferred*. New York: Bold Type Books, 2021, pp. 93–112.

[361] Chanda Prescod-Weinstein. "The Point of Science. Lessons from the Mauna". In: *The Disordered Cosmos. A Journey Into Dark Matter, Spacetime, and Dreams Deferred*. New York: Bold Type Books, 2021, pp. 213–233.

[362] Chanda Prescod-Weinstein. "Wages for Scientific Housework". In: *The Disordered Cosmos. A Journey Into Dark Matter, Spacetime, and Dreams Deferred*. New York: Bold Type Books, 2021, pp. 183–196.

[363] Chanda Prescod-Weinstein. "Who Is a Scientist?" In: *The Disordered Cosmos. A Journey Into Dark Matter, Spacetime, and Dreams Deferred*. New York: Bold Type Books, 2021, pp. 131–146.

[364] John Preskill. "Quantum computing and the entanglement frontier". In: (2012). arXiv: 1203.5813 [quant-ph].

[365] John Preskill. "Quantum Computing in the NISQ era and beyond". In: *Quantum* 2 (Aug. 2018), p. 79. ISSN: 2521-327X. DOI: 10.22331/q-2018-08-06-79. URL: https://doi.org/10.22331/q-2018-08-06-79.

[366] John Preskill. "Rapporteur Talk by J. Preskill: Quantum Entanglement and Quantum Computing. Discussion". In: *The Theory of the Quantum Wolrd. Proceedings of the 25th Solvay Conference on Physics*. Ed. by David Gross, Marc Henneaux, and Alexander Sevrin. Singapore: World Scientific, 2013, pp. 84–90.

[367] John Preskill. "Supremacy Now?" In: *Quantum Frontiers* (July 22, 2012). URL: https://quantumfrontiers.com/2012/07/22/supremacy-now/#more-444 (visited on 12/12/2021).

[368] John Preskill. *Why I Called It 'Quantum Supremacy'*. Quanta Magazine. Oct. 2, 2019. URL: https://www.quantamagazine.org/john-preskill-explains-quantum-supremacy-20191002/.

[369] Timothy Proctor, Melissa Revelle, Erik Nielsen, Kenneth Rudinger, Daniel Lobser, Peter Maunz, Robin Blume-Kohout, and Kevin Young. "Detecting and tracking drift in quantum information processors". In: *Nature Communications* 11.1 (2020), p. 5396. DOI: 10.1038/s41467-020-19074-4. URL: https://doi.org/10.1038/s41467-020-19074-4.

[370] Timothy Proctor, Kenneth Rudinger, Kevin Young, Erik Nielsen, and Robin Blume-Kohout. "Measuring the capabilities of quantum computers". In: *Nature Physics* 18.1 (Dec. 2021), pp. 75–79. DOI: 10.1038/s41567-021-01409-7. URL: https://doi.org/10.1038%2Fs41567-021-01409-7.

[371] Timothy Proctor, Kenneth Rudinger, Kevin Young, Mohan Sarovar, and Robin Blume-Kohout. "What Randomized Benchmarking Actually Measures". In: *Phys. Rev. Lett.* 119.13 (Sept. 2017), p. 130502. DOI: 10.1103/PhysRevLett.119.130502.

[372] C. M. Quintana, Yu Chen, D. Sank, A. G. Petukhov, T. C. White, Dvir Kafri, B. Chiaro, A. Megrant, R. Barends, B. Campbell, Z. Chen, A. Dunsworth, A. G. Fowler, R. Graff, E. Jeffrey, J. Kelly, E. Lucero, J. Y. Mutus, M. Neeley, C. Neill, P. J. J. O'Malley, P. Roushan, A. Shabani, V. N. Smelyanskiy, A. Vainsencher, J. Wenner, H. Neven, and John M. Martinis. "Observation of Classical-Quantum Crossover of $1/f$ Flux Noise and Its Paramagnetic Temperature Dependence". In: *Phys. Rev. Lett.* 118 (5 Jan. 2017), p. 057702. DOI: 10.1103/PhysRevLett.118.057702. URL: https://link.aps.org/doi/10.1103/PhysRevLett.118.057702.

[373] Robert Raussendorf and Hans J. Briegel. "A One-Way Quantum Computer". In: *Phys. Rev. Lett.* 86.22 (May 2001), pp. 5188–5191. DOI: 10.1103/PhysRevLett.86.5188.

[374] Matthew D Reed, Leonardo DiCarlo, Simon E Nigg, Luyan Sun, Luigi Frunzio, Steven M Girvin, and Robert J Schoelkopf. "Realization of three-qubit quantum error correction with superconducting circuits". In: *Nature* 482.7385 (2012), pp. 382–385.

[375] Philip Reinhold, Serge Rosenblum, Wen-Long Ma, Luigi Frunzio, Liang Jiang, and Robert J. Schoelkopf. "Error-corrected gates on an encoded qubit". In: *Nature Physics* 16.8 (June 2020), pp. 822–826. DOI: 10.1038/s41567-020-0931-8. URL: https://doi.org/10.1038%2Fs41567-020-0931-8.

[376] Rich Rines, Kevin Obenland, and Isaac Chuang. "Empirical determination of the simulation capacity of a near-term quantum computer". In: *arXiv:1905.10724* (May 2019).

[377] Rich Rines, Kevin Obenland, and Isaac Chuang. *Empirical determination of the simulation capacity of a near-term quantum computer*. 2019. DOI: 10.48550/ARXIV.1905.10724. URL: https://arxiv.org/abs/1905.10724.

[378] D Riste, M Dukalski, CA Watson, G De Lange, MJ Tiggelman, Ya M Blanter, Konrad W Lehnert, RN Schouten, and L DiCarlo. "Deterministic entanglement of superconducting qubits by parity measurement and feedback". In: *Nature* 502.7471 (2013), pp. 350–354.

[379] Ángel Rivas, Susana F Huelga, and Martin B Plenio. "Quantum non-Markovianity: characterization, quantification and detection". In: *Reports on Progress in Physics* 77.9 (Aug. 2014), p. 094001. DOI: 10.1088/0034-4885/77/9/094001. URL: https://doi.org/10.1088%2F0034-4885%2F77%2F9%2F094001.

[380] Ángel Rivas, Susana F. Huelga, and Martin B. Plenio. "Entanglement and Non-Markovianity of Quantum Evolutions". In: *Phys. Rev. Lett.* 105 (5 July 2010), p. 050403. DOI: 10.1103/PhysRevLett.105.050403. URL: https://link.aps.org/doi/10.1103/PhysRevLett.105.050403.

[381] Matana Roberts. *Coin Coin Chapter Four: Memphis*. Constellation, 2019.

[382] Matana Roberts. *Coin Coin Chapter One: Gens de Couleur Libres*. Constellation, 2011.

[383] Matana Roberts. *Coin Coin Chapter Three: river run thee*. Constellation, 2015.

[384] Matana Roberts. *Coin Coin Chapter Two: Mississippi Moonchile*. Constellation, 2013.

[385] Alan Robertson, Christopher Granade, Stephen D. Bartlett, and Steven T. Flammia. "Tailored Codes for Small Quantum Memories". In: *Phys. Rev. Applied* 8 (6 Dec. 2017), p. 064004. DOI: 10.1103/PhysRevApplied.8.064004. URL: https://link.aps.org/doi/10.1103/PhysRevApplied.8.064004.

[386] Cedric Robinson. *Black Marxism. The Making of the Black Radical Tradition*. London: Zed Books, 1983.

[387] Andrey V. Rodionov, Andrzej Veitia, R. Barends, J. Kelly, Daniel Sank, J. Wenner, John M. Martinis, Robert L. Kosut, and Alexander N. Korotkov. "Compressed sensing quantum process tomography for superconducting quantum gates". In: *Physical Review B* 90.14 (Oct. 2014). DOI: 10.1103/physrevb.90.144504. URL: https://doi.org/10.1103%2Fphysrevb.90.144504.

[388] M. A. Rol, F. Battistel, F. K. Malinowski, C. C. Bultink, B. M. Tarasinski, R. Vollmer, N. Haider, N. Muthusubramanian, A. Bruno, B. M. Terhal, and L. DiCarlo. "Fast, High-Fidelity Conditional-Phase Gate Exploiting Leakage Interference in Weakly Anharmonic Superconducting Qubits". In: *Phys. Rev. Lett.* 123.12 (Sept. 2019), p. 120502. DOI: 10.1103/PhysRevLett.123.120502.

[389] Troels F. Rønnow, Zhihui Wang, Joshua Job, Sergio Boixo, Sergei V. Isakov, David Wecker, John M. Martinis, Daniel A. Lidar, and Matthias Troyer. "Defining and detecting quantum speedup". In: *Science* 345.6195 (July 2014), pp. 420–424. (Visited on 04/18/2016).

[390] D. Rosenberg, D. Kim, R. Das, D. Yost, S. Gustavsson, D. Hover, P. Krantz, A. Melville, L. Racz, G. O. Samach, S. J. Weber, F. Yan, J. L. Yoder, A. J. Kerman, and W. D. Oliver. "3D integrated superconducting qubits". In: *npj Quantum Information* 3.1 (2017), p. 42. DOI: 10.1038/s41534-017-0044-0. URL: https://doi.org/10.1038/s41534-017-0044-0.

[391] Claire Rousay. *a softer focus*. American Dreams, 2021.

[392] Claire Rousay. *Twin Bed EP*. American Dreams, 2021.

[393] M. A. Rowe, D. Kielpinski, V. Meyer, C. A. Sackett, W. M. Itano, C. Monroe, and D. J. Wineland. "Experimental violation of a Bell's inequality with efficient detection". In: *Nature* 409.6822 (Feb. 2001), pp. 791–794. DOI: 10.1038/35057215.

[394] Antoine Royer. "Measurement of quantum states and the Wigner function". In: *Foundations of Physics* 19.1 (Jan. 1989), pp. 3–32. DOI: 10.1007/BF00737764.

[395] László Ruppert, Dániel Virosztek, and Katalin Hangos. "Optimal parameter estimation of Pauli channels". In: *Journal of Physics A: Mathematical and Theoretical* 45.26 (June 2012), p. 265305. DOI: 10.1088/1751-8113/45/26/265305. URL: https://doi.org/10.1088%2F1751-8113%2F45%2F26%2F265305.

[396] Y. Salathé, M. Mondal, M. Oppliger, J. Heinsoo, P. Kurpiers, A. Poto čnik, A. Mezzacapo, U. Las Heras, L. Lamata, E. Solano, S. Filipp, and A. Wallraff. "Digital Quantum Simulation of Spin Models with Circuit Quantum Electrodynamics". In: *Phys. Rev. X* 5 (2 June 2015), p. 021027. DOI: 10.1103/PhysRevX.5.021027.

[397] Gabriel Samach. "The Ubit Model. Decoherence in Real-Amplitude Quantum Theory". Supervised by William K. Wootters. B.A. Thesis. Williamstown, MA: Williams College, May 2015.

[398] Gabriel Samach, Steven Weber, David Hover, Danna Rosenberg, Jonilyn Yoder, David Kim, William Oliver, and Andrew Kerman. "Tunable XX-Coupling Between High Coherence Flux Qubits". In: *APS March Meeting Abstracts*. Vol. 2018. APS Meeting Abstracts. Jan. 2018, L33.013, p. L33.013.

[399] Gabriel O. Samach, Ami Greene, Johannes Borregaard, Matthias Christandl, Joseph Barreto, David K. Kim, Christopher M. McNally, Alexander Melville, Bethany M. Niedzielski, Youngkyu Sung, Danna Rosenberg, Mollie E. Schwartz, Jonilyn L. Yoder, Terry P. Orlando, Joel I-Jan Wang, Simon Gustavsson, Morten Kjaergaard, and William D. Oliver. *Lindblad Tomography of a Superconducting Quantum Processor*. 2021. DOI: 10.48550/ARXIV.2105.02338. URL: https://arxiv.org/abs/2105.02338.

[400] Yuval R Sanders, Joel J Wallman, and Barry C Sanders. "Bounding quantum gate error rate based on reported average fidelity". In: *New Journal of Physics* 18.1 (Dec. 2015), p. 012002. DOI: 10.1088/1367-2630/18/1/012002. URL: https://doi.org/10.1088%2F1367-2630%2F18%2F1%2F012002.

[401] Daniel Sank, R. Barends, Radoslaw C. Bialczak, Yu Chen, J. Kelly, M. Lenander, E. Lucero, Matteo Mariantoni, A. Megrant, M. Neeley, P. J. J. O'Malley, A. Vainsencher, H. Wang, J. Wenner, T. C. White, T. Yamamoto, Yi Yin, A. N. Cleland, and John M. Martinis. "Flux Noise Probed with Real Time Qubit Tomography in a Josephson Phase Qubit". In: *Phys. Rev. Lett.* 109 (6 Aug. 2012), p. 067001. DOI: 10.1103/PhysRevLett.109.067001. URL: http://link.aps.org/doi/10.1103/PhysRevLett.109.067001.

[402] T. van der Sar, Z. H. Wang, M. S. Blok, H. Bernien, T. H. Taminiau, D. M. Toyli, D. A. Lidar, D. D. Awschalom, R. Hanson, and V. V. Dobrovitski. "Decoherence-protected quantum gates for a hybrid solid-state spin register". In: *Nature* 484.7392 (Apr. 2012), pp. 82–86. DOI: 10.1038/nature10900. URL: https://doi.org/10.1038%2Fnature10900.

[403] Nicolas P. D. Sawaya, Mikhail Smelyanskiy, Jarrod R. McClean, and Alán Aspuru-Guzik. *Error Sensitivity to Environmental Noise in Quantum Circuits for Chemical State Preparation*. 2016. DOI: 10.48550/ARXIV.1602.01857. URL: https://arxiv.org/abs/1602.01857.

[404] Thomas Scheidl, Rupert Ursin, Johannes Kofler, Sven Ramelow, Xiao-Song Ma, Thomas Herbst, Lothar Ratschbacher, Alessandro Fedrizzi, Nathan K. Langford, Thomas Jennewein, and Anton Zeilinger. "Violation of local realism with freedom of choice". In: *Proceedings of the National Academy of Science* 107.46 (Nov. 2010), pp. 19708–19713. DOI: 10.1073/pnas.1002780107.

[405] Londa Schiebinger. *The Mind Has No Sex? Women in the Origins of Modern Science*. Cambridge: Harvard University Press, 1989.

[406] S. G. Schirmer, A. Kolli, and D. K. L. Oi. "Experimental Hamiltonian identification for controlled two-level systems". In: *Phys. Rev. A* 69 (5 May 2004), p. 050306. DOI: 10.1103/PhysRevA.69.050306. URL: https://link.aps.org/doi/10.1103/PhysRevA.69.050306.

[407] Sonia G. Schirmer and D. K. L. Oi. "Quantum system identification by Bayesian analysis of noisy data: Beyond Hamiltonian tomography". In: *Laser Physics* 20 (2009), pp. 1203–1209.

[408] Edwin Schrödinger. *The Interpretation of Quantum Mechanics. Dublin Seminars (1949–1955) and Other Unpublished Essays*. Woodbridge, CT: Ox Bow Press, 1995.

[409] Banjamin Schumacher. "Information from Quantum Measurements". In: *Complexity, Entropy, and the Physics of Information. The Proceedings of the 1988 Workshop on Complexity, Entropy, and the Physics of Information Held May–June, 1989 in Sante Fe, New Mexico*. Ed. by Wojciech H. Zurek. Redwood City, CA: Addison-Wesley, 1990, pp. 29–37.

[410] Benjamin Schumacher. "Quantum coding". In: *Phys. Rev. A* 51 (4 Apr. 1995), pp. 2738–2747. DOI: 10.1103/PhysRevA.51.2738. URL: https://link.aps.org/doi/10.1103/PhysRevA.51.2738.

[411] D. I. Schuster, A. Wallraff, A. Blais, L. Frunzio, R.-S. Huang, J. Majer, S. M. Girvin, and R. J. Schoelkopf. "ac Stark Shift and Dephasing of a Superconducting Qubit Strongly Coupled to a Cavity Field". In: *Phys. Rev. Lett.* 94 (12 Mar. 2005), p. 123602. DOI: 10.1103/PhysRevLett.94.123602. URL: https://link.aps.org/doi/10.1103/PhysRevLett.94.123602.

[412] Lucia Schwarz and S. J. van Enk. "Error models in quantum computation: An application of model selection". In: *Phys. Rev. A* 88 (3 Sept. 2013), p. 032318. DOI: 10.1103/PhysRevA.88.032318. URL: https://link.aps.org/doi/10.1103/PhysRevA.88.032318.

[413] Christian Schwemmer, Géza Tóth, Alexander Niggebaum, Tobias Moroder, David Gross, Otfried Gühne, and Harald Weinfurter. "Experimental Comparison of Efficient Tomography Schemes for a Six-Qubit State". In: *Phys. Rev. Lett.* 113 (4 July 2014), p. 040503. DOI: 10.1103/PhysRevLett.113.040503. URL: https://link.aps.org/doi/10.1103/PhysRevLett.113.040503.

[414] Daryl Michael Scott. *Contempt and Pity. Social Policy and the Image of the Damaged Black Psyche, 1880–1996*. New York: The University of North Carolina Press, 1997.

[415] K. Serniak, M. Hays, G. de Lange, S. Diamond, S. Shankar, L. D. Burkhart, L. Frunzio, M. Houzet, and M. H. Devoret. "Hot Nonequilibrium Quasiparticles in Transmon Qubits". In: *Phys. Rev. Lett.* 121 (15 Oct. 2018), p. 157701. DOI: 10.1103/PhysRevLett.121.157701. URL: https://link.aps.org/doi/10.1103/PhysRevLett.121.157701.

[416] William Shakespeare. "The Tragedy of King Lear. The Folio Text". In: *The Complete Works*. Ed. by Stanley Wells and Gary Taylor. 2nd ed. Oxford: Oxford University Press, 2005, pp. 1153–1184.

[417] Claude Elwood Shannon. "A Mathematical Theory of Communication". In: *Bell System Technical Journal* 27.3 (1982), pp. 379–423.

[418] Steven Shapin and Simon Schaffer. *Leviathan and the Air-Pump. Hobbes, Boyle, and the Experimental Life*. Princeton: Princeton University Press, 1985.

[419] Peter W. Shor. "Polynomial-Time Algorithms for Prime Factorization and Discrete Logarithms on a Quantum Computer". In: *SIAM Journal on Computing* 26.5 (Oct. 1997), pp. 1484–1509. DOI: 10.1137/s0097539795293172. URL: https://doi.org/10.1137%2Fs0097539795293172.

[420] Peter W. Shor. "Polynomial-Time Algorithms for Prime Factorization and Discrete Logarithms on a Quantum Computer". In: *SIAM Rev.* 41.2 (Jan. 1999), pp. 303–332. ISSN: 0036-1445. DOI: 10.1137/S0036144598347011.

[421] M. A. Sillanpää, T. Lehtinen, A. Paila, Yu. Makhlin, L. Roschier, and P. J. Hakonen. "Direct Observation of Josephson Capacitance". In: *Phys. Rev. Lett.* 95 (20 Nov. 2005), p. 206806. DOI: 10.1103/PhysRevLett.95.206806. URL: http://link.aps.org/doi/10.1103/PhysRevLett.95.206806.

[422] SOPHIE. *OIL OF EVERY PEARL'S UN-INSIDES*. Transgressive Records, 2018.

[423] SOPHIE. *PRODUCT*. Numbers, 2015.

[424] Ashley M. Stephens, William J. Munro, and Kae Nemoto. "High-threshold topological quantum error correction against biased noise". In: *Phys. Rev. A* 88 (6 Dec. 2013), p. 060301. DOI: 10.1103/PhysRevA.88.060301. URL: https://link.aps.org/doi/10.1103/PhysRevA.88.060301.

[425] Frederick W. Strauch, Philip R. Johnson, Alex J. Dragt, C. J. Lobb, J. R. Anderson, and F. C. Wellstood. "Quantum Logic Gates for Coupled Superconducting Phase Qubits". In: *Phys. Rev. Lett.* 91.16 (Oct. 2003), p. 167005. ISSN: 0031-9007. DOI: 10.1103/PhysRevLett.91.167005.

[426] J. Struck, C. Ölschläger, R. Le Targat, P. Soltan-Panahi, A. Eckardt, M. Lewenstein, P. Windpassinger, and K. Sengstock. "Quantum Simulation of Frustrated Classical Magnetism in Triangular Optical Lattices". In: *Science* 333.6045 (2011), pp. 996–999. DOI: 10.1126/science.1207239. eprint: https://www.science.org/doi/pdf/10.1126/science.1207239. URL: https://www.science.org/doi/abs/10.1126/science.1207239.

[427] E.C.G. Stueckelberg. "Quantum theory in real Hilbert space". In: *Helvetica Physica Acta* 33 (1960), pp. 727–752.

[428] Youngkyu Sung, Leon Ding, Jochen Braumüller, Antti Vepsäläinen, Bharath Kannan, Morten Kjaergaard, Ami Greene, Gabriel O. Samach, Chris McNally, David Kim, Alexander Melville, Bethany M. Niedzielski, Mollie E. Schwartz, Jonilyn L. Yoder, Terry P. Orlando, Simon Gustavsson, and William D. Oliver. "Realization of High-Fidelity CZ and ZZ-Free iSWAP Gates with a Tunable Coupler". In: *Phys. Rev. X* 11 (2 June 2021), p. 021058. DOI: 10.1103/PhysRevX.11.021058. URL: https://link.aps.org/doi/10.1103/PhysRevX.11.021058.

[429] *supremacy, n.* OED Online. URL: https://www-oed-com.libproxy.mit.edu/view/Entry/194796 (visited on 01/27/2022).

[430] Soraya Taghavi, Robert L. Kosut, and Daniel A. Lidar. "Channel-Optimized Quantum Error Correction". In: *IEEE Transactions on Information Theory* 56.3 (2010), pp. 1461–1473. DOI: 10.1109/TIT.2009.2039162.

[431] The Microphones. *Microphones in 2020*. P.W. Elveerum & Sun, 2009.

[432] *The Physics of Computation Conference*. MIT Endicott House. Mar. 21, 2018. URL: https://mitendicotthouse.org/physics-computation-conference/ (visited on 04/22/2022).

[433] Le Phuc Thinh, Philippe Faist, Jonas Helsen, David Elkouss, and Stephanie Wehner. "Practical and reliable error bars for quantum process tomography". In: *Phys. Rev. A* 99 (5 May 2019), p. 052311. DOI: 10.1103/PhysRevA.99.052311. URL: https://link.aps.org/doi/10.1103/PhysRevA.99.052311.

[434] Tommaso Toffoli. "How Cheap Can Mechanics' First Principles Be?" In: *Complexity, Entropy, and the Physics of Information. The Proceedings of the 1988 Workshop on Complexity, Entropy, and the Physics of Information Held May–June, 1989 in Sante Fe, New Mexico*. Ed. by Wojciech H. Zurek. Redwood City, CA: Addison-Wesley, 1990, pp. 301–318.

[435] Tommaso Toffoli. "Reversible computing". In: *Automata, Languages and Programming*. Ed. by Jaco de Bakker and Jan van Leeuwen. Berlin, Heidelberg: Springer Berlin Heidelberg, 1980, pp. 632–644. ISBN: 978-3-540-39346-7.

[436] Lars Tornberg and Göran Johansson. "Dispersive Charge and Flux Qubit Readout as a Quantum Measurement Process". In: *Journal of Low Temperature Physics* 146.1 (2007), pp. 227–252. ISSN: 1573-7357. DOI: 10.1007/s10909-006-9261-1. URL: http://dx.doi.org/10.1007/s10909-006-9261-1.

[437] G. Tóth, W. Wieczorek, D. Gross, R. Krischek, C. Schwemmer, and H. Weinfurter. "Permutationally Invariant Quantum Tomography". In: *Phys. Rev. Lett.* 105 (25 Dec. 2010), p. 250403. DOI: 10.1103/PhysRevLett.105.250403. URL: https://link.aps.org/doi/10.1103/PhysRevLett.105.250403.

[438] Sharon Traweek. *Beamtimes and Lifetimes. The World of High Energy Physicists*. Cambridge: Harvard University Press, 1988.

[439] Ivanka Trump. *It's official! The USA has achieved quantum supremacy!* Instagram post. Oct. 23, 2019. URL: https://www.instagram.com/p/B39gY-phOBp/ (visited on 12/12/2021).

[440] Anna Lowenhaupt Tsing. *The Mushroom at the End of the World. On the Possibility of Life in Capitalist Ruins*. Princeton: Princeton University Press, 2015.

[441] Eve Tuck and K. Wayne Yang. "Decolonization Is Not a Metaphor". In: *Decolonization: Indigeneity, Education & Society* 1.1 (2012), pp. 1–40.

[442] David K. Tuckett, Stephen D. Bartlett, and Steven T. Flammia. "Ultrahigh Error Threshold for Surface Codes with Biased Noise". In: *Phys. Rev. Lett.* 120 (5 Jan. 2018), p. 050505. DOI: 10.1103/PhysRevLett.120.050505. URL: https://link.aps.org/doi/10.1103/PhysRevLett.120.050505.

[443] David K. Tuckett, Stephen D. Bartlett, Steven T. Flammia, and Benjamin J. Brown. "Fault-Tolerant Thresholds for the Surface Code in Excess of 5% under Biased Noise". In: *Phys. Rev. Lett.* 124 (13 Mar. 2020), p. 130501. DOI: 10.1103/PhysRevLett.124.130501. URL: https://link.aps.org/doi/10.1103/PhysRevLett.124.130501.

[444] David K. Tuckett, Andrew S. Darmawan, Christopher T. Chubb, Sergey Bravyi, Stephen D. Bartlett, and Steven T. Flammia. "Tailoring Surface Codes for Highly Biased Noise". In: *Phys. Rev. X* 9 (4 Nov. 2019), p. 041031. DOI: 10.1103/PhysRevX.9.041031. URL: https://link.aps.org/doi/10.1103/PhysRevX.9.041031.

[445] A. M. Turing. "On Computable Numbers, with an Application to the Entscheidungsproblem". In: *Proceedings of the London Mathematical Society* s2-42.1 (Jan. 1937), pp. 230–265. ISSN: 0024-6115. DOI: 10.1112/plms/s2-42.1.230. eprint: https://academic.oup.com/plms/article-pdf/s2-42/1/230/4317544/s2-42-1-230.pdf. URL: https://doi.org/10.1112/plms/s2-42.1.230.

[446] A. M. Turing. "On Computable Numbers, with an Application to the Entscheidungsproblem". en. In: *Proc. London Math. Soc.* s2-42.1 (1937), pp. 230–265. ISSN: 1460-244X. DOI: 10.1112/plms/s2-42.1.230.

[447] *Unveiling our new Quantum AI campus*. Google Quantum AI. May 18, 2021. URL: https://blog.google/technology/ai/unveiling-our-new-quantum-ai-campus/ (visited on 07/13/2022).

[448] Lieven M. K. Vandersypen, Matthias Steffen, Gregory Breyta, Costantino S. Yannoni, Mark H. Sherwood, and Isaac L. Chuang. "Experimental realization of Shor's quantum factoring algorithm using nuclear magnetic resonance". In: *Nature* 414.6866 (Dec. 2001), pp. 883–887. DOI: 10.1038/414883a. URL: https://doi.org/10.1038%2F414883a.

[449] Farrokh Vatan and Colin Williams. "Optimal quantum circuits for general two-qubit gates". In: *Phys. Rev. A* 69.3 (Mar. 2004), p. 032315. DOI: 10.1103/PhysRevA.69.032315.

[450] Inés de Vega and Daniel Alonso. "Dynamics of non-Markovian open quantum systems". In: *Rev. Mod. Phys.* 89 (1 Jan. 2017), p. 015001. DOI: 10.1103/RevModPhys.89.015001. URL: https://link.aps.org/doi/10.1103/RevModPhys.89.015001.

[451] R Vijay, Chris Macklin, DH Slichter, SJ Weber, KW Murch, Ravi Naik, Alexander N Korotkov, and Irfan Siddiqi. "Stabilizing Rabi oscillations in a superconducting qubit using quantum feedback". In: *Nature* 490.7418 (2012), pp. 77–80.

[452] K. Vogel and H. Risken. "Determination of quasiprobability distributions in terms of probability distributions for the rotated quadrature phase". In: *Phys. Rev. A* 40 (5 Sept. 1989), pp. 2847–2849. DOI: 10.1103/PhysRevA.40.2847. URL: https://link.aps.org/doi/10.1103/PhysRevA.40.2847.

[453] John Von Neumann. *First Draft of a Report on the EDVAC*. Tech. rep. University of Pennsylvania, June 1945.

[454] Lana Wachowski and Lilly Wachowski. *The Matrix*. director Lana Wachowski and Lilly Wachowski. 1999.

[455] Joel Wallman, Chris Granade, Robin Harper, and Steven T. Flammia. "Estimating the coherence of noise". en. In: *New J. Phys.* 17.11 (Nov. 2015), p. 113020. ISSN: 1367-2630. DOI: 10.1088/1367-2630/17/11/113020.

[456] Joel J. Wallman. *Bounding experimental quantum error rates relative to fault-tolerant thresholds*. 2015. DOI: 10.48550/ARXIV.1511.00727. URL: https://arxiv.org/abs/1511.00727.

[457] Joel J. Wallman. "Randomized benchmarking with gate-dependent noise". en-GB. In: *Quantum* 2 (Jan. 2018), p. 47. DOI: 10.22331/q-2018-01-29-47.

[458] Joel J. Wallman and Joseph Emerson. "Noise tailoring for scalable quantum computation via randomized compiling". In: *Phys. Rev. A* 94 (5 Nov. 2016), p. 052325. DOI: 10.1103/PhysRevA.94.052325.

[459] Michael Walter, Brent Doran, David Gross, and Matthias Christandl. "Entanglement Polytopes: Multiparticle Entanglement from Single-Particle Information". In: *Science* 340.6137 (June 2013), pp. 1205–1208. DOI: 10.1126/science.1232957. URL: https://doi.org/10.1126%2Fscience.1232957.

[460] Joel I-Jan Wang, Daniel Rodan-Legrain, Landry Bretheau, Daniel L. Campbell, Bharath Kannan, David Kim, Morten Kjaergaard, Philip Krantz, Gabriel O. Samach, Fei Yan, Jonilyn L. Yoder, Kenji Watanabe, Takashi Taniguchi, Terry P. Orlando, Simon Gustavsson, Pablo Jarillo-Herrero, and William D. Oliver. "Coherent control of a hybrid superconducting circuit made with graphene-based van der Waals heterostructures". In: *Nature Nanotechnology* 14.2 (2019), pp. 120–125. DOI: 10.1038/s41565-018-0329-2. URL: https://doi.org/10.1038/s41565-018-0329-2.

[461] Zhi-Wei Wang, Yong-Sheng Zhang, Yun-Feng Huang, Xi-Feng Ren, and Guang-Can Guo. "Experimental realization of direct characterization of quantum dynamics". In: *Phys. Rev. A* 75 (4 Apr. 2007), p. 044304. DOI: 10.1103/PhysRevA.75.044304. URL: https://link.aps.org/doi/10.1103/PhysRevA.75.044304.

[462] T. F. Watson, S. G. J. Philips, E. Kawakami, D. R. Ward, P. Scarlino, M. Veldhorst, D. E. Savage, M. G. Lagally, Mark Friesen, S. N. Coppersmith, M. A. Eriksson, and L. M. K. Vandersypen. "A programmable two-qubit quantum processor in silicon". In: *Nature* 555.7698 (Feb. 2018), pp. 633–637. DOI: 10.1038/nature25766. URL: https://doi.org/10.1038%2Fnature25766.

[463] Steven J. Weber, Gabriel O. Samach, David Hover, Simon Gustavsson, David K. Kim, Alexander Melville, Danna Rosenberg, Adam P. Sears, Fei Yan, Jonilyn L. Yoder, William D. Oliver, and Andrew J. Kerman. "Coherent Coupled Qubits for Quantum Annealing". In: *Phys. Rev. Applied* 8 (1 July 2017), p. 014004. DOI: 10.1103/PhysRevApplied.8.014004. URL: https://link.aps.org/doi/10.1103/PhysRevApplied.8.014004.

[464] Stefan Weigert. "How to determine a quantum state by measurements: The Pauli problem for a particle with arbitrary potential". In: *Phys. Rev. A* 53 (4 Apr. 1996), pp. 2078–2083. DOI: 10.1103/PhysRevA.53.2078. URL: https://link.aps.org/doi/10.1103/PhysRevA.53.2078.

[465] Gregor Weihs, Thomas Jennewein, Christoph Simon, Harald Weinfurter, and Anton Zeilinger. "Violation of Bell's Inequality under Strict Einstein Locality Conditions". In: *Physical Review Letters* 81.23 (Dec. 1998), pp. 5039–5043. DOI: 10.1103/PhysRevLett.81.5039. arXiv: quant-ph/9810080 [quant-ph].

[466] Yaakov S. Weinstein, Timothy F. Havel, Joseph Emerson, Nicolas Boulant, Marcos Saraceno, Seth Lloyd, and David G. Cory. "Quantum process tomography of the quantum Fourier transform". In: *The Journal of Chemical Physics* 121.13 (Oct. 2004), pp. 6117–6133. DOI: 10.1063/1.1785151. URL: https://doi.org/10.1063%2F1.1785151.

[467] John Archibald Wheeler. "Beyond the Black Hole". In: *Some Strangeness in the Proportion. A Centennial Symposium to Celebrate the Achievements of Albert Einstein*. Ed. by Harry Woolf. Redwood City, CA: Addison-Wesley, 1979, pp. 341–375.

[468] John Archibald Wheeler. "Information, Physics, Quantum: The Search for Links". In: *Complexity, Entropy, and the Physics of Information. The Proceedings of the 1988 Workshop on Complexity, Entropy, and the Physics of Information Held May–June, 1989 in Sante Fe, New Mexico*. Ed. by Wojciech H. Zurek. Redwood City, CA: Addison-Wesley, 1990, pp. 3–28.

[469] Karoline Wiesner. "The careless use of language in quantum information". In: (2017). arXiv: 1705.06768 [physics.soc-ph].

[470] Mark M. Wilde. *Quantum Information Theory 2nd ed.* Cambridge University Press, 2017. DOI: 10.1017/9781316809976.

[471] M. M. Wolf, J. Eisert, T. S. Cubitt, and J. I. Cirac. "Assessing Non-Markovian Quantum Dynamics". In: *Phys. Rev. Lett.* 101 (15 Oct. 2008), p. 150402. DOI: 10.1103/PhysRevLett.101.150402. URL: https://link.aps.org/doi/10.1103/PhysRevLett.101.150402.

[472] W. K. Wootters and W. H. Zurek. "A single quantum cannot be cloned". In: *Nature* 299.5886 (1982), pp. 802–803. DOI: 10.1038/299802a0. URL: https://doi.org/10.1038/299802a0.

[473] William K. Wootters. Private correspondence.

[474] William K. Wootters. "Entanglement of Formation of an Arbitrary State of Two Qubits". In: *Phys. Rev. Lett.* 80.10 (Mar. 1998), pp. 2245–2248. DOI: 10.1103/PhysRevLett.80.2245.

[475] William K. Wootters. "Local Accessibility of Quantum States". In: *Complexity, Entropy, and the Physics of Information. The Proceedings of the 1988 Workshop on Complexity, Entropy, and the Physics of Information Held May–June, 1989 in Sante Fe, New Mexico*. Ed. by Wojciech H. Zurek. Redwood City, CA: Addison-Wesley, 1990, pp. 39–46.

[476] James R Wootton. "Benchmarking near-term devices with quantum error correction". In: *Quantum Science and Technology* 5.4 (July 2020), p. 044004. DOI: 10.1088/2058-9565/aba038. URL: https://doi.org/10.1088%2F2058-9565%2Faba038.

[477] K. Wright, K. M. Beck, S. Debnath, J. M. Amini, Y. Nam, N. Grzesiak, J.-S. Chen, N. C. Pisenti, M. Chmielewski, C. Collins, K. M. Hudek, J. Mizrahi, J. D. Wong-Campos, S. Allen, J. Apisdorf, P. Solomon, M. Williams, A. M. Ducore, A. Blinov, S. M. Kreikemeier, V. Chaplin, M. Keesan, C. Monroe, and J. Kim. "Benchmarking an 11-qubit quantum computer". In: *Nature Communications* 10.1 (Nov. 2019). DOI: 10.1038/s41467-019-13534-2. URL: https://doi.org/10.1038%2Fs41467-019-13534-2.

[478] Sylvia Wynter. "Unsettling the Coloniality of Being/Power/Truth/Freedom. Towards the Human, After Man, Its Overrepresentation–An Argument". In: *The New Centennial Review* 3.3 (2003), pp. 257–337.

[479] Xiaosi Xu, Qi Zhao, Xiao Yuan, and Simon C. Benjamin. "High-Threshold Code for Modular Hardware With Asymmetric Noise". In: *Phys. Rev. Applied* 12 (6 Dec. 2019), p. 064006. DOI: 10.1103/PhysRevApplied.12.064006. URL: https://link.aps.org/doi/10.1103/PhysRevApplied.12.064006.

[480] Fei Yan, Simon Gustavsson, Archana Kamal, Jeffrey Birenbaum, Adam P Sears, David Hover, Ted J. Gudmundsen, Danna Rosenberg, Gabriel Samach, S Weber, Jonilyn L. Yoder, Terry P. Orlando, John Clarke, Andrew J. Kerman, and William D. Oliver. "The flux qubit revisited to enhance coherence and reproducibility". In: *Nature Communications* 7 (Nov. 2016), pp. 12964–. URL: http://dx.doi.org/10.1038/ncomms12964.

[481] Fei Yan, Simon Gustavsson, Archana Kamal, Jeffrey Birenbaum, Adam P Sears, David Hover, Ted J. Gudmundsen, Danna Rosenberg, Gabriel Samach, S. Weber, Jonilyn L. Yoder, Terry P. Orlando, John Clarke, Andrew J. Kerman, and William D. Oliver. "The flux qubit revisited to enhance coherence and reproducibility". In: *Nature Communications* 7.1 (2016), p. 12964. DOI: 10.1038/ncomms12964. URL: https://doi.org/10.1038/ncomms12964.

[482] Kübra Yeter-Aydeniz, Eugene F. Dumitrescu, Alex J. McCaskey, Ryan S. Bennink, Raphael C. Pooser, and George Siopsis. "Scalar quantum field theories as a benchmark for near-term quantum computers". In: *Phys. Rev. A* 99 (3 Mar. 2019), p. 032306. DOI: 10.1103/PhysRevA.99.032306. URL: https://link.aps.org/doi/10.1103/PhysRevA.99.032306.

[483] Mingsheng Ying. *Foundations of Quantum Programming*. London: Elsevier, 2016.

[484] Renato Renner Yuxiang Yang and Giulio Chiribella. "Optimal universal programming of unitary gates". In: *arXiv:2007.10363* (2020). arXiv: 2007.10363 [quant-ph].

[485] Marko Žnidari č, Carlos Pineda, and Ignacio Garcıa-Mata. "Non-Markovian Behavior of Small and Large Complex Quantum Systems". In: *Phys. Rev. Lett.* 107 (8 Aug. 2011), p. 080404. DOI: 10.1103/PhysRevLett.107.080404. URL: https://link.aps.org/doi/10.1103/PhysRevLett.107.080404.

[486] V. Zakosarenko, N. Bondarenko, S. H. W. van der Ploeg, A. Izmalkov, S. Linzen, J. Kunert, M. Grajcar, E. Il'ichev, and H.-G. Meyer. "Realization of a classical counterpart of a scalable design for adiabatic quantum computation". In: *Applied Physics Letters* 90.2 (2007), p. 022501. DOI: 10.1063/1.2430693.

[487] Alessandro Zavatta, Silvia Viciani, and Marco Bellini. "Quantum-to-Classical Transition with Single-Photon-Added Coherent States of Light". In: *Science (New York, N.Y.)* 306 (Nov. 2004), pp. 660–2. DOI: 10.1126/science.1103190.

[488] Weiwei Zhou, Sophie Shermer, ErLing Gong, HongWei Xie, and Ming Zhang. "Identification of Markovian open system dynamics for qubit systems". In: *Chinese Science Bulletin* 57 (June 2012). DOI: 10.1007/s11434-012-5180-5.

[489] Mário Ziman. "Incomplete quantum process tomography and principle of maximal entropy". In: *Phys. Rev. A* 78 (3 Sept. 2008), p. 032118. DOI: 10.1103/PhysRevA.78.032118. URL: https://link.aps.org/doi/10.1103/PhysRevA.78.032118.

[490] Gary Zukav. *The Dancing Wu Li Masters*. New York: William Morrow and Company, 1979.

[491] Wojciech H. Zurek. "Foreword: Complexity, Entropy, and the Physics of Information — A Manifesto". In: *Complexity, Entropy, and the Physics of Information. The Proceedings of the 1988 Workshop on Complexity, Entropy, and the Physics of Information Held May–June, 1989 in Sante Fe, New Mexico*. Ed. by Wojciech H. Zurek. Redwood City, CA: Addison-Wesley, 1990, pp. vii–ix.